# ADAPTIVE CONTROL FOR SMART SOIL-STRUCTURE INTERACTION SYSTEMS WITH SEMI-ACTIVE DEVICES

A Dissertation

by

ZUHAIR ABD HACHEEM

Submitted to the Office of Graduate and Professional Studies of
Texas A&M University
in partial fulfillment of the requirements for the degree of

DOCTOR OF PHILOSOPHY

| | |
|---|---|
| Chair of Committee, | Charles Aubeny |
| Co-Chair of Committee, | Luciana Barroso |
| Committee Members, | Zenon Medina-Cetina |
| | Theofanis Strouboulis |
| Head of Department, | Robin Autenrieth |

August 2020

Major Subject: Civil Engineering

# ABSTRACT

Supplemental structural control has become a focus for researchers to improve structural performance and to maintain structural safety during hazardous events and corresponding loads. For structures without supplemental control systems, the dynamic interaction between the structure and the soil can have significant impact on the structure response, and the impact increases when structures are constructed on soft soil. Existing research has not deeply investigated soil-structure interaction effects in structures with smart control systems. The object of this research was to study the theory of the simple adaptive control (SAC) algorithm and magnetorheological (MR) damper to reduce the response for soil-structure interaction in performance-based building control design with hazard loads. Three main issues were investigated to accomplish this goal. First, many simplifications and hypotheses were utilized throughout this work to obtain the investigation computationally comprehensibly. Model reduction techniques were adopted to estimate the equivalent stiffness matrices for structures and foundations. For structures, the equivalent stiffness matrices for frame and frame shear wall systems were developed in the finite element software ETABS, as they relate to three-dimensional structures and their geometric and material properties. For soil, the equivalent stiffness matrices for rigid foundations with different soil profiles were determined using the finite element software ABAQUS. Next, the effect of SSI is numerically investigated for the variation of the period of structures (T), the structure's slenderness ratio ($\lambda$), the structure-to-soil stiffness ratio ($\sigma$), and set of earthquake loads. The mathematical model of the one-story building (SDOF) is used to

explore the general structure behavior under consideration. The results reveal that the SAC algorithm is capable to mitigate the responses of fixed base structures and SSI. Moreover, the responses and control forces of SSI systems increase with the increase in the slenderness ratio (λ). The SSI systems need to more cost of control effort and the control forces increase with increasing of the period of the fixed support structure (T). Finally, the SAC algorithm was found to be highly effective at maintaining structures experiencing SSI effects in the presence of variations in the structural systems (i.e., frame and frame shear wall systems) and soil stiffness. The performance of controlled structure changes when the soil stiffness varies from soft to medium, decreasing with decreases in soil stiffness. The performance also decreases as the stiffness of the structure increases. The SSI effect is very clear in structures constructed on soft soil, stiff structures, and frame shear wall systems.

# DEDICATION

To my country, and my family.

# ACKNOWLEDGEMENTS

I would like to thank my committee chair, Professor Aubeny, co-chair Professor Barroso, for all the support, significant advice, and kindness. This study would not have been achievable without their guidance. Moreover, my committee members, Professor Theofanis Strouboulis, and Professor Zenon Medina-Cetina, for their guidance and support throughout the course of this research.

Additionally, I want to express my gratitude for the Ministry of Higher Education and Scientific Research in Iraq (MOHESR) for financial support. Furthermore, I would like to thank my friends and colleagues and the department faculty and staff for the shared knowledge, discussions, and making my time at Texas A&M University a great experience. Finally, thanks to my family for their encouragement, their patience, and love.

# CONTRIBUTORS AND FUNDING SOURCES

## Contributors

This work was supervised by a dissertation committee consisting of Professor Charles Aubeny (advisor), Professor Luciana Barroso (co-advisor) and Professor Zenon Medina-Cetina of the Department of Civil Engineering and Professor Theofanis Strouboulis of the Department of Aerospace Engineering.

All work for the thesis was completed by the student independently.

## Funding Sources

Graduate study was supported by the Ministry of Higher Education and Scientific Research in Iraq (MOHESR). Its contents are solely the responsibility of the authors and do not necessarily represent the official views of the MOHESR.

TABLE OF CONTENTS

Page

LIST OF FIGURES

Page

LIST OF TABLES

Page

# 1. INTRODUCTION

Numerous severe hazard events such as seismic and winds loads may impact structures, inducing dynamic loads that can adversely influence their performance and even induce failure. The classical approach to designing for seismic or wind loads involves designing the structure to withstand the additional stresses and deformations induced by dynamic loading, with no explicit attempt to mitigate the dynamic response of the structure through energy dissipation. However, in the 1970's the concept of smart structures was introduced, with the intent of reducing dynamic stresses and deformations through various means of external energy dissipation. Smart structures consist of sensing and data acquisition technology, dampers and/or actuators, a control algorithm, and a control center (i.e., computer). This equipment works together to generate damping forces and improve structural performance during dynamic loading. Aside from purely passive systems, discussed subsequently, smart structures rely on a computational model to control the dynamic response of the structure. To a large degree, the computational models on which smart structures are based consider only the dynamic response of the structure; i.e., the dynamic response of the foundation and soil mass supporting the structure is not considered. This research investigates the effects the dynamic response of coupled structure-foundation-soil systems, and how this coupling effect can affect the performance of smart structures.

At the most basic level, the dynamic analysis of a structure models the system as an elastic superstructure supported by a rigid foundation, effectively neglecting the elastic response of the foundation. In actuality, foundations have a finite stiffness, and the dynamic

response of a coupled superstructure-foundation system can significantly differ from that of the superstructure alone. The mutual interaction of a structure and its supporting elastic foundation is termed ‘soil-structure interaction’ (SSI). The foundation under discussion here comprises a constructed foundation element, such as a spread footing or a pile, on or embedded into a semi-infinite elastic soil continuum. In principle, the elastic behavior of both the foundation element and the soil continuum can affect overall system response, especially in the case of pile foundations. However, the scope of this study is restricted to monolithic shallow foundations extending beneath the entire footprint of the structure. Following much of the published literature on this topic, the footing is taken as rigid. Thus, SSI effects in this study are considered within the context of a structure supported on a semi-infinite elastic soil continuum, with a rigid footing transmitting loads between the two sub-systems.

Investigating the influence of SSI on smart structure performance involves three major research thrusts:

1. Characterizing the elastic, semi-finite soil continuum as a single horizontal spring and a single rocking spring. These springs depend on soil stiffness, layering and other forms of heterogeneity, the soil profile depth, and the foundation shape and dimensions.
2. Coupling the soil springs to a single or multi-degree-of-freedom structural model. Based on this model, studies are conducted to develop basic insights into: (1) the conditions for which SSI materially influences structural response and (2) the relative significance of SSI effects.

3. Using the coupled soil-structure model, the performance of a smart structure relative to a conventional structure (with otherwise identical mass and stiffness characteristics) is investigated from three perspectives: (1) for the case of rigid supporting soil mass, (2) for the case of an elastic supporting soil mass when the control system algorithm assumes a rigid supporting soil mass, and (3) for the case of an elastic supporting soil mass when the control system algorithm accurately accounts for the elastic properties of the supporting soil mass. It is noted that the second case is most representative of the current state of practice; i.e. real soils always exhibit some degree of elastic behavior and most smart systems assume a rigid soil mass.

## 1.1 Soil-Structure Interaction

According to Mylonakis & Gazetas (2000), cases of significant damage attributed to SSI effects include earthquakes in Brancea in 1977 (Bucharest), Kobe in 1995 (Takatori, Fukiai), and Michoacan in 1985 (Mexico City). (Mylonakis & Gazetas, 2000). The Mexico City earthquake was particularly destructive, damaging all buildings 10 to 12 stories or higher that were built on soft clay because the SSI influence extended the time period from 1.0 sec to 2.0 sec (Reséndiz & Roesset, 1985) (see Figure 1-1). The 630 m elevated section of the Hanshin Expressway Route 3 in Kobe (Fukae) failed due to the SSI impact, as well (Gazetas, 1998). Celebi offered additional evidence of the SSI's role in building collapses resulting from the recent Adana-Ceyhan earthquake (1998) (Mylonakis & Gazetas, 2000). Table 1-1 lists other severe seismic events producing significant damage to buildings via the SSI effect.

The response of a building to seismic loads is influenced by interactions among three elements: the soil, structure, and foundation. SSI analysis estimates the combined response of these elements to a given seismic load. It is notable that the dynamic response of a structure constructed on soft soil should be different from that of the same structure founded on stiff soil. There are two important components of this variation. First, the SSI has more degrees of freedom, and thus a different dynamic behavior from that of a fixed support structure. Second, a vital portion of the vibrational energy of an SSI system can be dissipated by the soil medium or foundation damping. Researchers have indicated that there are two types of interactions to consider for these three elements when engaging in SSI analysis. First is the inertial interaction, which is caused by the inertia of the structure due to transformation of motion to the foundation. The second is called kinematic interaction, which results from interaction between the soil and foundation, causing foundation motion that is different from free-field motion (known as foundation input motion (FIM)) (J. Wolf & Hall, 1988), (J. P. Stewart, Fenves, & Seed, 1999), (J. P. Stewart, Seed, & Fenves, 1999).

Figure 1-2 introduces the typical standard shape of the acceleration response spectra curve currently recommended in seismic design codes. It is obvious that when the structure is massive or very stiff (e.g., frame shear trusses or shear wall structural systems) and the fixed support's period is located near Point A, the dynamic SSI effect can result in a vital amplification, so long as the united period of the SSI system is in the region of Point C. This phenomenon appears in structures such as nuclear reactors, massive turbine foundations, large vessels supported on short pedestals, and massive gravity dams that present notable amplification when the SSI is taken into account. Conversely, for every structure in which

the fixed support period is someplace between Points B and C, if the fixed support's period passes Point C, the SSI effect will cause significant attenuation. This can be seen in elevated water tanks, steel or RCC chimneys, etc. (see Figure 1-2). Therefore, relying on mass distribution, a dynamic characteristic of the soil and stiffness of the structure, the SSI can either amplify or attenuate a structure's response.

**Figure 1-1** Pounding of adjacent buildings in Mexico City (1985) due to the SSI (Bisch et al., 2012)

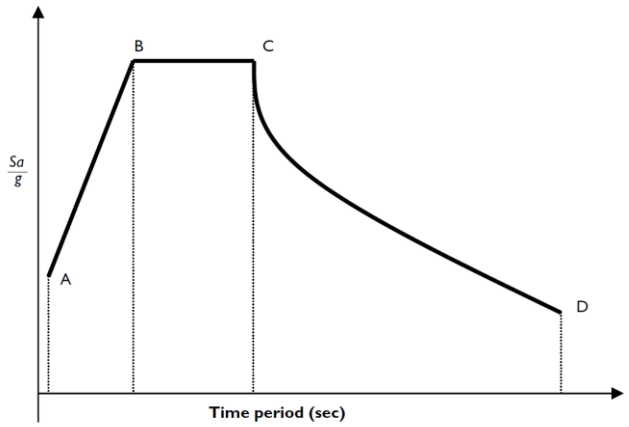


**Figure 1-2** General response spectra design curve for earthquakes (Chowdhury & Dasgupta, 2008).

**Table 1-1** Selected ground motions recorded at soft soil sites (Mylonakis & Gazetas, 2000)

| Station | Event Date | Geology | Magnitude (Ms) | Epicentral Distance (km) | Direction | PGA (g) | PGV (m/s) |
|---|---|---|---|---|---|---|---|
| Bucharest Research Inst. Basem. Bldg | Romania 3/4/77 | Soft Soil | 7.2 | 149 | NS<br>EW | 0.21<br>0.18 | 0.75<br>0.33 |
| Secretaria Communication & Transport. | | Soft Clay | | 376 | NS<br>EW | 0.10<br>0.17 | 0.39<br>0.61 |
| Central de Abastos Oficina | Michoacan 9/19/85 | Soft Clay | 8.1 | 384 | NS<br>EW | 0.08<br>0.07 | 0.42<br>0.35 |
| Central de Abastos Frigorifico | | Soft Clay | | 384 | NS<br>EW | 0.09<br>0.08 | 0.35<br>0.25 |
| Oakland Outer Harbor Wharf | Lorna Prieta 10/17/89 | Bay Mud | | 98 | N35E<br>S85W | 0.28<br>0.27 | 0.42<br>0.41 |
| Foster City Redwood Shores | | Bay Mud | 7.1 | 68 | NS<br>EW | 0.26<br>0.28 | 0.32<br>0.45 |
| San Francisco18-storey Commercial Bldg. | | Fill Over Bay Mud | | 99 | N80E<br>N10W | 0.13<br>0.16 | 0.17<br>0.16 |
| Emeryville Free Field South | | Bay Mud | | 97 | N10W<br>S80W | 0.21<br>0.26 | 0.21<br>0.21 |
| Treasure Island Naval Base | Lorna Prieta 10/17/89 | Fill | | 98 | EW<br>NS | 0.16<br>0.10 | 0.16<br>0.33 |
| San Francisco International Airport | | Bay Mud | | 79 | EW<br>NS | 0.33<br>0.23 | 0.29<br>0.26 |
| Colonia Roma | Acapulco 4/25/89 | Soft Clay | 6.9 | - | N90W<br>S00W | 0.06<br>0.05 | 0.12<br>0.11 |
| Kobe Fukiai | Kobe 1/17/95 | Soft Alluvium | 7.2 | 19 | EW | 0.80 | 1.3 |
| Kobe Takatori | | Soft Alluvium | | 10 | NS | 0.65 | 1.55 |

## 1.2 Smart Structures

One substantial challenge for civil engineers is to mitigate structural responses during dynamic loads such as severe seismic loads or strong winds. The classic design method has only a limited ability to efficiently resist dynamic loads, and the inherent damping in most structures tends to be relatively ineffective in dissipating external energy. Therefore, innovative smart structures and structural control methodologies have been adopted and implemented since the 1970s. Numerous studies have shown that the smart structure technique is a promising means of maintaining structures in the face of hazard loads (Housner et al., 1997) (Saaed, Nikolakopoulos, Jonasson, & Hedlund, 2015). In this methodology, an energy dissipation device is added to the structure and equipped to enhance its resistance capacity. This technique is an attractive option for increasing structural serviceability and safety because it can significantly improve a structure's seismic performance. Devices can be retrofitted into existing structures or implemented to sustain new buildings. Figure 1-3 lists energy dissipation devices and applications in smart structures. Smart structures consist of sensing and data acquisition technology, dampers and/or actuators, a control algorithm, and a control center (i.e., computer). All of this equipment works together to generate damping forces and maintain the structure during hazard loads. Figure 1-3 d and e illustrate a typical setup for a smart structure with an accumulated semi-active hydraulic damper (ASHD) device. The operating mechanisms of smart structures can be classified into four principal types: passive, active, semi-active, and hybrid.

### 1.2.1 Passive Control Systems

Passive control systems dissipate external energy, depending essentially on energy dissipation devices or base isolation. In the past, passive control was considered a smart system because it generates more damping forces, increasing in proportion to the quantity of the structural response. Usually, a passive system has limited intelligence because it cannot modify the load or structural response, and consequently often offers an inadequate control capacity. It is optimally attuned to save the structure versus a special dynamic load, and its performance is likely to be non-optimal in situations with different dynamic loads. An energy dissipation device is completely reliant on the relative motion of the structure and is administered only by the local structural response. Nevertheless, passive control devices are essentially stable, and operate without the need for structural response measures or any external energy; thus, they are comparatively easy to construct and design (Saaed et al., 2015).

### 1.2.2 Active Control Systems

Notwithstanding the reliability and comparative affordability of passive control devices, they generally are inadequate in terms of structural response and offer only a limited range of intelligence. For accurate structural response feedback, active control systems supply a higher level of performance than do passive control systems whose operation is completely administered by local structural responses (Housner et al., 1997). Active control systems require a great deal of energy to prevent impacts from severe natural hazards, and this is difficult to guarantee since energy equipment often collapses during such situations.

Furthermore, active control systems require sensors and controller devices to adapt a structure's response through the application of control forces. This may lead to an unstable or undesirable situation for the structural system. Active control systems do offer certain advantages such as intensified control effectiveness with no ideological limits on performance, as well as flexibility in the face of different hazard loads, the ability to sense excitation and automatically adapt to counterbalance, choosiness with regards to control purposes, designs that allow for the attainment of different goals such as safety or comfort, and a general applicability to different load cases. Active systems can be designed to overcome a broad frequency range in terms of loadings (Dyke, Spencer Jr, Quast, & Sain, 1995), and (Sivaselvan, Reinhorn, Shao, & Weinreber, 2008).

### 1.2.3 Semi-Active Control Systems

Semi-active control devices are the normal evolution of passive control. Ordinarily, they are called intelligent or controllable dampers because they involve adjustment systems that adapt their performances and responses. To enhance behavior, this type of system adapts the damper performance based on feedback information related to structural responses and loads. A semi-active system consists of sensors that read the input and/or output, a control computer that prepares the analysis and provides signals to control the actuators, a control actuator that commands the operation of the passive device, and the passive device itself (Cheng, Jiang, & Lou, 2008).

a) Four story base-isolated building

b) External retrofit of a building

c) Retrofit with fluid viscous dampers

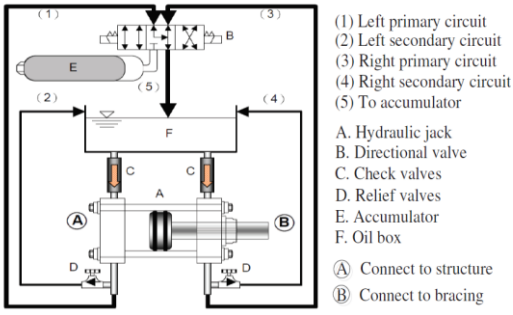


d) Schematic of an ASHD system

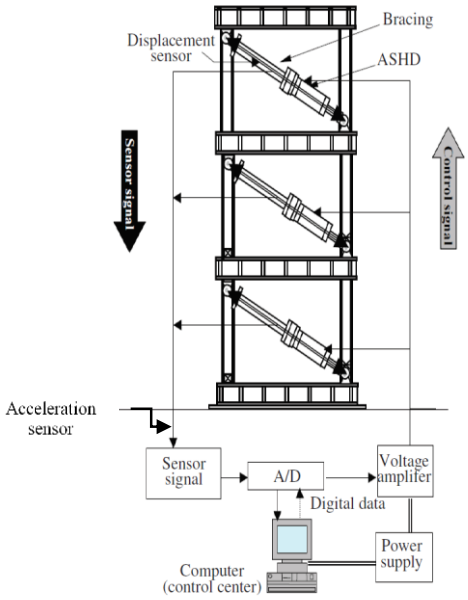


e) Setup of a typical smart structure with an ASHD system

**Figure 1-3** Different smart structure applications (Edrees, 2015).

In semi-active devices, an actuator is employed to manage the device's characteristics rather than directly subjecting the structure to the controlled force. Such devices require only simple energy sources such as batteries, which is significant because energy equipment often collapses under hazard loads, creating unstable structures. Notwithstanding this difficulty, semi-active systems are simple to produce, dependable in service, offer fail safety, and generally are better than passive systems (Housner et al., 1997).

The drawback of this type of device is that because it operates passively, its control effort is inadequate. However, it is promising because it mixes the characteristics of both active and passive devices (H.-J. Jung, Spencer Jr, Ni, & Lee, 2004).

### 1.2.4 Hybrid Control Systems

These control systems possess certain drawbacks; therefore, they should be organized in parallel or series arrangements to allow for their benefits while reducing the effects of their discrete disadvantages. These innovative arrangement systems are essentially defined as hybrid control and have been considered interesting solutions for hazard loads since the 1990s. In these systems, passive devices are used to obtain most of the response reduction needed to maintain the structure within the desired performance zone, while active implements are employed to modify and tune the response (e.g., minimizing acceleration and displacement to keep the structure safe). Hybrid systems have higher capacity and efficiency levels than do passive or active systems, and are more economical. Additionally, they are more reliable and require less power than do active systems because there is no need for substantial control forces, though power is still vital. Hybrid systems are very efficient

at protecting structures from various types of excitation with different frequencies and intensities (Housner et al., 1997), (Y.-L. Xu & He, 2017), (Cheng et al., 2008), and (Saaed et al., 2015).

## 1.3 Smart SSI Systems

Researchers have demonstrated that the SSI has a significant effect on the structural response if the structure in question is constructed on soft soil (Cheng & Suthiwong, 1996), (H. Li & Wang, 2011), and (Nazarimofrad & Zahrai, 2016). Despite the fact that there has been fast progress in the area of smart structure technology, application of such technology to the SSI problem has been insufficiently investigated. However, studies have shown that the SSI affects control performance, and a greater impact will be seen if the soil underneath the foundation is soft (Amini, Bitaraf, Nasab, & Javidan, 2018). In the present research, the SSI's impact on the effectiveness of a semi-active control device (i.e., an MR damper) and its employment via a simple adaptive control (SAC) algorithm are investigated for moments-resistant and frame-shear wall structural systems.

# 2. BACKGROUND

This research investigates the effect of soil-structure interaction (SSI) on structural control systems. To assess the current state of knowledge relevant to this research focus, extensive literature reviews were performed on the practical significance of SSI, the methods of analysis to predict SSI effects on conventional structures, the different categories of control systems, the instrumentation, equipment and algorithms utilized in the various control systems, and previous research investigation the effects of SSI on the performance of control systems. This chapter summarizes the findings of the literature review.

## 2.1 Soil Structure Interaction Systems in Buildings

Seismic soil structure interaction (SSI) is one of the most significant research areas in geotechnical earthquake engineering. Hadjian, Luco, and Tsai (1974) presented the earliest review on this topic, in which both the continuum and finite element methods were presented. These researchers also noted that these methods required solving problems of suitability, efficacy, and adequacy, while also recognizing that each is useful and applicable in special relevance cases (Hadjian, Luco, & Tsai, 1974). Kausel (2010) offered an excellent survey of the early history and analytical methods of static and dynamic SSI. This treatise focused on finding essential analytical solutions for shallow circular and rectangular foundations constructed for elastic half-space problems. It is of note that most of the studies reviewed adopted very versatile numerical methods (Kausel, 2010). Lou, Wang, Chen, and Zhai's (2011) review included recent research on SSI evaluation and analysis. This work

focused on analytical and numerical methods, experiments, prototype observations, site-city interactions, computer programs, and future research tendencies. The advantages, disadvantages, and applicability of the aforementioned topics were also discussed (Lou, Wang, Chen, & Zhai, 2011).

Roesset (2013) offered a useful description of the initial stages of SSI, demonstrating how the topic has developed and highlighting the advantages and disadvantages of the substructure and direct methods. This survey also illustrated the interaction effects among the various piles in a group pile. This work offered a critical historical perspicacity study that included material from 1920 to 2013, and clarified knowledge of interest to designers of nuclear power plants (Roesset, 2013). In Kavitha, Beena, and Narayanan's study (2016), SSI in lateral load pile analysis was reviewed, focusing on significant SSI parameters such as soil properties and profiles, ground surface inclination, and pile geometry and arrangement (Kavitha, Beena, & Narayanan, 2016). Sharma, Dasgupta, and Dey (2018) offered a comprehensive state-of-the-art review investigating the features and effects of seismic SSI and analyzing the different available design codes. This work also illustrated research on SSI methodologies, computational methods, and soil mathematical models in an effort to improve the essential body of knowledge on this topic (Sharma, Dasgupta, & Dey, 2018).

It is remarkable that the Kobe (Takatori, Fukiai) earthquake of 1995, Michoacan earthquake in 1985 (Mexico City (SCT)), and Brancea earthquake in 1977 (Bucharest) all resulted in damage stemming from SSI effects (Mylonakis & Gazetas, 2000). The Mexico earthquake in 1985 was especially destructive, damaging all buildings 10 to 12 stories in

height that were constructed on soft clay because the SSI effect increased the period of buildings from 1.0 sec to nearly 2.0 sec (Reséndiz & Roesset, 1985). The 630 m elevated highway section of Hanshin Expressway Route 3 in Kobe (Fukae section) also collapsed due to SSI effects (Gazetas, 1998). Celebi provided additional evidence of SSI's role in building collapses in the recent Adana-Ceyhan earthquake (Celebi, 1998).

There are two processes for analyzing SSI systems: direct and substructure. Figure 2-1 offers a sketch of both. The **direct method** depends on the finite element method to analyze the soil and structure in one mesh. The soil is assumed to be a continuum-based media, and discreteness is maintained using a plane strain element. The interaction region is described by interface elements and the structure model by beam elements. This method assumes that kinematic interaction is negligible and the free field ground motion and foundation will move together. The external forces of the system come from ground acceleration. One important advantage of this method is that it can analyze a system's nonlinear behavior.

The **substructure method** assumes that the soil and structure are independent of one another and have two separate mathematical models or substructures. In the contact area, each substructure has the same interaction force, but with an opposite direction. This system is very suitable for frequency domain analysis (J. Wolf & Hall, 1988), making the SSI system easy to solve by dividing it into discrete parts.

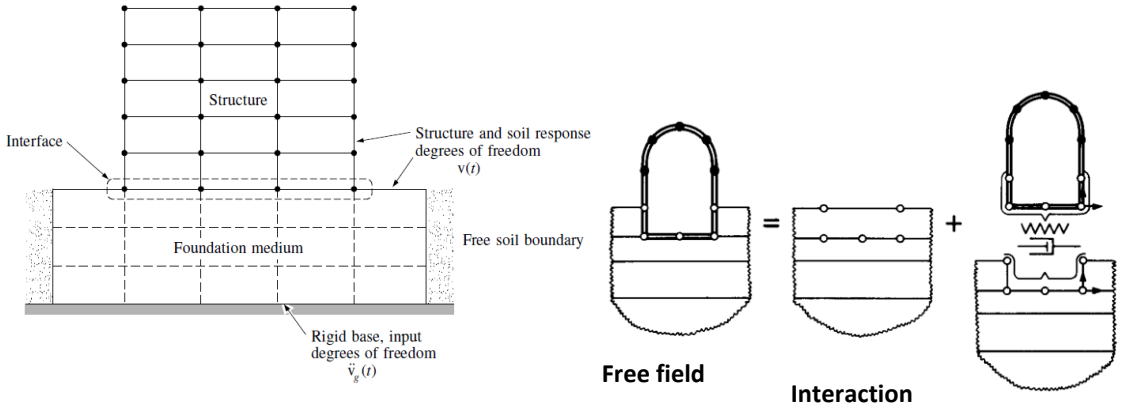


**Figure 2-1** Approaches to soil structure analysis: a) direct (Clough & Penzien, 1993) and b) substructure(J. Wolf & Hall, 1988).

## 2.2 Theoretical Background of Smart Structures

A smart structure or structural control has the ability to sense variations in environment loads or other characteristics of the system, diagnose any problem approaching a critical condition, use sensing and data acquisition systems to store and process information and make appropriate decisions regarding enhancing the system's performance, and maintain structural integrity, serviceability, and safety (Cheng et al., 2008). Smart structures can be classified based on their operational mechanisms, which fall into four main categories: passive, active, semi-active, and hybrid. (Saaed et al., 2015) and (Housner et al., 1997) documented excellent reviews of these control strategies and presented the advantages and disadvantages of each.

One significant control system commonly utilized for structural control is called a **passive control system**. In this mechanism, no external energy needs to dissipate from the input energy because the system includes energy dissipation devices. The dissipation

mechanism relies completely on the relative movement of the structure, and is regarded only as the structure's local response. Generally, passive systems can be termed limited intelligence systems because these mechanisms are unable to significantly reduce structural dynamic response and have a limited control capacity. Furthermore, passive systems cannot deal with uncertain loads, and their parameters are unable to change. However, passive control is inherently stable; there is no need for external energy to measure the structural response or for control system operation. They are also relatively easy to design and construct. A passive control system can be developed to protect the structure for a specific dynamic loading , but the control will be generally less effective for other dynamic loading conditions (Cheng et al., 2008), (Y.-L. Xu & He, 2017), (Housner et al., 1997), and (Saaed et al., 2015).

**Active control systems** overcome the weaknesses of passive control systems in many ways. Active systems adopt feedback control schemes in their operation. There are many advantages, such as the ability to sense a load and modify the control forces. They can also be designed for different purposes such as comfort or safety, and are able to utilize numerous loading excitations. They offer unlimited control effectiveness. However, these systems are very complex because they require sensors and controllers, and modify the dynamic behavior of a structure by changing the system's energy. They demand a significant amount of energy to mitigate dynamic excitation, which cannot be guaranteed during severe hazard loads. Generally, they are very sensitive to variations in structural parameters and may be unstable. Also, to produce substantial control forces, they required substantial energy. One popular device utilized for active control is the hydraulic actuator. (Dyke et al.,

1995), and (Sivaselvan et al., 2008) discuss the dynamic behavior and fluid nonlinearity of hydraulic actuators.

The **semi-active control system** is the natural extension of active and passive control**,** combining the positive features and advantages of both. Therefore, it is a very promising avenue of investigation. The essential improvement in performance comes from regulation of the damper behavior through a feedback mechanism. A semi-active control system consists of sensors, a computer controller, actuator, and passive damping device. In semi-active control, the actuator is used to modify the passive properties, instead of generating control forces on the building's system. Therefore, semi-active control systems need little power (such as a single b attery), which is a very significant feature, especially during hazard loads. Regardless of the complexity associated with semi-active control, such systems are easy to manufacture and offer high reliability and stability, as well as fail-safe mechanisms (Housner et al., 1997), (Y.-L. Xu & He, 2017).

A **hybrid control system** consists of a combination of arrangements in parallel or as part of a series of other control systems (i.e., passive, active, and semi-active controls). Thus, they can exploit the advantages of each system while minimizing the associated disadvantages. Since the 1990s, hybrid control systems have been considered the ideal solution for smart structures. In hybrid systems, passive devices can be utilized to achieve the main portion of structural response reduction, maintaining the building within the stability requirements. The active device only tunes and adjusts the final response of the structure. Hybrid control systems offer higher efficiency and a greater capacity than do passive systems, and are cheaper. Likewise, they require less energy and are more reliable

than active controls because there is no need for substantial control forces. They do, however, still require significant power. Hybrid control systems are more effective at protecting buildings than are other types of control systems when facing the same severe hazard loads (Cheng et al., 2008) and (Y.-L. Xu & He, 2017). Figure 2-2 classifies and summarizes the relevant control systems (Saaed et al., 2015).

Well-known examples of **semi-active devices** include electrorheological dampers (ER) and magnetorheological dampers (MR). ER dampers are filled with a special fluid that can change its properties when an electric field is applied. The special fluid inside MR dampers changes its properties when subjected to a magnetic field. Both feature feedback control systems for adjusting control forces and require very little power to operate. The ability to achieve a large yield stress is the main advantage of MR dampers over ER dampers. In terms of fluid viscosity, the MR fluid is a magnitude greater in terms of yield stress (over ER fluid). Therefore, the quantity of MR fluid required for operation is less than what is needed by an ER damper with the same capacity. Moreover, MR dampers are better than ER dampers in extreme temperatures, and in situations of contamination and breakdown (Spencer & Sain, 1997).

Numerous studies have investigated the behavior and dynamic modeling of MR damper devices. Spencer (1997) mentioned their significance in a review of dynamic models for MR dampers (Spencer Jr, Dyke, Sain, & Carlson, 1997). The Bouc-Wen (Wen, 1976), Bingham (R Stanway, Sproston, & Stevens, 1985), and Gamota and Filisko (Gamota & Filisko, 1991) models have all been thoroughly discussed. A modified Bouc-Wen model was established to describe the dynamic modeling of MR dampers. Figure 2-3 illustrates some

of the dynamic models used for MR dampers. Yang et al. (2002) developed a dynamic model for full-scale MR dampers and compared the prediction results with those obtained from experiments (Yang, Spencer Jr, Carlson, & Sain, 2002). That study demonstrated the excellent experimental calibration used to determine MR damper parameters. Jung (2004) achieved state-of-the-art implementation of MR dampers in smart structures (H.-J. Jung et al., 2004). In Tsang et al. (2006), a simplified inverse model for MR dampers was presented in order to calculate the voltage relied upon for the MR damper's feedback command (Tsang, Su, & Chandler, 2006).

Semi-active devices are resettable, and consist of a valve and two-way piston. In the case of a closed valve, the piston motion compresses the cylinder's fluid; in the case of an open valve, the fluid's energy dissipates. Barroso et al. (2003) investigated the application of semi-active devices for mitigating the structural response of steel moment-resisting frame systems under multi-level seismic loads (Barroso, Chase, & Hunt, 2003).

One the notable element of closed-loop control systems is the control algorithm, which calculates the control command by relying on the control law. Control devices generate and apply control forces to a building, depending on the control command. Control algorithms can be classified on the basis of gain, into either non-adaptive or adaptive groups. Control gains in adaptive control algorithms are estimated earlier and invariant with time. Optimal control mechanisms such as linear quadratic regulators (LQR) are one example of non-adaptive control algorithms. In adaptive control algorithms, control gains are unknown and variant with time. They are calculated on line, depending on the structural dynamic response. Adaptive control can be categorized according to structural parameters, as either

direct or indirect. With direct adaptive control structural parameters can be obtained explicitly, while indirect control implicitly obtains the structural parameters implicitly.

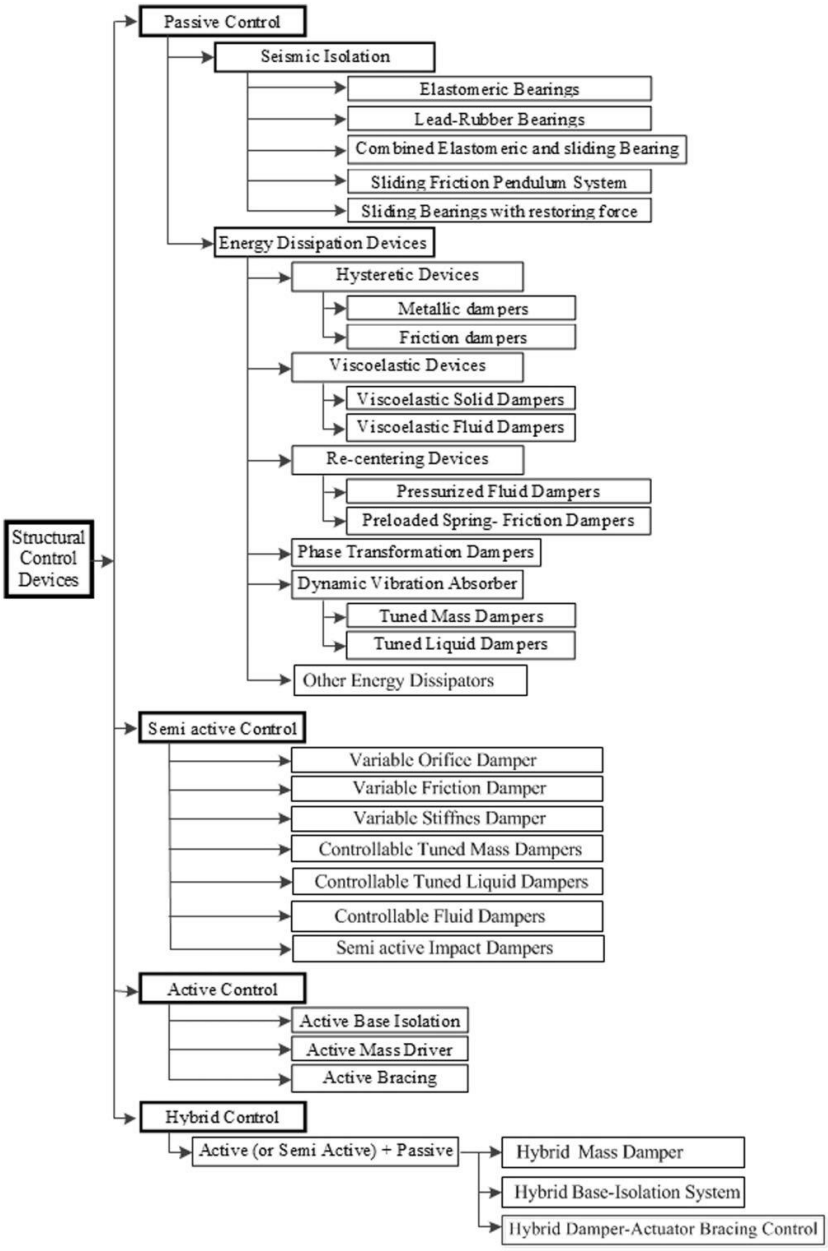


**Figure 2-2** Classifications of smart structures (Saaed et al., 2015).

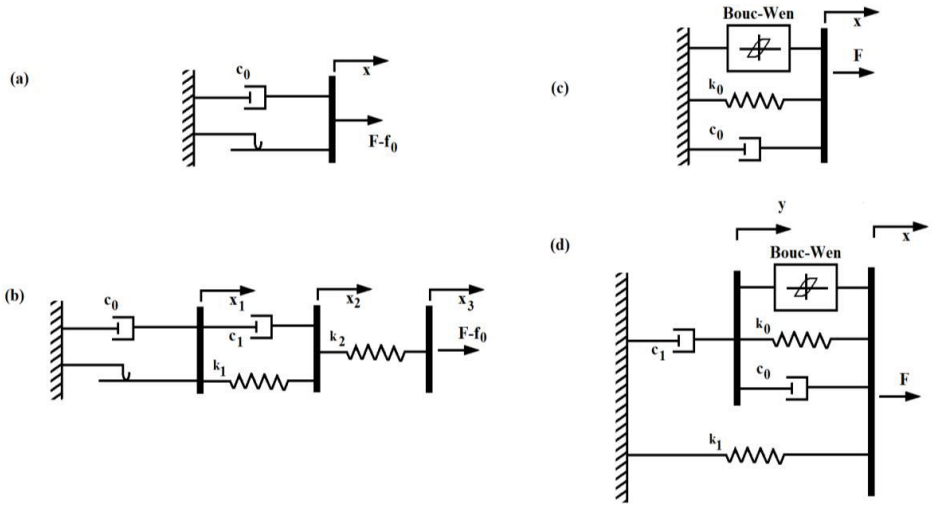


**Figure 2-3** Dynamic models of MR dampers: (a) Bingham, (b) Gamota and Filisko, (c) Bouc-Wen, (d) modified Bouc-Wen, as adapted from (Spencer Jr et al., 1997).

Model reference adaptive control (MRAC) and simple adaptive control (SAC) are excellent examples of the adaptive control algorithm.

SAC is an extension of the standard MRAC technique. Sobel et al. (1982) traced the development of the fundamental idea behind SAC (Sobel, Kaufman, & Mabius, 1982). SAC evolved in several subsequent studies (Bar-Kana, 1987) (BAR-KANA & Guez, 1990) (Bar-Kana & Kaufman, 1993) (Barkana, 2005) (Barkana, 2008) (Barkana, 2013) (Barkana, 2014) (Barkana, 2016a) (Barkana, 2016b) (Barkana, 2016c). The main feature is the modification of the limitations of the standard MRAC in order to deal with multiple-input-multiple-output (MIMO) systems that appear in full-state feedback, full-order observers, instability, and other cases. A block diagram of SAC appears in Figure 2-4. Barkana (2014) described the latest developments regarding the SAC method. That study also contained a comprehensive review and proof of MRAC's stability under typical conditions (Barkana, 2014).

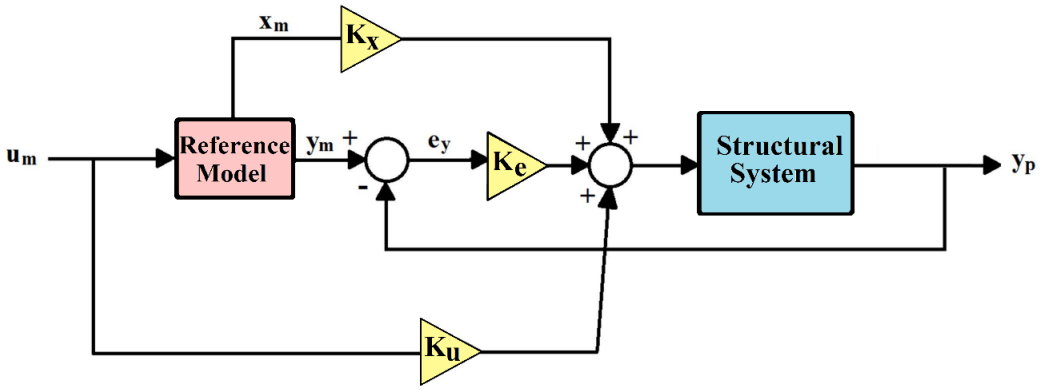


**Figure 2-4** Block diagram of SAC (Wysard Soares, 2019).

If the full state vector is available and the system is completely stable, MRAC performs a strict positive actual condition and is undoubtedly stable. Nevertheless, Barkana indicated that unmodeled dynamics, occurring when the structure's system is a higher order than the model reference. Have the potential to cause instability during noise or disturbances effects. SAC can be utilized with a remarkably decreased order model reference (as compared to the real system of the structure), and is beneficial to systems that are inclined towards instability. Furthermore, SAC has been proven to asymptotically confirm perfect tracking, and successfully evades the requirement of estimators.

Barkana (2016c) carried out an additional analytical study to address certain problems associated with diverging from adaptive gains stemming from the effects of disturbances. Prior to the aforementioned research, a sigma term was utilized to confirm stability during disturbance effects (Barkana, 2016c). However, this sigma term eliminated perfect tracking and introduced chaotic phenomena. In that study, Lyapunov's stability proof was incorporated with other methods and a parallel feedforward term presented to the SAC

formulation to include robustness and perfect tracking during non-ideal scenarios and disturbances (Barkana, 2016c). Since its appearance, SAC has been successfully utilized in numerous engineering applications involving structures. The results of these studies show that SAC is a promising means of dealing with variations in noise, system parameters, and disturbances.

## 2.3 Smart Structure Applications for SSI Systems

Structural control has recently gained in both recognition and interest. Civil engineers use control techniques to reduce the effects of hazard loads. SSI has significant impacts on the analysis and design of structures. This section presents a summary of the work related to SSI for systems that employ seismic control techniques.

Wong and Luco (1991) studied the effects of SSI on control rules and the effectiveness of active control. They modeled their structure as a uniform shear beam with a rigid foundation on half-elastic space. The seismic load was modeled as vertical shear waves. These researchers considered an absorbing boundary (i.e., active control) at the top of the beam. The active control was found to cancel the reflection of waves at the top, as well as resonance within the superstructure. The researchers found that the rocking changed the control rule related to the interaction of kinematic and inertial forces (Wong & Luco, 1991).

In 1992, Xu and Kwok examined the wind-induced motion of tall or slender structures equipped with tuned mass damper staking into account the effect of soil compliance under the foundation. Researchers applied a transfer matrix formulation to

analyses the soil-structure-mass damper interaction in the frequency domain. Numerical analyses illustrations indication that soil compliance will influence responses of structure and the performance of tuned mass dampers, relying on the properties of the structure, the type of structural response, the properties of the soil, and the nature of the excitation (Y. Xu & Kwok, 1992).

In 1993, Alam, and Baba published research describing a new algorithm for a bridge tower called robust active optimal control, to be used as protection against earthquakes with SSI, and studied parameter changes in the soil. These researchers demonstrated that optimal regulator control for a building with fixed support and without an observer was completely ineffective in soft soil. In addition, they found that SSI effects must be considered in the control algorithm, and optimal regulator control systems with SSI and an observer are robust for variations in the soil shear wave velocity (i.e., soil parameters) (Alam & Baba, 1993).

Wu, Wen-Hwa, and Smith (1993) developed new formulations of equations for internally (i.e., active tendon) and externally (i.e., active mass damper) controlled structural systems, including SSI in the frequency domain. The authors showed that the transfer functions for control force and ground motion must be multiplied by an SSI transfer function. For active mass dampers, the SSI transfer functions are the same as for control force and ground motion, while for active tendons these functions are not same. With active mass dampers, the control force acts like external ground motion in the active damper case and as an internal force in the active tendon scenario. Their work presented a comparison between these two control formulations, depending on a numerical example of the SDOF system. The

authors concluded that the active mass damper system was appropriate in terms of decreasing the system's response and minimizing dynamic energy (Wu & Smith, 1995).

In 1996, Cheng and Suthiwong developed a means of active control of seismic excitation for structures on embedded foundations. The researchers presented mathematical models with and without SSI for active control and applied the frequency property of layers and half-space of nonhomogeneous soil for SSI cases. They used optimal closed-loop theory that depended on a generalized performance index. The control rule involved the horizontal and rocking displacement of foundations for control systems with SSI effects. Time domain analysis was also applied using these mathematical models. The results showed the significant effect of the depth of the soil layer and foundation embedment on both rocking and structural response. The foundation's degrees of freedom gave additional modes that completely changed the structural behavior. The translation mode was found to have an important effect on low-rise buildings, while the rocking mode profoundly affected high-rise and/or massive buildings. For massive low-rise buildings, the two modes led to significant responses. In control systems without SSI effects, the reduction in response came from relative floor translation, but in systems with SSI, the reduction came from a decrease in rocking. Moreover, the efficiency of the active control decreased for buildings on soft soil (Cheng & Suthiwong, 1996).

In 1997, Smith and Wu presented an optimal control algorithm that included the effects of SSI and applied it in general control MDOF systems with SSI. The algorithm involved deriving the transfer functions for control force and ground motion to minimize the calculations required for structural response. The researchers also developed equivalent

MDOF with a fixed support model to represent the general MDOF with SSI system. To solve the optimal control gain for this type of system, they applied an iteration technique. The results showed that in terms of suppressing structural response, the new control algorithm that included SSI was more effective than the algorithm with a fixed support model, but it required more control force as compared to the results of the same algorithm using a fixed base system (Smith & WU, 1997).

In 1998, Luco presented an active control system for one-story structures with SSI. The method relied on modified equivalent 1-DOF oscillators that described the effects of both the control system and SSI. The researcher found that control reduces the relative horizontal displacement, rocking motion of the foundation, and internal deformation of the structure. For small control forces, the effects of SSI led to a decrease the structural deformation and control forces, while increasing the rocking motion and relative displacement of the foundation. For large control forces, SSI effects may lead to deformities in the structure larger than those calculated without SSI. The author also presented a simple method for including SSI effects in the control gain (Enrique Luco, 1998).

In 2000, Takewaki developed a new well-organized method for optimal viscous damper (VD) location in buildings with a tuned mass damper (TMD) considering SSI effects to amplify the building responses. The non-linear amplification of SSI is represented by an equivalent linear model and local interaction with the soil is combined with a horizontal dashpot and spring. The mathematical model included a description to hysteretic damping of the surface ground and radiation damping into the semi-infinite viscoelastic ground. Also, an original stiff direction search model is used to the interaction model with a TMD. Analytic

formulations of the inverse of the coefficient matrix (tridiagonal matrix) authorize one to calculate the transfer function and its derivative concerning to design variables very effectively. the results confirmed that simultaneous use of added viscous dampers and a TMD is very efficiently in the ratio of the fundamental natural period of the building to that of the surface ground and response reduction is a fundamental parameter for distinguishing the optimal damper position. Many examples without and with a TMD for different soil situations are given to prove the validity and efficiency of the introduced method (Takewaki, 2000).

Zhang, Cheng, and Jiang introduced the design of the intelligent control strategy to minimally employ the active energy and to maximally employ the passive damper. Therefore, the active controller serves for severe earthquakes and the passive controller of the hybrid system is intended for medium and small earthquakes, whenever the response of structure passes the origin values. In this research, the hybrid control system with this approach is investigated under and the ground motions created regarding the tectonic movements of seismic plates and existing earthquake records; the impact of SSI on the control performance is studied. Relying on analyses of 1-story and 6-story structures, it is summarized that the intelligent strategy is useful for the hybrid control, and SSI demands to be involved in the treatment of the intelligent hybrid system as well as other types of control for structures on soft soil (Xiaozhe Zhang, 2004), (XZ Zhang, Cheng, & Jiang, 2006).

In 2008, Liu, Chiang, Hwang, and Chu developed a mathematical model to predict wind-induced vibrations of a high-rise building with a tuned mass damper (TMD) when SSI is adopted. The model is established on time-domain analysis, and the numerical illustrations

are employed to evaluate the performance of a TMD for vibration reduction during wind loads. In this paper, the results show that the suggested model can reasonably predict the characteristics of the soil. It can more correctly estimate wind-induced responses of a structure with a TMD than fixed-base models. Likewise, if SSI is ignored, the performance of TMDs will be underestimated and structural vibrations will be overestimated. The researchers' conclusions emphasize that TMDs are useful devices in decreasing wind-induced oscillations of high-rise buildings. In particular, they are more efficient and operative for the higher soil stiffness (Liu, Chiang, Hwang, & Chu, 2008).

Lee et al (2009) performed an investigation to assess the effectiveness of an MR damper to mitigate the building seismic response including the SSI effects. Lee and Min studied an MR damper performance variance because of the variation of the building's natural period by creating its normalized response spectrum depending on the numerical analysis of many earthquakes and the building's natural period. Lee and Min also normalized the MR damper force by the structural base shear force, and its amplitude and evaluated decrement of response. Lee and Min evaluated numerically the characteristics of SSI system due to various soil conditions, and the increasing of the building's natural period relied on the response spectrum analysis. Lee and Min evaluated the numerical results with and without including the SSI effects for the building structure with an MR damper. In this study, comparative evaluations of simulations with and without SSI demonstrated that the SSI effect should be included (S. K. Lee et al., 2009).

In 2010, Li, Yu, Xiong, and Wang have developed the equations of motion for the soil-asymmetric structure-active multiple-tuned mass dampers (AMTMD) interaction

system in the frequency domain subjected to the earthquake loads using the Fourier transform. In this study, the standard for investigating the optimum factors of the AMTMD is selected as the minimization of the minimum values of the maximum displacement dynamic magnification elements (DMF) of the asymmetric building with the AMTMD. The calculation criterion of the efficiency of the AMTMD is elected as the ratio of the minimization of the minimum amounts of the maximum displacement DMF of the asymmetric building with the AMTMD to the maximum displacement DMF of the asymmetric building without the AMTMD. By applying these two criteria, the parametric studies for the effectiveness of the stiffness ratio of the soil to the building, the height-to-base ratio of the SSI system, the normalized eccentricity ratio (NER), torsional to translational frequency ratio (TTFR), and are then achieved on two the robustness and effectiveness of the AMTMD. Concurrently, the performance of an active-tuned mass damper (ATMD) with the optimum location is as well given and discussed the comparison with that of the AMTMD. Comprehensive numerical analyses indicate that both the ATMD and AMTMD can efficiently mitigate the torsional and translational responses of asymmetric buildings constructed on soft soil (C. Li, Yu, Xiong, & Wang, 2010).

Lin, Chang, and Wang investigated SSI effects on active control systems for irregular structures with torsional coupled buildings under an earthquake load. The researchers used an H∞ direct output feedback control algorithm to reduce the responses of the torsional coupled building, finding that the number of sensors and controllers and their locations relied on the degree of floor eccentricity. For a high two-way eccentricity, a one-way active tendon placed in one of two frames farthest away from the center of resistance was found to reduce

both torsional and translational responses. The SSI effect was dominated by the slenderness ratio of the building, as well as by the stiffness ratio of the soil to the building. They further suggested that a control system could still reduce a building's response to a high SSI effect and recommended that torsional coupling and SSI effects should be incorporated into the design of active control devices. This is particularly important for cases of tall buildings constructed on soft soil (Lin, Chang, & Wang, 2010).

Although rocking of shallow foundations may be designed to maintain many beneficial features such as self-centering, isolation, and, energy dissipation, current seismic design codes often avoid energy dissipation under foundations and nonlinear soil behavior. In 2011, Gajan and Saravanathiiban presented a comprehensive investigation to compares the performance of energy dissipation in foundation soil during rocking with the performance of structural energy dissipation devices during earthquakes. Numerical analyses were achieved to systematically study the seismic energy dissipation in structural elements and passive controlled energy dissipation devices embedded in the building. The numerical model was verified using shaking table laboratory results on the model of buildings with and without energy dissipation devices. The energy dissipation in the building, displacement, drift ratio, and the force demands on the structure are compared with energy dissipation features of rocking shallow foundations as discovered in centrifuge tests, where shallow foundations were permitted to rock on dry sandy soil stratum through dynamic loading. For the buildings with energy dissipating devices, about 70–90% of the seismic input energy is damped by devices, while foundation rocking damps about 30–90% of the total seismic input energy in foundation soil relying on the static safety factor. The

results show that, if suitably designed with stable capacity and tolerable settlements, opposing influences of foundation rocking can be reduced, while taking benefit of the desirable characteristics of foundation rocking and therefore they can be used as effective and economical seismic energy dissipation devices in buildings and bridges (Gajan & Saravanathiiban, 2011).

In 2011, Li and Wang presented an experimental study investigating the capability and feasibility of MR dampers commanded by a decentralized control algorithm for the seismic control of nonlinear structures that include SSI. The experimental model consisted of a two-story reinforced concrete RC frame, soil layers, a container, two MR dampers set in the first story, and a shaking table. Figure 2-5 shows the test setup. The model was subjected to different seismic excitations during the shaking table tests. Researchers treated the SSI as an additional external excitation and the nonlinear behavior of the test RC structures as an unknown nonlinear term. Li and Wang demonstrated that an MR damper can effectively reduce the response of an SSI system and infrastructure (i.e., soil response, pile response, and the earth pressure applied to the piles). The proposed decentralized algorithm was validated through the experiment (H. Li & Wang, 2011).

In 2011, Amini and Shadlou studied the effects of embedment depth using a substructure approach that included soil foundation structure interaction (SFSI) effects for earthquake excitation under plane strain conditions. They assumed the soil to be elastic, homogeneous, and isotropic, and the foundations to be rigid. Also, control devices were installed on each floor. The results showed that the $H_2$ norm of the transfer function of a control system with SFSI becomes larger as the shear wave velocity becomes smaller.

Moreover, according to Amini and Shadlou, SFSI effects should be considered in controller design (Amini & Shadlou, 2011).

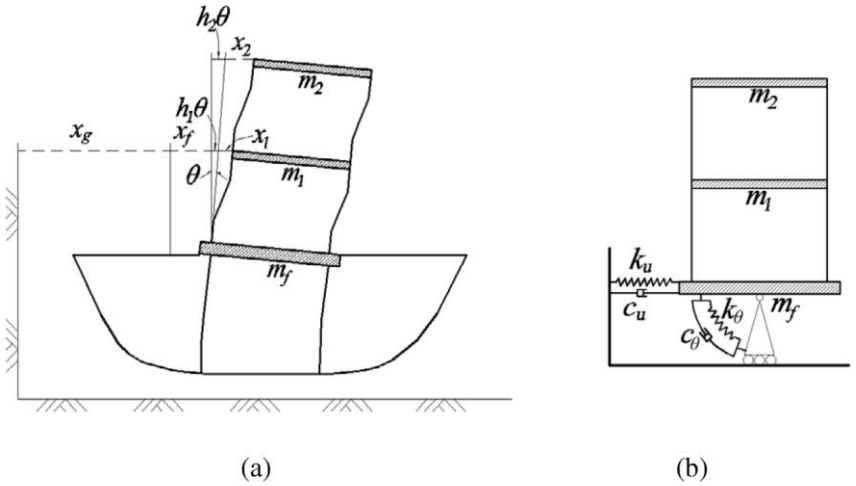


**Figure 2-5** SSI test setup: (a) experimental model and (b) mathematical model (H. Li & Wang, 2011).

In 2014, R. Jabary and Madabhushi presented experimental studies on the findings from several shaking table experiments carried out on 3 degrees of freedom sway frame building model provided with a range of TMD arrangements mutually located on the different stories of the building. The purpose of this research is to experimentally describe the effects of different tuned and de-tuned mass damper arrangements on the response of a multi-story building mutually located on fixed support and SSI. Experimental results recommend that locating of a TMD along the height of the building is crucial for its performance and that regardless of whether it is tuned to the SSI system characteristics, a

TMD may still increase the isolated building's response. This could possibly have significant inferences for existing and new buildings implemented with TMDs for seismic stability (R. Jabary & Madabhushi, 2014).

In 2015, R. Jabary and Madabhushi offered experimental investigations on the effects of TMDs on the response of a multi-story building considering dynamic SSI by a series of geotechnical centrifuge tests. Building's responses were mitigated for soil profiles, and a wide range of loads characteristics, damper configurations. The workability related to the use of TMDs in the damping of resonant buildings in light of unpredicted earthquake properties different from design earthquakes was experimentally proved. Tuning a TMD to SSI system characteristics rather than fixed-base structural characteristics were determined to double the improvement in damping and decrease the original peak response by approximately half. The possible performance of a de-tuned mass damper in light of important SSI was also proved (R. Jabary & Madabhushi, 2015).

Currently, real-time sub-structuring methods are an excellent experimental technique for examining large-size specimens in the lab. In this technique, the all experimented system is divided into two connected sections, the section of special attention or nonlinearity, which is experimented physically, and the remanding section which is experimented numerically. To carry out and to capture a comprehensive interface response, it is needed to compensate for transfer system dynamics, time-varying parameters within the physical substructures, nonlinearities, and uncertainties. Guo, Tang, Chen, and Li (2016) presented the sub-structuring technique and control implementation of the linear and the adaptive controllers for experimenting with the dynamic properties of the SSI system. This is hard to simulate as

an entire system in the laboratory because of the size and energy amount constraints of the laboratory abilities. Guo, Tang, Chen, and Li a modified linear sub-structuring controller (MLSC) as a substitute for the linear sub-structuring controller (LSC). The MLSC no needed to the perfect analytical model of the physical building that is necessitated by the LSC. The effects of parameter identification errors of the shaking table and the physical building on the control implementation of the MLSC are examined. Guo, Tang, Chen, and Li designed an adaptive controller to recompense for parameter identification errors, and the errors from the simplification of the physical model in the MLSC. To assess the adaptive controller and the performance of the MLSC, comparative emulation and laboratory tests were presented (Guo, Tang, Chen, & Li, 2016).

Nazarimofrad and Zahri developed a 3D mathematical model for irregular multistory frame structures using an active tendon control system to calculate structural responses. The SSI effect was included in and updated the equation of motion by modified mass, stiffness, and damping matrices. The model was applied to 10-story frame structures to calculate the response, depending on an LQR algorithm and active tendon system. The results indicated that when structures are built on soft soil, active control tendons are less effective in the reduction of structural responses under applied loads (Nazarimofrad & Zahrai, 2016).

Zhao, Wang, Du, and Liu investigated multistory buildings using optimally placed viscoelastic dampers (VEDs) that included the SSI effect. The researchers assumed an elastic system and employed frequency domain analysis for stationary random seismic excitations. A genetic algorithm (GA) was used to minimize the maximum response of the system to a specific amount of viscoelastic material, in order to obtain optimal VED designs for

multistory buildings. The cases studied included two typical elastic multistory buildings, different soil types, and a variety of embedment ratios for foundations demonstrating the optimum VED locations. Researchers were able to identify the optimum VED locations and obtained the best control for fixed support, but the findings indicated a reduction in the control efficiency for soft soil. The foundation embedment ratio had a significant effect on the efficiency of the VEDs. For soft soil, an increase in the embedment ratio was found to increase the dynamic interaction between the soil and foundation as a result of decreases in the efficiency of the VEDs. The SSI effect had a significant influence on the optimal placement of VEDs in multistory buildings. For stiff soil, the optimal locations were on the middle floors. As the stiffness of the soil decreased, the optimal locations moved to the top floors. When the soil stiffness increased, the optimization effect was also found to increase (Zhao, Wang, Du, & Liu, 2017).

In 2017, Nazarimofrad and Seyed introduced a mathematical model regarding the SSI effect to obtain the seismic performance of an irregular multi-story building having two Active Tuned Mass Dampers (ATMD) at the center of mass on the top floor. Researchers applied the model to examine the seismic response of 10 and 15-story asymmetric plan buildings in different cases utilizing LQR and fuzzy logic algorithms forces both ATMD. Likewise, both TMDs are utilized in the same position to compare. The results confirmed that utilizing both ATMDs on the top floor would decrease influenced response of the structure in the 10 and 15-story buildings constructed on soft (Nazarimofrad & Zahrai, 2017).

In 2017, Elias and Matsagar studied the effect of SSI on the dynamic responses of seismically isolated three-span continuous reinforced concrete (RC) bridge. Furthermore, researchers investigated the tuned mass damper(s) (TMD/s) is/are utilized to control unacceptable bearing displacement, considering the SSI effect. Researchers located the TMDs at the mid-span of the bridge and each tuned with a modal frequency while controlling up to first few modes as acceptable. They modeled the soil surrounding the foundation of the pier by frequency-independent coefficients and the dynamic analysis executed in the time domain applying the direct integration method. To particularize the effects of the SSI, the comparison study for the responses of the non-isolated, isolated and controlled isolated bridge are investigated. The results show that the soil encirclement the pier has important influences on the bearing displacement of the isolated RC bridges, and the seismic responses of isolated RC bridge decreased notably with the installation of the TMDs (Elias & Matsagar, 2017).

In 2017, Elias, Matsagat, and Datta investigated the control of chimneys construction on a flexible foundation for multi-mode wind response. They realized multi-mode control by utilizing distributed multiple tuned mass dampers (d-MTMDs). In this study, a reinforced concrete (RC) chimney is represented by an assembly of beam elements, all assumed to have a constant diameter through the element length, and SSI is considered. The soil is modeled in one layer under the annular raft foundation external and internal diameters 40 m and 15 m, respectively, and 2.5 m in depth. The mathematical model for the raft and surrounding soil utilized frequency-independent dashpots and springs. The time domain analysis used Newmark's method of average acceleration for the complex damped system. The

comparison study to the performance of the d-MTMDs with different cases of arbitrarily installed distributed MTMDs (ad-MTMDs), d-MTMDs controlling the fundamental modal responses (d-MTMDs-1), and single tuned mass damper (STMD) is presented. Also, to examine the effectiveness in the STMD, d-MTMDs-1, ad-MTMDs, and d-MTMDs cases, the displacement and acceleration response at the top of the chimney subjected to wind forces are calculated. The results indicate that the d-MTMDs are more effective than the STMD, d-MTMDs-1, and ad-MTMDs while adopting the equal total mass of the TMD(s). Moreover, the soil type considerably affects the wind response of the chimney with a flexible foundation and the design parameters of the STMD/ d-MTMDs-1/ ad-MTMDs/ d-MTMDs (Elias, Matsagar, & Datta, 2017).

In 2017, Bekdas and Nigdeli presented the study to offer an optimization method for optimum design of tuned mass dampers (TMDs) performed to seismic buildings including SSI effects. In this approach, two metaheuristic algorithms such as bat algorithm and harmony search algorithm were utilized. The present methods assess the time-domain analysis of the building and study the results during different earthquakes loads. The optimum design variables defined as damping ratio, period, and mass, of TMD were examined for the design constraint (limitation of the scaled stroke of TMD) and the optimization objective (minimization of the maximum displacement of building). The single degree of freedom structures for structure periods, different soil properties and damping ratios is used to investigate the proposed methods. Also, a 40-story high-rise building was explored. In 40-story building, the optimally tuned TMDs are operative to mitigate the critical response up to 25%. The recommended approaches are both practical and possible,

but bat algorithm has benefits on the minimization of the optimization objective and obtaining a specific optimum value (Bekdaş & Nigdeli, 2017).

In 2018, Raz and Gopal performed experimental investigations on Tuned Mass Damper (TMD are useful structural control device) and their performances in systems including dynamic SSI effects. A few experimental studies existed on the investigation of TMDs. Researchers are employed the Geotechnical centrifuge tests to study the effects of single and multiple TMDs in an SSI system with a variation of the story positioning. Researchers indicated the optimal story positioning criteria, and the results show that story positioning effects TMD performance more than the number of TMDs. Also, Non-optimal story positioning was found to have the potential of reducing damping efficiency, encouraging lengthier high-intensity motion, and increasing peak response of structures (R. N. Jabary & Madabhushi, 2018).

In 2018, Sun studies the control of monopile offshore wind turbines subjected to multi-hazards including wind, earthquake, and wave presented a semi-active tuned mass damper (STMD) with tunable natural frequency and damping ratio to control the dynamic response. Sun established a new fully coupled analytical model of the monopile offshore wind turbine with an STMD and formulated the seismic loading, hydrodynamic, and aerodynamic models. In this study, the soil effects and damage are respected. Additionally, it employed the National Renewable Energy Lab monopile 5 MW baseline wind turbine model to examine the performance of the STMD. For comparison, a passive tuned mass damper (TMD) is used. The numerical analyses results show that before damage occurs, the wind and wave-induced response is more dominant than the earthquake-induced response.

The results found that with damage present in the tower and the foundation, the nacelle and the tower response is amplified rapidly and the natural frequency is reduced noticeably. Consequently, the passive TMD with fixed parameters becomes off-tuned and loses its effectiveness. In contrast, the STMD reflected in real-time shows logical effectiveness in controlling the dynamic response of the monopile offshore wind turbines under multi-hazards and damage with a smaller stroke (Sun, 2018).

In 2018, Buckley, Watson, Cahill, Jaksic, and Pakrashi presented research to investigate the potential of using a Tuned Liquid Column Damper (TLCD) to mitigate structural oscillations of a wind turbine tower. The effect of TLCD on wind turbine towers, considering the SSI for a monopile foundation, was modeled mathematically and compared laboratory experiments were achieved to verify these results. The tower of the turbine is modeled as an Euler beam with a group of springs at the boundary to simulate the SSI. TLCD design was achieved employing such a model and the decrease in tower vibrations because of the distribution of TLCD was then studied for different loading conditions in the time and frequency domains. The performance of TLCDs for mitigating structural vibrations was studied for detuned and tuned situations. The response of a small-scale prototype was simulated along with that of a full-scale turbine. Then, the parametric studies around the variations of inputs associated with uncertainties were carried out. Also, experiments were performed on a scaled model turbine to measure the performance of the TLCD. The functionalism of placing a TLCD in a full-scale turbine was investigated (Buckley, Watson, Cahill, Jaksic, & Pakrashi, 2018).

In 2018, Amin, Bitaraf, Nasab, and Javidan studied the effects of SSI on the control of structures. In this research, simple adaptive control (SAC) was used with MR dampers. The SSI effect was studied from different aspects, focusing on control forces and the effectiveness of SAC in the control of SSI systems. The structure models included a 2D frame using a beam column element, and the shallow foundation models featured a beam element on a spring (or Winkler foundation) for the horizontal, vertical, and rocking positions (with all elements and models from OpenSees). The results showed that the structure without SSI underestimated the control forces and controlled structure responses. A fragility analysis indicated that there was a significant difference between the probabilities of failure for fixed-base and SSI systems. As a consequence, SSI was found to have a significant effect on structural control, especially in buildings constructed on soft soil (Amini et al., 2018).

The research is still required to study the control system effect to reduce the system responses during hazard loads for smart SSI systems. This thesis investigates the performance of the advanced control algorithm and a magnetorheological damper on the behavior of dynamic SSI systems for different types of soil, soil profile, and types of structural systems.

## 2.4 Fundamentals Concepts of the Dynamic SSI System

### 2.4.1 Introduction

Commonly, conventional analysis of the seismic responses of structures assumes that in practice a structure is supported by a fixed base (i.e., a very rigid base support); this is an

ideal hypothesis since in most conditions, the soil is flexible (i.e., a flexible-base support). This hypothesis is sensible only when the structure is constructed on rocky soil or when the relative stiffness of the soil compared to the structure is extremely high. Otherwise, the soil's behavior can have two different effects on the structural response: first, adjustment of the free-field motion (i.e., ground motion not affected by the presence of the structure) at the foundation of the structure; and second, deformation of the soil from the dynamic structural response. The former is known as kinematic interaction, while the latter is referred to as inertial interaction. Together, the whole process is generally known as the SSI. The principal notion supporting site response analysis is that free-field motion relies on the characteristics of the soil profile and comprehensive rigidity of the soil layers. The stiffness of the layer can vary the amplitude of the ground motion and frequency content. The fundamentals concepts comprising the dynamic SSI are investigated below.

### 2.4.2 Dynamic Behavior of Fixed and Flexibly Supported Structures

In 1985, Wolf demonstrated the salient characteristics of the SSI (see Figure 2-6) by comparing the seismic response of a structure constructed on rock with that of the same structure with a rigid base (i.e., comprehensive side walls and a raft foundation) embedded in soil. In Figure 2-6, earthquake waves with a horizontal motion are denoted with solid signs. They diffuse vertically into the rock from the structure. The magnitude of motion is evaluated according to the lengths of the solid signs. In Figure 2-6, motion at Point A at the rock ground surface is adopted as a benchmark (John P. Wolf, 1985).

In a structure constructed on rock (which can be considered nearly a fixed-base support), differences in the motions at Points A and B are almost indistinguishable. Thus, the motion read at the benchmark Point A can be followed straight to the bottom of the structure. If the lateral structural rigidity is significant, the earthquake at the bottom will create a horizontal acceleration that is fixed over the rise of the structure. Hence, an overturning moment and transverse shear force will grow at the bottom.

Because the rock is rigid, the rocking moment and horizontal shear force generate additional deformation in and around the ground. Therefore, the rigid foundation is joined to the rock and creates transits along the side through the rock's lateral motion. Conversely, a structure embedded in soil shows an obviously different dynamic behavior when compared to the structure constructed on rock. The difference is essentially associated with the reality that the motion at Point O (i.e., the bottom center) varies from that at benchmark Point A, due to three key concepts outlined below.

The first is known as free-field motion, which is the motion of the site without the presence of any excavations and/or structures. As illustrated in Figure 2-6 (c), the soft soil stratum covering the rock decreases the motion at Point C, as indicated by $\ddot{u}_g$, which is equal to the motion at benchmark Point A if there is no soil on top of the rock (see Figure 2-6 (b)). Wave propagation within the soil stratum is accompanied by attenuation or amplification of the free-field motion. Depending on the excitation frequency, the motion normally increases. As a result, motion at Points E and D (signified by $\ddot{u}_{g,b}$), resting on the surface of the interface between the soil and structure, varies from that of Point C (see Figure 2-6 (c)). Estimation of the free-field motion requires a site response investigation.

Constructing a rigid foundation in soil modifies the motion at the bottom, which may then undergo additional rocking and some average swaying displacement (see Figure 2-6 (d)). The coupled rocking and swaying responses cause a change in horizontal acceleration with the elevation of the structure. This concept is essentially a consequence of the stiffness contrast between the foundation and neighboring soil, and also happens when there is a massless foundation; in such cases it is defined as kinematic interaction (see the following section entitled Kinematic Interaction). Finally, the transverse overturning moment and shear force following from the inertial forces create extra deformation in the neighboring soil, which adjusts the input motion at the bottom center at Point O (see Figure 2-6 (e)). This interaction between the structure and its neighboring soil is called inertial interaction (see the section below entitled Inertial Interaction).

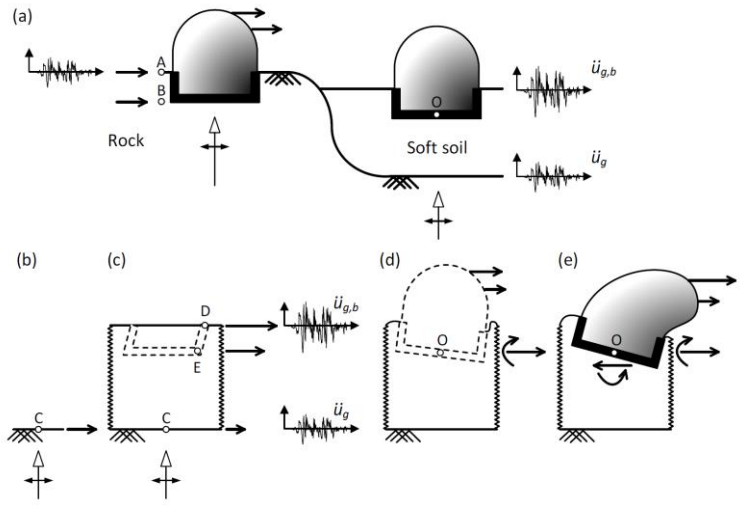


**Figure 2-6** Seismic responses of structures built on rock and soil: (a) sites, (b) rock outcropping, (c) free field, (d) kinematic interaction, and (e) inertial interaction(John P. Wolf, 1985) (Lu, 2016).

### 2.4.3 Kinematic Interaction

The impact of kinematic interaction mainly arises from the stiffness difference between the soil and foundation. In the free field, when there is no structure, the particles of soil obey the motion pattern caused by wave propagation. One assumes that a foundation constructed upon or embedded in the soil is very stiff, such that it cannot adapt to the displacement of the free field pattern; this creates a foundation motion that is different from the free-field motion if the mass of the foundation is ignored.

Figure 2-7 describes situations where the kinematic interaction concept dominates. In all sketches, the foundations are assumed to be massless and the dotted curves describe the free-field motion.

As displayed in Figure 2-7 (a), which shows a typical pile subjected to shear waves, the amplitude progresses while the diffusion moves vertically up within the soil media. The pile's flexural stiffness restrains it from following the free-field motion, trying to adjust the displacements of soil related to the free-field displacements in the region of the pile body. Conversely, the soil movement around the pile creates bending moments that may pose a risk to the pile’s stability.

For massless embedded foundations, Figure 2-7 (b) and (c) illustrate a comparison between the effects of the frequency components of a motion on the foundation's response. It appears from Figure 2-7 (b) that when subjected to a high-frequency motion that changes laterally, the kinematic forces exerted on the foundation emanate out, dropping from the foundation unchanged by the wave motion. In contrast, during lower-frequency motion, the foundation tends to sway and rock, increasing the **foundation input motion** (**FIM**) caused

by swaying and rocking displacements, even though the free-field motion is completely lateral (see Figure 2-7(c)). In spite of the fact that kinematic interaction is more common in embedded foundations, particularly those that are deep, there are situations where this influence is also notable in shallow foundations. For instance, Figure 2-7(d) illustrates how the in-plane stiffness of a shallow foundation does not permit it to obey the displacement pattern in the soil underneath the foundation. Similarly, Figure 2-7(e) and (f) confirm that excitation frequency has an important influence on the foundation's response, identical to the demonstrations provided in Figure 2-7 (b) and (c).

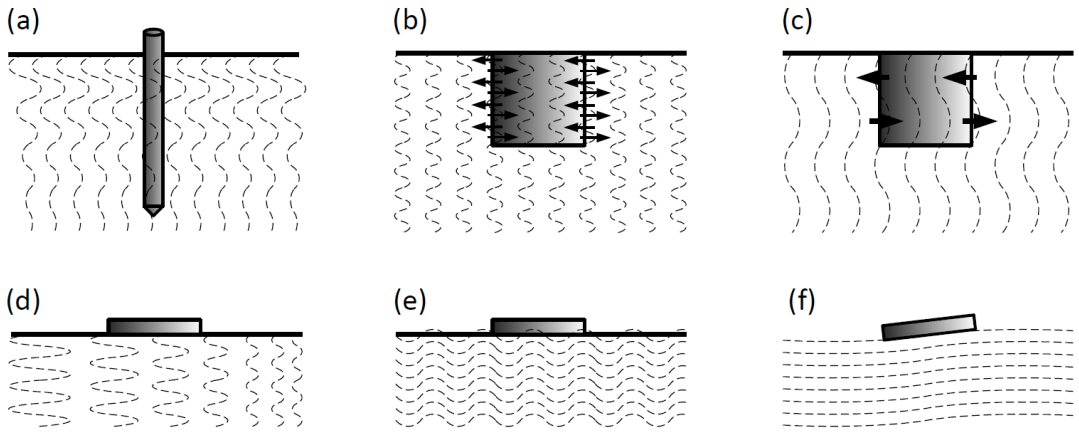


**Figure 2-7** Kinematic interaction influence for deep and shallow foundations (Lu, 2016).

Generally, the way kinematic interaction influences a foundation's behavior relies on the predominant wavelength corresponding to the foundation's dimensions. For high-frequency movements in which wavelengths are very small relative to the features of the

foundation's dimensions, the contribution to the foundation's response is relatively insignificant (see Figure 2-7(a), (b), and (e)). For this reason, a foundation can be imagined as a high-period pass (i.e., low-frequency pass) filter applied to the high-frequency elements of the free-field motion (FEMA, 2005). This filtering influence is more notable for short-period structures influenced essentially by high-frequency motion, leading to a significant decrease in such structures' seismic demands.

When the dimensions of the foundation are similar to the wavelength, a kinematic interaction will lead to a change in the foundation's vibration modes (see Figure 2-7(c) and (f)). If, however, the feature foundation dimension becomes adequately small in relation to the wavelength, the kinematic interaction's influence can be sensibly neglected. Figure 2-7(d) displays the principle known as the base-slab averaging effect, which is also effective at low periods. It must be specified that kinematic interaction does not occur in all situations. For instance, if the shallow foundations shown in Figure 2-7(d), (e), and (f) are loaded by the seismic waves represented in Figure 2-7 (a), (b), and (c), a kinematic interaction will not occur.

### 2.4.4 Inertial Interaction

A structure is animated by inertial forces, and the foundation input motion is generated inside the structure by an inertial interaction event. The essential coupled characteristics resulting from this interaction are presented below. First, the inertia-induced transverse overturning moment and shear force generated at the bottom of the foundation produce deformation in the soil joining with that which comes from the free-field motion.

Deformation size is regulated by the obedience of the soil and vibration amplitude. Presentation of deformable soil under the foundation causes the whole SSI system to be more flexible, and consequently have a longer period.

The excited foundation operates as a finite reference of vibration that sends waves propagating from the soil to infinity. With a shallow foundation, the swaying displacement response (uh) shown in Figure 2-8 (a) produces dilatational P-waves (P) and shear S-waves (S) through extension and compression at the vertical interfaces and friction at the horizontal interface between the nearby soil and foundation. In terms of the rocking mode of vibration with the angle of rotation (θ), P-waves fundamentally result from compressive stresses transferred from the base of the foundation to the soil (see Figure 2-8 (b)).

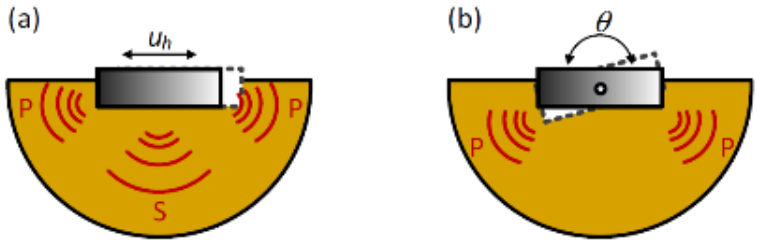


**Figure 2-8** Foundation vibration in (a) swaying and (b) rocking modes as inertial interaction dissipates wave energy into the surrounding soil domain (Lu, 2016).

Inertial interaction forms two principal types of wave energy dissipation. The first is a consequence of geometric mitigation through wave propagation where an extension of the wave front from a point reference occurs. This process is normally called radiation damping

because foundation vibration radiates waves throughout the soil domain. The second process references nonlinear soil behavior and is named hysteretic damping. If the foundation uplift is subtracted, the influence of the foundation on the soil and attendant vertical vibration motion dissipates a portion of the kinetic energy given on the foundation (Adamidis, Gazetas, Anastasopoulos, & Argyrou, 2014). Together, the coupled principal characteristics of inertial interaction are lengthening of the vibration period and introduction of hysteretic and radiation soil damping into the system.

### 2.4.5 Methods of Analysis

#### 2.4.5.1 Direct Method

The most rigorous method of analyzing a dynamic SSI system is applying the direct method, which involves modeling the whole SSI system in the time domain, including wave propagation, transmission across interfaces, boundary conditions, locative variation in the soil characteristics, and geometric and material nonlinearities. Direct methods normally use finite element method (FEM) techniques, where the entire SSI system is modeled and analyzed as a whole. Figure 2-9 schematically explains this SSI analysis by FEM, which consists of the soil and foundation usually being described as a continuum (e.g., plane strain elements), structural elements (e.g., a frame element), boundaries of the soil mesh, and interface elements situated between the soil and foundation.

The equation of motion (EOM) for an SSI system in a finite element model is described by:

$$[\boldsymbol{M}]\{\ddot{\boldsymbol{Y}}\} + [\boldsymbol{C}]\{\dot{\boldsymbol{Y}}\} + [\boldsymbol{K}]\{\boldsymbol{Y}\} = -[\boldsymbol{M}]\{\ddot{\boldsymbol{u}}_{\boldsymbol{g}}\} \quad 2\text{-}1$$

where [M], $[C]$, and $[K]$ are the mass, damping, and stiffness matrices, respectively; $\{\ddot{Y}\}$, $\{\dot{Y}\}$, and $\{Y\}$ are the acceleration, velocity, and displacement vectors regarding the degrees of freedom of the nodes in the finite element mesh of the SSI system, respectively; and $\{\ddot{u}_g\}$ is the ground acceleration vector. Despite the fact that the direct method can model the soil and structure with equal levels of accuracy, it normally requires substantial computational effort and is not simple to use in preliminary design. Therefore, structural engineers more often employ the practical substructure method explained below.

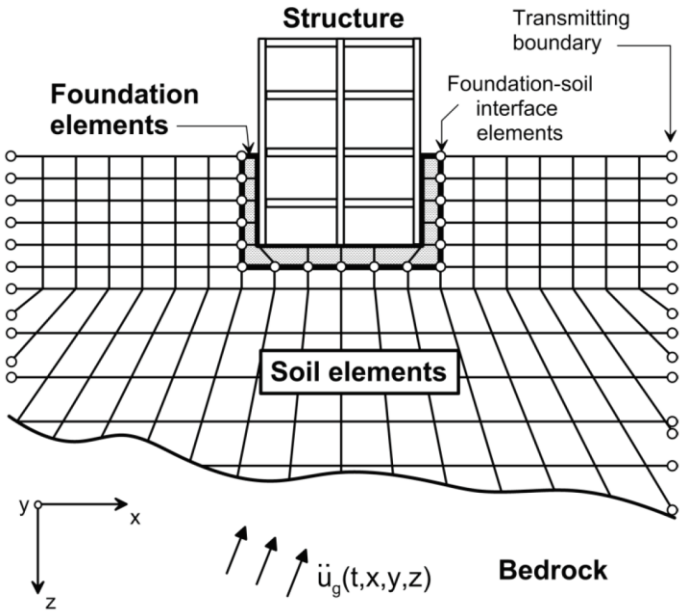


**Figure 2-9** Typical schematic of a FEM and the types of elements used in an SSI analysis (J. Stewart et al., 2012).

### 2.4.5.2 Substructure Method

The substructure approach is also named the multi-step method; it is where an SSI problem is determined by mixing solutions from kinematic and inertial interaction concepts described earlier (see Figure 2-10).

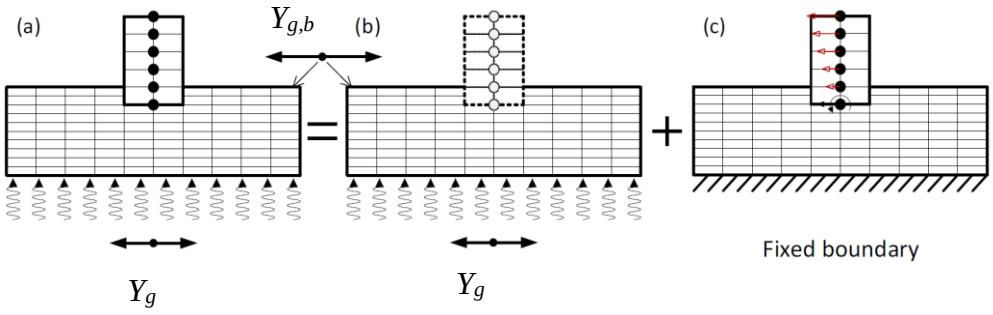


**Figure 2-10** Analysis of (a) an SSI problem can be broken down into (b) a kinematic interaction analysis and (c) an inertial interaction analysis (Lu, 2016).

In a kinematic interaction analysis, seismic loads are subjected to the base of the SSI model where the structure and foundation are assumed to include stiffness but are massless (see Figure 2-10 (b)). The EOM for a kinematic interaction can be described by:

$$[\boldsymbol{M_{soil}}]\{\ddot{\boldsymbol{Y}}_{\boldsymbol{KI}}\} + [\boldsymbol{K}]\{\boldsymbol{Y_{KI}}\} = -[\boldsymbol{M_{soil}}]\{\ddot{\boldsymbol{Y}}_{\boldsymbol{g}}\} \quad 2\text{-}2$$

where $[M_{soil}]$ is a mass matrix within which are notes conformable to the structure, the foundation is zero, and the index KI indicates kinematic interaction.

Analytically, the EOM for inertial interaction can be removed from Equation (2.1) by subtracting the elements for the kinematic interaction shown in Equation (2.2):

$$[\boldsymbol{M}]\{\ddot{\boldsymbol{Y}}_{\boldsymbol{II}}\} + [\boldsymbol{K}]\{\boldsymbol{Y}_{\boldsymbol{II}}\} = -[\boldsymbol{M}_{\boldsymbol{structure}}]\{\ddot{\boldsymbol{Y}}_{\boldsymbol{g}} + \ddot{\boldsymbol{Y}}_{\boldsymbol{KI}}\} \quad 2\text{-}3$$

where $\{Y_{II}\} = \{Y\} - \{Y_{KI}\}$ is the inertial interaction aspect of the displacement vector $\{Y\}$, and $[M_{structure}] = [M] - [M_{soil}]$. It is of note that for the degrees of freedom communicating with the structure-foundation system, $\{Y_{KI}\} + \{Y_g\}$ is decreased to the foundation input motion. Especially important for a surface foundation applied to coherent vertically propagating shear waves, $\{Y_{KI}\} + \{Y_g\}$ at the foundation elevation is equal to $\{Y_{g,b}\}$, which is the motion at the ground surface in the free field.

From a practical point of view, to clarify an SSI analysis, the soil medium is normally substituted with the named impedance function that captures the stiffness and damping features of the soil-foundation interaction when subject to vibration at different frequencies. These frequency-dependent impedance functions are mathematically described by springs with complex stiffnesses. In such cases, the methods given in

Figure 2-10 can employ an even simpler SSI model. Kramer and Stewart presented an approach consisting of the following three steps (see Figure 2-11) (Bozorgnia & Bertero, 2004).

1. Determine the foundation input motion, which relies on the stiffness and geometry of the soil and foundation.
2. Estimate the impedance function that for the simple case of a rigid foundation is purely a function of elastic soil characteristics (e.g., Poisson's ratio and stiffness), foundation geometry, soil layers, and wave frequency.
3. Implement a dynamic analysis of the SSI system subjected to the foundation input motion.

Figure 2-11 and Figure 2-12 graphically illustrate the substructure method of analyzing an SSI system employing both rigid and flexible foundation suppositions. It is obvious that the solution to kinematic interaction is powerful foundation input motion. Inertial interaction solves the response of an SSI system where the structure (i.e., incorporating foundation) is moved by the foundation input motion and combines with the neighboring soil. The total response of the SSI system is computed from the interaction analyses.

### 2.4.6 Seismic Design Guidelines for SSI Systems

The SSI was initially described in the US ATC-3 report (Council & California, 1978), which was the forerunner of the National Earthquake Hazard Reduction Program (NEHRP) seismic service. An easy method for applying the SSI was recommended in the ATC-3; it involved applying the decreased design base shear associated with the fixed support value. The advantageous influence of the SSI is why SSI requirements work as optional design parameters and were never integrated into the design codes. Another reason why code practice does not incorporate SSI effects is the uncertainty regarding SSI influence, which continues to be debatable.

#### 2.4.6.1 SSI in Eurocode design codes

Notwithstanding the fact that no special design techniques are offered, Eurocode 8 (EN, 2004) provides a qualitative explanation of SSI effects in its Annex D and certifies

subsequent cases where SSI impacts may be damaging and should be adopted in the design, including:

1. Buildings where P-Δ (i.e., second order) influences play a vital role;
2. Deep-seated foundations or massive structures, like silos, bridge piers, and offshore caissons;
3. Slender or tall buildings, like chimneys and towers; and
4. Structures constructed on extremely soft soil with an average shear wave velocity of less than 100 m/s.

Annex C gives the pile-head stiffness that can be employed for SSI computations with piled foundations.

#### 2.4.6.2 SSI in US Design Codes

SSI necessities now exist in many significant American seismic design codes (i.e., (FEMA, 2005); (A. Engineers, 2010); (J. Stewart et al., 2012)). The subsequent offerings in these codes for basic SSI processes have been performed in current displacement- and force-based designs of structures.

The NEHRP has suggested certain requirements for seismic guidance in new structures and other buildings. These include a method for taking into account the SSI to estimate the equivalent lateral force (Agency, 2003). By obtaining an effective period regarding the first mode of vibration, a decrease in base shear is presented that leads to a decrease in overturning moments and lateral forces. The most effective period to be applied in the response spectrum is determined by:

$$\frac{T_{ssi}}{T_s} = \sqrt{1 + \frac{\bar{k}}{K_y}\left(1 + \frac{\bar{h}^2}{K_\theta}\right)} \qquad 2\text{-}4$$

where $T_{ssi}/T_s$ is the period ratio, $T_{ssi}$ is the period of the SSI system, Ts is the fundamental period of the fixed support building, $\bar{h}$ is the height of the building (defined as 0.7 times the total height for multi-story structures, and one-story buildings are named the total height), $\bar{k}$ is the stiffness of the fixed-support building, Ky is the lateral stiffness of the foundation, and Kθ is the rocking stiffness of the foundation.

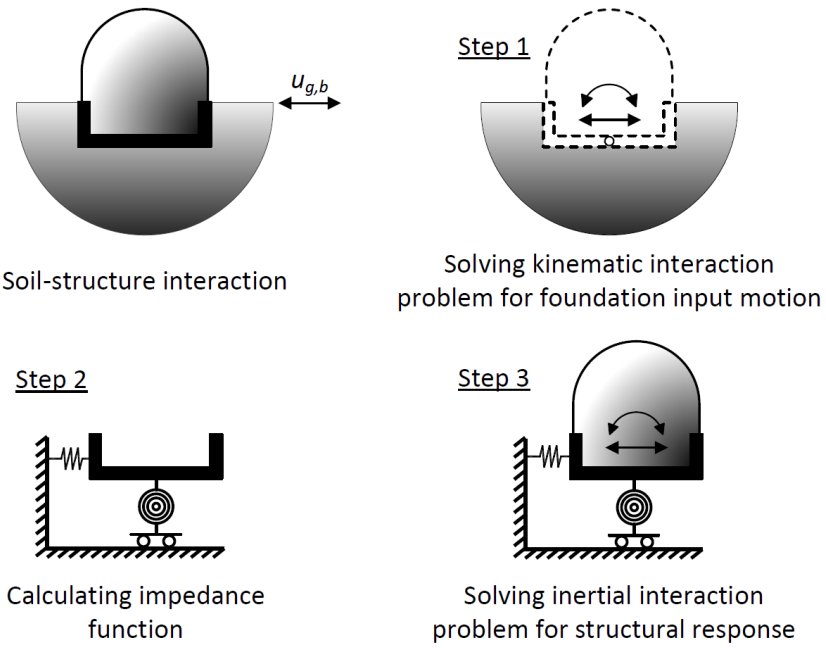


**Figure 2-11** Substructure approach to an SSI problem that utilizes an impedance function (Bozorgnia & Bertero, 2004) (Lu, 2016).

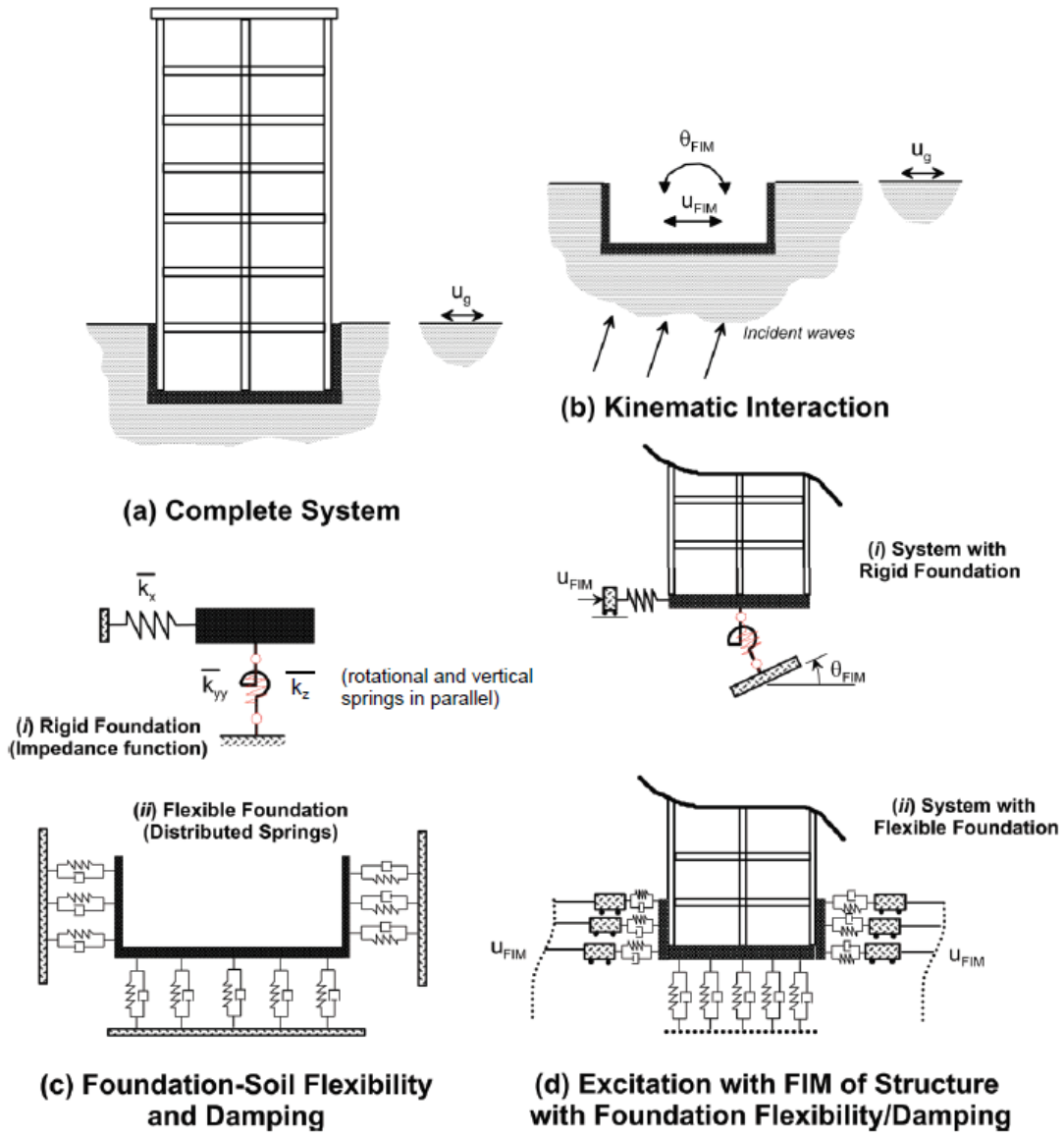


**Figure 2-12** Schematic illustration of a substructure approach to the analysis of soil structure interaction using either (i) rigid or (ii) flexible foundation assumptions (J. Stewart et al., 2012).

*2.4.6.2.1 Displacement-Based Methods*

For existing buildings, US seismic design guidelines have relied on pushover (i.e., nonlinear static) methods. The different pushover methods are as follows: coefficient, capacity spectrum, linearization, and improved coefficient (i.e., displacement modification) (FEMA, 2005) (A. S. o. C. Engineers, 2013). SSI approaches have been realized in recent methods from the, which then developed into the ASCE (2013). A displacement-based method requires a pair of significant elements: a pushover (i.e., capacity) curve and a demand (i.e., design response) spectrum. Both are considered in spectral acceleration (Sa) versus spectral displacement (Sd) or ADRS form.

The pushover curve can be inferred from an incremental pushover computation where an MDOF SSI system in equilibrium is exposed to a static lateral load case. The total system is pushed statically until a specific displacement (normally estimated at the roof) is achieved (see Figure 2-13). The mobilized base shear (i.e., the cumulative horizontal load H) can be plotted with the roof displacement $\Delta$ to indicate the nonlinear level of the building.

The seismic performance of a structure is evaluated by mixing the seismic demand spectrum and capacity curve into the ADRS pattern. This requires the MDOF system to be converted into an equivalent SDOF system (the fundamental mode of the MDOF system is normally chosen). To value the nonlinear response, the demand spectrum should be decreased from its elastic match without consideration of the SSI's impacts. Each nonlinear spectrum or an equivalent elastic spectrum can be applied as the demand spectrum. The impacts of the SSI on the demand spectrum are measured in the ASCE (2013) by decreases in demand for inertial and kinematic interaction, as discussed below.

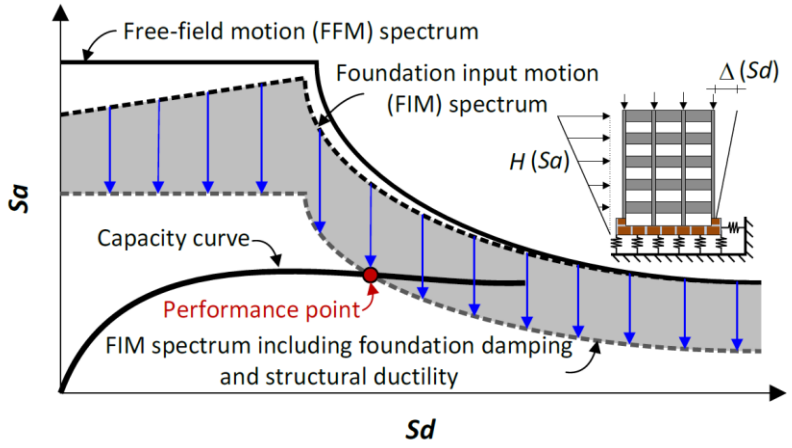


**Figure 2-13** Schematic showing the SSI's impacts on displacement-based methods for evaluating nonlinear structural performance (Lu, 2016).

Mathematically, the foundation input motion (FIM) in kinematic interaction can be estimated by averaging the number of transfer functions represented as frequency-dependent ratios of FIM Fourier amplitudes to those of the free-field motion (FFM). The ASCE (2013) advises that a decreased response spectrum can be applied to estimate the kinematic interaction. This is dependent upon the relationship between the transfer function ordinates (i.e., the amplitude ratios of FIM/FFM) and the response spectral ratios of the FIM/FFM at frequencies lower than 5Hz (Veletsos & Prasad, 1989). The ratio for the response spectra (RRS) is defined for base-slab averaging ($RRS_{bsa}$) and embedment ($RRS_e$) influences, but the entire decrease in FFM spectral ordinates cannot be higher than 50%.

The transfer function (and thus the $RRS_{bsa}$) for vertically propagating waves is determined by:

$$\boldsymbol{RRS_{bsa} = 0.25 + 0.75\left\{\frac{1}{b_0^2}\left[1 - exp\left(-2b_0^2\right)B_{bsa}\right]\right\}^{0.5}} \quad 2\text{-}5$$

where

$$B_{bsa} = \begin{cases} 1 + b_0^2 + b_0^4 + \frac{b_0^6}{2} + \frac{b_0^8}{4} + \frac{b_0^{10}}{12}, & if\ b_0 \le 1 \\ exp(2b_0^2)\left[\frac{1}{\sqrt{\pi} b_0}\left[1 - \frac{1}{16 b_0^2}\right]\right], & if\ b_0 > 1 \end{cases}$$

$b_0 = 0.0001\left[\frac{2\pi b_e}{T_{ssi}}\right]$, and $b_e = \sqrt{A} \le 260$ ft (the effective dimension of the foundation).

Tssi is the fundamental period of the SSI that cannot be used if less than 0.2 s is applied in Equation (2.13). The low-period cutoff of 0.2 s is defined by the above-discussed frequency of 5Hz, so that the RRS agrees in terms of fit with the transfer function. With regards to the RRS term for the embedment foundation, RRSe is defined as:

$$\boldsymbol{RRS_e = 0.25 + 0.75 \cos\left(\frac{2\pi e}{T_{ssi} V_s}\right) \ge 0.5} \qquad \text{2-6}$$

where e is the embedment depth of the foundation (in ft).

The ASCE (2013) lists the subsequent states where decreases due to the kinematic interaction impact are not permitted:

- Buildings having flexible diaphragms where decreases are not allowed for the base-slab averaging influence ($RRS_{bsa} = 1$);
- Buildings constructed on hard rock sites ($RRS_e = 1$);
- Buildings constructed on soft clay sites (RRS = 1); and
- Buildings with foundation parts that are not laterally linked, where decreases are not allowed for both influences (RRS = 1).

In the (FEMA, 2005) and ASCE (2013), the decreased seismic demand spectrum is assessed for a similar viscous damping ratio due to the mixed impact of structural yielding and SSI in inertial interaction (see Equation (2.15)).

$$\boldsymbol{\xi_0 = \xi_f + \frac{\xi_s}{[T_{ssi,eff}/T_{s,eff}]^3} \leq 20\%} \quad \text{2-7}$$

where $\xi_f$ is the foundation damping ratio that can be determined from Figure 2-15, and $T_{ssi,eff}/T_{s,eff}$ is the effective period lengthening ratio estimated at maximum post-yield displacement.

$$\boldsymbol{\frac{T_{ssi,eff}}{T_{s,eff}} = \left[1 + \frac{1}{\mu}\left[\left[\frac{T_{ssi}}{T_s}\right]^2 - 1\right]\right]^{0.5}} \quad \text{2-8}$$

where $T_{ssi}/T_s$ is the period lengthening of the SSI as defined by Equation (2.5), and $\mu$ is a ductility factor that includes the degree of nonlinearity due to yielding in buildings.

When decreasing an elastic design spectrum from 5%, its damped match is offered as a damping coefficient. The decreased demand spectrum is taken by dividing the 5% damped spectrum by a damping coefficient.

*2.4.6.2.2 Force-Based Methods*

The NEHRP (BSSC, 2009) and (A. Engineers, 2010) (see Chapter 19) adopt a force-based design methodology that combines the SSI with the equivalent lateral force method. The ASCE (2010) ignores the impact of the kinematic interaction's focus on period lengthening and adjusted damping that occurs from inertial interaction.

Figure 2-14 explains the inertial impact on a design's seismic spectrum. The base shear (V) reduction is determined by:

$$\Delta V = \left[C_s - C_{s,ssi}\left(\frac{\xi_s}{\xi_{ssi}}\right)^{0.4}\right]\overline{W} \leq 0.3C_s\overline{W} \quad \text{2-9}$$

where Cs is the seismic response coefficient or the design pseudo-acceleration (Sa) normalized by gravity acceleration (g); the subscripts ssi and s denote an SSI system and fixed-support system, respectively; the damping ratio ξ is normally taken as 5%; and $\overline{W}$ is the effective seismic weight of the building, ordinarily taken as 70% of the total seismic weight for buildings established on raft foundations that lean on the ground's surface or are embedded wherever the impact of contact between the soil and sidewalls is considered unimportant.

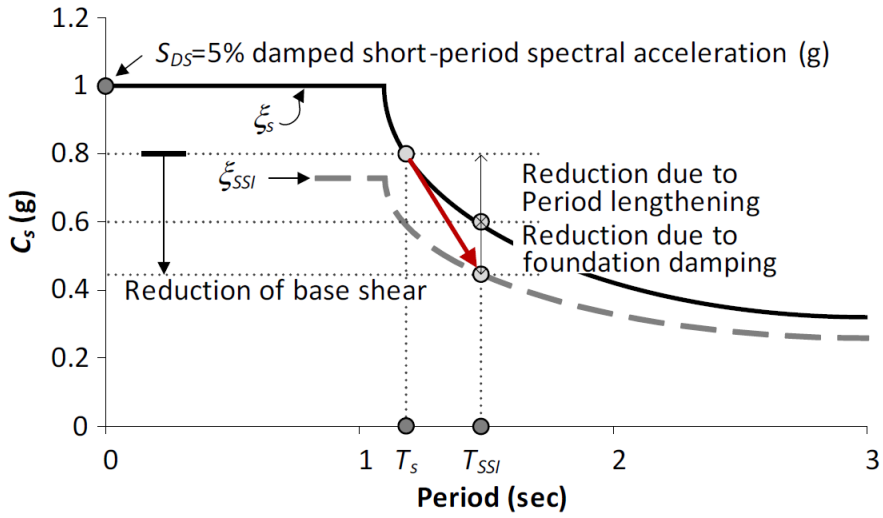


**Figure 2-14** Impacts of period lengthening and foundation damping on a design's spectral ordinates for the SSI (Lu, 2016).

According to (Veletsos & Meek, 1974), the period of an SSI system ($T_{ssi}$) can be estimated by:

$$\boldsymbol{T_{ssi} = T\sqrt{1 + \frac{25\alpha R_h \bar{h}}{V_s^2 T_s^2}\left(1 + \frac{1.12 R_h \bar{h}^2}{\alpha_\theta R_\theta^3}\right)}} \qquad 2\text{-}10$$

where:

α is the relative weight density of the building and the soil is determined as:

$\alpha = \frac{\bar{W}}{\gamma A \bar{h}}$ , and Rh and Rθ are geometric properties of the foundation and are determined by:

$R_h = \sqrt{\frac{A}{\pi}}$ And $R_\theta = \sqrt[4]{\frac{4I}{\pi}}$

where A is the area of the foundation; I is the moment of inertia of the foundation about an axis normal to the direction in which the building is analyzed; αθ is the foundation stiffness modifier for the rocking motion, as defined in Table 2-1; and Vs is the shear wave velocity.

**Table 2-1** Values for αθ (A. Engineers, 2010).

| $R_\theta/V_sT_s$ | $\alpha_\theta$ |
|---|---|
| < 0.05 | 1.0 |
| 0.15 | 0.85 |
| 0.35 | 0.7 |
| 0.5 | 0.6 |

The effective damping of the SSI is determined by:

$$\boldsymbol{\xi_{ssi} = \xi_f + \frac{\xi_s}{(T_{ssi}/T_s)^3}} \qquad 2\text{-}11$$

where ξf is the foundation damping factor as estimated in Figure 2-15.

The ASCE (2010) and BSSC (2009) consider the strain-dependent foundation stiffness and damping factor by linking them to the peak spectral ordinate (SDS), which corresponds to the short period value on a 5% damped design acceleration spectrum (see Figure 2-14).

The graphical solution in  is inferred by utilizing the (Veletsos & Nair, 1975) damping formulation as a function of the building's slenderness ratio ($\bar{h}/r$), peak spectral acceleration (SDS), and period ratio of $T_{ssi}/T_s$. The equivalent foundation radius r is defined by:

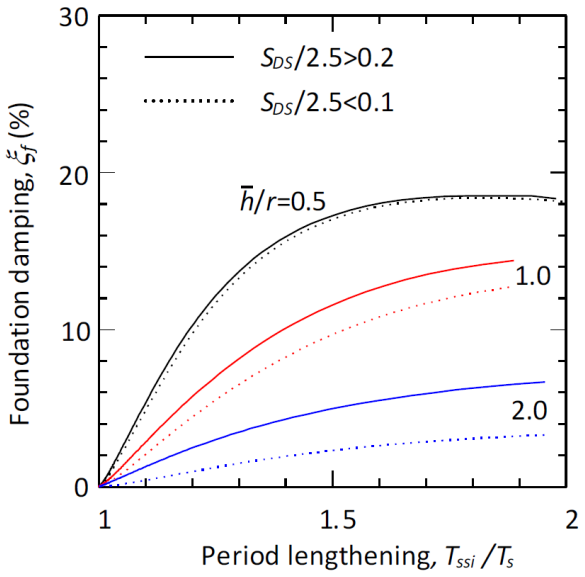


**Figure 2-15** Foundation damping factor (ASCE, 2010).

$$\boldsymbol{r} = \begin{cases} \boldsymbol{R_h}, & \boldsymbol{if}\ \frac{\bar{h}}{L} \leq \mathbf{0.5} \\ \boldsymbol{R_\theta}, & \boldsymbol{if}\ \frac{\bar{h}}{L} \geq \mathbf{1.0} \end{cases} \quad \text{2-12}$$

where L is the overall foundation's side length in the direction of analysis.

Linear interpolation can be used to determine r and z for intermediate values of $S_{DS}$ and $\bar{h}/L$. The ASCE (2010) recommends that the effective damping of an SSI system determined by Equation (2.8) should be $20\% \leq \xi_{ssi} \leq 5\%\ \xi_s$. Force-based methods always appear to decrease base shear because the design spectrum has a fixed and descending element above a wide length of periods. In modal analysis, application of the SSI is additionally permitted with methods similar to equivalent lateral load analysis but particularly employed in the fundamental mode of response. Considering that higher mode responses are basically unchanged by the SSI, the participation of higher modes is estimated by relying on the fixed-support supposition (Bielak, 1976).

The specified SSI methods for calculating the design's base shear are suitable for linear SSI systems where yielding is eliminated. Seismic design guidelines support nonlinear hysteretic behavior occurring in structural elements to dissipate seismic energy via plastic deformation. The ASCE (2010) provides an easy equation for the seismic response parameter that considers the contributions of nonlinear structural behavior (see Chapter 12):

$$\boldsymbol{C_s} = \frac{\boldsymbol{S_{DS}}}{(\boldsymbol{R/I})} \quad \text{2-13}$$

where R is a response modification factor that estimates the ductility of a structure and decreases the base shear, and I is a significance factor (I =1 in normal structures). The R factor may reflect the advantageous impact of the SSI, and adjusting the base shear to estimate for both ductility and the SSI maybe not be conservative in some situations (Crouse,

2002). Ghannad and Jahankhah (2007) confirmed that utilizing the R factor formulation depends on a fixed-support supposition for SSI systems, guiding a higher ductility demand than the target value (Ghannad & Jahankhah, 2007).

### 2.4.7 Summary of SSI Effects

The dynamic interaction between structure and soil can be divided into two categories: inertial and kinematic. Initial SSI progress was motivated by the seismic design of nuclear power plants. Structures constructed on flexible soil show different dynamic responses related to their fixed support. This variation results from kinematic and inertial interactions. Prior interaction event outcomes in deviations of the FIM from free-field motion normally lead to a higher damping and period of vibration for the SSI system. Despite the fact that a direct method does work as a strict SSI procedure, design codes normally use a substructure method that mixes the solutions obtained from both interaction analyses.

Kinematic interaction is mentioned as the difference in ground motion due to the behavior of a hard foundation with or without mass and inertial interactions; it is a deformation of the soil resulting from affected moments and base shear from the structure. The relative significance of these coupled elements relies on the type of incoming wave field and foundation features. Because the normal mass of the soil excavated to build a foundation is similar to the structure's mass, kinematic interaction can be neglected except when the foundation replaced is extremely stiff (Scawthorn & Chen, 2002). Consequently, the kinematic part of the SSI analysis is normally of interest in designs for the oil industry, nuclear power plants, and off-shore structures. Also, for motions that are not strong at high

frequencies, the input motion can be considered nearly identical to that of the free field. The influence of kinematic interaction is ordinarily far more complex to strictly estimate than that of inertial interaction.

The impacts of kinematic interaction are insignificant for shallow foundations in a seismic condition consisting only of dilatational waves or vertically propagating shear waves. Base averaging and kinematic interaction impacts usually filter out high frequencies. In the field, soil characteristics are notably changeable and difficult to estimate with any level of certainty. Consequently, a soil model that is simple to apply and computationally effective is attractive because it allows the user to manage sensitivity investigations and estimate the influence of a variety of subsurface situations on the seismic responses of the structures being simulated (John P Wolf, 1994). Adding springs and dashpots to the bottom of the structure is the easiest way to capture the flexible boundary condition for estimating seismic requirements. The outcomes for a uniform half-space are very acceptable. A finite element analysis of the SSI provides more sensible results but is very difficult for daily engineering uses.

Seismic design guidelines recommend situations in which the SSI should be adopted. The NEHRP commentary on the interaction effects for SSI systems noted that within the normal parameter range for buildings subjected to seismic loads, the outcomes are insignificant to the period. This is a reasonably accurate simplifying assumption that allows practical designs to utilize the static stiffness. In terms of response, the stiffness characteristics of the soil are less important than the stiffness and mass aspects of the structure (Arefi, 2008).

The SSI is crucial for stiff superstructures constructed on soft soil. Generally, the rocking portion of the SSI is most important for laterally stiff structures (e.g., structures with shear walls), especially those constructed on soft soil (J. P. Stewart, Kim, Bielak, Dobry, & Power, 2003). In this case, the influence of frequency dependence is not normally high because the frequency of this mode of vibration is generally low and not in the domain where influences are significant. Interaction influences for higher vibration modes are small. Inertial interaction is significant for the fundamental model because it has high cooperation between the base moment and shear.

The fundamental period of flexible-support structures is longer than that of fixed-support structures. Also, damping is higher for SSI systems than for fixed-support structures. The total displacement of a structure is larger in the SSI and can be very significant for pounding buildings; with respect to the SSI, drifts and damage to structural elements are greater than in fixed-support structures (Chambers, 1998). The response of the SSI system is extremely sensitive to the magnitude of the seismic load. A severe earthquake can induce significant nonlinearity and plastic deformations in SSI systems, decreasing the stiffness and increasing the damping throughout a small earthquake. Under some seismic loads and with certain characteristics and site conditions, the SSI can cause a damaging influence on structures (Gazetas & Mylonakis, 2001) (Mylonakis & Gazetas, 2000).

## 2.5 Building Structural Systems

### 2.5.1 Introduction

Multi-story buildings must be stabilized against lateral loads (e.g., wind and earthquakes) that should become critical load conditions in the building design. There are many types of structural systems can realize this need. Such systems rely on a classic rigid joined frame system. The essential philosophy supporting these structural systems is to increase the structural rigidity against lateral and vertical loads (Günel & Ilgin, 2014).

### 2.5.2 Classification of Structural Systems

Structural systems can be categorized by the construction materials used in the buildings: steel, reinforced concrete, or composite. For efficiency, Khan classified structural systems for tall buildings according to their height (see Figure 2-16).

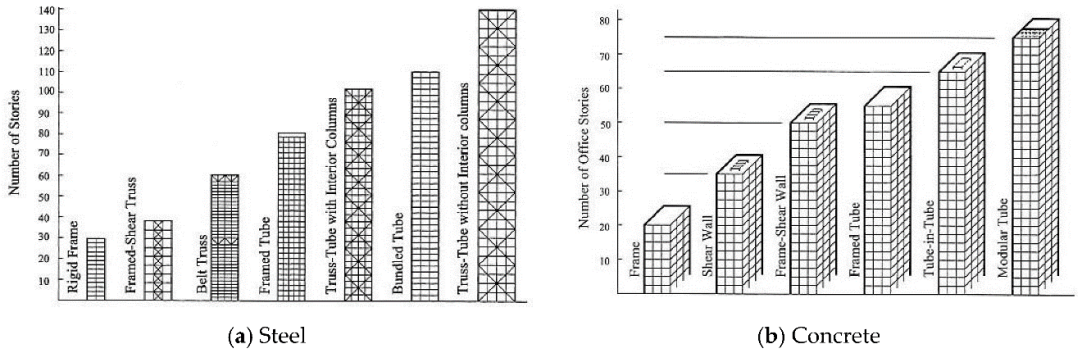


**Figure 2-16** Classification of tall building structural systems by Fazlur Kha (M. Ali & Moon, 2018).

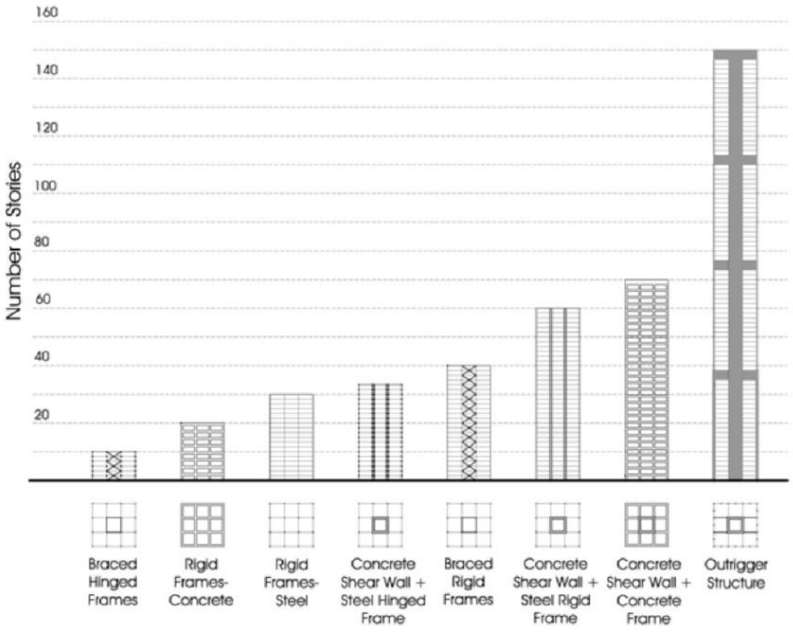


**Figure 2-17** Interior structures (M. Ali & Moon, 2018).

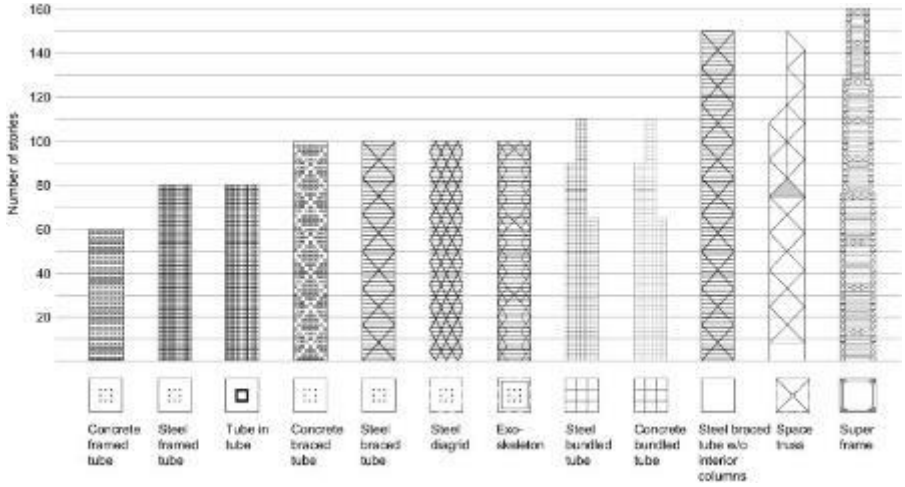


**Figure 2-18** Exterior structures (M. Ali & Moon, 2018).

According to (M. Ali & Moon, 2018) and (M. M. Ali & Moon, 2007), structural systems can be classified into two broad categories: exterior and interior structures. This classification depends on the distribution of elements comprising the lateral load resistance system used.

Figure 2-17 and Figure 2-18 summarize these classifications. Building structural systems can also be classified by their structural behavior under lateral loads. These classifications are further explained below (Günel & Ilgin, 2014).

Rigid frame or moment-resisting frame systems are used in reinforced concrete, steel, and composite buildings. These systems contain beams and columns without bracing (see Figure 2-19). The stiffness and resistance capacity of a rigid frame system in response to lateral and vertical loads come from the flexural rigidity of the columns and beams. Such systems depend on the rigid joining of beams and columns during the loading effect. Therefore, reinforced concrete is a perfect material for steel structures to use in strengthening their beam-column joints. In rigid frame systems, structural stiffness increases with the dimensions of the cross-section and flexural rigidity of the columns and beams. It decreases with their spacing and length. In terms of economics and efficiency, rigid frame systems can be used to resist lateral (i.e., earthquake and wind) and vertical (i.e., dead and live) loads in buildings up to 25 stories.

In reinforced concrete buildings, flat slab systems are very common. They consist of columns and slabs of a constant thickness and without beams. Shear walls can be used with or without columns. To reduce the punching shear effect and offer an architectural advantage, gussets or column capitals (see Figure 2-20 b and c) can be used on the upper

ends of columns. Because slabs have a low flexural stiffness, the flat slab system may be inadequate to resist lateral loads (as compared to the rigid frame system). Consequently, shear walls can be added to reinforce this low flexural stiffness and increase lateral resistance, protecting the flat slab system against lateral loads.

A core system is often utilized in reinforced concrete structures. It forms a concrete core from a shear wall, resisting both lateral and vertical loads (see Figure 2-21). Generally, a core system is comprised of an open core wall that is partially closed due to the use of beams and/or slabs. This strengthens the torsional and lateral rigidities of the structure. A core system that is partially closed satisfies rigidity needs against bending and shear. Core systems are very effective at resisting earthquake and wind loads in multi-story buildings up to 20 stories tall.

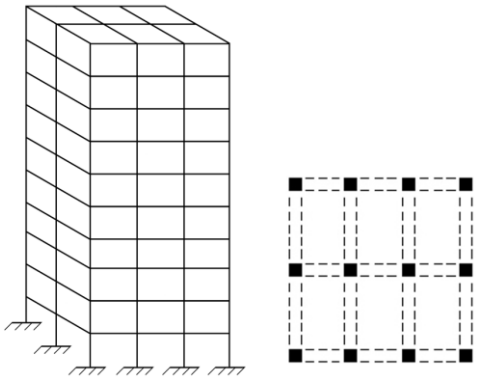

**Figure 2-19** Rigid frame system (Günel & Ilgin, 2014).

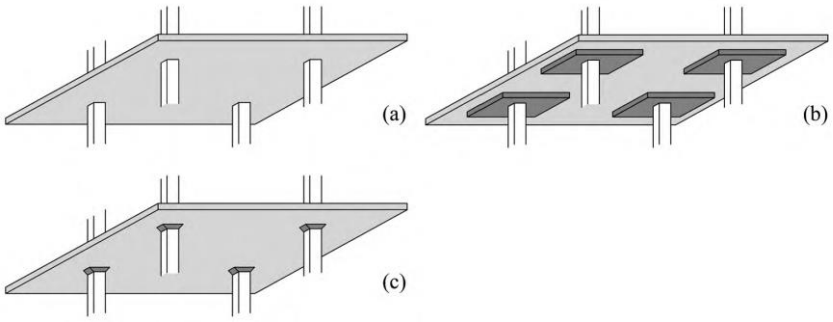


**Figure 2-20** Flat plate/slab systems: (a) without column capitals, (b) with column capitals, and (c) with gussets (Günel & Ilgin, 2014).

Shear wall systems are most often applied in reinforced concrete buildings. This type of system includes reinforced concrete shear walls that can be either solid or have openings. Shear wall systems can be considered cantilever beams with fixed base support, resisting both horizontal and vertical loads (see Figure 2-22). Due to the general behavior of the cantilever, the drift on the top floors is greater than on the bottom floors. Consequently, in very high-rise buildings it can be complicated to control the drift on the top floors. From economic and efficiency perspectives, the shear wall system provides rigidity adequate to resist lateral loads in buildings of 35 stories or less.

Economically speaking, the rigid frame system is inadequately rigid to accommodate lateral loads in buildings of more than 25 stories, due to significant displacement from the bending of columns. A building's height can be increased, however, by installing shear trusses and/or shear walls on the rigid frame system to resist lateral loads (see Figure 2-23). The combination of a frame system and shear trusses and/or shear walls is known as a shear frame system.

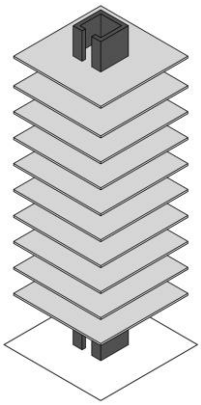

**Figure 2-21** Core system (Günel & Ilgin, 2014).

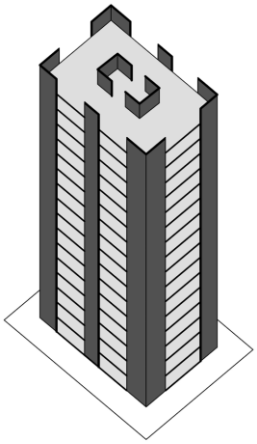

**Figure 2-22** Shear wall system (Günel & Ilgin, 2014).

This type of system can be divided into two categories:

- Shear truss frame systems (see Figure 2-23 a), and
- Shear wall frame systems (see Figure 2-23 b).

Shear truss frame systems include rigid frame systems and diagonal braces like vertical trusses, while shear wall frame systems are rigid frame systems with reinforced concrete shear walls either with or without openings. Stairwell and elevator core designs often feature shear trusses and/or shear walls. In this type of situation, a shear frame system with a structural core is known as a core frame system. Shear wall and truss frame systems with cores are called core wall and core truss frame systems, respectively. These cores increase a building's rigidity, allowing it to accommodate torsional and lateral loads. In terms of efficiency and economics, shear frame systems provide adequate rigidity to resist lateral loads in buildings of 40 stories or less.

Mega column (e.g., mega frame, space truss) systems include composite and concrete columns and/or shear walls that have sizeable sections and considerable height. They can resist both horizontal and vertical loads (see Figure 2-24). The horizontal connections are both essential and significant because floor slabs do not have adequate stiffness to behave as rigid diaphragms. Therefore, mega braces, belts, and Vierendeel frames are used. In this technique, mega columns and/or shear walls are linked to resist lateral loads (see Figure 2-24 a). According to (Günel & Ilgin, 2014), mega column systems can also be called mega frame systems, depending on their appearance and function (see Figure 2-24 a); they're called space truss systems when mega braces enhance the mega columns (see Figure 2-24 b). In terms of economics and efficiency, mega column systems can be used to resist both horizontal and vertical loads in buildings with more than 40 stories.

Mega core systems include reinforced concrete and composite core shear walls with substantial cross-sections, adding continual height to buildings (see Figure 2-25). Mega core

systems resist both lateral and vertical loads. Therefore, columns and/or shear walls on the perimeter of this type of building are unnecessary. In this system, floor slabs provide support like cantilevers linked to core shear walls (see Figure 2-25 a). Likewise, mega core systems corroborate strengthened cantilever slabs (see Figure 2-25 b).

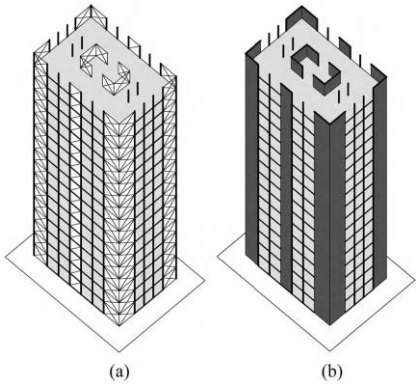


**Figure 2-23** (a) Shear truss (brace) frame system, and (b) shear wall frame system (Günel & Ilgin, 2014).

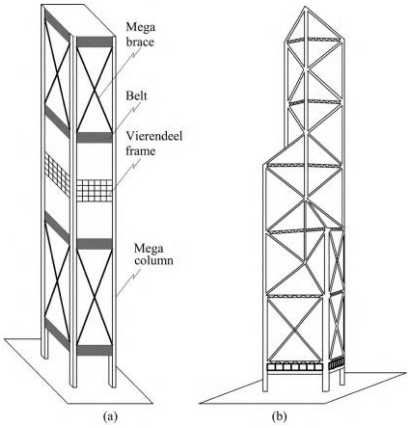


**Figure 2-24** Mega column (mega frame, space truss) system (Günel & Ilgin, 2014).

In such situations, discontinuous perimeter columns and core shear walls support the floor slabs. Strengthened cantilever slabs support perimeter columns, which are duplicated on certain stories. Strengthened cantilever slabs extend from the core to carry the story loads. In terms of both economics and efficiency, mega core systems can be used to resist lateral and vertical loads of more than 40 stories.

Outriggered frame systems rely on a combination of outriggers to frame shear wall and core frame systems, linking the core to exterior columns. The outrigger is a structural element linked to the exterior columns on one or more levels in a building in order to increase its structural rigidity (see Figure 2-26). The outrigger enhances the core shear truss or wall against bending by generating axial compression and tension on the exterior columns. In this method, the system is guaranteed to exhibit cantilever tube behavior and increased rigidity in shear frame systems. Moreover, the system has a significant effect on decreasing a building's drift. Belts include a horizontal shear truss or wall of sufficient rigidity in terms of both shear and flexure, and a depth similar to that of the outrigger (see Figure 2-26). These belts connect exterior columns to one another and enhance the system's efficiency by balancing the column loads along the perimeter. Both economically and in terms of efficiency, outriggered frame systems can resist both lateral and vertical loads in buildings of more than 40 stories.

In the 1960s, Fazlur Rahman Khan, the father of tubular design, developed the tube system (see Figure 2-27). A tube system consists of a hollow box column that can be considered a cantilever beam; it exhibits a tubular behavior rather than a horizontal load. The tube system depends on the rigid frame system and can be considered a frame with the

ability to resist horizontal loads through its use of the building's exterior facade. In 1966, the 43-story Plaza on Dewitt in Chicago was the first building to use the tube system.

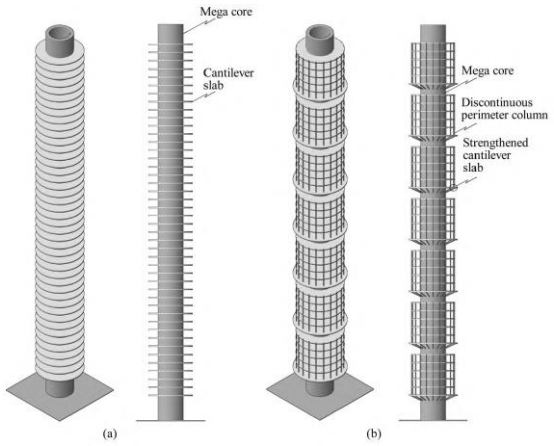


**Figure 2-25** Slabs in the mega core system: (a) cantilever slab and (b) supported cantilever slab (Günel & Ilgin, 2014).

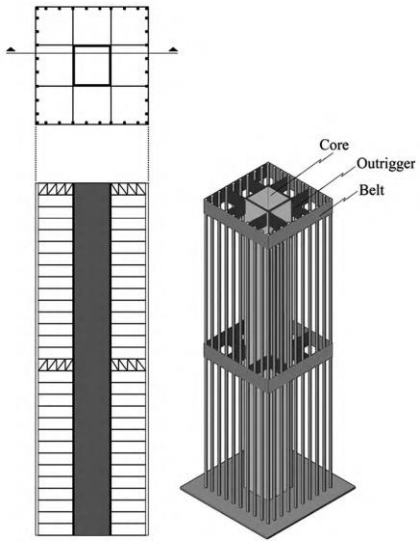


**Figure 2-26** Outriggered frame system (Günel & Ilgin, 2014).

Framed tube systems are also known as perforated or Vierendeel tube systems (see Figure 2-28). They have closely spaced exterior columns with 1.5 to 4.5 m centers, which is a significant feature. These columns are connected by deep spandrel beams at the floor level. To ensure framed tube system behavior, the designer increases the size of the exterior columns and spandrel beams. The framed tube system does not exhibit perfect tubular cantilever behavior due to the flexibility of the spandrel beams. The true behavior of framed tube systems can be described as something between frame and vertical cantilever behavior.

The narrow bay spacing of exterior columns seen in framed tube systems can prevent an outside view from the interior of a building. To increase bay spacing without decreasing the tubular behavior, the trussed tube system was developed. In this type of system, braces are added to the exterior columns (see Figure 2-29).

Fazlur Rahman Khan designed the trussed tube system by innovating on the framed tube system. The bracing of the exterior columns serves to develop and increase the structural stiffness. The trussed tube system increase the height of a building by providing less bay spacing than the framed tube system. In steel or composite structures, this system is applied through diagonal or X-braces on the building's facade (see Figure 2-29 a). Trussed tube systems can be utilized in reinforced concrete structures by filling the bay spacing with reinforced concrete shear walls, constituting the diagonal or X-brace on the facade of the building (see Figure 2-29 b).

Tube-in-tube systems enhance the stiffness of a tube system in terms of both lateral and vertical loads. This type of system consists of a core tube inside the building and a second exterior tube. The main lateral and vertical loads are carried by the exterior tube

because it has more rigidity than the interior tube. The diaphragm of the building joins the interior and exterior tubes which together respond to lateral loads. The resistance to earthquake and wind is similar to that of frame and frame shear wall systems, but tube-in-tube systems have more stiffness than do rigid frame systems.

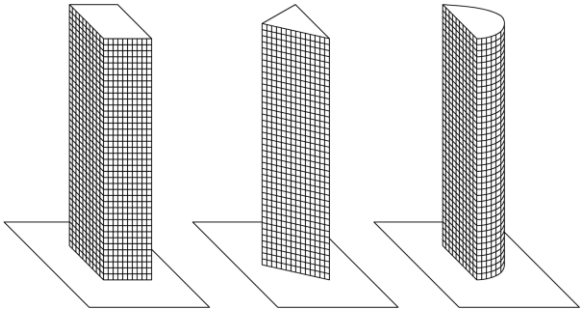

**Figure 2-27** Tube systems (Günel & Ilgin, 2014).

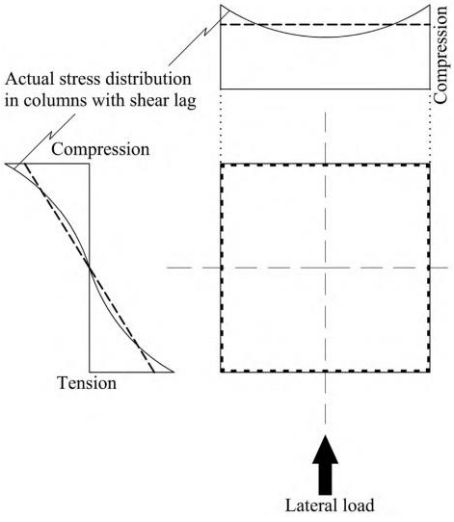


**Figure 2-28** Distribution of tension and shear lag in the perimeter columns of a framed tube system (Günel & Ilgin, 2014).

Bundled tube systems consist of a combination tube, trussed tube, and/or framed tube system working together as a united tube (see Figure 2-30). These systems offer a number of advantages, such as the architectural freedom to design tubes with different heights; the opportunity to employ wider column spacing of a desired height, as compared to the framed tube system; and the substantial facility to organize the aspect ratio. The bundled tube system also provides setbacks of various dimensions and shapes by ending the tubes at a desirable rise. In this system, different shapes can be generated by arranging single tubes in different forms of triangles or rectangles.

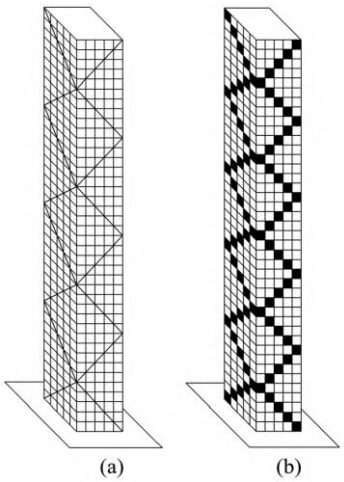


**Figure 2-29** Trussed tube systems in (a) steel or composite, and (b) reinforced concrete (Günel & Ilgin, 2014).

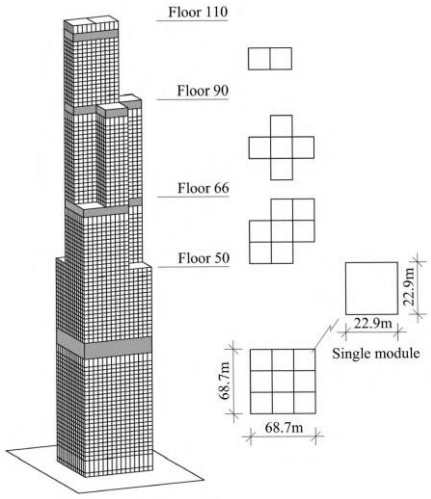


**Figure 2-30** Willis Tower, Chicago, USA, 1974 (photo courtesy of Antony Wood/CTBUH) (Günel & Ilgin, 2014).

### 2.5.3 Lateral Load Resistance Systems

Aside from a structural system's ability to resist loads, structural engineers normally understand lateral load resistance systems as consisting of vertical elements, horizontal elements, and the foundation. Figure 2-31 illustrates all of these. Vertical elements are represented by the columns and shear walls that transmit loads (e.g., gravity and seismic and wind loads) from the elevated levels to the building's foundation (Moehle, 2015). Typically, horizontal elements include floor diaphragms, collectors, and any chords. Likewise, they can also involve horizontal or diagonal bracing and truss elements.

#### 2.5.3.1 Diaphragms

The essential function of a diaphragm is to carry and transfer loads to other elements such as columns and shear walls. They are horizontal elements that distribute wind and

seismic forces to the vertical elements of a lateral load resistance system and tie them together (see Figure 2-31). ACI 318-14 highlighted additional functions of diaphragms, such as:

- Resisting gravity loads,
- Providing lateral support to vertical elements,
- Resisting out-of-plane forces,
- Resisting thrust from inclined columns,
- Transferring lateral inertial forces to the vertical elements of a seismic force resistance system,
- Transferring forces through the diaphragm, and
- Supporting soil pressure below ground.

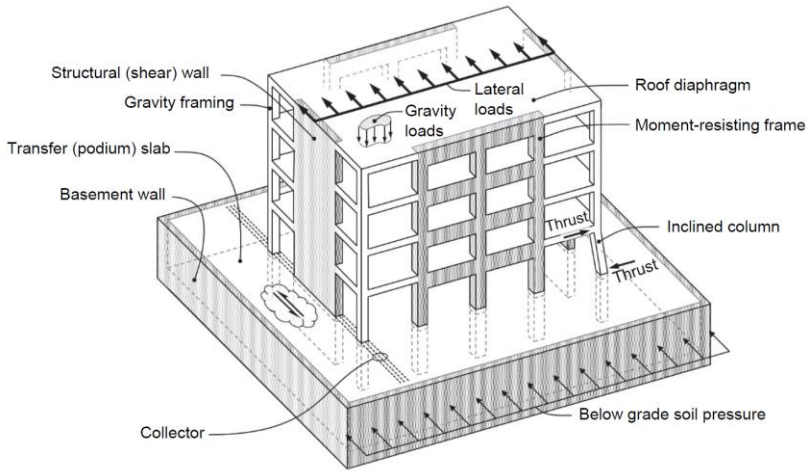


**Figure 2-31** Fundamental parts of a building's structural system, including horizontal elements (diaphragms), vertical elements (walls and frames), the foundation, and diaphragms (Moehle, 2015).

Diaphragms can carry and distribute forces between the vertical elements of a seismic force resistance system. For instance, shear walls and frames that behave independently have different deflected shapes under lateral loads (Moehle, Hooper, Kelly, & Meyer, 2010). When shear walls and frames are connected by a diaphragm, the stiffness of that diaphragm imposes a compatibility of displacement (see Figure 2-32). Consequently, the validity and efficiency of a building are highly reliant on the performance of its diaphragms. Usually, a diaphragm is constructed from concrete, wood, steel, or a combination of these materials. When diaphragms have openings, they should be arranged to avoid damage to the diaphragm from a large transfer of forces.

#### 2.5.3.2 Diaphragm Behavior

According to ASCE 7, reinforced concrete diaphragms and concrete-filled metal decks have span-to-depth ratios of 3 or lower in buildings with no horizontal irregularities, as defined in ASCE 7 Table 12.3-1. They are permitted to be idealized as rigid. Otherwise, a flexible diaphragm model must be used (A. S. o. C. Engineers, 2013). Figure 2-33 shows a diaphragm with a span-to-depth ratio greater than 3. In rigid diaphragms, the distribution of horizontal forces relies on the relative stiffness of the lateral load resistance system. A rigid diaphragm serves as a lateral resistance load system with same amount of deflection, because of its high stiffness. Rigid diaphragms are able to transfer torsion, shear, and forces based on their high stiffness and rigid bodies. They are constructed from reinforced concrete, precast concrete, or composite steel.

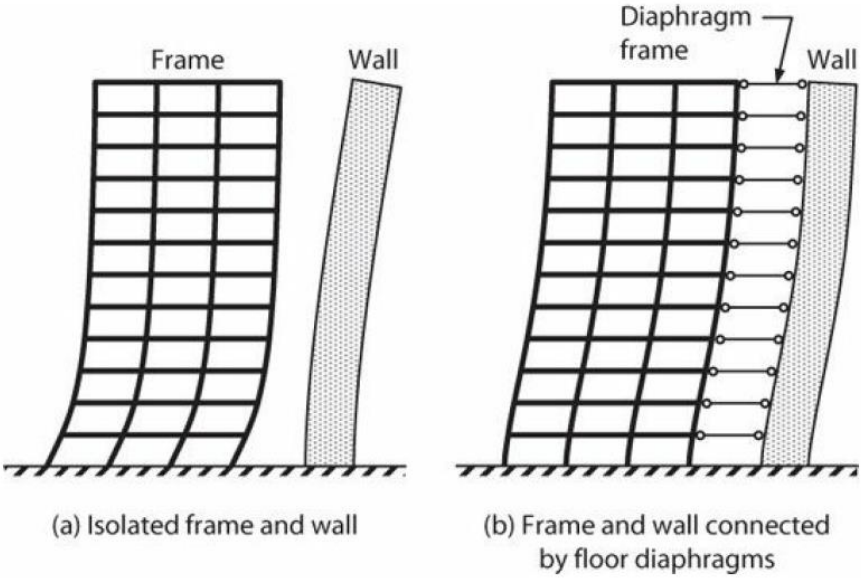


**Figure 2-32** Diaphragms developing transfer forces by imposing displacement compatibility on different vertical elements of a seismic force resistance system (Moehle et al., 2010).

In flexible diaphragms, the distribution of horizontal forces is independent of the relative stiffness of the lateral load resistance system. In designing flexible diaphragms, they can be assumed to be like simple beams between supports, distributing horizontal forces to the lateral load resistance system by relying on tributary width. Flexible diaphragms are unable to distribute torsion or rotational forces, and are constructed from wood, diagonally sheathed wood, sheathed wood, etc. Slender diaphragms between long spaces of lateral load resistance systems should be designed as flexible diaphragms. The design displacements and forces can then be influenced by the diaphragm's flexibility (see Figure 2-33).

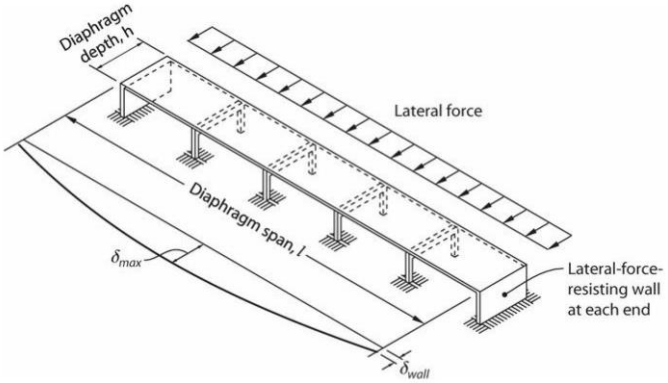


**Figure 2-33** Example of a flexible diaphragm with a high aspect ratio (Moehle, 2015).

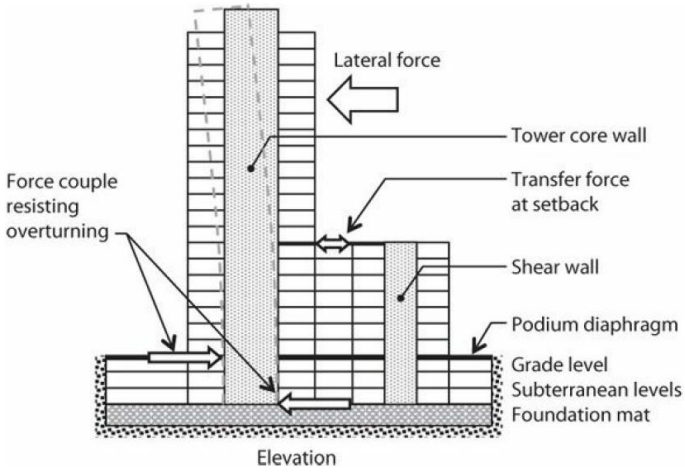


**Figure 2-34** Diaphragm transfer forces at irregularities in the vertical elements of a seismic force resistance system (Moehle, 2015).

Commonly, large diaphragm transfer forces occur at discontinuities or offsets of the vertical elements in a building. Figure 2-34 shows vertical discontinuities in a building at a podium level at grade, and a setback in the building's profile. In such cases, an analysis of the structure should utilize the flexible diaphragm model to produce accurate results, since a rigid diaphragm might unrealistically calculate large transfer forces (Moehle et al., 2010).

#### 2.5.3.3 Shear Walls

Shear walls can resist combinations of horizontal and vertical loads during static and dynamic conditions. The selection of shear walls as the essential seismic force resistance element relies on cost, constructability, seismic performance, and functionality. Typically, in low- to mid-rise buildings, moment-resisting frame systems are less cost effective than are shear wall systems. Generally, shear walls contribute remarkable stiffness to a building, enhance performance, and allow for longer spans under code drift limitations. A shear wall's circumference of elevator cores and stairs provide a dual function of including both vertical and horizontal resistance. Figure 2-35 shows different types of shear walls (Taranath, 2009).

#### 2.5.3.4 Shear Wall Configurations

There are numerous ways to configure shear walls; some are shown in Figure 2-36. Relatively speaking, rectangular sections are very simple to construct and design, but very thin sections should be avoided because they feature poor efficiency and low quality. Barbell walls consist of rectangular sections with boundary columns that enhance resistance, increase stability, and frame the wall. However, boundary columns may increase construction costs and result in architectural difficulties. To generate complex geometries for shear walls such as C, L, I, and T cross-sections, a combination of wall segments can be utilized. Core walls envelop stairs, elevators, and other zones, and have beams over openings. In the direction of lateral shear force, any orthogonal wall sections are assumed to behave as tension or compression flanges, while parallel wall sections are assumed to behave

as a web, resisting axial force, moment, and shear (Moehle, Ghodsi, Hooper, Fields, & Gedhada, 2011).

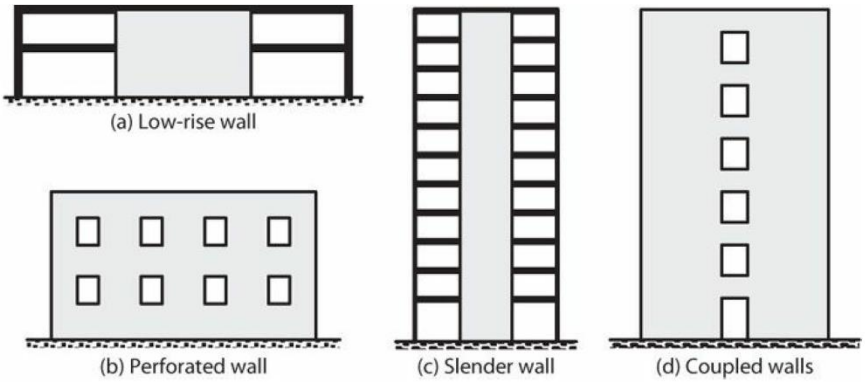


**Figure 2-35** Illustration of shear walls (Moehle et al., 2011).

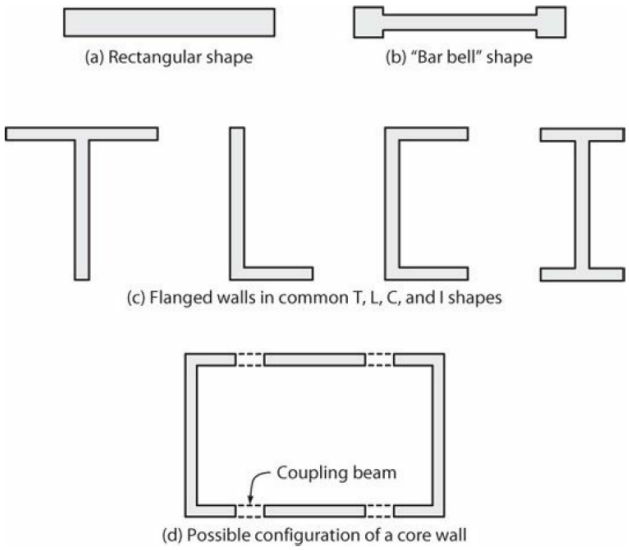


**Figure 2-36** Various wall cross-sections (Moehle et al., 2011).

### 2.5.3.5 Shear Wall–Frame Interaction

The lateral stiffness of a building can be enhanced by utilizing shear walls with rigid frame systems because of the interaction between the two. To understand the behavior of a framed shear wall system, one should investigate each system separately. The shear wall has a flexural mode deformation with concavity downwind and the slope is greatest at the top, while a rigid frame system has a shear mode deformation with concavity upwind and the slope is greatest at the bottom (see Figure 2-37). When a rigid frame system and shear wall are linked by a rigid connection, the deformation of the new system has a flat S curve. In other words, it has a shear deformation shape at the top and a bending deformation shape at the bottom. Consequently, the lateral load is resisted mainly by the rigid frame system on the top part of the building and the shear wall on the bottom.

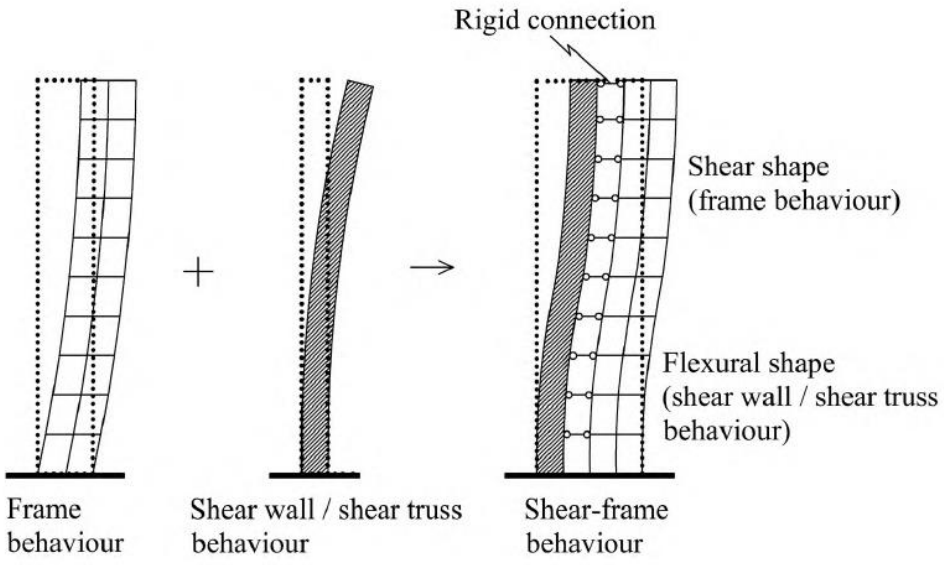


**Figure 2-37** Shear wall–frame interaction (Günel & Ilgin, 2014).

### 2.5.3.6 Shear Wall Aspect Ratio

The predictable behavior of a wall relies on the wall's aspect ratio (H/L). Generally, the definition of a slender wall ($H/L \geq 2.0$) is one that behaves like a flexural cantilever beam and has ductile flexural yielding. In contrast, squat walls ($H/L \leq 0.5$) resist lateral forces (depending on the diagonal strut mechanism) and have shear failure. Walls with intermediate aspect ratios ($0.5 \leq H/L \leq 2.0$) have both shear and bending stiffness components (Moehle et al., 2011).

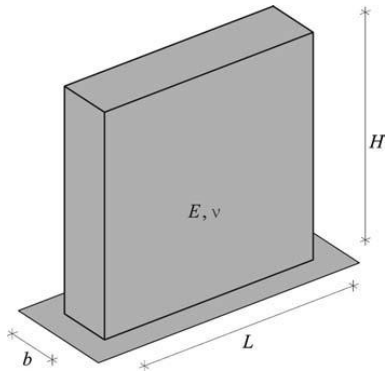


**Figure 2-38** Shear wall with fixed support (Neuenhofer, 2006).

### 2.5.3.7 Lateral Stiffness of Shear Walls

The deep beam is a very common structural model used to describe prismatic and solid shear walls. Figure 2-38 presents a typical shear wall with fixed support (Neuenhofer, 2006). In deep beam theory, cross-sections are supposed to keep to the same plane after deformation. Shear wall stiffness can be obtained by determining the wall's flexibility and

calculating the inverse to determine the stiffness. The wall's lateral displacement can be identified according to the principle of virtual forces, taking the sum of the shear and flexural deformations (see Figure 2-39).

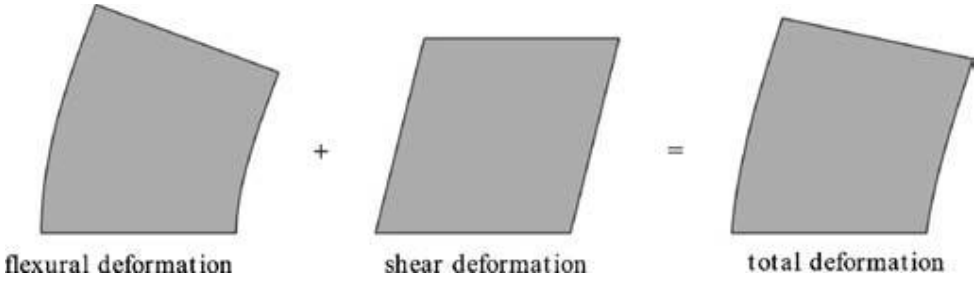


**Figure 2-39** Shear wall deformation (Neuenhofer, 2006).

$$\Delta_{total} = \Delta_{flex} + \Delta_{shear} = \frac{PH^3}{3EI} + \alpha\frac{PH}{GA}, \boldsymbol{P = 1} \qquad 2\text{-}14$$

where:

I is the moment of inertia = bL3/12,

A is the shear area (i.e., the area of the cross-section), and

E and G are the modulus of elasticity and shear modulus, respectively. They are related by E = 2(1+υ) G.

Where υ is the Poisson's ratio = 0.25, and α = 1.2.

Flexural deformation adopts the cantilever beam's behavior and shear deformation uses the shape factor, which relies on the distribution of shear stresses over the cross-section.

$$\Delta_{total} = \Delta_{flex} + \Delta_{shear} = \frac{P}{Eb}\left[4\left(\frac{H}{L}\right)^3 + 3\left(\frac{H}{L}\right)\right], \boldsymbol{P = 1} \qquad 2\text{-}15$$

From this equation, how the relative contributions of flexural and shear deformation affect the total deformation can be investigated. Figure 2-40 illustrates this relationship.

$\frac{\Delta_{flex}}{\Delta_{total}} = \frac{4(H/L)^2}{3+4(H/L)^2}$ And $\frac{\Delta_{shear}}{\Delta_{total}} = \frac{3}{3+4(H/L)^2}$

It is clear that shear deformation controls in small aspect ratios, and for large aspect ratios, flexural deformation dominates.

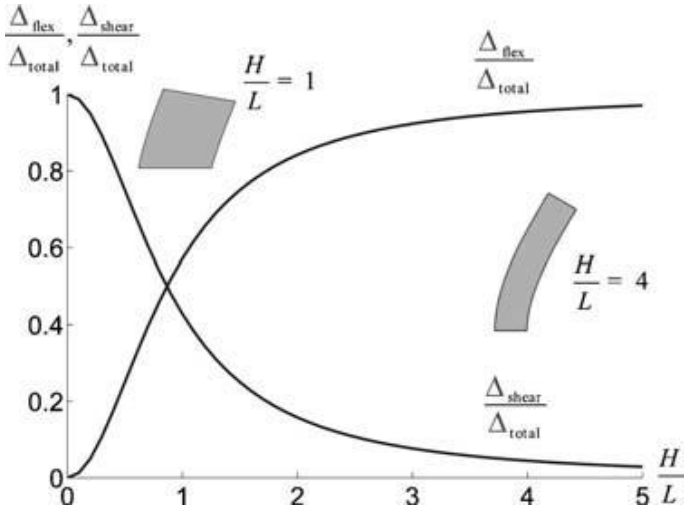


**Figure 2-40** Relative contributions of shear and flexural deformation to the total (Neuenhofer, 2006).

# 3. MOTIVATION AND SIGNIFICANCE

## 3.1 Problem Statement

A smart structure system has the facility to sense any variation in the environment loads or system properties, diagnose any problem at critical conditions, use sensing and data acquisition systems to store and process data and make an appropriate decision to improve system performance and to maintain structural integrity, serviceability, and safety. The importance of the dynamic soil-structure interaction system for traditional building structures has long been investigated by researchers, which have determined that the interaction has a significant effect on the tall buildings constructed on soft soil. However, the advent of smart structural systems necessitates an expansion of the field. Smart structural systems dynamically vary their effective stiffness and damping during a dynamic loading event, so the same results and conditions for traditional structures with soil-structure interaction effects no longer apply. Research is still needed to study the control system effect to reduce the system responses during hazard loads. Based on the advanced control algorithm (simple adaptive control) and effective damper (magnetorheological damper), the purpose of this study to investigate the performance these advanced control algorithm and MR damper on the behavior of dynamic soil-structure interaction system for different types of soil, soil profile and types of structural systems.

## 3.2 Research Objectives

The proposed research will evaluate the impact of soil structure interaction effects on the performance of structural systems with supplemental control systems in the presence of parameter uncertainty. The work will consider impact on both the structural system as well as on the control system design and performance, and identifying key criteria that are important in their design and evaluation.

## 3.3 Research Questions

The theory of control has recently been presented in soil structure interaction of building. However, several practical questions arise when dealing with smart soil structure interaction systems with simple adaptive control algorithm and MR damper.

- What are the important modeling, simulation, and design considerations for systems with significant soil-structure interaction effects?
- What is the impact of neglecting soil-structure interaction effects in evaluating the response of a controlled structure?
    a. Under what conditions is it important to consider soil-structure interaction effects when analyzing controlled structures? Are these the same conditions as for uncontrolled structures?
    b. How do simple adaptive control systems designed on fixed-supported-structures basis perform on structures having soil-structure interaction effects?
    c. What is the change in the cost of control effort that can occur when taking into account soil-structure interaction effects?

- What is the effectiveness of the simple-adaptive control strategy (SAC) for systems with significant soil-structure interaction effects in the presence of variations in the structure and soil conditions?
    a. How does the performance of controlled buildings change when the properties of the soil vary (soft vs medium)? What is the impact on the control system?
    b. How does the performance change when the building properties vary?

To answer all these questions, the research presents parametric study and cases study in this research.

### 3.4 Significance

Multi-story buildings are essential to people lives and the failure of them lead to loss lives and money during hazard loads. Prevent a building collapse on the hazard loads is one of the most significant challenges of the civil engineer. Control strategies and smart dampers can be useful to maintain structural safety and avoid failure. Structural control can provide a high level of serviceability and comfort. Moreover, it gives the designer more facility to increase building's flexibility and reduce construction cost. The SSI has significant impact on structure responses and it has not deeply investigated in previous studies.

In this study, the stiffness' parameters of soils and soil profiles are going to be investigated because these have great effects on the evaluation of foundation stiffness. The foundation stiffness leads to increase the responses of SSI system comprising with fixed support structures, especially for soft and medium soils. The SSI effect increases with decrease foundation stiffness.

The ISS effect increases while increasing the structural rigidity even with medium soils (not only for soft soils). Therefore, the structural rigidity will be studied. For the multi-story buildings, frame and frame shear wall structure types are widely used; however, these types of structures are going to be also investigated.

SAC algorithm and MR dampers used in this research to investigate the effect of SSI on previous parameters of soils and structures types. The SAC and the MR damper have high ability to maintain structures. The SAC is suitable to maintain large structures with multiple actuators and sensors (MIMO system), and it is not depending on the evaluation of the system parameters. In addition, the calculations of the SAC do not rely on full state feedback or observers and the order of the reference model may be much smaller than the system order. The MR damper has a highly reliable operation and can be viewed as a fail-safe, and it gave the adaptability of active devices without requiring to high power sources. Moreover, it becomes passive damper when hardware malfunction occurs.

## 3.5 Research Overview

Chapters 1, 2 and 3 are displayed the introduction, background, motivation and significance, and objectives of the research.

Chapter 4 discusses and presents the theoretical basis necessary for the development of smart structure and emphasis on the control algorithms, and control devices adopted in this research.

In chapter 5, SSI dynamic analysis, structural characterization and modeling assumptions are presented and discussed. Model reduction techniques are presented, implemented and validated for the structure and soil foundation.

In chapter 6 parametric study, adaptive control approach is developed to control a portal frame system. An initial investigation where a control scheme based on the SAC algorithm is developed and implemented, aiming to mitigate seismic responses of a portal frame system. Following the initial investigation, a comprehensive parametric study is conducted considering a portal frame with and without SSI, and different four soil profiles.

In chapter 7 Frame, Frame shear wall, semi-active adaptive control schemes based in SAC adaptive control are proposed. Cases study are conducted considering a frame and frame shear wall structural systems as the main structural configuration to be controlled. The SAC adaptive algorithm is implemented to control this structural systems, considering SSI effects with different four soil profiles.

# 4. SMART STRUCTURE

## 4.1 Introduction

The employment of smart structure for mitigating the responses of structures, under the impacts of hazard loadings, has become an attractive methodology, although further research is needed to fully develop the full potential of these technologies.

A smart structure or structural control has the ability to sense variations in environment loads or other characteristics of the system, diagnose any problem approaching a critical condition, use sensing and data acquisition systems to store and process information and make appropriate decisions regarding enhancing the system's performance, and maintain structural integrity, serviceability, and safety (Cheng et al., 2008).

## 4.2 Control Algorithms

Control devices (i.e., passive, active, semi-active, and hybrid) maintain buildings in response to different hazard loads. For such devices to achieve a high level of efficiency, practical control algorithms are needed. This section provides the fundamental theories, mathematical models, and utilization specifics for a variety of control algorithms. The algorithms employed for the present research and demonstrated below, and include the optimal control method (with an emphasis on the linear quadratic regulator algorithm) and adaptive control method (with an emphasis on the SAC algorithm).

### 4.2.1 Optimal Control Method

The words “optimal control” indicate a best choice or design. However, depending on the criteria and conditions, any stable control system can be considered optimal. To begin the search for an optimal solution, one must define the job, establish the necessary mathematical models, and identify all possible alternatives. For example, assume there are parameters in terms of stiffness, mass, and damping matrices that can be modified within specified requirements. Structural engineers can simultaneously redesign the structural parameters and control system while maintaining the system’s dynamic stability. In other words, the simultaneous optimization of the structure and control parameters minimizes the control energy required. Optimal control is determined by establishing a control law to satisfy the optimality criteria and specifications (Skelton, 1988). What is known as optimal is determined by the engineers and expressed in a mathematical form that identifies the best options for the design objectives. Optimal control is the common control method and can easily be used for structures (Dorf & Bishop, 2011).

#### 4.2.1.1 Linear Quadratic Regulator

Generally, an optimal control system is concerned with minimizing the performance index J (i.e., the cost function) defined by Eq. 4-1. In other words, optimal control determines a control variable u(t) that allows the system to follow an optimal trajectory x(t), which minimizes the performance index (Skelton, 1988). The linear quadratic regulator (LQR) is a significant type of optimal control method that follows an appropriate control solution, satisfying the minimum quadratic performance index for a linear system (Burns, 2001).

$$\boldsymbol{J = \int_{t0}^{t1} h\big(x(t), u(t)\big)dt} \quad \text{4-1}$$

A calculus of variations of other mathematical optimization techniques can be applied to solve this quadratic performance index, leading to the well-known matrix called the Riccati equation. The following summarizes of the main equations used in the LQR algorithm (Franklin, Powell, & Emami-Naeini, 2015).

Linear system

$$\boldsymbol{\dot{x} = Ax + Bu} \quad \text{4-2}$$

Quadratic performance index

$$\boldsymbol{J = \int_{t0}^{t1} (x^T Q x + u^T R u) dt} \quad \text{4-3}$$

Optimal u

$$\boldsymbol{u = -Kx} \quad \text{4-4}$$

Gain K

$$\boldsymbol{K = R^{-1} B^T P} \quad \text{4-5}$$

Algebraic Riccatti equation

$$\boldsymbol{PA + A^T P + Q - PBR^{-1} B^T P = 0} \quad \text{4-6}$$

where:

P is the unique solution to the algebraic Riccatti equation,

Q is a symmetric semi-definite matrix ($2n \times 2n$),

R is a symmetric and positive definite matrix ($n \times m$),

n is the number of degrees of freedom, and

m is the number of actuators.

The controller can tune with changing Q and R matrices. For example, when R is very small, this leads to fast convergence and high control efforts, and is used to weight the energy for each actuator. A Q matrix is used to weight the energy for displacements and velocities for each floor. If the model of the system is well defined and all of the states are available for feedback, LQR stability is guaranteed. The observer can reconstruct the states when it is not possible to measure them all. In this case, the system is still guaranteed to be stable, but the margins are small. As mentioned above, P is a unique solution that can be determined by the matrix factorizations. Arnold and Laub (1984) developed a very effective method for solving these algebraic equations (Arnold & Laub, 1984). Figure 4-1 presents the feedback control system for the LQR algorithm. The gain matrix (K) can be directly calculated by the MATLAB function lqr (A, B, Q, and R) (Franklin et al., 2015) and (Dorf & Bishop, 2011).

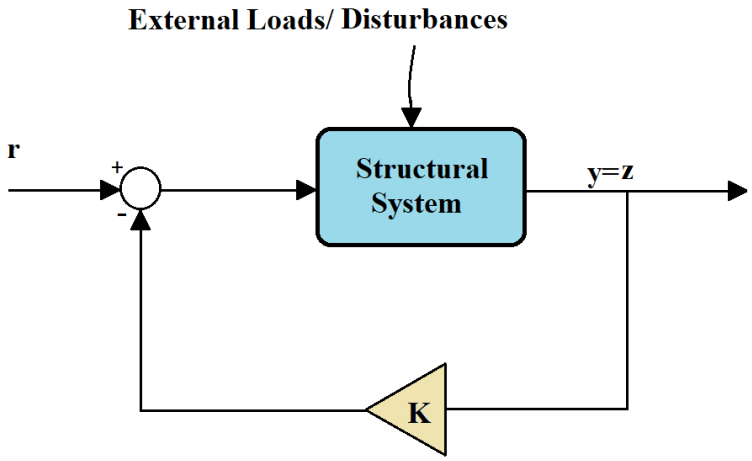


**Figure 4-1** System with feedback for the LQR algorithm (Wysard Soares, 2019).

### 4.2.2 Simple Adaptive Control

Adaptive control is a type of control method that has the ability to adjust the system parameters, allowing for adaptive control to modify its behavior in response to changes in external disturbances or the dynamic performance of the system. Application of an adaptive control involves the following steps:

- Identify a controller,
- Define a performance criterion,
- Evaluate online the performance related to the desired behavior, and
- Evaluate online the controller parameters to force performance tracking for the desired behavior.

Adaptive control methods can be divided into two principle categories: direct (or implicit) and indirect (or explicit). In direct methods, the control parameters are estimated directly depending on the error between the response system and desired response (i.e., direct methods adjust the adaptation system without explicit calculation of system parameters). Indirect methods require explicit evaluation of the system parameters to adjust the adaptation method. Direct methods offer more advantages than do indirect methods, such as employment, speed, and applicability to MIMO systems.

SAC is an algorithm for the adaptive control method that can be applied in large structural systems and employed in this research to mitigate structural responses. SAC is an example of direct model reference adaptive control (MRAC). It depends on the command generator tracker (CGT) approach and Lyapunov's stability theory (Kaufman, Barkana, &

Sobel, 2012). Figure 4-2 includes a typical block diagram for MRAC. SAC has many advantages over other MRSC types, such as:

- SAC is suitable to structure with multiple actuators and sensors (for MIMO systems).
- SAC does not depend on the evaluation of system parameters.
- The calculations do not rely on full-state feedback or observers.
- The order of the reference model may be much smaller than the system order.

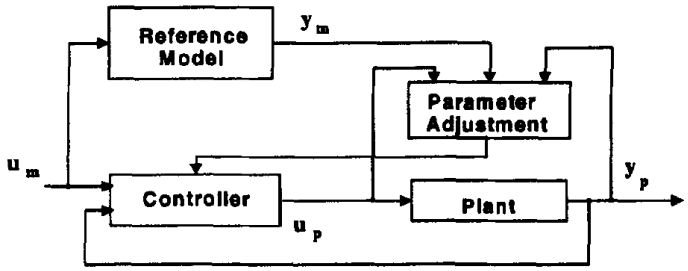


**Figure 4-2** Block diagram of a model reference adaptive control (MRAC) (Housner et al., 1997).

These significant properties make SAC very attractive for structural systems (Kaufman et al., 2012). In the SAC algorithm, the desired structural responses are described by a well-defined reference model. The purpose of this algorithm is to drive the system to track the response of the reference model. To guarantee that the system's trajectory tracks the reference model's response, the structural response is compared with the reference model's response and the necessary controller parameter modifications are estimated. Since 1982, the SAC algorithm has been employed successfully in a variety of control problems

such as flight control (Morse & Ossman, 1990) , helicopters, missiles (BAR-KANA & Guez, 1990), motor control (Shibata, Sun, Fujinaka, & Maruoka, 1996), and flexible structures (Bar-Kana & Kaufman, 1993).

In 1982, Kaufman and Mabius presented the SAC algorithm and Barkana and Kaufman improved upon it (1993). This method can obtain the performance of any system asymptotic to the perfect desired performance described by a reference model. (Sobel et al., 1982) demonstrated that SAC can be used to benefit systems with a notable change in characteristics or high uncertainty during sudden load changes (Sobel et al., 1982). Its comprehensibility and ease make SAC especially attractive to designers dealing with practical implementations. In SAC, the conditions are less challenging with guaranteed asymptotic tracking, in contrast to classic control in linear time-invariant (LTI) systems.

The advanced SAC algorithm is superior to classic control (Bar-Kana & Kaufman, 1993). Specifically, the control parameters are estimated for the particular problem through adaptive controllers; therefore, asymptotic adaptive tracking with no general LTI tracking solution is reasonable (Barkana, 2005). Commonly with SAC, a lower-order model can be employed and there is no need for an estimator. Moreover, prior knowledge of the controlled system is needed for common adaptive control methods, but not easily available, particularly for large structural systems. However, in SAC there is no need for prior knowledge. Consequently, its application is extended (Barkana & Kaufman, 1993).

Figure 4-3 presents a block diagram of SAC. Feedback on the error between the system and model reference responses, feedforward of the model states, and disturbances are all utilized in this mechanism to control the system's performance (Barkana, 2016c).

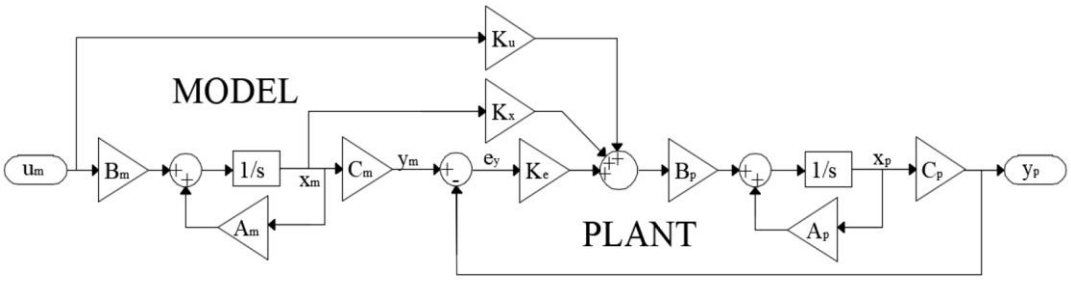


**Figure 4-3** Block diagram of a simple adaptive control (Barkana, 2016).

The controlled system or plant (i.e., the structure) is described by the governing equations.

$$\dot{\boldsymbol{x}}_{\boldsymbol{s}}(\boldsymbol{t}) = \boldsymbol{A}_{\boldsymbol{s}}\boldsymbol{x}_{\boldsymbol{s}}(\boldsymbol{t}) + \boldsymbol{B}_{\boldsymbol{s}}\boldsymbol{u}_{\boldsymbol{s}}(\boldsymbol{t}) + \boldsymbol{d}_{\boldsymbol{i}}(\boldsymbol{t}) \quad 4\text{-}7$$

$$\boldsymbol{y}_{\boldsymbol{s}}(\boldsymbol{t}) = \boldsymbol{C}_{\boldsymbol{s}}\boldsymbol{x}_{\boldsymbol{s}}(\boldsymbol{t}) + \boldsymbol{d}_{\boldsymbol{0}}(\boldsymbol{t}) \quad 4\text{-}8$$

where Ap is the state matrix, Bp is the input matrix, and Cp is the output matrix for the system. The xs variable is the system's n-state vector (n is the number of dimensions of the state), us is the m-input control vector (m is the number of dimensions of the input control vector), ys is the system m-output vector, and do and di are the input and output disturbances, respectively.

The system's output is required to follow the output of the reference model, which is represented by the governing equations.

$$\dot{\boldsymbol{x}}_{\boldsymbol{m}}(\boldsymbol{t}) = \boldsymbol{A}_{\boldsymbol{m}}\boldsymbol{x}_{\boldsymbol{m}}(\boldsymbol{t}) + \boldsymbol{B}_{\boldsymbol{m}}\boldsymbol{u}_{\boldsymbol{m}}(\boldsymbol{t}) + \boldsymbol{d}_{\boldsymbol{i}}(\boldsymbol{t}) \quad 4\text{-}9$$

$$\boldsymbol{y}_{\boldsymbol{m}}(\boldsymbol{t}) = \boldsymbol{C}_{\boldsymbol{m}}\boldsymbol{x}_{\boldsymbol{m}}(\boldsymbol{t}) \quad 4\text{-}10$$

where Am is the state matrix, Bm is the input matrix, and Cm is the output matrix for the reference model. The xm variable is the model n-state vector, um is the m-input

command vector, and ym is the model m-output vector. The model reference state dimension can be less than the system state dimension, but it must have sufficient dimensions to develop the required control command for the system. Nevertheless, the order of the system output is equal to the order of the model reference output because yp follows ym. It must be noted that for large structures with a significant degree of freedom, SAC is not required to determine all states because the order of model reference (m) can be less than the order of the system (n). The adaptive gains in SAC are time-varying and used to force the tracking error to zero.

The control law and adaptive gains are represented by:

$$\boldsymbol{u_p(t) = K(t)r(t)} \quad \text{4-11}$$

where

$K(t) = [K_e(t) \quad K_x(t) \quad K_u(t)]$

And $r^T(t) = [y_m - y_s \quad x_m^T(t) \quad u_m^T(t)]$.

The gain K(t) can be calculated from the sum of the integral (KI(t)) and proportional gains (Kp(t)).

$$\boldsymbol{\dot{K}_I(t) = \big(y_m(t) - y_s(t)\big)r^T T - \sigma K_I(t)} \quad \text{4-12}$$

$$\boldsymbol{K_P(t) = \big(y_m(t) - y_s(t)\big)r^T \bar{T}} \quad \text{4-13}$$

where $T$ and $\bar{T}$ are designated positive definite matrices and can be tuned to the adaptation rate.

An integral gain is needed for the tracking and stability of the plant, while the proportional gain controls the increasing convergence rate of the error between the system and model reference to zero. The coefficient σ in above equation is employed to save the

integral gain from attaining divergence or a very large amount, and the existence of the disturbance may be very small (Barkana, 2005).

SAC's promised stability relies on the transfer function of the system, which is almost strictly positive real (ASPR), something that several real systems cannot be confirmed to satisfy. A system can be defined as ASPR if it exists again in a closed-loop system that confirms that the original system is strictly positive real (SPR). In old formulations of SAC, an σ parameter was adopted to ensure stability during the disturbance effect. It has been noted that the σ parameter can reduce perfect tracking and cause chaotic phenomena. In 2016, Barkana presented a parallel feedforward (PFC) expression to ensure perfect tracking and robustness during disturbances and non-ideal situations, dropping the σ parameter and gain components (Barkana, 2016c).

$$\dot{\boldsymbol{K}}_{\boldsymbol{e}} = \boldsymbol{e}_{\boldsymbol{y}}(\boldsymbol{t})\boldsymbol{e}_{\boldsymbol{y}}(\boldsymbol{t})^{\boldsymbol{T}}\boldsymbol{\Gamma}_{\boldsymbol{e}} \quad \text{4-14}$$

$$\dot{\boldsymbol{K}}_{\boldsymbol{x}} = \boldsymbol{e}_{\boldsymbol{y}}(\boldsymbol{t})\boldsymbol{x}_{\boldsymbol{m}}(\boldsymbol{t})^{\boldsymbol{T}}\boldsymbol{\Gamma}_{\boldsymbol{x}} \quad \text{4-15}$$

$$\dot{\boldsymbol{K}}_{\boldsymbol{e}} = \boldsymbol{e}_{\boldsymbol{y}}(\boldsymbol{t})\boldsymbol{u}_{\boldsymbol{m}}(\boldsymbol{t})^{\boldsymbol{T}}\boldsymbol{\Gamma}_{\boldsymbol{u}} \quad \text{4-16}$$

#### 4.2.2.1 Designing a Reference Model for SAC

To consider the SAC algorithm, a reference model must be defined; this can be any mathematical model developed in such a way that its responses are a specific desirable performance. In this section, two design examples from current research are investigated. Bitaraf demonstrated an excellent mathematical model that can describe the controlling structural performance under any hazard load (Amini et al., 2018; Bitaraf, 2011). This model has a number of design features. The first is that there is no need to measure the external

signal loads on the structural system from earthquakes or wind. Additionally, the reference model's behavior continually outperforms the behavior of the controlled structural system, and does not rely on external signal loads.

Generally, essential design features recognize the limitation of energy-dissipating devices (i.e., control devices). For instance, MR dampers can generate control forces with lower- and upper-limit capacities. Bitaraf defined the reference model for the SAC algorithm as a structural system having responses within a limited range, which can be described by:

$$\boldsymbol{y_m = y_S} \qquad \boldsymbol{if\ |y_s| < Y_{max}} \qquad \text{4-17}$$

$$\boldsymbol{y_m = Y_{max}} \qquad \boldsymbol{if\ |y_s| \geq Y_{max}} \qquad \text{4-18}$$

where Ymax is the vector of the maximum satisfactory value for the reference model's responses. It is clear that the reference model assumes that all values less than Ymax are suitable, and others will be neglected. When the structural system's response is less than Ymax, the error between the responses of the structural system and reference model is equal to zero. When the structural system's response is greater than Ymax, the purpose of the SAC algorithm is to minimize the error and make the structural system's response fall within the range defined by Ymax. In the above definition for SAC, there is no need to measure the external signal loads on the structural system. The SAC algorithm never increases the response of the controlled structural system to the uncontrolled system and is not reliant on the properties of the disturbance. The reference model illustrated by Equations (4.17) and (4.18) matches well with the organization of the SAC algorithm, controlling the structural systems implemented with the MR damper with regards to its conditions.

The Ymax term may have any value greater than or equal to zero ($Y_{max} \geq 0$). Bitaraf suggested the minimum values for the displacement and drift of floors can be reached by selecting that Ymax be equal to zero. Nevertheless, if Ymax is set to equal zero, the values estimated for an acceleration of the structural system may not be in a satisfactory domain. Consequently, the best value for Ymax depends on the goal of the analysis. Additionally, the input command um is considered to be zero. The reference model's responses can be determined from the output of the reference model, as follows:

$$\boldsymbol{x_m} = \begin{bmatrix} \boldsymbol{X_m} \\ \boldsymbol{\dot{X}_m} \end{bmatrix} = \begin{bmatrix} \int \boldsymbol{\dot{X}_m dt} \\ \boldsymbol{\dot{X}_m} \end{bmatrix} = \begin{bmatrix} \int \boldsymbol{y_m dt} \\ \boldsymbol{y_m} \end{bmatrix} \quad \text{4-19}$$

where $X_m$ and $\dot{X}_m$ are the displacement and velocity of the reference model, respectively. Figure 4-4 displays a block diagram of the reference model established by Bitaraf that allows the SAC algorithm to have the structure's performance (Bitaraf, 2011).

Another design example for the reference model was offered by Al-Fahdawi. This design adopted the optimal control theory, and particularly the LQR, to estimate the desired output of the reference model with the assumption of invariable system parameters (Al-Fahdawi, Barroso, & Soares, 2018).

## 4.3 Control Devices

In recent decades, structural engineers have been using energy dissipating devices (e.g., passive, active, and semi-active control devices) to mitigate the influence of hazard loads on structural damage. Active control devices have the ability to adaptively deal with any variation in the structural properties or external excitations, but their significant energy

requirements, reliability, and stability are still the topics of primary importance to civil engineers (Kerber, Hurlebaus, Beadle, & Stöbener, 2007). In comparison, passive control devices are very effective but have low damping capacity and adaptability. Semi-active devices are substitutional strategies that maintain buildings against external hazard loads (e.g., earthquakes and wind). In this portion of the study, the features of semi-active devices are described in detail and different models of their dynamic behavior studied.

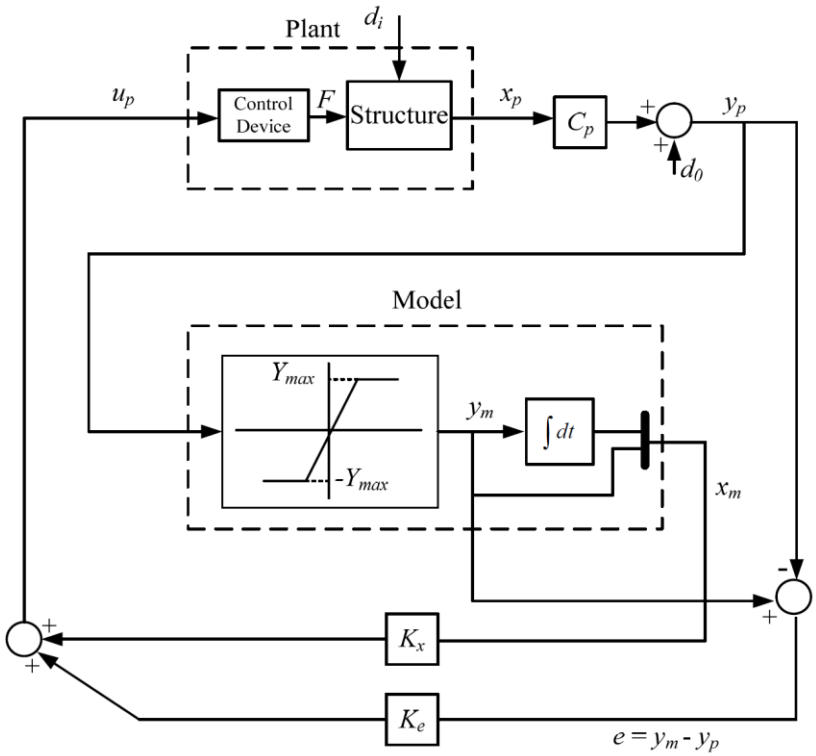


**Figure 4-4** Block diagram of SAC for optimizing structural performance (Bitaraf, 2011).

### 4.3.1 Semi-Active Devices

Semi-active control devices can contribute to the adaptability and versatility of active control devices and the reliability of passive control devices. Semi-active devices outperform other types because they require only a small amount of external energy to operate and cannot inherently make a structure unstable. Numerous semi-active control devices (e.g., fluid viscous dampers, friction control devices, electrorheological (ER) fluid dampers, magnetorheological (MR) dampers) have been utilized to maintain buildings, corresponding to their hazard loads. In this section, the semi-active device called an MR damper is investigated.

#### 4.3.1.1 Magnetorheological Dampers

In recent years, semi-active devices have received significant attention because they offer the adaptability of active devices without requiring connection to large power sources. MR dampers are one of the most promising semi-active devices that use MR fluids to produce controllable damper forces. MR dampers are highly reliable and can be viewed as a fail-safe. They become passive dampers when hardware malfunction occurs. Figure 4-5 shows the schematics of an MR damper. They allow rapid changes to damping characteristics (H.-J. Jung et al., 2004).

If MR fluid is subjected to a magnetic field, particles disseminated in that fluid are rearranged and a particle series develops. In milliseconds, the fluid then switches from being free flowing to a semi-solid and exhibiting a visco-plastic performance (see Figure 4-6). MR dampers are effective at eliminating vibration in many implementations, due to the

simplicity of the mechanism, high limit, low energy requirements, high damping force range, and substantial stability, reliability, and robustness. Likewise, such devices are comparatively economical to produce and maintain and are impervious to temperature variations. Therefore, they can be employed for outdoor and indoor uses alike.

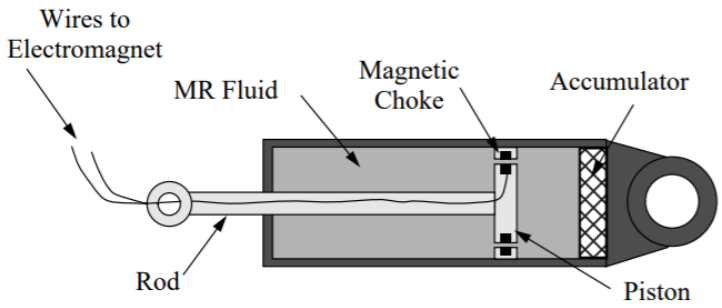


**Figure 4-5** Magnetorheological damper (Spencer Jr et al., 1997).

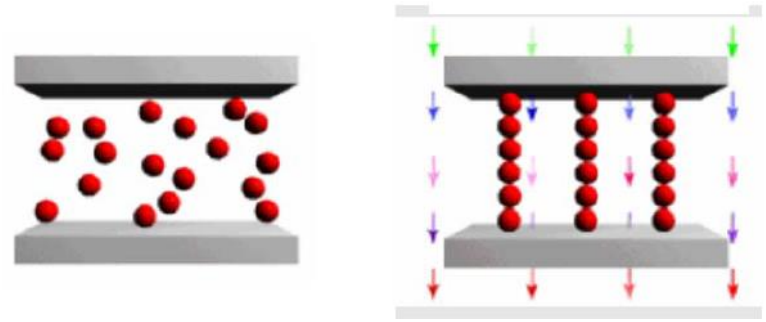

**Figure 4-6** Chain-like structure formation in MR fluid after application of a magnetic field (LORD Corporation).

Figure 4-7 displays a sketch of a commercial 20-ton MR damper. As mentioned above, one advantage of MR dampers is that they are qualified applicants for mitigating structural vibrations and have been examined in several studies demonstrating their ability to maintain buildings in the face of seismic effect (Dyke & Spencer Jr, 1996) (Spencer Jr et al., 1997) (Sahasrabudhe & Nagarajaiah, 2005) (H. J. Jung, Choi, Spencer Jr, & Lee, 2006) (Shook, Roschke, & Ozbulut, 2008).

Modeling the dynamic behavior of MR dampers is an essential challenge due to the device's inherent nonlinearity. There are two categories of mathematical models for the dynamic behavior of MR dampers: parametric and nonparametric. Neural network and fuzzy logic (i.e., intelligent) models are nonparametric methods applied to depict the dynamic behavior of MR dampers (Chang & Roschke, 1998), (Wang & Liao, 2004) and fuzzy logic-based models (Kim, Langari, & Hurlebaus, 2009). Several parametric models have been adopted to estimate the dynamic behavior of MR dampers, such as the nonlinear hysteretic bi-viscous model (Kamath & Werely, 1997), hyperbolic tangent model (Christenson, Lin, Emmons, & Bass, 2008), Bingham model (D.-Y. Lee & Wereley, 2000) and Bouc-Wen hysteresis model (Jansen & Dyke, 2000). This research focuses only on parametric models.

Normally, the Bingham model is utilized to depict MR dampers because it is easy to achieve and straightforward. However, the elastic properties of the fluid at low shear rates and small deformations cannot be verified and the nonlinear force-velocity result cannot be represented (H.-J. Jung et al., 2004). In the nonlinear hysteretic bi-viscous model, the MR damper's behavior can be adequately captured, but to fit the practical conditions, it is necessary that more comprehensive research be conducted (H.-J. Jung et al., 2004). The

hyperbolic tangent model can identify the nonlinear forces of large MR dampers, but its equations are more complex than those of other suggested models. Spencer et al. (1997) offered a simple Bouc-Wen model to capture and characterize the behavior of MR fluid dampers. In this model, the force displacement and force velocity behaviors can be predicted very strongly, and the analytical results match with experiment-based tests. However, this model cannot capture the force roll off when the velocities are small and the velocity and acceleration are in opposite directions. Spencer et al. (1997) introduced a modified version of the Bouc-Wen model to overcome this disadvantage. The modified Bouc-Wen model has a very high level of efficiency, but its equations are complicated. In the present research, the simple Bouc-Wen model was adopted to depict the dynamic behavior of the MR damper.

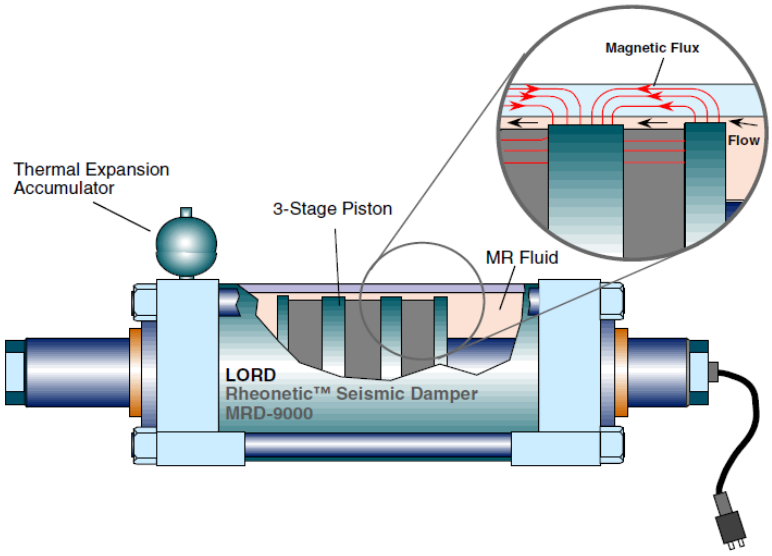


**Figure 4-7** Schematic of a prototype 20-ton large-scale MR fluid damper (LORD Corporation).

#### 4.3.1.2 Bingham Model

The Bingham model is an extremely common dynamic model used to demonstrate the behavior of MR dampers. It was presented by Stanway et al. (1987) to indicate the behavior of ER fluids (RSJL Stanway, Sproston, & Stevens, 1987). Spencer et al. (1997) applied the Bingham model to MR dampers. Figure 4-8 offers a simple schematic diagram of the Bingham model. The force generated by the MR damper is given by:

$$\boldsymbol{f = f_y sgn(\dot{x}) + c_0 \dot{x}} \quad \text{4-20}$$

$$\boldsymbol{f_y = f_{ya} + f_{yb} u} \quad \text{4-21}$$

$$\boldsymbol{c_0 = c_{0a} + c_{0b} u} \quad \text{4-22}$$

where fy is the yield force, c0 is the coefficient of damping, and x is the velocity of the MR damper. Equations (4.21) and (4.22) indicate that the parameters fy and c0 depend on the applied voltage u (and functions of u).

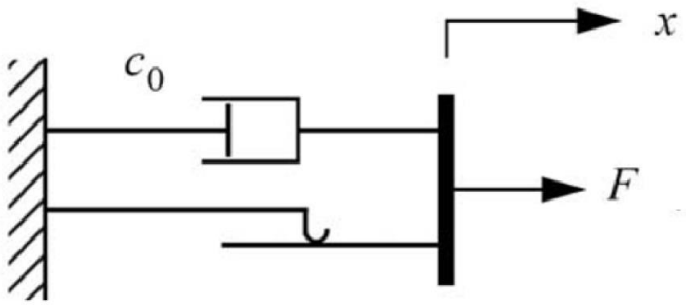


**Figure 4-8** Bingham model of an MR Damper (H.-J. Jung et al., 2004).

#### 4.3.1.3 Simple Bouc-Wen Model

To understand the full advantage of an MR damper, a nonlinear model of the damper's behavior should be chosen from the literature. In the present research, a simple Bouc-Wen model was selected. Figure 4-9 shows this mechanical model (Wen, 1976). The force of the MR damper was:

$$\boldsymbol{f = C_0\dot{x} + \alpha z} \quad \text{4-23}$$

$$\boldsymbol{C_0 = C_{0a} + C_{0b}u} \quad \text{4-24}$$

$$\boldsymbol{\alpha = \alpha_a + \alpha_b u} \quad \text{4-25}$$

$$\boldsymbol{\dot{u} = -\eta(u - v)} \quad \text{4-26}$$

$$\boldsymbol{\dot{z} = -\gamma|\dot{x}|z|z|^{(n-1)} - \beta\dot{x}|z|^n + A\dot{x}} \quad \text{4-27}$$

where $f$ and $\dot{x}$ are the MR damper's force and velocity, respectively, C0 is the viscous damping, and the z variable is the hysteretic behavior. The variables γ, β, n, and A are adjustable shape parameters (Kim et al., 2009). The model parameters α and C0 depend on the voltage (v), and u and v are the input and output voltages, respectively. The αa, αb, C0a, and C0b variables are calculation parameters that rely on voltage; the result is a magnetic field (Spencer Jr et al., 1997). The inverse model of the MR damper was used to determine the necessary MR damper voltage that will generate the forces estimated from the SAC algorithm (Tse & Chang, 2004).

$$\boldsymbol{z \cong sign(\dot{x})\left[\frac{A}{\gamma+\beta}\right]^{1/n}} \quad \text{4-28}$$

$$\boldsymbol{u = \frac{f - C_{0a}\dot{x} - \alpha_a z}{C_{0b}\dot{x} + \alpha_b z}} \quad \text{4-29}$$

$$\boldsymbol{v = u + \frac{\dot{u}}{\eta}} \quad \text{4-30}$$

Figure 4-9 shows a schematic of the simple Bouc-Wen model, and Table 4-1 lists the properties of the 1000 kN MR damper used in this research.

**Table 4-1** 1000 kN MR Damper parameters for the simple Bouc-Wen model (Bitaraf, 2011).

| Parameter | Value | Parameter | Value |
|---|---|---|---|
| $C_{0a}$ | 4.4 x $10^2$ (Ns/m) | $\alpha_b$ | 4.9615 x $10^7$ (N/mV) |
| $C_{0b}$ | 4.4 x $10^3$ (Ns/mV) | $\beta$ | 300 ($m^{-1}$) |
| $\alpha_a$ | 1.087 x $10^7$ (N/m) | $\gamma$ | 300 ($m^{-1}$) |
| $V_{max}$ | 10 (V) | n | 1 |
| A | 1.2 | $\eta$ | 50 ($S^{-1}$) |

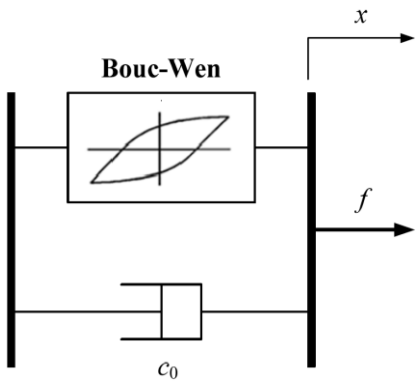


**Figure 4-9** Schematic of the simple Bouc-Wen model of the MR damper (Jung et al., 2004).

#### 4.3.1.4 Modified Bouc-Wen Model

Figure 4-10 presents a schematic of the standardized version of the modified Bouc-Wen model of the MR damper. According to (Yang et al., 2002), the MR damper's force can be evaluated by:

$$\boldsymbol{F = \alpha z + c_0(\dot{x} - \dot{y}) + k_0(x - y) + k_1(x - x_0) = c_1\dot{y} + k_1(x - x_0)} \quad \text{4-31}$$

The z and y variables are determined as:

$$\boldsymbol{y = \frac{1}{c_0 + c_1}\{\alpha z + c_0\dot{x} + k_0(x - y)\}} \quad \text{4-32}$$

and

$$\boldsymbol{\dot{z} = -\gamma|\dot{x} - \dot{y}|z|z|^{n-1} - \beta(\dot{x} - \dot{y})|z|^n + A(\dot{x} - \dot{y})} \quad \text{4-33}$$

where k0 is the stiffness and c0 is the viscous damping at large velocities. The c1 variable is the viscous damping at low velocities, and k1 is the accumulator stiffness. Yang et al. (2002) introduced a third-order polynomial to calculate the parameters α, c0, and c1, depending on the input current i (i.e., the functions of i) for full-scale MR dampers.

$$\boldsymbol{\alpha(i) = 16566i^3 - 87071i^2 + 168326i + 15114} \quad \text{4-34}$$

$$\boldsymbol{c_0(i) = 437097i^3 + 154540i^2 + 1641376i + 457741} \quad \text{4-35}$$

$$\boldsymbol{c_1(i) = -9363108i^3 + 5334183i^2 + 48788640i - 2791630} \quad \text{4-36}$$

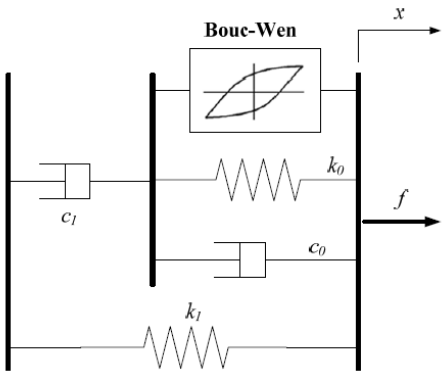


**Figure 4-10** Schematic of the modified Bouc-Wen model of the MR damper (Jung et al., 2004).

As stated above, to generate the force (F) required by the MR damper, the inverse model must be applied to estimate the desired electrical current. Under the assumption that the stiffnesses are negligible and z can be approximated as its ultimate hysteretic strength, (Tsang et al., 2006) demonstrated how the desired current (i) can be determined.

$$\boldsymbol{i(t) = -\frac{2}{3} ln\left[1 - \frac{-|F| + |\widetilde{F}_{\eta}|}{1.5 \times 10^{5}}\right]} \quad \text{4-37}$$

$$\boldsymbol{\widetilde{F}_{\eta}(t) = \frac{c_0(t-\Delta t)c_1(t-\Delta t)}{c_0(t-\Delta t)+c_1(t-\Delta t)}\dot{x}(t)} \quad \text{4-38}$$

Equations (4.31) through (4.38) predict the current and force. The A and n parameters are given. Table 4-2 provides the parameters for the simple Bouc-Wen model for the full-scale MR damper with a 200 kN capacity that was selected in (Yang et al., 2002). Researchers modified the parameter values by applying the least-squares method because they could not be obtained directly from the literature (Crassidis & Junkins, 2011). Some values for force were determined using the equations from the modified Bouc-Wen model. Subsequently, the fittest values for the parameters c0a, c0b, αa, αb were estimated by employing the least-squares method to reduce the error between the modified and simple Bouc-Wen models (Yang et al., 2002).

**Table 4-2** 200 kN MR Damper parameters for the simple Bouc-Wen model (Bitaraf, 2011).

| Parameter | Value | Parameter | Value |
|---|---|---|---|
| $C_{0a}$ | 13760 (Ns/m) | $\alpha_b$ | 4904 (N/mV) |
| $C_{0b}$ | 12553 (Ns/mV) | β | 100.1 ($m^{-1}$) |
| $\alpha_a$ | 103690 (N/m) | γ | 3819.4 ($m^{-1}$) |
| A | 833.45 | n | 2.39832 |
| η | 31.4 ($S^{-1}$) | | |

**Table 4-3** 200 kN MR Damper parameters for the modified Bouc-Wen model (Bitaraf, 2011).

| Parameter | Value | Parameter | Value |
|---|---|---|---|
| $k_0$ | 13760 (N/m) | η | 31.4 ($S^{-1}$) |
| $X_0$ | 12553 (m) | β | 100.1 ($m^{-1}$) |
| $k_1$ | 617.31(N/m) | γ | 647.46 ($m^{-1}$) |
| A | 2679 ($m^{-1}$) | n | 10 |

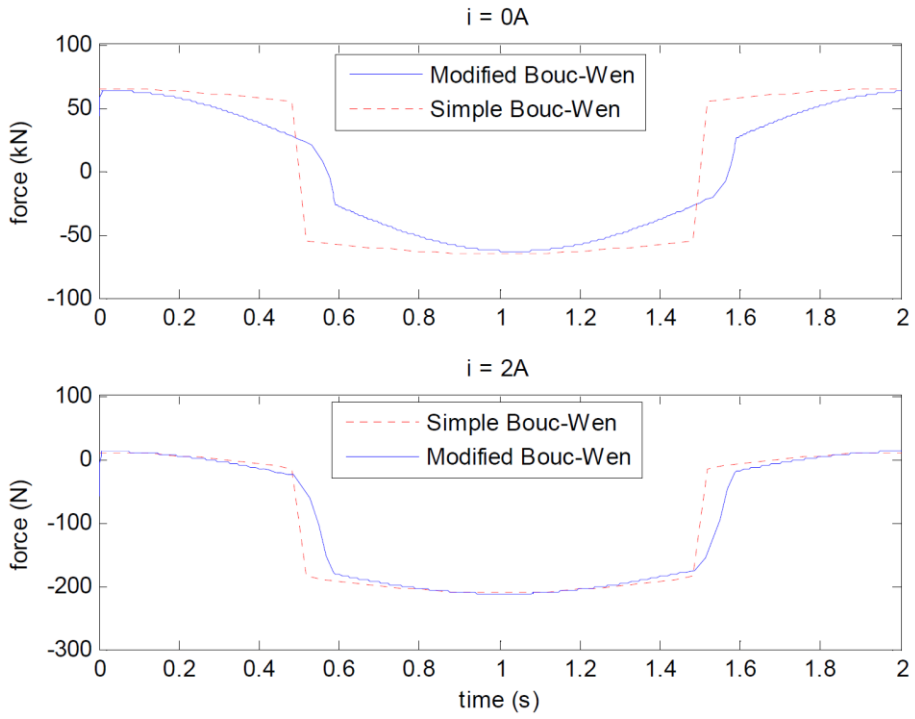


**Figure 4-11** Comparison of the MR damper's behavior using modified and simple Bouc-Wen models (Bitaraf, 2011).

The sinusoidal displacement excitation with 0.5 Hz and a 2.54 cm (1 inch) amplitude was used to generate the MR damper's force and capacity; the values were 200 kN for both. A comparison of the simple and modified Bouc-Wen models can be found in

Figure 4-11, which together model the full-scale MR damper's behavior. The simple Bouc-Wen model is obviously satisfactory for modeling an MR damper in practical applications. Table 4-3 displays the MR damper's parameters for the modified Bouc-Wen model.

# 5. MODELLING OF DYNAMIC SSI SYSTEMS

## 5.1 Introduction

This section describes the dynamic analysis of the methodological and conceptual principles essential for the development of an SSI system, followed by an explanation of the significant related parameters. Finally, model reduction procedures used to determine equivalent stiffness matrices for the structure and foundation are discussed and presented. Hypotheses and simplifications utilized to develop computationally efficient algorithms are presented.

The finite element software ETABS (Computers and Structures, 2019) was used to compute equivalent stiffness matrices for frame and frame shear wall systems. The formulations considered the three-dimensional structure, material properties, and geometry of the structural system. The equivalent stiffness matrices for foundations with different soil profiles were estimated using the finite element software ABAQUS. Lastly, the stiffness and mass matrices for frame and frame shear wall systems and foundations were exported to MATLAB and SIMULINK (Mathworks, 2019).

## 5.2 General Equations of Motion

Building structures are usually simulated into equivalent MDOF models during the preliminary seismic design step. One uncomplicated and widely adopted model called the shear building model has been used to investigate the seismic responses of multi-story buildings. This type of model was chosen here, due to its ability to capture the general

behavior and higher mode effects without expanding the calculation effort. The properties needed to describe a shear building model equivalent for a full-frame model can easily be evaluated. Figure 5-1 illustrates a typical shear building model, where each floor represents a lumped mass attached by springs that only undergoes shear deformation when a lateral load is applied.

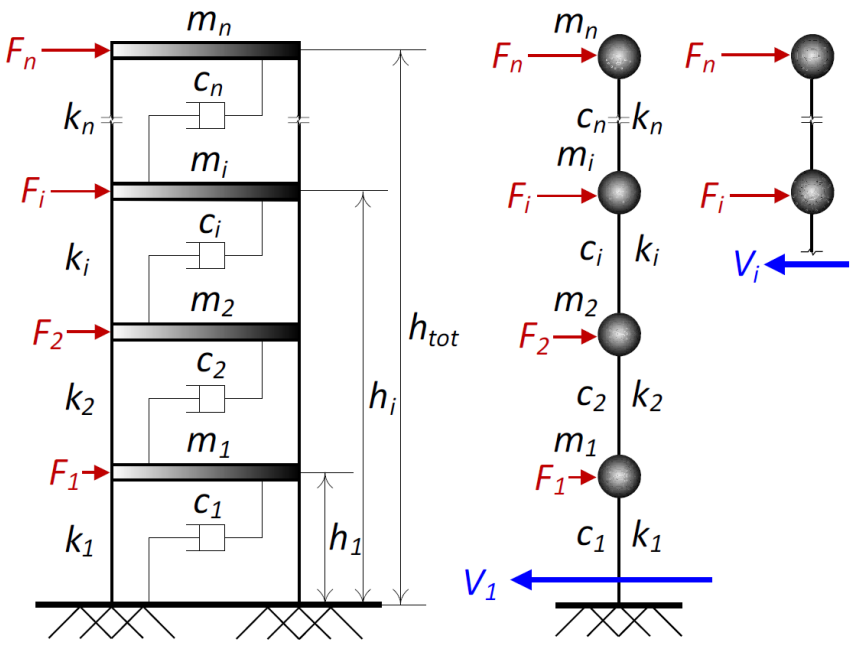


**Figure 5-1** Typical shear building model with fixed support (Lu, 2016).

In shear building models, the lateral stiffness of every floor is assumed to be proportional to the story's shear force, Vi. This can be obtained by subjecting force equilibrium with an applied equivalent lateral force. In most building codes, lateral seismic

force distributions follow a style similar to the first mode-deflected shape of an MDOF system. At story i, the design's lateral force Fi can be estimated by:

$$\boldsymbol{F_i = \frac{w_i h_i^k}{\sum_{j=1}^{n} w_j h_j^k} V} \quad \text{5-1}$$

where V is the total design base shear ( = V1); hi and wi are the height of the floor and effective weight at level i from the ground, respectively; n is the number of stories; and the term k is a function of the building's fundamental period Ts, essentially used to describe the influences of higher modes. Table 5-1 shows the k values regarding each force pattern. According to ASCE (A. Engineers, 2010), and (A. S. o. C. Engineers, 2013), the fundamental period of a building (i.e., the MDOF) in its fixed support condition can be calculated by applying the following equation:

$$\boldsymbol{T_s = C_t h_{tot}^x} \quad \text{5-2}$$

where htot is the total elevation of the building (i.e., the MDOF), while the coefficients Ct and x are associated with the type of the structural system, as displayed in Table 5-2.

**Table 5-1** Lateral load patterns determined by index k.

| Lateral load pattern | Exponent k |
|---|---|
| Concentric | N/A (A single load applied at roof) |
| Rectangular | 0 |
| Trapezoidal | $0.5 + 0.2T_s$ |
| Eurocode 8 | 1 |
| IBC-2012 | 1, if $T_s < 0.5$ sec |
| IBC-2012 | 2, if $T_s > 2.5$ sec |
| IBC-2012 | $1 + 0.5(T_s - 0.5)$, other $T_s$ |
| Parabolic | $1 + 0.8T_s$ |

**Table 5-2** Quantities of Ct and x for various structural systems (A. Engineers, 2010).

| Structural type | $C_t$ | x |
|---|---|---|
| Steel moment resisting frame | 0.0724 | 0.8 |
| Concrete moment resisting frame | 0.0466 | 0.9 |
| Steel brace frames | 0.0731 | 0.75 |
| All other structural systems | 0.0488 | 0.75 |

Figure 5-2 (a) illustrates an entire two-dimensional SSI system where a multi-story shear frame model is constructed on a rigid foundation that stands on a soil half-space and is exposed to the horizontal component of seismic excitation. It was assumed that horizontal motion was generated by a shear wave that propagated vertically. In this type of case, kinematic interaction would not occur.

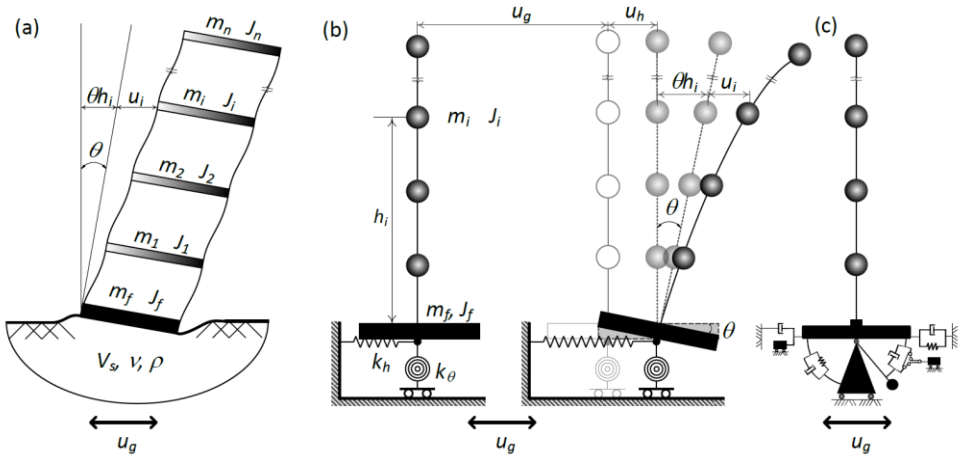


**Figure 5-2** Soil-structure interaction models: (a) multi-story shear frame resting on a soil half-space, (b) equivalent MDOF structure supported by soil impedance functions, and (c) soil half-space replaced by a cone-based discrete element model (Lu, 2016).

A foundation may be directly subjected to free-field ground motion (signified by ug). The whole SSI model can be analyzed through simplified models by converting the shear frame into an equivalent MDOF building model and replacing the soil half-space with equivalent springs and dampers (see Figure 5-2 (b) and (c)). The equation of motion of fixed support for a buildings system under seismic loading can be written as:

$$[\boldsymbol{M_s}]\{\ddot{\boldsymbol{x}}\} + [\boldsymbol{C_s}]\{\dot{\boldsymbol{x}}\} + [\boldsymbol{K_s}]\{\boldsymbol{x}\} = -[\boldsymbol{M_s}]\{\boldsymbol{E}\}\ddot{\boldsymbol{x}}_{\boldsymbol{g}} \quad 5\text{-}3$$

where [Ms], [Cs], and [Ks] are the mass, damping, and stiffness matrices of the building, respectively; $\{E\}$ is a vector with elements equal to one; and $\ddot{x}_g$ is the ground acceleration. For SSI systems, the foundation's degree of freedom must be added, and the equation of motion can be written as:

$$\begin{bmatrix} [\boldsymbol{M_s}] & \{\boldsymbol{m}\} & \{\boldsymbol{mh}\} \\ \{\boldsymbol{m}\}^T & \boldsymbol{S1} & \boldsymbol{S2} \\ \{\boldsymbol{mh}\}^T & \boldsymbol{S2} & \boldsymbol{S4} \end{bmatrix} \begin{Bmatrix} \{\ddot{\boldsymbol{x}}\} \\ \ddot{\boldsymbol{x}}_f \\ \ddot{\boldsymbol{\varphi}}_f \end{Bmatrix} + \begin{bmatrix} [\boldsymbol{C_s}] & \{\boldsymbol{0}\} & \{\boldsymbol{0}\} \\ \{\boldsymbol{0}\}^T & \boldsymbol{C_{xx}} & \boldsymbol{C_{x\varphi}} \\ \{\boldsymbol{0}\}^T & \boldsymbol{C_{\varphi x}} & \boldsymbol{C_{\varphi\varphi}} \end{bmatrix} \begin{Bmatrix} \{\dot{\boldsymbol{x}}\} \\ \dot{\boldsymbol{x}}_f \\ \dot{\boldsymbol{\varphi}}_f \end{Bmatrix} + \begin{bmatrix} [\boldsymbol{K_s}] & \{\boldsymbol{0}\} & \{\boldsymbol{0}\} \\ \{\boldsymbol{0}\}^T & \boldsymbol{k_{xx}} & \boldsymbol{k_{x\varphi}} \\ \{\boldsymbol{0}\}^T & \boldsymbol{k_{\varphi x}} & \boldsymbol{k_{\varphi\varphi}} \end{bmatrix} \begin{Bmatrix} \{\boldsymbol{x}\} \\ \boldsymbol{x}_f \\ \boldsymbol{\varphi}_f \end{Bmatrix}$$

$$= -\left\{\{\boldsymbol{m}\}, \boldsymbol{S1}, \boldsymbol{S2}\right\}^{\boldsymbol{T}} \ddot{\boldsymbol{x}}_{\boldsymbol{g}} \quad 5\text{-}4$$

or:

$$[\boldsymbol{M_{SSI}}]\{\ddot{\boldsymbol{x}}_{\boldsymbol{SSI}}\} + [\boldsymbol{C_{SSI}}]\{\dot{\boldsymbol{x}}_{\boldsymbol{SSI}}\} + [\boldsymbol{K_{SSI}}]\{\boldsymbol{x}_{\boldsymbol{SSI}}\} = -\{\boldsymbol{E_{SSI}}\}\ddot{\boldsymbol{x}}_{\boldsymbol{g}} \quad 5\text{-}5$$

where:

$S1 = m_f + \sum_{i=1}^{n} m_i \;\; , \;\; S2 = \sum_{i=1}^{n} m_i h_i \;\; , \quad S4 = I_{yf} + \sum_{i=1}^{n} I_{yi} m_i h_i^2$

$\{E_{SSI}\} = \left\{\{m\}, S1, S2\right\}^T$

$\{m\} = \{m_1, m_2, \dots, m_n\}^T$

$\{mh\} = \{m_1 h_1, m_2 h_2, \dots, m_n h_n\}^T$

and $m_f$ and $I_f$ are mass and the mass moment of inertial of foundation, respectively.

$$x_{SSI} = \begin{Bmatrix} \{x\} \\ x_f \\ \varphi \end{Bmatrix}$$

$x_f$ and $\varphi$ are the horizontal translation and rotation of the foundation;

$k_{xx}, k_{x\varphi}, k_{\varphi x}$, and $k_{\varphi\varphi}$ are the stiffness coefficients of the foundation; and

$C_{xx}, C_{x\varphi}, C_{\varphi x}$, and $C_{\varphi\varphi}$ are the damping coefficients of the foundation.

For three-dimensional systems, the degree of freedoms in the Y direction and torsion must be added, and the equation of motion can be written as:

$$\begin{bmatrix} [\boldsymbol{m}] & [\boldsymbol{0}] & [\boldsymbol{0}] \\ [\boldsymbol{0}] & [\boldsymbol{m}] & [\boldsymbol{0}] \\ [\boldsymbol{0}] & [\boldsymbol{0}] & [\boldsymbol{J}] \end{bmatrix} \begin{Bmatrix} \{\ddot{\boldsymbol{x}}\} \\ \{\ddot{\boldsymbol{y}}\} \\ \{\ddot{\boldsymbol{\theta}}\} \end{Bmatrix} + \begin{bmatrix} [\boldsymbol{C_{xx}}] & [\boldsymbol{C_{xy}}] & [\boldsymbol{C_{x\theta}}] \\ [\boldsymbol{C_{yx}}] & [\boldsymbol{C_{yy}}] & [\boldsymbol{C_{y\theta}}] \\ [\boldsymbol{C_{\theta x}}] & [\boldsymbol{C_{\theta y}}] & [\boldsymbol{C_{\theta\theta}}] \end{bmatrix} \begin{Bmatrix} \{\dot{\boldsymbol{x}}\} \\ \{\dot{\boldsymbol{y}}\} \\ \{\dot{\boldsymbol{\theta}}\} \end{Bmatrix} +$$

$$\begin{bmatrix} [\boldsymbol{K_{xx}}] & [\boldsymbol{K_{xy}}] & [\boldsymbol{K_{x\theta}}] \\ [\boldsymbol{K_{yx}}] & [\boldsymbol{K_{yy}}] & [\boldsymbol{K_{y\theta}}] \\ [\boldsymbol{K_{\theta x}}] & [\boldsymbol{K_{\theta y}}] & [\boldsymbol{K_{\theta\theta}}] \end{bmatrix} \begin{Bmatrix} \{\boldsymbol{x}\} \\ \{\boldsymbol{y}\} \\ \{\boldsymbol{\theta}\} \end{Bmatrix} = \begin{Bmatrix} \{\boldsymbol{f_x}\} \\ \{\boldsymbol{f_y}\} \\ \{\boldsymbol{f_\theta}\} \end{Bmatrix} \quad \text{5-6}$$

or

$$[\boldsymbol{M_s}]\{\ddot{\boldsymbol{q}}\} + [\boldsymbol{C_s}]\{\dot{\boldsymbol{q}}\} + [\boldsymbol{K_s}]\{\boldsymbol{q}\} = \{\boldsymbol{f}\} \quad \text{5-7}$$

where

$$[M_s] = \begin{bmatrix} [m] & [0] & [0] \\ [0] & [m] & [0] \\ [0] & [0] & [J] \end{bmatrix}, [C_s] = \begin{bmatrix} [C_{xx}] & [C_{xy}] & [C_{x\theta}] \\ [C_{yx}] & [C_{yy}] & [C_{y\theta}] \\ [C_{\theta x}] & [C_{\theta y}] & [C_{\theta\theta}] \end{bmatrix}, \text{ and}$$

$$[K_s] = \begin{bmatrix} [K_{xx}] & [K_{xy}] & [K_{x\theta}] \\ [K_{yx}] & [K_{yy}] & [K_{y\theta}] \\ [K_{\theta x}] & [K_{\theta y}] & [K_{\theta\theta}] \end{bmatrix}$$

$$\{q\}^T = \{x_1 \quad x_2 \quad \cdots \quad x_n \quad y_1 \quad y_2 \quad \cdots \quad y_n \quad \theta_1 \quad \theta_2 \quad \cdots \quad \theta_n\}^T$$

$$\{f\}^T = \{f_{x1} \quad f_{x2} \quad \cdots \quad f_{xn} \quad f_{y1} \quad f_{y2} \quad \cdots \quad f_{yn} \quad f_{\theta 1} \quad f_{\theta 2} \quad \cdots \quad f_{\theta n}\}^T$$

$$\{f\}^T = -[M_s]\{E\}\ddot{q}_g$$

where:

$x_1, x_2, \ldots x_n$ are horizontal translation displacements in the X direction;

$y_1, y_2, \ldots y_n$ are horizontal translation displacements in the Y direction;

$\theta_1, \theta_2, \ldots \theta_n$ are torsional translation displacements;

$\{f\}$ is the load vector;

$[m]$ is the mass of the inertial slab matrix (diagonal matrix) in the X and Y directions; and

$[J]$ is the mass torsion of the inertial slab matrix (diagonal matrix).

$\{E\}$ is the earthquake influence coefficients vector for fixed base structure.

For three-dimensional SSI systems, the degree of foundation must be added, and the equation of motion can be written as:

$$[\boldsymbol{M_{SSI}}]\{\ddot{\boldsymbol{q}}_{\boldsymbol{SSI}}\} + [\boldsymbol{C_{SSI}}]\{\dot{\boldsymbol{q}}_{\boldsymbol{SSI}}\} + [\boldsymbol{K_{SSI}}]\{\boldsymbol{q_{SSI}}\} = -\{\boldsymbol{E_{SSI}}\}\ddot{\boldsymbol{q}}_{\boldsymbol{g}} \qquad 5\text{-}8$$

where:

$$[M_{SSI}] = \begin{bmatrix} [M_s] & [MH] \\ [MH]^T & [M_f] \end{bmatrix}$$

$$[MH] = \begin{bmatrix} \{m\} & \{0\} & \{0\} & \{mh\} & \{0\} \\ \{0\} & \{m\} & \{0\} & \{0\} & \{mh\} \\ \{0\} & \{0\} & \{J\} & \{0\} & \{0\} \end{bmatrix}$$

$$\{m\} = \{m_1, m_2, \ldots, m_n\}^T$$

$$\{mh\} = \{m_1h_1, m_2h_2, \ldots, m_nh_n\}^T$$

$$\{J\} = \{J_1, J_2, \ldots, J_n\}^T$$

$$[M_f] = \begin{bmatrix} S1 & 0 & 0 & S2 & 0 \\ 0 & S1 & 0 & 0 & S2 \\ 0 & 0 & S3 & 0 & 0 \\ S2 & 0 & 0 & S4 & 0 \\ 0 & S2 & 0 & 0 & S5 \end{bmatrix}$$

$S1 = m_f + \sum_{i=1}^{n} m_i$ , $S2 = \sum_{i=1}^{n} m_i h_i$ , $S3 = J_f + \sum_{i=1}^{n} J_i$ ,

$S4 = I_{yf} + \sum_{i=1}^{n} I_{yi} m_i h_i^2$ , $S5 = I_{xf} + \sum_{i=1}^{n} I_{xi} m_i h_i^2$

$m_f$ is the foundation mass

$m_i$ is the mass slab of i floor

$h_i$ is the height of i floor (from ground to center of floor see Figure 5-2)

$I_{yf}$, $I_{xf}$ , and $J_f$ foundation mass moment of inertia in x, y, and z directions respectively

$I_{yi}$, $I_{xi}$ , and $J_i$ slab mass moment of inertia of i floor in x, y, and z directions respectively

$$[K_{SSI}] = \begin{bmatrix} [K_s] & [0] \\ [0] & [K_{soil}] \end{bmatrix}, \quad [K_{soil}] = diagonal[k_{xx} \quad k_{yy} \quad k_t \quad k_{\varphi\varphi} \quad k_{\vartheta\vartheta}]$$

$[C_{SSI}] = \alpha[M_{SSI}] + \beta[K_{SSI}]$ Rayleigh damping

$\{E_{SSI}\} = \{\{m\}, \{m\}, \{J\}, S1, S1, S3, S2, S2\}^T$

$\{q_{SSI}\}^T$

$= \{x_1 \quad x_2 \quad \cdots \quad x_n, \quad y_1 \quad y_2 \quad \cdots \quad y_n, \quad \theta_1 \quad \theta_2 \quad \cdots \quad \theta_n, x_f \quad y_f \quad \theta_f \quad \varphi_{xf} \quad \varphi_{yf}\}^T$

$x_f$ is the horizontal foundation translation displacements in the X direction;

$y_f$ is the horizontal foundation translation displacements in the Y direction;

$\theta_f$ is the torsional foundation translation displacements;

$\varphi_{xf}$ is the rocking foundation in the X direction; and

$\varphi_{yf}$ is the rocking foundation in the Y direction.

kxx and kyy are the equivalent soil stiffnesses in the X and Y directions, respectively.

kt is the equivalent torsion soil stiffness in the Z direction.

$k_{\varphi\varphi}$ and $k_{\vartheta\vartheta}$ are the equivalent moment soil stiffnesses in the X and Y direction, respectively.

## 5.3 Equations of Motion in State-Space Form

The equations of motion for fixed support structures and soil structure interaction systems can be formulated in state-space form (Cheng et al., 2008). The state-space form for a fixed support structure is:

$$\{\boldsymbol{z}\} = \begin{Bmatrix}\{\boldsymbol{q}\}\\ \{\dot{\boldsymbol{q}}\}\end{Bmatrix} \tag{5-9}$$

$$\{\dot{\boldsymbol{z}}\} = [\boldsymbol{A}]\{\boldsymbol{z}\} + [\boldsymbol{B}]\ddot{\boldsymbol{q}}_{\boldsymbol{g}} + [\boldsymbol{B}_{\boldsymbol{c}}]\{\boldsymbol{f}_{\boldsymbol{c}}\} \tag{5-10}$$

where:

$$[A] = \begin{bmatrix}[0] & [I]\\ -[M]^{-1}[K] & -[M]^{-1}[C]\end{bmatrix}$$

$$[B] = \begin{bmatrix}[0]\\ -[E]\end{bmatrix}$$

$$[B_c] = \begin{bmatrix}[0]\\ [M]^{-1}[\delta]\end{bmatrix}$$

$[\delta]$ the matrix controlling device placement and inclination; and

$\{f_c\}$ is the control force.

The output equation is:

$$\{\boldsymbol{Y}\} = [\boldsymbol{C}]\{\boldsymbol{z}\} + [\boldsymbol{D}]\{\boldsymbol{f}_{\boldsymbol{c}}\} \tag{5-11}$$

Where

$[C] = [I],\ [D] = [0]$

The state-space form for soil structure interaction is:

$$\{\boldsymbol{Z_{SSI}}\} = \begin{Bmatrix} \boldsymbol{q_{SSI}} \\ \boldsymbol{\dot{q}_{SSI}} \end{Bmatrix} \quad 5\text{-}12$$

$$\{\boldsymbol{\dot{Z}_{SSI}}\} = [\boldsymbol{A_{SSI}}]\{\boldsymbol{Z_{SSI}}\} + [\boldsymbol{B_{SSI}}]\boldsymbol{\ddot{q}_g} + [\boldsymbol{B_{cSSI}}]\{\boldsymbol{f_{cSSI}}\} \quad 5\text{-}13$$

where:

$$[A_{SSI}] = \begin{bmatrix} [0] & [I] \\ -[M_{SSI}]^{-1}[K_{SSI}] & -[M_{SSI}]^{-1}[C_{SSI}] \end{bmatrix}$$

$$[B_{SSI}] = \begin{bmatrix} [0] \\ -[E_{SSI}] \end{bmatrix}$$

$$[B_{cSSI}] = \begin{bmatrix} [0] \\ [M_{SSI}]^{-1}[\delta_{SSI}] \end{bmatrix}$$

$[\delta_{SSI}]$ is the matrix responsible for control device placement and inclination; and

$\{f_{cSSI}\}$ is the control force of the soil structure interaction system.

The output equation for a soil structure interaction system is:

$$\{\boldsymbol{Y_{SSI}}\} = [\boldsymbol{C_{SSI}}]\{\boldsymbol{z}\} + [\boldsymbol{D_{SSI}}]\{\boldsymbol{f_{cSSI}}\} \quad 5\text{-}14$$

where

$$[C_{SSI}] = [I],\ [D_{SSI}] = [0]$$

A MATLAB/SIMULINK version 2016a software package obtained from Texas A&M University was used to simulate the numerical solution for dynamic systems. Most of the differential equations were solved utilizing the ODE45 function, which uses an explicit Runge-Kutta method with variable steps (Dormand & Prince, 1980). The technique is powerful for solving the largest non-stiff differential equations. Whenever a differential equation presents stiff behavior, the ODE15s function should be applied. ODE15s is an implicit solver technique with a variable step that computes the solution at the next time step.

## 5.4 Significant Parameters

Prior studies have confirmed that dynamic SSI effects can be effectively characterized in terms of appropriate dimensionless parameters. These parameters characterize the structure, soil characteristics, and seismic loads (e.g.,(Veletsos & Nair, 1975), (John P Wolf, 1994).

### 5.4.1 Structure to Soil Stiffness Ratio

The structure to soil stiffness ratio, σ = h/(VsT), can be employed as a relative index for identifying when SSI impacts will become important. In this definition, h is the building height (for practical purposes, h = 0.7htot (see Figure 5-1)), Vs is the shear wave velocity of the soil, and T is the fixed-base structure period. Figure 5-3 illustrates the relationship between $\bar{T}/T$ and σ.

$$\boldsymbol{\sigma = \frac{h}{V_s T}} \qquad 5\text{-}15$$

When σ is greater than 0.1, the SSI can significantly increase the period of the structure and damping of the fixed-base structure system. However, when σ is less than 0.1, the SSI will not modify the period of the structure and damping of the system. The SSI effects will modify the design base shear increase or decrease reliance on the seismic load (i.e., the slope of the spectral curve). This will lead to a change in the distribution of forces and deformation in the structure corresponding to a fixed-base system. Consequently, the use of SSI analysis will be most important for stiff structural systems like braced and shear wall frame systems. It is essential to remember that the structure to soil stiffness ratio is an estimated relative index and not an ideal standard. Also, when σ is less than 0.1, the

corresponding distribution of shear forces and moments in a structure can change in relation to the fixed-base condition, particularly in underground structures, dual systems, and structures with significant higher-mode responses.

### 5.4.2 Slenderness Ratio

The slenderness ratio, λ, structure height to foundation width ratio, and slenderness ratio, λ = H/B, are important parameters.

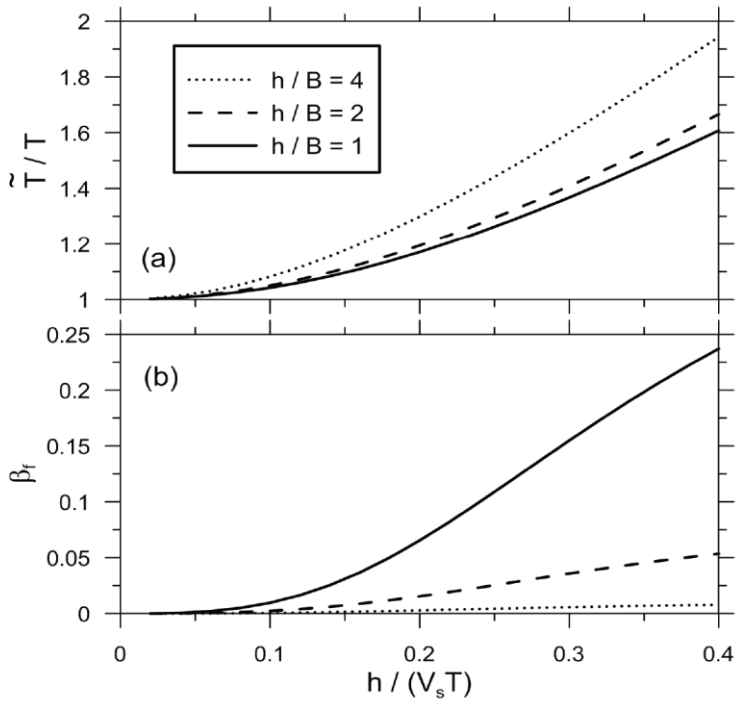


**Figure 5-3** Plot of the period lengthening ratio and foundation damping (βf ) versus structure to soil stiffness ratio for square foundations (J. Stewart et al., 2012).

When σ is greater than 0.1, the natural period and damping characteristics of the system are sensitive to λ, as shown in Figure 5-3.

### 5.4.3 Foundation Width to Length Ratio

The foundation width to length ratio, B/L, is defined as the foundation aspect ratio. For a constant value H/B ratio, period lengthening is recognized as reducing purely with B/L because of the extended area of the foundation, which leads to an increase in the foundation's stiffness.

When all parameters are fixed, the period lengthening amplifies with increases in the slenderness ratio, H/B, because of the increased foundation rotation, θ, and overturning moment. This means that inertial SSI impacts are more significant in tall or slender buildings that have high structure to soil stiffness ratios (σ > 0.1). For fixed slenderness ratios, period lengthening is noted to decrease reasonably with the foundation aspect ratio because of increases in the soil stiffness normal to the direction of loading.

### 5.4.4 Structure to Soil Mass Ratio

The structure to soil mass ratio $\bar{m}$ is:

$$\bar{m} = \frac{\sum_{i=1}^{n} m_i}{\rho h_{tot} B L} \qquad 5\text{-}16$$

where ρ is the mass density of the soil and Af is the area of the foundation.

### 5.4.5 Structure to Foundation Mass Ratio

$$\bar{m}_f = \frac{m_f}{\sum_{i=1}^{n} m_i} \quad 5\text{-}17$$

### 5.4.6 Poisson's Ratio

Poisson's ratio of the Soil.

### 5.4.7 Damping Ratio

The damaging of structure, ξs, and the damaging of soil, ξg.

### 5.4.8 Maximum Inter-story Ductility Ratio

The maximum inter-story ductility ratio is defined for any story i in Figure 5-2 as:

$$\mu_i = \frac{\Delta u_{i,max}}{\Delta u_{i,y}} \quad 5\text{-}18$$

where

Δui,max is the maximum inter-story distortion (i.e., (ui – ui-1)max); and

Δui,y is the inter-story distortion at the onset of yielding in the ith story.

### 5.4.9 Slope of Response Spectrum Curve

Figure 5-4 summarizes the influence of the response spectrum curve slope, μ. When σ is greater than 0.1 and μ is greater than zero, the SSI increases in response. Conversely, when σ is greater than 0.1 and μ is less than zero, the SSI decreases in response. In general, most earthquakes have an ascending branch of the spectrum (i.e., a positive slope) in the

short time period when T is less than 1; therefore, the SSI will have a significant effect on increasing the responses of structures with those periods (Moghaddasi, Cubrinovski, Pampanin, Carr, & Chase, 2010).

The SSI impacts the base shear depending on the slope of the spectrum carve. Thus, if the slope of the spectrum is positive, the base shear will increase. If the slope of the spectrum is negative, the base shear will decrease. For buildings with relatively short periods on the increasing portion of the spectrum, use of $\bar{S}_a$ (i.e., a flexible base) instead of $S_a$ (i.e., a fixed base) typically results in increased base shear.

Figure 5-4 explains the impact of inertial SSI on the base shear of a structure. The curve describes the change in pseudo-spectral acceleration versus period on both linear and log scales because the base shear for an elastic response is usually calculated depending on the pseudo-spectral acceleration of the first mode. For an SSI, the pseudo-spectral acceleration, $\bar{S}_a$, is estimated by accessing the spectrum curve for an elongated period, $\bar{T}$, at the corresponding effective damping ratio, $\beta_0$. For short period structures on the increasing portion of the spectrum, the utility of $\bar{S}_a$ (i.e., a flexible base) instead of $S_a$ (i.e., a fixed base) typically results in increased base shear. Conversely, inertial SSI can reduce the base shear in long period structures (J. Stewart et al., 2012).

The possible scope of the σ values can be calculated by Equations (5.2) and (5.15) for different soil sites; such sites are categorized into several groups according to the average shear wave velocity of the top 30 meters of the sites' Vs values (see Table 5-3).

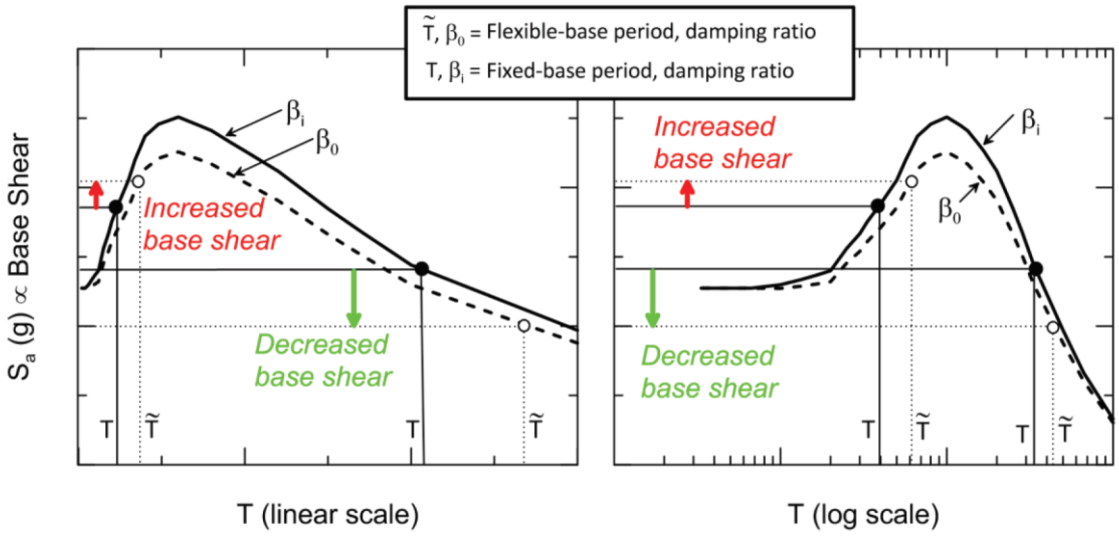


**Figure 5-4** Inertial SSI effects on spectral acceleration (base shear) associated with period lengthening and changes in damping (J. Stewart et al., 2012).

**Table 5-3** Site soil classifications according to (A. S. o. C. Engineers, 2013).

| Site class | Soil profile name | $V_{s,30}$ (m/s) | ν |
|---|---|---|---|
| A | Hard rock | >1500 | N/A |
| B | Rock | 760-1500 | N/A |
| C | Very dense soil | 360-760 | 0.33 |
| D | Stiff soil | 180-360 | 0.4 |
| E | Soft soil | <180 | 0.5 |

Figure 5-5 explains the possible variety of σ values for different types of multi-story buildings found on various site classes, according to IBC (2012). To include a wide variety of SSI conditions, the X-axis in Figure 5-5 begins at 90 m/s, describing the average value of Site Class E, and ends at 1,500 m/s, which describes a fixed support condition for common structures found on Site Class A. It can be observed in Figure 5-5 that for a presented shear wave velocity, a larger structure to soil stiffness ratio, σ, value is always required for tall

buildings. While the maximum amount of σ for frame structures is about 2, it has been confirmed that σ can increase up to 3 for other structural systems. ATC (2005) recommends that for traditional buildings, $\bar{m}$ should range between 0.3 and 0.6 (FEMA, 2005).

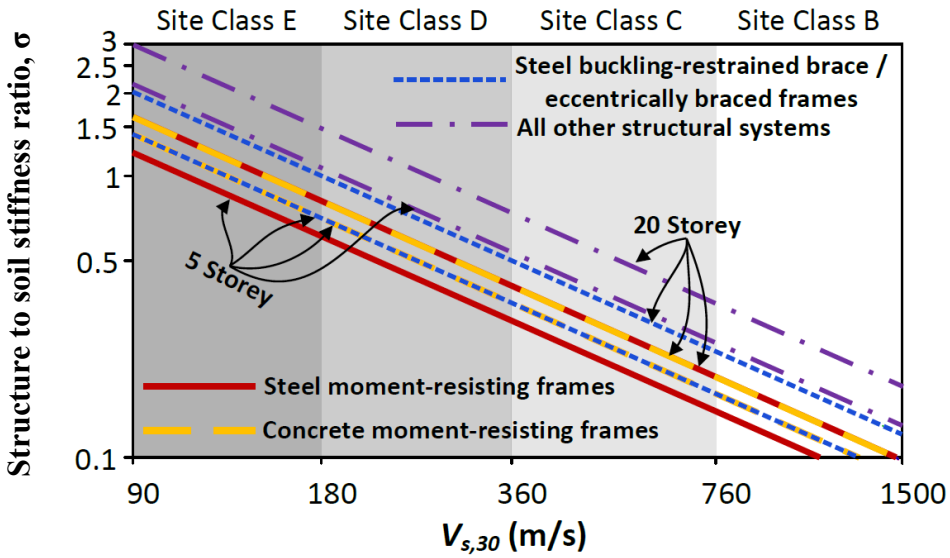


**Figure 5-5** Practical range of structure to soil stiffness ratio , σ, for various types of structures located on different soil sites, according to IBC (2012).

## 5.5 Equivalent Stiffness Matrix for Frame and Frame Shear Wall Systems

Consider the frame shear wall structural system shown in Figure 5-6. The structure coordinate system can be defined by load and displacement vectors. In matrix form, the load vector P and displacement vector Δ can be written as:

$$\{\boldsymbol{P}\} = \begin{Bmatrix} \boldsymbol{P_1} \\ \boldsymbol{P_2} \\ \boldsymbol{P_3} \end{Bmatrix} \qquad 5\text{-}19$$

$$\{\Delta\} = \begin{Bmatrix} \Delta_1 \\ \Delta_2 \\ \Delta_3 \end{Bmatrix} \quad 5\text{-}20$$

The flexibility coefficient estimates the displacement at some point on the structure that results from being subjected to a united load at that or some other point. Specifically, the flexibility coefficient $f_{ij}$ gives the amount of the ith displacement that results from a united value of the ith load. The total array of flexibility coefficients can be set in the form of a flexibility matrix (West, 1989).

$$\begin{Bmatrix} \Delta_1 \\ \Delta_2 \\ \Delta_3 \end{Bmatrix} = \begin{bmatrix} f_{11} & f_{12} & f_{13} \\ f_{21} & f_{22} & f_{23} \\ f_{31} & f_{32} & f_{33} \end{bmatrix} \begin{Bmatrix} P_1 \\ P_2 \\ P_3 \end{Bmatrix} \quad 5\text{-}21$$

or

$$\{\Delta\} = [f]\{P\} \quad 5\text{-}22$$

The inversion of the flexibility matrix F gives a stiffness matrix K for the frame shear wall structural system (i.e., lateral forces and corresponding lateral displacements).

$$\{P\} = [K]\{\Delta\} \quad 5\text{-}23$$

The equivalent stiffness matrix for frame and frame shear wall systems is calculated depending on the unit load method, using the finite element software ETABS (Computers and Structures, 2019) and considering the three-dimensional structure, material properties, and geometry of the structural system (see Figure 5-7) (Seetharamulu, 2014).

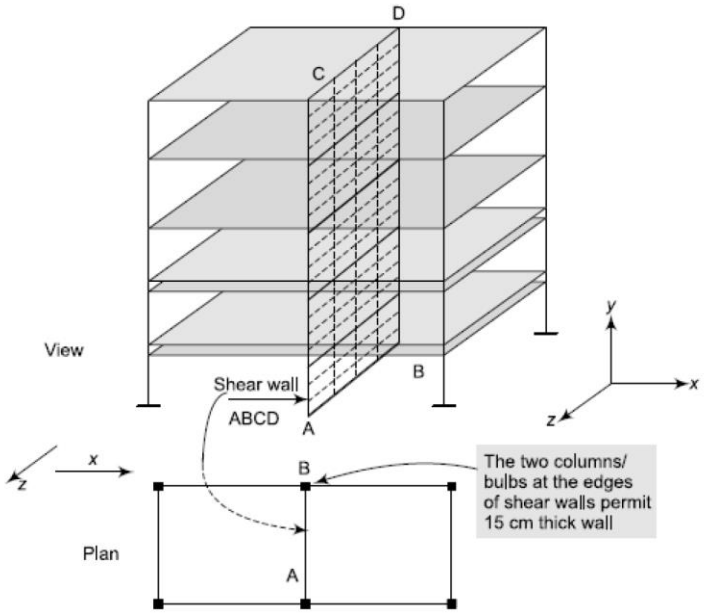


**Figure 5-6** Typical frame shear wall structure system (Seetharamulu, 2014).

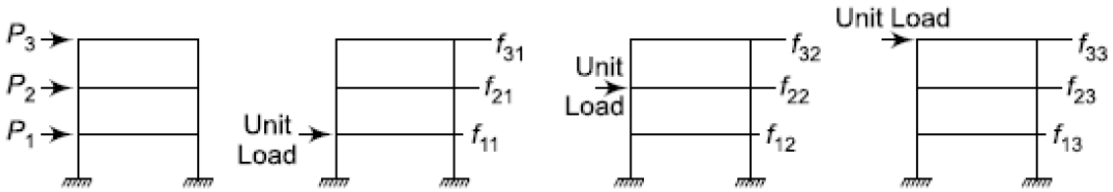


**Figure 5-7** Unit load method for determining the flexibility matrix (Seetharamulu, 2014).

## 5.6 Equivalent Stiffness Matrix for Rigid Foundations

The finite element analysis method was developed to evaluate the equivalent stiffness matrix of soil media for rigid foundations. As an initial approach, in this research the results from the numerical analyses were validated by comparing them to the analytic solution for elastic half-space. To estimate the affected bedrock depth, several sets of

numerical analyses with different depths were performed using the ABAQUS software. The second set of analyses examined the impact of soil layers on variations in equivalent soil stiffness. The last set of analyses investigated the influence of changing the models of elasticity with linear and parabolic depths for clay and sand, respectively.

For all analyses, the foundation was assumed to be a perfectly rigid body (see Figure 5-8). It was also assumed that there were no deformations in the body and the soils were a linear elastic and single-phase material. ABAQUS has special rigid elements that help the user to employ a group of elements or nodes as a reference node. The reference node is inserted at the center of the foundation and displacements or rotations applied. The equivalent stiffness matrix is then calculated from the basic principle of the stiffness method when applied to unite a displacement or rotation in one direction (and not in the other) for all displacements and rotations (West, 1989).

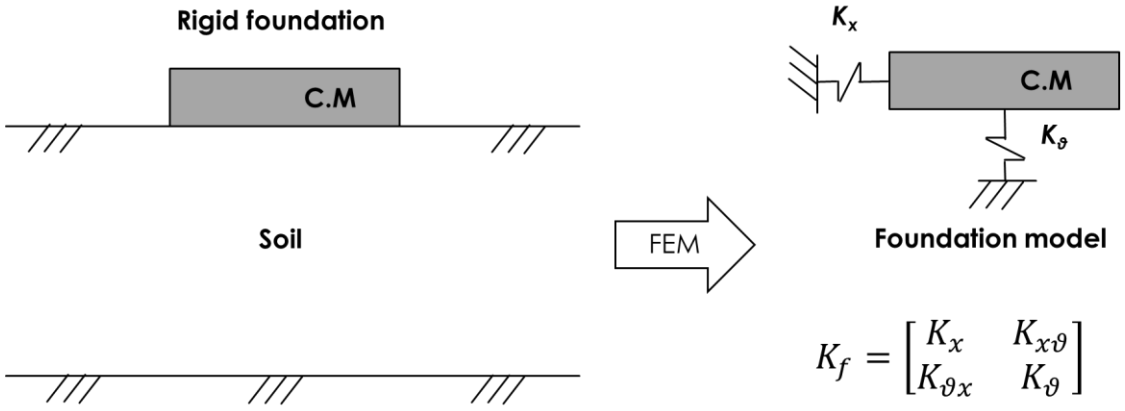


**Figure 5-8** Equivalent stiffness matrix of soil media for a rigid foundation.

# 6. PARAMETRIC STUDIES ON PORTAL FRAME STRUCTURE

## 6.1 Introduction

This section focuses on the modeling and analysis of a dynamic soil structure interaction system for a single degree of freedom system. An MR damper and SAC algorithm were utilized to study efficiency and performance. Two types of reference models, a fixed-base support structure and SSI, were used to demonstrate the difference in maintaining structures during various earthquake loads. Four soil profiles were employed in this parametric study.

## 6.2 Methodology of Portal Frame System

A mathematical simulation using an SSI system subjected to a suite of four earthquake motions with different features was considered in order to clarify the effects of SSI on structural response.

For geotechnical parametric study, the structure model is a SDOF lumped mass system (see Equation 5.3, and Figure 6-1 a) characterized by a fundamental period T = 0.2 sec, with equivalent viscous damping (C) characterized by a damping ratio $\zeta$ = C/Ccrit = 5%. The mass of the structure is based on a 17.7-m square concrete slab by 0.2-m thick slab (M = 153.3 ton). The structure stiffness k calculated from T, and M. The Equation 5.3 can rewrite for SDOF system

$$\boldsymbol{M\ddot{x} + c\dot{x} + kx = -M\ddot{x}_g} \quad \text{6-1}$$

SSI is introduced (Figure 6-1 b) into the model by adding one horizontal spring-dashpot characterized by a spring constant $K_x$ and viscous damping $C_f$, and one rocking spring-dashpot characterized by spring constant $K_\theta$ and viscous damping $C_\theta$ (three degree of freedom). System response is now governed by Equation 5.5, which now becomes:

$$\begin{bmatrix} \boldsymbol{M} & \boldsymbol{M} & \boldsymbol{M \cdot H} \\ \boldsymbol{M} & \boldsymbol{(M + M_f)} & \boldsymbol{M \cdot H} \\ \boldsymbol{M \cdot H} & \boldsymbol{M \cdot H} & \boldsymbol{(I_f + I_s \cdot H^2)} \end{bmatrix} \begin{Bmatrix} \ddot{\boldsymbol{x}} \\ \ddot{\boldsymbol{x}}_{\boldsymbol{f}} \\ \ddot{\boldsymbol{\theta}}_{\boldsymbol{f}} \end{Bmatrix} + \begin{bmatrix} \boldsymbol{C} & \boldsymbol{0} & \boldsymbol{0} \\ \boldsymbol{0} & \boldsymbol{C_f} & \boldsymbol{0} \\ \boldsymbol{0} & \boldsymbol{0} & \boldsymbol{C_\theta} \end{bmatrix} \begin{Bmatrix} \dot{\boldsymbol{x}} \\ \dot{\boldsymbol{x}}_{\boldsymbol{f}} \\ \dot{\boldsymbol{\theta}}_{\boldsymbol{f}} \end{Bmatrix} + \begin{bmatrix} \boldsymbol{k} & \boldsymbol{0} & \boldsymbol{0} \\ \boldsymbol{0} & \boldsymbol{k_x} & \boldsymbol{0} \\ \boldsymbol{0} & \boldsymbol{0} & \boldsymbol{k_\theta} \end{bmatrix} \begin{Bmatrix} \boldsymbol{x} \\ \boldsymbol{x}_{\boldsymbol{f}} \\ \boldsymbol{\theta}_{\boldsymbol{f}} \end{Bmatrix}$$

$$= -\{\boldsymbol{M}, \boldsymbol{(M + M_f)}, \boldsymbol{M \cdot H}\}^{\boldsymbol{T}} \ddot{\boldsymbol{x}}_{\boldsymbol{g}}$$

6-2

The foundation stiffness parameters $K_x$ and $K_\theta$ were determined from finite element studies for various soil profiles as will be discussed subsequently. In this parametric study, the damping matrix was derived in terms of a Rayleigh damping formulation. The finite element model (see Chapter 5) was utilized in the analyses to evaluate the equivalent soil stiffness. The mass moment of inertia for slab and foundation, $I_s$ and $I_f$, respectively.

The ABAQUS finite element software package was employed to determine the equivalent stiffness matrices of the various soil profiles (see Chapter 5).The foundation stiffness elements (see section 6.11 and Equation 6.23) are dependent on foundation width (B = 17.7) (see Figure 6-1 b). The mass matrix in this equation is influenced by building height H. The parametric study to be presented is conducted for two values of slenderness ratio, H/B = 0.5 and 1.0. For Structural parametric study see Section 6.12.

Finally, the SSI model was imported to a control scheme under a group of four earthquake ground motions and different soil profiles (see Sections 6.5 and 6.11) in order to

investigate the variability of the responses of the control and uncontrolled systems (see Sections 6.6, 6.7, 6.8, 6.9, and 6.10).

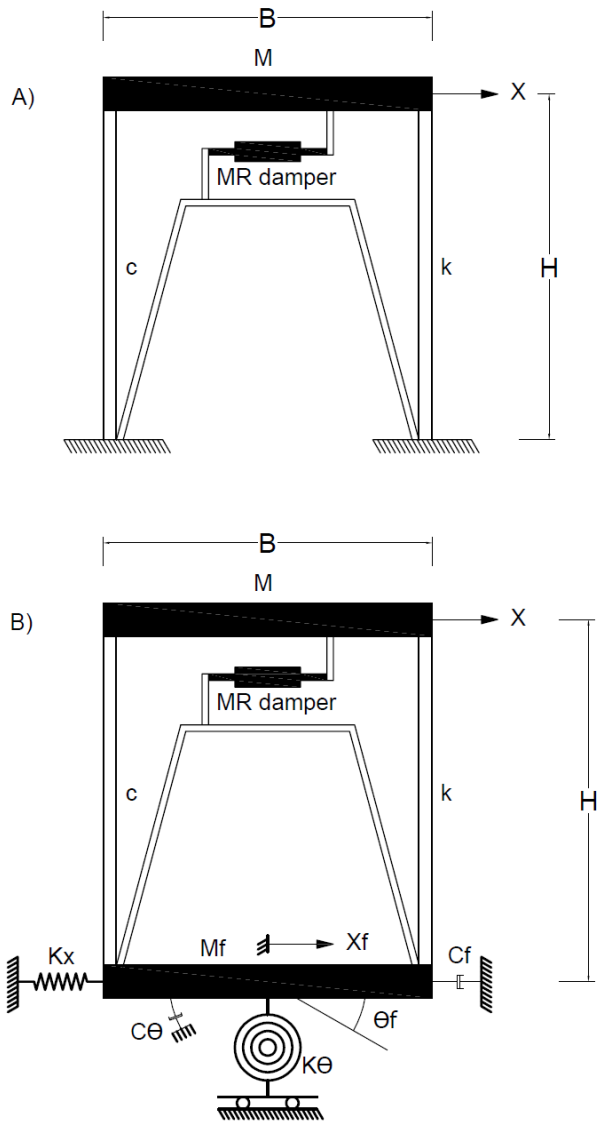


**Figure 6-1** Mathematical model and schematics of the device in the building: a) fixed-base structure and b) SSI.

The SAC algorithm and MR damper employed in this chapter. Table 4-1 show the parameter of the MR damper with 1000 kN capacity. A closed-form solution programmed in MATLAB and SIMULINK was used.

## 6.3 The Case Studies

The following summary of the case studies adopted in this chapter are:

- The earthquake suite (four earthquake see section 6.5)
- The control cases for SAC algorithm (two cases of reference model, Fixed – SSI and SSI – SSI, see sections 6.6 and 6.7)
- The geotechnical case studies (four soil profiles see section 6.11)
- The geometry of the structure by using two value of the structures slenderness ratio ($\lambda$, = H/B = 0.5, 1 see section 6.12)

## 6.4 The Parametric Studies

### 6.4.1 The Geotechnical Parameters

- Depth ratio, Z/B (0, 0.1, 0.25, 0.5, 1, and 1.25) for soil layers profiles.
- The surface shear modulus, Ga (15, 25, 35, 50, 70, and 100 MPa) for sand and clay soil profiles.

### 6.4.2 The Structural Parameters

- Structural period (Ts = 0.1, 0.2, 0.4, 0.6, 0.8, 1 sec.).

## 6.5 Earthquake Suite

To estimate the effectiveness of the simple adaptive control, four different earthquakes were implemented to a single degree of freedom system, including SSI effects (see Figure 6-1). The earthquakes selected have various intrinsic characteristics. Figure 6-5 displays the accelerated time histories of these earthquakes. A suite of four earthquake motions recorded on different types of soil profiles were employed in the time-history simulations. The records were constrained as follows: (i) the magnitudes ranged from 4.73 to 5.9, (ii) the closest source-to-site distance was from 11.1 to 6 km, and (iii) the peak ground acceleration (PGA) was between 8.0132E-02 and 1.1259E-01 (g). A review of the basic properties of the earthquakes can be found in Table 6-1.

**Table 6-1** Earthquake characteristics.

| Name | RNS | Year | Station | Magnitude | PGA (g) | Hypocenter Depth (km) |
|---|---|---|---|---|---|---|
| Taiwan SMART1(5) | 311 | 1981 | SMART1 O01 | 5.9 | 1.1259E-01 | 11.1 |
| Mammoth Lakes-07 | 252 | 1980 | Green Church | 4.73 | 1.6415E-01 | 6 |
| Livermore-02 | 218 | 1980 | Antioch - 510 G St | 5.42 | 8.0132E-02 | 14.5 |
| Borrego | 9 | 1942 | El Centro Array #9 | 6.5 | 5.2247E-02 | 8 |

## 6.6 Design of the SAC algorithm

The SAC methodology is to make a system that tracks the response of the reference model (see Chapter 4). In this section, two types of reference models were adopted to investigate the effects of SSI on the behavior of the SAC algorithm. For the fixed support structure, the reference model and system with the fixed base assumption is adopted (Fixed-

Fixed). The optimal control theory especially the linear quadratic regulator (LQR) is utilized to estimate the desired output (see Figure 6-2). For the SSI system, the two reference models cases have adopted fixed base structure (Fixed-SSI see Figure 6-3) and SSI (SSI-SSI see Figure 6-4). Also, the optimal control theory (LQR) algorithm is used to estimate the desired output of the reference models.

## 6.7 Control Scheme Design and Implementation

The control scheme formed for the SSI system was constituted of sensors measuring transverse displacements at the center of the floor, center of the foundation, and rocking at the center of the foundation.

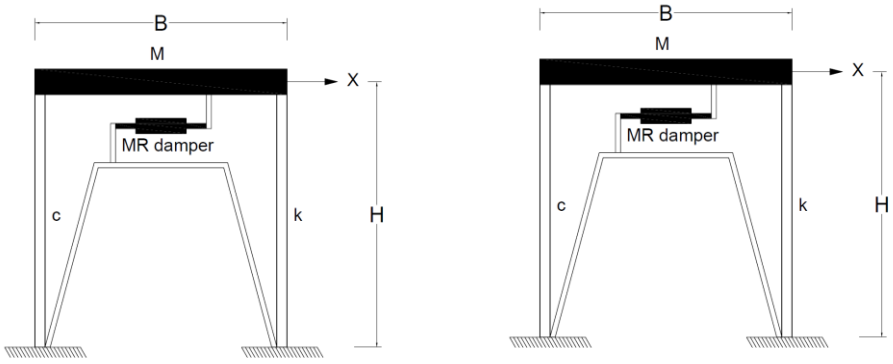


A) The reference model with the fixed support structure assumption

B) The boundary conditions of the superstructure

**Figure 6-2** Design of the SAC algorithm for fixed base structure with Fixed- SSI assumption.

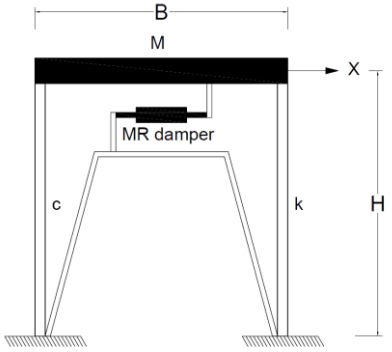


A) The reference model with the fixed support structure assumption

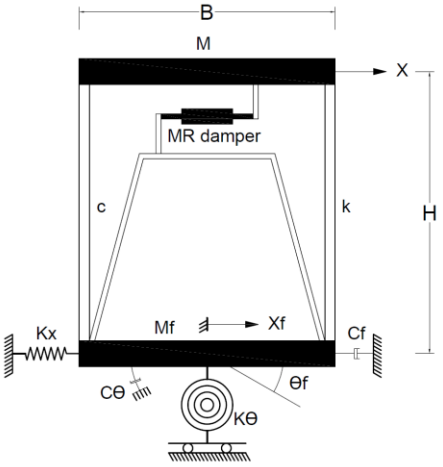


B) The boundary conditions of the superstructure

**Figure 6-3** Design of the SAC algorithm for SSI system with Fixed- SSI assumption.

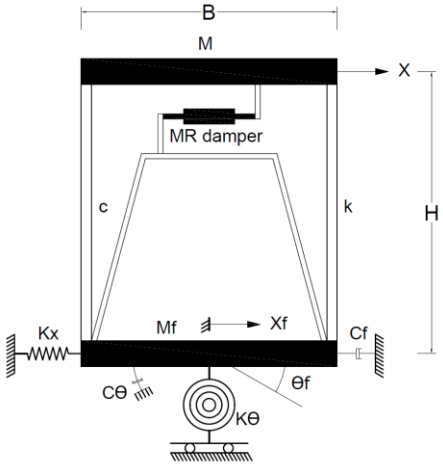


A) The reference model with the SSI assumption

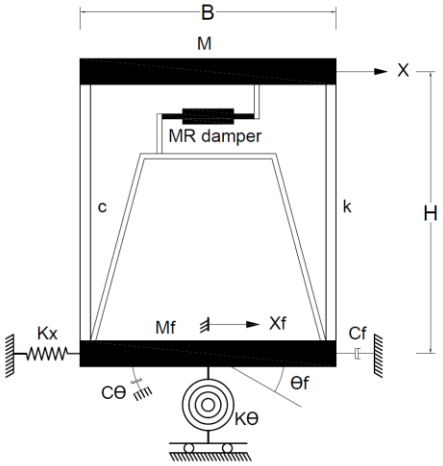


B) The boundary conditions of the superstructure

**Figure 6-4** Design of the SAC algorithm for SSI system with SSI - SSI assumption.

For the fixed-base system, there was one sensor measuring transverse displacement at the center of the floor. For both systems, a control device was placed between the floor and foundation. Figure 6-1 presents a schematic of the device's installation on the floor for both the fixed and flexible base structure systems. Parametric studies were carried out based on a one-story building with fixed and flexible support and different soil profiles. The section of soil profile presents all parameters for each soil profile.

The SAC algorithm was utilized as the main control strategy for this adaptive control scheme. An MR damper was employed as a semi-active device, and the reference model was implemented according to the Al-Fahdawi design. This design adopted the optimal control theory (i.e., LQR) to determine the desired output of the reference model, according to the hypothesis of invariable system parameters (Al-Fahdawi et al., 2018).

The LQR constants for the reference model were:

$\rho = 10^{-10}$, $Q = I$

The SAC constants were: $\Gamma_e = 10^{10}$ , $\Gamma_x = 10^{10}$, $\Gamma_u = 10^{10}$

## 6.8 Performance Evaluation Criteria

The performance evaluation criteria described by Equations (3) to (13) were utilized; these were chosen from the criteria established by (Ohtori, Christenson, Spencer Jr, & Dyke, 2004). Criteria J1, J2, J3, J4, and J5 calculated the performance in terms of normalized peak responses. Criteria J6, J7, J8, and J9 estimated the performance in terms of normed responses; these are given by Equations (6.3) to (6.13).

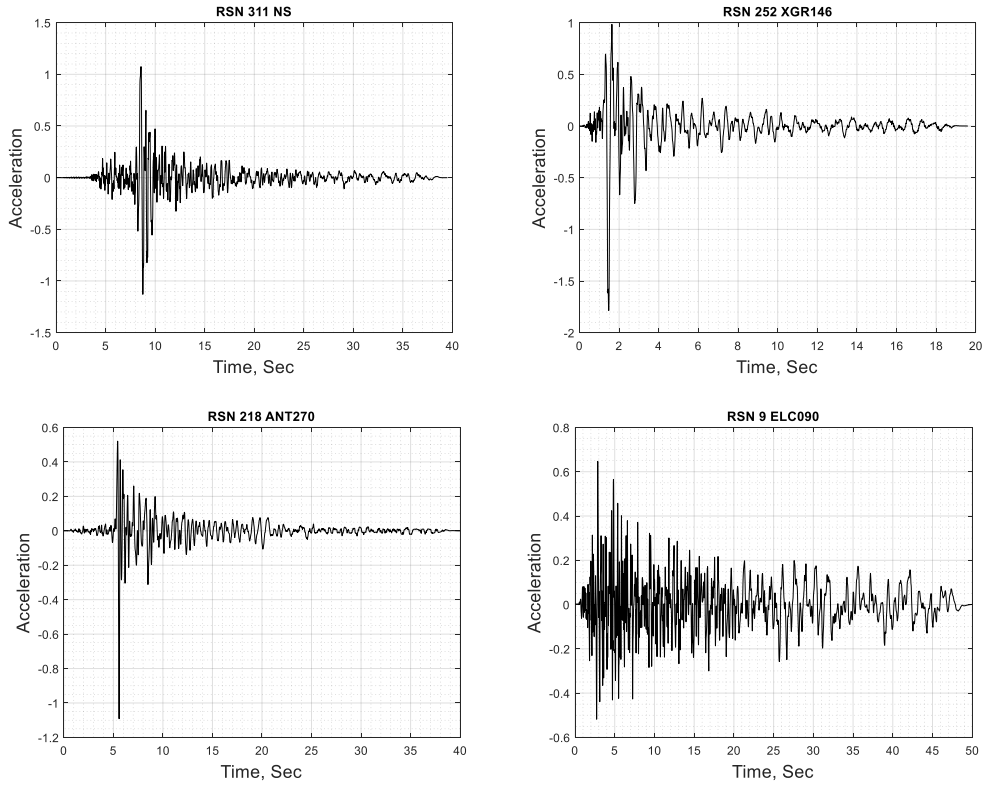


**Figure 6-5** Acceleration time history of the earthquake suite adopted in the investigations.

$$J_1 = max\left\{\frac{max(|x_i(t)|)}{x_{uncnt}}\right\}$$ is the normalized peak displacement 6-3

$$J_2 = max\left\{\frac{max\frac{|d_i(t)|}{h_i}}{d_{uncnt}}\right\}$$ is the peak normalized inter-story drift 6-4

$$J_3 = max\left\{\frac{max(|\ddot{x}_i(t)|)}{\ddot{x}_{uncnt}}\right\}$$ is the normalized peak acceleration 6-5

$$J_4 = \frac{max(|f_i(t)|)}{W}$$ is the normalized peak control force 6-6

$$J_5 = \frac{max(|\sum m_i\ddot{x}_i(t)|)}{F_b}$$ is the normalized peak base shear 6-7

$J_6 = max\left\{max\frac{\|x_i(t)\|}{\|x_{uncnt}\|}\right\}$ is the normed displacement 6-8

$J_7 = max\left\{\frac{max\frac{\|d_i(t)\|}{h_i}}{\|d_{uncnt}\|}\right\}$ is the normed inter-story drift ratio 6-9

$J_8 = max\left\{\frac{max\|\ddot{x}_i(t)\|}{\|\ddot{x}_{uncnt}\|}\right\}$ is the normed acceleration 6-10

$J_9 = max\left\{\frac{\|\sum m_i\ddot{x}_i(t)\|}{\|F_b\|}\right\}$ is the peak normalized base shear 6-11

$J_{10} =$ is the number of devices 6-12

$J_{11} =$ is the number of sensors 6-13

## 6.9 Normalization of SSI results

The normalized SSI results were divided into two groups: uncontrolled and controlled ratios corresponding to the fixed support system. Following are the definitions of these ratios.

Uncontrolled Systems

Max. Disp. Ratio = $(max(|\bar{\delta}_{unc}|)/max(|\delta_{fixedunc}|))$ 6-14

Max. Acc. Ratio = $(max\left(\left|\bar{\ddot{\delta}}_{unc}\right|\right)/max(|\ddot{\delta}_{fixedunc}|))$ 6-15

Max. Base Shear Ratio = $\left(max(|\bar{V}_{unc}|)\right)/max(|V_{unc}|)$ 6-16

Controlled Systems

Max. Disp. Ratio = $(max(|\bar{\delta}_{con}|)/max(|\delta_{fixedcon}|))$ 6-17

Max. Acc. Ratio = $(max\left(\left|\bar{\ddot{\delta}}_{con}\right|\right)/max(|\ddot{\delta}_{fixedcon}|))$ 6-18

Max. Control Force Ratio ($R_f = \sum|F_{SSI}|/\sum|F_{fixed}|$) 6-19

Max. Base Shear Ratio = $\left(\boldsymbol{max}(|\bar{\boldsymbol{V}}_{\boldsymbol{con}}|)\right)/\boldsymbol{max}(|\boldsymbol{V}_{\boldsymbol{con}}|)$ 6-20

where:

$\bar{\delta}_{unc}$ is the displacement of the uncontrolled SSI

$\bar{\delta}_{con}$ is the displacement of the controlled SSI

$\delta_{fixedunc}$ is the displacement of the uncontrolled fixed

$\delta_{fixedcon}$ is the displacement of the controlled fixed

$\bar{\ddot{\delta}}_{unc}$ is the acceleration of the uncontrolled SSI

$\bar{\ddot{\delta}}_{con}$ is the acceleration of the controlled SSI

$\ddot{\delta}_{fixedunc}$ is the acceleration of the uncontrolled fixed

$\ddot{\delta}_{fixedcon}$ is the acceleration of the controlled fixed

$F_{fixed}$ is the control force of the fixed system

$F_{SSI}$ is the control force of the SSI system

$\bar{V}_{unc}$ is Base Shear of the uncontrolled SSI

$\bar{V}_{con}$ is Base Shear of the controlled SSI

$V_{unc}$ is Base Shear of uncontrolled fixed

$V_{con}$ is Base Shear of controlled fixed

## 6.10 Normalization of Foundation Results

The normalization of the foundation control response to uncontrolled conditions was also investigated in this research. Following are definitions of these ratios.

$\boldsymbol{X_F = max}\left\{\frac{\boldsymbol{max}(|\boldsymbol{foux_i(t)}|)}{\boldsymbol{foux_{uncnt}}}\right\}$ is the normalized peak foundation displacement 6-21

$\boldsymbol{Y_F = max\left\{\frac{max(|fouy_i(t)|)}{fouy_{uncnt}}\right\}}$ is the normalized peak foundation displacement 6-22

$\boldsymbol{\Phi_X = max\left\{\frac{max(|fou\theta_i(t)|)}{fou\theta_{uncnt}}\right\}}$ is the normalized peak foundation rocking 6-23

$\boldsymbol{\Phi_Y = max\left\{\frac{max(|fou\phi_i(t)|)}{fou\phi_{uncnt}}\right\}}$ is the normalized peak foundation rocking 6-24

where:

$foux_i$ is the foundation displacement of the controlled SSI in the X direction

$foux_{uncnt}$ is the foundation displacement of the uncontrolled SSI in the X direction

$fouy_i$ is the foundation displacement of the controlled SSI in the Y direction

$fouy_{uncnt}$ is the foundation displacement of the uncontrolled SSI in the Y direction

$fou\theta_i$ is the foundation rotation displacement of the controlled SSI in the Y direction

$fou\theta_{uncnt}$ is the foundation rotation displacement of the uncontrolled SSI in the Y direction

$fou\phi_i$ is the foundation rotation displacement of the controlled SSI in the X direction

$fou\phi_{uncnt}$ is the foundation rotation displacement of the uncontrolled SSI in the X direction

## 6.11 Geotechnical Parametric Studies

The soil profiles described the change in soil properties with depth. In this section, soil layer, linear (i.e., clay), and parabolic (i.e., sand) profiles were adopted to model variations in soil stiffness with depth. The first two soil profiles consisted of two layers, soft and medium, with difference arrangements; the second two soil profiles modeled the shear modules of the soil varieties: parabolic for sand and linear for clay. Figure 6-6, Figure 6-7, Figure 6-14, and Figure 6-15 show these soil profiles. The equivalent soil stiffness matrices

of the rigid foundation were calculated by ABAQUS finite element software and written as a diagonal matrix (see Chapter 5).

$$[\boldsymbol{K_{soil}}] = \begin{bmatrix} \boldsymbol{k_{xx}} & \boldsymbol{0} \\ \boldsymbol{0} & \boldsymbol{k_{\theta\theta}} \end{bmatrix} \quad \text{6-25}$$

where:

kxx is the equivalent soil stiffness in the X direction

$k_{\theta\theta}$ is the equivalent soil rocking stiffness in the Y direction

### 6.11.1 The Soil Layer Profiles Cases

Common soil profiles consisting of medium top and soft bottom or soft top and medium bottom layers were investigated. Figure 6-6, and Figure 6-7 display the soil profiles implemented. The simulation of the finite element analysis assumed a square foundation with a 17.7 m width; the soil stiffness properties varied with increases in depth ratio (Z/D). Figure 6-8, Figure 6-9, Figure 6-10, and Figure 6-11 present the variations in elements of the equivalent soil stiffness matrices by depth ratio for the two types of soil profile.

Table 6-2 and Figure 6-12 summarize the relationship between the system parameters and effect of variations in depth ratio (Z/D) on the time period ratio for the medium top and soft bottom layer system. It appears from Figure 6-12 that an increase in the depth ratio resulted in a decrease in the time period ratio. Moreover, an increase in the slenderness ratio (λ) led to an increase in the time period ratio. Similarly, for the soft top and medium bottom layer system, Table 6-2 and Figure 6-13 present that an increase in the depth ratio led to an increase in the time period ratio, while an increase in the slenderness ratio led to an increase in the time period ratio.

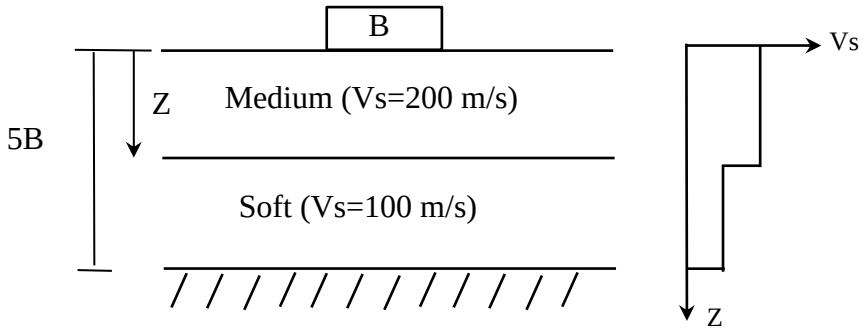


**Figure 6-6** Soil profile of medium top and soft bottom layers.

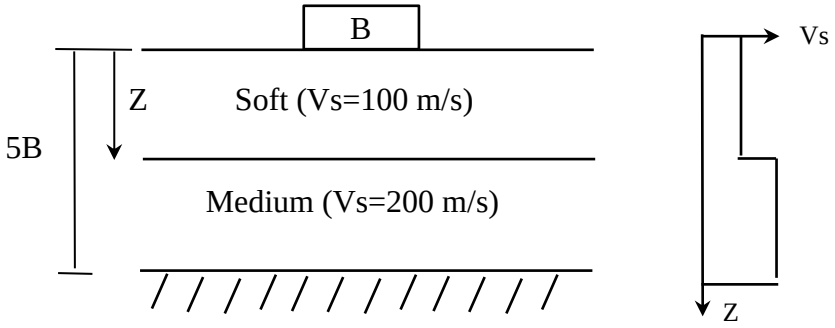


**Figure 6-7** Soil profile of soft top and medium bottom layers.

Where: B = width of the foundation, Z = thickness of first layer, total thickness of soil (5B), and Z/B = normalized thickness of first layer.

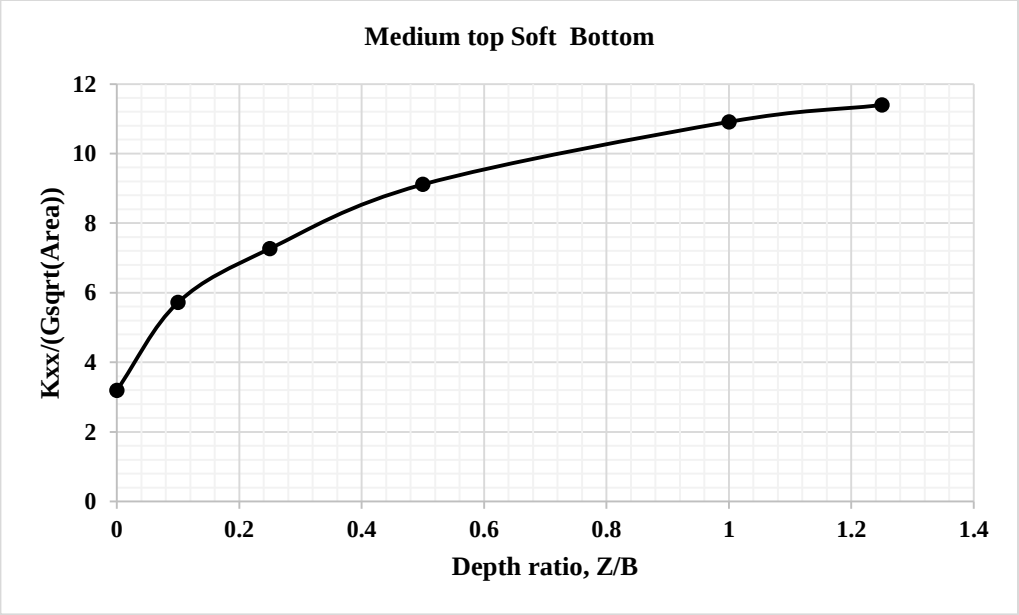


**Figure 6-8** Variations in the stiffness of the foundation in the X direction corresponding to the Z/B ratio.

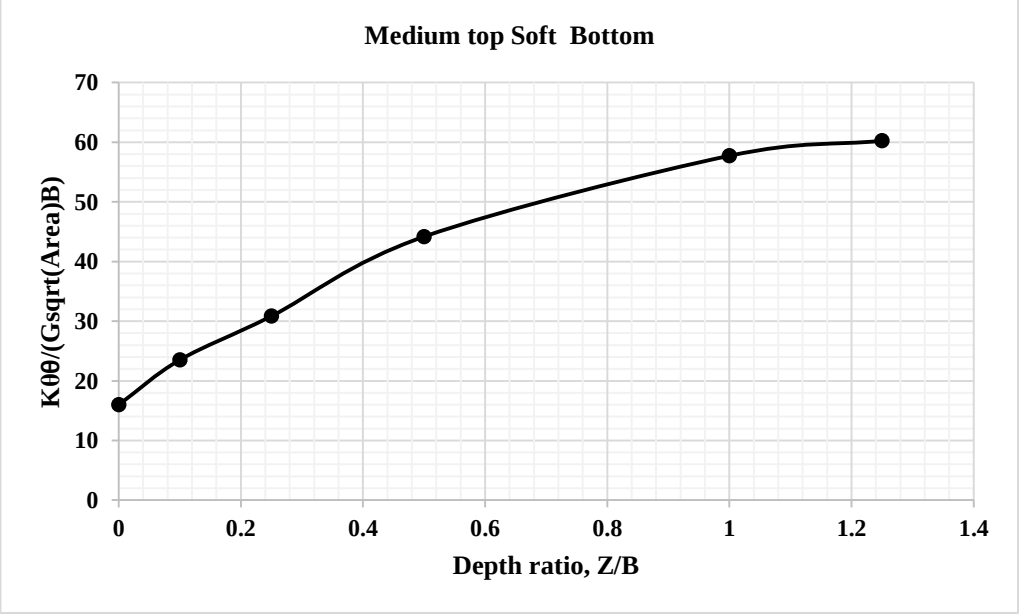


**Figure 6-9** Variations in the rocking stiffness of the foundation in the Y direction corresponding to the Z/B ratio.

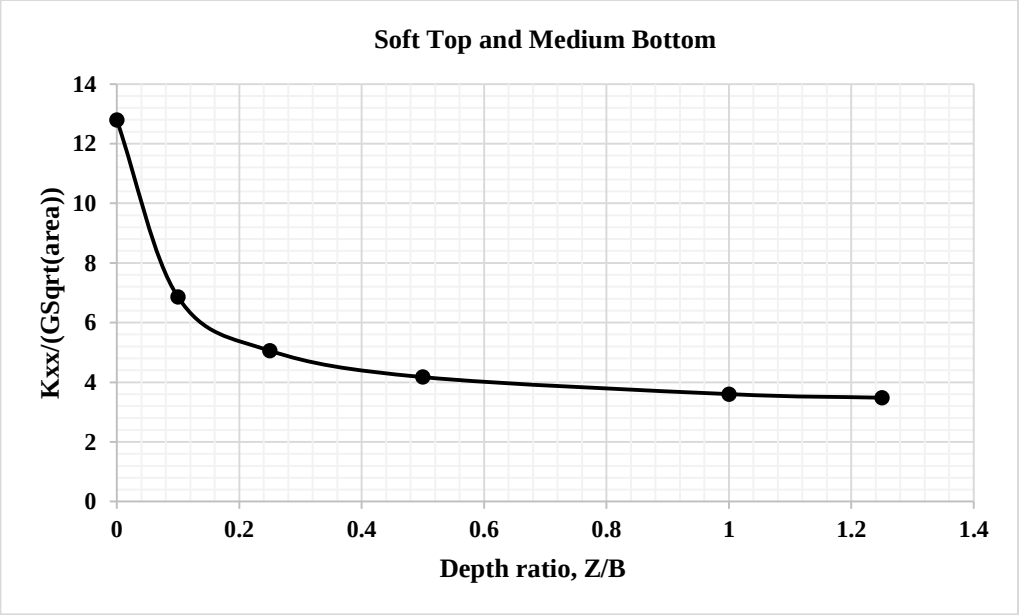


**Figure 6-10** Variations in stiffness of the foundation in the X direction corresponding to the Z/B ratio.

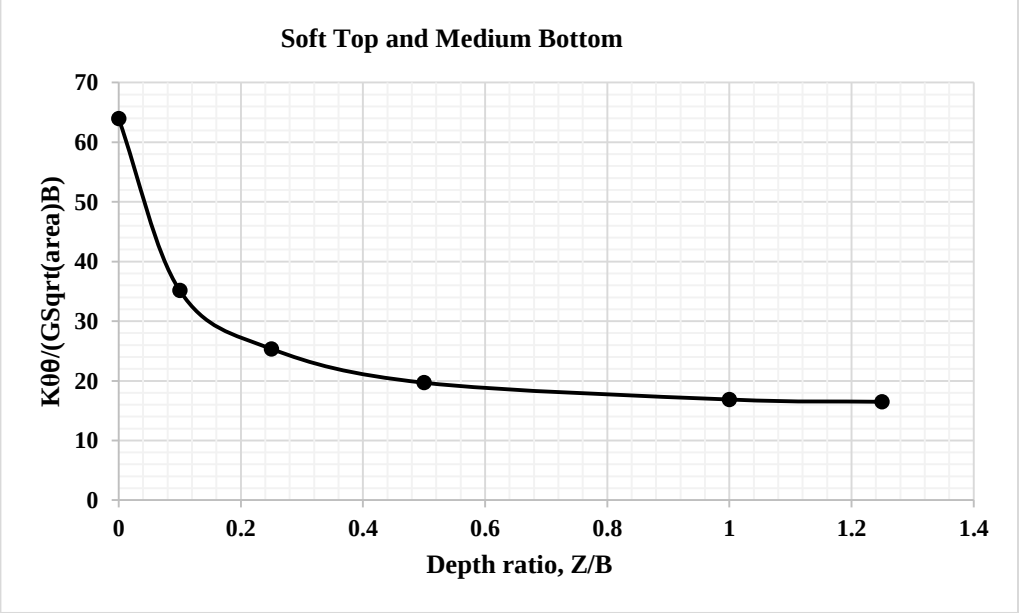


**Figure 6-11** Variation in the momentary stiffness of the foundation in the Y direction corresponding to the Z/B ratio.

**Table 6-2** Relationships among system parameters.

| Z/B | Medium top and soft bottom | | Soft top and medium bottom | |
|---|---|---|---|---|
| | λ = 1 | λ = 0.5 | λ = 1 | λ = 0.5 |
| | $\bar{T}/T$ | $\bar{T}/T$ | $\bar{T}/T$ | $\bar{T}/T$ |
| 0 | 1.7558 | 1.3747 | 1.2277 | 1.1007 |
| 0.1 | 1.5336 | 1.2402 | 1.3924 | 1.1821 |
| 0.25 | 1.4251 | 1.1883 | 1.5174 | 1.2453 |
| 0.5 | 1.3169 | 1.1421 | 1.6323 | 1.3016 |
| 1 | 1.2531 | 1.1146 | 1.7159 | 1.3462 |
| 1.25 | 1.2433 | 1.1099 | 1.7306 | 1.3553 |

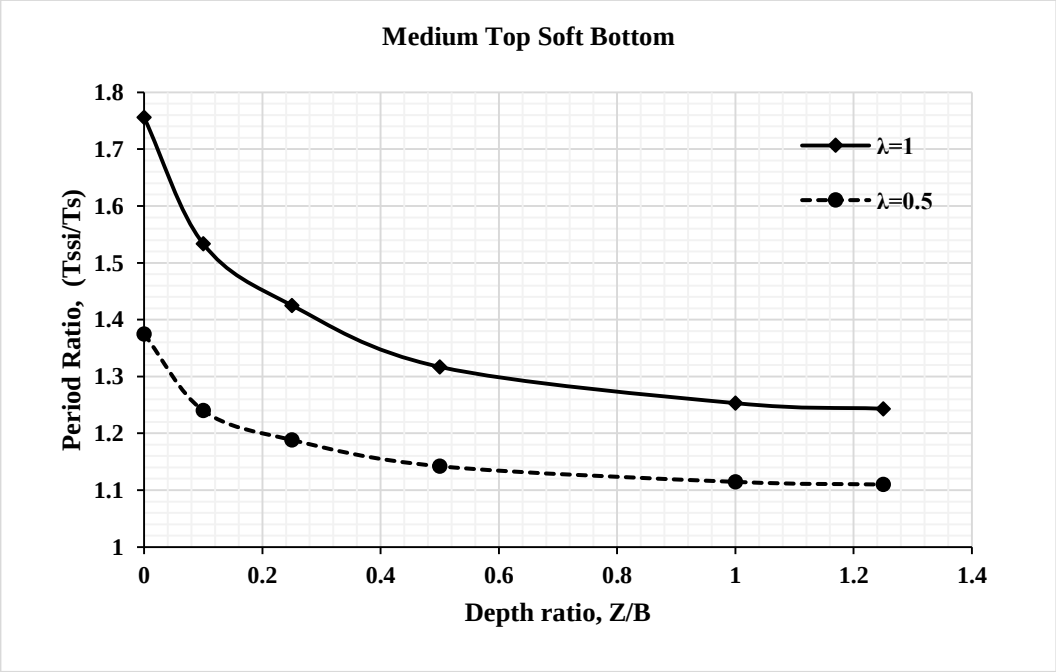


**Figure 6-12** Variations in the time period ratio depending on the Z/B and λ ratios for the medium top and soft bottom layers.

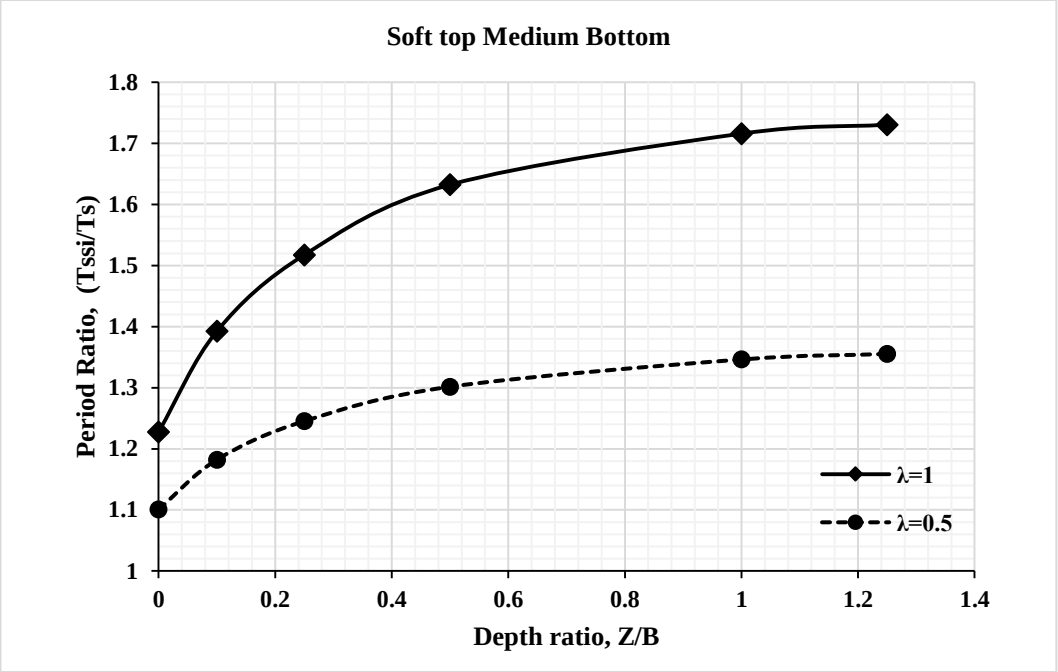


**Figure 6-13** Variations in the time period ratio depending on the Z/B and λ ratios for the soft top and medium bottom layers.

The SDOF constructed on the soil layer profiles had a constant time period (T = 0.2), showing that in the medium top and soft bottom soil profiles, the period ratio decreased with an increase in the depth ratio. Conversely, the soft top and medium bottom soil profiles showed that the period ratio increased with an increase in the depth ratio. The slenderness ratio (λ) increased the period ratio for both soil profiles (see Figure 6-12, Figure 6-13, and Table 6-2).

### 6.11.2 The Sand and Clay Soil Profiles Cases

Other common soil profiles for sand and clay were represented by linear and parabolic variations in the shear modulus, G, with depth, as shown in Figure 6-14 and

Figure 6-15. The horizontal and rocking stiffnesses were determined using finite element analysis for a square foundation with a 17.7 m width; the results are displayed in Figure 6-16, Figure 6-17, Figure 6-18, and Figure 6-19.

Table 6-3 presents variations in the time period ratio depending on the parameter G. Figure 6-20 and Figure 6-21 illustrate the relationship between the system parameters and effect of increases in Shear modulus, G with depth in terms of the time period ratio. For clay soil, it appears from Figure 6-20 that an increase in G led to a decrease in the time period ratio because of the increase in soil stiffness. Moreover, an increase in the slenderness ratio (λ) led to an increase in the time period ratio. For sand, Figure 6-21 shows a similar variation of G.

The SDOF constructed on the soil profiles had a constant time period (T = 0.2), showing that in the sand and clay soil profiles the period ratio decreased with an increase in the depth ratio. Furthermore, an increase in the slenderness ratio (λ) increased the period ratio for both soil profiles (see Figure 6-20 and Figure 6-21 and Table 6-3).

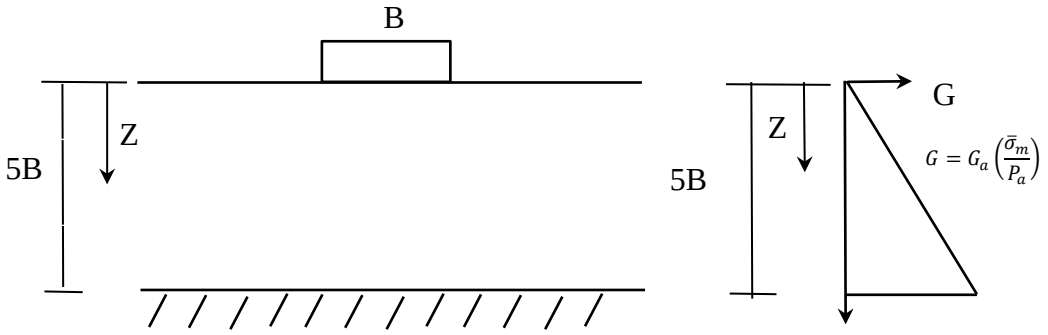


**Figure 6-14** Variations of shear modulus, G with depth for clay (linear).

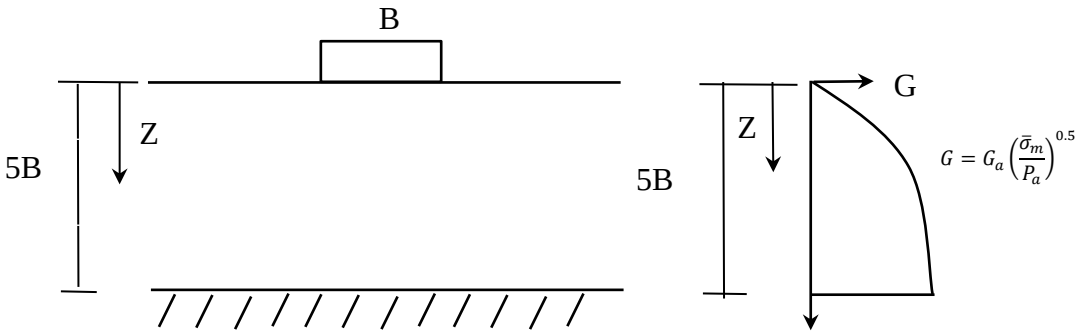


**Figure 6-15** Variations of shear modulus, G with depth for sand (parabolic).

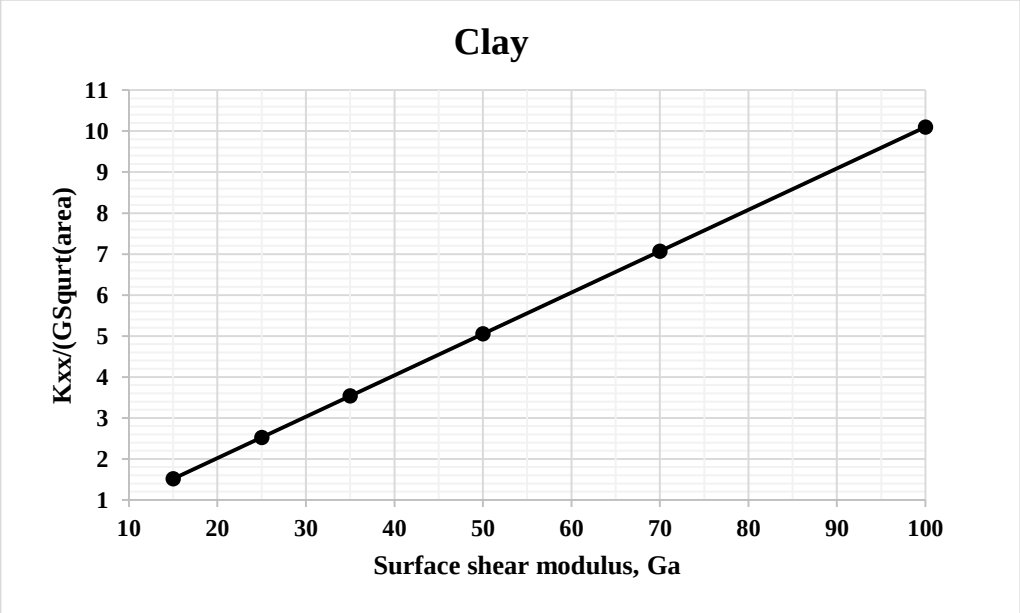


**Figure 6-16** Variations in the stiffness of the foundation in the X direction corresponding to surface shear modulus, Ga for clay soil.

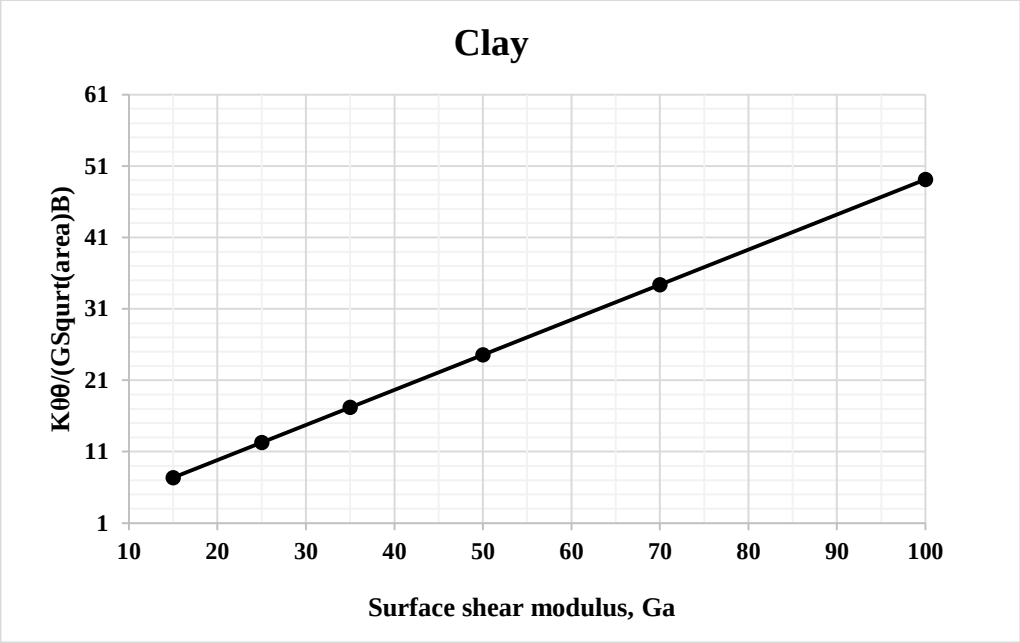


**Figure 6-17** Variations in rocking stiffness of the foundation in the Y direction corresponding to surface shear modulus, Ga for clay soil.

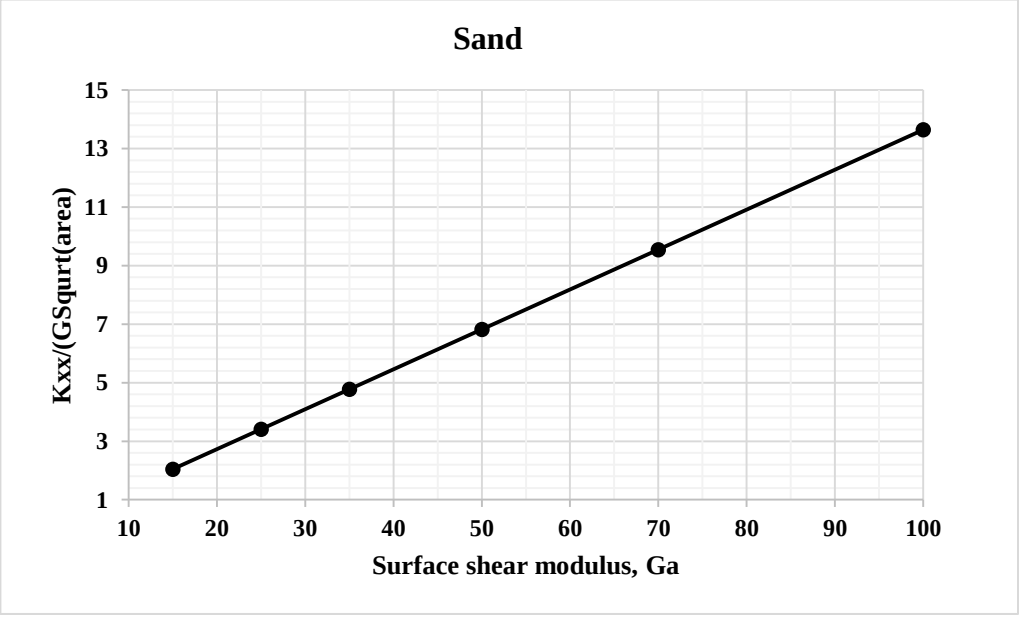


**Figure 6-18** Variations in the stiffness of the foundation in the X direction corresponding to the surface shear modulus, Ga for sand soil.

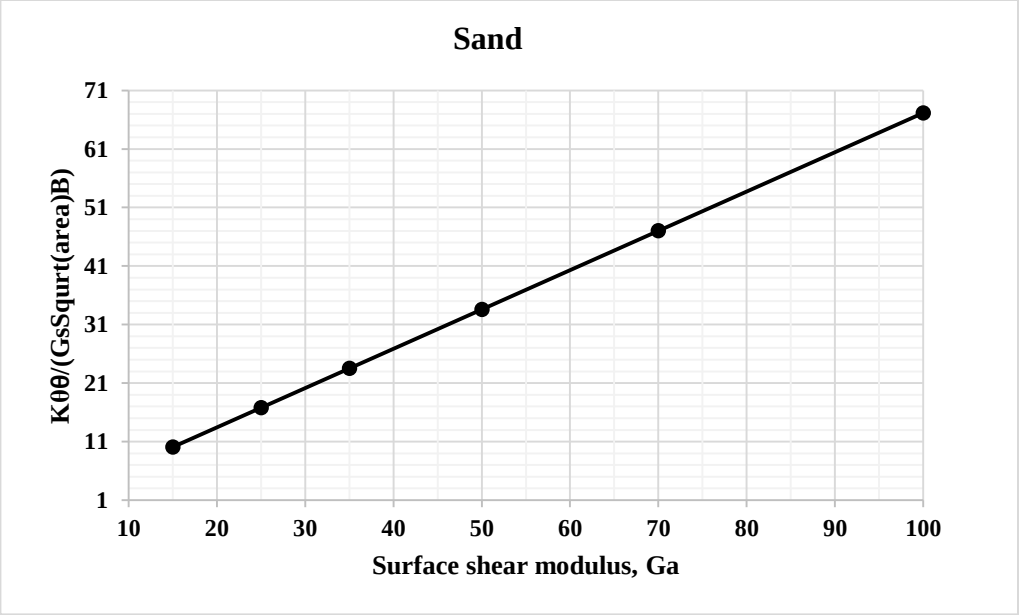


**Figure 6-19** Variations in the rocking stiffness of the foundation in the Y direction corresponding to the surface shear modulus, Ga for sand soil.

**Table 6-3** Relationships among the system parameters.

| $G_a$ | Clay (linear) | | Sand (parabola) | |
|---|---|---|---|---|
| | λ = 1 | λ = 0.5 | λ = 1 | λ = 0.5 |
| | $\bar{T}/T$ | $\bar{T}/T$ | $\bar{T}/T$ | $\bar{T}/T$ |
| 15 | 2.3543 | 1.7217 | 2.0779 | 1.5583 |
| 25 | 1.9254 | 1.4678 | 1.7248 | 1.3559 |
| 35 | 1.7097 | 1.3463 | 1.5498 | 1.2611 |
| 50 | 1.5288 | 1.2491 | 1.4052 | 1.1864 |
| 70 | 1.396 | 1.1811 | 1.3006 | 1.1348 |
| 100 | 1.2883 | 1.1284 | 1.2169 | 1.0952 |

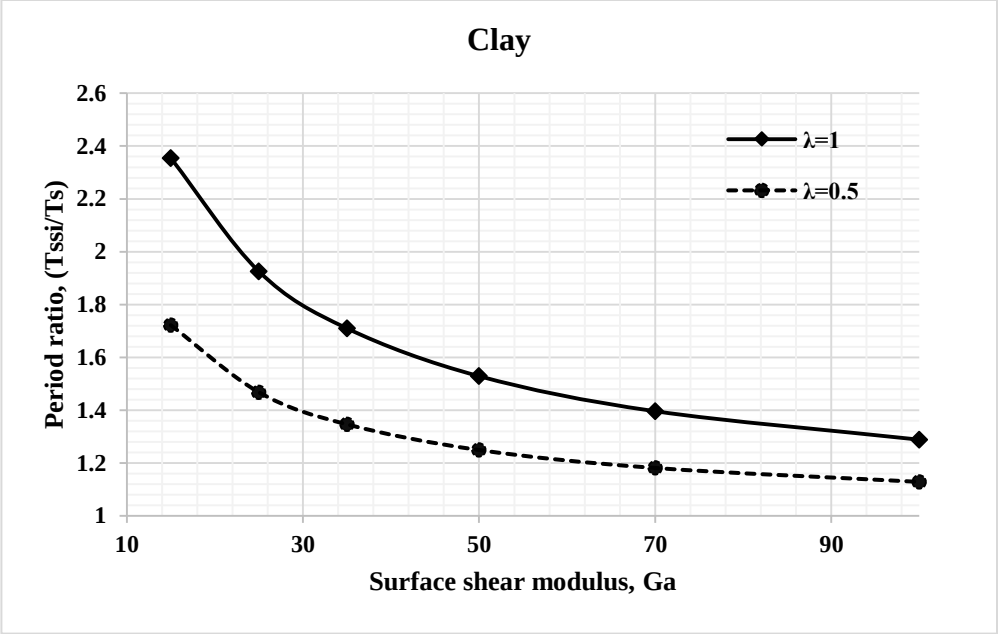


**Figure 6-20** Variations in the time period ratio depending on the surface shear modulus, Ga and λ ratios for clay soil.

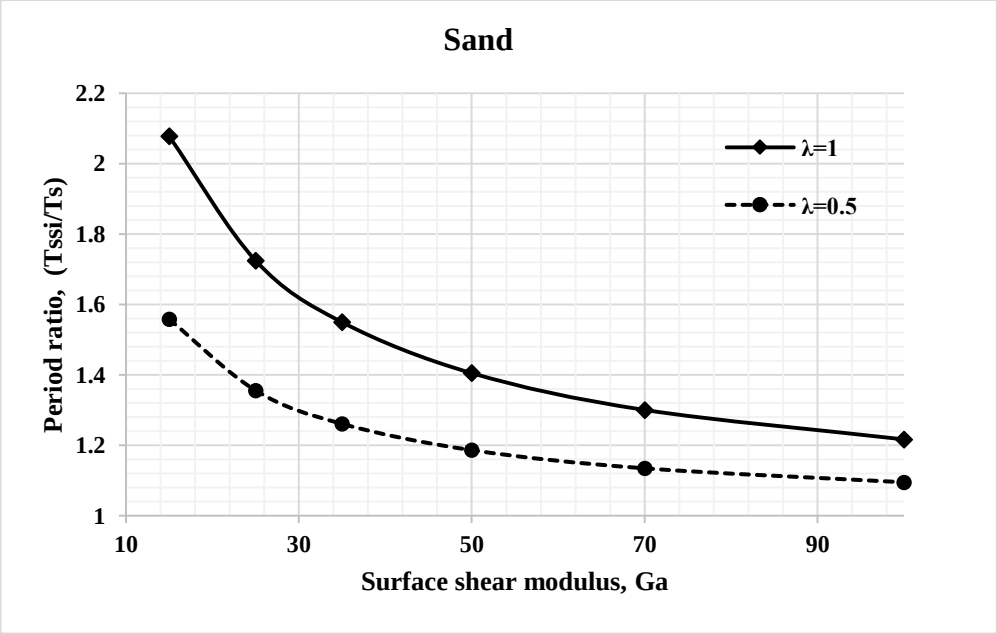


**Figure 6-21** Variations in the time period ratio depending on the surface shear modulus Ga and λ ratios for sand soil.

## 6.12 Structural Parametric Study

The structural parametric study is carried out based on the one story building for fixed and flexible base and the mathematical model is illustrated in Figure 6-1. The series of parameters are: the time period of fixed support structure (T = 0.1, 0.2, 0.4, 0.6, 0.8, and 1 sec), the structure's slenderness ratio (λ = 0.5, and 1), and the earthquake loads. The soil assumed as a soft soil with constant shear velocity (Vs = 100 m/s). Table 6-4 shows ratio of natural time period of SSI system to fixed support structure and Figure 6-22 show the relation between parameters of systems in this study.

**Table 6-4** Relationships among the structure parameters.

| Ts | slenderness ratio (λ = H/B) | | | |
|---|---|---|---|---|
| | λ = 0.5 | | λ = 1 | |
| | $\sigma = \frac{h}{(V_s T)}$ | $\frac{\bar{T}}{T}$ | $\sigma = \frac{h}{(V_s T)}$ | $\frac{\bar{T}}{T}$ |
| 0.1 | 0.5900 | 2.1789 | 1.1800 | 3.0774 |
| 0.2 | 0.2950 | 1.3747 | 0.5900 | 1.7558 |
| 0.4 | 0.1475 | 1.1007 | 0.2950 | 1.2277 |
| 0.6 | 0.0983 | 1.0452 | 0.1967 | 1.1058 |
| 0.8 | 0.0737 | 1.0255 | 0.1475 | 1.0605 |
| 1.0 | 0.0590 | 1.0164 | 0.1180 | 1.0390 |

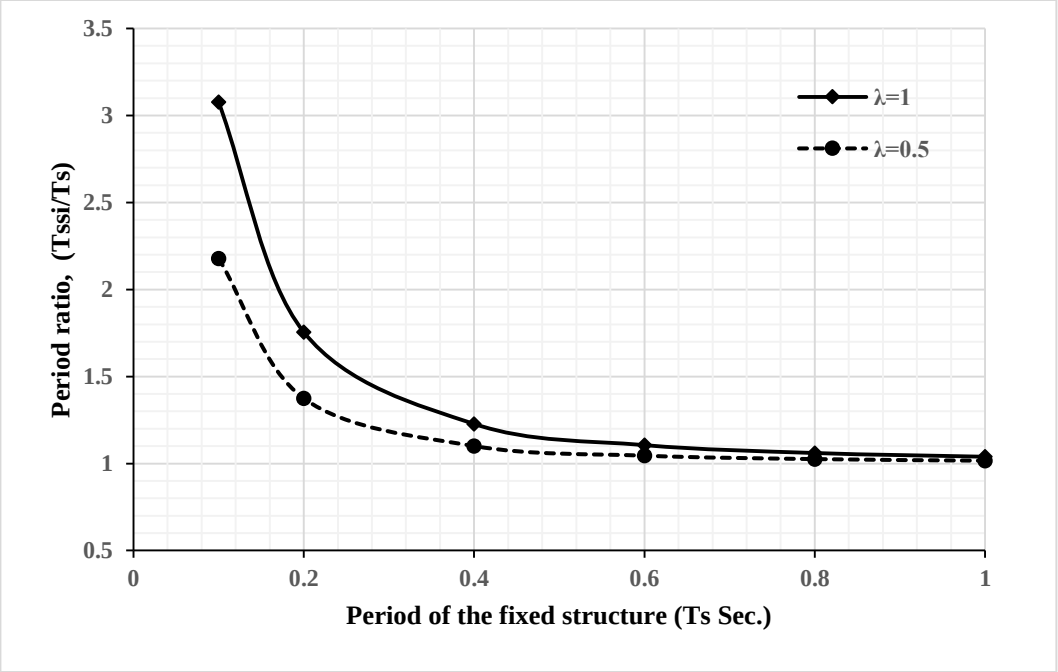


**Figure 6-22** Variations in the time period ratio depending on the structural period of fixed base structure (Ts) and slenderness (λ) ratio.

## 6.13 Results and Discussion

### 6.13.1 Uncontrolled Systems

The displacements of uncontrolled systems were investigated based on the maximum displacement ratio. Figure 6-23 offers a conceptual summary of the behavior observed in the SSI system. The Figure 6-23 explains that in order to determine whether the SSI consideration was beneficial or detrimental, the responses of the two systems, the original fixed-base system and SSI system, had to be compared using the displacement spectrum of the input earthquake.

The period of the SSI system was always higher than the period of the fixed-base system (TSSI > TS); therefore, the response of the SSI system shifted to the response at TSSI

on the earthquake spectrum. Obviously, this relied on the earthquake spectrum in place of the fundamental period of the fixed-base system. The SSI system might have had either beneficial or detrimental effects.

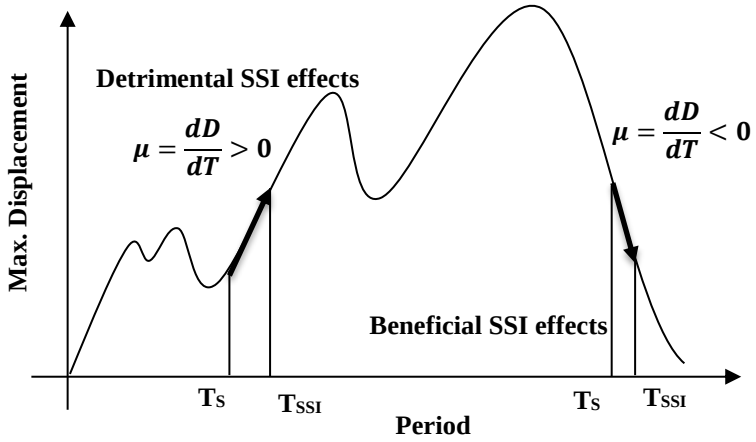


**Figure 6-23** Conceptual presentation of the SSI's detrimental and beneficial effects.

For geotechnical parametric study, the soil with medium top and soft bottom layers showed displacement ratios for all earthquakes with a slender ratio of λ = 1, varying within a range of 1.6271 to 0.6443; when the slender ratio was λ = 0.5, the displacement ratio varied from 1.6340 to 0.7055. Layered soil with a soft top and medium bottom profile showed a displacement ratio for all earthquakes with a slender ratio of λ = 1, varying from 1.5842 to 0.6630; when the slender ratio was λ = 0.5, the displacement ratio varied from 1.6528 to 0.7021. For clay soil profiles, the results revealed that the displacement ratio for all earthquakes with a slender ratio of λ = 1 ranged from 1.7701 to 0.6568; when the slender ratio was λ = 0.5, the displacement ratio ranged from 1.6551 to 0.7031. For sand soil profiles,

the results indicated that the displacement ratio for all earthquakes with a slender ratio of λ = 1 ranged from 1.6797 to 0.6369; when the slender ratio was λ = 0.5, the displacement ratio varied from 1.6514 to 0.7043. Figure 6-24, Figure 6-25, Figure 6-26, and Figure 6-27 display the results for different soil profiles.

For structural parametric study, the results showed that the displacement ratio for all earthquakes with a slender ratio of λ = 1 ranged from 2.6032 to 0.6023; when the slender ratio was λ = 0.5, the displacement ratio varied from 2.2029 to 0.6865. Figure 6-28 show the results for different value to the time period of fixed base structure (Ts).

### 6.13.2 Controlled Systems

#### 6.13.2.1 Maximum Control Force Ratio

For geotechnical parametric study, the medium top and soft bottom soil profiles with the SSI-SSI reference model for the control system, the results illustrate that the maximum control force ratio for all earthquakes with a slender ratio (both λ = 1 and λ = 0.5) decreased with an increase in depth ratio, ranging for λ = 1 from 1.8910 to 1.1022 and for λ = 0.5 from 1.6799 to 1.0213; however, the control force ratio increased with an increase in slenderness ratio. Similarly, for the fixed-SSI reference model with more control force, the maximum control force ratio ranged for λ = 1 from 2.1866 to 1.2369 and for λ = 0.5 from 1.8462 to 1.1365.

For soft top and medium bottom soil profiles with the SSI-SSI reference model for a control system, the results illustrate that the maximum control force ratio for all earthquakes with a slender ratio (both λ = 1 and λ = 0.5) increased with an increase in the depth ratio,

ranging for λ = 1 from 2.0234 to 1.0898 and for λ = 0.5 from 1.6339 to 1.0114; however, the control force ratio increased with an increase in the slender ratio. Similarly, for the fixed-SSI reference model with more control force, the control force ratio for λ = 1 ranged from 2.1832 to 1.2218 and for λ = 0.5 from 1.7878 to 1.1247.

For clay (linear) soil profiles with the SSI-SSI reference model for the control system, the results illustrate that the maximum control force ratio for all earthquakes with a slender ratio (both λ = 1 and λ = 0.5) decreased with an increase in the shear modulus, for λ = 1 ranging from 2.4792 to 1.1215 and for λ = 0.5 from 2.2762 to 1.0369; however, the control force ratio increased with an increase in the slender ratio. Similarly, for the fixed-SSI reference model with more control force, the variation ranged for λ = 1 from 2.9330 to 1.2699 and for λ = 0.5 from 2.5629 to 1.1562.

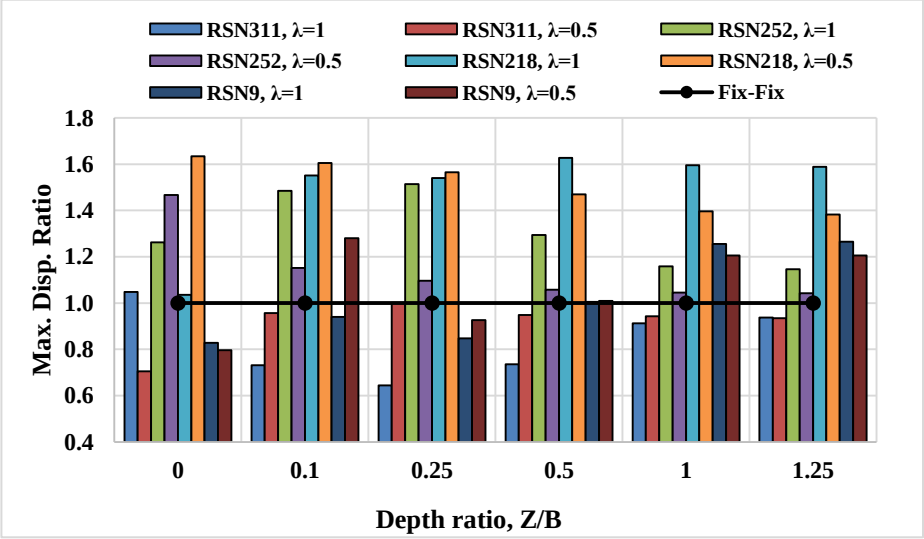


**Figure 6-24** Variations in the maximum displacement ratio for medium top and soft bottom soil profiles with the earthquake suite.

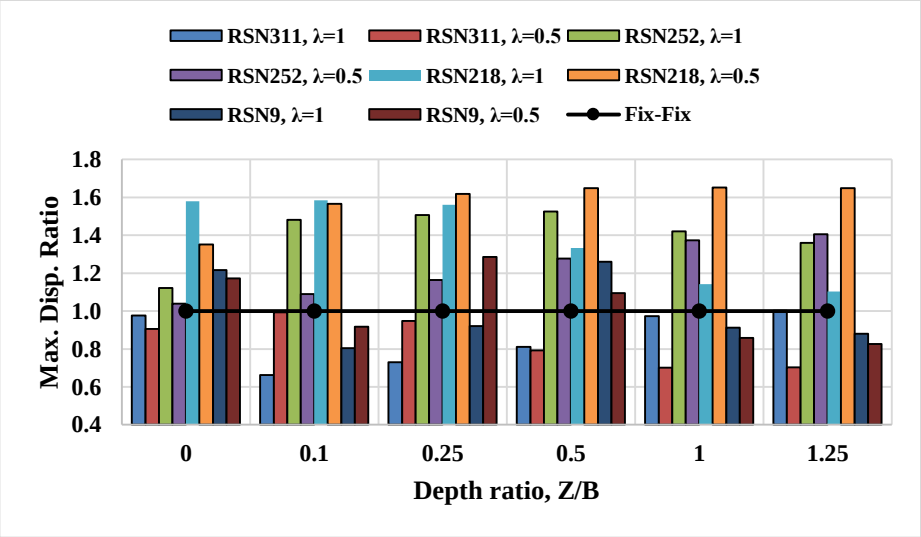


**Figure 6-25** Variations in the maximum displacement ratio for soft top and medium bottom soil profiles with the earthquake suite.

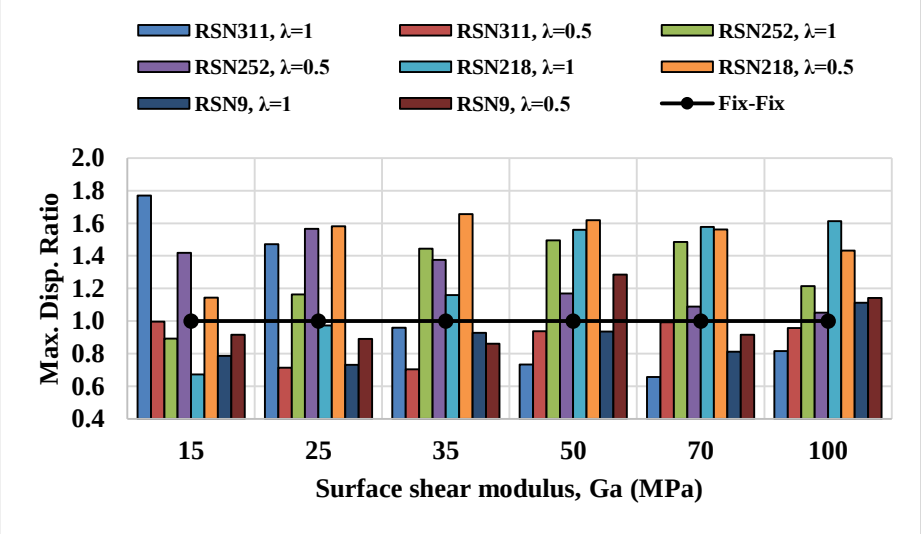


**Figure 6-26** Variations in the maximum displacement ratio for clay soil profiles with the earthquake suite.

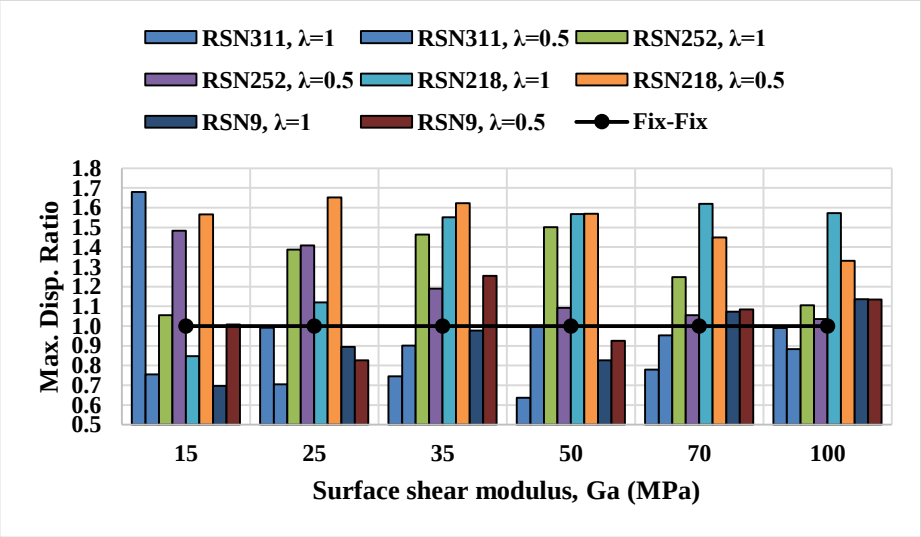


**Figure 6-27** Variations in the maximum displacement ratio for the sand soil profiles with the earthquake suite.

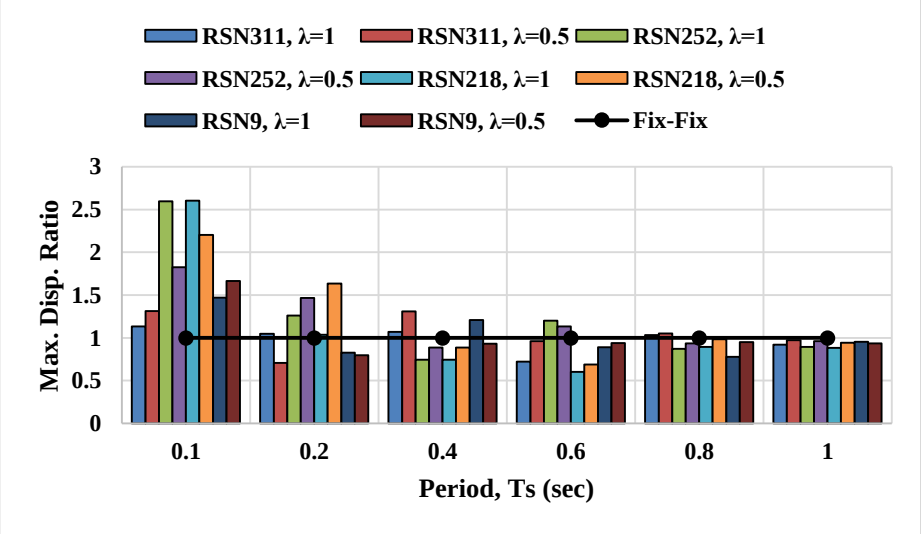


**Figure 6-28** Variations in the maximum displacement ratio for the structural parameter with the earthquake suite.

For the sand (parabolic) soil profiles with the SSI-SSI reference model for the control system, the results illustrate that the maximum control force ratio for all earthquakes with a slender ratio (both $\lambda = 1$ and $\lambda = 0.5$) decreased with an increase in shear modulus, ranging for $\lambda = 1$ from 2.1030 to 1.0814 and for $\lambda = 0.5$ from 2.0813 to 1.0059; however, the control force ratio increased with an increase in the slender ratio. Similarly, for the fixed-SSI reference model with more control force, the maximum control force ratio ranged for $\lambda = 1$ from 2.4647 to 1.2119 and for $\lambda = 0.5$ from 2.3010 to 1.1180. All figures illustrating the control force ratios for all soil profiles are available in Appendix A.

For structural parametric study with the SSI-SSI reference model for the control system, the results show that the maximum control force ratio for all earthquakes with a slender ratio (both $\lambda = 1$ and $\lambda = 0.5$) decreased with an increase in the period of fixed base structure (Ts), ranging for $\lambda = 1$ from 2.2959 to 1.0212 and for $\lambda = 0.5$ from 3.1726 to 1.0590; however, the control force ratio increased with an increase in the slender ratio. Similarly, for the fixed-SSI reference model with more control force, the maximum control force ratio ranged for $\lambda = 1$ from 3.2210 to 1.2194 and for $\lambda = 0.5$ from 3.2200 to 1.1199. All figures illustrating the control force ratios are available in Appendix A.

#### 6.13.2.2 Maximum Control Displacement Ratio

For geotechnical parametric study, the medium top and soft bottom soil profiles with the SSI-SSI reference model for the control system, the results show that the maximum displacement ratio under the earthquake suite with different slender ratios (both $\lambda = 1$ and $\lambda = 0.5$) decreased with an increase in the depth ratio, ranging for $\lambda = 1$ from 2.0965 to 1.2740

and for $\lambda = 0.5$ from 1.7862 to 1.1616; however, the displacement ratio increased with an increase in the slender ratio. Similarly, for the fixed-SSI reference model, the maximum displacement ratio decreased with an increase in the depth ratio, but to a lesser extent, ranging for $\lambda = 1$ from 2.0051 to 1.2259 and for $\lambda = 0.5$ from 1.6912 to 1.1211.

For the soft top and medium bottom soil profiles with the SSI-SSI reference model for the control system, the results show that the maximum displacement ratio under the earthquake suite with different slender ratios (both $\lambda = 1$ and $\lambda = 0.5$) increased with an increase in the depth ratio, ranging for $\lambda = 1$ from 1.9991 to 1.2616 and for $\lambda = 0.5$ from 1.7522 to 1.1510; however, the displacement ratio increased with an increase in the slender ratio. Similarly, for the fixed-SSI reference model, the maximum displacement ratio decreased with an increase in the depth ratio, but to a lesser extent, ranging for $\lambda = 1$ from 1.9097 to 1.2119 and for $\lambda = 0.5$ from 1.6586 to 1.1107.

For the clay (linear) soil profiles with the SSI-SSI reference model for the control system, the results show that the maximum displacement ratio under the earthquake suite with different slender ratios (both $\lambda = 1$ and $\lambda = 0.5$) decreased with an increase in the shear modulus, ranging for $\lambda = 1$ from 3.5617 to 1.3173 and for $\lambda = 0.5$ from 2.0406 to 1.1821; however, the displacement ratio increased with an increase in the slender ratio. Similarly, for the fixed-SSI reference model, the maximum displacement ratio decreased with an increase in the shear modulus, but to a lesser extent, ranging for $\lambda = 1$ from 3.3727 to 1.2736 and for $\lambda = 0.5$ from 2.0009 to 1.1427.

For the sand (parabolic) soil profiles with the SSI-SSI reference model for the control system, the results show that the maximum displacement ratio under the earthquake suite

with different slender ratios (both $\lambda = 1$ and $\lambda = 0.5$) decreased with an increase in the shear modulus, ranging for $\lambda = 1$ from 3.2094 to 1.2517 and for $\lambda = 0.5$ from 1.9964 to 1.1446; however, the displacement ratio increased with an increase in the slender ratio. Similarly, for the fixed-SSI reference model, the maximum displacement ratio decreased with an increase in the shear modulus, but to a lesser extent, ranging for $\lambda = 1$ from 2.9926 to 1.2016 and for $\lambda = 0.5$ from 1.8891 to 1.1042. The figures illustrating the displacement ratios for all soil profiles are available in Appendix A.

For structural parametric study with the SSI-SSI reference model for the control system, the results indication that the maximum displacement ratio under the earthquake suite with different slender ratios (both $\lambda = 1$ and $\lambda = 0.5$) decreased with an increase in the period of fixed base structure (Ts), ranging for $\lambda = 1$ from 2.6404 to 1.3031 and for $\lambda = 0.5$ from 2.6223 to 1.2433; however, the displacement ratio increased with an increase in the slender ratio. Similarly, for the fixed-SSI reference model, the maximum displacement ratio decreased with an increase in the period of fixed base structure (Ts), but to a lesser extent, ranging for $\lambda = 1$ from 2.6157 to 1.1727 and for $\lambda = 0.5$ from 2.5387 to 1.1298. The figures illustrating the displacement ratios are available in Appendix A.

### 6.13.3 Normalization of Foundation Results

The results indicate that the SAC algorithm and MR damper can effectively reduce the response of the foundation. For geotechnical parametric study, the medium top and soft bottom soil profiles with the SSI-SSI reference model for the control system, the results show that the maximum horizontal and rocking displacement ratios of the foundation under

the earthquake suite with different slender ratios (both $\lambda = 1$ and $\lambda = 0.5$) decreased with an increase in the depth ratio; variations in the horizontal displacement ratio ranged for $\lambda = 1$ from 0.9390 to 0.4566 and for $\lambda = 0.5$ from 0.8801 to 0.4270. Variations in the rocking ratio ranged for $\lambda = 1$ from 0.9654 to 0.4369 and for $\lambda = 0.5$ from 0.8641 to 0.3960. However, the horizontal and rocking displacement ratios of the foundation increased with an increase in the slenderness ratio. Similarly, for the fixed-SSI reference model, the maximum horizontal and rocking displacement ratios of the foundation decreased with an increase in the shear modulus; variations in the horizontal displacement ratio ranged for $\lambda = 1$ from 0.9376 to 0.4335 and for $\lambda = 0.5$ from 0.8771 to 0.3968. Variations in the rocking ratio ranged for $\lambda = 1$ from 0.9594 to 0.4114 and for $\lambda = 0.5$ from 0.8660 to 0.3645. However, the responses of the fixed-SSI reference model were less than the responses of the SSI-SSI reference model.

For the soft top and medium bottom soil profiles with the SSI-SSI reference model for the control system, the results show that the maximum horizontal and rocking displacement ratios of the foundation under the earthquake suite with different slender ratios (both $\lambda = 1$ and $\lambda = 0.5$) increased with an increase in the depth ratio. Variations in the horizontal displacement ratio ranged for $\lambda = 1$ from 0.89854 to 0.4750 and for $\lambda = 0.5$ from 0.8681 to 0.4282. Variations in the rocking ratio ranged for $\lambda = 1$ from 0.92265 to 0.4485 and for $\lambda = 0.5$ from 0.8301 to 0.4031. However, the displacement and rocking ratios of the foundation increased with an increase in the slenderness ratios. Similarly, for the fixed-SSI reference model, the maximum horizontal and rocking displacement ratios of the foundation decreased with an increase in the shear modulus. Variations in the horizontal displacement ratio ranged for $\lambda = 1$ from 0.8963 to 0.4496 and for $\lambda = 0.5$ from 0.8616 to 0.3998. Variations

in the rocking ratio ranged for $\lambda = 1$ from 0.9182 to 0.4209 and for $\lambda = 0.5$ from 0.8287 to 0.3701. However, the responses of the fixed-SSI reference model were less than the responses of the SSI-SSI reference model.

For the clay (linear) soil profiles with the SSI-SSI reference model for the control system, the results show that the maximum horizontal and rocking displacement ratios of the foundation under the earthquake suite with different slender ratios (both $\lambda = 1$ and $\lambda = 0.5$) decreased with an increase in the shear modulus. Variations in the horizontal displacement ratio ranged for $\lambda = 1$ from 1.0005 to 0.5282 and for $\lambda = 0.5$ from 0.8709 to 0.4616. Variations in the rocking ratio ranged for $\lambda = 1$ from 1.0136 to 0.5028 and for $\lambda = 0.5$ from 0.8945 to 0.4401. However, the displacement and rocking ratios of the foundation increased with an increase in the slenderness ratio. Similarly, for the fixed-SSI reference model, the maximum horizontal and rocking displacement ratios of the foundation decreased with an increase in the shear modulus. Variations in the horizontal displacement ratio ranged for $\lambda = 1$ from 1.0036 to 0.5080 and for $\lambda = 0.5$ from 0.8633 to 0.4304. Variations in the rocking ratio ranged for $\lambda = 1$ from 1.0195 to 0.4785 and for $\lambda = 0.5$ from 0.8837 to 0.4055. However, the responses of the fixed-SSI reference model were less than the responses of the SSI-SSI reference model.

For the sand (parabolic) soil profiles with the SSI-SSI reference model for the control system, the results show that the maximum horizontal and rocking displacement ratios of the foundation under the earthquake suite with different slender ratios (both $\lambda = 1$ and $\lambda = 0.5$) decreased with an increase in the shear modulus. Variations in the horizontal displacement ratio ranged for $\lambda = 1$ from 0.9838 to 0.5028 and for $\lambda = 0.5$ from 0.8353 to 0.4381. Variations

in the rocking ratio ranged for λ = 1 from 0.9861 to 0.4769 and for λ = 0.5 from 0.8194 to 0.4144. However, the displacement and rocking ratios of the foundation increased with an increase in the slenderness ratio. Similarly, for the fixed-SSI reference model, the maximum horizontal and rocking displacement ratios of the foundation decreased with an increase in the shear modulus. Variations in the horizontal displacement ratio ranged for λ = 1 from 0.9848 to 0.4764 and for λ = 0.5 from 0.8630 to 0.4083. Variations in the rocking ratio ranged for λ = 1 from 0.9873 to 0.4451 and for λ = 0.5 from 0.8312 to 0.3803. However, the responses of the fixed-SSI reference model were less than the responses of the SSI-SSI reference model. The figures for all soil profiles are available in Appendix B.

For structural parametric study with the SSI-SSI reference model for the control system, the results indication that the maximum horizontal and rocking displacement ratios of the foundation under the earthquake suite with different slender ratios (both λ = 1 and λ = 0.5) increased with an increase in the period of fixed base structure (Ts). Variations in the horizontal displacement ratio ranged for λ = 1 from 2.2561 to 0.5786 and for λ = 0.5 from 2.2313 to 0.3161. Variations in the rocking ratio ranged for λ = 1 from 2.4523 to 0.3727 and for λ = 0.5 from 2.1306 to 0.4225. However, the displacement and rocking ratios of the foundation increased with an increase in the slenderness ratio. Similarly, for the fixed-SSI reference model, the maximum horizontal and rocking displacement ratios of the foundation increased with an increase in the period of fixed base structure (Ts). Variations in the horizontal displacement ratio ranged for λ = 1 from 2.4630 to 0.4362 and for λ = 0.5 from 2.4190 to 0.3036. Variations in the rocking ratio ranged for λ = 1 from 2.7113 to 0.3866 and for λ = 0.5 from 2.2777 to 0.2694. However, the responses of the fixed-SSI reference model

were less than the responses of the SSI-SSI reference model. The horizontal and rocking displacement ratios of the foundation when greater than one, which means the response of the control system greater than uncontrolled. It comes from the effect of control force on the foundation. The figures are available in Appendix B.

### 6.13.4 Performance Evaluation Criteria

The results of the performance evaluation criteria obtained in the parametric study for the SDOF with the fixed-base support and SSI systems with different soil profiles are presented and discussed below. Tables give the J1, J3, J4, J6, and J8 performance criteria values for the soil profiles are available in Appendix C.

The results of the J1, J3, J6, and J8 performance criteria indicate that the fixed-SSI reference model was more effective than the SSI-SSI reference model in reducing response, but with more control force (J4 for the fixed-SSI was greater than J4 for the SSI-SSI) for all soil profiles. The efficiency of the SAC algorithm decreased with an increase in the slenderness ratio ($\lambda$). Moreover, the SAC algorithm's efficiency increased with an increase in the soil stiffness and it increased with an increase in the period ratio of fixed base structure (Ts).

# 7. SMART FRAME AND FRAME SHEAR WALL SYSTEMS

## 7.1 Introduction

This section emphasizes the modeling and analysis of dynamic soil structure interaction (SSI) systems for three-dimensional multi-story buildings with frame and frame shear wall systems. The SAC algorithm and MR dampers were employed to investigate the performers and their efficiency levels. Two types of reference model (i.e., fixed and SSI) are presented to identify differences in maintaining structures during hazard load. Additionally, four soil profiles were used in this study.

## 7.2 Description of The Structural Models

The structural models adopted here were frame and frame shear wall systems employed in the previous literature (Shiming & Gang, 1998). Figure 7-1 shows these two types of structural system. Each had the same plan, and all buildings had 12 stories. The height of each floor was 3.6 m. The raft foundation was 32.4 m long, 17.7 m wide, and 0.8 m thick. The sizes of the cross-sections of the beams, columns, and shear walls are shown in Table 7-1 and Table 7-2. Table 7-3 displays the strengths of the concrete for each floor. Figure 7-2 and Figure 7-3 demonstrate the three-dimensional finite-element models of the frame and frame shear wall buildings in ETABS (version 18). The models were represented by three-dimensional beam elements; shell elements were used to model the beams, columns, walls, and slabs. Using the inverse flexibility matrix method (see Chapter 5), all element stiffness matrices were obtained from the finite element model and summed at the

mass center of the diaphragm to estimate the equivalent global stiffness matrix. The natural damping of the building was a function of the stiffness and mass matrices of the structural and SSI systems. The Raleigh damping method was adopted to estimate the damping matrices, assuming a 2% modal damping ratio in the first and second modes for the fixed and SSI systems. Figure 7-4 and Figure 7-5 display the mode shapes determined for the frame and frame shear wall buildings with fixed support, and Table 7-4 presents their modal characteristics. In this research, a linear model of the building was adopted for dynamic analysis. The finite element method was employed to determine the equivalent soil stiffness matrix using the ABAQUS finite element software package to calculate the equivalent stiffness matrices of the various soil profiles (see Chapter 5). The soil-foundation interface surface was modeled by a tie element in ABAQUS. The rigid foundation was simulated by a three-dimensional rigid element and soil media formed as a three-dimensional brick element. Lastly, the SSI model was imported to a control scheme under two earthquake ground motions and four different soil profiles in order to study the variability of the responses of the controlled and uncontrolled systems (see Chapter 5). Then, all data were input into MATLAB and SIMULINK (R2019b) software to produce the final results.

**Table 7-1** Cross-section of beams and column for frame structure.

| Floor | Column (mm) | Beam 1 | Beam 2 |
|---|---|---|---|
| 1~3 | 400X700 | 250X700 | 250X400 |
| 4~6 | 400X 600 | 250X700 | 250X400 |
| 7~12 | 400X500 | 250X700 | 250X400 |

**Table 7-2** Cross-section of beams, column, and shear wall for frame shear wall structure.

| Floor | Column (mm) | Thickness of Shear-wall (mm) | Beam 1 | Beam 2 |
|---|---|---|---|---|
| 1~4 | 400X700 | 200 | 250X700 | 250X400 |
| 5~7 | 400X 600 | 200 | 250X700 | 250X400 |
| 8~12 | 400X500 | 180 | 250X700 | 250X400 |

**Table 7-3** Strengths of concrete.

| Floor | 1~4 | 5~7 | 8~12 |
|---|---|---|---|
| Grade of Concrete | C35 | C30 | C25 |

**Table 7-4** Time period per building.

| Period | T1 | T2 | T3 | T4 | T5 | T6 | T7 | T8 | T9 |
|---|---|---|---|---|---|---|---|---|---|
| Frame shear wall building system | 1.183 | 0.719 | 0.539 | 0.326 | 0.183 | 0.152 | 0.136 | 0.092 | 0.085 |
| Frame building system | 1.636 | 1.488 | 1.349 | 0.572 | 0.515 | 0.473 | 0.336 | 0.296 | 0.276 |

## 7.3 Equation of motion

The equation of motion 5.7 of three dimensional frame and frame Shear wall Systems with fixed base under seismic loading can be rewritten as:

$$[\boldsymbol{M_s}]\{\ddot{\boldsymbol{q}}\} + [\boldsymbol{C_s}]\{\dot{\boldsymbol{q}}\} + [\boldsymbol{K_s}]\{\boldsymbol{q}\} = -[\boldsymbol{M_s}]\{\boldsymbol{E}\}\ddot{\boldsymbol{q}}_{\boldsymbol{g}} \qquad 7\text{-}1$$

where [Ms], [Cs], and [Ks] are the mass, damping, and stiffness matrices of the building, respectively; $\{E\}$ is a vector with elements equal to one; and $\ddot{q}_g$ is the ground acceleration.

$$[M_s] = \begin{bmatrix} [m] & [0] & [0] \\ [0] & [m] & [0] \\ [0] & [0] & [J] \end{bmatrix}$$ (36X36 dimension)

$[m]$ is the mass of the inertial slab matrix (diagonal matrix) in the X and Y directions (12X12 dimension) which calculated using ETABS 18; and

$[J]$ is the mass torsion of the inertial slab matrix (diagonal matrix) (12X12 dimension) which calculated using ETABS 18.

$[K_s] = \begin{bmatrix} [K_{xx}] & [K_{xy}] & [K_{x\theta}] \\ [K_{yx}] & [K_{yy}] & [K_{y\theta}] \\ [K_{\theta x}] & [K_{\theta y}] & [K_{\theta\theta}] \end{bmatrix}$ (36X36 dimension) calculated using ETABS 18.

$[C_S] = \alpha[M_S] + \beta[K_S]$ Rayleigh damping (36X36 dimension)

SSI is introduced for three diminution into the model by adding five stiffness components two horizontal (Kx, and Ky), two rocking (Kφφ and Kθθ) , and torsional (Kt ) (the foundation's degree of freedom). System response is now governed by Equation 5.8, which now becomes:

$$[\boldsymbol{M_{SSI}}]\{\ddot{\boldsymbol{q}}_{\boldsymbol{SSI}}\} + [\boldsymbol{C_{SSI}}]\{\dot{\boldsymbol{q}}_{\boldsymbol{SSI}}\} + [\boldsymbol{K_{SSI}}]\{\boldsymbol{q}_{\boldsymbol{SSI}}\} = -\{\boldsymbol{E_{SSI}}\}\ddot{\boldsymbol{q}}_{\boldsymbol{g}} \quad 7\text{-}2$$

where:

$[M_{SSI}] = \begin{bmatrix} [M_s] & [MH] \\ [MH]^T & [M_f] \end{bmatrix}$ (41X41 dimension), $[MH] = \begin{bmatrix} \{m\} & \{0\} & \{0\} & \{mh\} & \{0\} \\ \{0\} & \{m\} & \{0\} & \{0\} & \{mh\} \\ \{0\} & \{0\} & \{J\} & \{0\} & \{0\} \end{bmatrix}$

(41X5 dimension)

$\{m\} = \{m_1, m_2, \dots, m_{12}\}^T$ , $\{mh\} = \{m_1h_1, m_2h_2, \dots, m_{12}h_{12}\}^T$, $\{J\} = \{J_1, J_2, \dots, J_{12}\}^T$

$[M_f] = \begin{bmatrix} S1 & 0 & 0 & S2 & 0 \\ 0 & S1 & 0 & 0 & S2 \\ 0 & 0 & S3 & 0 & 0 \\ S2 & 0 & 0 & S4 & 0 \\ 0 & S2 & 0 & 0 & S5 \end{bmatrix}$ (5X5 dimension)

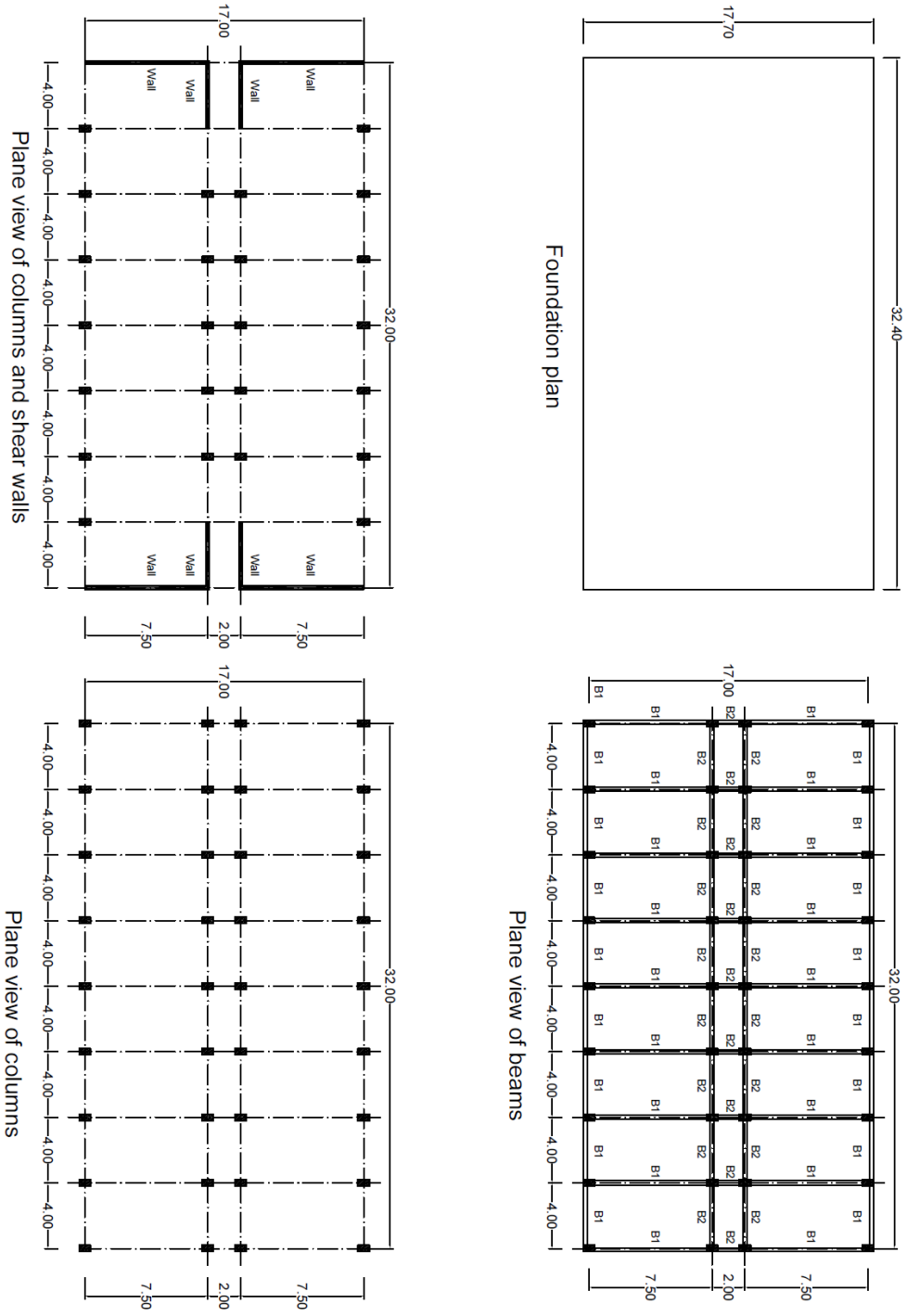


**Figure 7-1** Structural systems.

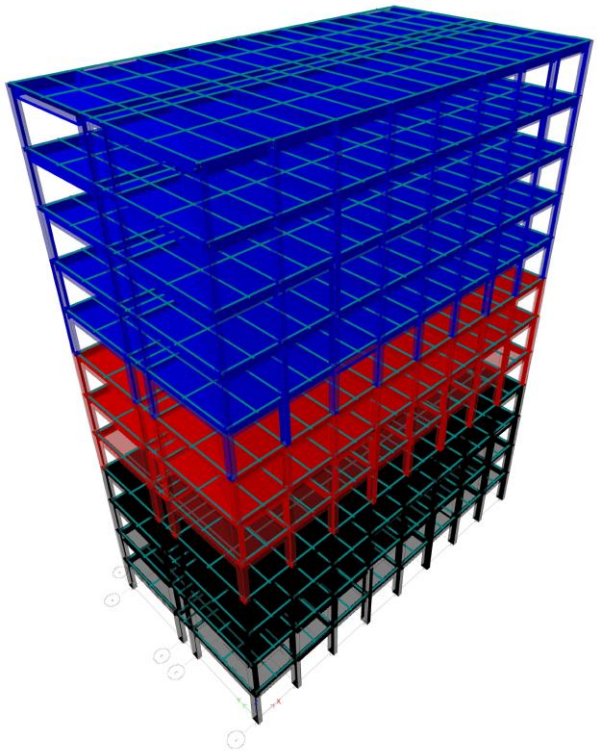

**Figure 7-2** Finite element mode of the frame building using ETABS 18.

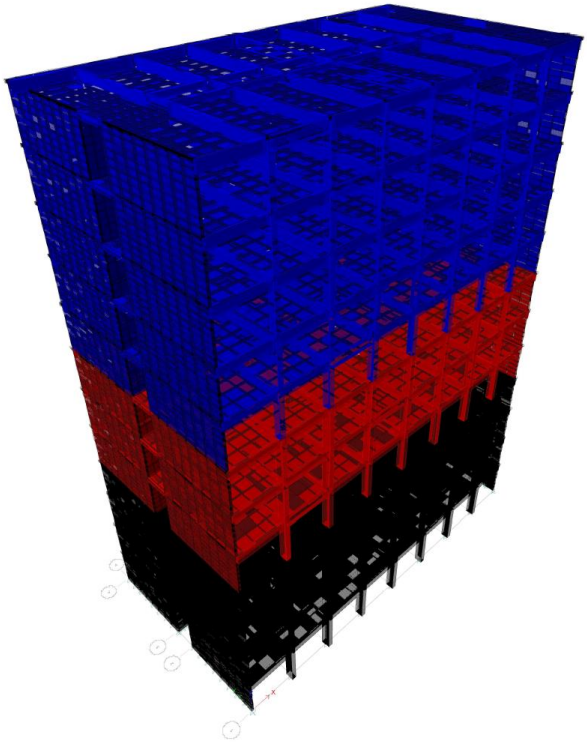

**Figure 7-3** Finite element mode of the frame shear wall building using ETABS 18.

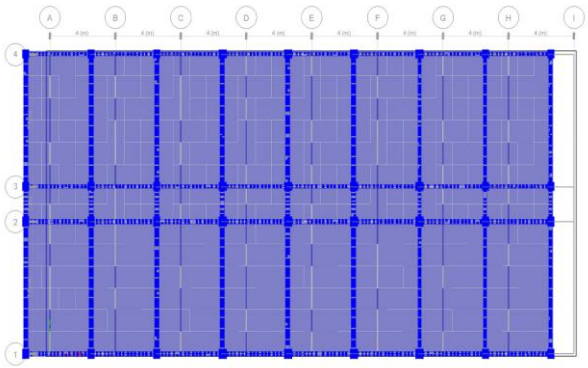

A) Top view of Mode 1: period 1.636

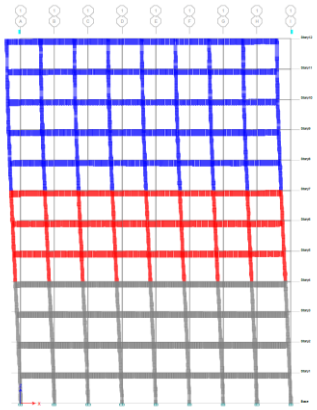

B) Side view of Mode 1: period 1.636

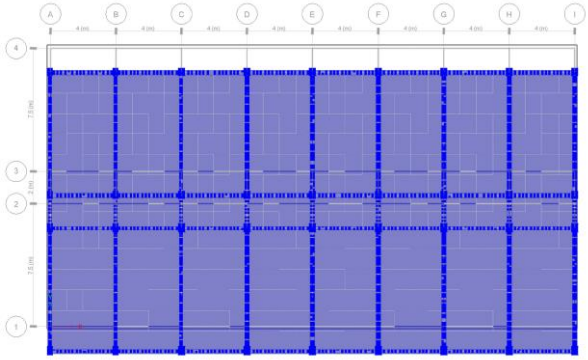

C) Top view of Mode 2: period 1.488

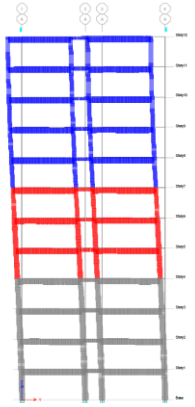

D) Side view of Mode 2: period 1.488

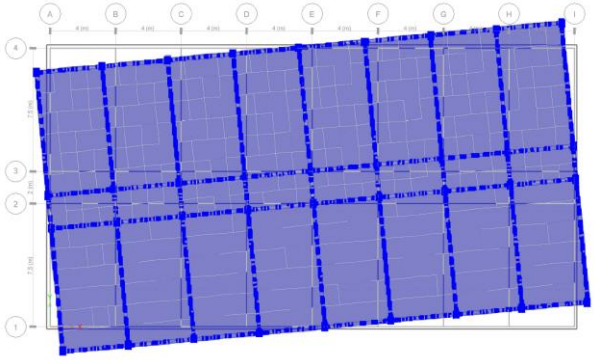

E) Top view of Mode 3: period 1.349

**Figure 7-4** Mode shapes for the frame wall building using ETABS 18.

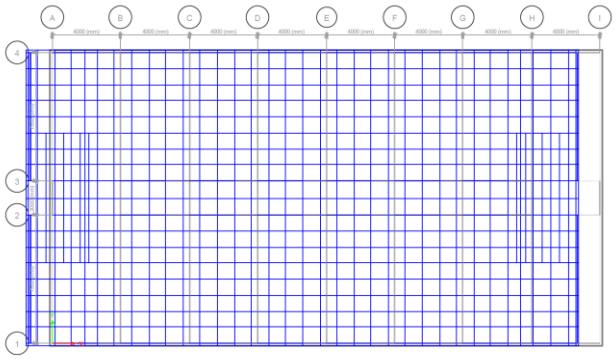

A) Top view of Mode 1: period 1.183

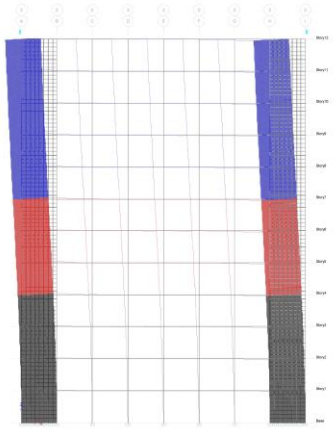

B) Side view of Mode 1: period 1.183

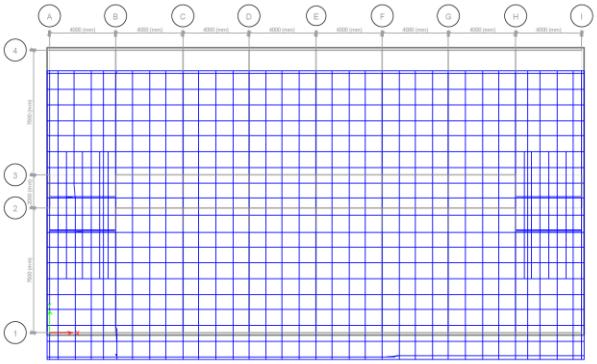

C) Top view of Mode 2: period 0.719

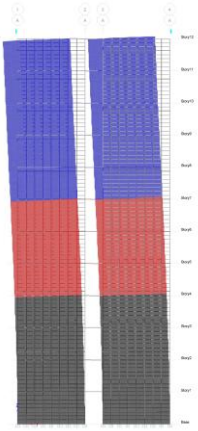

D) Side view of Mode 2: period 0.719

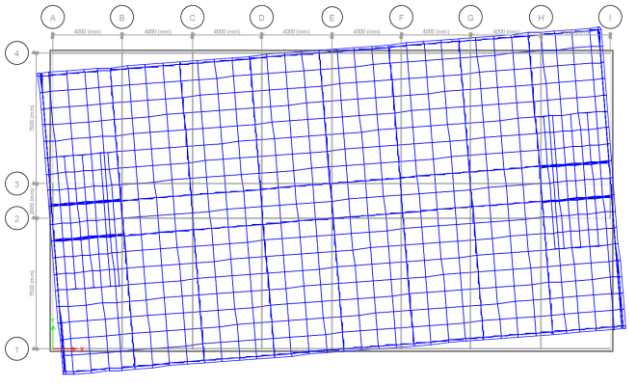

E) Top view of Mode 3: period 0.539

**Figure 7-5** Mode shapes for the frame shear wall building using ETABS 18.

$S1 = m_f + \sum_{i=1}^{12} m_i$ , $S2 = \sum_{i=1}^{12} m_i h_i$ , $S3 = J_f + \sum_{i=1}^{12} J_i$ ,

$S4 = I_{yf} + \sum_{i=1}^{12} I_{yi} m_i h_i^2$ , $S5 = I_{xf} + \sum_{i=1}^{12} I_{xi} m_i h_i^2$

where:

$[M_{SSI}] = \begin{bmatrix} [M_s] & [MH] \\ [MH]^T & [M_f] \end{bmatrix}$ (41X41 dimension), $[MH] = \begin{bmatrix} \{m\} & \{0\} & \{0\} & \{mh\} & \{0\} \\ \{0\} & \{m\} & \{0\} & \{0\} & \{mh\} \\ \{0\} & \{0\} & \{J\} & \{0\} & \{0\} \end{bmatrix}$

(41X5 dimension)

$\{m\} = \{m_1, m_2, \dots, m_{12}\}^T$ , $\{mh\} = \{m_1 h_1, m_2 h_2, \dots, m_{12} h_{12}\}^T$, $\{J\} = \{J_1, J_2, \dots, J_{12}\}^T$

$[M_f] = \begin{bmatrix} S1 & 0 & 0 & S2 & 0 \\ 0 & S1 & 0 & 0 & S2 \\ 0 & 0 & S3 & 0 & 0 \\ S2 & 0 & 0 & S4 & 0 \\ 0 & S2 & 0 & 0 & S5 \end{bmatrix}$ (5X5 dimension)

$S1 = m_f + \sum_{i=1}^{12} m_i$ , $S2 = \sum_{i=1}^{12} m_i h_i$ , $S3 = J_f + \sum_{i=1}^{12} J_i$ ,

$S4 = I_{yf} + \sum_{i=1}^{12} I_{yi} m_i h_i^2$ , $S5 = I_{xf} + \sum_{i=1}^{12} I_{xi} m_i h_i^2$

$m_f$ is the foundation mass

$m_i$ is the mass slab of i floor

$h_i$ is the height of i floor (from ground to center of floor see Figure 5-2)

$I_{yf}$, $I_{xf}$ , and $J_f$ foundation mass moment of inertia in x, y, and z directions respectively

$I_{yi}$, $I_{xi}$ , and $J_i$ slab mass moment of inertia of i floor in x, y, and z directions respectively

$[K_{SSI}] = \begin{bmatrix} [K_s] & [0] \\ [0] & [K_{soil}] \end{bmatrix}$ (41X41 dimension)

$[K_{soil}] = diagonal[k_{xx} \quad k_{yy} \quad k_t \quad k_{\varphi\varphi} \quad k_{\vartheta\vartheta}]$ (5X5 dimension)

kxx and kyy are the equivalent soil stiffnesses in the X and Y directions, respectively.

kt is the equivalent torsion soil stiffness in the Z direction.

$k_{\varphi\varphi}$ and $k_{\vartheta\vartheta}$ are the equivalent moment soil stiffnesses in the X and Y direction, respectively.

$[C_{SSI}] = \alpha[M_{SSI}] + \beta[K_{SSI}]$ Rayleigh damping (41X41 dimension)

$\{E_{SSI}\} = \{\{m\}, \{m\}, \{J\}, S1, S1, S3, S2, S2\}^T$ (41X1 dimension)

$\{q_{SSI}\}^T =$

$\{x_1 \quad x_2 \quad \cdots \quad x_{12}, \quad y_1 \quad y_2 \quad \cdots \quad y_{12}, \quad \theta_1 \quad \theta_2 \quad \cdots \quad \theta_{12}, x_f \quad y_f \quad \theta_f \quad \varphi_{xf} \quad \varphi_{yf}\}^T$

(41X1 dimension) displacement vector

## 7.4 The Case Studies

The following summary of the case studies adopted in this chapter are:

- The earthquake suite (two earthquake see section 7.6)
- The geotechnical case studies (four soil profiles see section 7.7)
- The control cases for SAC algorithm (two cases of reference model, Fixed – SSI and SSI – SSI, see sections 7.8 and 7.9)
- The structure cases studies (frame and frame shear wall structural systems see Figure 7-1)

## 7.5 The Parametric Studies

The geotechnical parameters are

- Depth ratio, Z/B (0, 0.1, 0.25, 0.5, 1, and 1.25) for soil layers profiles.

- The surface shear modulus, Ga (15, 25, 35, 50, 70, and 100 MPa) for sand and clay soil profiles.

## 7.6 Earthquake Suite

To assess the effectiveness of the simple adaptive control, two different earthquakes were applied to the frame and frame shear wall systems, including SSI effects (see Figure 7-1). The earthquakes were attributed various intrinsic characteristics. Figure 7-6 displays their acceleration time histories. Two earthquake motions recorded on different types of soil profile were used in the time history simulations. The records were constrained as follows: (i) magnitudes ranged from 5.2 to 6.6, (ii) closest source-to-site distance was 5 to 7.15 km, and (iii) peak ground acceleration (PGA) was between 2.2911E-01 and 2.5588E-01 (g). A review of the basic earthquake properties is included in Table 7-5.

**Table 7-5** Earthquake characteristics.

| Name | RNS | Year | Station | Magnitude | PGA (g) | Hypocenter depth (km) |
|---|---|---|---|---|---|---|
| Managua, Nicaragua-02 | 96 | 1972 | Managua, ESSO | 5.2 | 2.2911E-01 | 5 |
| Corinth, Greece | 313 | 1981 | Corinth | 6.6 | 2.5588E-01 | 7.15 |

## 7.7 Geotechnical Parametric Studies

Soil profiles describe changes in soil property with depth. In this section, soil layer, linear (i.e., clay), and parabolic (i.e., sand) profiles were adopted to model variations in soil stiffness with depth. The first two soil profiles consisted of two layers, soft and medium,

with different arrangements; the second two soil profiles modeled the shear moduli of the soil varieties: parabolic for sand and linear for clay. Figure 7-7, Figure 7-8, Figure 7-13, and Figure 7-14 show these soil profiles. The equivalent soil stiffness matrix $[K_{soil}]$ of the rigid foundation were calculated by the ABAQUS finite element software and written as a 5 x 5 diagonal matrix (see Chapter 5).

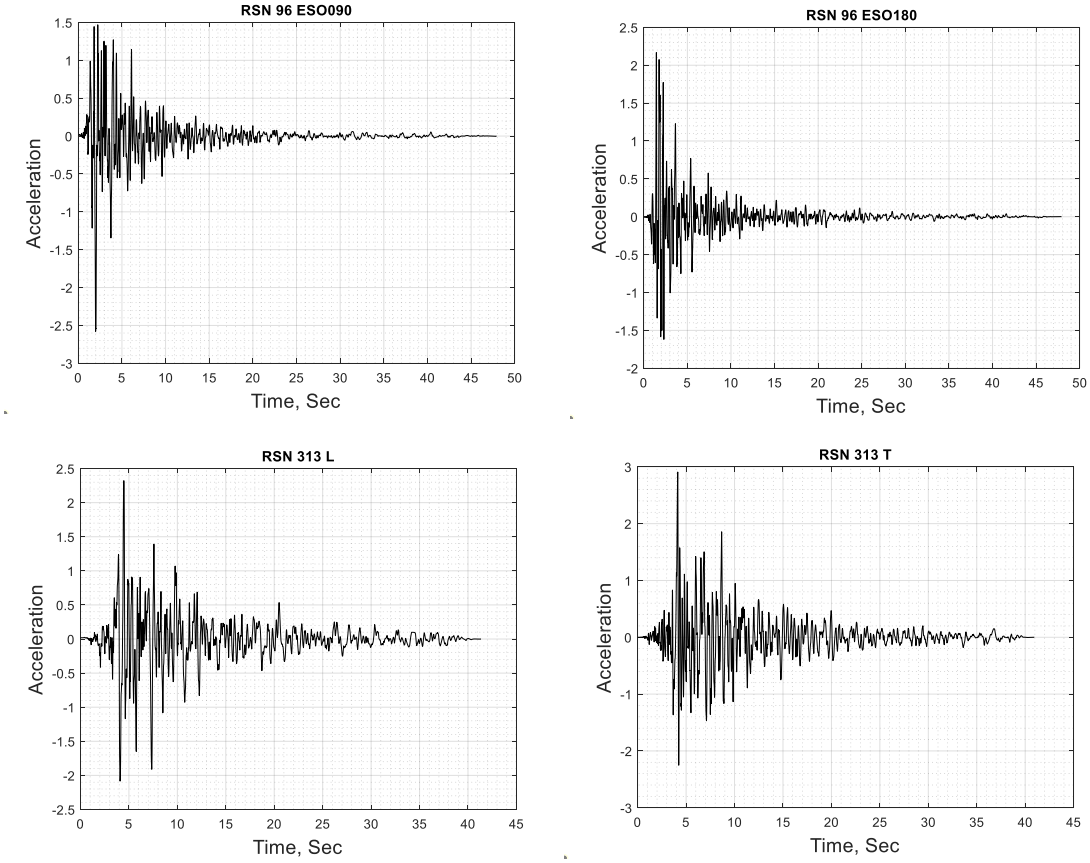


**Figure 7-6** Acceleration time history of the earthquake suite in two directions.

$$[\boldsymbol{K_{soil}}] = \boldsymbol{diagonal}[\boldsymbol{k_{xx}} \quad \boldsymbol{k_{yy}} \quad \boldsymbol{k_t} \quad \boldsymbol{k_{\varphi\varphi}} \quad \boldsymbol{k_{\vartheta\vartheta}}] \qquad 7\text{-}3$$

where: kxx and kyy are the equivalent soil stiffnesses in the X and Y directions, respectively. kt is the equivalent torsion soil stiffness in the Z direction. $k_{\varphi\varphi}$ and $k_{\vartheta\vartheta}$ are the equivalent moment soil stiffnesses in the X and Y direction, respectively.

### 7.7.1 The Soil Layer Profiles Cases

Common soil profiles consisting of medium top and soft bottom or soft top and medium bottom layers were investigated. Figure 7-7 and Figure 7-8 display the soil profiles considered. The simulation of the finite element analysis assumed a rectangular foundation with a 32.4 m length, 17.7 m width, and 0.8 m thickness; the soil stiffness properties varied with increases in depth ratio (Z/B). Figure 7-9 and Figure 7-10 present the variations in elements of the equivalent soil stiffness matrices by depth ratio for the two types of soil.

Table 7-6 and Table 7-7 and Figure 7-11 summarize the relationships among the system parameters and effect of variations by depth ratio (Z/B) for the time period ratios of the medium top and soft bottom layer system. As seen in Figure 7-10, an increase in the depth ratio led to in a decrease in the time period ratio. Furthermore, an increase in the structure stiffness led to an increase in the fundamental time period ratio (i.e., the time period ratio of the frame shear wall building system was greater than that of the frame building system). Similarly, for the soft top and medium bottom layer soil profiles, Table 7-8 and Table 7-9 and Figure 7-12 show that an increase in the depth ratio led to an increase in the fundamental time period ratio, while an increase in the structure's stiffness led to an increase in the time period ratio.

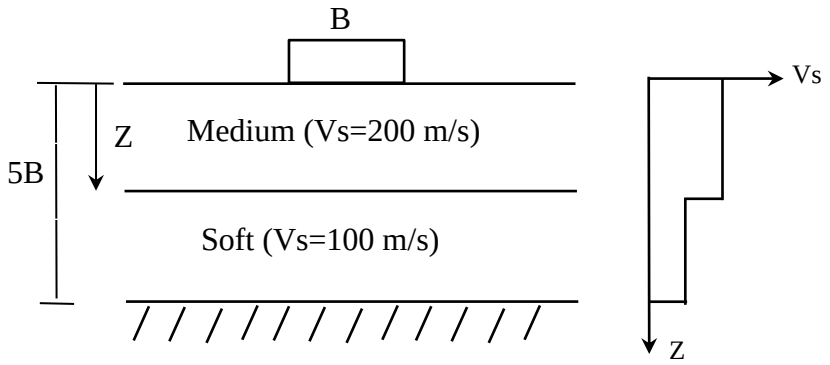


**Figure 7-7** Soil profile of the medium top and soft bottom layers.

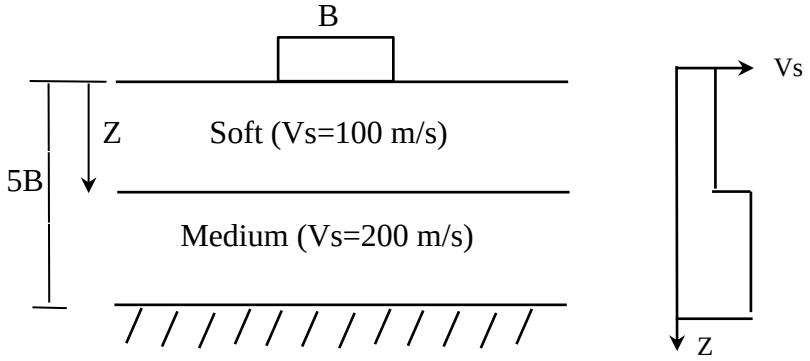


**Figure 7-8** Soil profile of the soft top and medium bottom layers.

where: B = the width of the foundation, Z = the thickness of the first layer, the total thickness of the soil (5B), and Z/B = the normalized thickness of first layer.

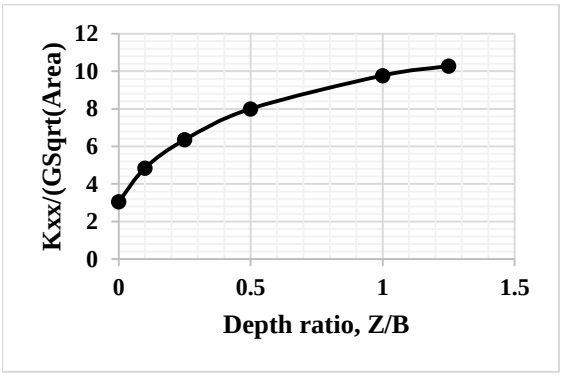


a) Horizontal stiffness of soil in the X direction

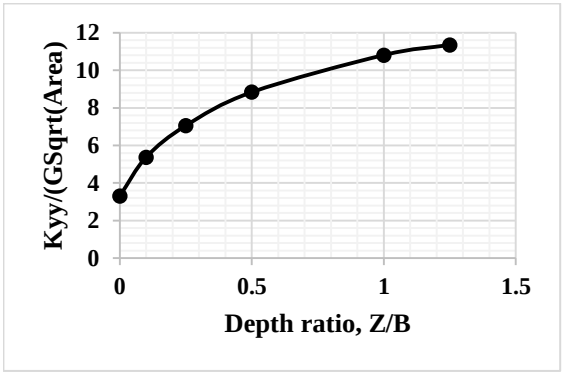


b) Horizontal stiffness of soil in the Y direction

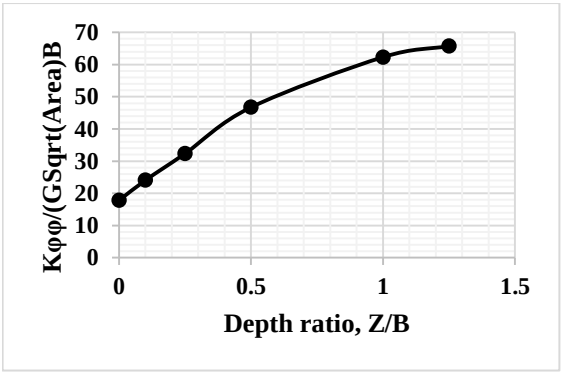


c) Rocking stiffness of soil in the X direction

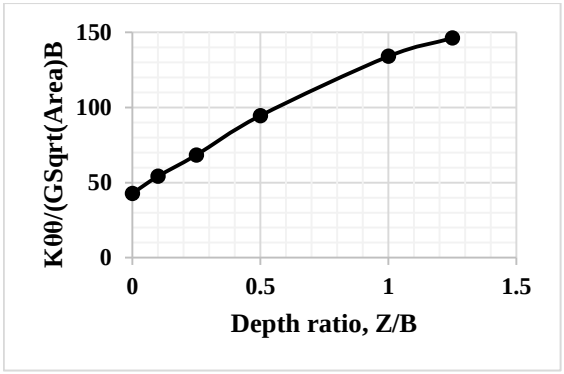


d) Rocking stiffness of soil in the Y direction

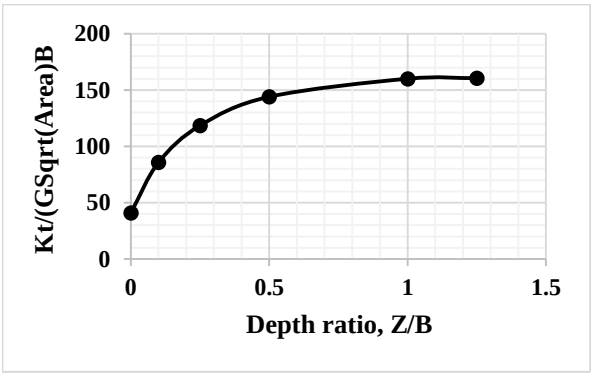


d) Torsion stiffness of soil in the Z direction

**Figure 7-9** Stiffness matrix elements for the soil profile of medium top and soft bottom layers.

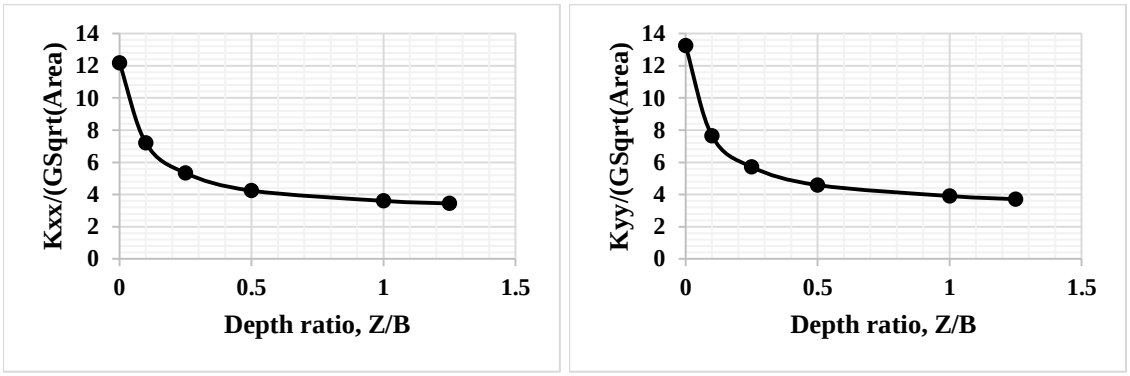


a) Horizontal stiffness of soil in the X direction b) Horizontal stiffness of soil in the Y direction

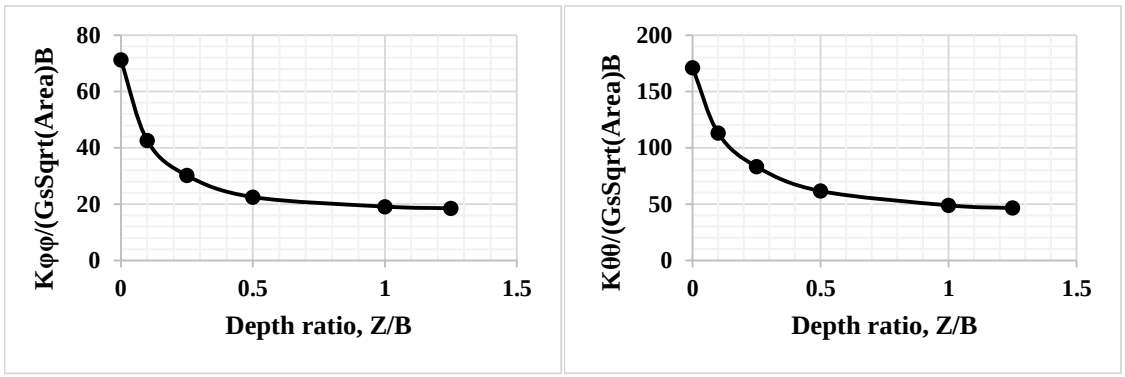


c) Rocking stiffness of soil in the X direction d) Rocking stiffness of soil in the Y direction

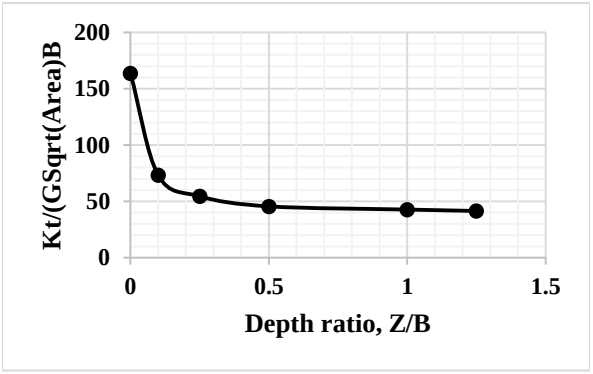


d) Torsion stiffness of soil in the Z direction

**Figure 7-10** Stiffness matrix elements for the soil profile of soft top and medium bottom layers.

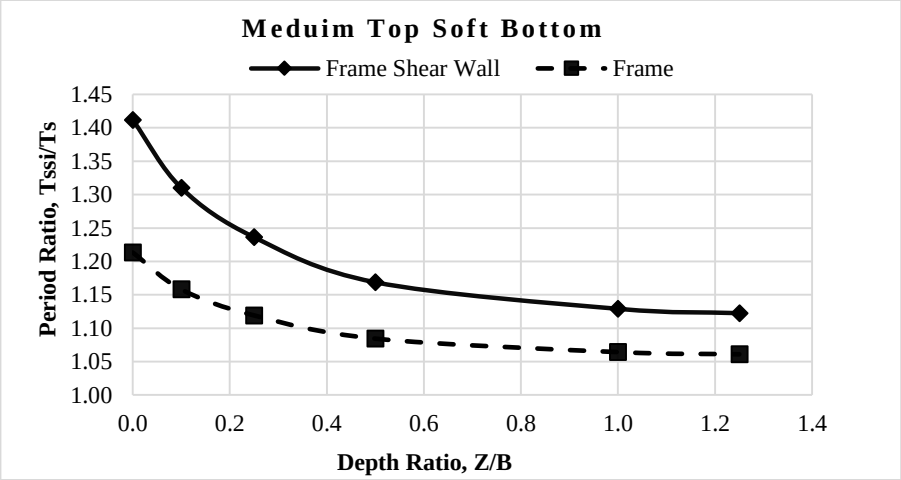


**Figure 7-11** Period ratio (the fundamental period of the SSI mode to fundamental period of the fixed support structure) to the depth ratio of a medium top and soft bottom layer of soil.

**Table 7-6** Period ratios for frame buildings on medium top and soft bottom layers.

| Z/B | $\frac{\bar{T}_1}{T_1}$ | $\frac{\bar{T}_2}{T_2}$ | $\frac{\bar{T}_3}{T_3}$ | $\frac{\bar{T}_4}{T_4}$ | $\frac{\bar{T}_5}{T_5}$ | $\frac{\bar{T}_6}{T_6}$ | $\frac{\bar{T}_7}{T_7}$ | $\frac{\bar{T}_8}{T_8}$ | $\frac{\bar{T}_9}{T_9}$ | $\frac{\bar{T}_{10}}{T_{10}}$ | $\frac{\bar{T}_{11}}{T_{11}}$ | $\frac{\bar{T}_{12}}{T_{12}}$ |
|---|---|---|---|---|---|---|---|---|---|---|---|---|
| 0.00 | 1.2133 | 1.1218 | 1.0180 | 1.0383 | 1.0412 | 1.0246 | 1.0733 | 1.1339 | 1.1780 | 1.1387 | 1.2153 | 1.2130 |
| 0.10 | 1.1581 | 1.0929 | 1.0085 | 1.0230 | 1.0242 | 1.0113 | 1.0368 | 1.0327 | 1.1516 | 1.1199 | 1.1879 | 1.1571 |
| 0.25 | 1.1192 | 1.0737 | 1.0062 | 1.0170 | 1.0181 | 1.0081 | 1.0238 | 1.0235 | 1.0342 | 1.1158 | 1.1775 | 1.1407 |
| 0.50 | 1.0844 | 1.0546 | 1.0051 | 1.0130 | 1.0143 | 1.0066 | 1.0166 | 1.0181 | 1.0070 | 1.0225 | 1.1288 | 1.1319 |
| 1.00 | 1.0643 | 1.0398 | 1.0046 | 1.0104 | 1.0116 | 1.0059 | 1.0127 | 1.0143 | 1.0063 | 1.0126 | 1.0171 | 1.1116 |
| 1.25 | 1.0610 | 1.0368 | 1.0045 | 1.0099 | 1.0110 | 1.0059 | 1.0120 | 1.0135 | 1.0063 | 1.0117 | 1.0161 | 1.0864 |

**Table 7-7** Period ratios for frame shear wall buildings on medium top and soft bottom layers.

| Z/B | $\frac{\bar{T}_1}{T_1}$ | $\frac{\bar{T}_2}{T_2}$ | $\frac{\bar{T}_3}{T_3}$ | $\frac{\bar{T}_4}{T_4}$ | $\frac{\bar{T}_5}{T_5}$ | $\frac{\bar{T}_6}{T_6}$ | $\frac{\bar{T}_7}{T_7}$ | $\frac{\bar{T}_8}{T_8}$ | $\frac{\bar{T}_9}{T_9}$ | $\frac{\bar{T}_{10}}{T_{10}}$ | $\frac{\bar{T}_{11}}{T_{11}}$ | $\frac{\bar{T}_{12}}{T_{12}}$ |
|---|---|---|---|---|---|---|---|---|---|---|---|---|
| 0.00 | 1.4118 | 1.4889 | 1.1273 | 1.1971 | 1.7781 | 1.9832 | 1.7187 | 2.3018 | 1.7922 | 2.0273 | 1.8898 | 1.7980 |
| 0.10 | 1.3101 | 1.3826 | 1.0584 | 1.1275 | 1.5963 | 1.7078 | 1.5593 | 1.8627 | 1.6567 | 1.9679 | 1.8098 | 1.6710 |
| 0.25 | 1.2362 | 1.3091 | 1.0417 | 1.0969 | 1.4477 | 1.5931 | 1.4677 | 1.7239 | 1.5574 | 1.9146 | 1.7176 | 1.5870 |
| 0.50 | 1.1688 | 1.2336 | 1.0341 | 1.0743 | 1.2737 | 1.5164 | 1.3978 | 1.6573 | 1.4705 | 1.8557 | 1.5744 | 1.5581 |
| 1.00 | 1.1290 | 1.1729 | 1.0306 | 1.0593 | 1.2002 | 1.3908 | 1.3451 | 1.6263 | 1.4002 | 1.7966 | 1.4228 | 1.5408 |
| 1.25 | 1.1225 | 1.1604 | 1.0305 | 1.0562 | 1.1900 | 1.3627 | 1.3331 | 1.6255 | 1.3843 | 1.7809 | 1.4099 | 1.5130 |

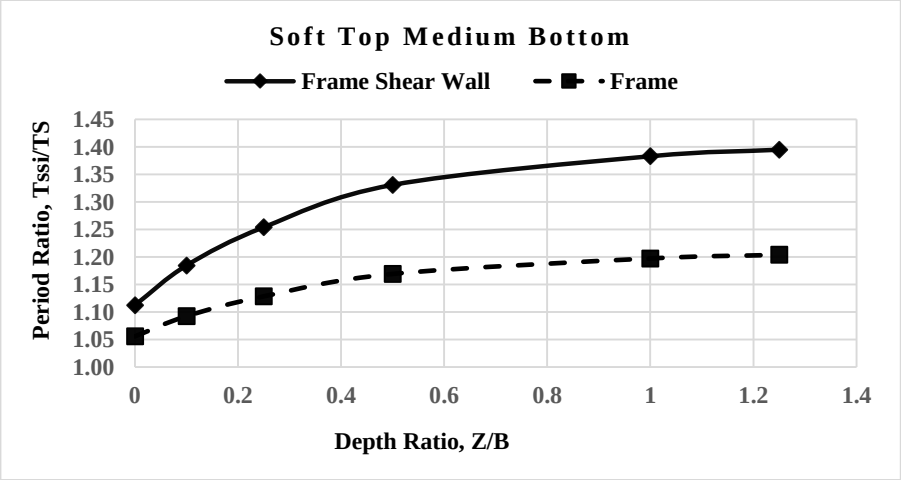


**Figure 7-12** Period ratio (the fundamental period of the SSI mode to fundamental period of the fixed support structure) to the depth ratio of a soft top and medium bottom layer.

**Table 7-8** Period ratios for frame buildings on soft top and medium bottom layers.

| Z/B | $\frac{\bar{T}_1}{T_1}$ | $\frac{\bar{T}_2}{T_2}$ | $\frac{\bar{T}_3}{T_3}$ | $\frac{\bar{T}_4}{T_4}$ | $\frac{\bar{T}_5}{T_5}$ | $\frac{\bar{T}_6}{T_6}$ | $\frac{\bar{T}_7}{T_7}$ | $\frac{\bar{T}_8}{T_8}$ | $\frac{\bar{T}_9}{T_9}$ | $\frac{\bar{T}_{10}}{T_{10}}$ | $\frac{\bar{T}_{11}}{T_{11}}$ | $\frac{\bar{T}_{12}}{T_{12}}$ |
|---|---|---|---|---|---|---|---|---|---|---|---|---|
| 0 | 1.0558 | 1.0315 | 1.0045 | 1.0083 | 1.0094 | 1.0058 | 1.0103 | 1.0114 | 1.0061 | 1.0095 | 1.0133 | 1.0505 |
| 0.1 | 1.0925 | 1.0488 | 1.0100 | 1.0145 | 1.0166 | 1.0133 | 1.0186 | 1.0205 | 1.0147 | 1.0383 | 1.1579 | 1.1371 |
| 0.25 | 1.1286 | 1.0657 | 1.0135 | 1.0202 | 1.0226 | 1.0181 | 1.0280 | 1.0286 | 1.0630 | 1.1292 | 1.1829 | 1.1524 |
| 0.5 | 1.1693 | 1.0865 | 1.0162 | 1.0264 | 1.0287 | 1.0219 | 1.0427 | 1.0571 | 1.1577 | 1.1347 | 1.1937 | 1.1704 |
| 1 | 1.1974 | 1.1066 | 1.0172 | 1.0319 | 1.0343 | 1.0235 | 1.0603 | 1.1094 | 1.1668 | 1.1370 | 1.2031 | 1.1888 |
| 1.25 | 1.2039 | 1.1119 | 1.0178 | 1.0336 | 1.0363 | 1.0242 | 1.0656 | 1.1192 | 1.1700 | 1.1381 | 1.2062 | 1.1958 |

**Table 7-9** Period ratios for frame shear wall buildings on soft top and medium bottom layers.

| Z/B | $\frac{\bar{T}_1}{T_1}$ | $\frac{\bar{T}_2}{T_2}$ | $\frac{\bar{T}_3}{T_3}$ | $\frac{\bar{T}_4}{T_4}$ | $\frac{\bar{T}_5}{T_5}$ | $\frac{\bar{T}_6}{T_6}$ | $\frac{\bar{T}_7}{T_7}$ | $\frac{\bar{T}_8}{T_8}$ | $\frac{\bar{T}_9}{T_9}$ | $\frac{\bar{T}_{10}}{T_{10}}$ | $\frac{\bar{T}_{11}}{T_{11}}$ | $\frac{\bar{T}_{12}}{T_{12}}$ |
|---|---|---|---|---|---|---|---|---|---|---|---|---|
| 0 | 1.1124 | 1.1382 | 1.0299 | 1.0479 | 1.1615 | 1.3219 | 1.2987 | 1.6200 | 1.3371 | 1.7271 | 1.3910 | 1.4901 |
| 0.1 | 1.1845 | 1.2101 | 1.0687 | 1.0827 | 1.3176 | 1.5630 | 1.4283 | 1.9420 | 1.5070 | 1.8839 | 1.5655 | 1.6358 |
| 0.25 | 1.2541 | 1.2779 | 1.0940 | 1.1133 | 1.4867 | 1.6797 | 1.5300 | 2.1088 | 1.6000 | 1.9506 | 1.6356 | 1.7588 |
| 0.5 | 1.3309 | 1.3586 | 1.1136 | 1.1436 | 1.6366 | 1.7875 | 1.6134 | 2.2199 | 1.6785 | 1.9886 | 1.7609 | 1.7847 |
| 1 | 1.3830 | 1.4334 | 1.1216 | 1.1680 | 1.7257 | 1.8783 | 1.6629 | 2.2729 | 1.7417 | 2.0097 | 1.8461 | 1.7929 |
| 1.25 | 1.3949 | 1.4530 | 1.1254 | 1.1755 | 1.7458 | 1.9099 | 1.6786 | 2.2925 | 1.7592 | 2.0149 | 1.8634 | 1.7964 |

For the frame and frame shear wall systems constructed on medium top and soft bottom soil profiles, the period ratio decreased with an increase in the depth ratio. Conversely, the soft top and medium bottom soil profiles indicated that the period ratio increased with an increase in the depth ratio. Also, a structure's stiffness increased the period ratio for both soil profiles (see Figure 7-11 and Figure 7-12, and Table 7-6, Table 7-7, Table 7-8, and Table 7-9).

### 7.7.2 The Sand and Clay Soil Profiles Cases

Other common soil profiles for sand and clay were represented by linear and parabolic variations in the shear modulus with depth, G, as shown in Figure 7-13 and Figure 7-14. The horizontal, rocking, and torsion stiffnesses were calculated using finite element analysis for a rectangular foundation 32.4 m long, 17.7 m wide, and 0.8 m thick; the results are displayed in Figure 7-15 and Figure 7-16. Table 7-10, Table 7-11, Table 7-12, and Table 7-13 present variations in the time period ratio depending on the parameter G. Figure 7-17 and Figure 7-18 illustrate the relationships among the system parameters and the effect of increases in G with depth in terms of the fundamental time period ratio. For clay soil, it can be seen from Figure 7-17 that an increase in G led to a decrease in the time period ratio because of the increase in soil stiffness. Moreover, an increase in the structure's stiffness led to an increase in the time period ratio. For sand, Figure 7-18 shows a similar variation of G. Also, the fundamental time period ratio for the clay soil profiles was greater than the time period ratio for sand soil profiles.

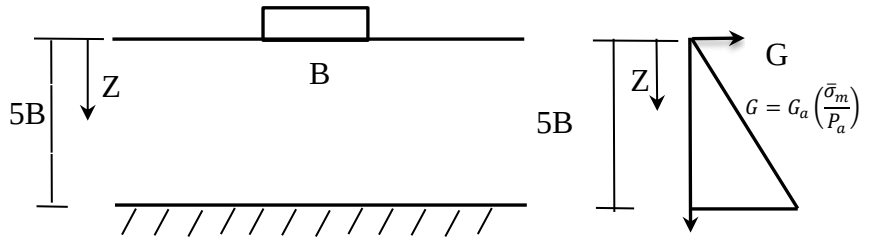


**Figure 7-13** Variations in G with depth for clay (linear).

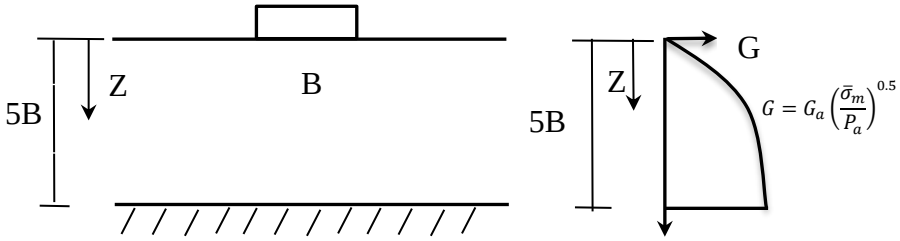


**Figure 7-14** Variations in G with depth for sand (parabola).

The frame and frame shear wall systems constructed on the selected soil profiles show that in sand and clay soil, the period ratio decreased with an increase in the depth ratio. An increase in the structure's stiffness increased the period ratio for both soil profiles (see Figure 7-17 and Figure 7-18 and Table 7-11 and Table 7-12). Figure 7-11, Figure 7-12, Figure 7-17, and Figure 7-18 illustrate the variation in period ratio for the frame and frame shear wall systems under different soil profiles. Table 7-6 to Table 7-13 indicate the period ratios of the first 12 modes of the structural systems. From these figures and tables, it is clear that the period ratio increased with a decrease in soil stiffness. For all cases, the period ratio of the frame shear wall structural system was greater than that of the frame system due to the difference in structure stiffness; this difference is particularly clear on soft soil.

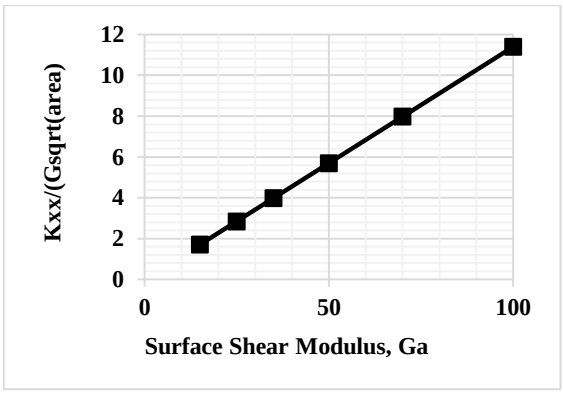


a) Horizontal stiffness of soil in the X direction

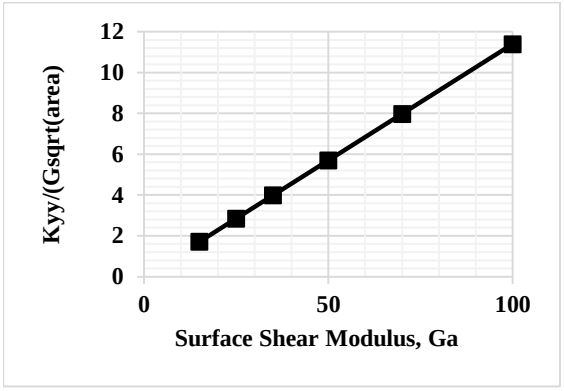


b) Horizontal stiffness of soil in the Y direction

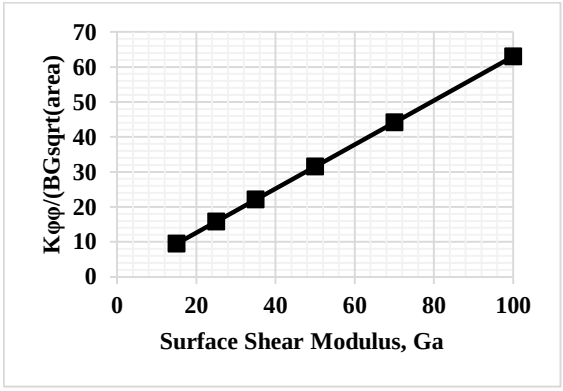


c) Rocking stiffness of soil in the X direction

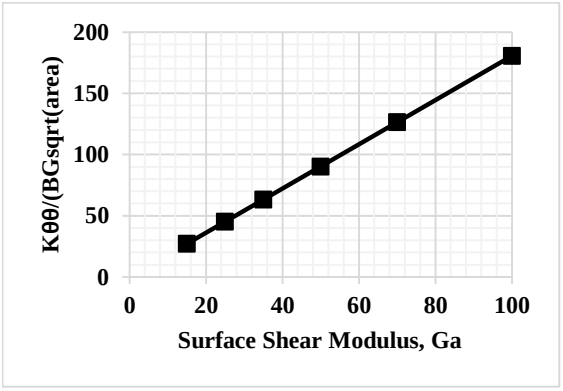


d) Rocking stiffness of soil in the Y direction

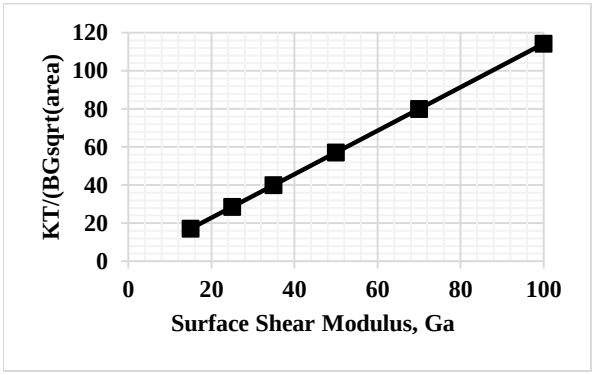


e) Torsion stiffness of soil in the Z direction

**Figure 7-15** Stiffness matrix elements for the soil profile of clay (linear).

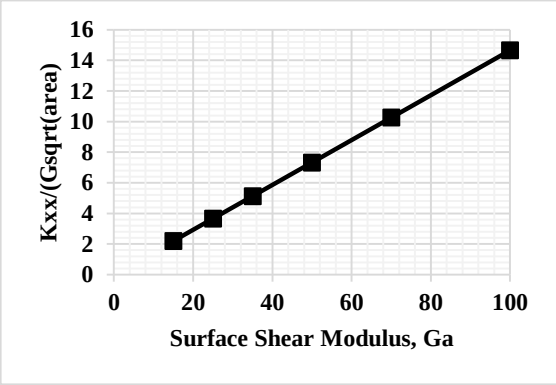


a) Horizontal stiffness of soil in the X direction

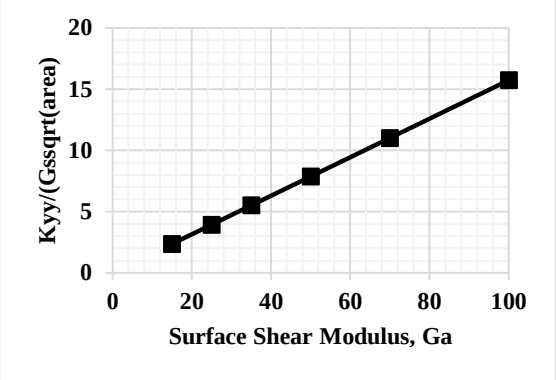


b) Horizontal stiffness of soil in the Y direction

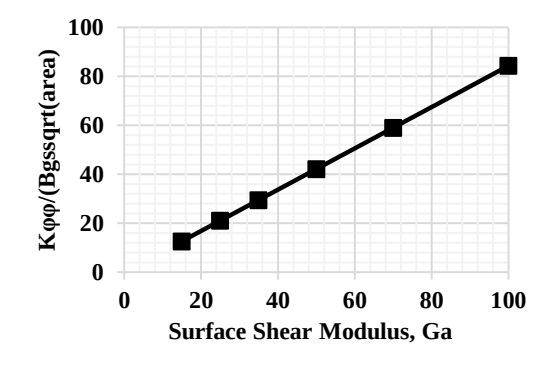


c) Rocking stiffness of soil in the X direction

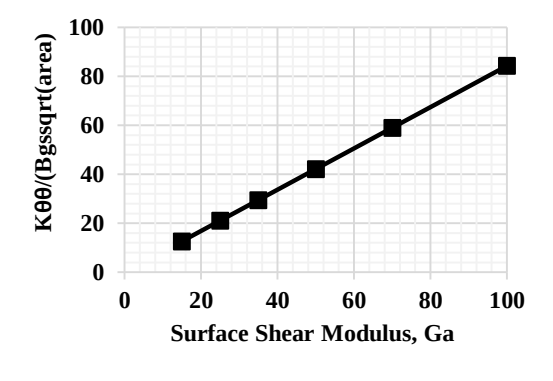


d) Rocking stiffness of soil in the Y direction

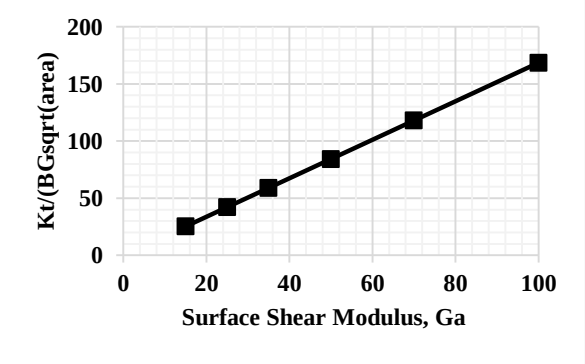


e) Torsion stiffness of soil in the Z direction

**Figure 7-16** Stiffness matrix elements for the soil profile of sand (parabola).

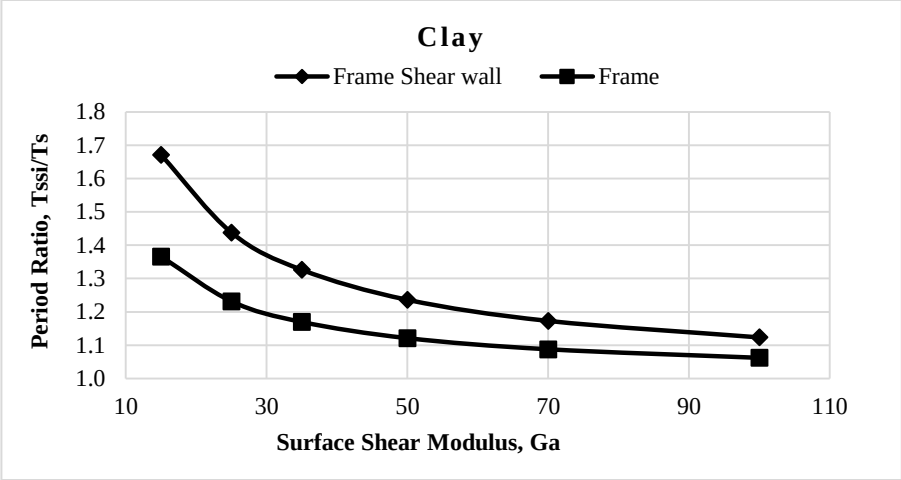


**Figure 7-17** Period ratio of the fundamental SSI mode for a fixed support structure with a soil profile of clay (linear).

**Table 7-10** Period ratios for frame buildings on clay (linear).

| Ga Mpa | $\frac{\bar{T}_1}{T_1}$ | $\frac{\bar{T}_2}{T_2}$ | $\frac{\bar{T}_3}{T_3}$ | $\frac{\bar{T}_4}{T_4}$ | $\frac{\bar{T}_5}{T_5}$ | $\frac{\bar{T}_6}{T_6}$ | $\frac{\bar{T}_7}{T_7}$ | $\frac{\bar{T}_8}{T_8}$ | $\frac{\bar{T}_9}{T_9}$ | $\frac{\bar{T}_{10}}{T_{10}}$ | $\frac{\bar{T}_{11}}{T_{11}}$ | $\frac{\bar{T}_{12}}{T_{12}}$ |
|---|---|---|---|---|---|---|---|---|---|---|---|---|
| 15 | 1.3660 | 1.1965 | 1.0436 | 1.0728 | 1.0825 | 1.0643 | 1.0821 | 1.1181 | 1.1229 | 1.2075 | 1.3566 | 1.2863 |
| 25 | 1.2316 | 1.1206 | 1.0259 | 1.0398 | 1.0453 | 1.0363 | 1.0454 | 1.0630 | 1.0463 | 1.0697 | 1.1722 | 1.1944 |
| 35 | 1.1696 | 1.0870 | 1.0184 | 1.0272 | 1.0311 | 1.0252 | 1.0314 | 1.0416 | 1.0302 | 1.0394 | 1.0696 | 1.0899 |
| 50 | 1.1211 | 1.0613 | 1.0129 | 1.0185 | 1.0212 | 1.0172 | 1.0214 | 1.0272 | 1.0196 | 1.0232 | 1.0377 | 1.0270 |
| 70 | 1.0877 | 1.0440 | 1.0092 | 1.0129 | 1.0148 | 1.0121 | 1.0151 | 1.0185 | 1.0134 | 1.0148 | 1.0233 | 1.0174 |
| 100 | 1.0620 | 1.0309 | 1.0064 | 1.0089 | 1.0102 | 1.0084 | 1.0104 | 1.0125 | 1.0090 | 1.0096 | 1.0148 | 1.0112 |

**Table 7-11** Linear period ratios for frame shear wall buildings on clay (linear).

| Ga Mpa | $\frac{\bar{T}_1}{T_1}$ | $\frac{\bar{T}_2}{T_2}$ | $\frac{\bar{T}_3}{T_3}$ | $\frac{\bar{T}_4}{T_4}$ | $\frac{\bar{T}_5}{T_5}$ | $\frac{\bar{T}_6}{T_6}$ | $\frac{\bar{T}_7}{T_7}$ | $\frac{\bar{T}_8}{T_8}$ | $\frac{\bar{T}_9}{T_9}$ | $\frac{\bar{T}_{10}}{T_{10}}$ | $\frac{\bar{T}_{11}}{T_{11}}$ | $\frac{\bar{T}_{12}}{T_{12}}$ |
|---|---|---|---|---|---|---|---|---|---|---|---|---|
| 15 | 1.6710 | 1.7516 | 1.3138 | 1.3501 | 2.0380 | 1.7178 | 2.0180 | 2.5175 | 2.3904 | 2.1338 | 2.2045 | 1.8451 |
| 25 | 1.4378 | 1.4891 | 1.1838 | 1.2008 | 1.6619 | 1.5111 | 1.7732 | 2.2513 | 2.1915 | 2.0816 | 2.1631 | 1.8126 |
| 35 | 1.3260 | 1.3631 | 1.1286 | 1.1400 | 1.4840 | 1.3721 | 1.6251 | 2.0340 | 2.0085 | 2.0301 | 2.1199 | 1.7793 |
| 50 | 1.2361 | 1.2618 | 1.0881 | 1.0962 | 1.3436 | 1.2453 | 1.4888 | 1.7860 | 1.7792 | 1.9563 | 2.0539 | 1.7291 |
| 70 | 1.1728 | 1.1907 | 1.0618 | 1.0679 | 1.2456 | 1.1715 | 1.3559 | 1.5561 | 1.5582 | 1.8673 | 1.9691 | 1.6636 |
| 100 | 1.1233 | 1.1354 | 1.0426 | 1.0471 | 1.1696 | 1.1145 | 1.2446 | 1.3321 | 1.3485 | 1.7570 | 1.8511 | 1.5737 |

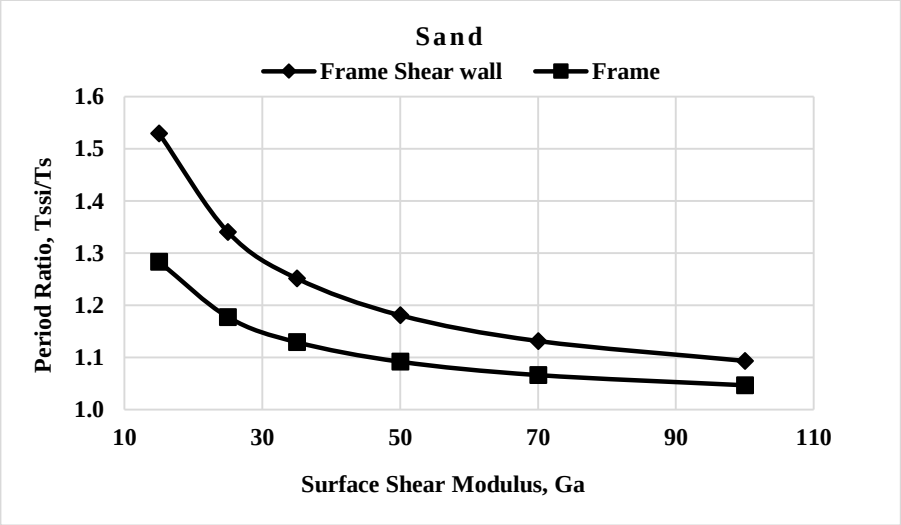


**Figure 7-18** Period ratio of a fundamental SSI mode for a fixed support structure on sand (parabola).

**Table 7-12** Period ratios for frame buildings on sand (parabola).

| Ga Mpa | $\frac{\bar{T}_1}{T_1}$ | $\frac{\bar{T}_2}{T_2}$ | $\frac{\bar{T}_3}{T_3}$ | $\frac{\bar{T}_4}{T_4}$ | $\frac{\bar{T}_5}{T_5}$ | $\frac{\bar{T}_6}{T_6}$ | $\frac{\bar{T}_7}{T_7}$ | $\frac{\bar{T}_8}{T_8}$ | $\frac{\bar{T}_9}{T_9}$ | $\frac{\bar{T}_{10}}{T_{10}}$ | $\frac{\bar{T}_{11}}{T_{11}}$ | $\frac{\bar{T}_{12}}{T_{12}}$ |
|---|---|---|---|---|---|---|---|---|---|---|---|---|
| 15 | 1.2838 | 1.1590 | 1.0294 | 1.0536 | 1.0609 | 1.0416 | 1.0609 | 1.0869 | 1.0544 | 1.1364 | 1.2881 | 1.2437 |
| 25 | 1.1776 | 1.0972 | 1.0175 | 1.0298 | 1.0340 | 1.0238 | 1.0343 | 1.0462 | 1.0283 | 1.0449 | 1.0884 | 1.1386 |
| 35 | 1.1294 | 1.0699 | 1.0125 | 1.0206 | 1.0236 | 1.0167 | 1.0238 | 1.0309 | 1.0189 | 1.0268 | 1.0443 | 1.0259 |
| 50 | 1.0920 | 1.0492 | 1.0087 | 1.0141 | 1.0161 | 1.0115 | 1.0163 | 1.0204 | 1.0126 | 1.0165 | 1.0261 | 1.0163 |
| 70 | 1.0664 | 1.0353 | 1.0062 | 1.0099 | 1.0113 | 1.0081 | 1.0115 | 1.0140 | 1.0087 | 1.0108 | 1.0168 | 1.0108 |
| 100 | 1.0468 | 1.0248 | 1.0043 | 1.0068 | 1.0078 | 1.0056 | 1.0080 | 1.0095 | 1.0059 | 1.0072 | 1.0109 | 1.0072 |

**Table 7-13** Period ratios for frame shear wall buildings on sand (parabola).

| Ga Mpa | $\frac{\bar{T}_1}{T_1}$ | $\frac{\bar{T}_2}{T_2}$ | $\frac{\bar{T}_3}{T_3}$ | $\frac{\bar{T}_4}{T_4}$ | $\frac{\bar{T}_5}{T_5}$ | $\frac{\bar{T}_6}{T_6}$ | $\frac{\bar{T}_7}{T_7}$ | $\frac{\bar{T}_8}{T_8}$ | $\frac{\bar{T}_9}{T_9}$ | $\frac{\bar{T}_{10}}{T_{10}}$ | $\frac{\bar{T}_{11}}{T_{11}}$ | $\frac{\bar{T}_{12}}{T_{12}}$ |
|---|---|---|---|---|---|---|---|---|---|---|---|---|
| 15 | 1.5295 | 1.6254 | 1.2092 | 1.2664 | 1.8352 | 1.5729 | 1.8820 | 2.4159 | 2.2879 | 2.1118 | 2.1860 | 1.8220 |
| 25 | 1.3406 | 1.4021 | 1.1216 | 1.1532 | 1.5226 | 1.3774 | 1.6280 | 2.1134 | 2.0378 | 2.0453 | 2.1303 | 1.7731 |
| 35 | 1.2516 | 1.2964 | 1.0851 | 1.1072 | 1.3791 | 1.2730 | 1.4751 | 1.8815 | 1.8281 | 1.9811 | 2.0726 | 1.7237 |
| 50 | 1.1810 | 1.2125 | 1.0585 | 1.0739 | 1.2668 | 1.1878 | 1.3377 | 1.6332 | 1.5952 | 1.8925 | 1.9873 | 1.6518 |
| 70 | 1.1317 | 1.1542 | 1.0413 | 1.0523 | 1.1890 | 1.1287 | 1.2362 | 1.4140 | 1.3931 | 1.7918 | 1.8794 | 1.5647 |
| 100 | 1.0936 | 1.1091 | 1.0286 | 1.0363 | 1.1297 | 1.0850 | 1.1579 | 1.2064 | 1.2693 | 1.6556 | 1.6875 | 1.4627 |

## 7.8 Design of the SAC algorithm

The SAC algorithm is based on obtaining a system that tracks the desired response (i.e., the response of the reference model) (see Chapter 4). In this section, two types of reference model were utilized to study the influence of SSI on the behavior of the SAC algorithm. The reference model with the fixed base structure assumption was employed for the fixed support structure (Fixed-Fixed). Optimal control theory, especially the linear quadratic regulator (LQR), was used to determine the desired output (see Figure 7-19). For the SSI system, two reference models were chosen for the fixed base support structure (Fixed-SSI) and SSI (SSI-SSI). Furthermore, the optimal control theory (i.e., LQR) algorithm was applied to determine the desired output of the reference models (see Figure 7-20, and Figure 7-21).

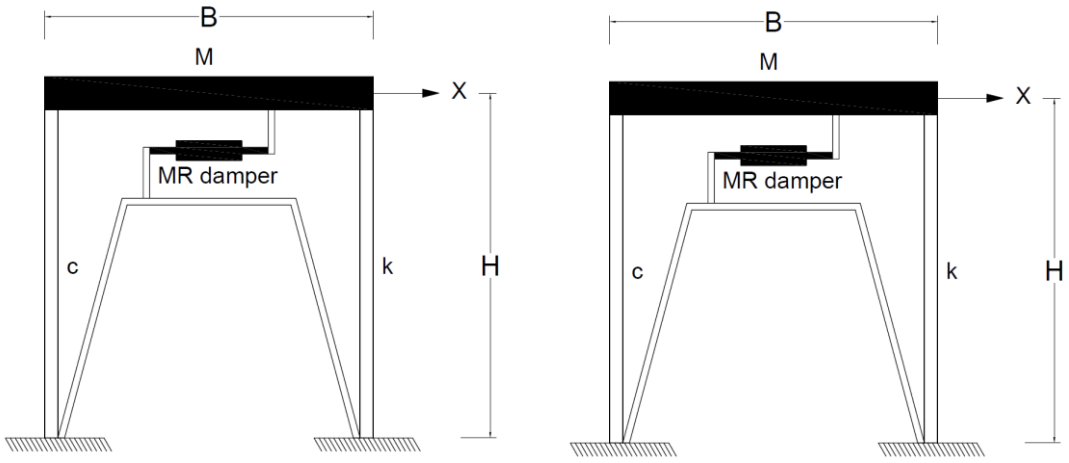


A) The reference model with the fixed support structure assumption

B) The boundary conditions of the superstructure

**Figure 7-19** Design of the SAC algorithm for fixed base structure with Fixed- Fixed assumption.

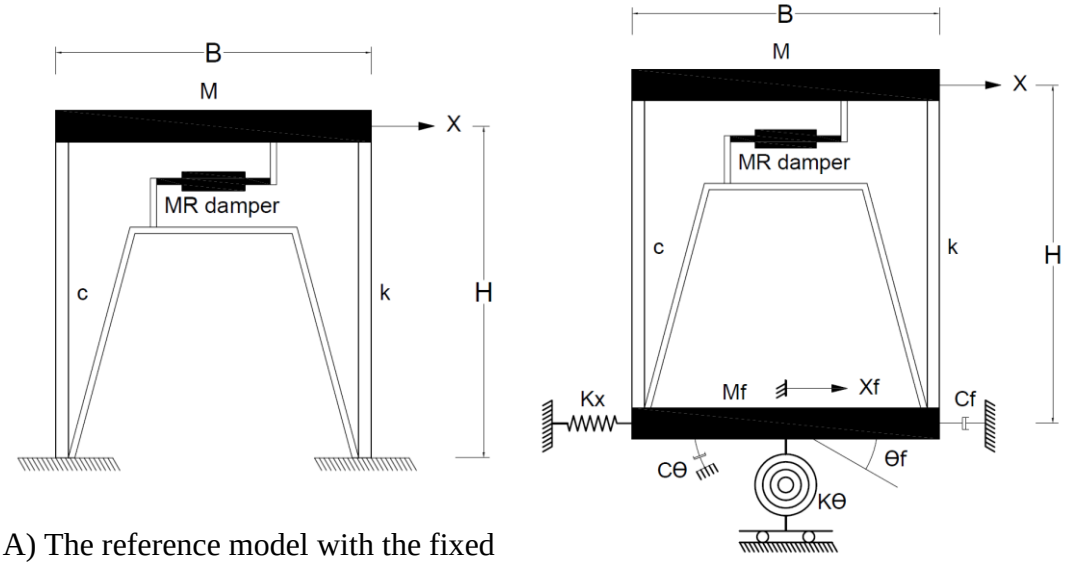


A) The reference model with the fixed support structure assumption

B) The boundary conditions of the superstructure

**Figure 7-20** Design of the SAC algorithm for SSI system with Fixed- SSI assumption.

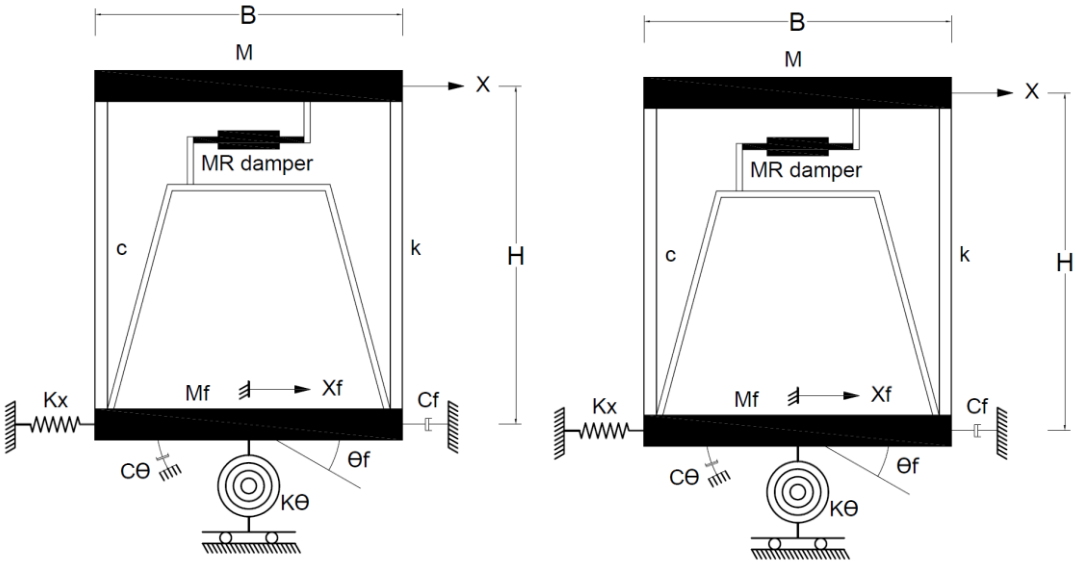


A) The reference model with the SSI assumption

B) The boundary conditions of the superstructure

**Figure 7-21** Design of the SAC algorithm for SSI system with SSI - SSI assumption.

## 7.9 Control Scheme Design and Implementation

The control scheme formed for the SSI system was constituted of sensors measuring transverse displacements in two directions at the center of each floor and two directions at the center of the foundation, and rocking in two direction at the center of the foundation. For the fixed base system, there were sensors measuring transverse displacements at the center of the floor in two directions. For both systems, control devices (1000 kN MR damper see Table 4-1) were placed between the floors in two directions; on the first floor, they were placed between the floor and foundation in two directions. Figure 7-22 presents a schematic of the device's installation on the floor for both the fixed and flexible base structure systems in the X direction. Parametric studies were carried out based on a multi-story building with fixed and flexible supports and different soil profiles. The section of soil profile presents all parameters for each soil profile.

The SAC algorithm was employed as the main control method for this adaptive control scheme. An MR damper was used as a semi-active device, and the reference model was utilized according to the Al-Fahdawi design. This design adopted the optimal control theory (i.e., LQR) to estimate the desired output of the reference model, according to the assumption of invariable system parameters (Al-Fahdawi et al., 2018).

The LQR constants for the reference model were:

$\rho = 10^{-10}, Q = I$

The SAC constants were:

$\Gamma_e = 10^{12}$ , $\Gamma_x = 10^{12}, \Gamma_u = 10^{12}$

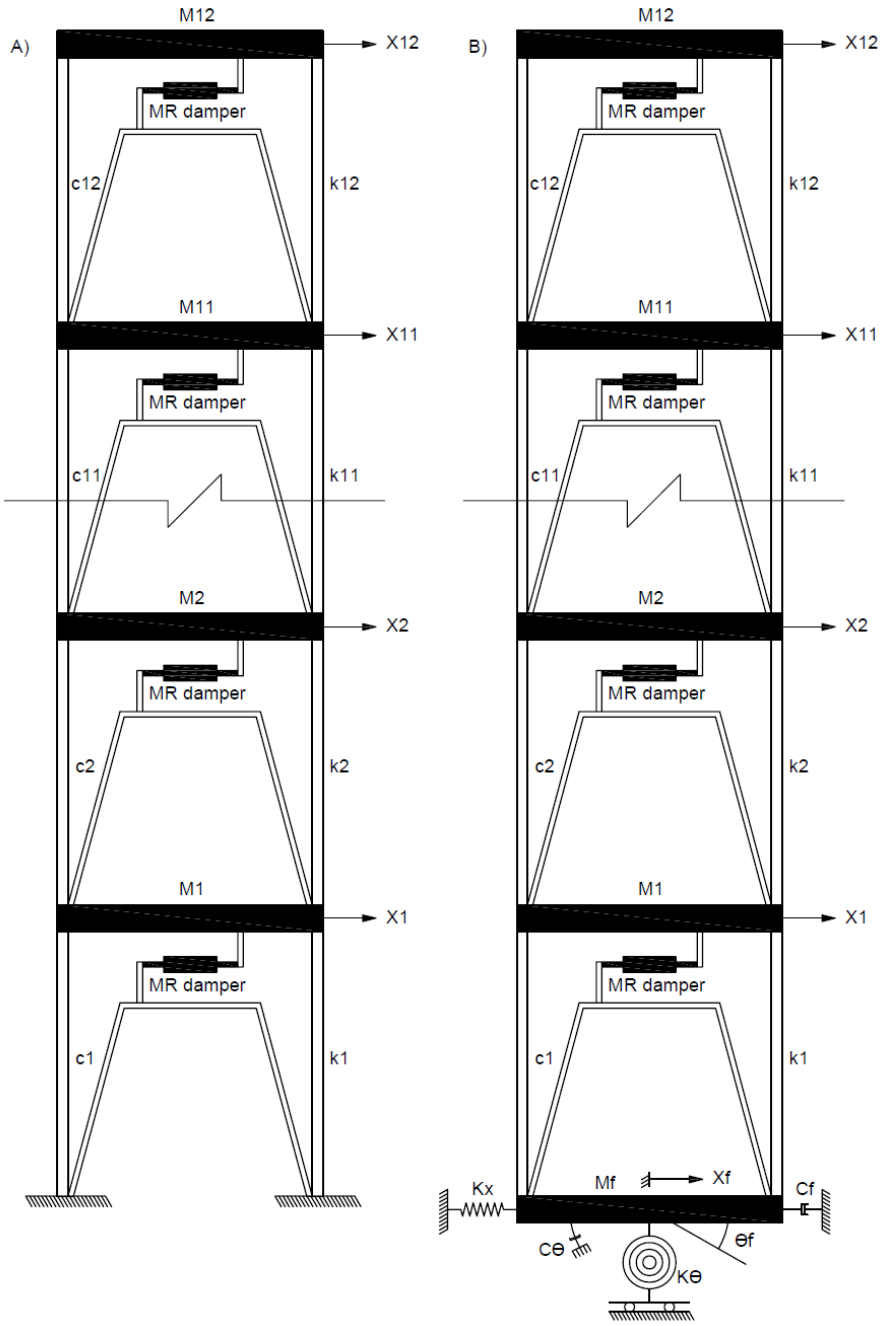


**Figure 7-22** Presents a schematic of the device's installation on the floor for both the fixed and flexible base structure systems in the X direction, A) fixed base structure, B) SSI.

## 7.10 Results and Discussion

In this section, the responses of the controlled and uncontrolled systems for the frame and frame shear wall systems are investigated. Two types of reference model were adopted for the SAC algorithm (i.e., fixed-SSI and SSI-SSI) to analyze the common design. The seismic input was in two primary directions, X and Y, with and without SSI.

### 7.10.1 Maximum Displacements of Floors

As mentioned in Chapter 6, the floor displacements of SSI systems rely on the earthquake spectrum in place of the fundamental period relied upon by fixed base system. The figures in Appendix G illustrate the floor displacement envelope of the fixed support structure and SSI for the controlled and uncontrolled systems. Soils with medium top and soft bottom layers showed floor displacement envelopes in the two primary directions (i.e., X and Y) for controlled and uncontrolled decreases with an increase in the depth ratio for both structural systems under the two earthquake loads. The SSI system was indistinguishable from the fixed base system when the soil was very stiff. Generally, the behaviors of the clay and sand soil profiles were similar to soils with medium top and soft bottom layers.

Layered soil with a soft top and medium bottom layer profile showed displacement envelopes in the two primary directions (i.e., X and Y) for the controlled and uncontrolled decreases with a decrease in the depth ratio for both structural systems under the two earthquake loads. Also, the SSI system was identical to the fixed base system when the soil was very stiff. For all soil profiles, reductions in the control systems in the floor

displacements with a fixed SSI reference model were greater than the reductions in the SSI-SSI reference model. Also, the floor displacements for the frame structural system were greater than the floor displacements for the frame shear wall structural system because of the difference in structural stiffness (i.e., fundamental period).

### 7.10.2 Maximum Interstory Drift

This section discusses the maximum interstory drift of the controlled and uncontrolled systems for the frame and frame shear wall systems. The figures in Appendix G illustrate the interstory drift envelope of the fixed support structure and SSI for the controlled and uncontrolled systems. Soils with medium top and soft bottom layers showed interstory drift envelopes in the two primary directions (i.e., X and Y) for controlled and uncontrolled decreases with an increase in the depth ratio for both structural systems under the two earthquake loads. The SSI system was indistinguishable from the fixed base system when the soil was very stiff. Generally, the behaviors of the clay and sand soil profiles were similar to soils with medium top and soft bottom layers.

Layered soils with soft top and medium bottom layers showed interstory drift envelopes in the two primary directions (i.e., X and Y) for controlled and uncontrolled decreases with a decrease in the depth ratio for the frame and frame shear wall structural systems under the two earthquake loads. Moreover, the SSI system was identical to the fixed base system when the soil was very stiff. For all soil profiles, the reduction in controlled systems in the interstory drift envelopes with the fixed SSI reference model were greater than the reductions in interstory drift envelopes of the SSI-SSI reference model. Also, the

interstory drift envelopes for the frame structural systems were greater than the floor displacements for the frame shear wall structural systems, due to the difference in structural stiffness (i.e., fundamental period).

### 7.10.3 Maximum Acceleration of Floors

In this section, the maximum acceleration or acceleration envelope of controlled and uncontrolled systems for frame and frame shear wall systems are discussed. The figures in Appendix G illustrate the acceleration envelope of the fixed support structure and SSI for controlled and uncontrolled systems. Soils with medium top and soft bottom layers showed acceleration envelopes in the two primary directions (i.e., X and Y) for controlled and uncontrolled decreases with an increase in the depth ratio for both structural systems under the two earthquake loads. The SSI system was indistinguishable from the fixed base system when the soil was very stiff. Generally, the behaviors of the clay and sand soil profiles were similar to soils with medium top and soft bottom layers.

Layered soils with soft top and medium bottom layers showed acceleration envelopes in the two primary directions (i.e., X and Y) for controlled and uncontrolled decreases with a decrease in the depth ratio for the frame and frame shear wall structural systems under the two earthquake loads. Moreover, the SSI system was identical to the fixed base system when the soil was very stiff. For all soil profiles, the reductions in control systems in the acceleration envelopes with the fixed SSI reference model were greater than reductions in the acceleration envelopes of the SSI-SSI reference model. Moreover, the acceleration envelopes for frame structural systems were greater than the floor displacements for the

frame shear wall structural systems, due to differences in structural stiffness (i.e., fundamental period).

### 7.10.4 Uncontrolled Systems

The SSI system may have either a beneficial or detrimental effect on the response riling of the properties of external excitation.

#### 7.10.4.1 Maximum Displacement and Drift Ratios

The results of the frame and frame shear wall systems on all soil profiles show that the majority of maximum displacement and drift ratios for the SSI were greater than the maximum drift ratio of the fixed base structure. See the Tables in Appendix E.

#### 7.10.4.2 Maximum Acceleration and Base Shear Ratios

The results of the frame and frame shear wall systems on all soil profiles demonstrate that the difference between the changes in fixed base structures and SSI systems increased or decreased based on the external excitation characteristics. For the frame and frame shear wall systems, the majority of the maximum acceleration and base shear ratios of the SSI were greater than the maximum acceleration and base shear ratios of the fixed base structures under all earthquake loads. See the Tables in Appendix E.

### 7.10.5 Control Systems

#### 7.10.5.1 Maximum Drift Ratio

The results of the frame and frame shear wall systems on all soil profiles show that the maximum drift ratio of the SSI-SSI reference model was greater than the maximum drift ratio of the fixed SSI reference model. For the frame systems, the maximum drift ratios of both reference models in the X and Y directions were greater than the maximum drift ratio of the fixed base structure. For the frame shear wall systems, the majority of the maximum drift ratios of both reference models was greater than the maximum drift ratio of the fixed base structure under all earthquake loads. See the figures in Appendix H.

#### 7.10.5.2 Maximum Base Shear Ratio

The results of the frame and frame shear wall systems on all soil profiles demonstrate that the difference in changes in the SSI-SSI and fixed SSI reference models increased or decreased depending on the external excitation characteristics. For the frame systems, the majority of the maximum base shear ratios for both reference models were greater than the maximum base shear ratio of the fixed support structure under all earthquake loads. For the frame shear wall systems modeled in the Managua, Nicaragua ’02 earthquake, the majority of maximum base shear ratios for both reference models was greater than the maximum base shear ratio of the fixed support structural system. Also, for the frame shear wall systems modeled in the Corinth, Greece earthquake, the maximum base shear ratios of both reference models in the X direction were less than the maximum base shear ratio of the fixed support structure. However, the majority of the maximum base shear ratios in the Y direction for

both reference models were greater than the maximum base shear ratios of the fixed support structural system. See the figures in Appendix H.

#### 7.10.5.3 Maximum Control Force Ratio

The results of the frame and frame shear wall systems for all soil profiles demonstrate that the maximum control force ratio of the SSI-SSI reference model was less than the maximum control force ratio of the fixed SSI reference model. For frame systems modeled in the Managua, Nicaragua ’02 earthquake, the maximum control force ratios for the reference models in the X direction were less than the maximum control force ratio of the fixed support structure. However, the majority of the maximum control force ratios in the Y direction for both reference models were greater than the maximum control force ratio of the fixed support structural system. For frame systems modeled in the Corinth, Greece earthquake, the maximum control force ratio of the fixed SSI reference model was greater than the maximum control force ratio of the fixed support structural system, but the SSI-SSI reference model had a lower maximum control force ratio for the fixed support structural system in the X direction. In the Y direction, the majority to the maximum control force ratios for both reference models were greater than the maximum control force ratio of the fixed support structural system. For the frame shear wall systems, the majority of the maximum control force ratios for both reference models were greater than the maximum control force ratio of the fixed support structure under all earthquake loads. See the figures in Appendix H.

### 7.10.6 Normalization of Foundation Results

The results indicate that the SAC algorithm and MR damper can effectively reduce the response of a foundation. The results of the frame and frame shear wall systems on all soil profiles demonstrate that the majority of the maximum horizontal and rocking displacement ratios of the fixed SSI reference model were less than the maximum horizontal and rocking displacement ratios of the SSI-SSI reference model. For frame systems, the maximum horizontal and rocking displacement ratios for both reference models were less than one (i.e., the control responses were less than the uncontrolled responses). For the frame shear wall systems, some of the maximum horizontal and rocking displacement ratios for both reference models were greater than one, and the majority of the maximum horizontal and rocking displacement ratios of both reference models were less than one. See the figures in Appendix F.

### 7.10.7 Performance Evaluation Criteria

The results of the performance evaluation criteria obtained in the parametric study for the MDOF systems (both frame and frame shear wall structures) with different soil profiles are presented and discussed here. For all soil profiles, the results show that the majority of the performance evaluation criteria of the SSI-SSI reference model were greater than the performance evaluation criteria of the fixed SSI reference model. Therefore, the results indicate that the fixed SSI reference model was more effective than the SSI-SSI reference model in reducing response; however, it requires more control force. The SAC

algorithm's efficiency decreased with an increase in the period ratio (i.e., a decrease in the soil stiffness). The results are available in Appendix D.

# 8. CONCLUSIONS AND FUTURE WORKS

## 8.1 Introduction

The objective of this research was to study the effects of soil-structure interaction on control systems using the SAC algorithm with an MR damper for performance-based building control design with hazard loads. Three main issues were investigated to accomplish this goal. First, many hypotheses and simplifications were employed throughout this work to make the investigation computationally understandable. Model reduction methods were adopted to determine equivalent stiffness matrices for structures and foundations. For structures, the equivalent stiffness matrices for frame and frame shear wall systems were formulated in the finite element software ETABS, as they relate to three-dimensional structures and their geometric and material properties. For soil, the equivalent stiffness matrices for rigid foundations with different soil profiles were calculated using the finite element software ABAQUS. Then, the stiffness and mass matrices for the frame and frame shear wall systems and foundations were exported to MATLAB and SIMULINK (see Chapter 5).

Next, it was determined that neglecting the SSI effects in control design can lead to the underestimation of structural response. The significant SSI system parameters (e.g., structure to soil stiffness ratio, $\sigma$, slenderness ratio, $\lambda$, etc., see Chapter 5) play an important role in changing the dynamic behavior of structures during external excitation and control design. There is a significant difference in the SAC systems designed for fixed-base

structures as opposed to those experiencing SSI effects. SSIs require more control effort than do fixed-base structures (see Chapter 6).

Finally, the SAC algorithm was found to be highly effective at maintaining structures experiencing SSI effects in the presence of variations in the structure and soil properties. The performance of a controlled structure can be significantly affected when the soil stiffness is in the soft to medium range, with progressively worse structural performance occurring with decreasing soil stiffness. Structural performance is also adversely affected as the stiffness of the structure increases (i.e., the performance of SAC in frame shear wall structural system is less than the performance of SAC in frame system). The SSI effect is very clear in structures constructed on soft soil, stiff structures, and frame shear wall systems (see Chapter 7).

## 8.2 Conclusions

### 8.2.1 The Portal Frame System

#### 8.2.1.1 Uncontrolled Systems

- The period of the SSI system was always greater than the period of the fixed base system (TSSI > TS); consequently, the response of the SSI system changed to the response at TSSI on the earthquake spectrum. Clearly, this relied on the earthquake spectrum being in the position of the fundamental period of the fixed base system. Therefore, the SSI system may have either beneficial or detrimental influence.

#### 8.2.1.2 Controlled Systems

##### *8.2.1.2.1 Maximum Control Force Ratio*

- The results indicate that the maximum control force ratio decreased with an increase in soil stiffness.
- The results indicate that the maximum control force ratio decreased with an increase in the period of fixed base structure (Ts).
- The control force ratio increased with an increase in the slenderness ratio.
- The maximum control force ratio of the Fixed-SSI reference model was greater than that of the SSI-SSI reference model.
- The maximum control force ratio of the SSI was greater than that of the fixed base structure.

##### *8.2.1.2.2 Maximum Control Displacement Ratio*

- The results show that the maximum displacement ratio under the earthquake suite with different slenderness ratios decreased with an increase in the soil stiffness.
- The results show that the maximum displacement ratio under the earthquake suite with different slenderness ratios decreased with an increase in the period of fixed base structure (Ts).
- The maximum displacement ratio of the SSI-SSI reference model was greater than that of the Fixed-SSI reference model.
- The maximum displacement ratio increased with an increase in the slenderness ratio.

- The maximum displacement ratio of the SSI was greater than that of the fixed base structure.

#### 8.2.1.3 Normalization of the Foundation Results

The normalization of the horizontal and rocking displacements of foundation are calculated according to equations 6-21 to 6-24.

- The results indicate that the SAC algorithm and MR damper could effectively reduce the response (horizontal and rocking displacements) of a foundation.

#### 8.2.1.4 Performance Evaluation Criteria

- The results of the J1, J3, J6, and J8 performance criteria indicate that for all soil profiles, the Fixed-SSI reference model was more effective than the SSI-SSI reference model in reducing responses (displacements, velocities, accelerations, etc.), but with more control force (i.e., J4 for the Fixed-SSI was greater than J4 for the SSI-SSI).
- The efficiency of the SAC algorithm decreased with an increase in the slenderness ratio ($\lambda$).
- The SAC algorithm's efficiency increased with an increase in the soil stiffness.
- The SAC algorithm's efficiency increased with an increase in the period of fixed base structure (Ts).

### 8.2.2 Smart Frame and Frame Shear Wall Systems

#### 8.2.2.1 Comparison of Controlled and Uncontrolled Systems

##### *8.2.2.1.1 Maximum Displacement of Floors*

- The floor displacement envelopes for controlled and uncontrolled systems decreased with an increase in soil stiffness.
- The reduction of control system floor displacement was greater in the Fixed-SSI reference model than in the SSI-SSI reference model.
- The floor displacement in frame structural systems was greater than in frame shear wall structural systems because of the difference in structural stiffness (i.e., the fundamental period).

##### *8.2.2.1.2 Maximum Inter-story Drift*

- The inter-story drift envelopes for controlled and uncontrolled systems decreased with an increase in soil stiffness.
- The reduction of inter-story drift in controlled systems was greater in the Fixed-SSI reference model than in the SSI-SSI reference model.
- The inter-story drift in frame structural systems was greater than in frame shear wall structural systems because of the difference in structural stiffness (i.e., the fundamental period).

*8.2.2.1.3 Maximum Acceleration of Floors*

- The acceleration envelopes for controlled and uncontrolled systems decreased with an increase in soil stiffness.
- The reduction in the acceleration envelopes of controlled systems in the Fixed-SSI reference model was greater than in the SSI-SSI reference model.
- The acceleration envelopes for frame structural systems were greater than the floor displacements in frame shear wall structural systems due to the difference in structural stiffness (i.e., the fundamental period).

### 8.2.2.2 Uncontrolled Systems

*8.2.2.2.1 Maximum Displacement and Drift Ratios*

- The majority of maximum SSI displacement and drift values were greater than the maximum drift ratio value for the fixed base structure.

*8.2.2.2.2 Maximum Acceleration and Base Shear Ratios*

- The results demonstrate that the difference in change between the fixed-base structure and SSI system increased or decreased depending on the external excitation characteristics.
- The majority of the maximum SSI acceleration and base shear ratios were greater than those of the fixed base structure.

#### 8.2.2.3 Controlled Systems

##### *8.2.2.3.1 Maximum Drift Ratio*

- The results show that the maximum drift ratio for the SSI-SSI reference model was greater than that of the Fixed-SSI reference model.
- The majority of the maximum drift ratios for both SSI reference models were greater than those of the fixed base structure.

##### *8.2.2.3.2 Maximum Base Shear Ratio*

- The results demonstrate that the difference between the SSI-SSI and Fixed-SSI reference models was that the change increased or decreased depending on the characteristics of the external excitation.
- For frame systems, the majority of the maximum base shear ratios of both reference models were greater than those of the fixed support structure.

##### *8.2.2.3.3 Maximum Control Force Ratio*

- The results demonstrate that the maximum control force ratio of the SSI-SSI reference model was less than that of the Fixed-SSI reference model.
- For frame systems, the maximum control force ratios for both reference models varied to be more or less than that of the fixed support structure due to the external load characteristics.
- For the frame shear wall systems, the majority of the maximum control force ratios for both reference models were greater than those of the fixed support structure.

#### 8.2.2.4 Normalization of Foundation Results

The normalization of the horizontal and rocking displacements of foundation are calculated according to equations 6-21 to 6-24 in the two directions X and Y.

- The results indicate that the SAC algorithm and MR damper can effectively reduce the foundation response.
- The results demonstrate that the responses of the Fixed-SSI reference model were less than those of the SSI-SSI reference model but required more control cost.
- The SAC algorithm was more efficient at reducing the responses of frame systems than frame shear wall systems.

#### 8.2.2.5 Performance Evaluation Criteria

- The results show that the majority of performance evaluation criteria for the SSI-SSI reference model were greater than those of the Fixed-SSI reference model. Therefore, the Fixed-SSI reference model was more effective than the SSI-SSI reference model at reducing response but did require more control force.
- The SAC algorithm's efficiency decreased with an increase in the period ratio (i.e., a decrease in the soil stiffness).

## 8.3 Recommendations for Future Research

The future research needed regarding smart soil-structure interaction systems has been organized here into two general thematic areas. The first involves nonlinear soil-

structure interaction, and the second includes recommendations for using other advanced theories of control. Following is a description of each.

### 8.3.1 Nonlinear soil-structure interaction

The nonlinear SSI system can include material and geometric nonlinearities in the structure, foundation, and soil. The main reasons for nonlinearity are:

1. The yielding of seismic force-resisting elements in the structure;
2. The yielding of soil and strength loss due to liquefaction or cyclic softening (i.e., increases in pore water pressure);
3. Gaps occurring between the soil and foundation, such as separation of foundation sidewalls from the surrounding soil or foundation uplift; and
4. The yielding of foundation elements.

These special effects must be calculated and response history analyses implemented in the time domain. The current knowledge of this topic is inadequate and these subjects are under-researched. The majority of work has focused on nonlinear SSI due to nonlinear structure behavior and equivalent linear soil (Type 1) or nonlinear soil/gapping with linear structures (Types 2 and 3).

#### 8.3.1.1 Nonlinear Structures and Equivalent Linear Soil

The majority of research has focused on nonlinearities in structures because the constitutive relations of soil are very complex and neglect wave reflections at problem boundaries. If the foundation is over-designed or if structural yielding progresses at

relatively low intensity seismic loads, considerable material nonlinearities in the foundation and soil may not appear. Therefore, the equivalent linear model of soil can be used to analyze these cases.

#### 8.3.1.2 Nonlinearity in the Foundation and Soil

An enormous body of experimental and analytical evidence has demonstrated that geometric and material nonlinearities in the soil and foundation may be advantageous to seismic analyses of a structure. Therefore, some researchers have suggested modifying the concept of foundation design to allow for significant yielding in the soil near the foundation, or the foundation itself to dissipate energy and maintain the structure (Gazetas, 2006; Gajan and Kutter, 2008). This requires the control of displacement and rocking. Consequently, the analysis and design method for soil nonlinearity includes optimization of the trade-offs between the advantageous effects of soil yielding (particularly with respect to energy dissipation) and damaging effects of displacement or residual rocking. Soil-structure interaction research has thus considered how nonlinear soil and foundation behavior can be categorized into two methods, as discussed below.

##### *8.3.1.2.1 Beam-on-Nonlinear Winkler Foundation Models*

Beam-on-Nonlinear Winkler Foundation (BNWF) models have been implemented for static and dynamic analyses of SSI systems with different types of foundations (Matlock, 1970; Cox et al., 1974, Penzien, 1970; Nogami et al., 1992; Boulanger et al., 1999). Significant advantages that BNWF models have over continuum models are based on the

former's ability to represent soil-structure interaction systems through one-dimensional nonlinear springs distributed throughout the interface domain. The parameters of BNWF models rely on soil properties, the stiffness of the foundation, geometry of the system, frequency, response mode, and strain level. One limitation of this method is related to its one-dimensional nature. A spring responds only to loads acting parallel to its axis; consequently, loads acting in a perpendicular direction do not affect the response of the spring. Therefore, the concept of plastic potential and the flow rule cannot be clearly united. However, the BNWF method is common because of its ease and predictive ability with regards to different problems. The linear analysis is related to linear springs that can be coupled with damper elements and gapping (Chopra and Yim, 1985). Nonlinear springs for shallow foundations have been implemented in combination with gapping and damper elements (Allotey, 2003; Naggar, 2007; Raychowdhury and Hutchinson, 2009). BNWF models have several parameters describing their behavior.

*8.3.1.2.2 Plasticity Based Macro-Element Models*

Plasticity Based Macro-Element models represent a modern development with implementation in the nonlinear analysis of rigid foundations (Nova and Montrasio, 1991). This type of model mixes elements from both BNWF and continuum formulations. A macro-element model represents an element located at the interface between a rigid foundation and soil media to describe the energy dissipation and soil behavior corresponding to an SSI system. From a numerical analysis point of view, a macro-element is placed at the foundation-soil interface and describes the rigid foundation and soil domain. This concept is

known as a contact interface model (CIM) and was developed by Gajan and Kutter (2009). The advantage of a macro-element model is its constitutive relationship that tracks the contacts of the soil-foundation interface and geometry of the gap. Moreover, CIMs capture nonlinear behavior between cyclic loads and displacements in SSI systems in complex cyclic loading conditions. The main advantage of a CIM over a BNWF model is the coupling in the vertical load, shear, and moment capacities. Coupling between the moment and vertical capacities is made by gap formation. In other words, the moment capacity typically happens after a gap has developed, making it possible for the vertical capacity to drop.

### 8.3.2 Theory of Control

#### 8.3.2.1 Intelligent Control

Intelligent control employs methods from the areas of artificial intelligence, operations research, and automatic control in order to sense, judge, treat, and perform smartly. Intelligent control can be thought of as self-organizing or adaptive systems that learn through intercommunication with their environment, with certain *a priori* information. There are four main methodologies associated with intelligent control that have been established: artificial neural network, fuzzy logic, fuzzy-neural, and neural-fuzzy.

#### 8.3.2.2 Stochastic Control

Stochastic control deals with the existence of uncertainty both in the noise and observations that drive the development of a system. It employs Bayesian probability theory, which argues that random noise associated with probability distribution affects the

estimation and observation of state variables. Stochastic control designs the time paths of control variables that perform the desired control requirements with minimum cost despite the behavior of the noise.

#### 8.3.2.3 Sliding mode control

Sliding mode control is a type of nonlinear control that changes the dynamics of a nonlinear system by implementing a discontinuous or set value control signal that slides along the normal behavior of the system. The control law is intentionally varied throughout the control process, according to certain defined laws that depend on the current location in the state space. Consequently, sliding mode control is a variable structure control approach.

# REFERENCES


Adamidis, O., Gazetas, G., Anastasopoulos, I., & Argyrou, C. (2014). Equivalent-linear stiffness and damping in rocking of circular and strip foundations. *Bulletin of Earthquake Engineering, 12*(3), 1177-1200. doi:10.1007/s10518-013-9554-0

Agency, F. E. M. (2003). *NEHRP recommended provisions for seismic regulations for new buildings and other structures*: Fema.

Al-Fahdawi, O. A., Barroso, L. R., & Soares, R. W. (2018). *Utilizing the Adaptive Control in Mitigating the Seismic Response of Adjacent Buildings Connected with MR Dampers.* Paper presented at the 2018 Annual American Control Conference (ACC).

Alam, S. S., & Baba, S. (1993). Robust active optimal control scheme including soil-structure interaction. *Journal of Structural Engineering, 119*(9), 2533-2551. doi:Doi 10.1061/(Asce)0733-9445(1993)119:9(2533)

Ali, M., & Moon, K. (2018). Advances in Structural Systems for Tall Buildings: Emerging Developments for Contemporary Urban Giants. *Buildings, 8*(8), 104.

Ali, M. M., & Moon, K. S. (2007). Structural developments in tall buildings: current trends and future prospects. *Architectural science review, 50*(3), 205-223.

Amini, F., Bitaraf, M., Nasab, M. S. E., & Javidan, M. M. (2018). Impacts of soil-structure interaction on the structural control of nonlinear systems using adaptive control approach. *Engineering Structures, 157,* 1-13.

Amini, F., & Shadlou, M. (2011). Embedment effects of flexible foundations on control of structures. *Soil Dynamics and Earthquake Engineering, 31*(8), 1081-1093.

Arefi, M. J. (2008). Effects of soil-structure interaction on the seismic response of existing RC frame buildings. *Istituto Universitario di Studi Superiori di Pavia, Università degli Studi di Pavia*.

Arnold, W. F., & Laub, A. J. (1984). Generalized eigenproblem algorithms and software for algebraic Riccati equations. *Proceedings of the IEEE, 72*(12), 1746-1754.

Bar-Kana, I. (1987). On parallel feedforward and simplified adaptive control. In *Adaptive Systems in Control and Signal Processing 1986* (pp. 99-104): Elsevier.

Bar-Kana, I., & Guez, A. (1990). Simple adaptive control for a class of non-linear systems with application to robotics. *International Journal of Control, 52*(1), 77-99.

Bar-Kana, I., & Kaufman, H. (1993). Simple adaptive control of large flexible space structures. *IEEE Transactions on Aerospace and Electronic Systems, 29*(4), 1137-1149.

Barkana, I. (2005). Gain conditions and convergence of simple adaptive control. *International Journal of Adaptive Control and Signal Processing, 19*(1), 13-40.

Barkana, I. (2008). *A modified invariance principle and gain convergence in adaptive control.* Paper presented at the 2008 IEEE 25th Convention of Electrical and Electronics Engineers in Israel.

Barkana, I. (2013). Extensions in adaptive model tracking with mitigated passivity conditions. *Chinese Journal of Aeronautics, 26*(1), 136-150.

Barkana, I. (2014). Simple adaptive control–a stable direct model reference adaptive control methodology–brief survey. *International Journal of Adaptive Control and Signal Processing, 28*(7-8), 567-603.

Barkana, I. (2016a). Adaptive control? But is so simple! *Journal of Intelligent & Robotic Systems, 83*(1), 3-34.

Barkana, I. (2016b). Parallel feedforward and simple adaptive control of flexible structures: First-order pole instead of collocated velocity sensors? *Journal of Aerospace Engineering, 29*(2), 04015039.

Barkana, I. (2016c). Robustness and perfect tracking in simple adaptive control. *International Journal of Adaptive Control and Signal Processing, 30*(8-10), 1118-1151.

Barroso, L. R., Chase, J. G., & Hunt, S. (2003). Resettable smart dampers for multi-level seismic hazard mitigation of steel moment frames. *Journal of Structural Control, 10*(1), 41-58.

Bekdaş, G., & Nigdeli, S. M. (2017). Metaheuristic based optimization of tuned mass dampers under earthquake excitation by considering soil-structure interaction. *Soil Dynamics and Earthquake Engineering, 92*, 443-461.

Bielak, J. (1976). Modal analysis for building-soil interaction. *Journal of the engineering mechanics division, 102*(5), 771-786.

Bisch, P., Carvalho, E., Degee, H., Fajfar, P., Fardis, M., Franchin, P., . . . Plumier, A. (2012). Eurocode 8: seismic design of buildings worked examples. *Luxembourg: Publications Office of the European Union*.

Bitaraf, M. (2011). *Enhancing the structural performance with active and semi-active devices using adaptive control strategy*: Texas A&M University.

Bozorgnia, Y., & Bertero, V. V. (2004). *Earthquake engineering: from engineering seismology to performance-based engineering*: CRC press.

Buckley, T., Watson, P., Cahill, P., Jaksic, V., & Pakrashi, V. (2018). Mitigating the structural vibrations of wind turbines using tuned liquid column damper considering soil-structure interaction. *Renewable Energy, 120*, 322-341.

Burns, R. (2001). *Advanced control engineering*: Elsevier.

Celebi, M. (1998). Turkish earthquakes: two reports. Lessons from the Adana-Ceyhan quake and the Dinar aftershock. *EERI newsletter, 32*(9), 8.

Chambers, J. (1998). A distributed spring soil model for dynamic soil-structure interaction analysis. *ME Thesis, Dept. of Civil Engineering, University of Canterbury, Christchurch, New Zealand*.

Chang, C.-C., & Roschke, P. (1998). Neural network modeling of a magnetorheological damper. *Journal of intelligent material systems and structures, 9*(9), 755-764.

Cheng, F. Y., Jiang, H., & Lou, K. (2008). *Smart structures: innovative systems for seismic response control*: CRC press.

Cheng, F. Y., & Suthiwong, S. (1996). Active control for seismic-resistant structures on embedded foundation in layered half space. *NSF Report, US Department of Commerce, National Technical Information Service, Springfield, VA, NTIS NO. PB97-121354*.

Chowdhury, I., & Dasgupta, S. P. (2008). *Dynamics of structure and foundation-A unified approach: 1. Fundamentals*: Crc Press.

Christenson, R., Lin, Y. Z., Emmons, A., & Bass, B. (2008). Large-scale experimental verification of semiactive control through real-time hybrid simulation. *Journal of Structural Engineering, 134*(4), 522-534.

Clough, R. W., & Penzien, J. (1993). Dynamics of structures, MacGraw-Hill. *Inc Editor*.

Council, A. T., & California, S. E. A. o. (1978). *Tentative provisions for the development of seismic regulations for buildings: a cooperative effort with the design professions, building code interests, and the research community* (Vol. 3): Department of Commerce, National Bureau of Standards.

Crassidis, J. L., & Junkins, J. L. (2011). *Optimal estimation of dynamic systems*: CRC press.

Crouse, C. (2002). *Commentary on soil-structure interaction in US seismic provisions.* Paper presented at the Proc. 7th US national conference on earthquake engineering.

Dorf, R. C., & Bishop, R. H. (2011). *Modern control systems. 12th ed. Richard C. Dorf, Robert H. Bishop* (12th ed. ed.): Pearson Prentice Hall.

Dormand, J. R., & Prince, P. J. (1980). A family of embedded Runge-Kutta formulae. *Journal of computational and applied mathematics*, *6*(1), 19-26.

Dyke, S., & Spencer Jr, B. (1996). *Seismic response control using multiple MR dampers.* Paper presented at the Proceedings of the 2nd international workshop on structural control.

Dyke, S., Spencer Jr, B., Quast, P., & Sain, M. (1995). Role of control-structure interaction in protective system design. *Journal of engineering mechanics, 121*(2), 322-338.

Edrees, T. (2015). *Structural control and identification of civil engineering structures.* Luleå tekniska universitet,

Elias, S., & Matsagar, V. (2017). Effectiveness of tuned mass dampers in seismic response control of isolated bridges including soil-structure interaction. *Latin American Journal of Solids and Structures, 14*(13), 2324-2341.

Elias, S., Matsagar, V., & Datta, T. (2017). Distributed multiple tuned mass dampers for wind response control of chimney with flexible foundation. *Procedia engineering, 199*, 1641-1646.

En, C. (2004). 5 Design of structures for earthquake resistance–Part 5: Foundations, retaining structures and geotechnical aspects. In: Brussels.

Engineers, A. (2010). Minimum design loads for buildings and other structures. *ASCE 7, 10*.

Engineers, A. S. o. C. (2013). *Minimum Design Loads for Buildings and Other Structures, Standard ASCE/SEI 7-10*: Amer Soc Of Civil Engin.

Enrique Luco, J. (1998). A simple model for structural control including soil–structure interaction effects. *Earthquake engineering & structural dynamics, 27*(3), 225-242.

Fema, A. (2005). 440, Improvement of nonlinear static seismic analysis procedures. *FEMA-440, Redwood City, 7*(9), 11.

Franklin, G. F., Powell, J. D., & Emami-Naeini, A. (2015). *Feedback control of dynamic systems. Seventh edition. Global edition. Gene Franklin, J. David Powell, Abbas Emami-Naeini; Gobal edition contributions by Danjay H. S* (Seventh edition. ed.): Pearson Education Limited.

Gajan, S., & Saravanathiiban, D. S. (2011). Modeling of energy dissipation in structural devices and foundation soil during seismic loading. *Soil Dynamics and Earthquake Engineering, 31*(8), 1106-1122.

Gamota, D., & Filisko, F. (1991). Dynamic mechanical studies of electrorheological materials: moderate frequencies. *Journal of rheology, 35*(3), 399-425.

Gazetas, G. (1998). *Seismic soil-structure interaction: New evidence and emerging issues State of the Art Paper.* Paper presented at the Geotechnical Earthquake Engineering and Soil Dynamics Geo-Institute ASCE Conference.

Gazetas, G., & Mylonakis, G. (2001). Soil-structure interaction effects on elastic and inelastic structures.

Ghannad, M., & Jahankhah, H. (2007). Site-dependent strength reduction factors for soil-structure systems. *Soil Dynamics and Earthquake Engineering, 27*(2), 99-110.

Günel, M. H., & Ilgin, H. E. (2014). *Tall buildings: structural systems and aerodynamic form*: Routledge.

Guo, J., Tang, Z., Chen, S., & Li, Z. (2016). Control strategy for the substructuring testing systems to simulate soil-structure interaction. *Smart Structures and Systems, 18*(6), 1169-1188.

Hadjian, A., Luco, J., & Tsai, N. (1974). Soil-structure interaction: continuum or finite element? *Nuclear Engineering and Design, 31*(2), 151-167.

Housner, G. W., Bergman, L. A., Caughey, T. K., Chassiakos, A. G., Claus, R. O., Masri, S. F., . . . Yao, J. T. (1997). Structural control: past, present, and future. *Journal of engineering mechanics, 123*(9), 897-971.

Jabary, R., & Madabhushi, S. (2014). *An experimental investigation of soil-structure interaction in a sway frame structure with tuned mass dampers.* Paper presented at the Proceedings of the International Conference on Structural Dynamic, EURODYN.

Jabary, R., & Madabhushi, S. (2015). Tuned mass damper effects on the response of multi-storied structures observed in geotechnical centrifuge tests. *Soil Dynamics and Earthquake Engineering, 77*, 373-380.

Jabary, R. N., & Madabhushi, G. S. (2018). Tuned mass damper positioning effects on the seismic response of a soil-MDOF-structure system. *Journal of Earthquake Engineering, 22*(2), 281-302.

Jansen, L. M., & Dyke, S. J. (2000). Semiactive control strategies for MR dampers: comparative study. *Journal of engineering mechanics, 126*(8), 795-803.

Jung, H.-J., Spencer Jr, B., Ni, Y., & Lee, I. (2004). State-of-the-art of semiactive control systems using MR fluid dampers in civil engineering applications. *Structural Engineering and Mechanics, 17*(3-4), 493-526.

Jung, H. J., Choi, K. M., Spencer Jr, B. F., & Lee, I. W. (2006). Application of some semi-active control algorithms to a smart base-isolated building employing MR dampers. *Structural Control and Health Monitoring: The Official Journal of the International Association for Structural Control and Monitoring and of the European Association for the Control of Structures, 13*(2-3), 693-704.

Kamath, G. M., & Werely, N. M. (1997). Nonlinear viscoelastic-plastic mechanisms-based model of an electrorheological damper. *Journal of guidance, control, and dynamics, 20*(6), 1125-1132.

Kaufman, H., Barkana, I., & Sobel, K. (2012). *Direct adaptive control algorithms: theory and applications*: Springer Science & Business Media.

Kausel, E. (2010). Early history of soil–structure interaction. *Soil Dynamics and Earthquake Engineering, 30*(9), 822-832.

Kavitha, P., Beena, K., & Narayanan, K. (2016). A review on soil–structure interaction analysis of laterally loaded piles. *Innovative Infrastructure Solutions, 1*(1), 14.

Kerber, F., Hurlebaus, S., Beadle, B., & Stöbener, U. (2007). Control concepts for an active vibration isolation system. *Mechanical Systems and Signal Processing, 21*(8), 3042-3059.

Kim, Y., Langari, R., & Hurlebaus, S. (2009). Semiactive nonlinear control of a building with a magnetorheological damper system. *Mechanical Systems and Signal Processing, 23*(2), 300-315.

Lee, D.-Y., & Wereley, N. M. (2000). *Analysis of electro-and magneto-rheological flow mode dampers using Herschel-Bulkley model.* Paper presented at the Smart Structures and Materials 2000: Damping and Isolation.

Lee, S. K., Lee, S. H., Min, K. W., Moon, B. W., Youn, K. J., & Hwang, J. S. (2009). Performance evaluation of an MR damper in building structures considering soil–structure interaction effects. *The Structural Design of Tall and Special Buildings, 18*(1), 105-115.

Li, C., Yu, Z., Xiong, X., & Wang, C. (2010). Active multiple-tuned mass dampers for asymmetric structures considering soil–structure interaction. *Structural Control and Health Monitoring: The Official Journal of the International Association for Structural Control and Monitoring and of the European Association for the Control of Structures, 17*(4), 452-472.

Li, H., & Wang, J. (2011). Experimental investigation of the seismic control of a nonlinear soil-structure system using MR dampers. *Smart Materials and Structures*, *20*(8), 085026.

Lin, C.-C., Chang, C.-C., & Wang, J.-F. (2010). Active control of irregular buildings considering soil–structure interaction effects. *Soil Dynamics and Earthquake Engineering*, *30*(3), 98-109.

Liu, M.-Y., Chiang, W.-L., Hwang, J.-H., & Chu, C.-R. (2008). Wind-induced vibration of high-rise building with tuned mass damper including soil–structure interaction. *Journal of Wind Engineering and Industrial Aerodynamics*, *96*(6-7), 1092-1102.

Lou, M., Wang, H., Chen, X., & Zhai, Y. (2011). Structure–soil–structure interaction: literature review. *Soil Dynamics and Earthquake Engineering*, *31*(12), 1724-1731.

Lu, Y. (2016). *Seismic soil-structure interaction in performance-based design.* University of Nottingham,

Moehle, J. P. (2015). *Seismic design of reinforced concrete buildings*: McGraw-Hill Education New York.

Moehle, J. P., Ghodsi, T., Hooper, J. D., Fields, D. C., & Gedhada, R. (2011). Seismic design of cast-in-place concrete special structural walls and coupling beams. *NEHRP Seismic Design Technical Brief No, 6*.

Moehle, J. P., Hooper, J. D., Kelly, D. J., & Meyer, T. R. (2010). Seismic Design of cast-in-place concrete diaphragms, chords, and collectors. *Seismic design technical brief, US Department of Commerce, Building and Fire Research Laboratory, National Institute of Standards and Technology*.

Moghaddasi, M., Cubrinovski, M., Pampanin, S., Carr, A., & Chase, J. (2010). A robust probabilistic evaluation of soil-foundation-structure interaction effects on structural response. *Soil-Foundation-Structure Interaction*, 77-84.

Morse, W., & Ossman, K. (1990). Model following reconfigurable flight control system for the AFTI/F-16. *Journal of guidance, control, and dynamics, 13*(6), 969-976.

Mylonakis, G., & Gazetas, G. (2000). Seismic soil-structure interaction: beneficial or detrimental? *Journal of Earthquake Engineering, 4*(3), 277-301.

Nazarimofrad, E., & Zahrai, S. M. (2016). Seismic control of irregular multistory buildings using active tendons considering soil–structure interaction effect. *Soil Dynamics and Earthquake Engineering, 89*, 100-115.

Nazarimofrad, E., & Zahrai, S. M. (2017). Fuzzy control of asymmetric plan buildings with active tuned mass damper considering soil-structure interaction. *Soil Dynamics and Earthquake Engineering*.

Neuenhofer, A. (2006). Lateral stiffness of shear walls with openings. *Journal of Structural Engineering, 132*(11), 1846-1851.

Ohtori, Y., Christenson, R., Spencer Jr, B., & Dyke, S. (2004). Benchmark control problems for seismically excited nonlinear buildings. *Journal of engineering mechanics, 130*(4), 366-385.

Reséndiz, D., & Roesset, J. (1985). *Soil-structure interaction in Mexico City during the 1985 earthquakes.* Paper presented at the The Mexico Earthquakes—1985: Factors Involved and Lessons Learned.

Roesset, J. M. (2013). Soil structure interaction the early stages. *淡江理工學刊, 16*(1), 1-8.

Saaed, T. E., Nikolakopoulos, G., Jonasson, J.-E., & Hedlund, H. (2015). A state-of-the-art review of structural control systems. *Journal of Vibration and Control, 21*(5), 919-937.

Sahasrabudhe, S., & Nagarajaiah, S. (2005). Experimental study of sliding base-isolated buildings with magnetorheological dampers in near-fault earthquakes. *Journal of Structural Engineering, 131*(7), 1025-1034.

Scawthorn, C., & Chen, W.-F. (2002). *Earthquake engineering handbook*: CRC press.

Seetharamulu, K. (2014). *Dynamic Analysis of Skeletal Structures: Force and Displacement Methods and Iterative Techniques*. New York: McGraw-Hill Education.

Sharma, N., Dasgupta, K., & Dey, A. (2018). A state-of-the-art review on seismic SSI studies on building structures. *Innovative Infrastructure Solutions, 3*(1), 22.

Shibata, H., Sun, Y., Fujinaka, T., & Maruoka, G. (1996). *Discrete-time algorithm for generalized simplified adaptive control and its application to DC motor control.* Paper presented at the Proceedings of the 1996 IEEE IECON. 22nd International Conference on Industrial Electronics, Control, and Instrumentation.

Shiming, W., & Gang, G. (1998). Dynamic soil-structure interaction for high-rise buildings. In *Developments in geotechnical engineering* (Vol. 83, pp. 203-216): Elsevier.

Shook, D., Roschke, P., & Ozbulut, O. (2008). Superelastic semi-active damping of a base-isolated structure. *Structural Control and Health Monitoring: The Official Journal of the International Association for Structural Control and Monitoring and of the European Association for the Control of Structures, 15*(5), 746-768.

Sivaselvan, M. V., Reinhorn, A. M., Shao, X., & Weinreber, S. (2008). Dynamic force control with hydraulic actuators using added compliance and displacement compensation. *Earthquake engineering & structural dynamics, 37*(15), 1785-1800.

Skelton, R. E. (1988). *Dynamic systems control : linear systems analysis and synthesis. Robert E. Skelton*: Wiley.

Smith, H. A., & WU, W. H. (1997). Effective optimal structural control of soil–structure interaction systems. *Earthquake engineering & structural dynamics, 26*(5), 549-570.

Sobel, K., Kaufman, H., & Mabius, L. (1982). Implicit adaptive control for a class of MIMO systems. *IEEE Transactions on Aerospace and Electronic Systems*(5), 576-590.

Spencer, B., & Sain, M. K. (1997). Controlling buildings: a new frontier in feedback. *IEEE Control Systems Magazine, 17*(6), 19-35.

Spencer Jr, B., Dyke, S., Sain, M., & Carlson, J. (1997). Phenomenological model for magnetorheological dampers. *Journal of engineering mechanics, 123*(3), 230-238.

Stanway, R., Sproston, J., & Stevens, N. (1985). Non-linear identification of an electro-rheological vibration damper. *IFAC Proceedings Volumes, 18*(5), 195-200.

Stanway, R., Sproston, J., & Stevens, N. (1987). Non-linear modelling of an electro-rheological vibration damper. *Journal of Electrostatics, 20*(2), 167-184.

Stewart, J., Crouse, C., Hutchinson, T. C., Lizundia, B., Naeim, F., & Ostadan, F. (2012). *Soil-structure interaction for building structures*. Retrieved from

Stewart, J. P., Fenves, G. L., & Seed, R. B. (1999). Seismic soil-structure interaction in buildings. I: Analytical methods. *Journal of Geotechnical and Geoenvironmental Engineering, 125*(1), 26-37.

Stewart, J. P., Kim, S., Bielak, J., Dobry, R., & Power, M. S. (2003). Revisions to soil-structure interaction procedures in NEHRP design provisions. *Earthquake Spectra, 19*(3), 677-696.

Stewart, J. P., Seed, R. B., & Fenves, G. L. (1999). Seismic soil-structure interaction in buildings. II: Empirical findings. *Journal of Geotechnical and Geoenvironmental Engineering, 125*(1), 38-48.

Sun, C. (2018). Semi-active control of monopile offshore wind turbines under multi-hazards. *Mechanical Systems and Signal Processing, 99*, 285-305. doi:10.1016/j.ymssp.2017.06.016

Takewaki, I. (2000). Soil–structure random response reduction via TMD-VD simultaneous use. *Computer methods in applied mechanics and engineering, 190*(5-7), 677-690.

Taranath, B. S. (2009). *Reinforced concrete design of tall buildings*: CRC press.

Tsang, H., Su, R., & Chandler, A. (2006). Simplified inverse dynamics models for MR fluid dampers. *Engineering Structures, 28*(3), 327-341.

Tse, T., & Chang, C. (2004). Shear-mode rotary magnetorheological damper for small-scale structural control experiments. *Journal of Structural Engineering, 130*(6), 904-911.

Veletsos, A. S., & Meek, J. W. (1974). Dynamic behaviour of building-foundation systems. *Earthquake engineering & structural dynamics, 3*(2), 121-138.

Veletsos, A. S., & Nair, V. (1975). Seismic interaction of structures on hysteretic foundations. *Journal of the Structural Division, 101*(1), 109-129.

Veletsos, A. S., & Prasad, A. M. (1989). Seismic interaction of structures and soils: stochastic approach. *Journal of Structural Engineering, 115*(4), 935-956.

Wang, D., & Liao, W. (2004). Modeling and control of magnetorheological fluid dampers using neural networks. *Smart Materials and Structures, 14*(1), 111.

Wen, Y.-K. (1976). Method for random vibration of hysteretic systems. *Journal of the engineering mechanics division, 102*(2), 249-263.

West, H. H. (1989). Analysis of Structures: An Integration of Classical and Modern Methods.

Wolf, J., & Hall, W. (1988). *Soil-structure-interaction analysis in time domain*: A Division of Simon & Schuster.

Wolf, J. P. (1985). *Dynamic soil-structure interaction. John P. Wolf*: Prentice-Hall.

Wolf, J. P. (1994). *Foundation vibration analysis using simple physical models*: Pearson Education.

Wong, H., & Luco, J. (1991). Structural control including soil-structure interaction effects. *Journal of engineering mechanics, 117*(10), 2237-2250. doi:Doi 10.1061/(Asce)0733-9399(1991)117:10(2237)

Wu, W.-H., & Smith, H. A. (1995). Comparison of SSI effects on externally and internally controlled systems. *Smart Materials and Structures, 4*(1A), A158.

Wysard Soares, R. (2019). *Adaptive Control to Reduce the Dynamic Response of Bridges Considering Parametric Changes.*

Xu, Y.-L., & He, J. (2017). *Smart civil structures*: CRC Press.

Xu, Y., & Kwok, K. (1992). Wind-induced response of soil-structure-damper systems. *Journal of Wind Engineering and Industrial Aerodynamics, 43*(1-3), 2057-2068.

Yang, G., Spencer Jr, B., Carlson, J., & Sain, M. (2002). Large-scale MR fluid dampers: modeling and dynamic performance considerations. *Engineering Structures, 24*(3), 309-323.

Zhang, X. (2004). Intelligent hybrid damper-actuator bracing control (HDABC) with deterministic and nondeterministic seismic input, soil-structure interaction, and tectonic movements. *Proceedings of the Third International Conference on Earthquake Engineering*, 685-692.

Zhang, X., Cheng, F., & Jiang, H. (2006). Hybrid actuator–damper–bracing control (HDABC) system with intelligent strategy and soil–structure interaction. *Engineering Structures, 28*(14), 2010-2022.

Zhao, X., Wang, S., Du, D., & Liu, W. (2017). Optimal Design of Viscoelastic Dampers in Frame Structures considering Soil-Structure Interaction Effect. *Shock and vibration, 2017*. doi:Artn 962908310.1155/2017/9629083

APPENDIX A

MAX. CONTROL FORCE RATIO AND MAX. DISP. RATIO

Geotechnical paramedic study

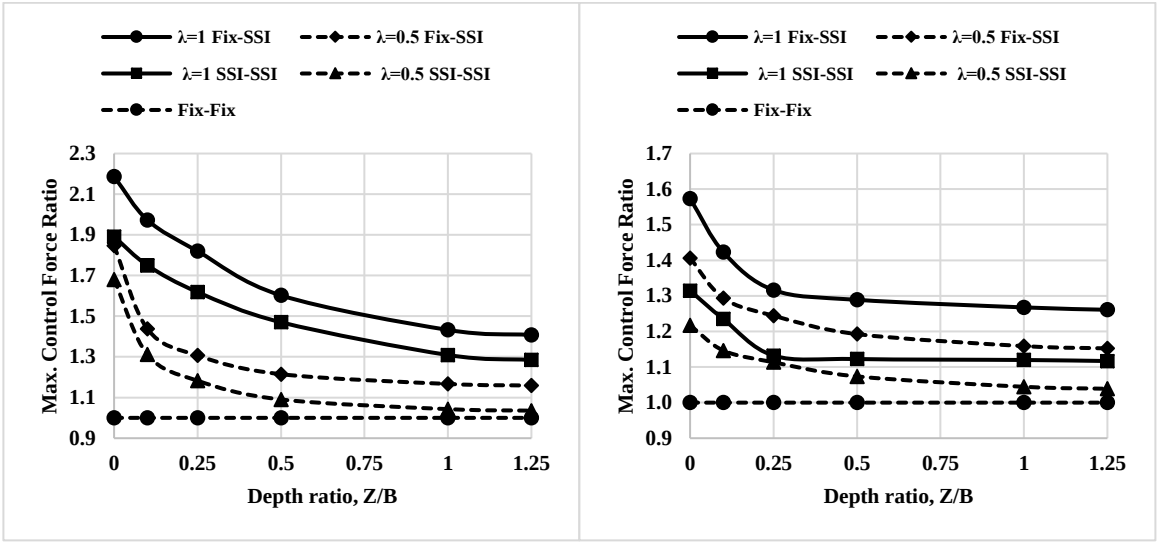


Taiwan SMART1 (5), 1/29/1981, SMART1 O01, NS  Mammoth Lakes-07, 5/27/1980, Green Church, 146

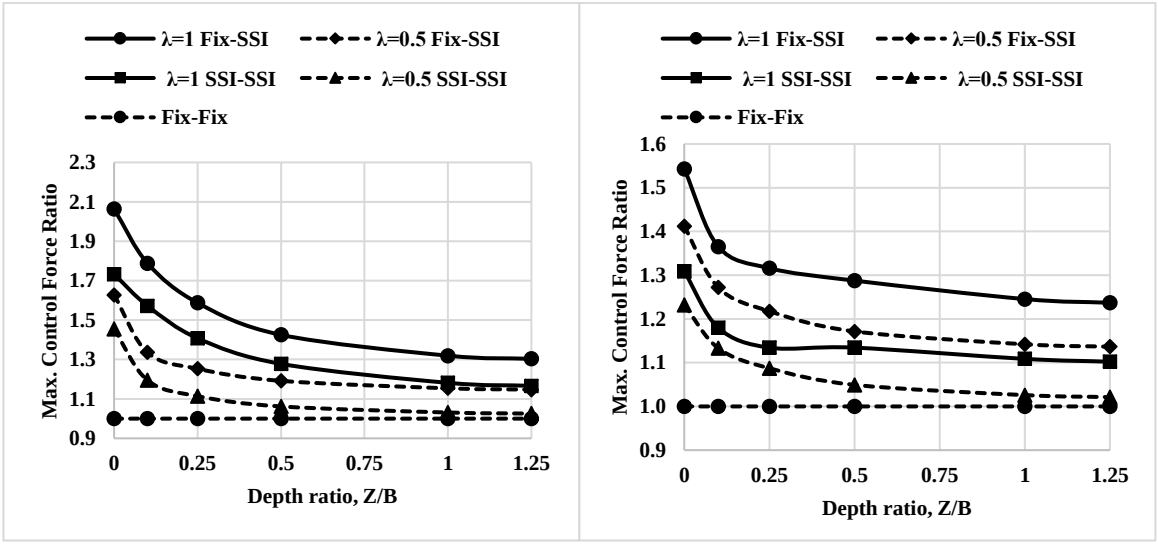


Livermore-02, 1/27/1980, Antioch - 510 G St, 270  Borrego, 10/21/1942, El Centro Array #9, 0

**Figure A-1** Max. control force ratio for medium soil top and soft soil bottom under different earthquakes

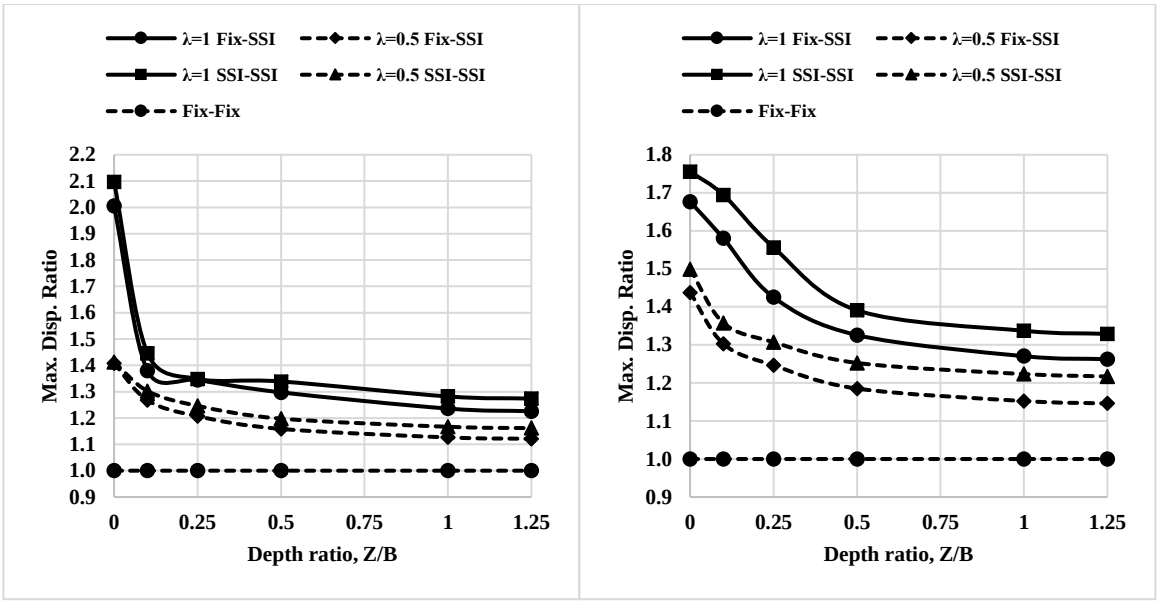


Taiwan SMART1 (5), 1/29/1981, SMART1 O01, NS

Mammoth Lakes-07, 5/27/1980, Green Church, 146

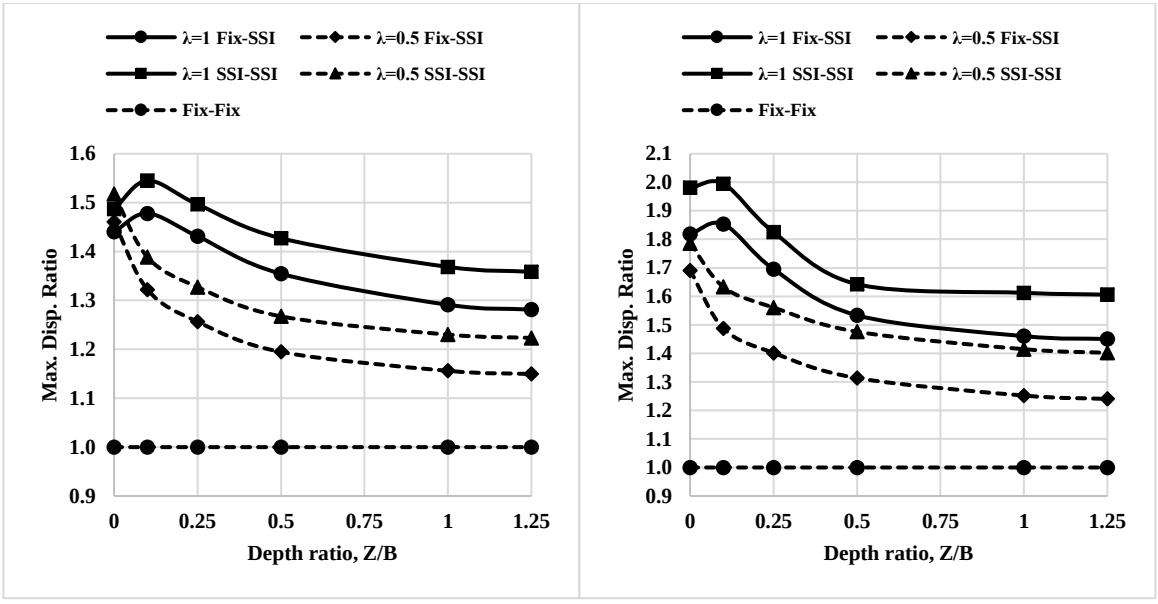


Livermore-02, 1/27/1980, Antioch - 510 G St, 270

Borrego, 10/21/1942, El Centro Array #9, 0

**Figure A-2** Max. displacement ratio for medium soil top and soft soil bottom under different earthquakes

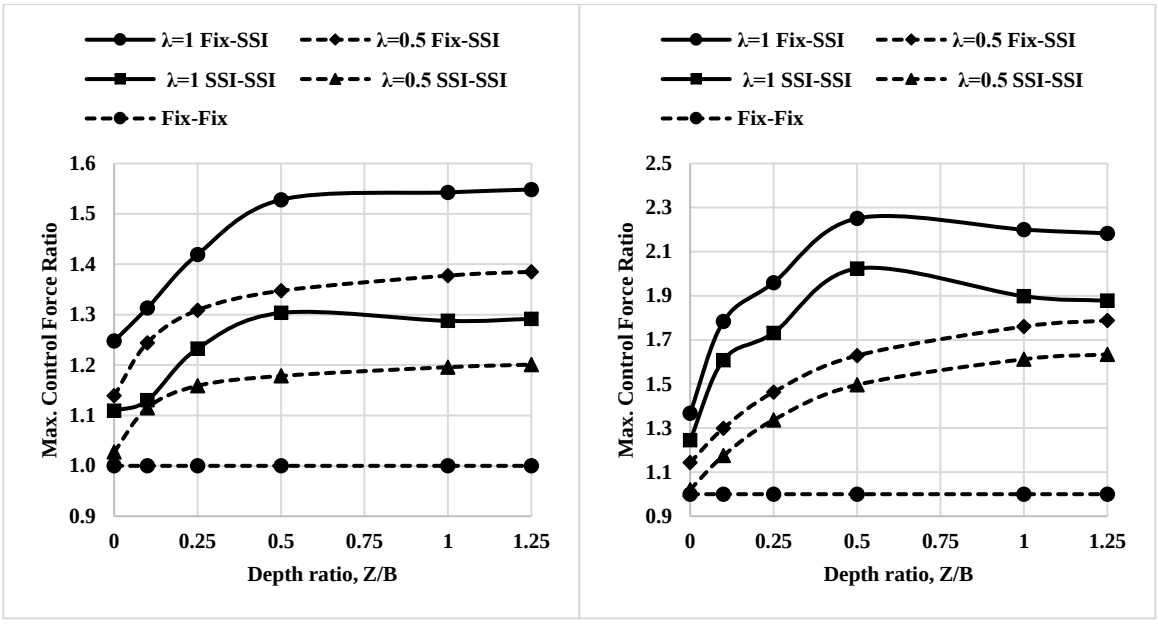


Taiwan SMART1 (5), 1/29/1981, SMART1 O01, NS  Mammoth Lakes-07, 5/27/1980, Green Church, 146

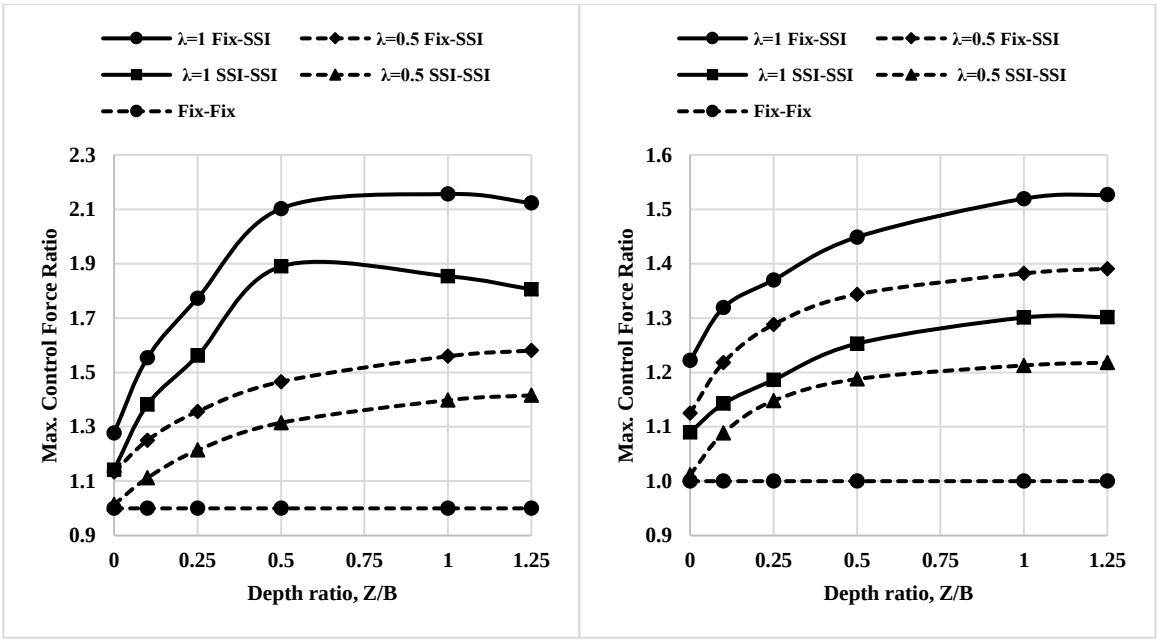


Livermore-02, 1/27/1980, Antioch - 510 G St, 270  Borrego, 10/21/1942, El Centro Array #9, 0

**Figure A-3** Max. control force ratio for soft soil top and medium soil bottom under different earthquakes

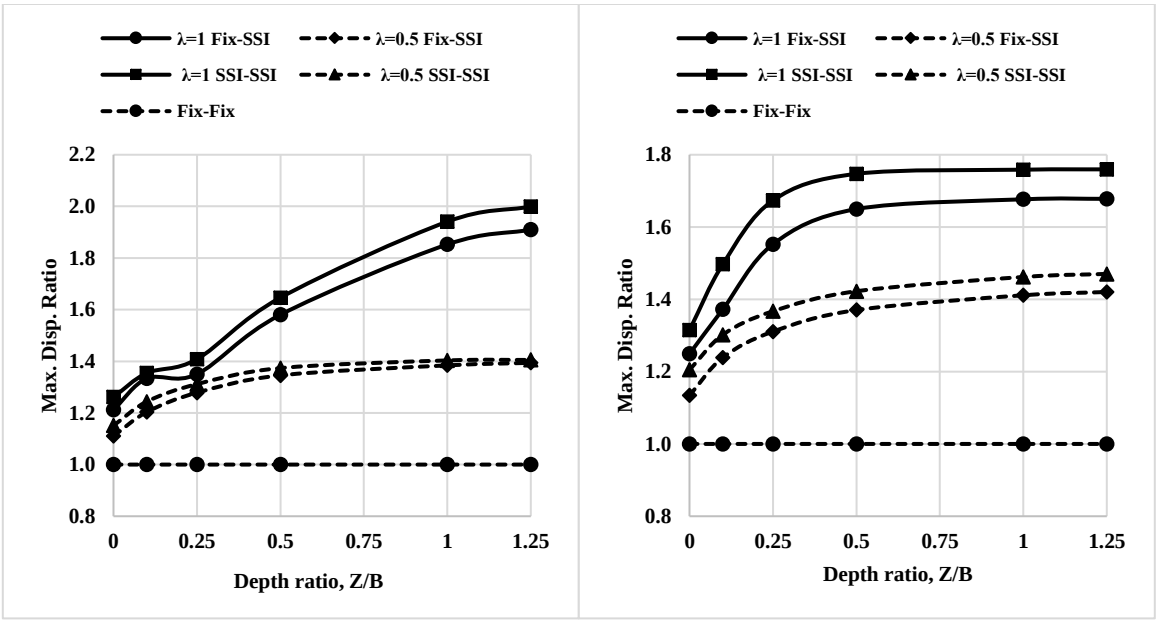


Taiwan SMART1 (5), 1/29/1981, SMART1 O01, NS  Mammoth Lakes-07, 5/27/1980, Green Church, 146

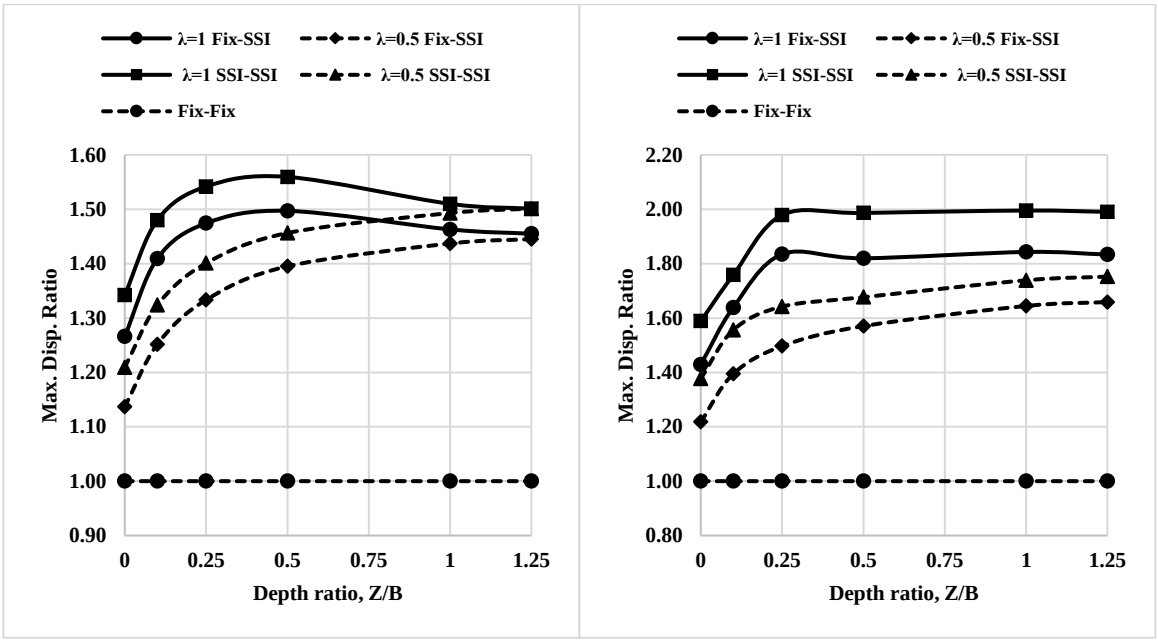


Livermore-02, 1/27/1980, Antioch - 510 G St, 270  Borrego, 10/21/1942, El Centro Array #9, 0

**Figure A-4** Max. displacement ratio for soft soil top and medium soil bottom under different earthquakes

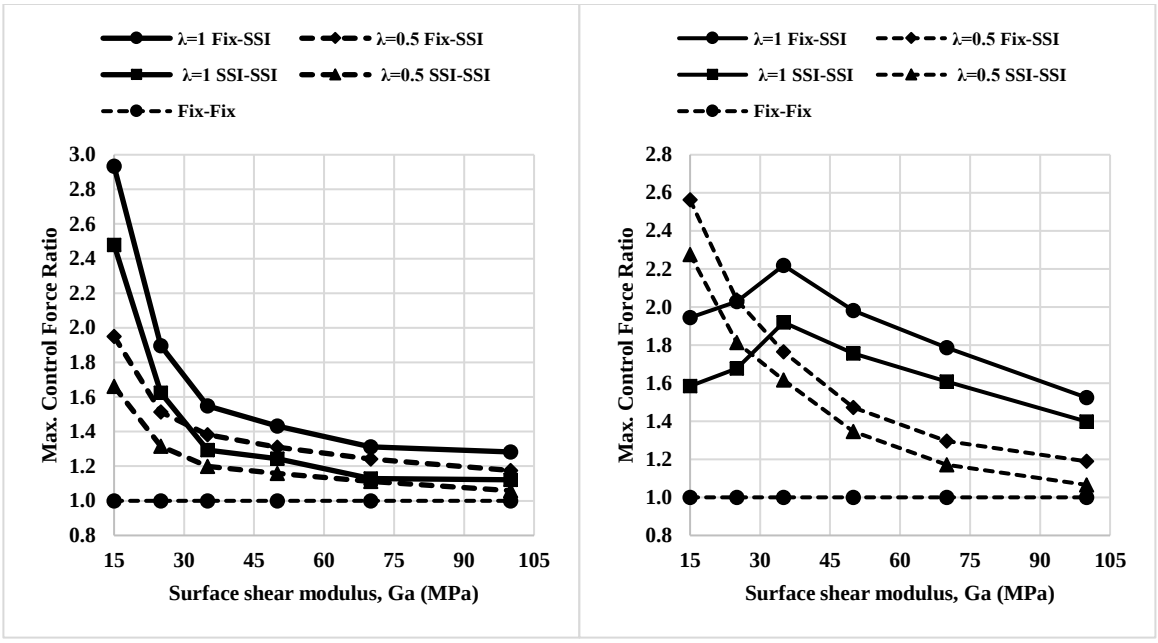


Taiwan SMART1 (5), 1/29/1981, SMART1 O01, NS  Mammoth Lakes-07, 5/27/1980, Green Church, 146

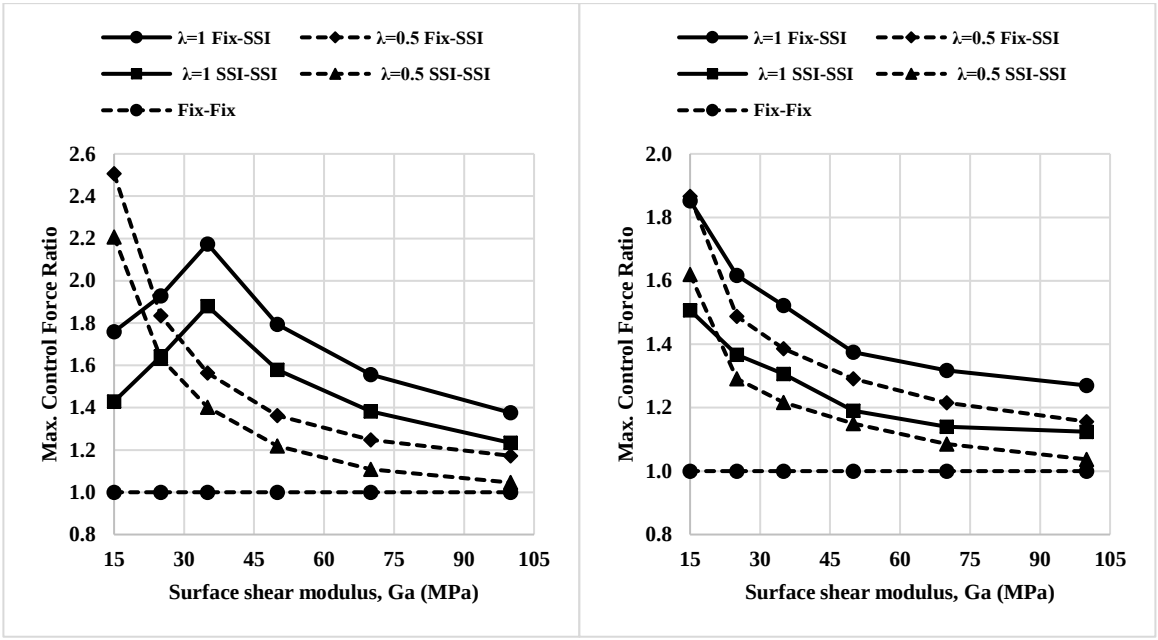


Livermore-02, 1/27/1980, Antioch - 510 G St, 270  Borrego, 10/21/1942, El Centro Array #9, 0

**Figure A-5** Max. control force ratio for clay soil (linear) under different earthquakes

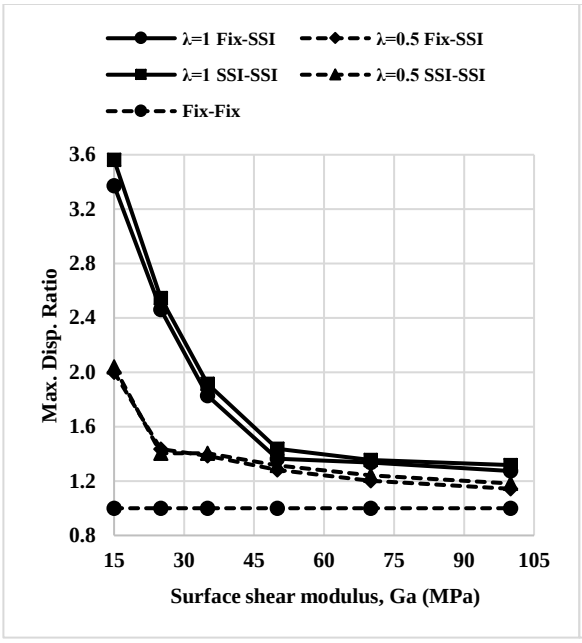


Taiwan SMART1 (5), 1/29/1981, SMART1 O01, NS

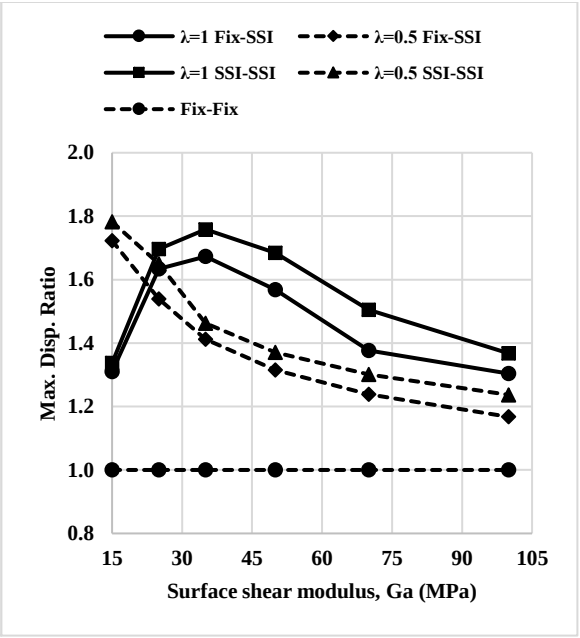


Mammoth Lakes-07, 5/27/1980, Green Church, 146

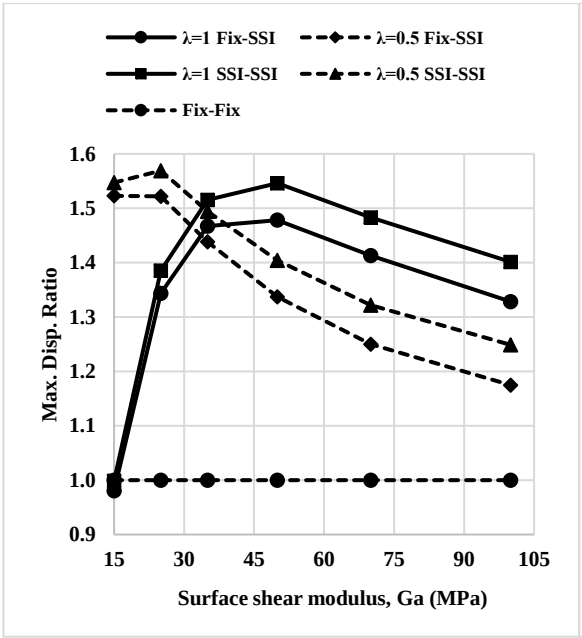


Livermore-02, 1/27/1980, Antioch - 510 G St, 270

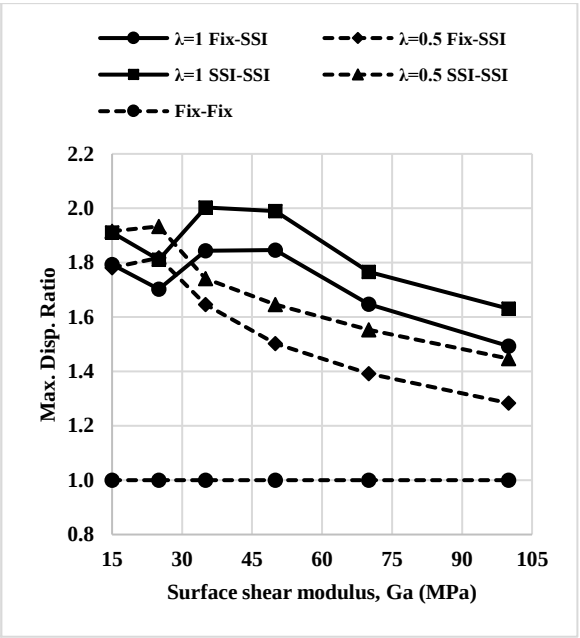


Borrego, 10/21/1942, El Centro Array #9, 0

**Figure A-6** Max. displacement ratio for clay soil (linear) under different earthquakes.

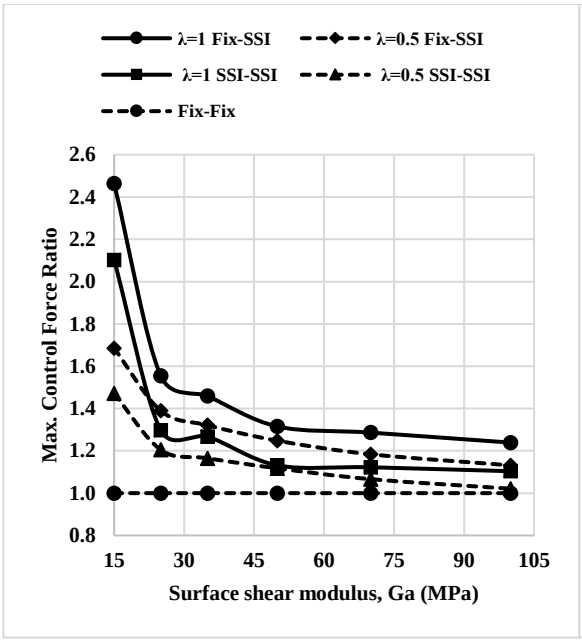


Taiwan SMART1 (5), 1/29/1981, SMART1 O01, NS

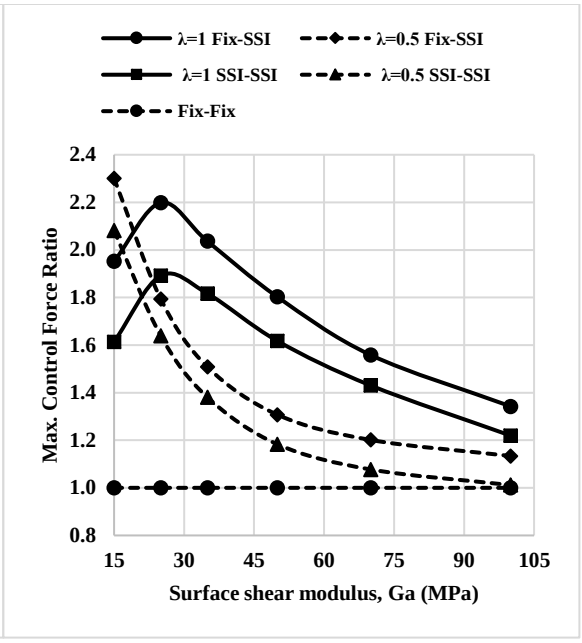


Mammoth Lakes-07, 5/27/1980, Green Church, 146

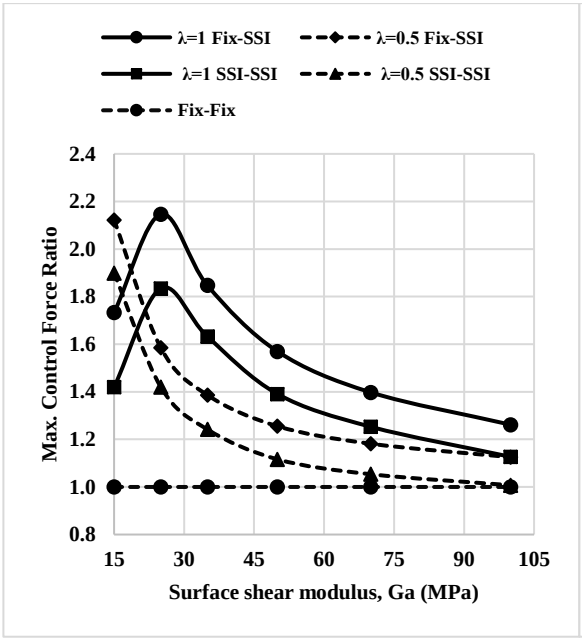


Livermore-02, 1/27/1980, Antioch - 510 G St, 270

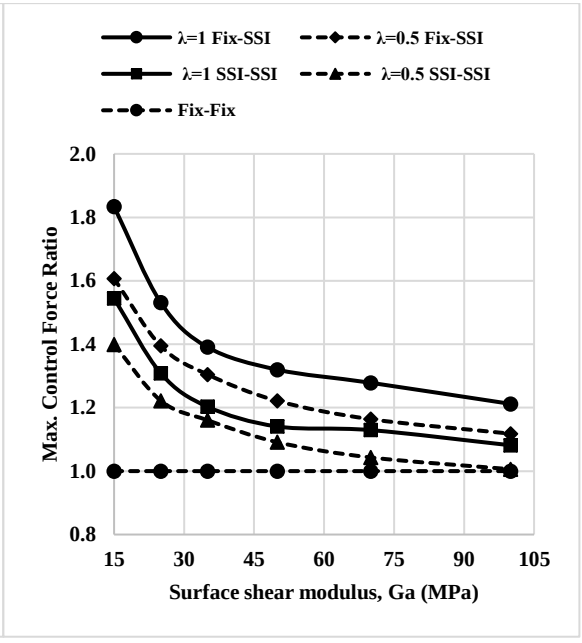


Borrego, 10/21/1942, El Centro Array #9, 0

**Figure A-7** Max. control force ratio for sand soil (parabola) under different earthquakes

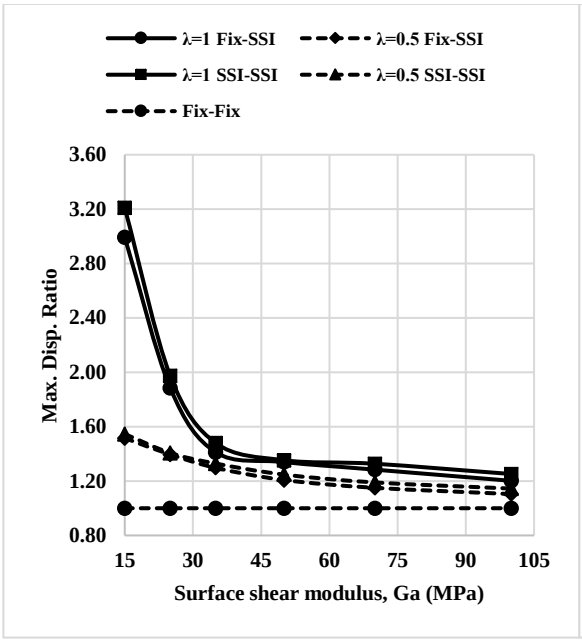


Taiwan SMART1 (5), 1/29/1981, SMART1 O01, NS

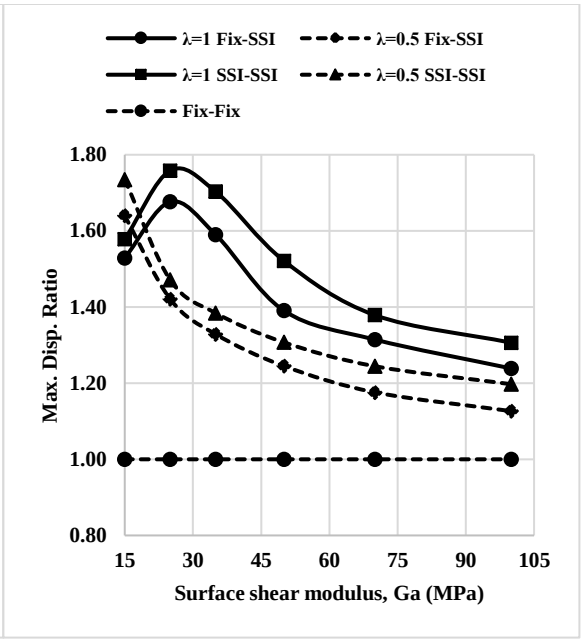


Mammoth Lakes-07, 5/27/1980, Green Church, 146

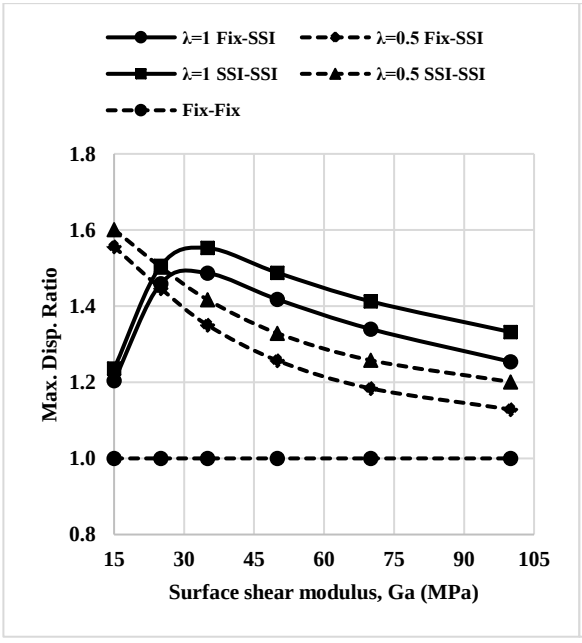


Livermore-02, 1/27/1980, Antioch - 510 G St, 270

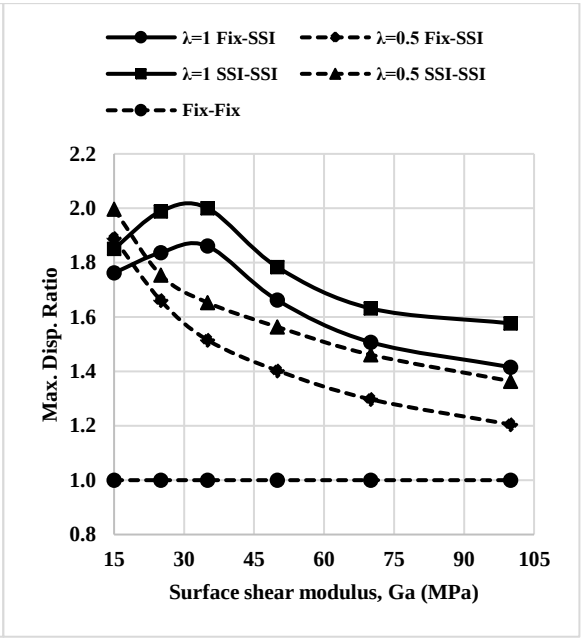


Borrego, 10/21/1942, El Centro Array #9, 0

**Figure A-8** Max. displacement ratio for sand soil (parabola) under different earthquakes.

Structural paramedic study.

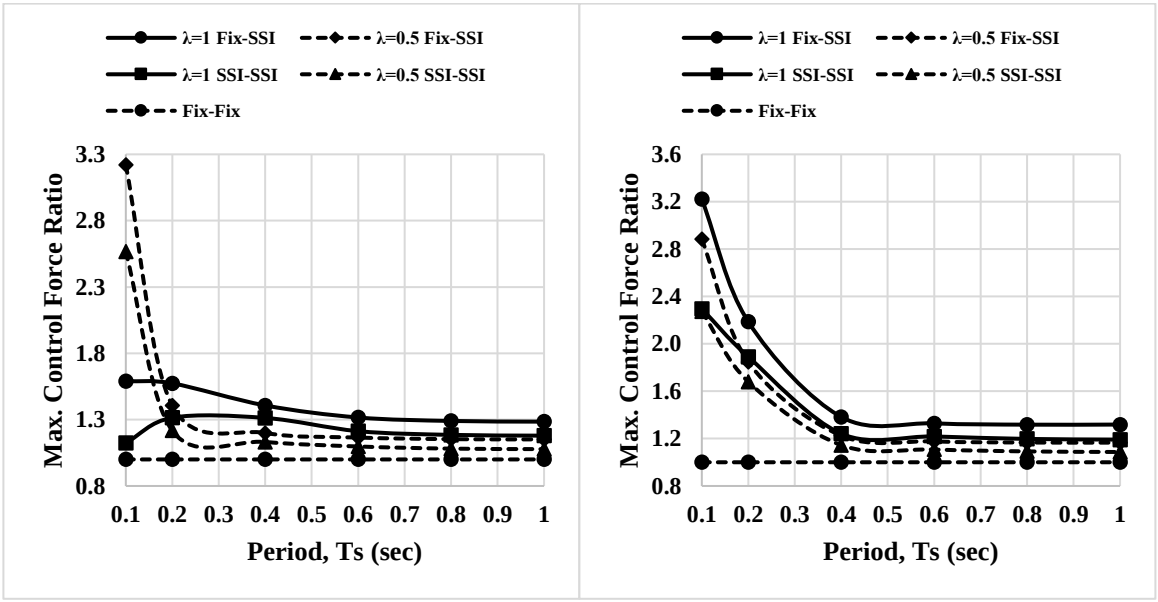


Taiwan SMART1 (5), 1/29/1981, SMART1 O01, NS  Mammoth Lakes-07, 5/27/1980, Green Church, 146

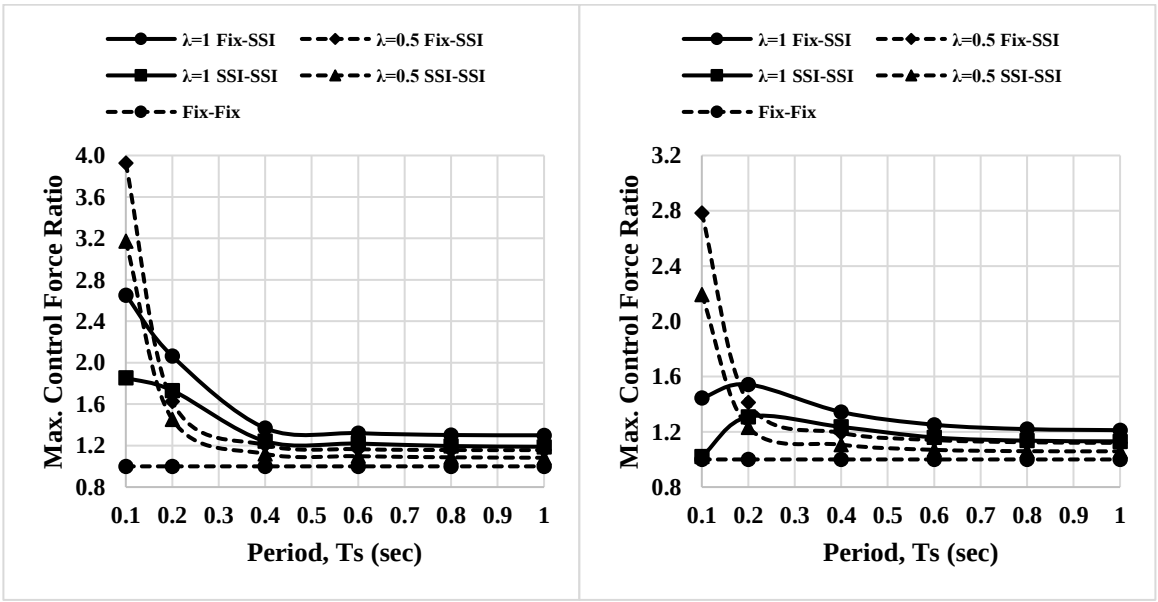


Livermore-02, 1/27/1980, Antioch - 510 G St, 270  Borrego, 10/21/1942, El Centro Array #9, 0

**Figure A-9** Max. control force ratio for structural parametric study under different earthquakes.

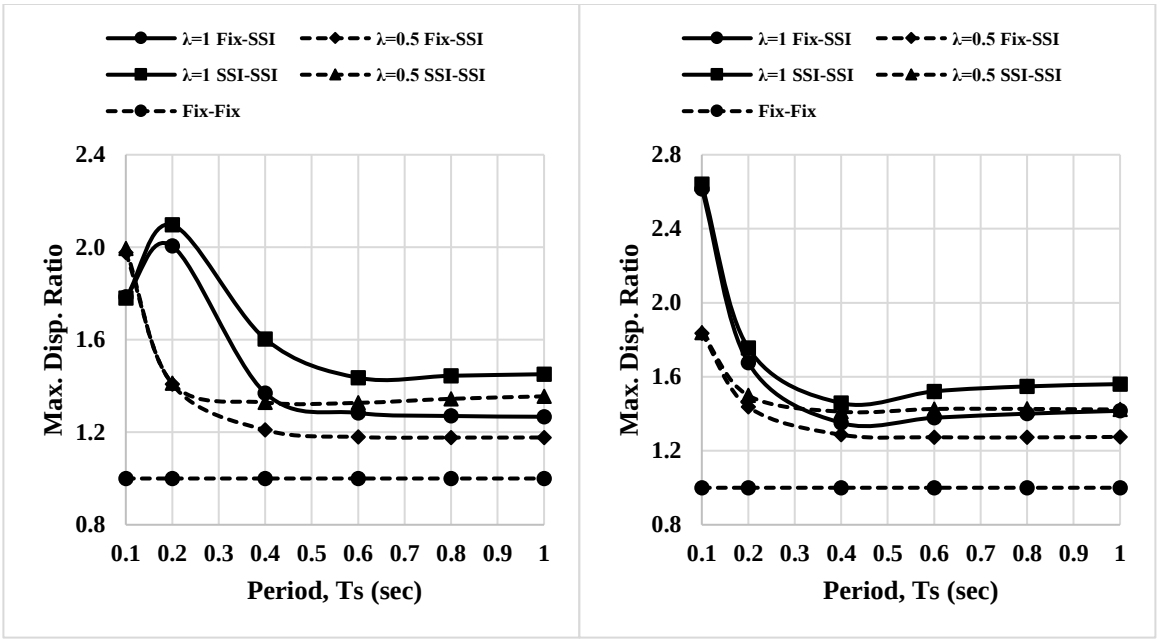


Taiwan SMART1 (5), 1/29/1981, SMART1 O01, NS  Mammoth Lakes-07, 5/27/1980, Green Church, 146

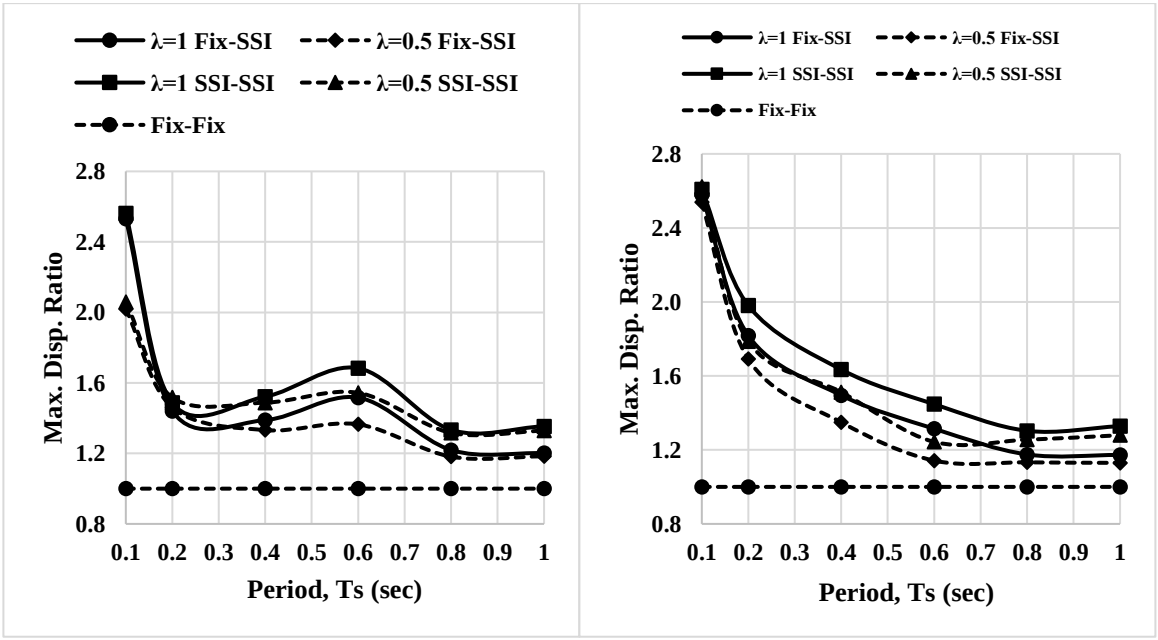


Livermore-02, 1/27/1980, Antioch - 510 G St, 270  Borrego, 10/21/1942, El Centro Array #9, 0

**Figure A-10** Max. displacement ratio for structural parametric study under different earthquakes.

APPENDIX B

NORMALIZED OF FOUNDATION RESULTS CHAPTER 6

Geotechnical paramedic study clay (linear) soil profile

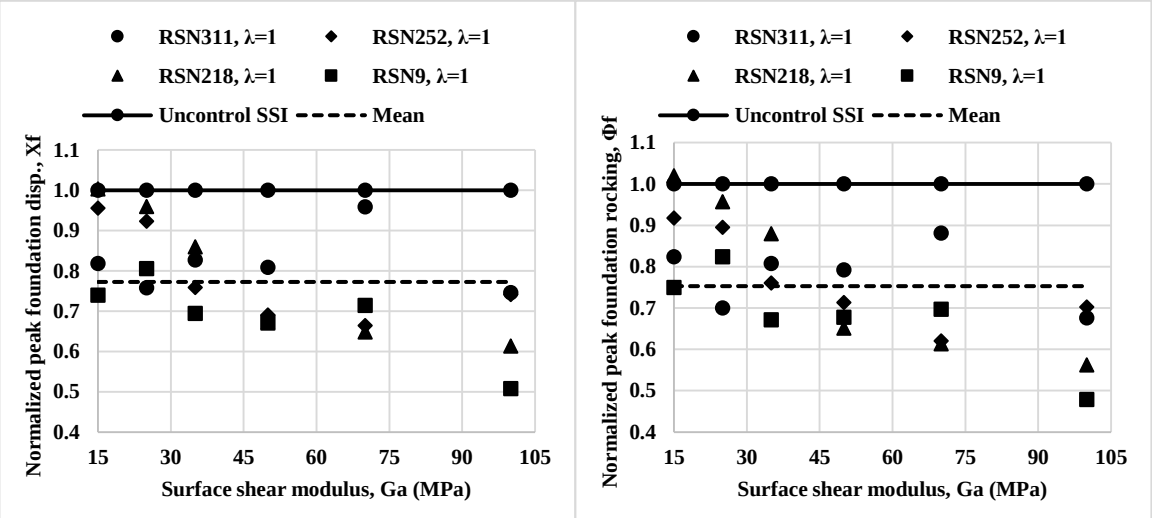


**Figure B-1** Normalization of horizontal and rocking foundation displacement for Fixed-SSI reference model and λ = 1.

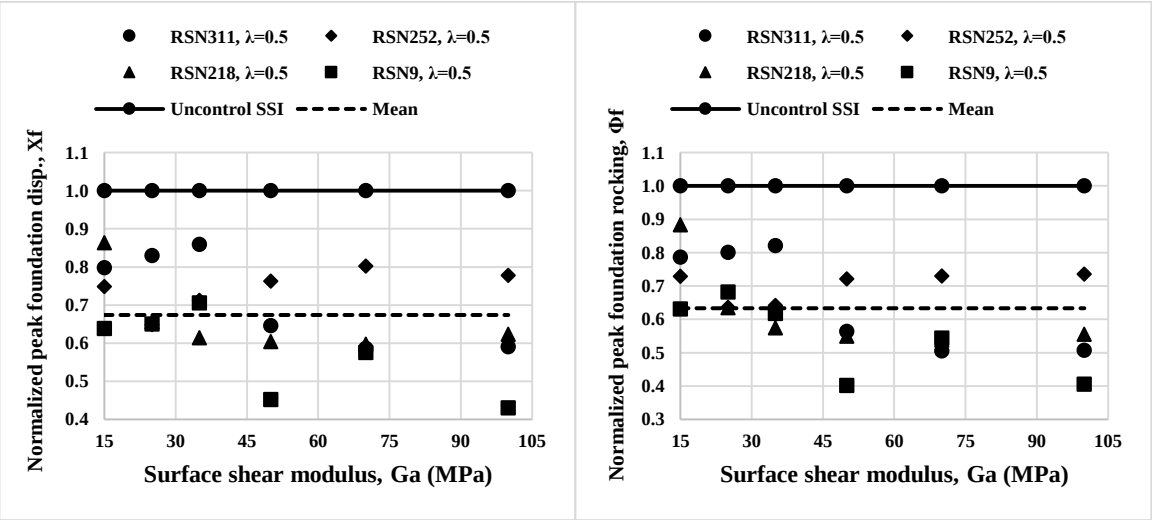


**Figure B-2** Normalization of horizontal and rocking foundation displacement for Fixed-SSI reference model and λ = 0.5.

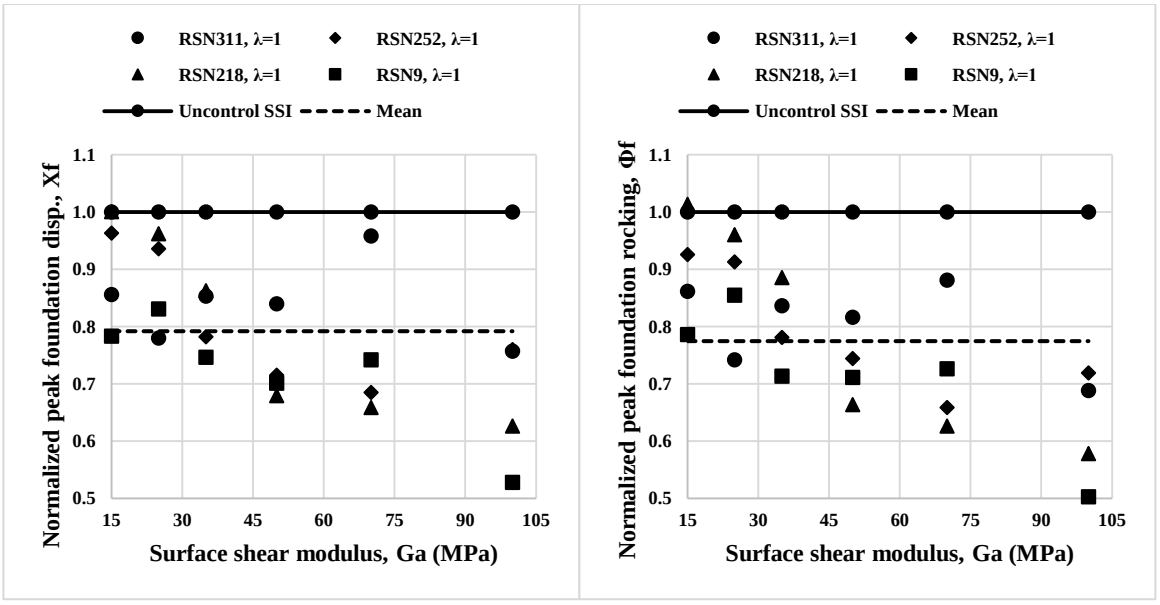


**Figure B-3** Normalization of horizontal and rocking foundation displacement for SSI-SSI reference model and $\lambda = 1$.

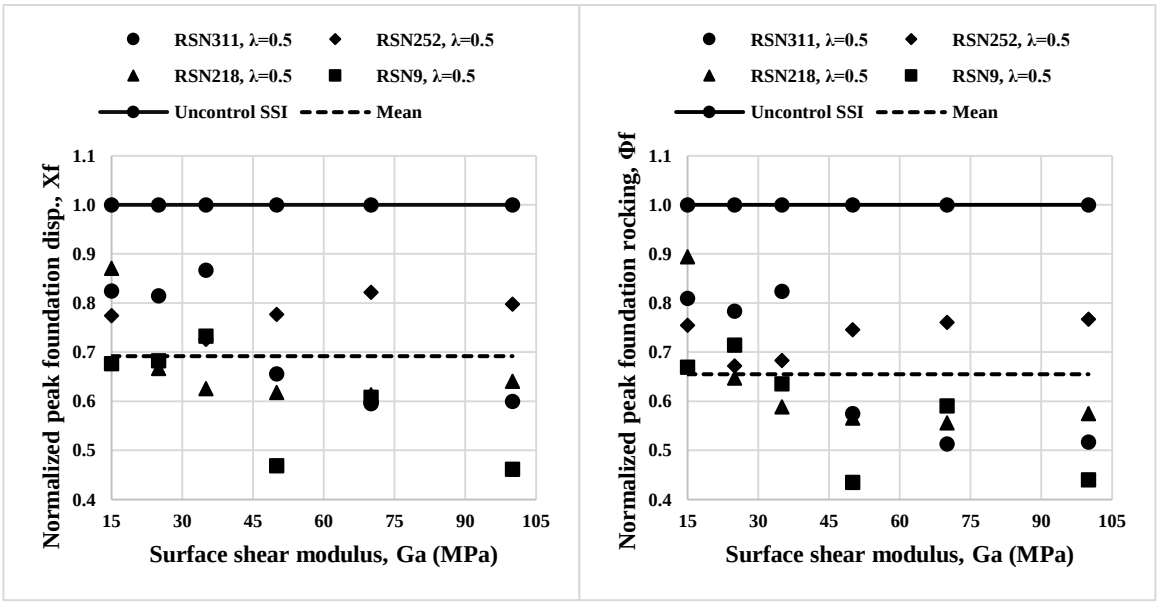


**Figure B-4** Normalization of horizontal and rocking foundation displacement for SSI-SSI reference model and $\lambda = 0.5$.

Medium soil top and soft soil bottom soil profile

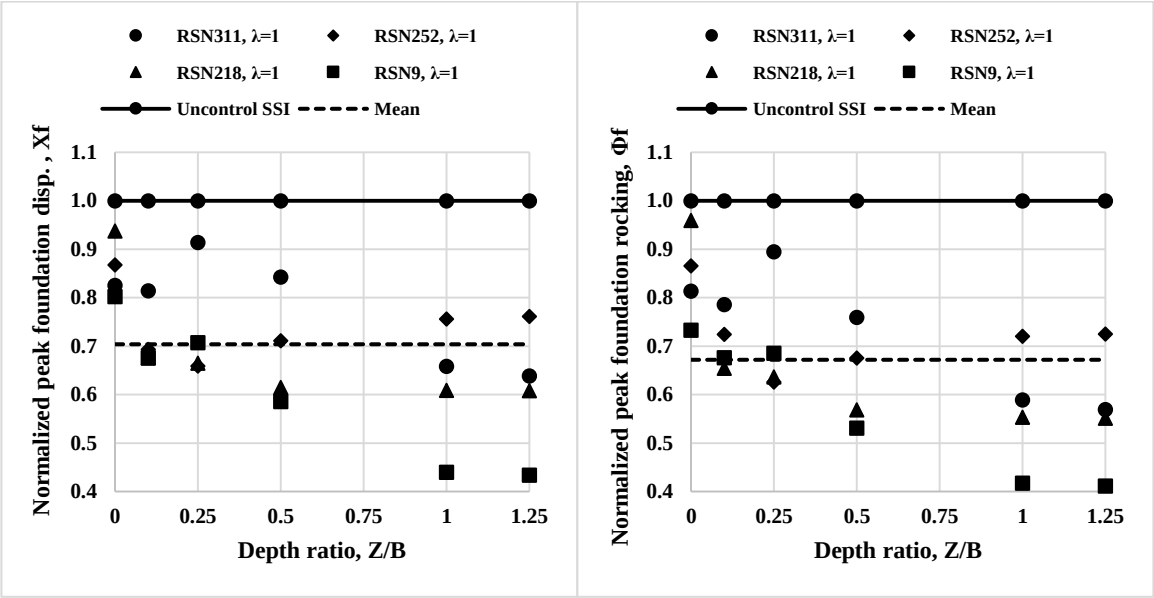


**Figure B-5** Normalization of horizontal and rocking foundation displacement for Fixed-SSI reference model and λ = 1.

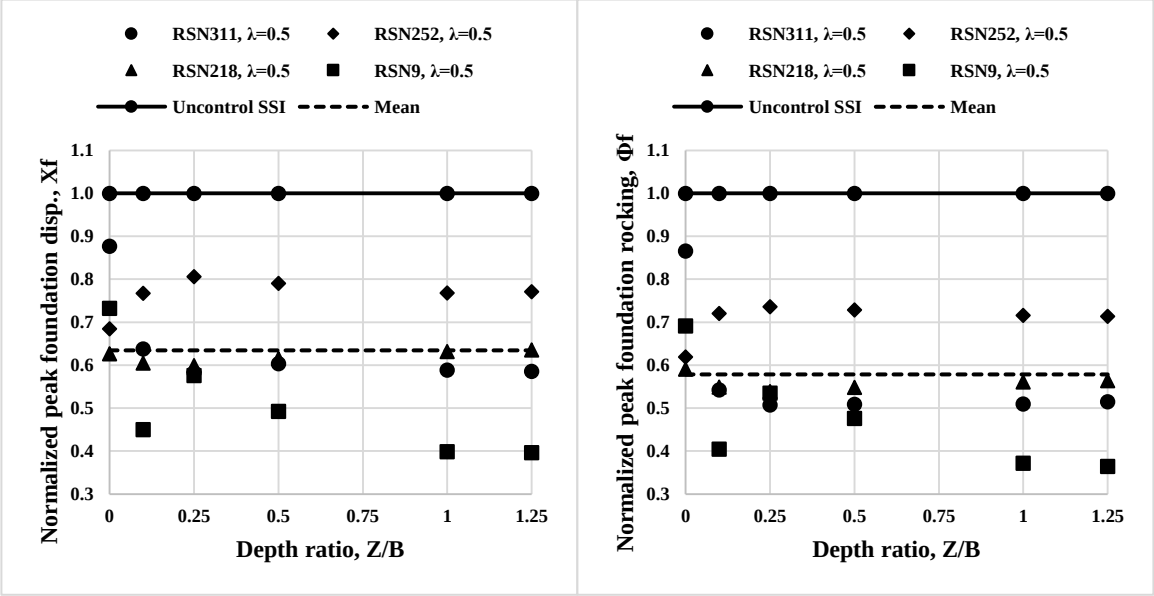


**Figure B-6** Normalization of horizontal and rocking foundation displacement for Fixed-SSI reference model and λ = 0.5.

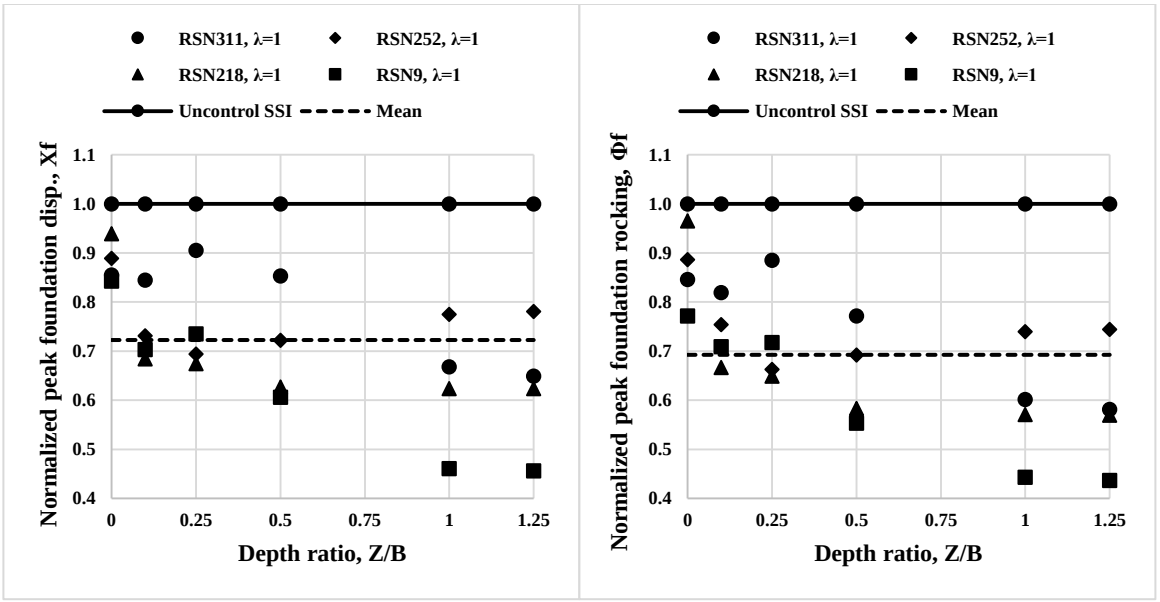


**Figure B-7** Normalization of horizontal and rocking foundation displacement for SSI-SSI reference model and $\lambda = 1$.

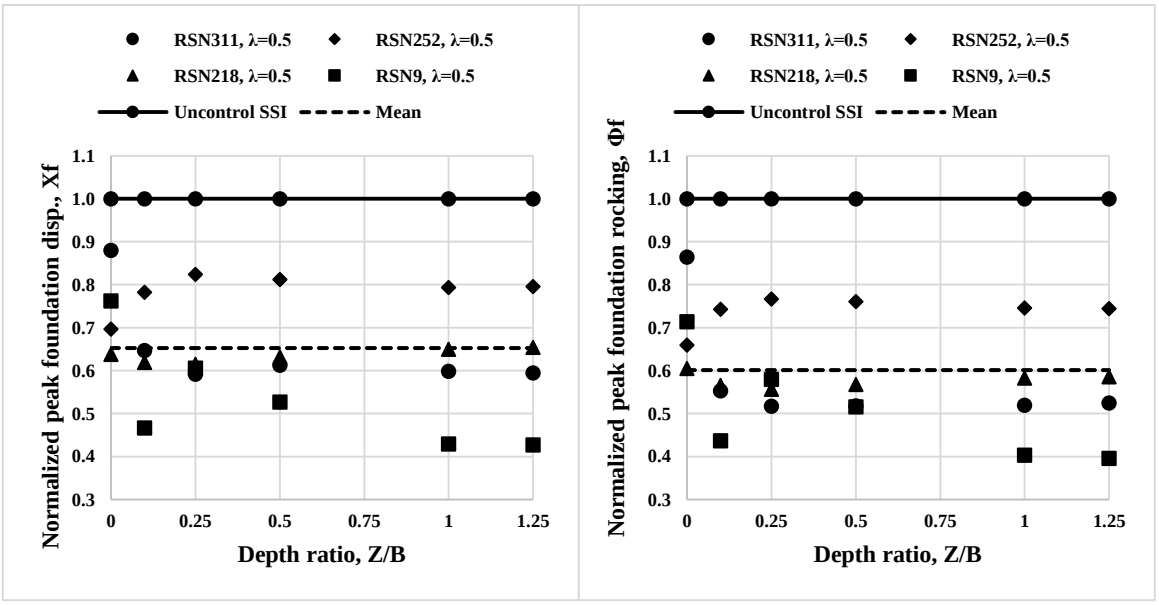


**Figure B-8** Normalization of horizontal and rocking foundation displacement for SSI-SSI reference model and $\lambda = 0.5$.

Sand (parabola) soil profile

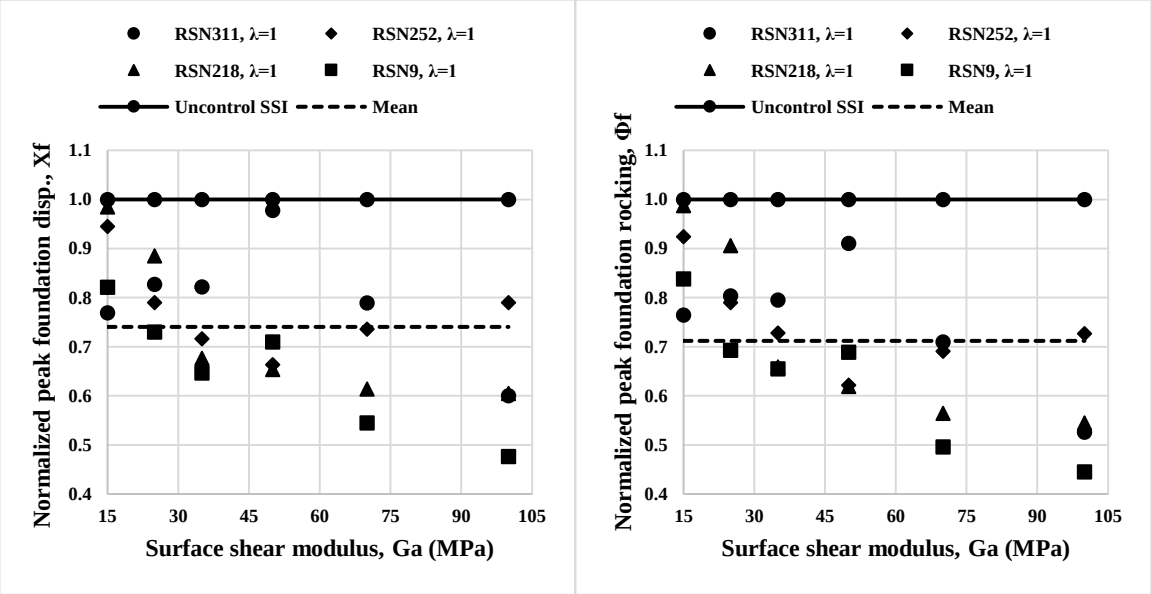


**Figure B-9** Normalization of horizontal and rocking foundation displacement for Fixed-SSI reference model and $\lambda = 1$.

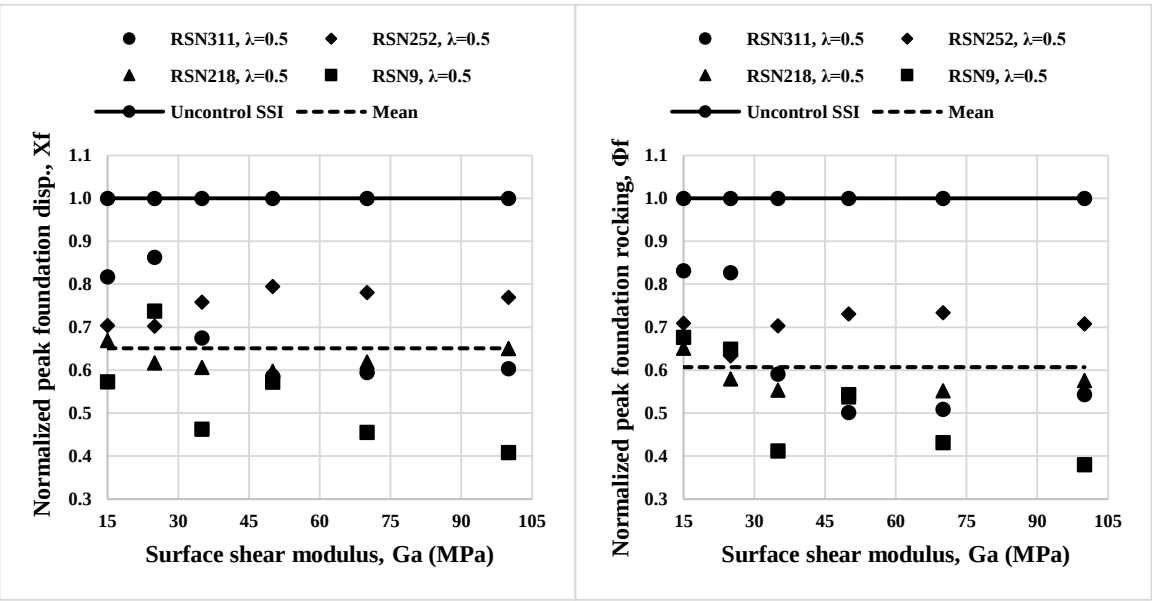


**Figure B-10** Normalization of horizontal and rocking foundation displacement for Fixed-SSI reference model and $\lambda = 0.5$.

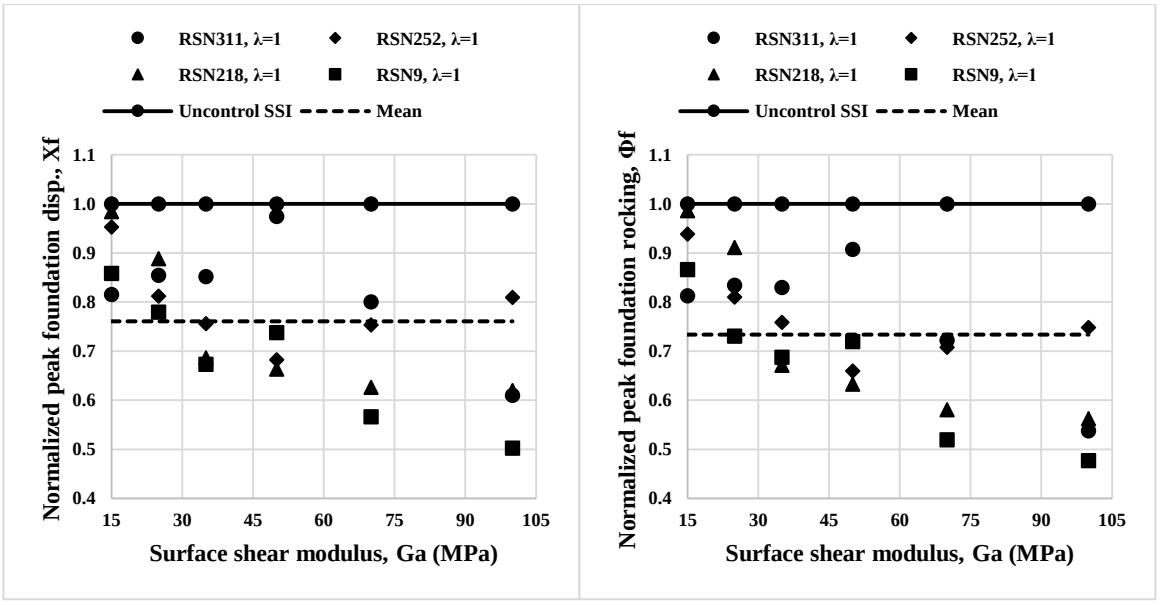


**Figure B-11** Normalization of horizontal and rocking foundation displacement for SSI-SSI reference model and $\lambda = 1$.

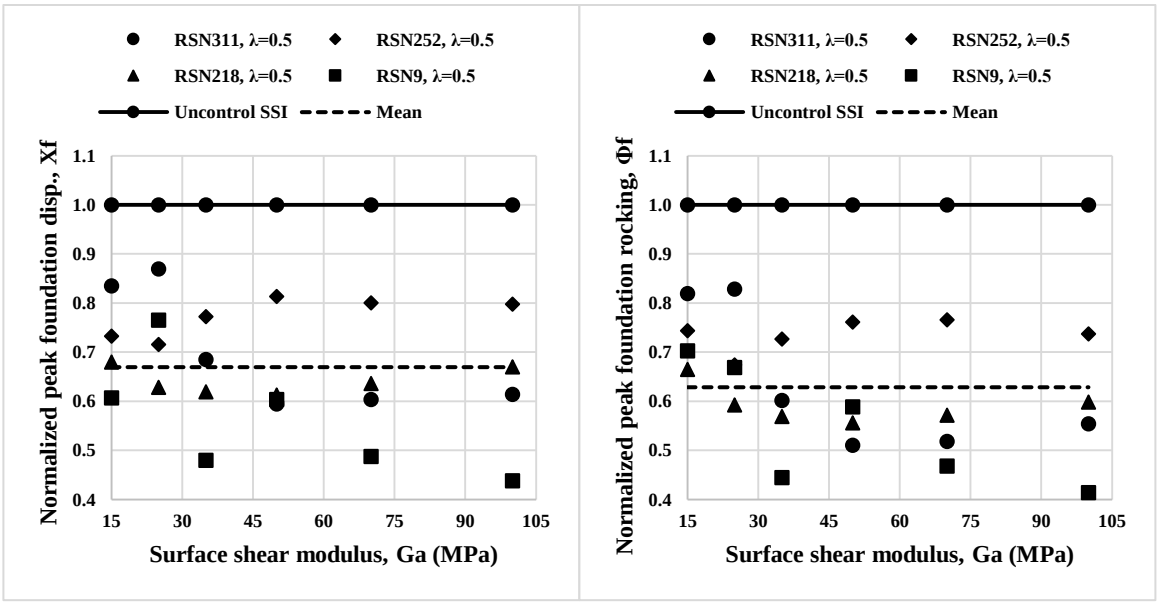


**Figure B-12** Normalization of horizontal and rocking foundation displacement for SSI-SSI reference model and $\lambda = 0.5$.

Soft soil top and medium soil bottom soil profile

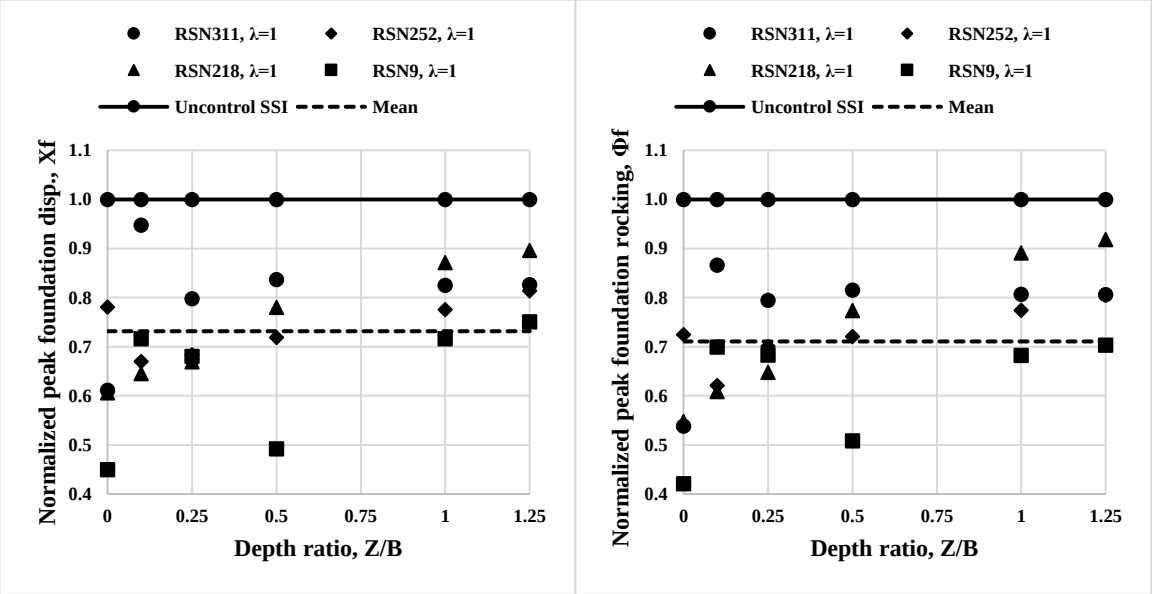


**Figure B-13** Normalization of horizontal and rocking foundation displacement for Fixed-SSI reference model and λ = 1.

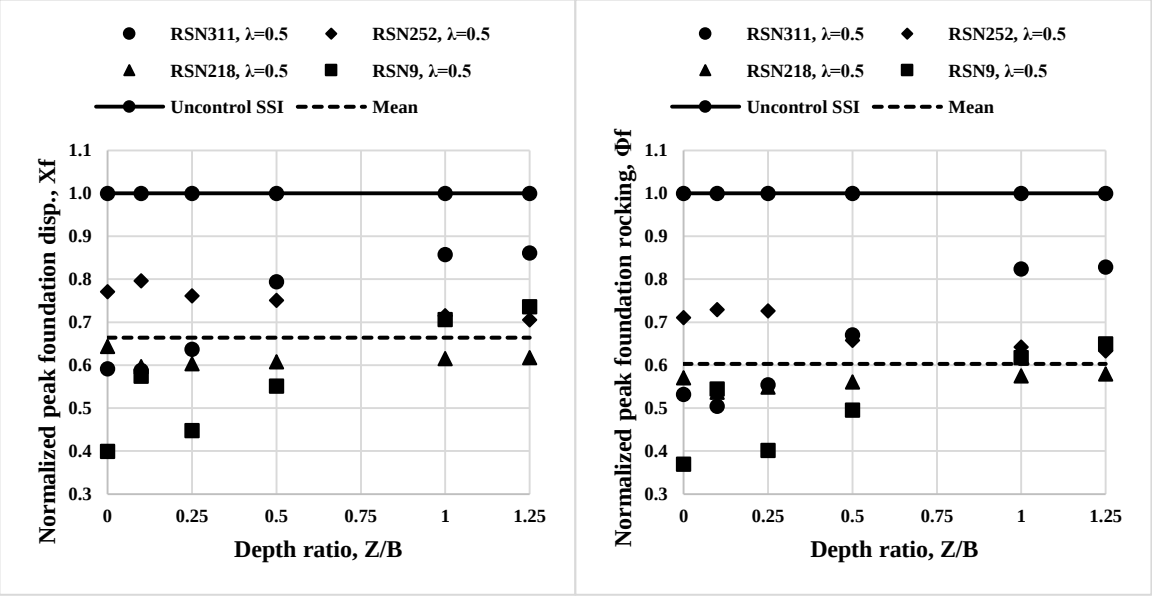


**Figure B-14** Normalization of horizontal and rocking foundation displacement for Fixed-SSI reference model and λ = 0.5.

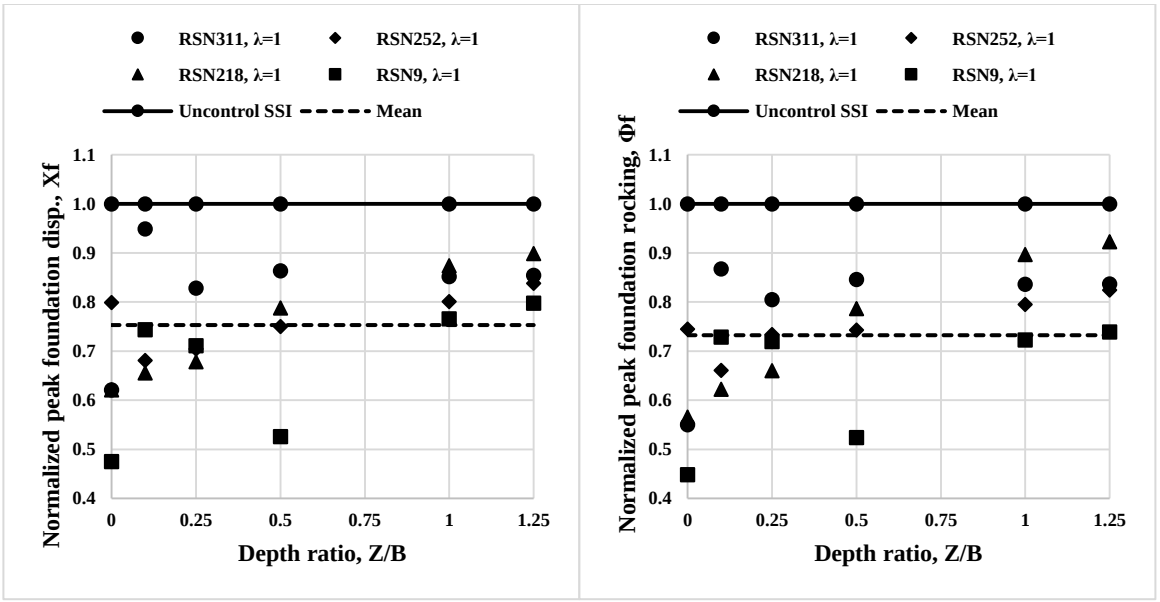


**Figure B-15** Normalization of horizontal and rocking foundation displacement for SSI-SSI reference model and $\lambda = 1$.

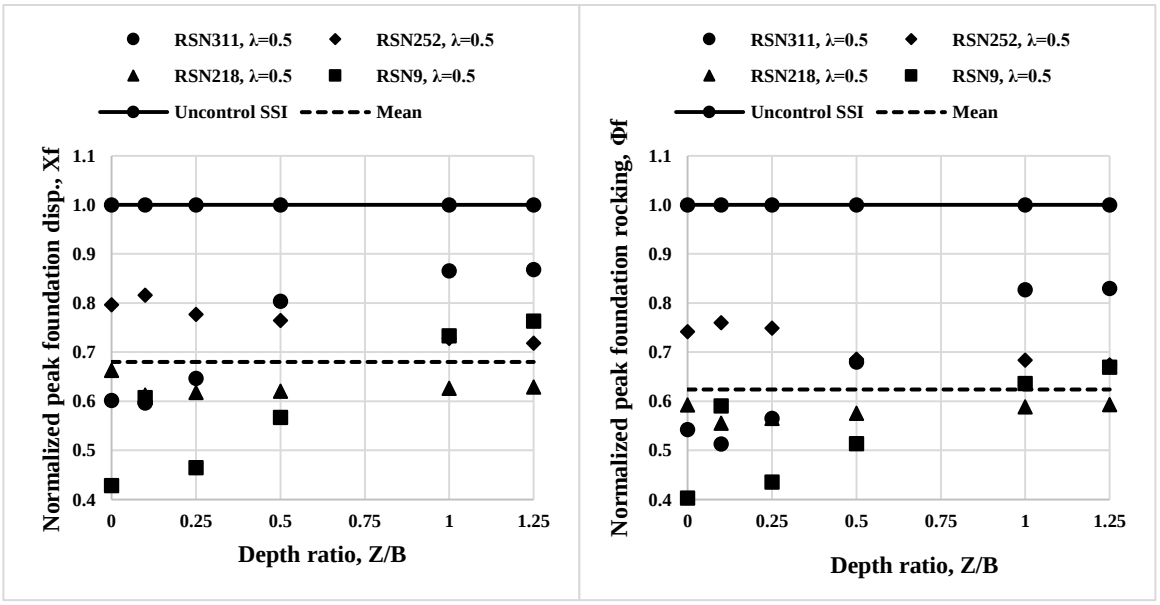


**Figure B-16** Normalization of horizontal and rocking foundation displacement for SSI-SSI reference model and $\lambda = 0.5$.

Normalization of foundation results for structure paramedic study

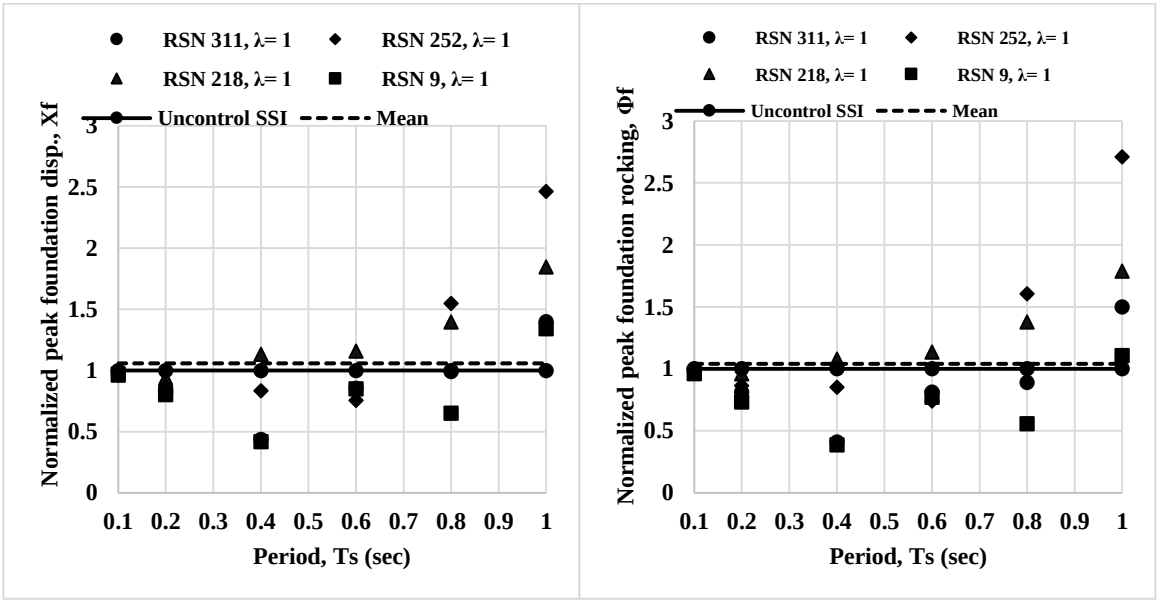


**Figure B-17** Normalization of horizontal and rocking foundation displacement for Fixed-SSI reference model and λ = 1.

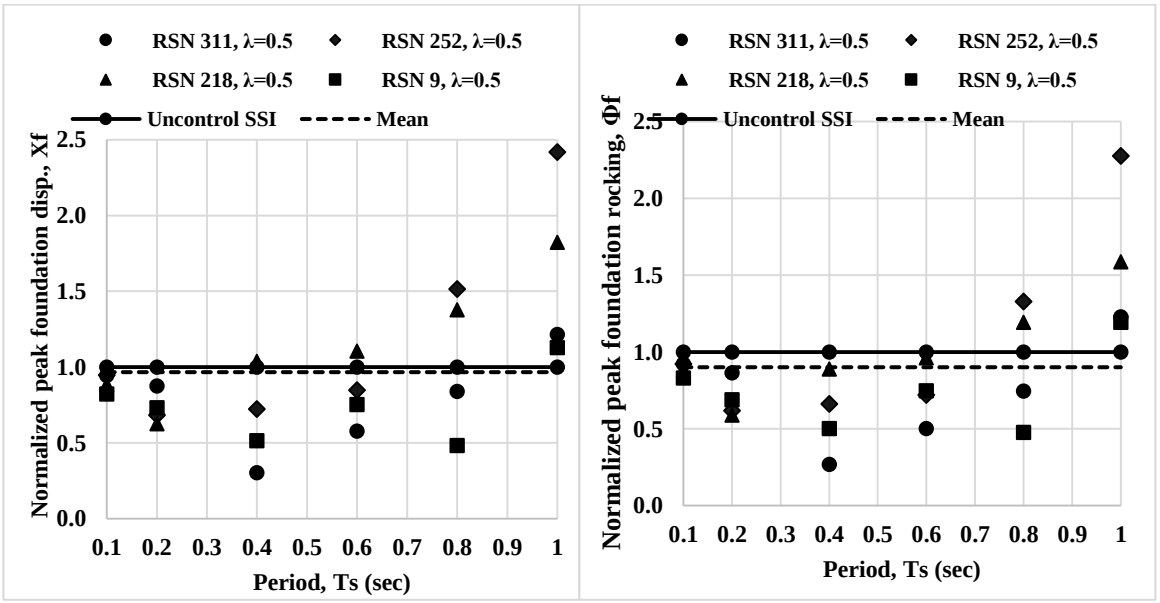


**Figure B-18** Normalization of horizontal and rocking foundation displacement for Fixed-SSI reference model and λ = 0.5.

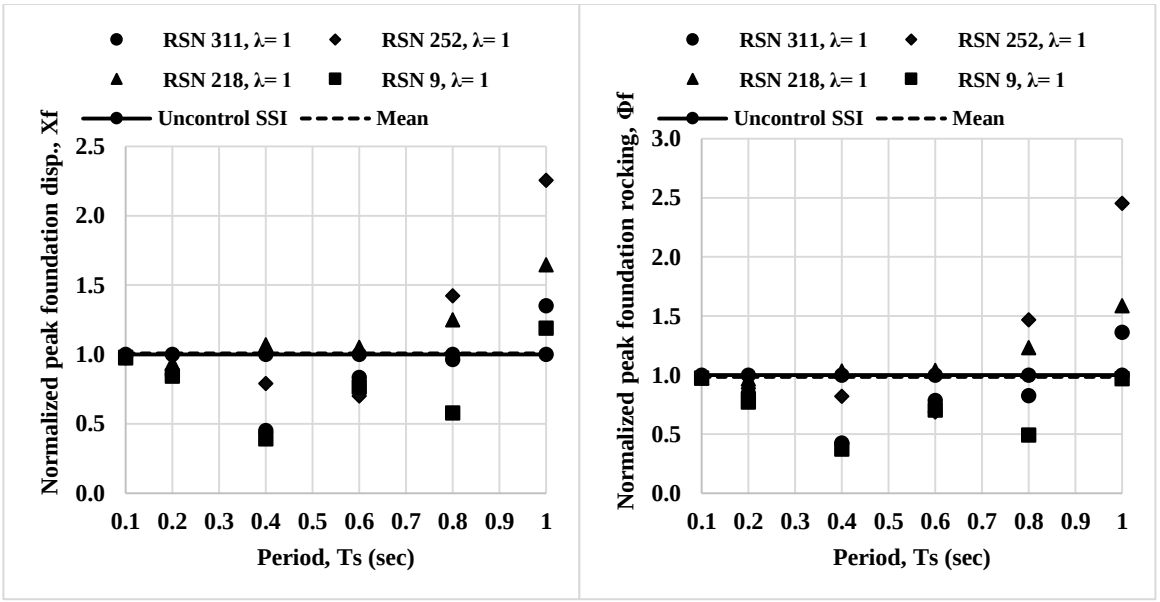


**Figure B-19** Normalization of horizontal and rocking foundation displacement for SSI-SSI reference model and λ = 1.

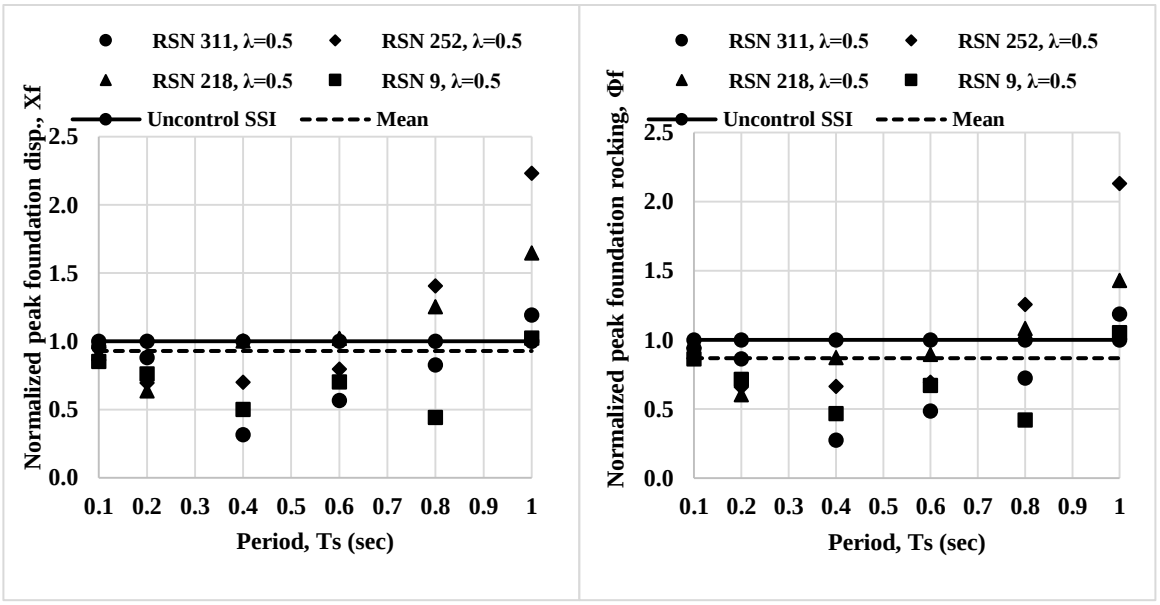


**Figure B-20** Normalization of horizontal and rocking foundation displacement for SSI-SSI reference model and λ = 0.5.

APPENDIX C

PERFORMANCE EVALUATION CRITERIA OF CHAPTER 6

Geotechnical paramedic study

**Table C-1** Clay (linear) soil profile with Fixed-SSI reference model and λ (H/B) = 1.

| Earthquakes | Structure | system | J1 | J3 | J4 | J6 | J8 |
|---|---|---|---|---|---|---|---|
| Taiwan SMART1(5), 1/29/1981, SMART1 O01, NS RSN 311 | Fixed | support | 0.4132 | 0.3286 | 0.0543 | 0.4029 | 0.2321 |
| | SSI Ga | 15 | 0.7872 | 0.8313 | 0.1210 | 0.6303 | 0.6585 |
| | | 25 | 0.6907 | 0.8477 | 0.1048 | 0.5773 | 0.5795 |
| | | 35 | 0.7879 | 0.8184 | 0.0766 | 0.7057 | 0.6748 |
| | | 50 | 0.7687 | 0.9618 | 0.0660 | 0.5940 | 0.5045 |
| | | 70 | 0.8412 | 0.6342 | 0.0685 | 0.7320 | 0.6376 |
| | | 100 | 0.6453 | 0.4857 | 0.0664 | 0.5030 | 0.3818 |
| Mammoth Lakes-07, 5/27/1980, Green Church, 146 RSN 252 | Fixed | support | 0.6048 | 0.3954 | 0.0846 | 0.4229 | 0.2437 |
| | SSI Ga | 15 | 0.8886 | 0.9269 | 0.0744 | 0.6834 | 0.7184 |
| | | 25 | 0.8492 | 0.9720 | 0.1090 | 0.7124 | 0.7414 |
| | | 35 | 0.7002 | 0.7288 | 0.1263 | 0.5063 | 0.5234 |
| | | 50 | 0.6346 | 0.5676 | 0.1341 | 0.3936 | 0.3916 |
| | | 70 | 0.5607 | 0.4303 | 0.1332 | 0.3723 | 0.3413 |
| | | 100 | 0.6498 | 0.5588 | 0.1248 | 0.2872 | 0.2351 |
| Livermore-02, 1/27/1980, Antioch - 510 G St, 270 RSN 218 | Fixed | support | 0.6269 | 0.3962 | 0.0633 | 0.3071 | 0.1788 |
| | SSI Ga | 15 | 0.9136 | 0.8227 | 0.0360 | 0.6887 | 0.6806 |
| | | 25 | 0.8650 | 0.8080 | 0.0601 | 0.5883 | 0.6074 |
| | | 35 | 0.7935 | 0.8129 | 0.0750 | 0.5172 | 0.5299 |
| | | 50 | 0.5940 | 0.6491 | 0.0847 | 0.4364 | 0.4383 |
| | | 70 | 0.5617 | 0.6090 | 0.0869 | 0.3735 | 0.3554 |
| | | 100 | 0.5164 | 0.5014 | 0.0851 | 0.3491 | 0.3088 |
| Borrego, 10/21/1942, El Centro Array #9, 0 RSN 9 | Fixed | support | 0.3132 | 0.2066 | 0.0396 | 0.2709 | 0.1887 |
| | SSI Ga | 15 | 0.7142 | 1.1442 | 0.0352 | 0.6351 | 0.7719 |
| | | 25 | 0.7289 | 1.0427 | 0.0430 | 0.5740 | 0.6814 |
| | | 35 | 0.6229 | 0.6815 | 0.0488 | 0.5182 | 0.5270 |
| | | 50 | 0.6186 | 0.5737 | 0.0528 | 0.4671 | 0.4497 |
| | | 70 | 0.6364 | 0.5587 | 0.0499 | 0.5119 | 0.4835 |
| | | 100 | 0.4201 | 0.3842 | 0.0519 | 0.3364 | 0.2995 |

**Table C-2** Clay (linear) soil profile with Fixed-SSI reference model and λ (H/B) = 0.5.

| Earthquakes | Structure | system | J1 | J3 | J4 | J6 | J8 |
|---|---|---|---|---|---|---|---|
| Taiwan SMART1(5), 1/29/1981, SMART1 O01, NS RSN 311 | Fixed | support | 0.4132 | 0.3286 | 0.0543 | 0.4029 | 0.2321 |
| | SSI Ga | 15 | 0.8292 | 0.6103 | 0.1065 | 0.7297 | 0.6390 |
| | | 25 | 0.8303 | 0.9422 | 0.0732 | 0.6415 | 0.5170 |
| | | 35 | 0.8136 | 0.5107 | 0.0703 | 0.6514 | 0.5018 |
| | | 50 | 0.5648 | 0.4202 | 0.0698 | 0.4821 | 0.3529 |
| | | 70 | 0.5005 | 0.3731 | 0.0651 | 0.3193 | 0.2183 |
| | | 100 | 0.4935 | 0.3523 | 0.0598 | 0.3495 | 0.2260 |
| Mammoth Lakes-07, 5/27/1980, Green Church, 146 RSN 252 | Fixed | support | 0.6048 | 0.3954 | 0.0846 | 0.4229 | 0.2437 |
| | SSI Ga | 15 | 0.7340 | 0.6322 | 0.1572 | 0.4898 | 0.4888 |
| | | 25 | 0.5947 | 0.4837 | 0.1492 | 0.4486 | 0.4205 |
| | | 35 | 0.6203 | 0.4970 | 0.1394 | 0.3158 | 0.2699 |
| | | 50 | 0.6804 | 0.5293 | 0.1266 | 0.3408 | 0.2727 |
| | | 70 | 0.6875 | 0.4875 | 0.1155 | 0.5137 | 0.3974 |
| | | 100 | 0.6713 | 0.5474 | 0.1065 | 0.5307 | 0.3912 |
| Livermore-02, 1/27/1980, Antioch - 510 G St,270 RSN 218 | Fixed | support | 0.6269 | 0.3962 | 0.0633 | 0.3071 | 0.1788 |
| | SSI Ga | 15 | 0.8354 | 0.8161 | 0.0957 | 0.5039 | 0.5091 |
| | | 25 | 0.6033 | 0.6615 | 0.0959 | 0.4069 | 0.3931 |
| | | 35 | 0.5447 | 0.5555 | 0.0921 | 0.3300 | 0.3018 |
| | | 50 | 0.5178 | 0.4786 | 0.0869 | 0.3088 | 0.2614 |
| | | 70 | 0.5016 | 0.4219 | 0.0816 | 0.3021 | 0.2380 |
| | | 100 | 0.5141 | 0.4021 | 0.0766 | 0.3451 | 0.2564 |
| Borrego, 10/21/1942, El Centro Array #9, 0 RSN 9 | Fixed | support | 0.3132 | 0.2066 | 0.0396 | 0.2709 | 0.1887 |
| | SSI Ga | 15 | 0.6091 | 0.5792 | 0.0601 | 0.5211 | 0.5172 |
| | | 25 | 0.6388 | 0.6572 | 0.0575 | 0.5173 | 0.5069 |
| | | 35 | 0.5993 | 0.5620 | 0.0516 | 0.5053 | 0.4627 |
| | | 50 | 0.3665 | 0.3553 | 0.0533 | 0.2836 | 0.2515 |
| | | 70 | 0.4759 | 0.4006 | 0.0511 | 0.3718 | 0.3230 |
| | | 100 | 0.3524 | 0.3038 | 0.0483 | 0.3474 | 0.2900 |

**Table C-3** Clay (linear) soil profile with SSI-SSI reference model and λ (H/B) = 1.

| Earthquakes | Structure | system | J1 | J3 | J4 | J6 | J8 |
|---|---|---|---|---|---|---|---|
| Taiwan SMART1(5), 1/29/1981, SMART1 O01, NS RSN 311 | Fixed | support | 0.4132 | 0.3286 | 0.0543 | 0.4029 | 0.2321 |
| | SSI Ga | 15 | 0.8314 | 0.8679 | 0.0959 | 0.6883 | 0.7097 |
| | | 25 | 0.7144 | 0.8703 | 0.0848 | 0.6278 | 0.6262 |
| | | 35 | 0.8253 | 0.8644 | 0.0620 | 0.7437 | 0.7135 |
| | | 50 | 0.8090 | 0.9902 | 0.0523 | 0.6253 | 0.5403 |
| | | 70 | 0.8528 | 0.6744 | 0.0572 | 0.7626 | 0.6763 |
| | | 100 | 0.6674 | 0.5276 | 0.0574 | 0.5298 | 0.4186 |
| Mammoth Lakes-07, 5/27/1980, Green Church, 146 RSN 252 | Fixed | support | 0.6048 | 0.3954 | 0.0846 | 0.4229 | 0.2437 |
| | SSI Ga | 15 | 0.9070 | 0.9126 | 0.0566 | 0.7344 | 0.7603 |
| | | 25 | 0.8814 | 0.9940 | 0.0872 | 0.7562 | 0.7794 |
| | | 35 | 0.7360 | 0.7574 | 0.1044 | 0.5589 | 0.5738 |
| | | 50 | 0.6816 | 0.5945 | 0.1116 | 0.4400 | 0.4364 |
| | | 70 | 0.6130 | 0.4737 | 0.1135 | 0.4163 | 0.3865 |
| | | 100 | 0.6816 | 0.5979 | 0.1079 | 0.3197 | 0.2680 |
| Livermore-02, 1/27/1980, Antioch - 510 G St, 270 RSN 218 | Fixed | support | 0.6269 | 0.3962 | 0.0633 | 0.3071 | 0.1788 |
| | SSI Ga | 15 | 0.9307 | 0.8165 | 0.0270 | 0.7334 | 0.7278 |
| | | 25 | 0.8918 | 0.8445 | 0.0473 | 0.6346 | 0.6527 |
| | | 35 | 0.8199 | 0.8506 | 0.0606 | 0.5706 | 0.5835 |
| | | 50 | 0.6213 | 0.6917 | 0.0705 | 0.4870 | 0.4881 |
| | | 70 | 0.5896 | 0.6585 | 0.0737 | 0.4161 | 0.3987 |
| | | 100 | 0.5449 | 0.5531 | 0.0736 | 0.3885 | 0.3500 |
| Borrego, 10/21/1942, El Centro Array #9, 0 RSN 9 | Fixed | support | 0.3132 | 0.2066 | 0.0396 | 0.2709 | 0.1887 |
| | SSI Ga | 15 | 0.7612 | 1.1166 | 0.0281 | 0.6893 | 0.7930 |
| | | 25 | 0.7754 | 1.0537 | 0.0351 | 0.6212 | 0.7084 |
| | | 35 | 0.6765 | 0.7126 | 0.0421 | 0.5656 | 0.5732 |
| | | 50 | 0.6667 | 0.6220 | 0.0454 | 0.5081 | 0.4914 |
| | | 70 | 0.6823 | 0.5851 | 0.0435 | 0.5493 | 0.5246 |
| | | 100 | 0.4588 | 0.4187 | 0.0452 | 0.3659 | 0.3321 |

**Table C-4** Clay (linear) soil profile with SSI-SSI reference model and λ (H/B) = 0.5.

| Earthquakes | Structure | system | J1 | J3 | J4 | J6 | J8 |
|---|---|---|---|---|---|---|---|
| Taiwan SMART1(5), 1/29/1981, SMART1 O01, NS RSN 311 | Fixed | support | 0.4132 | 0.3286 | 0.0543 | 0.4029 | 0.2321 |
| | SSI Ga | 15 | 0.8456 | 0.5851 | 0.0888 | 0.7481 | 0.6626 |
| | | 25 | 0.8125 | 0.9551 | 0.0595 | 0.6576 | 0.5400 |
| | | 35 | 0.8253 | 0.5396 | 0.0598 | 0.6719 | 0.5340 |
| | | 50 | 0.5791 | 0.4494 | 0.0617 | 0.5046 | 0.3871 |
| | | 70 | 0.5171 | 0.3987 | 0.0595 | 0.3359 | 0.2422 |
| | | 100 | 0.5105 | 0.3886 | 0.0556 | 0.3680 | 0.2524 |
| Mammoth Lakes-07, 5/27/1980, Green Church, 146 RSN 252 | Fixed | support | 0.6048 | 0.3954 | 0.0846 | 0.4229 | 0.2437 |
| | SSI Ga | 15 | 0.7594 | 0.6497 | 0.1330 | 0.5302 | 0.5302 |
| | | 25 | 0.6378 | 0.5228 | 0.1269 | 0.4906 | 0.4649 |
| | | 35 | 0.6425 | 0.5437 | 0.1201 | 0.3487 | 0.3055 |
| | | 50 | 0.7093 | 0.5831 | 0.1103 | 0.3722 | 0.3050 |
| | | 70 | 0.7222 | 0.5319 | 0.1022 | 0.5549 | 0.4410 |
| | | 100 | 0.7112 | 0.5999 | 0.0955 | 0.5702 | 0.4336 |
| Livermore-02, 1/27/1980, Antioch - 510 G St, 270 RSN 218 | Fixed | support | 0.6269 | 0.3962 | 0.0633 | 0.3071 | 0.1788 |
| | SSI Ga | 15 | 0.8487 | 0.8468 | 0.0793 | 0.5444 | 0.5525 |
| | | 25 | 0.6221 | 0.7031 | 0.0813 | 0.4457 | 0.4334 |
| | | 35 | 0.5660 | 0.6007 | 0.0793 | 0.3627 | 0.3367 |
| | | 50 | 0.5438 | 0.5284 | 0.0759 | 0.3396 | 0.2945 |
| | | 70 | 0.5303 | 0.4745 | 0.0720 | 0.3311 | 0.2695 |
| | | 100 | 0.5465 | 0.4592 | 0.0682 | 0.3772 | 0.2923 |
| Borrego, 10/21/1942, El Centro Array #9, 0 RSN 9 | Fixed | support | 0.3132 | 0.2066 | 0.0396 | 0.2709 | 0.1887 |
| | SSI Ga | 15 | 0.6550 | 0.6074 | 0.0512 | 0.5522 | 0.5477 |
| | | 25 | 0.6794 | 0.6898 | 0.0503 | 0.5471 | 0.5372 |
| | | 35 | 0.6338 | 0.5907 | 0.0451 | 0.5387 | 0.5017 |
| | | 50 | 0.4014 | 0.3831 | 0.0474 | 0.3054 | 0.2767 |
| | | 70 | 0.5311 | 0.4577 | 0.0463 | 0.4001 | 0.3560 |
| | | 100 | 0.3974 | 0.3481 | 0.0442 | 0.3734 | 0.3208 |

**Table C-5** Medium soil top and soft soil bottom soil profile with Fixed-SSI reference model and λ (H/B) = 1.

| Earthquakes | Structure system | | J1 | J3 | J4 | J6 | J8 |
|---|---|---|---|---|---|---|---|
| Taiwan SMART1(5), 1/29/1981, SMART1 O01, NS RSN 311 | Fixed | support | 0.4132 | 0.3286 | 0.0543 | 0.4029 | 0.2321 |
| | SSI Z/B | 0 | 0.7908 | 0.7670 | 0.0837 | 0.6598 | 0.6186 |
| | | 0.1 | 0.7800 | 0.9371 | 0.0646 | 0.5906 | 0.4995 |
| | | 0.25 | 0.8624 | 0.7105 | 0.0677 | 0.7003 | 0.6041 |
| | | 0.5 | 0.7295 | 0.5657 | 0.0655 | 0.5494 | 0.4266 |
| | | 1 | 0.5596 | 0.3968 | 0.0669 | 0.4711 | 0.3480 |
| | | 1.25 | 0.5408 | 0.3751 | 0.0666 | 0.4693 | 0.3430 |
| Mammoth Lakes-07, 5/27/1980, Green Church, 146 RSN 252 | Fixed | support | 0.6048 | 0.3954 | 0.0846 | 0.4229 | 0.2437 |
| | SSI Z/B | 0 | 0.8031 | 0.7231 | 0.1231 | 0.5070 | 0.5290 |
| | | 0.1 | 0.6438 | 0.5444 | 0.1328 | 0.3960 | 0.3955 |
| | | 0.25 | 0.5696 | 0.4491 | 0.1333 | 0.4224 | 0.3976 |
| | | 0.5 | 0.6197 | 0.5284 | 0.1274 | 0.2963 | 0.2497 |
| | | 1 | 0.6632 | 0.6010 | 0.1218 | 0.3225 | 0.2577 |
| | | 1.25 | 0.6666 | 0.6138 | 0.1206 | 0.3496 | 0.2800 |
| Livermore-02, 1/27/1980, Antioch - 510 G St, 270 RSN 218 | Fixed | support | 0.6269 | 0.3962 | 0.0633 | 0.3071 | 0.1788 |
| | SSI Z/B | 0 | 0.8722 | 0.8287 | 0.0719 | 0.5734 | 0.5946 |
| | | 0.1 | 0.5971 | 0.6546 | 0.0835 | 0.4402 | 0.4428 |
| | | 0.25 | 0.5827 | 0.6332 | 0.0861 | 0.3785 | 0.3645 |
| | | 0.5 | 0.5219 | 0.5216 | 0.0860 | 0.3483 | 0.3179 |
| | | 1 | 0.5075 | 0.4721 | 0.0836 | 0.3036 | 0.2589 |
| | | 1.25 | 0.5056 | 0.4641 | 0.0832 | 0.3016 | 0.2552 |
| Borrego, 10/21/1942, El Centro Array #9, 0 RSN 9 | Fixed | support | 0.3132 | 0.2066 | 0.0396 | 0.2709 | 0.1887 |
| | SSI Z/B | 0 | 0.6883 | 0.8020 | 0.0479 | 0.5721 | 0.5982 |
| | | 0.1 | 0.6172 | 0.5516 | 0.0524 | 0.4664 | 0.4461 |
| | | 0.25 | 0.6269 | 0.5195 | 0.0506 | 0.5189 | 0.4919 |
| | | 0.5 | 0.4777 | 0.4416 | 0.0514 | 0.4179 | 0.3763 |
| | | 1 | 0.3647 | 0.3399 | 0.0522 | 0.2797 | 0.2480 |
| | | 1.25 | 0.3591 | 0.3390 | 0.0521 | 0.2782 | 0.2467 |

**Table C-6** Medium soil top and soft soil bottom profile with Fixed-SSI reference model and λ (H/B) = 0.5.

| Earthquakes | Structure | system | J1 | J3 | J4 | J6 | J8 |
|---|---|---|---|---|---|---|---|
| Taiwan SMART1(5), 1/29/1981, SMART1 O01, NS RSN 311 | Fixed | support | 0.4132 | 0.3286 | 0.0543 | 0.4029 | 0.2321 |
| | SSI Z/B | 0 | 0.8244 | 0.5589 | 0.0726 | 0.7252 | 0.5730 |
| | | 0.1 | 0.5479 | 0.4010 | 0.0686 | 0.4784 | 0.3469 |
| | | 0.25 | 0.4981 | 0.3790 | 0.0657 | 0.3210 | 0.2196 |
| | | 0.5 | 0.5046 | 0.3572 | 0.0608 | 0.3595 | 0.2371 |
| | | 1 | 0.4938 | 0.3714 | 0.0598 | 0.3505 | 0.2238 |
| | | 1.25 | 0.4958 | 0.3670 | 0.0597 | 0.3532 | 0.2245 |
| Mammoth Lakes-07, 5/27/1980, Green Church, 146 RSN 252 | Fixed | support | 0.6048 | 0.3954 | 0.0846 | 0.4229 | 0.2437 |
| | SSI Z/B | 0 | 0.5927 | 0.4812 | 0.1430 | 0.3387 | 0.2950 |
| | | 0.1 | 0.6846 | 0.5174 | 0.1255 | 0.3691 | 0.2967 |
| | | 0.25 | 0.6874 | 0.4852 | 0.1173 | 0.5042 | 0.3936 |
| | | 0.5 | 0.6779 | 0.5291 | 0.1085 | 0.5426 | 0.4107 |
| | | 1 | 0.6667 | 0.5399 | 0.1039 | 0.5153 | 0.3668 |
| | | 1.25 | 0.6646 | 0.5377 | 0.1030 | 0.5077 | 0.3564 |
| Livermore-02, 1/27/1980, Antioch - 510 G St, 270 RSN 218 | Fixed | support | 0.6269 | 0.3962 | 0.0633 | 0.3071 | 0.1788 |
| | SSI Z/B | 0 | 0.5604 | 0.5876 | 0.0936 | 0.3578 | 0.3309 |
| | | 0.1 | 0.5165 | 0.4729 | 0.0856 | 0.3092 | 0.2600 |
| | | 0.25 | 0.5034 | 0.4290 | 0.0818 | 0.3052 | 0.2425 |
| | | 0.5 | 0.5099 | 0.4082 | 0.0779 | 0.3305 | 0.2504 |
| | | 1 | 0.5189 | 0.3910 | 0.0752 | 0.3457 | 0.2501 |
| | | 1.25 | 0.5215 | 0.3872 | 0.0747 | 0.3443 | 0.2466 |
| Borrego, 10/21/1942, El Centro Array #9, 0 RSN 9 | Fixed | support | 0.3132 | 0.2066 | 0.0396 | 0.2709 | 0.1887 |
| | SSI Z/B | 0 | 0.6649 | 0.5480 | 0.0528 | 0.5129 | 0.4772 |
| | | 0.1 | 0.3640 | 0.3462 | 0.0524 | 0.2861 | 0.2528 |
| | | 0.25 | 0.4738 | 0.3837 | 0.0513 | 0.3713 | 0.3246 |
| | | 0.5 | 0.4075 | 0.3585 | 0.0491 | 0.3277 | 0.2759 |
| | | 1 | 0.3255 | 0.2849 | 0.0475 | 0.3520 | 0.2896 |
| | | 1.25 | 0.3225 | 0.2821 | 0.0471 | 0.3511 | 0.2871 |

**Table C-7** Medium soil top and soft soil bottom profile with SSI-SSI reference model and λ (H/B) = 1.

| Earthquakes | Structure | system | J1 | J3 | J4 | J6 | J8 |
|---|---|---|---|---|---|---|---|
| Taiwan SMART1(5), 1/29/1981, SMART1 O01, NS RSN 311 | Fixed | support | 0.4132 | 0.3286 | 0.0543 | 0.4029 | 0.2321 |
| | SSI Z/B | 0 | 0.8268 | 0.8131 | 0.0683 | 0.6982 | 0.6577 |
| | | 0.1 | 0.8171 | 0.9509 | 0.0511 | 0.6216 | 0.5348 |
| | | 0.25 | 0.8649 | 0.7447 | 0.0558 | 0.7288 | 0.6386 |
| | | 0.5 | 0.7528 | 0.6096 | 0.0555 | 0.5764 | 0.4632 |
| | | 1 | 0.5805 | 0.4369 | 0.0589 | 0.4986 | 0.3856 |
| | | 1.25 | 0.5620 | 0.4202 | 0.0591 | 0.4971 | 0.3808 |
| Mammoth Lakes-07, 5/27/1980, Green Church, 146 RSN 252 | Fixed | support | 0.6048 | 0.3954 | 0.0846 | 0.4229 | 0.2437 |
| | SSI Z/B | 0 | 0.8411 | 0.7471 | 0.1009 | 0.5558 | 0.5756 |
| | | 0.1 | 0.6903 | 0.5718 | 0.1104 | 0.4428 | 0.4401 |
| | | 0.25 | 0.6220 | 0.4842 | 0.1130 | 0.4703 | 0.4464 |
| | | 0.5 | 0.6502 | 0.5648 | 0.1097 | 0.3315 | 0.2859 |
| | | 1 | 0.6980 | 0.6469 | 0.1062 | 0.3566 | 0.2924 |
| | | 1.25 | 0.7018 | 0.6606 | 0.1054 | 0.3857 | 0.3170 |
| Livermore-02, 1/27/1980, Antioch - 510 G St, 270 RSN 218 | Fixed | support | 0.6269 | 0.3962 | 0.0633 | 0.3071 | 0.1788 |
| | SSI Z/B | 0 | 0.9004 | 0.8651 | 0.0577 | 0.6210 | 0.6418 |
| | | 0.1 | 0.6242 | 0.6969 | 0.0693 | 0.4912 | 0.4930 |
| | | 0.25 | 0.6093 | 0.6812 | 0.0726 | 0.4211 | 0.4076 |
| | | 0.5 | 0.5499 | 0.5717 | 0.0739 | 0.3879 | 0.3593 |
| | | 1 | 0.5379 | 0.5255 | 0.0729 | 0.3376 | 0.2943 |
| | | 1.25 | 0.5361 | 0.5177 | 0.0727 | 0.3352 | 0.2903 |
| Borrego, 10/21/1942, El Centro Array #9, 0 RSN 9 | Fixed | support | 0.3132 | 0.2066 | 0.0396 | 0.2709 | 0.1887 |
| | SSI Z/B | 0 | 0.7498 | 0.8488 | 0.0405 | 0.6161 | 0.6380 |
| | | 0.1 | 0.6644 | 0.5950 | 0.0449 | 0.5074 | 0.4884 |
| | | 0.25 | 0.6749 | 0.5395 | 0.0440 | 0.5557 | 0.5315 |
| | | 0.5 | 0.5117 | 0.4756 | 0.0443 | 0.4535 | 0.4160 |
| | | 1 | 0.4026 | 0.3772 | 0.0460 | 0.3046 | 0.2752 |
| | | 1.25 | 0.3977 | 0.3773 | 0.0461 | 0.3028 | 0.2738 |

**Table C-8** Medium soil top and soft soil bottom profile with SSI -SSI reference model and $\lambda$ (H/B) = 0.5.

| Earthquakes | Structure | system | J1 | J3 | J4 | J6 | J8 |
|---|---|---|---|---|---|---|---|
| Taiwan SMART1(5), 1/29/1981, SMART1 O01, NS RSN 311 | Fixed | support | 0.4132 | 0.3286 | 0.0543 | 0.4029 | 0.2321 |
| | SSI Z/B | 0 | 0.8269 | 0.5875 | 0.0612 | 0.7454 | 0.6050 |
| | | 0.1 | 0.5630 | 0.4297 | 0.0609 | 0.5012 | 0.3814 |
| | | 0.25 | 0.5144 | 0.4065 | 0.0599 | 0.3375 | 0.2434 |
| | | 0.5 | 0.5217 | 0.3915 | 0.0564 | 0.3785 | 0.2643 |
| | | 1 | 0.5116 | 0.4093 | 0.0544 | 0.3693 | 0.2503 |
| | | 1.25 | 0.5138 | 0.4052 | 0.0540 | 0.3721 | 0.2511 |
| Mammoth Lakes-07, 5/27/1980, Green Church, 146 RSN 252 | Fixed | support | 0.6048 | 0.3954 | 0.0846 | 0.4229 | 0.2437 |
| | SSI Z/B | 0 | 0.6179 | 0.5079 | 0.1229 | 0.3734 | 0.3326 |
| | | 0.1 | 0.7135 | 0.5716 | 0.1095 | 0.4024 | 0.3313 |
| | | 0.25 | 0.7211 | 0.5210 | 0.1036 | 0.5449 | 0.4367 |
| | | 0.5 | 0.7164 | 0.5786 | 0.0971 | 0.5837 | 0.4552 |
| | | 1 | 0.7077 | 0.5922 | 0.0937 | 0.5535 | 0.4071 |
| | | 1.25 | 0.7058 | 0.5906 | 0.0930 | 0.5452 | 0.3958 |
| Livermore-02, 1/27/1980, Antioch - 510 G St, 270 RSN 218 | Fixed | support | 0.6269 | 0.3962 | 0.0633 | 0.3071 | 0.1788 |
| | SSI Z/B | 0 | 0.5821 | 0.6327 | 0.0802 | 0.3930 | 0.3681 |
| | | 0.1 | 0.5424 | 0.5223 | 0.0748 | 0.3398 | 0.2931 |
| | | 0.25 | 0.5318 | 0.4809 | 0.0721 | 0.3346 | 0.2744 |
| | | 0.5 | 0.5409 | 0.4641 | 0.0693 | 0.3614 | 0.2850 |
| | | 1 | 0.5522 | 0.4482 | 0.0671 | 0.3778 | 0.2859 |
| | | 1.25 | 0.5551 | 0.4445 | 0.0667 | 0.3761 | 0.2821 |
| Borrego, 10/21/1942, El Centro Array #9, 0 RSN 9 | Fixed | support | 0.3132 | 0.2066 | 0.0396 | 0.2709 | 0.1887 |
| | SSI Z/B | 0 | 0.7023 | 0.5743 | 0.0462 | 0.5443 | 0.5136 |
| | | 0.1 | 0.3995 | 0.3721 | 0.0468 | 0.3081 | 0.2784 |
| | | 0.25 | 0.5276 | 0.4369 | 0.0464 | 0.3994 | 0.3577 |
| | | 0.5 | 0.4579 | 0.4101 | 0.0448 | 0.3523 | 0.3048 |
| | | 1 | 0.3677 | 0.3273 | 0.0435 | 0.3786 | 0.3211 |
| | | 1.25 | 0.3645 | 0.3249 | 0.0432 | 0.3776 | 0.3185 |

**Table C-9** Sand (parabola) profile with Fixed-SSI reference model and λ (H/B) = 1.

| Earthquakes | Structure | system | J1 | J3 | J4 | J6 | J8 |
|---|---|---|---|---|---|---|---|
| Taiwan SMART1(5), 1/29/1981, SMART1 O01, NS RSN 311 | Fixed | support | 0.4132 | 0.3286 | 0.0543 | 0.4029 | 0.2321 |
| | SSI Ga | 15 | 0.7361 | 0.7817 | 0.1131 | 0.5964 | 0.6033 |
| | | 25 | 0.7849 | 0.7908 | 0.0790 | 0.6954 | 0.6610 |
| | | 35 | 0.7829 | 0.9747 | 0.0656 | 0.5661 | 0.4791 |
| | | 50 | 0.8691 | 0.6532 | 0.0685 | 0.7304 | 0.6418 |
| | | 70 | 0.6803 | 0.5107 | 0.0663 | 0.5172 | 0.3963 |
| | | 100 | 0.5014 | 0.3461 | 0.0655 | 0.4060 | 0.2828 |
| Mammoth Lakes-07, 5/27/1980, Green Church, 146 RSN 252 | Fixed | support | 0.6048 | 0.3954 | 0.0846 | 0.4229 | 0.2437 |
| | SSI Ga | 15 | 0.8767 | 0.9847 | 0.0950 | 0.6484 | 0.6646 |
| | | 25 | 0.7302 | 0.7375 | 0.1253 | 0.5200 | 0.5396 |
| | | 35 | 0.6568 | 0.6046 | 0.1340 | 0.3906 | 0.3916 |
| | | 50 | 0.5604 | 0.4389 | 0.1334 | 0.3918 | 0.3609 |
| | | 70 | 0.6366 | 0.5564 | 0.1259 | 0.2885 | 0.2397 |
| | | 100 | 0.6776 | 0.5611 | 0.1177 | 0.4415 | 0.3580 |
| Livermore-02, 1/27/1980, Antioch - 510 G St, 270 RSN 218 | Fixed | support | 0.6269 | 0.3962 | 0.0633 | 0.3071 | 0.1788 |
| | SSI Ga | 15 | 0.8900 | 0.8132 | 0.0497 | 0.6706 | 0.6817 |
| | | 25 | 0.8161 | 0.8191 | 0.0740 | 0.5439 | 0.5593 |
| | | 35 | 0.6009 | 0.6499 | 0.0841 | 0.4265 | 0.4327 |
| | | 50 | 0.5671 | 0.6173 | 0.0870 | 0.3733 | 0.3571 |
| | | 70 | 0.5185 | 0.5108 | 0.0854 | 0.3578 | 0.3216 |
| | | 100 | 0.4997 | 0.4436 | 0.0815 | 0.3096 | 0.2551 |
| Borrego, 10/21/1942, El Centro Array #9, 0 RSN 9 | Fixed | support | 0.3132 | 0.2066 | 0.0396 | 0.2709 | 0.1887 |
| | SSI Ga | 15 | 0.7925 | 0.9100 | 0.0407 | 0.5492 | 0.6380 |
| | | 25 | 0.6433 | 0.7201 | 0.0487 | 0.5390 | 0.5540 |
| | | 35 | 0.5959 | 0.5164 | 0.0526 | 0.4497 | 0.4355 |
| | | 50 | 0.6302 | 0.5599 | 0.0503 | 0.5144 | 0.4876 |
| | | 70 | 0.4398 | 0.4067 | 0.0517 | 0.3693 | 0.3301 |
| | | 100 | 0.3903 | 0.3573 | 0.0513 | 0.3080 | 0.2723 |

**Table C-10** Sand (parabola) profile with Fixed-SSI reference model and λ (H/B) = 0.5.

| Earthquakes | Structure | system | J1 | J3 | J4 | J6 | J8 |
|---|---|---|---|---|---|---|---|
| Taiwan SMART1(5), 1/29/1981, SMART1 O01, NS RSN 311 | Fixed | support | 0.4132 | 0.3286 | 0.0543 | 0.4029 | 0.2321 |
| | SSI Ga | 15 | 0.8294 | 0.9496 | 0.0757 | 0.5823 | 0.4806 |
| | | 25 | 0.8186 | 0.5209 | 0.0712 | 0.6776 | 0.5255 |
| | | 35 | 0.5944 | 0.4359 | 0.0703 | 0.4830 | 0.3570 |
| | | 50 | 0.4990 | 0.3768 | 0.0658 | 0.3190 | 0.2185 |
| | | 70 | 0.4985 | 0.3460 | 0.0603 | 0.3532 | 0.2304 |
| | | 100 | 0.5162 | 0.3892 | 0.0588 | 0.3714 | 0.2330 |
| Mammoth Lakes-07, 5/27/1980, Green Church, 146 RSN 252 | Fixed | support | 0.6048 | 0.3954 | 0.0846 | 0.4229 | 0.2437 |
| | SSI Ga | 15 | 0.6689 | 0.5107 | 0.1524 | 0.3825 | 0.3711 |
| | | 25 | 0.6096 | 0.4898 | 0.1405 | 0.3209 | 0.2760 |
| | | 35 | 0.6756 | 0.5164 | 0.1285 | 0.3145 | 0.2523 |
| | | 50 | 0.6887 | 0.4781 | 0.1164 | 0.5063 | 0.3934 |
| | | 70 | 0.6743 | 0.5403 | 0.1075 | 0.5364 | 0.4001 |
| | | 100 | 0.6576 | 0.5294 | 0.1001 | 0.4850 | 0.3279 |
| Livermore-02, 1/27/1980, Antioch - 510 G St, 270 RSN 218 | Fixed | support | 0.6269 | 0.3962 | 0.0633 | 0.3071 | 0.1788 |
| | SSI Ga | 15 | 0.6228 | 0.6647 | 0.0974 | 0.4093 | 0.4100 |
| | | 25 | 0.5491 | 0.5662 | 0.0927 | 0.3331 | 0.3055 |
| | | 35 | 0.5214 | 0.4896 | 0.0877 | 0.3161 | 0.2701 |
| | | 50 | 0.5023 | 0.4260 | 0.0821 | 0.3040 | 0.2410 |
| | | 70 | 0.5119 | 0.4053 | 0.0772 | 0.3400 | 0.2552 |
| | | 100 | 0.5316 | 0.3770 | 0.0732 | 0.3364 | 0.2335 |
| Borrego, 10/21/1942, El Centro Array #9, 0 RSN 9 | Fixed | support | 0.3132 | 0.2066 | 0.0396 | 0.2709 | 0.1887 |
| | SSI Ga | 15 | 0.5867 | 0.6403 | 0.0591 | 0.4525 | 0.4388 |
| | | 25 | 0.6297 | 0.5792 | 0.0519 | 0.5140 | 0.4738 |
| | | 35 | 0.3781 | 0.3775 | 0.0536 | 0.2947 | 0.2620 |
| | | 50 | 0.4749 | 0.3932 | 0.0514 | 0.3721 | 0.3254 |
| | | 70 | 0.3746 | 0.3271 | 0.0487 | 0.3388 | 0.2843 |
| | | 100 | 0.3325 | 0.2935 | 0.0459 | 0.3457 | 0.2767 |

**Table C-11** Sand (parabola) profile with SSI-SSI reference model and λ (H/B) = 1.

| Earthquakes | Structure | system | J1 | J3 | J4 | J6 | J8 |
|---|---|---|---|---|---|---|---|
| Taiwan SMART1(5), 1/29/1981, SMART1 O01, NS RSN 311 | Fixed | support | 0.4132 | 0.3286 | 0.0543 | 0.4029 | 0.2321 |
| | SSI Ga | 15 | 0.7894 | 0.7915 | 0.0920 | 0.6534 | 0.6571 |
| | | 25 | 0.8218 | 0.8390 | 0.0642 | 0.7333 | 0.6998 |
| | | 35 | 0.8205 | 1.0079 | 0.0519 | 0.5976 | 0.5148 |
| | | 50 | 0.8778 | 0.6887 | 0.0570 | 0.7608 | 0.6796 |
| | | 70 | 0.7032 | 0.5504 | 0.0566 | 0.5439 | 0.4327 |
| | | 100 | 0.5223 | 0.3685 | 0.0587 | 0.4302 | 0.3153 |
| Mammoth Lakes-07, 5/27/1980, Green Church, 146 RSN 252 | Fixed | support | 0.6048 | 0.3954 | 0.0846 | 0.4229 | 0.2437 |
| | SSI Ga | 15 | 0.9048 | 1.0090 | 0.0744 | 0.6987 | 0.7099 |
| | | 25 | 0.7660 | 0.7678 | 0.1033 | 0.5721 | 0.5895 |
| | | 35 | 0.7035 | 0.6324 | 0.1111 | 0.4382 | 0.4375 |
| | | 50 | 0.6131 | 0.4832 | 0.1135 | 0.4377 | 0.4082 |
| | | 70 | 0.6678 | 0.5932 | 0.1086 | 0.3220 | 0.2737 |
| | | 100 | 0.7146 | 0.6085 | 0.1035 | 0.4837 | 0.4029 |
| Livermore-02, 1/27/1980, Antioch - 510 G St, 270 RSN 218 | Fixed | support | 0.6269 | 0.3962 | 0.0633 | 0.3071 | 0.1788 |
| | SSI Ga | 15 | 0.9132 | 0.8387 | 0.0384 | 0.7104 | 0.7232 |
| | | 25 | 0.8421 | 0.8571 | 0.0596 | 0.5958 | 0.6113 |
| | | 35 | 0.6275 | 0.6920 | 0.0698 | 0.4772 | 0.4826 |
| | | 50 | 0.5951 | 0.6665 | 0.0737 | 0.4159 | 0.4003 |
| | | 70 | 0.5466 | 0.5617 | 0.0737 | 0.3984 | 0.3641 |
| | | 100 | 0.5308 | 0.4978 | 0.0715 | 0.3430 | 0.2904 |
| Borrego, 10/21/1942, El Centro Array #9, 0 RSN 9 | Fixed | support | 0.3132 | 0.2066 | 0.0396 | 0.2709 | 0.1887 |
| | SSI Ga | 15 | 0.8325 | 0.9060 | 0.0326 | 0.6027 | 0.6729 |
| | | 25 | 0.6964 | 0.7467 | 0.0419 | 0.5856 | 0.5984 |
| | | 35 | 0.6407 | 0.5595 | 0.0450 | 0.4912 | 0.4775 |
| | | 50 | 0.6763 | 0.5848 | 0.0438 | 0.5517 | 0.5282 |
| | | 70 | 0.4761 | 0.4399 | 0.0448 | 0.4014 | 0.3657 |
| | | 100 | 0.4346 | 0.4012 | 0.0458 | 0.3344 | 0.3019 |

**Table C-12** Sand (parabola) profile with SSI-SSI reference model and λ (H/B) = 0.5.

| Earthquakes | Structure | system | J1 | J3 | J4 | J6 | J8 |
|---|---|---|---|---|---|---|---|
| Taiwan SMART1(5), 1/29/1981, SMART1 O01, NS RSN 311 | Fixed | support | 0.4132 | 0.3286 | 0.0543 | 0.4029 | 0.2321 |
| | SSI Ga | 15 | 0.8459 | 0.9297 | 0.0608 | 0.5996 | 0.5037 |
| | | 25 | 0.8253 | 0.5485 | 0.0602 | 0.6980 | 0.5578 |
| | | 35 | 0.6088 | 0.4674 | 0.0616 | 0.5048 | 0.3900 |
| | | 50 | 0.5155 | 0.4033 | 0.0600 | 0.3356 | 0.2423 |
| | | 70 | 0.5155 | 0.3810 | 0.0561 | 0.3719 | 0.2571 |
| | | 100 | 0.5351 | 0.4280 | 0.0534 | 0.3911 | 0.2609 |
| Mammoth Lakes-07, 5/27/1980, Green Church, 146 RSN 252 | Fixed | support | 0.6048 | 0.3954 | 0.0846 | 0.4229 | 0.2437 |
| | SSI Ga | 15 | 0.7075 | 0.5469 | 0.1283 | 0.4213 | 0.4109 |
| | | 25 | 0.6312 | 0.5345 | 0.1209 | 0.3543 | 0.3122 |
| | | 35 | 0.7039 | 0.5660 | 0.1118 | 0.3442 | 0.2825 |
| | | 50 | 0.7231 | 0.5195 | 0.1029 | 0.5473 | 0.4368 |
| | | 70 | 0.7136 | 0.5935 | 0.0963 | 0.5768 | 0.4435 |
| | | 100 | 0.6989 | 0.5830 | 0.0907 | 0.5201 | 0.3645 |
| Livermore-02, 1/27/1980, Antioch - 510 G St, 270 RSN 218 | Fixed | support | 0.6269 | 0.3962 | 0.0633 | 0.3071 | 0.1788 |
| | SSI Ga | 15 | 0.6409 | 0.7012 | 0.0822 | 0.4505 | 0.4523 |
| | | 25 | 0.5705 | 0.6114 | 0.0796 | 0.3661 | 0.3404 |
| | | 35 | 0.5473 | 0.5386 | 0.0764 | 0.3477 | 0.3040 |
| | | 50 | 0.5310 | 0.4782 | 0.0724 | 0.3333 | 0.2728 |
| | | 70 | 0.5439 | 0.4619 | 0.0688 | 0.3718 | 0.2908 |
| | | 100 | 0.5657 | 0.4347 | 0.0656 | 0.3671 | 0.2675 |
| Borrego, 10/21/1942, El Centro Array #9, 0 RSN 9 | Fixed | support | 0.3132 | 0.2066 | 0.0396 | 0.2709 | 0.1887 |
| | SSI Ga | 15 | 0.6200 | 0.6689 | 0.0510 | 0.4838 | 0.4709 |
| | | 25 | 0.6653 | 0.6090 | 0.0454 | 0.5471 | 0.5125 |
| | | 35 | 0.4125 | 0.4041 | 0.0475 | 0.3173 | 0.2881 |
| | | 50 | 0.5292 | 0.4489 | 0.0465 | 0.4004 | 0.3586 |
| | | 70 | 0.4220 | 0.3745 | 0.0445 | 0.3642 | 0.3143 |
| | | 100 | 0.3765 | 0.3393 | 0.0422 | 0.3716 | 0.3076 |

**Table C-13** Soft soil top and medium soil bottom profile with Fixed-SSI reference model and λ (H/B) = 1.

| Earthquakes | Structure | system | J1 | J3 | J4 | J6 | J8 |
|---|---|---|---|---|---|---|---|
| Taiwan SMART1(5), 1/29/1981, SMART1 O01, NS RSN 311 | Fixed | support | 0.4132 | 0.3286 | 0.0543 | 0.4029 | 0.2321 |
| | SSI Z/B | 0 | 0.5128 | 0.3514 | 0.0657 | 0.4445 | 0.3160 |
| | | 0.1 | 0.8310 | 0.6228 | 0.0686 | 0.7275 | 0.6333 |
| | | 0.25 | 0.7642 | 0.9948 | 0.0665 | 0.6080 | 0.5174 |
| | | 0.5 | 0.8053 | 0.9283 | 0.0681 | 0.5951 | 0.5331 |
| | | 1 | 0.7870 | 0.8199 | 0.0771 | 0.7041 | 0.6765 |
| | | 1.25 | 0.7873 | 0.7939 | 0.0794 | 0.6917 | 0.6611 |
| Mammoth Lakes-07, 5/27/1980, Green Church, 146 RSN 252 | Fixed | support | 0.6048 | 0.3954 | 0.0846 | 0.4229 | 0.2437 |
| | SSI Z/B | 0 | 0.6740 | 0.5700 | 0.1190 | 0.4050 | 0.3267 |
| | | 0.1 | 0.5605 | 0.4347 | 0.1333 | 0.3633 | 0.3309 |
| | | 0.25 | 0.6228 | 0.5318 | 0.1346 | 0.3949 | 0.3918 |
| | | 0.5 | 0.6544 | 0.7705 | 0.1304 | 0.3962 | 0.4053 |
| | | 1 | 0.7137 | 0.7548 | 0.1259 | 0.5157 | 0.5345 |
| | | 1.25 | 0.7464 | 0.7486 | 0.1246 | 0.5227 | 0.5442 |
| Livermore-02, 1/27/1980, Antioch - 510 G St, 270 RSN 218 | Fixed | support | 0.6269 | 0.3962 | 0.0633 | 0.3071 | 0.1788 |
| | SSI Z/B | 0 | 0.5025 | 0.4524 | 0.0822 | 0.3066 | 0.2557 |
| | | 0.1 | 0.5576 | 0.6033 | 0.0871 | 0.3711 | 0.3524 |
| | | 0.25 | 0.5920 | 0.6489 | 0.0852 | 0.4287 | 0.4284 |
| | | 0.5 | 0.7037 | 0.7535 | 0.0800 | 0.3584 | 0.3653 |
| | | 1 | 0.8030 | 0.8159 | 0.0742 | 0.5310 | 0.5445 |
| | | 1.25 | 0.8264 | 0.8204 | 0.0732 | 0.5545 | 0.5708 |
| Borrego, 10/21/1942, El Centro Array #9, 0 RSN 9 | Fixed | support | 0.3132 | 0.2066 | 0.0396 | 0.2709 | 0.1887 |
| | SSI Z/B | 0 | 0.3681 | 0.3462 | 0.0516 | 0.2922 | 0.2586 |
| | | 0.1 | 0.6379 | 0.5601 | 0.0499 | 0.5086 | 0.4806 |
| | | 0.25 | 0.6245 | 0.6052 | 0.0529 | 0.4711 | 0.4528 |
| | | 0.5 | 0.4520 | 0.4955 | 0.0507 | 0.4049 | 0.4027 |
| | | 1 | 0.6327 | 0.6872 | 0.0483 | 0.5288 | 0.5387 |
| | | 1.25 | 0.6527 | 0.7472 | 0.0483 | 0.5483 | 0.5647 |

**Table C-14** Soft soil top and medium soil bottom profile with Fixed-SSI reference model and λ (H/B) = 0.5.

| Earthquakes | Structure | system | J1 | J3 | J4 | J6 | J8 |
|---|---|---|---|---|---|---|---|
| Taiwan SMART1(5), 1/29/1981, SMART1 O01, NS RSN 311 | Fixed | support | 0.4132 | 0.3286 | 0.0543 | 0.4029 | 0.2321 |
| | SSI Z/B | 0 | 0.5065 | 0.3793 | 0.0591 | 0.3623 | 0.2281 |
| | | 0.1 | 0.5002 | 0.3706 | 0.0654 | 0.3184 | 0.2179 |
| | | 0.25 | 0.5567 | 0.4147 | 0.0698 | 0.4806 | 0.3506 |
| | | 0.5 | 0.7008 | 0.5085 | 0.0690 | 0.5315 | 0.4039 |
| | | 1 | 0.8145 | 0.5087 | 0.0700 | 0.6517 | 0.5013 |
| | | 1.25 | 0.8196 | 0.5195 | 0.0708 | 0.6768 | 0.5240 |
| Mammoth Lakes-07, 5/27/1980, Green Church, 146 RSN 252 | Fixed | support | 0.6048 | 0.3954 | 0.0846 | 0.4229 | 0.2437 |
| | SSI Z/B | 0 | 0.6603 | 0.5296 | 0.1012 | 0.4923 | 0.3370 |
| | | 0.1 | 0.6876 | 0.4806 | 0.1156 | 0.5118 | 0.3961 |
| | | 0.25 | 0.6812 | 0.5321 | 0.1259 | 0.3517 | 0.2812 |
| | | 0.5 | 0.6492 | 0.5134 | 0.1341 | 0.2956 | 0.2428 |
| | | 1 | 0.6212 | 0.4967 | 0.1393 | 0.3162 | 0.2703 |
| | | 1.25 | 0.6112 | 0.4954 | 0.1403 | 0.3211 | 0.2762 |
| Livermore-02, 1/27/1980, Antioch - 510 G St, 270 RSN 218 | Fixed | support | 0.6269 | 0.3962 | 0.0633 | 0.3071 | 0.1788 |
| | SSI Z/B | 0 | 0.5271 | 0.3800 | 0.0737 | 0.3399 | 0.2387 |
| | | 0.1 | 0.5012 | 0.4222 | 0.0818 | 0.3021 | 0.2382 |
| | | 0.25 | 0.5167 | 0.4749 | 0.0868 | 0.3080 | 0.2600 |
| | | 0.5 | 0.5305 | 0.5207 | 0.0898 | 0.3650 | 0.3259 |
| | | 1 | 0.5450 | 0.5570 | 0.0918 | 0.3305 | 0.3023 |
| | | 1.25 | 0.5493 | 0.5673 | 0.0923 | 0.3333 | 0.3056 |
| Borrego, 10/21/1942, El Centro Array #9, 0 RSN 9 | Fixed | support | 0.3132 | 0.2066 | 0.0396 | 0.2709 | 0.1887 |
| | SSI Z/B | 0 | 0.3255 | 0.2823 | 0.0464 | 0.3482 | 0.2809 |
| | | 0.1 | 0.4757 | 0.4003 | 0.0513 | 0.3719 | 0.3239 |
| | | 0.25 | 0.3647 | 0.3501 | 0.0534 | 0.2831 | 0.2509 |
| | | 0.5 | 0.4493 | 0.4536 | 0.0532 | 0.3794 | 0.3382 |
| | | 1 | 0.5995 | 0.5618 | 0.0513 | 0.5058 | 0.4626 |
| | | 1.25 | 0.6289 | 0.5778 | 0.0516 | 0.5145 | 0.4737 |

**Table C-15** Soft soil top and medium soil bottom profile with SSI-SSI reference model and λ (H/B) = 1.

| Earthquakes | Structure | system | J1 | J3 | J4 | J6 | J8 |
|---|---|---|---|---|---|---|---|
| Taiwan SMART1(5), 1/29/1981, SMART1 O01, NS RSN 311 | Fixed | support | 0.4132 | 0.3286 | 0.0543 | 0.4029 | 0.2321 |
| | SSI Z/B | 0 | 0.5338 | 0.3784 | 0.0589 | 0.4708 | 0.3518 |
| | | 0.1 | 0.8439 | 0.6638 | 0.0574 | 0.7586 | 0.6724 |
| | | 0.25 | 0.7970 | 1.0230 | 0.0529 | 0.6393 | 0.5531 |
| | | 0.5 | 0.8391 | 0.9693 | 0.0540 | 0.6300 | 0.5702 |
| | | 1 | 0.8245 | 0.8668 | 0.0625 | 0.7418 | 0.7145 |
| | | 1.25 | 0.8241 | 0.8425 | 0.0646 | 0.7295 | 0.6991 |
| Mammoth Lakes-07, 5/27/1980, Green Church, 146 RSN 252 | Fixed | support | 0.6048 | 0.3954 | 0.0846 | 0.4229 | 0.2437 |
| | SSI Z/B | 0 | 0.7094 | 0.6160 | 0.1044 | 0.4448 | 0.3685 |
| | | 0.1 | 0.6114 | 0.4785 | 0.1137 | 0.4066 | 0.3756 |
| | | 0.25 | 0.6713 | 0.5578 | 0.1122 | 0.4407 | 0.4363 |
| | | 0.5 | 0.6930 | 0.7960 | 0.1097 | 0.4458 | 0.4530 |
| | | 1 | 0.7486 | 0.7829 | 0.1039 | 0.5683 | 0.5846 |
| | | 1.25 | 0.7827 | 0.7779 | 0.1025 | 0.5743 | 0.5933 |
| Livermore-02, 1/27/1980, Antioch - 510 G St, 270 RSN 218 | Fixed | support | 0.6269 | 0.3962 | 0.0633 | 0.3071 | 0.1788 |
| | SSI Z/B | 0 | 0.5327 | 0.5061 | 0.0720 | 0.3401 | 0.2909 |
| | | 0.1 | 0.5856 | 0.6531 | 0.0739 | 0.4137 | 0.3957 |
| | | 0.25 | 0.6191 | 0.6924 | 0.0710 | 0.4781 | 0.4768 |
| | | 0.5 | 0.7330 | 0.7953 | 0.0656 | 0.4056 | 0.4122 |
| | | 1 | 0.8288 | 0.8539 | 0.0597 | 0.5839 | 0.5976 |
| | | 1.25 | 0.8526 | 0.8587 | 0.0588 | 0.6057 | 0.6220 |
| Borrego, 10/21/1942, El Centro Array #9, 0 RSN 9 | Fixed | support | 0.3132 | 0.2066 | 0.0396 | 0.2709 | 0.1887 |
| | SSI Z/B | 0 | 0.4092 | 0.3864 | 0.0458 | 0.3176 | 0.2868 |
| | | 0.1 | 0.6844 | 0.5876 | 0.0434 | 0.5463 | 0.5221 |
| | | 0.25 | 0.6736 | 0.6567 | 0.0456 | 0.5114 | 0.4938 |
| | | 0.5 | 0.4934 | 0.5292 | 0.0440 | 0.4473 | 0.4453 |
| | | 1 | 0.6850 | 0.7129 | 0.0417 | 0.5759 | 0.5846 |
| | | 1.25 | 0.7086 | 0.7684 | 0.0413 | 0.5944 | 0.6086 |

**Table C-16** Soft soil top and medium soil bottom profile with SSI-SSI reference model and λ (H/B) = 0.5.

| Earthquakes | Structure | system | J1 | J3 | J4 | J6 | J8 |
|---|---|---|---|---|---|---|---|
| Taiwan SMART1(5), 1/29/1981, SMART1 O01, NS RSN 311 | Fixed | support | 0.4132 | 0.3286 | 0.0543 | 0.4029 | 0.2321 |
| | SSI Z/B | 0 | 0.5249 | 0.4160 | 0.0535 | 0.3814 | 0.2553 |
| | | 0.1 | 0.5170 | 0.3962 | 0.0597 | 0.3352 | 0.2418 |
| | | 0.25 | 0.5712 | 0.4428 | 0.0618 | 0.5034 | 0.3850 |
| | | 0.5 | 0.7155 | 0.5506 | 0.0591 | 0.5519 | 0.4350 |
| | | 1 | 0.8258 | 0.5368 | 0.0596 | 0.6720 | 0.5334 |
| | | 1.25 | 0.8262 | 0.5469 | 0.0599 | 0.6971 | 0.5561 |
| Mammoth Lakes-07, 5/27/1980, Green Church, 146 RSN 252 | Fixed | support | 0.6048 | 0.3954 | 0.0846 | 0.4229 | 0.2437 |
| | SSI Z/B | 0 | 0.7016 | 0.5816 | 0.0917 | 0.5281 | 0.3745 |
| | | 0.1 | 0.7226 | 0.5253 | 0.1023 | 0.5532 | 0.4398 |
| | | 0.25 | 0.7105 | 0.5873 | 0.1098 | 0.3839 | 0.3144 |
| | | 0.5 | 0.6738 | 0.5628 | 0.1160 | 0.3255 | 0.2743 |
| | | 1 | 0.6435 | 0.5409 | 0.1199 | 0.3492 | 0.3059 |
| | | 1.25 | 0.6327 | 0.5336 | 0.1207 | 0.3545 | 0.3124 |
| Livermore-02, 1/27/1980, Antioch - 510 G St, 270 RSN 218 | Fixed | support | 0.6269 | 0.3962 | 0.0633 | 0.3071 | 0.1788 |
| | SSI Z/B | 0 | 0.5608 | 0.4374 | 0.0660 | 0.3710 | 0.2733 |
| | | 0.1 | 0.5301 | 0.4748 | 0.0722 | 0.3312 | 0.2699 |
| | | 0.25 | 0.5428 | 0.5251 | 0.0758 | 0.3386 | 0.2930 |
| | | 0.5 | 0.5538 | 0.5676 | 0.0778 | 0.4015 | 0.3653 |
| | | 1 | 0.5662 | 0.6022 | 0.0790 | 0.3632 | 0.3372 |
| | | 1.25 | 0.5706 | 0.6125 | 0.0792 | 0.3662 | 0.3405 |
| Borrego, 10/21/1942, El Centro Array #9, 0 RSN 9 | Fixed | support | 0.3132 | 0.2066 | 0.0396 | 0.2709 | 0.1887 |
| | SSI Z/B | 0 | 0.3680 | 0.3264 | 0.0425 | 0.3743 | 0.3120 |
| | | 0.1 | 0.5307 | 0.4567 | 0.0464 | 0.4003 | 0.3569 |
| | | 0.25 | 0.4000 | 0.3770 | 0.0476 | 0.3049 | 0.2762 |
| | | 0.5 | 0.4797 | 0.4786 | 0.0467 | 0.4073 | 0.3708 |
| | | 1 | 0.6339 | 0.5908 | 0.0448 | 0.5392 | 0.5017 |
| | | 1.25 | 0.6644 | 0.6077 | 0.0451 | 0.5477 | 0.5125 |

Structure paramedic study

**Table C-17** Fixed-SSI reference model and λ (H/B) = 1.

| | | SSI System | | | | |
|---|---|---|---|---|---|---|
| Earthquakes | Ts | J1 | J3 | J4 | J6 | J8 |
| Taiwan SMART1(5), 1/29/1981, SMART1 O01, NS RSN 311 | 0.1 | 1.010035 | 1.263292 | 0.015403 | 0.942607 | 0.958887 |
| | 0.2 | 0.790776 | 0.767031 | 0.083665 | 0.659834 | 0.618621 |
| | 0.4 | 0.251584 | 0.299566 | 0.160699 | 0.134094 | 0.153996 |
| | 0.6 | 0.350817 | 0.356315 | 0.167125 | 0.185129 | 0.280829 |
| | 0.8 | 0.259682 | 0.401096 | 0.159517 | 0.069094 | 0.182072 |
| | 1 | 0.300963 | 0.453657 | 0.152752 | 0.101435 | 0.319569 |
| Mammoth Lakes-07, 5/27/1980, Green Church, 146 RSN 252 | Ts | J1 | J3 | J4 | J6 | J8 |
| | 0.1 | 0.965727 | 1.043173 | 0.039578 | 0.917353 | 0.919092 |
| | 0.2 | 0.80314 | 0.723101 | 0.123145 | 0.506978 | 0.52904 |
| | 0.4 | 0.485691 | 0.500808 | 0.185134 | 0.232823 | 0.301348 |
| | 0.6 | 0.238007 | 0.530255 | 0.178448 | 0.075344 | 0.172139 |
| | 0.8 | 0.30094 | 0.580723 | 0.186873 | 0.085849 | 0.280025 |
| | 1 | 0.336607 | 0.668835 | 0.190215 | 0.119849 | 0.435855 |
| Livermore-02, 1/27/1980, Antioch - 510 G St, 270 RSN 218 | Ts | J1 | J3 | J4 | J6 | J8 |
| | 0.1 | 0.957585 | 0.95928 | 0.022745 | 0.935301 | 0.933121 |
| | 0.2 | 0.872232 | 0.828715 | 0.071878 | 0.573397 | 0.594579 |
| | 0.4 | 0.575287 | 0.732524 | 0.102268 | 0.295099 | 0.404174 |
| | 0.6 | 0.291318 | 0.657176 | 0.114443 | 0.172833 | 0.33318 |
| | 0.8 | 0.185687 | 0.594517 | 0.115868 | 0.078317 | 0.25215 |
| | 1 | 0.161786 | 0.591935 | 0.115877 | 0.055511 | 0.258423 |
| Borrego, 10/21/1942, El Centro Array #9, 0 RSN 9 | Ts | J1 | J3 | J4 | J6 | J8 |
| | 0.1 | 0.96367 | 1.023638 | 0.017081 | 0.924987 | 0.952958 |
| | 0.2 | 0.688324 | 0.801983 | 0.047863 | 0.572115 | 0.598194 |
| | 0.4 | 0.215944 | 0.253484 | 0.060688 | 0.172381 | 0.205811 |
| | 0.6 | 0.221928 | 0.254368 | 0.06582 | 0.185113 | 0.263762 |
| | 0.8 | 0.107371 | 0.322154 | 0.065893 | 0.108876 | 0.210651 |
| | 1 | 0.155734 | 0.300209 | 0.065746 | 0.152626 | 0.324226 |

**Table C-18** Fixed-SSI reference model and λ (H/B) = 0.5.

| SSI System | | | | | | |
|---|---|---|---|---|---|---|
| Earthquakes | Ts | J1 | J3 | J4 | J6 | J8 |
| Taiwan SMART1(5), 1/29/1981, SMART1 O01, NS RSN 311 | 0.1 | 0.965004 | 0.95938 | 0.049685 | 0.776083 | 0.733875 |
| | 0.2 | 0.824424 | 0.558862 | 0.072631 | 0.725216 | 0.572985 |
| | 0.4 | 0.181896 | 0.170919 | 0.136532 | 0.105342 | 0.108745 |
| | 0.6 | 0.24275 | 0.29 | 0.146324 | 0.152173 | 0.232297 |
| | 0.8 | 0.23614 | 0.352283 | 0.13855 | 0.076375 | 0.19587 |
| | 1 | 0.264572 | 0.407099 | 0.132202 | 0.10728 | 0.321095 |
| Mammoth Lakes-07, 5/27/1980, Green Church, 146 RSN 252 | Ts | J1 | J3 | J4 | J6 | J8 |
| | 0.1 | 0.964572 | 0.978661 | 0.0629 | 0.835086 | 0.756804 |
| | 0.2 | 0.592686 | 0.481247 | 0.142972 | 0.338684 | 0.295034 |
| | 0.4 | 0.387865 | 0.411743 | 0.165759 | 0.140975 | 0.184138 |
| | 0.6 | 0.232918 | 0.450065 | 0.174199 | 0.066834 | 0.151467 |
| | 0.8 | 0.254253 | 0.527834 | 0.179396 | 0.084977 | 0.276838 |
| | 1 | 0.282082 | 0.623366 | 0.181479 | 0.107235 | 0.406841 |
| Livermore-02, 1/27/1980, Antioch - 510 G St, 270 RSN 218 | Ts | J1 | J3 | J4 | J6 | J8 |
| | 0.1 | 0.902892 | 0.887904 | 0.048532 | 0.760342 | 0.71576 |
| | 0.2 | 0.560417 | 0.587564 | 0.09362 | 0.357803 | 0.330921 |
| | 0.4 | 0.462389 | 0.603642 | 0.103659 | 0.331688 | 0.420924 |
| | 0.6 | 0.230034 | 0.645825 | 0.111212 | 0.102177 | 0.210219 |
| | 0.8 | 0.16301 | 0.599125 | 0.110792 | 0.077206 | 0.251967 |
| | 1 | 0.148868 | 0.611721 | 0.109779 | 0.046796 | 0.231675 |
| Borrego, 10/21/1942, El Centro Array #9, 0 RSN 9 | Ts | J1 | J3 | J4 | J6 | J8 |
| | 0.1 | 0.837556 | 0.754342 | 0.043491 | 0.762263 | 0.740676 |
| | 0.2 | 0.66494 | 0.548031 | 0.052789 | 0.512918 | 0.47716 |
| | 0.4 | 0.252685 | 0.356249 | 0.06254 | 0.228841 | 0.253699 |
| | 0.6 | 0.182272 | 0.326129 | 0.062207 | 0.215126 | 0.29921 |
| | 0.8 | 0.084784 | 0.358294 | 0.060293 | 0.084422 | 0.178867 |
| | 1 | 0.153261 | 0.342981 | 0.059305 | 0.133925 | 0.315821 |

**Table C-19** SSI-SSI reference model and λ (H/B) = 1.

| SSI System | | | | | | |
|---|---|---|---|---|---|---|
| Earthquakes | Ts | J1 | J3 | J4 | J6 | J8 |
| Taiwan SMART1(5), 1/29/1981, SMART1 O01, NS RSN 311 | 0.1 | 1.006285 | 1.189376 | 0.010507 | 0.957895 | 0.965357 |
| | 0.2 | 0.826799 | 0.813059 | 0.068302 | 0.698211 | 0.657731 |
| | 0.4 | 0.294547 | 0.335342 | 0.148421 | 0.154961 | 0.175723 |
| | 0.6 | 0.392393 | 0.382786 | 0.156476 | 0.209764 | 0.309438 |
| | 0.8 | 0.295246 | 0.442085 | 0.148031 | 0.078578 | 0.197929 |
| | 1 | 0.344633 | 0.496909 | 0.140697 | 0.1161 | 0.345289 |
| Mammoth Lakes-07, 5/27/1980, Green Church, 146 RSN 252 | Ts | J1 | J3 | J4 | J6 | J8 |
| | 0.1 | 0.974865 | 1.025027 | 0.027761 | 0.940559 | 0.941219 |
| | 0.2 | 0.841123 | 0.747072 | 0.100938 | 0.555829 | 0.575627 |
| | 0.4 | 0.524192 | 0.527807 | 0.162901 | 0.260567 | 0.32131 |
| | 0.6 | 0.262608 | 0.554791 | 0.158825 | 0.086306 | 0.18173 |
| | 0.8 | 0.33263 | 0.602361 | 0.167223 | 0.098069 | 0.293683 |
| | 1 | 0.370969 | 0.689957 | 0.170391 | 0.136225 | 0.455419 |
| Livermore-02, 1/27/1980, Antioch - 510 G St, 270 RSN 218 | Ts | J1 | J3 | J4 | J6 | J8 |
| | 0.1 | 0.969208 | 0.971101 | 0.015843 | 0.953653 | 0.952153 |
| | 0.2 | 0.900415 | 0.865135 | 0.057703 | 0.620967 | 0.641775 |
| | 0.4 | 0.630334 | 0.780025 | 0.089483 | 0.328964 | 0.428791 |
| | 0.6 | 0.323395 | 0.689999 | 0.102237 | 0.197941 | 0.353177 |
| | 0.8 | 0.203137 | 0.617003 | 0.10352 | 0.09015 | 0.265778 |
| | 1 | 0.182294 | 0.610507 | 0.103201 | 0.06391 | 0.271489 |
| Borrego, 10/21/1942, El Centro Array #9, 0 RSN 9 | Ts | J1 | J3 | J4 | J6 | J8 |
| | 0.1 | 0.974565 | 1.002051 | 0.011869 | 0.945733 | 0.961338 |
| | 0.2 | 0.749812 | 0.848811 | 0.040474 | 0.616085 | 0.638043 |
| | 0.4 | 0.236041 | 0.273894 | 0.053471 | 0.19108 | 0.223055 |
| | 0.6 | 0.244359 | 0.261344 | 0.058021 | 0.205167 | 0.282056 |
| | 0.8 | 0.119052 | 0.325935 | 0.057762 | 0.122184 | 0.223915 |
| | 1 | 0.176427 | 0.303251 | 0.057289 | 0.172999 | 0.343646 |

**Table C-20** SSI-SSI reference model and λ (H/B) = 0.5.

| SSI System | | | | | | |
|---|---|---|---|---|---|---|
| Earthquakes | Ts | J1 | J3 | J4 | J6 | J8 |
| Taiwan SMART1(5), 1/29/1981, SMART1 O01, NS RSN 311 | 0.1 | 0.973733 | 0.958454 | 0.037653 | 0.8106 | 0.777279 |
| | 0.2 | 0.826919 | 0.587461 | 0.061152 | 0.745397 | 0.604986 |
| | 0.4 | 0.19978 | 0.198838 | 0.128125 | 0.120782 | 0.122866 |
| | 0.6 | 0.273174 | 0.333625 | 0.140265 | 0.173395 | 0.257365 |
| | 0.8 | 0.269793 | 0.389879 | 0.132195 | 0.087365 | 0.214034 |
| | 1 | 0.304535 | 0.447466 | 0.124376 | 0.123549 | 0.348465 |
| Mammoth Lakes-07, 5/27/1980, Green Church, 146 RSN 252 | Ts | J1 | J3 | J4 | J6 | J8 |
| | 0.1 | 0.965568 | 0.979798 | 0.046989 | 0.854294 | 0.790651 |
| | 0.2 | 0.617941 | 0.507912 | 0.122853 | 0.373427 | 0.332626 |
| | 0.4 | 0.425425 | 0.449263 | 0.154972 | 0.158428 | 0.201704 |
| | 0.6 | 0.260888 | 0.483974 | 0.157892 | 0.076952 | 0.163009 |
| | 0.8 | 0.28503 | 0.559465 | 0.163216 | 0.097833 | 0.295338 |
| | 1 | 0.314833 | 0.655045 | 0.164906 | 0.122976 | 0.43197 |
| Livermore-02, 1/27/1980, Antioch - 510 G St, 270 RSN 218 | Ts | J1 | J3 | J4 | J6 | J8 |
| | 0.1 | 0.92075 | 0.909969 | 0.037103 | 0.794931 | 0.759577 |
| | 0.2 | 0.582124 | 0.632653 | 0.080247 | 0.392991 | 0.368072 |
| | 0.4 | 0.516456 | 0.650559 | 0.093466 | 0.368418 | 0.454265 |
| | 0.6 | 0.260155 | 0.678116 | 0.10135 | 0.116851 | 0.223821 |
| | 0.8 | 0.18164 | 0.619988 | 0.100641 | 0.089037 | 0.266273 |
| | 1 | 0.167193 | 0.627979 | 0.099331 | 0.05405 | 0.243799 |
| Borrego, 10/21/1942, El Centro Array #9, 0 RSN 9 | Ts | J1 | J3 | J4 | J6 | J8 |
| | 0.1 | 0.86515 | 0.80086 | 0.033565 | 0.798103 | 0.780488 |
| | 0.2 | 0.702313 | 0.574317 | 0.04621 | 0.54427 | 0.51363 |
| | 0.4 | 0.283161 | 0.372047 | 0.056094 | 0.250112 | 0.27388 |
| | 0.6 | 0.198449 | 0.341253 | 0.056233 | 0.236804 | 0.319506 |
| | 0.8 | 0.093943 | 0.372037 | 0.054133 | 0.094195 | 0.189779 |
| | 1 | 0.173548 | 0.354735 | 0.052784 | 0.15099 | 0.333966 |

**Table C-21** Fixed base reference model and Fixed base system.

| | | | Fixed | base | Structure | |
|---|---|---|---|---|---|---|
| Earthquakes | Ts | J1 | J3 | J4 | J6 | J8 |
| Taiwan SMART1(5), 1/29/1981, SMART1 O01, NS RSN 311 | 0.1 | 0.640322 | 0.409174 | 0.023511 | 0.597052 | 0.293268 |
| | 0.2 | 0.413166 | 0.328596 | 0.054307 | 0.402919 | 0.232101 |
| | 0.4 | 0.196718 | 0.239541 | 0.117853 | 0.111606 | 0.110943 |
| | 0.6 | 0.197738 | 0.292949 | 0.123218 | 0.149172 | 0.224384 |
| | 0.8 | 0.210753 | 0.395485 | 0.115291 | 0.079328 | 0.205523 |
| | 1 | 0.218309 | 0.418603 | 0.108679 | 0.093921 | 0.307978 |
| Mammoth Lakes-07, 5/27/1980, Green Church, 146 RSN 252 | Ts | J1 | J3 | J4 | J6 | J8 |
| | 0.1 | 0.9589 | 0.671115 | 0.022832 | 0.837462 | 0.433493 |
| | 0.2 | 0.604785 | 0.395448 | 0.084606 | 0.422895 | 0.243701 |
| | 0.4 | 0.267448 | 0.283573 | 0.132637 | 0.156371 | 0.173393 |
| | 0.6 | 0.207316 | 0.411436 | 0.146831 | 0.079548 | 0.167199 |
| | 0.8 | 0.187107 | 0.501214 | 0.150382 | 0.08539 | 0.256801 |
| | 1 | 0.212717 | 0.569689 | 0.151159 | 0.082468 | 0.338549 |
| Livermore-02, 1/27/1980, Antioch - 510 G St, 270 RSN 218 | Ts | J1 | J3 | J4 | J6 | J8 |
| | 0.1 | 0.984889 | 0.847434 | 0.014359 | 0.92673 | 0.461046 |
| | 0.2 | 0.62688 | 0.396151 | 0.063297 | 0.307098 | 0.17876 |
| | 0.4 | 0.307798 | 0.385389 | 0.08893 | 0.186969 | 0.199715 |
| | 0.6 | 0.115701 | 0.371974 | 0.092629 | 0.070159 | 0.129213 |
| | 0.8 | 0.135968 | 0.457369 | 0.090886 | 0.06107 | 0.181648 |
| | 1 | 0.118796 | 0.474821 | 0.089432 | 0.039564 | 0.17961 |
| Borrego, 10/21/1942, El Centro Array #9, 0 RSN 9 | Ts | J1 | J3 | J4 | J6 | J8 |
| | 0.1 | 0.549475 | 0.403574 | 0.016316 | 0.624339 | 0.366279 |
| | 0.2 | 0.313218 | 0.206623 | 0.039635 | 0.27093 | 0.188741 |
| | 0.4 | 0.174739 | 0.275499 | 0.052648 | 0.16792 | 0.170235 |
| | 0.6 | 0.150112 | 0.366309 | 0.050264 | 0.143384 | 0.196851 |
| | 0.8 | 0.071029 | 0.314268 | 0.047758 | 0.073297 | 0.144904 |
| | 1 | 0.12679 | 0.518353 | 0.046479 | 0.103271 | 0.253385 |

# APPENDIX D

## PERFORMANCE EVALUATION CRITERIA OF CHAPTER 7

Frame Building under Earthquake Managua Nicaragua-02, 12/23/1972, Managua

**Table D-1** Medium top and soft bottom soil profile with SSI-SSI reference model.

| Z/B | Dir. | J1 | J2 | J3 | J4 | J5 | J6 | J7 | J8 | J9 |
|---|---|---|---|---|---|---|---|---|---|---|
| 0 | X | 0.9516 | 0.7657 | 0.6355 | 0.0194 | 0.9983 | 0.8247 | 0.6796 | 0.5071 | 0.8251 |
| 0 | Y | 0.8882 | 0.8296 | 0.7170 | 0.0194 | 0.9640 | 0.7180 | 0.7117 | 0.5541 | 0.7302 |
| 0.1 | X | 0.9174 | 0.7819 | 0.8775 | 0.0194 | 1.0000 | 0.8016 | 0.7403 | 0.6049 | 0.8606 |
| 0.1 | Y | 0.8784 | 0.8676 | 0.8300 | 0.0194 | 0.9864 | 0.7225 | 0.7151 | 0.5681 | 0.7320 |
| 0.25 | X | 0.9130 | 0.8006 | 0.8726 | 0.0185 | 1.0030 | 0.8029 | 0.7609 | 0.7562 | 0.8800 |
| 0.25 | Y | 0.8870 | 0.8508 | 1.1199 | 0.0193 | 0.9873 | 0.7382 | 0.7259 | 0.6180 | 0.7402 |
| 0.5 | X | 0.8990 | 0.7823 | 0.8870 | 0.0190 | 1.0053 | 0.7894 | 0.7580 | 0.6664 | 0.8838 |
| 0.5 | Y | 0.8790 | 0.8632 | 0.8862 | 0.0194 | 0.9681 | 0.7478 | 0.7277 | 0.6243 | 0.7485 |
| 1 | X | 0.8934 | 0.8006 | 1.0788 | 0.0184 | 1.0043 | 0.7842 | 0.7586 | 0.8032 | 0.8875 |
| 1 | Y | 0.8773 | 0.8757 | 1.1966 | 0.0194 | 0.9779 | 0.7543 | 0.7317 | 0.6433 | 0.7582 |
| 1.25 | X | 0.9002 | 0.8017 | 1.0549 | 0.0187 | 1.0032 | 0.7839 | 0.7612 | 0.8025 | 0.8879 |
| 1.25 | Y | 0.8758 | 0.8573 | 0.9591 | 0.0194 | 0.9742 | 0.7576 | 0.7356 | 0.6482 | 0.7620 |
| Fixed | X | 0.8611 | 0.7965 | 1.1755 | 0.0194 | 0.9978 | 0.6463 | 0.6429 | 0.7617 | 0.8410 |
| | Y | 0.8320 | 0.7884 | 1.0746 | 0.0194 | 0.9605 | 0.6492 | 0.6426 | 0.6362 | 0.7072 |

**Table D-2** Medium top and soft bottom soil profile with Fixed-SSI reference model

| Z/B | Dir. | J1 | J2 | J3 | J4 | J5 | J6 | J7 | J8 | J9 |
|---|---|---|---|---|---|---|---|---|---|---|
| 0 | X | 0.9332 | 0.7233 | 0.6270 | 0.0190 | 1.0036 | 0.7937 | 0.6502 | 0.4882 | 0.8101 |
| 0 | Y | 0.8606 | 0.8152 | 0.7500 | 0.0194 | 0.9908 | 0.6651 | 0.6597 | 0.5240 | 0.6875 |
| 0.1 | X | 0.8957 | 0.7463 | 0.8608 | 0.0194 | 1.0080 | 0.7646 | 0.7049 | 0.5609 | 0.8446 |
| 0.1 | Y | 0.8504 | 0.8406 | 0.8239 | 0.0194 | 0.9950 | 0.6765 | 0.6696 | 0.5404 | 0.6954 |
| 0.25 | X | 0.8955 | 0.7439 | 0.8952 | 0.0190 | 1.0086 | 0.7643 | 0.7243 | 0.7413 | 0.8650 |
| 0.25 | Y | 0.8601 | 0.8188 | 1.1052 | 0.0194 | 0.9842 | 0.6948 | 0.6827 | 0.5887 | 0.7073 |
| 0.5 | X | 0.8818 | 0.7919 | 0.8282 | 0.0185 | 1.0127 | 0.7556 | 0.7227 | 0.6550 | 0.8741 |
| 0.5 | Y | 0.8516 | 0.8342 | 0.8853 | 0.0194 | 0.9707 | 0.7041 | 0.6852 | 0.6134 | 0.7181 |
| 1 | X | 0.8710 | 0.7840 | 0.9618 | 0.0188 | 0.9922 | 0.7491 | 0.7237 | 0.7790 | 0.8754 |
| 1 | Y | 0.8517 | 0.8269 | 1.0782 | 0.0194 | 0.9714 | 0.7171 | 0.6948 | 0.6136 | 0.7313 |
| 1.25 | X | 0.8757 | 0.7744 | 1.0834 | 0.0193 | 1.0003 | 0.7417 | 0.7183 | 0.7959 | 0.8737 |
| 1.25 | Y | 0.8457 | 0.8278 | 0.9358 | 0.0194 | 0.9673 | 0.7166 | 0.6951 | 0.6183 | 0.7316 |
| Fixed | X | 0.8611 | 0.7965 | 1.1755 | 0.0194 | 0.9978 | 0.6463 | 0.6429 | 0.7617 | 0.8410 |
| | Y | 0.8320 | 0.7884 | 1.0746 | 0.0194 | 0.9605 | 0.6492 | 0.6426 | 0.6362 | 0.7072 |

Earthquake Managua Nicaragua-02, 12/23/1972, Managua (RSN 96)

**Table D-3** Soft top and medium bottom soil profile with SSI-SSI reference model.

| Z/B | Dir. | J1 | J2 | J3 | J4 | J5 | J6 | J7 | J8 | J9 |
|---|---|---|---|---|---|---|---|---|---|---|
| 0 | X | 0.8926 | 0.7910 | 1.1388 | 0.0182 | 0.9998 | 0.7766 | 0.7558 | 0.8485 | 0.8874 |
| 0 | Y | 0.8723 | 0.8590 | 1.1194 | 0.0194 | 0.9621 | 0.7538 | 0.7340 | 0.6554 | 0.7626 |
| 0.1 | X | 0.9168 | 0.7774 | 0.8247 | 0.0188 | 1.0056 | 0.7928 | 0.7576 | 0.7050 | 0.8830 |
| 0.1 | Y | 0.8800 | 0.8614 | 0.8630 | 0.0194 | 0.9803 | 0.7480 | 0.7251 | 0.6123 | 0.7485 |
| 0.25 | X | 0.9071 | 0.8231 | 0.7946 | 0.0194 | 0.9983 | 0.8006 | 0.7493 | 0.6811 | 0.8727 |
| 0.25 | Y | 0.8839 | 0.8628 | 0.8561 | 0.0194 | 0.9817 | 0.7405 | 0.7279 | 0.6336 | 0.7439 |
| 0.5 | X | 0.9362 | 0.7587 | 0.8438 | 0.0191 | 1.0069 | 0.8098 | 0.7300 | 0.5813 | 0.8477 |
| 0.5 | Y | 0.8882 | 0.8626 | 1.0146 | 0.0194 | 0.9895 | 0.7252 | 0.7175 | 0.6574 | 0.7375 |
| 1 | X | 0.9178 | 0.7707 | 0.5524 | 0.0194 | 0.9980 | 0.8266 | 0.7169 | 0.5089 | 0.8352 |
| 1 | Y | 0.8892 | 0.8662 | 0.7709 | 0.0193 | 0.9868 | 0.7162 | 0.7102 | 0.6051 | 0.7310 |
| 1.25 | X | 0.9538 | 0.7578 | 0.5620 | 0.0192 | 0.9998 | 0.8308 | 0.7098 | 0.5019 | 0.8357 |
| 1.25 | Y | 0.8919 | 0.8638 | 0.7891 | 0.0194 | 0.9876 | 0.7146 | 0.7091 | 0.6131 | 0.7293 |
| Fixed | X | 0.8611 | 0.7965 | 1.1755 | 0.0194 | 0.9978 | 0.6463 | 0.6429 | 0.7617 | 0.8410 |
| | Y | 0.8320 | 0.7884 | 1.0746 | 0.0194 | 0.9605 | 0.6492 | 0.6426 | 0.6362 | 0.7072 |

**Table D-4** Soft top and medium bottom soil profile with Fixed-SSI reference model.

| Z/B | Dir. | J1 | J2 | J3 | J4 | J5 | J6 | J7 | J8 | J9 |
|---|---|---|---|---|---|---|---|---|---|---|
| 0 | X | 0.8700 | 0.7804 | 1.1344 | 0.0193 | 1.0026 | 0.7334 | 0.7129 | 0.8266 | 0.8742 |
| 0 | Y | 0.8464 | 0.8296 | 1.1049 | 0.0194 | 0.9564 | 0.7108 | 0.6918 | 0.6499 | 0.7313 |
| 0.1 | X | 0.8936 | 0.7762 | 0.9176 | 0.0190 | 0.9968 | 0.7529 | 0.7188 | 0.6885 | 0.8671 |
| 0.1 | Y | 0.8515 | 0.8361 | 0.9053 | 0.0194 | 0.9689 | 0.7070 | 0.6851 | 0.5850 | 0.7178 |
| 0.25 | X | 0.8956 | 0.8147 | 0.7503 | 0.0187 | 1.0016 | 0.7588 | 0.7116 | 0.6549 | 0.8569 |
| 0.25 | Y | 0.8560 | 0.8299 | 0.8612 | 0.0194 | 0.9799 | 0.6947 | 0.6827 | 0.6148 | 0.7111 |
| 0.5 | X | 0.9264 | 0.7362 | 0.8654 | 0.0194 | 1.0039 | 0.7715 | 0.6928 | 0.5701 | 0.8313 |
| 0.5 | Y | 0.8611 | 0.8288 | 1.0179 | 0.0194 | 0.9909 | 0.6796 | 0.6721 | 0.6182 | 0.7017 |
| 1 | X | 0.9103 | 0.7538 | 0.5249 | 0.0194 | 1.0010 | 0.7962 | 0.6854 | 0.4713 | 0.8241 |
| 1 | Y | 0.8642 | 0.8361 | 0.8319 | 0.0194 | 0.9886 | 0.6657 | 0.6604 | 0.5767 | 0.6897 |
| 1.25 | X | 0.9423 | 0.7389 | 0.5206 | 0.0194 | 1.0009 | 0.8018 | 0.6788 | 0.4738 | 0.8221 |
| 1.25 | Y | 0.8655 | 0.8378 | 0.7815 | 0.0194 | 0.9924 | 0.6666 | 0.6614 | 0.5759 | 0.6901 |
| Fixed | X | 0.8611 | 0.7965 | 1.1755 | 0.0194 | 0.9978 | 0.6463 | 0.6429 | 0.7617 | 0.8410 |
| | Y | 0.8320 | 0.7884 | 1.0746 | 0.0194 | 0.9605 | 0.6492 | 0.6426 | 0.6362 | 0.7072 |

Earthquake Corinth Greece, 2/24/1981, Corinth (RSN 313)

**Table D-5** Medium top and soft bottom soil profile with SSI-SSI reference model.

| Z/B | Dir. | J1 | J2 | J3 | J4 | J5 | J6 | J7 | J8 | J9 |
|---|---|---|---|---|---|---|---|---|---|---|
| 0 | X | 0.8767 | 0.8076 | 0.6450 | 0.0178 | 1.0086 | 0.8172 | 0.8120 | 0.6432 | 0.8572 |
| 0 | Y | 0.7684 | 0.6909 | 0.7551 | 0.0188 | 0.6598 | 0.7041 | 0.6503 | 0.5086 | 0.6585 |
| 0.1 | X | 0.8561 | 0.8707 | 0.7170 | 0.0184 | 0.9697 | 0.7886 | 0.7857 | 0.6652 | 0.8325 |
| 0.1 | Y | 0.7806 | 0.7022 | 0.7666 | 0.0188 | 0.7137 | 0.6845 | 0.6629 | 0.5579 | 0.6697 |
| 0.25 | X | 0.8822 | 0.8763 | 0.9686 | 0.0188 | 0.9983 | 0.7772 | 0.7720 | 0.7950 | 0.8277 |
| 0.25 | Y | 0.8302 | 0.6791 | 0.7706 | 0.0191 | 0.7593 | 0.6985 | 0.6800 | 0.5966 | 0.6939 |
| 0.5 | X | 0.7653 | 0.8780 | 0.8794 | 0.0158 | 0.9992 | 0.7579 | 0.7513 | 0.7760 | 0.8175 |
| 0.5 | Y | 0.8257 | 0.6863 | 0.7115 | 0.0175 | 0.8070 | 0.7386 | 0.7082 | 0.6201 | 0.7299 |
| 1 | X | 0.7865 | 0.9339 | 0.9566 | 0.0170 | 1.0059 | 0.7463 | 0.7401 | 0.8727 | 0.8175 |
| 1 | Y | 0.8223 | 0.6872 | 0.7692 | 0.0194 | 0.8408 | 0.7534 | 0.7169 | 0.6467 | 0.7427 |
| 1.25 | X | 0.7995 | 0.9150 | 1.3581 | 0.0175 | 0.9927 | 0.7504 | 0.7440 | 0.8257 | 0.8199 |
| 1.25 | Y | 0.8194 | 0.6901 | 0.7784 | 0.0193 | 0.8429 | 0.7507 | 0.7143 | 0.6557 | 0.7417 |
| Fixed | X | 0.8191 | 0.8852 | 0.9032 | 0.0194 | 0.9933 | 0.6899 | 0.6866 | 0.6748 | 0.8058 |
| | Y | 0.7426 | 0.6441 | 0.8533 | 0.0193 | 0.8989 | 0.7366 | 0.6929 | 0.6282 | 0.7450 |

**Table D-6** Medium top and soft bottom soil profile with Fixed-SSI reference model.

| Z/B | Dir. | J1 | J2 | J3 | J4 | J5 | J6 | J7 | J8 | J9 |
|---|---|---|---|---|---|---|---|---|---|---|
| 0 | X | 0.8405 | 0.7918 | 0.6644 | 0.0194 | 1.0154 | 0.7773 | 0.7720 | 0.6163 | 0.8289 |
| 0 | Y | 0.7463 | 0.6480 | 0.7155 | 0.0194 | 0.6130 | 0.6509 | 0.6012 | 0.4668 | 0.6137 |
| 0.1 | X | 0.8136 | 0.8506 | 0.5835 | 0.0194 | 0.9870 | 0.7485 | 0.7457 | 0.6285 | 0.8043 |
| 0.1 | Y | 0.7509 | 0.6508 | 0.7574 | 0.0193 | 0.7202 | 0.6270 | 0.6075 | 0.5428 | 0.6227 |
| 0.25 | X | 0.8688 | 0.8623 | 0.8085 | 0.0194 | 1.0049 | 0.7316 | 0.7265 | 0.8189 | 0.7976 |
| 0.25 | Y | 0.7974 | 0.6428 | 0.7583 | 0.0193 | 0.7466 | 0.6472 | 0.6300 | 0.5686 | 0.6525 |
| 0.5 | X | 0.7408 | 0.8486 | 0.8827 | 0.0191 | 1.0001 | 0.7154 | 0.7099 | 0.8074 | 0.7914 |
| 0.5 | Y | 0.7904 | 0.6433 | 0.6990 | 0.0194 | 0.8059 | 0.6920 | 0.6630 | 0.6056 | 0.6938 |
| 1 | X | 0.75611 | 0.9041 | 1.0142 | 0.0194 | 0.9938 | 0.7098 | 0.704 | 0.80211 | 0.7942 |
| 1 | Y | 0.7853 | 0.6449 | 0.6977 | 0.0184 | 0.83687 | 0.70706 | 0.67306 | 0.637 | 0.7074 |
| 1.25 | X | 0.7646 | 0.9009 | 1.0439 | 0.0181 | 0.9962 | 0.7126 | 0.7071 | 0.8528 | 0.7982 |
| 1.25 | Y | 0.7846 | 0.6490 | 0.8047 | 0.0192 | 0.8397 | 0.7071 | 0.6730 | 0.6310 | 0.7086 |
| Fixed | X | 0.8191 | 0.8852 | 0.9032 | 0.0194 | 0.9933 | 0.6899 | 0.6866 | 0.6748 | 0.8058 |
| | Y | 0.7426 | 0.6441 | 0.8533 | 0.0193 | 0.8989 | 0.7366 | 0.6929 | 0.6282 | 0.7450 |

Earthquake Corinth Greece, 2/24/1981, Corinth (RSN 313)

**Table D-7** Soft top and medium bottom soil profile with SSI-SSI reference model.

| Z/B | Dir. | J1 | J2 | J3 | J4 | J5 | J6 | J7 | J8 | J9 |
|---|---|---|---|---|---|---|---|---|---|---|
| 0 | X | 0.7961 | 0.9424 | 1.0275 | 0.0166 | 0.9988 | 0.7527 | 0.7465 | 0.8245 | 0.8239 |
| 0 | Y | 0.8164 | 0.6869 | 0.7144 | 0.0194 | 0.8697 | 0.7452 | 0.7103 | 0.6647 | 0.7395 |
| 0.1 | X | 0.7693 | 0.8580 | 0.9908 | 0.0188 | 1.0010 | 0.7622 | 0.7561 | 0.7852 | 0.8215 |
| 0.1 | Y | 0.8228 | 0.6825 | 0.6984 | 0.0178 | 0.8136 | 0.7440 | 0.7024 | 0.6157 | 0.7284 |
| 0.25 | X | 0.8573 | 0.9017 | 0.8633 | 0.0174 | 1.0384 | 0.7780 | 0.7737 | 0.7796 | 0.8297 |
| 0.25 | Y | 0.8256 | 0.6830 | 0.7618 | 0.0182 | 0.7921 | 0.7081 | 0.6684 | 0.5756 | 0.6876 |
| 0.5 | X | 0.8550 | 0.8728 | 0.6976 | 0.0185 | 0.9816 | 0.7984 | 0.7963 | 0.6874 | 0.8444 |
| 0.5 | Y | 0.7870 | 0.6981 | 0.8006 | 0.0194 | 0.7230 | 0.6792 | 0.6445 | 0.5227 | 0.6534 |
| 1 | X | 0.8742 | 0.8218 | 0.6731 | 0.0181 | 0.9562 | 0.8155 | 0.8136 | 0.6245 | 0.8609 |
| 1 | Y | 0.7645 | 0.7550 | 0.7879 | 0.0190 | 0.6689 | 0.6869 | 0.6463 | 0.5172 | 0.6519 |
| 1.25 | X | 0.8769 | 0.8032 | 0.7026 | 0.0169 | 0.9852 | 0.8149 | 0.8125 | 0.6907 | 0.8601 |
| 1.25 | Y | 0.7613 | 0.7146 | 0.6863 | 0.0187 | 0.6619 | 0.6912 | 0.6469 | 0.5088 | 0.6528 |
| Fixed | X | 0.8191 | 0.8852 | 0.9032 | 0.0194 | 0.9933 | 0.6899 | 0.6866 | 0.6748 | 0.8058 |
| | Y | 0.7426 | 0.6441 | 0.8533 | 0.0193 | 0.8989 | 0.7366 | 0.6929 | 0.6282 | 0.7450 |

**Table D-8** Soft top and medium bottom soil profile with Fixed-SSI reference model.

| Z/B | Dir. | J1 | J2 | J3 | J4 | J5 | J6 | J7 | J8 | J9 |
|---|---|---|---|---|---|---|---|---|---|---|
| 0 | X | 0.7706 | 0.9127 | 1.0358 | 0.0186 | 1.0071 | 0.7097 | 0.7040 | 0.8380 | 0.7994 |
| 0 | Y | 0.7809 | 0.6474 | 0.7664 | 0.0194 | 0.8634 | 0.7045 | 0.6715 | 0.6401 | 0.7092 |
| 0.1 | X | 0.7530 | 0.8510 | 0.8530 | 0.0194 | 1.0008 | 0.7201 | 0.7151 | 0.7575 | 0.7937 |
| 0.1 | Y | 0.7860 | 0.6393 | 0.7551 | 0.0191 | 0.8080 | 0.6980 | 0.6586 | 0.5976 | 0.6929 |
| 0.25 | X | 0.8420 | 0.8931 | 0.9661 | 0.0194 | 1.0026 | 0.7357 | 0.7322 | 0.7665 | 0.8002 |
| 0.25 | Y | 0.7915 | 0.6386 | 0.7778 | 0.0194 | 0.7921 | 0.6601 | 0.6228 | 0.5450 | 0.6497 |
| 0.5 | X | 0.8277 | 0.8678 | 0.7053 | 0.0190 | 0.9868 | 0.7561 | 0.7548 | 0.6887 | 0.8140 |
| 0.5 | Y | 0.7503 | 0.6519 | 0.7372 | 0.0194 | 0.7198 | 0.6235 | 0.5920 | 0.5014 | 0.6086 |
| 1 | X | 0.8382 | 0.8080 | 0.6819 | 0.0194 | 0.9570 | 0.7731 | 0.7717 | 0.6163 | 0.8316 |
| 1 | Y | 0.7361 | 0.6990 | 0.7581 | 0.0194 | 0.6448 | 0.6303 | 0.5933 | 0.4906 | 0.6054 |
| 1.25 | X | 0.8401 | 0.7718 | 0.6842 | 0.0178 | 0.9823 | 0.7760 | 0.7734 | 0.6769 | 0.8324 |
| 1.25 | Y | 0.7307 | 0.6807 | 0.6189 | 0.0194 | 0.6172 | 0.6368 | 0.5960 | 0.4711 | 0.6077 |
| Fixed | X | 0.8191 | 0.8852 | 0.9032 | 0.0194 | 0.9933 | 0.6899 | 0.6866 | 0.6748 | 0.8058 |
| | Y | 0.7426 | 0.6441 | 0.8533 | 0.0193 | 0.8989 | 0.7366 | 0.6929 | 0.6282 | 0.7450 |

Earthquake Managua Nicaragua-02, 12/23/1972, Managua (RSN 96)

**Table D-9** Clay (linear) soil profile with SSI-SSI reference model.

| Ga | Dir. | J1 | J2 | J3 | J4 | J5 | J6 | J7 | J8 | J9 |
|---|---|---|---|---|---|---|---|---|---|---|
| 15 | X | 0.8058 | 0.7568 | 0.9772 | 0.0194 | 1.003 | 0.8928 | 0.545 | 0.5059 | 0.8342 |
| 15 | Y | 0.9072 | 0.8675 | 0.8705 | 0.0194 | 0.8601 | 0.7533 | 0.7463 | 0.6358 | 0.7766 |
| 25 | X | 0.9032 | 0.7457 | 0.9717 | 0.0192 | 1.0018 | 0.8401 | 0.6769 | 0.5318 | 0.8242 |
| 25 | Y | 0.8897 | 0.8479 | 0.7968 | 0.0194 | 0.9831 | 0.7104 | 0.703 | 0.5992 | 0.7227 |
| 35 | X | 0.9476 | 0.7399 | 0.8162 | 0.0192 | 1.0037 | 0.8181 | 0.7294 | 0.5788 | 0.8424 |
| 35 | Y | 0.8907 | 0.8602 | 1.0614 | 0.0194 | 0.9915 | 0.7247 | 0.7171 | 0.651 | 0.7387 |
| 50 | X | 0.913 | 0.8082 | 0.8773 | 0.0192 | 0.9948 | 0.794 | 0.7482 | 0.7766 | 0.8728 |
| 50 | Y | 0.8806 | 0.8583 | 0.9559 | 0.0194 | 0.986 | 0.7398 | 0.7242 | 0.6325 | 0.7431 |
| 70 | X | 0.9058 | 0.7858 | 0.8219 | 0.0189 | 1.0032 | 0.7925 | 0.7611 | 0.6937 | 0.886 |
| 70 | Y | 0.8762 | 0.8615 | 0.9231 | 0.0193 | 0.9736 | 0.7529 | 0.729 | 0.6182 | 0.7527 |
| 100 | X | 0.8931 | 0.7863 | 0.9623 | 0.0194 | 0.9924 | 0.7836 | 0.7616 | 0.8299 | 0.8915 |
| 100 | Y | 0.8739 | 0.8603 | 1.0745 | 0.0194 | 0.9707 | 0.7519 | 0.7316 | 0.6482 | 0.7595 |
| Fixed | X | 0.8611 | 0.7965 | 1.1755 | 0.0194 | 0.9978 | 0.6463 | 0.6429 | 0.7617 | 0.8410 |
|  | Y | 0.8320 | 0.7884 | 1.0746 | 0.0194 | 0.9605 | 0.6492 | 0.6426 | 0.6362 | 0.7072 |

**Table D-10** Clay (linear) soil profile with Fixed-SSI reference model.

| Ga | Dir. | J1 | J2 | J3 | J4 | J5 | J6 | J7 | J8 | J9 |
|---|---|---|---|---|---|---|---|---|---|---|
| 15 | X | 0.7800 | 0.7508 | 0.9854 | 0.0194 | 1.0038 | 0.8776 | 0.5073 | 0.4844 | 0.8231 |
| 15 | Y | 0.8835 | 0.8439 | 0.8454 | 0.0194 | 0.8444 | 0.7063 | 0.6996 | 0.5997 | 0.7374 |
| 25 | X | 0.8997 | 0.7091 | 1.0470 | 0.0194 | 1.0026 | 0.8119 | 0.6472 | 0.5271 | 0.8101 |
| 25 | Y | 0.8645 | 0.8339 | 0.7666 | 0.0194 | 1.0065 | 0.6607 | 0.6541 | 0.5623 | 0.6824 |
| 35 | X | 0.9219 | 0.7237 | 0.8359 | 0.0194 | 1.0006 | 0.7767 | 0.6889 | 0.5564 | 0.8260 |
| 35 | Y | 0.8655 | 0.8294 | 1.0882 | 0.0193 | 0.9876 | 0.6791 | 0.6717 | 0.6247 | 0.7034 |
| 50 | X | 0.8921 | 0.7695 | 0.8606 | 0.0194 | 1.0144 | 0.7605 | 0.7162 | 0.7128 | 0.8602 |
| 50 | Y | 0.8542 | 0.8298 | 0.8749 | 0.0194 | 0.9767 | 0.6953 | 0.6804 | 0.6028 | 0.7100 |
| 70 | X | 0.8818 | 0.7775 | 0.9507 | 0.0193 | 1.0025 | 0.7530 | 0.7225 | 0.6765 | 0.8729 |
| 70 | Y | 0.8475 | 0.8299 | 0.9217 | 0.0194 | 0.9660 | 0.7121 | 0.6890 | 0.5927 | 0.7232 |
| 100 | X | 0.8728 | 0.7908 | 0.9266 | 0.0186 | 0.9920 | 0.7449 | 0.7239 | 0.8402 | 0.8759 |
| 100 | Y | 0.8470 | 0.8150 | 0.9823 | 0.0194 | 0.9588 | 0.7102 | 0.6909 | 0.6351 | 0.7305 |
| Fixed | X | 0.8611 | 0.7965 | 1.1755 | 0.0194 | 0.9978 | 0.6463 | 0.6429 | 0.7617 | 0.8410 |
|  | Y | 0.8320 | 0.7884 | 1.0746 | 0.0194 | 0.9605 | 0.6492 | 0.6426 | 0.6362 | 0.7072 |

Earthquake Managua Nicaragua-02, 12/23/1972, Managua (RSN 96)

**Table D-11** Sand (parabola) soil profile with SSI-SSI reference model.

| Ga | Dir. | J1 | J2 | J3 | J4 | J5 | J6 | J7 | J8 | J9 |
|---|---|---|---|---|---|---|---|---|---|---|
| 15 | X | 0.7742 | 0.6613 | 0.9314 | 0.0194 | 1.0022 | 0.8821 | 0.6286 | 0.5272 | 0.8268 |
| 15 | Y | 0.9027 | 0.8290 | 0.9248 | 0.0192 | 0.9231 | 0.7514 | 0.7409 | 0.6464 | 0.7567 |
| 25 | X | 0.9142 | 0.7351 | 0.8000 | 0.0192 | 1.0025 | 0.8260 | 0.7223 | 0.5502 | 0.8356 |
| 25 | Y | 0.8881 | 0.8702 | 0.8314 | 0.0192 | 0.9985 | 0.7205 | 0.7146 | 0.6243 | 0.7363 |
| 35 | X | 0.9112 | 0.8216 | 0.7422 | 0.0188 | 1.0209 | 0.7929 | 0.7411 | 0.6566 | 0.8654 |
| 35 | Y | 0.8810 | 0.8602 | 0.8690 | 0.0194 | 0.9800 | 0.7394 | 0.7289 | 0.6296 | 0.7441 |
| 50 | X | 0.9131 | 0.7798 | 0.8564 | 0.0188 | 1.0164 | 0.7921 | 0.7578 | 0.7067 | 0.8835 |
| 50 | Y | 0.8803 | 0.8616 | 0.9277 | 0.0194 | 0.9817 | 0.7481 | 0.7252 | 0.6148 | 0.7485 |
| 70 | X | 0.8888 | 0.7827 | 0.9032 | 0.0186 | 0.9983 | 0.7881 | 0.7630 | 0.7596 | 0.8908 |
| 70 | Y | 0.8779 | 0.8570 | 0.9935 | 0.0194 | 0.9707 | 0.7557 | 0.7335 | 0.6499 | 0.7601 |
| 100 | X | 0.8939 | 0.7770 | 0.9509 | 0.0194 | 0.9982 | 0.7624 | 0.7469 | 0.8370 | 0.8839 |
| 100 | Y | 0.8748 | 0.8545 | 1.1028 | 0.0194 | 0.9713 | 0.7390 | 0.7233 | 0.6938 | 0.7550 |
| Fixed | X | 0.8611 | 0.7965 | 1.1755 | 0.0194 | 0.9978 | 0.6463 | 0.6429 | 0.7617 | 0.8410 |
|  | Y | 0.8320 | 0.7884 | 1.0746 | 0.0194 | 0.9605 | 0.6492 | 0.6426 | 0.6362 | 0.7072 |

**Table D-12** Sand (parabola) soil profile with Fixed-SSI reference model.

| Ga | Dir. | J1 | J2 | J3 | J4 | J5 | J6 | J7 | J8 | J9 |
|---|---|---|---|---|---|---|---|---|---|---|
| 15 | X | 0.7546 | 0.6525 | 0.9607 | 0.0194 | 1.0031 | 0.8607 | 0.6038 | 0.5023 | 0.8155 |
| 15 | Y | 0.8788 | 0.8057 | 0.9938 | 0.0194 | 0.9182 | 0.7021 | 0.6919 | 0.6197 | 0.7161 |
| 25 | X | 0.9066 | 0.7267 | 0.7293 | 0.0194 | 0.9959 | 0.7872 | 0.6856 | 0.5163 | 0.8206 |
| 25 | Y | 0.8608 | 0.8341 | 0.8562 | 0.0194 | 0.9918 | 0.6705 | 0.6646 | 0.6060 | 0.6965 |
| 35 | X | 0.8938 | 0.8058 | 0.7206 | 0.0187 | 1.0167 | 0.7611 | 0.7089 | 0.6338 | 0.8535 |
| 35 | Y | 0.8536 | 0.8277 | 0.8669 | 0.0192 | 0.9773 | 0.6917 | 0.6820 | 0.6042 | 0.7094 |
| 50 | X | 0.8979 | 0.7670 | 1.0118 | 0.0194 | 0.9812 | 0.7570 | 0.7243 | 0.7118 | 0.8725 |
| 50 | Y | 0.8519 | 0.8379 | 0.8953 | 0.0193 | 0.9733 | 0.7075 | 0.6856 | 0.5889 | 0.7195 |
| 70 | X | 0.8729 | 0.7937 | 0.8894 | 0.0183 | 0.9963 | 0.7533 | 0.7278 | 0.7388 | 0.8803 |
| 70 | Y | 0.8480 | 0.8270 | 1.0145 | 0.0194 | 0.9702 | 0.7164 | 0.6944 | 0.6222 | 0.7313 |
| 100 | X | 0.8689 | 0.7845 | 1.0177 | 0.0194 | 1.0020 | 0.7214 | 0.7070 | 0.8748 | 0.8709 |
| 100 | Y | 0.8478 | 0.8196 | 1.0115 | 0.0194 | 0.9575 | 0.7003 | 0.6852 | 0.6567 | 0.7262 |
| Fixed | X | 0.8611 | 0.7965 | 1.1755 | 0.0194 | 0.9978 | 0.6463 | 0.6429 | 0.7617 | 0.8410 |
|  | Y | 0.8320 | 0.7884 | 1.0746 | 0.0194 | 0.9605 | 0.6492 | 0.6426 | 0.6362 | 0.7072 |

Earthquake Corinth Greece, 2/24/1981, Corinth (RSN 313)

**Table D-13** Clay (linear) soil profile with SSI-SSI reference model.

| Ga | Dir. | J1 | J2 | J3 | J4 | J5 | J6 | J7 | J8 | J9 |
|---|---|---|---|---|---|---|---|---|---|---|
| 15 | X | 0.8958 | 0.8195 | 1.1806 | 0.0175 | 0.9850 | 0.8808 | 0.8777 | 0.7391 | 0.8919 |
| 15 | Y | 0.8274 | 0.6942 | 0.7536 | 0.0168 | 0.7338 | 0.7800 | 0.7062 | 0.5580 | 0.7452 |
| 25 | X | 0.8810 | 0.7942 | 0.8949 | 0.0171 | 1.0090 | 0.8225 | 0.8153 | 0.6486 | 0.8565 |
| 25 | Y | 0.7820 | 0.7015 | 0.7800 | 0.0192 | 0.6571 | 0.6967 | 0.6425 | 0.4982 | 0.6512 |
| 35 | X | 0.8636 | 0.8996 | 0.6696 | 0.0185 | 0.9739 | 0.8031 | 0.8017 | 0.6980 | 0.8501 |
| 35 | Y | 0.7746 | 0.7130 | 0.7002 | 0.0194 | 0.7025 | 0.6786 | 0.6392 | 0.5139 | 0.6483 |
| 50 | X | 0.8882 | 0.8753 | 0.9022 | 0.0192 | 1.0066 | 0.7735 | 0.7687 | 0.8501 | 0.8259 |
| 50 | Y | 0.8278 | 0.6945 | 0.7584 | 0.0192 | 0.8015 | 0.7200 | 0.6783 | 0.5799 | 0.6997 |
| 70 | X | 0.7629 | 0.8575 | 0.9480 | 0.0188 | 1.0029 | 0.7555 | 0.7503 | 0.8213 | 0.8170 |
| 70 | Y | 0.8223 | 0.6836 | 0.7383 | 0.0189 | 0.8254 | 0.7498 | 0.7086 | 0.6268 | 0.7354 |
| 100 | X | 0.7966 | 0.9651 | 1.0730 | 0.0175 | 1.0108 | 0.7480 | 0.7425 | 0.8599 | 0.8202 |
| 100 | Y | 0.8179 | 0.6933 | 0.7680 | 0.0190 | 0.8657 | 0.7471 | 0.7114 | 0.6541 | 0.7400 |
| Fixed | X | 0.8191 | 0.8852 | 0.9032 | 0.0194 | 0.9933 | 0.6899 | 0.6866 | 0.6748 | 0.8058 |
|  | Y | 0.7426 | 0.6441 | 0.8533 | 0.0193 | 0.8989 | 0.7366 | 0.6929 | 0.6282 | 0.7450 |

**Table D-14** Clay (linear) soil profile with Fixed-SSI reference model.

| Ga | Dir. | J1 | J2 | J3 | J4 | J5 | J6 | J7 | J8 | J9 |
|---|---|---|---|---|---|---|---|---|---|---|
| 15 | X | 0.88095 | 0.8069 | 1.10997 | 0.01937 | 0.9868 | 0.84565 | 0.8431 | 0.758 | 0.8664 |
| 15 | Y | 0.82469 | 0.662 | 0.70881 | 0.01939 | 0.7264 | 0.73857 | 0.6674 | 0.523 | 0.7104 |
| 25 | X | 0.85049 | 0.7629 | 0.91405 | 0.01847 | 0.9958 | 0.78146 | 0.7749 | 0.6261 | 0.8272 |
| 25 | Y | 0.75236 | 0.6604 | 0.72255 | 0.01939 | 0.616 | 0.64186 | 0.5918 | 0.4652 | 0.6054 |
| 35 | X | 0.83064 | 0.8618 | 0.77043 | 0.01939 | 0.9902 | 0.76098 | 0.7595 | 0.6558 | 0.8197 |
| 35 | Y | 0.73847 | 0.6637 | 0.72792 | 0.0193 | 0.7085 | 0.62352 | 0.5873 | 0.4788 | 0.6035 |
| 50 | X | 0.86415 | 0.8807 | 0.89536 | 0.01939 | 1.011 | 0.7325 | 0.7273 | 0.8289 | 0.7983 |
| 50 | Y | 0.79306 | 0.6457 | 0.73074 | 0.01917 | 0.8018 | 0.67076 | 0.6321 | 0.5525 | 0.6608 |
| 70 | X | 0.74838 | 0.8358 | 0.96384 | 0.01747 | 0.9919 | 0.71846 | 0.713 | 0.8038 | 0.7925 |
| 70 | Y | 0.78891 | 0.6349 | 0.80042 | 0.01939 | 0.8244 | 0.70313 | 0.6641 | 0.6045 | 0.6997 |
| 100 | X | 0.75984 | 0.9157 | 1.12927 | 0.01939 | 0.9978 | 0.70785 | 0.7028 | 0.8315 | 0.7958 |
| 100 | Y | 0.7812 | 0.6477 | 0.7939 | 0.01879 | 0.8732 | 0.70326 | 0.6687 | 0.6347 | 0.7064 |
| Fixed | X | 0.8191 | 0.8852 | 0.9032 | 0.0194 | 0.9933 | 0.6899 | 0.6866 | 0.6748 | 0.8058 |
|  | Y | 0.7426 | 0.6441 | 0.8533 | 0.0193 | 0.8989 | 0.7366 | 0.6929 | 0.6282 | 0.7450 |

Earthquake Corinth Greece, 2/24/1981, Corinth (RSN 313)

**Table D-15** Sand (parabola) soil profile with SSI-SSI reference model.

| Ga | Dir. | J1 | J2 | J3 | J4 | J5 | J6 | J7 | J8 | J9 |
|---|---|---|---|---|---|---|---|---|---|---|
| 15 | X | 0.8836 | 0.8447 | 0.9822 | 0.0179 | 1.0001 | 0.8456 | 0.8346 | 0.6003 | 0.8624 |
| 15 | Y | 0.7701 | 0.7256 | 0.6829 | 0.0185 | 0.6575 | 0.7364 | 0.6707 | 0.5242 | 0.6899 |
| 25 | X | 0.8691 | 0.8379 | 0.7213 | 0.0194 | 0.9755 | 0.8087 | 0.8065 | 0.6022 | 0.8572 |
| 25 | Y | 0.7828 | 0.7174 | 0.7455 | 0.0187 | 0.6770 | 0.6797 | 0.6396 | 0.5120 | 0.6463 |
| 35 | X | 0.8525 | 0.9163 | 0.9088 | 0.0193 | 1.0121 | 0.7767 | 0.7728 | 0.7767 | 0.8277 |
| 35 | Y | 0.8128 | 0.6985 | 0.8268 | 0.0194 | 0.7851 | 0.7008 | 0.6629 | 0.5633 | 0.6808 |
| 50 | X | 0.7698 | 0.8560 | 0.7753 | 0.0185 | 1.0004 | 0.7613 | 0.7559 | 0.7917 | 0.8198 |
| 50 | Y | 0.8212 | 0.6790 | 0.6909 | 0.0178 | 0.8139 | 0.7439 | 0.7034 | 0.6133 | 0.7295 |
| 70 | X | 0.7887 | 0.9306 | 1.0599 | 0.0183 | 1.0030 | 0.7527 | 0.7472 | 0.8281 | 0.8209 |
| 70 | Y | 0.8196 | 0.6943 | 0.8197 | 0.0189 | 0.8538 | 0.7491 | 0.7126 | 0.6555 | 0.7409 |
| 100 | X | 0.7959 | 0.9360 | 0.9582 | 0.0182 | 1.0004 | 0.7500 | 0.7442 | 0.8249 | 0.8261 |
| 100 | Y | 0.8138 | 0.6885 | 0.7490 | 0.0175 | 0.8842 | 0.7422 | 0.7074 | 0.6784 | 0.7389 |
| Fixed | X | 0.8191 | 0.8852 | 0.9032 | 0.0194 | 0.9933 | 0.6899 | 0.6866 | 0.6748 | 0.8058 |
|  | Y | 0.7426 | 0.6441 | 0.8533 | 0.0193 | 0.8989 | 0.7366 | 0.6929 | 0.6282 | 0.7450 |

**Table D-16** Sand (parabola) soil profile with Fixed-SSI reference model.

| Ga | Dir. | J1 | J2 | J3 | J4 | J5 | J6 | J7 | J8 | J9 |
|---|---|---|---|---|---|---|---|---|---|---|
| 15 | X | 0.8587 | 0.8134 | 1.0994 | 0.0194 | 1.0059 | 0.8070 | 0.7965 | 0.5816 | 0.8332 |
| 15 | Y | 0.7559 | 0.6920 | 0.6593 | 0.0189 | 0.6286 | 0.6869 | 0.6252 | 0.4850 | 0.6484 |
| 25 | X | 0.8392 | 0.8251 | 0.7516 | 0.0194 | 0.9648 | 0.7682 | 0.7664 | 0.5708 | 0.8275 |
| 25 | Y | 0.7480 | 0.6807 | 0.7982 | 0.0187 | 0.6736 | 0.6224 | 0.5857 | 0.4906 | 0.5998 |
| 35 | X | 0.8395 | 0.8970 | 0.8485 | 0.0194 | 1.0121 | 0.7345 | 0.7314 | 0.7613 | 0.7992 |
| 35 | Y | 0.7836 | 0.6441 | 0.8259 | 0.0178 | 0.7792 | 0.6517 | 0.6161 | 0.5291 | 0.6415 |
| 50 | X | 0.7584 | 0.8348 | 0.8307 | 0.0187 | 1.0010 | 0.7214 | 0.7159 | 0.7611 | 0.7940 |
| 50 | Y | 0.7859 | 0.6292 | 0.7236 | 0.0188 | 0.8097 | 0.7004 | 0.6619 | 0.5906 | 0.6957 |
| 70 | X | 0.7492 | 0.9160 | 0.9914 | 0.0182 | 0.9965 | 0.7084 | 0.7035 | 0.8823 | 0.7939 |
| 70 | Y | 0.7824 | 0.6448 | 0.8238 | 0.0189 | 0.8610 | 0.7032 | 0.6682 | 0.6424 | 0.7061 |
| 100 | X | 0.7819 | 0.9175 | 0.9453 | 0.0192 | 0.9919 | 0.7108 | 0.7060 | 0.8928 | 0.8037 |
| 100 | Y | 0.7781 | 0.6507 | 0.7687 | 0.0194 | 0.8844 | 0.7007 | 0.6675 | 0.6540 | 0.7080 |
| Fixed | X | 0.8191 | 0.8852 | 0.9032 | 0.0194 | 0.9933 | 0.6899 | 0.6866 | 0.6748 | 0.8058 |
|  | Y | 0.7426 | 0.6441 | 0.8533 | 0.0193 | 0.8989 | 0.7366 | 0.6929 | 0.6282 | 0.7450 |

Frame Shear Wall Building

Earthquake Managua Nicaragua-02, 12/23/1972, Managua (RSN 96)

**Table D-17** Medium top and soft bottom soil profile with SSI-SSI reference model.

| Z/B | Dir. | J1 | J2 | J3 | J4 | J5 | J6 | J7 | J8 | J9 |
|---|---|---|---|---|---|---|---|---|---|---|
| 0 | X | 0.8481 | 0.7717 | 0.9544 | 0.0178 | 0.7467 | 0.6442 | 0.6481 | 0.8262 | 0.6782 |
| 0 | Y | 0.8579 | 0.9106 | 0.8376 | 0.0166 | 0.9607 | 0.7783 | 0.7516 | 0.5694 | 0.8215 |
| 0.1 | X | 0.8117 | 0.7504 | 1.0132 | 0.0178 | 0.6463 | 0.7351 | 0.6236 | 0.5331 | 0.4951 |
| 0.1 | Y | 0.8282 | 0.8400 | 0.7499 | 0.0178 | 0.9320 | 0.7168 | 0.7283 | 0.7478 | 0.8396 |
| 0.25 | X | 0.7876 | 0.7297 | 0.4964 | 0.0178 | 0.5948 | 0.7129 | 0.5627 | 0.3792 | 0.4503 |
| 0.25 | Y | 0.7716 | 0.7662 | 0.7156 | 0.0177 | 0.7838 | 0.6946 | 0.6767 | 0.4336 | 0.6143 |
| 0.5 | X | 0.7679 | 0.6954 | 0.7902 | 0.0178 | 0.5032 | 0.6497 | 0.5664 | 0.4278 | 0.4639 |
| 0.5 | Y | 0.7813 | 0.8172 | 0.9358 | 0.0173 | 0.9490 | 0.6166 | 0.6239 | 0.8497 | 0.6559 |
| 1 | X | 0.7651 | 0.7436 | 0.9037 | 0.0178 | 0.6004 | 0.5671 | 0.5234 | 0.5316 | 0.4358 |
| 1 | Y | 0.8024 | 0.8988 | 0.9946 | 0.0174 | 0.9391 | 0.6240 | 0.6463 | 1.0862 | 0.7899 |
| 1.25 | X | 0.7715 | 0.7499 | 0.9203 | 0.0178 | 0.6157 | 0.5541 | 0.5118 | 0.4508 | 0.4347 |
| 1.25 | Y | 0.8857 | 0.9245 | 1.0747 | 0.0174 | 0.9085 | 0.6549 | 0.6772 | 1.0312 | 0.8434 |
| Fixed | X | 0.8751 | 0.8961 | 0.7134 | 0.0178 | 0.9181 | 0.6154 | 0.5985 | 0.4850 | 0.6282 |
| | Y | 0.9320 | 0.9517 | 0.7451 | 0.0168 | 0.9752 | 0.4682 | 0.4743 | 0.5048 | 0.5730 |

**Table D-18** Medium top and soft bottom soil profile with Fixed-SSI reference model.

| Z/B | Dir. | J1 | J2 | J3 | J4 | J5 | J6 | J7 | J8 | J9 |
|---|---|---|---|---|---|---|---|---|---|---|
| 0 | X | 0.8664 | 0.7371 | 0.9550 | 0.0178 | 0.7283 | 0.6147 | 0.6172 | 0.8301 | 0.6560 |
| 0 | Y | 0.8469 | 0.9285 | 0.7797 | 0.0175 | 0.9655 | 0.7183 | 0.6983 | 0.5729 | 0.8279 |
| 0.1 | X | 0.7318 | 0.6172 | 0.9637 | 0.0178 | 0.6057 | 0.6311 | 0.5333 | 0.5077 | 0.4548 |
| 0.1 | Y | 0.7463 | 0.7661 | 0.7096 | 0.0176 | 0.9339 | 0.6168 | 0.6280 | 0.6959 | 0.8049 |
| 0.25 | X | 0.6624 | 0.6345 | 0.4465 | 0.0178 | 0.5425 | 0.6104 | 0.4828 | 0.3548 | 0.4310 |
| 0.25 | Y | 0.6690 | 0.6238 | 0.7012 | 0.0178 | 0.7934 | 0.5419 | 0.5244 | 0.4088 | 0.6048 |
| 0.5 | X | 0.6369 | 0.6335 | 0.7530 | 0.0178 | 0.5127 | 0.5285 | 0.4631 | 0.4136 | 0.4435 |
| 0.5 | Y | 0.6839 | 0.7398 | 0.9222 | 0.0178 | 0.9321 | 0.4698 | 0.4736 | 0.8771 | 0.6339 |
| 1 | X | 0.6813 | 0.6195 | 0.9086 | 0.0178 | 0.6222 | 0.4420 | 0.4106 | 0.4781 | 0.4260 |
| 1 | Y | 0.6858 | 0.7620 | 0.9947 | 0.0174 | 0.9160 | 0.4891 | 0.5080 | 1.1069 | 0.7962 |
| 1.25 | X | 0.6934 | 0.6472 | 0.9172 | 0.0178 | 0.6396 | 0.4275 | 0.3970 | 0.4041 | 0.4257 |
| 1.25 | Y | 0.6959 | 0.7372 | 1.1041 | 0.0175 | 0.8823 | 0.5370 | 0.5555 | 1.0549 | 0.8398 |
| Fixed | X | 0.8751 | 0.8961 | 0.7134 | 0.0178 | 0.9181 | 0.6154 | 0.5985 | 0.4850 | 0.6282 |
| | Y | 0.9320 | 0.9517 | 0.7451 | 0.0168 | 0.9752 | 0.4682 | 0.4743 | 0.5048 | 0.5730 |

Earthquake Managua Nicaragua-02, 12/23/1972, Managua (RSN 96)

**Table D-19** Soft top and medium bottom soil profile with SSI-SSI reference model.

| Z/B | Dir. | J1 | J2 | J3 | J4 | J5 | J6 | J7 | J8 | J9 |
|---|---|---|---|---|---|---|---|---|---|---|
| 0 | X | 0.7973 | 0.7938 | 0.6886 | 0.0178 | 0.6578 | 0.5402 | 0.5043 | 0.3812 | 0.4474 |
| 0 | Y | 0.8599 | 0.9346 | 1.1451 | 0.0177 | 0.9073 | 0.6855 | 0.7161 | 0.8069 | 0.7565 |
| 0.1 | X | 0.7618 | 0.6967 | 0.7494 | 0.0178 | 0.5186 | 0.6747 | 0.5614 | 0.4433 | 0.4554 |
| 0.1 | Y | 0.7667 | 0.8221 | 0.7388 | 0.0171 | 1.0125 | 0.6152 | 0.6204 | 0.6411 | 0.5940 |
| 0.25 | X | 0.7813 | 0.7220 | 0.6201 | 0.0178 | 0.6315 | 0.6998 | 0.5676 | 0.4238 | 0.4560 |
| 0.25 | Y | 0.8990 | 0.9026 | 0.9308 | 0.0178 | 0.8743 | 0.7292 | 0.7079 | 0.5767 | 0.6377 |
| 0.5 | X | 0.8367 | 0.7944 | 0.7698 | 0.0178 | 0.6905 | 0.7209 | 0.6377 | 0.5293 | 0.5514 |
| 0.5 | Y | 0.9338 | 1.0264 | 0.7658 | 0.0177 | 1.0395 | 0.6924 | 0.7011 | 0.7256 | 0.7219 |
| 1 | X | 0.8502 | 0.8139 | 1.1477 | 0.0178 | 0.7514 | 0.6626 | 0.6163 | 0.5470 | 0.5725 |
| 1 | Y | 0.8732 | 0.9765 | 0.8169 | 0.0173 | 0.8911 | 0.7629 | 0.7545 | 0.6234 | 0.8193 |
| 1.25 | X | 0.8670 | 0.8200 | 1.1456 | 0.0178 | 0.7670 | 0.6489 | 0.6162 | 0.5758 | 0.5812 |
| 1.25 | Y | 0.8450 | 0.9278 | 0.7257 | 0.0171 | 0.9820 | 0.7512 | 0.7105 | 0.4910 | 0.7066 |
| Fixed | X | 0.8751 | 0.8961 | 0.7134 | 0.0178 | 0.9181 | 0.6154 | 0.5985 | 0.4850 | 0.6282 |
| | Y | 0.9320 | 0.9517 | 0.7451 | 0.0168 | 0.9752 | 0.4682 | 0.4743 | 0.5048 | 0.5730 |

**Table D-20** Soft top and medium bottom soil profile with Fixed-SSI reference model.

| Z/B | Dir. | J1 | J2 | J3 | J4 | J5 | J6 | J7 | J8 | J9 |
|---|---|---|---|---|---|---|---|---|---|---|
| 0 | X | 0.7119 | 0.6743 | 0.6630 | 0.0178 | 0.6780 | 0.4101 | 0.3844 | 0.3953 | 0.4336 |
| 0 | Y | 0.7007 | 0.7798 | 1.1573 | 0.0174 | 0.9037 | 0.5683 | 0.5649 | 0.7508 | 0.7241 |
| 0.1 | X | 0.6388 | 0.6180 | 0.7076 | 0.0178 | 0.4899 | 0.5583 | 0.4668 | 0.4009 | 0.4339 |
| 0.1 | Y | 0.6247 | 0.6528 | 0.7395 | 0.0176 | 1.0097 | 0.4388 | 0.4391 | 0.6254 | 0.5658 |
| 0.25 | X | 0.6701 | 0.6144 | 0.5604 | 0.0178 | 0.5858 | 0.6032 | 0.4898 | 0.3744 | 0.4283 |
| 0.25 | Y | 0.7805 | 0.7994 | 0.9040 | 0.0178 | 0.8495 | 0.5692 | 0.5471 | 0.5555 | 0.6142 |
| 0.5 | X | 0.7545 | 0.6616 | 0.7739 | 0.0178 | 0.6554 | 0.6429 | 0.5676 | 0.5062 | 0.5139 |
| 0.5 | Y | 0.8467 | 0.9099 | 0.7322 | 0.0178 | 1.0548 | 0.5605 | 0.5648 | 0.6717 | 0.6980 |
| 1 | X | 0.8603 | 0.7949 | 1.0746 | 0.0178 | 0.7193 | 0.6256 | 0.5830 | 0.5297 | 0.5521 |
| 1 | Y | 0.8091 | 0.8674 | 0.7798 | 0.0176 | 0.8809 | 0.6709 | 0.6650 | 0.5835 | 0.8166 |
| 1.25 | X | 0.8768 | 0.7980 | 1.0768 | 0.0178 | 0.7368 | 0.6185 | 0.5869 | 0.5537 | 0.5611 |
| 1.25 | Y | 0.8055 | 0.8498 | 0.6997 | 0.0175 | 0.9727 | 0.6839 | 0.6477 | 0.4537 | 0.6969 |
| Fixed | X | 0.8751 | 0.8961 | 0.7134 | 0.0178 | 0.9181 | 0.6154 | 0.5985 | 0.4850 | 0.6282 |
| | Y | 0.9320 | 0.9517 | 0.7451 | 0.0168 | 0.9752 | 0.4682 | 0.4743 | 0.5048 | 0.5730 |

Earthquake Managua Nicaragua-02, 12/23/1972, Managua (RSN 96)

**Table D-21** Medium top and soft bottom soil profile with SSI-SSI reference model.

| Z/B | Dir. | J1 | J2 | J3 | J4 | J5 | J6 | J7 | J8 | J9 |
|---|---|---|---|---|---|---|---|---|---|---|
| 0 | X | 0.7557 | 0.7466 | 0.7690 | 0.0178 | 0.7147 | 0.6297 | 0.6186 | 0.4716 | 0.5440 |
| 0 | Y | 0.9011 | 0.9133 | 0.9326 | 0.0178 | 1.0381 | 0.7436 | 0.7248 | 0.7047 | 0.8301 |
| 0.1 | X | 0.7831 | 0.7624 | 0.7304 | 0.0178 | 0.9690 | 0.6546 | 0.6477 | 0.7234 | 0.6884 |
| 0.1 | Y | 0.8973 | 0.8772 | 0.6668 | 0.0178 | 0.8437 | 0.7002 | 0.6560 | 0.4816 | 0.6406 |
| 0.25 | X | 0.9224 | 0.9228 | 0.8890 | 0.0178 | 0.9063 | 0.7612 | 0.7305 | 0.7928 | 0.6937 |
| 0.25 | Y | 0.9277 | 0.9199 | 0.6924 | 0.0178 | 0.6462 | 0.6730 | 0.6512 | 0.4339 | 0.5667 |
| 0.5 | X | 0.7452 | 0.7964 | 0.8266 | 0.0178 | 0.9156 | 0.7076 | 0.7009 | 0.6203 | 0.6905 |
| 0.5 | Y | 0.8830 | 0.8866 | 0.6744 | 0.0178 | 0.8637 | 0.6919 | 0.6923 | 0.6745 | 0.7029 |
| 1 | X | 0.7237 | 0.6724 | 0.5569 | 0.0178 | 0.8823 | 0.6099 | 0.5971 | 0.4559 | 0.5266 |
| 1 | Y | 0.8344 | 0.8435 | 0.9601 | 0.0178 | 0.7535 | 0.6935 | 0.6948 | 0.7268 | 0.5496 |
| 1.25 | X | 0.6870 | 0.6470 | 0.6825 | 0.0178 | 0.9074 | 0.5899 | 0.5764 | 0.4661 | 0.5096 |
| 1.25 | Y | 0.8504 | 0.8605 | 1.0551 | 0.0178 | 0.7948 | 0.6680 | 0.6696 | 0.6946 | 0.5175 |
| Fixed | X | 0.9337 | 0.8849 | 0.8363 | 0.0178 | 0.9659 | 0.6182 | 0.6139 | 0.5678 | 0.6840 |
| | Y | 0.9383 | 0.9396 | 1.0992 | 0.0178 | 0.7980 | 0.7506 | 0.7394 | 0.6828 | 0.7742 |

**Table D-22** Medium top and soft bottom soil profile with Fixed-SSI reference model.

| Z/B | Dir. | J1 | J2 | J3 | J4 | J5 | J6 | J7 | J8 | J9 |
|---|---|---|---|---|---|---|---|---|---|---|
| 0 | X | 0.6179 | 0.6019 | 0.7127 | 0.0178 | 0.7271 | 0.5630 | 0.5514 | 0.4374 | 0.5108 |
| 0 | Y | 0.8690 | 0.8751 | 0.9029 | 0.0178 | 1.0445 | 0.7070 | 0.6943 | 0.6900 | 0.8322 |
| 0.1 | X | 0.7672 | 0.7144 | 0.7289 | 0.0178 | 0.9773 | 0.6144 | 0.6050 | 0.6703 | 0.6672 |
| 0.1 | Y | 0.8449 | 0.8110 | 0.6360 | 0.0178 | 0.8300 | 0.6691 | 0.6186 | 0.4734 | 0.6438 |
| 0.25 | X | 0.8015 | 0.7698 | 0.8882 | 0.0178 | 0.9096 | 0.6532 | 0.6273 | 0.7666 | 0.6747 |
| 0.25 | Y | 0.8548 | 0.8309 | 0.6264 | 0.0178 | 0.6105 | 0.6346 | 0.6054 | 0.3928 | 0.5353 |
| 0.5 | X | 0.6526 | 0.6663 | 0.8424 | 0.0178 | 0.9140 | 0.5552 | 0.5493 | 0.6064 | 0.6648 |
| 0.5 | Y | 0.8030 | 0.8059 | 0.6475 | 0.0178 | 0.8556 | 0.6680 | 0.6678 | 0.6609 | 0.6760 |
| 1 | X | 0.6180 | 0.5900 | 0.5556 | 0.0178 | 0.8857 | 0.4178 | 0.4088 | 0.4661 | 0.5129 |
| 1 | Y | 0.7595 | 0.7660 | 0.9753 | 0.0178 | 0.7564 | 0.5318 | 0.5340 | 0.6972 | 0.5086 |
| 1.25 | X | 0.5846 | 0.5745 | 0.6920 | 0.0178 | 0.9150 | 0.3935 | 0.3839 | 0.4571 | 0.4983 |
| 1.25 | Y | 0.7835 | 0.7882 | 1.0609 | 0.0178 | 0.8072 | 0.5124 | 0.5149 | 0.6625 | 0.4761 |
| Fixed | X | 0.9337 | 0.8849 | 0.8363 | 0.0178 | 0.9659 | 0.6182 | 0.6139 | 0.5678 | 0.6840 |
| | Y | 0.9383 | 0.9396 | 1.0992 | 0.0178 | 0.7980 | 0.7506 | 0.7394 | 0.6828 | 0.7742 |

Earthquake Corinth Greece, 2/24/1981, Corinth (RSN 313)

**Table D-23** Soft top and medium bottom soil profile with SSI-SSI reference model.

| Z/B | Dir. | J1 | J2 | J3 | J4 | J5 | J6 | J7 | J8 | J9 |
|---|---|---|---|---|---|---|---|---|---|---|
| 0 | X | 0.6317 | 0.5911 | 0.6445 | 0.0178 | 0.9742 | 0.5657 | 0.5542 | 0.4196 | 0.5100 |
| 0 | Y | 0.8974 | 0.9693 | 0.8842 | 0.0178 | 0.8705 | 0.6906 | 0.6921 | 0.7795 | 0.5718 |
| 0.1 | X | 0.7721 | 0.8113 | 0.7869 | 0.0178 | 0.8906 | 0.6596 | 0.6570 | 0.7425 | 0.6922 |
| 0.1 | Y | 0.8271 | 0.7915 | 0.5711 | 0.0178 | 0.6093 | 0.7158 | 0.7113 | 0.5028 | 0.6051 |
| 0.25 | X | 0.7936 | 0.7679 | 0.9010 | 0.0178 | 1.0217 | 0.7428 | 0.7297 | 0.7916 | 0.7704 |
| 0.25 | Y | 0.8930 | 0.8629 | 0.7086 | 0.0178 | 0.8502 | 0.7230 | 0.7267 | 0.7781 | 0.7951 |
| 0.5 | X | 0.6806 | 0.6298 | 0.6310 | 0.0178 | 0.7841 | 0.6375 | 0.6002 | 0.4644 | 0.5869 |
| 0.5 | Y | 0.9268 | 0.9313 | 0.7636 | 0.0178 | 0.9007 | 0.8351 | 0.8010 | 0.6606 | 0.8078 |
| 1 | X | 0.6032 | 0.5440 | 0.4841 | 0.0178 | 0.5638 | 0.6230 | 0.5836 | 0.3374 | 0.4806 |
| 1 | Y | 0.9140 | 0.9558 | 0.8553 | 0.0178 | 1.0343 | 0.8528 | 0.8552 | 0.8781 | 1.0081 |
| 1.25 | X | 0.5846 | 0.5463 | 0.4858 | 0.0178 | 0.5749 | 0.5767 | 0.5280 | 0.2958 | 0.4471 |
| 1.25 | Y | 0.9130 | 0.9548 | 0.8979 | 0.0178 | 1.0372 | 0.8013 | 0.7053 | 0.5126 | 0.7634 |
| Fixed | X | 0.9337 | 0.8849 | 0.8363 | 0.0178 | 0.9659 | 0.6182 | 0.6139 | 0.5678 | 0.6840 |
| | Y | 0.9383 | 0.9396 | 1.0992 | 0.0178 | 0.7980 | 0.7506 | 0.7394 | 0.6828 | 0.7742 |

**Table D-24** Soft top and medium bottom soil profile with SSI-SSI reference model.

| Z/B | Dir. | J1 | J2 | J3 | J4 | J5 | J6 | J7 | J8 | J9 |
|---|---|---|---|---|---|---|---|---|---|---|
| 0 | X | 0.5456 | 0.5331 | 0.5963 | 0.0178 | 0.9777 | 0.3788 | 0.3708 | 0.4045 | 0.4993 |
| 0 | Y | 0.8235 | 0.8884 | 0.8983 | 0.0178 | 0.8660 | 0.5609 | 0.5653 | 0.7612 | 0.5435 |
| 0.1 | X | 0.6804 | 0.7256 | 0.8347 | 0.0178 | 0.8889 | 0.5487 | 0.5465 | 0.7486 | 0.6684 |
| 0.1 | Y | 0.7486 | 0.7089 | 0.5538 | 0.0178 | 0.5709 | 0.6270 | 0.6211 | 0.4672 | 0.5695 |
| 0.25 | X | 0.7921 | 0.7471 | 0.9020 | 0.0178 | 1.0327 | 0.6993 | 0.6872 | 0.7638 | 0.7502 |
| 0.25 | Y | 0.8085 | 0.7828 | 0.6834 | 0.0178 | 0.8398 | 0.7164 | 0.7194 | 0.7571 | 0.7794 |
| 0.5 | X | 0.6664 | 0.5889 | 0.6720 | 0.0178 | 0.7909 | 0.5939 | 0.5579 | 0.4684 | 0.5665 |
| 0.5 | Y | 0.9029 | 0.9127 | 0.7304 | 0.0178 | 0.8849 | 0.8141 | 0.7696 | 0.6221 | 0.7926 |
| 1 | X | 0.5311 | 0.5042 | 0.5430 | 0.0178 | 0.5676 | 0.5172 | 0.4840 | 0.3290 | 0.4613 |
| 1 | Y | 0.9344 | 0.9772 | 0.8278 | 0.0178 | 1.0353 | 0.8260 | 0.8354 | 0.8589 | 0.9956 |
| 1.25 | X | 0.5454 | 0.4945 | 0.4797 | 0.0178 | 0.5803 | 0.5211 | 0.4765 | 0.2876 | 0.4272 |
| 1.25 | Y | 0.9510 | 0.9929 | 0.8756 | 0.0178 | 1.0380 | 0.7913 | 0.7051 | 0.5038 | 0.7606 |
| Fixed | X | 0.9337 | 0.8849 | 0.8363 | 0.0178 | 0.9659 | 0.6182 | 0.6139 | 0.5678 | 0.6840 |
| | Y | 0.9383 | 0.9396 | 1.0992 | 0.0178 | 0.7980 | 0.7506 | 0.7394 | 0.6828 | 0.7742 |

Earthquake Managua Nicaragua-02, 12/23/1972, Managua (RSN 96)

**Table D-25** Clay (linear) soil profile with SSI-SSI reference model.

| Ga | Dir. | J1 | J2 | J3 | J4 | J5 | J6 | J7 | J8 | J9 |
|---|---|---|---|---|---|---|---|---|---|---|
| 15 | X | 0.8666 | 0.8825 | 0.9546 | 0.0178 | 0.6703 | 0.7200 | 0.5840 | 0.4520 | 0.4777 |
| 15 | Y | 1.0080 | 0.9800 | 0.9513 | 0.0178 | 0.9690 | 0.8532 | 0.8511 | 0.6802 | 0.7868 |
| 25 | X | 0.8322 | 0.7880 | 0.9400 | 0.0178 | 0.7506 | 0.6661 | 0.6661 | 0.7766 | 0.6810 |
| 25 | Y | 0.8755 | 0.9702 | 0.7584 | 0.0167 | 1.0167 | 0.7955 | 0.7881 | 0.7056 | 0.9219 |
| 35 | X | 0.8372 | 0.8122 | 0.8412 | 0.0178 | 0.7137 | 0.7387 | 0.6809 | 0.5883 | 0.5995 |
| 35 | Y | 0.9061 | 0.9557 | 0.7543 | 0.0175 | 0.9071 | 0.6830 | 0.6870 | 0.6747 | 0.6765 |
| 50 | X | 0.7743 | 0.7205 | 0.5528 | 0.0178 | 0.6183 | 0.7017 | 0.5518 | 0.3775 | 0.4430 |
| 50 | Y | 0.8076 | 0.8304 | 0.6874 | 0.0178 | 0.7600 | 0.7177 | 0.7120 | 0.6169 | 0.6380 |
| 70 | X | 0.7544 | 0.6847 | 0.7119 | 0.0178 | 0.4922 | 0.6617 | 0.5692 | 0.4251 | 0.4671 |
| 70 | Y | 0.7631 | 0.8395 | 0.9597 | 0.0172 | 0.9727 | 0.5742 | 0.5833 | 0.7302 | 0.6026 |
| 100 | X | 0.7708 | 0.7796 | 0.8673 | 0.0178 | 0.6330 | 0.5562 | 0.5136 | 0.4394 | 0.4435 |
| 100 | Y | 0.8392 | 0.9073 | 1.0409 | 0.0175 | 0.8740 | 0.6832 | 0.7089 | 0.8822 | 0.8269 |
| Fixed | X | 0.8751 | 0.8961 | 0.7134 | 0.0178 | 0.9181 | 0.6154 | 0.5985 | 0.4850 | 0.6282 |
| | Y | 0.9320 | 0.9517 | 0.7451 | 0.0168 | 0.9752 | 0.4682 | 0.4743 | 0.5048 | 0.5730 |

**Table D-26** Clay (linear) soil profile with Fixed-SSI reference model.

| Ga | Dir. | J1 | J2 | J3 | J4 | J5 | J6 | J7 | J8 | J9 |
|---|---|---|---|---|---|---|---|---|---|---|
| 15 | X | 0.8109 | 0.7838 | 0.8823 | 0.0178 | 0.6247 | 0.6491 | 0.4960 | 0.4197 | 0.4570 |
| 15 | Y | 0.9517 | 0.9008 | 0.9446 | 0.0178 | 0.9656 | 0.6760 | 0.6519 | 0.6481 | 0.7685 |
| 25 | X | 0.8280 | 0.7420 | 0.9114 | 0.0178 | 0.7499 | 0.6349 | 0.6351 | 0.7761 | 0.6580 |
| 25 | Y | 0.8563 | 0.9293 | 0.7437 | 0.0176 | 1.0244 | 0.7381 | 0.7325 | 0.7008 | 0.9199 |
| 35 | X | 0.7715 | 0.7060 | 0.8482 | 0.0178 | 0.6804 | 0.6476 | 0.5972 | 0.5680 | 0.5707 |
| 35 | Y | 0.8257 | 0.8813 | 0.7245 | 0.0177 | 0.9163 | 0.5507 | 0.5518 | 0.6409 | 0.6601 |
| 50 | X | 0.6594 | 0.5973 | 0.5098 | 0.0178 | 0.5706 | 0.6064 | 0.4769 | 0.3402 | 0.4199 |
| 50 | Y | 0.6540 | 0.6329 | 0.6643 | 0.0178 | 0.7058 | 0.5459 | 0.5322 | 0.5600 | 0.5919 |
| 70 | X | 0.6356 | 0.6439 | 0.6678 | 0.0178 | 0.5017 | 0.5473 | 0.4742 | 0.4210 | 0.4469 |
| 70 | Y | 0.6466 | 0.6777 | 0.9720 | 0.0172 | 0.9662 | 0.4241 | 0.4311 | 0.7149 | 0.5946 |
| 100 | X | 0.6934 | 0.6558 | 0.8454 | 0.0178 | 0.6567 | 0.4289 | 0.3985 | 0.4023 | 0.4350 |
| 100 | Y | 0.6692 | 0.7593 | 1.0425 | 0.0173 | 0.8709 | 0.5733 | 0.5792 | 0.8348 | 0.7862 |
| Fixed | X | 0.8751 | 0.8961 | 0.7134 | 0.0178 | 0.9181 | 0.6154 | 0.5985 | 0.4850 | 0.6282 |
| | Y | 0.9320 | 0.9517 | 0.7451 | 0.0168 | 0.9752 | 0.4682 | 0.4743 | 0.5048 | 0.5730 |

Earthquake Managua Nicaragua-02, 12/23/1972, Managua (RSN 96)

**Table D-27** Sand (parabola) soil profile with SSI-SSI reference model.

| Ga | Dir. | J1 | J2 | J3 | J4 | J5 | J6 | J7 | J8 | J9 |
|---|---|---|---|---|---|---|---|---|---|---|
| 15 | X | 0.8274 | 0.8255 | 0.8576 | 0.0178 | 0.5940 | 0.6782 | 0.6306 | 0.4417 | 0.5689 |
| 15 | Y | 0.9083 | 0.8878 | 0.8211 | 0.0174 | 0.7256 | 0.7570 | 0.7598 | 0.9496 | 0.8121 |
| 25 | X | 0.8359 | 0.8217 | 0.9799 | 0.0178 | 0.6025 | 0.6851 | 0.6275 | 0.5568 | 0.5822 |
| 25 | Y | 0.8403 | 0.8634 | 0.7372 | 0.0174 | 0.6516 | 0.7304 | 0.7289 | 0.5850 | 0.7671 |
| 35 | X | 0.7851 | 0.7293 | 0.6220 | 0.0178 | 0.5641 | 0.6888 | 0.5722 | 0.4532 | 0.4713 |
| 35 | Y | 0.8788 | 0.9175 | 1.0509 | 0.0178 | 0.6409 | 0.7402 | 0.7493 | 0.8046 | 0.7587 |
| 50 | X | 0.7583 | 0.6914 | 0.7556 | 0.0178 | 0.5520 | 0.6717 | 0.5593 | 0.4430 | 0.4583 |
| 50 | Y | 0.7548 | 0.7915 | 0.8027 | 0.0171 | 0.4748 | 0.6044 | 0.6108 | 0.6859 | 0.6044 |
| 70 | X | 0.7582 | 0.7503 | 0.9313 | 0.0178 | 0.4680 | 0.5735 | 0.5241 | 0.4984 | 0.4386 |
| 70 | Y | 0.8460 | 0.9767 | 1.1369 | 0.0173 | 0.5940 | 0.6698 | 0.7006 | 0.9591 | 0.8941 |
| 100 | X | 0.8444 | 0.8409 | 0.7702 | 0.0178 | 0.4430 | 0.5366 | 0.5061 | 0.3590 | 0.4687 |
| 100 | Y | 0.8609 | 0.9296 | 1.0000 | 0.0178 | 0.6262 | 0.6781 | 0.6289 | 0.6075 | 0.6376 |
| Fixed | X | 0.8751 | 0.8961 | 0.7134 | 0.0178 | 0.9181 | 0.6154 | 0.5985 | 0.4850 | 0.6282 |
| | Y | 0.9320 | 0.9517 | 0.7451 | 0.0168 | 0.9752 | 0.4682 | 0.4743 | 0.5048 | 0.5730 |

**Table D-28** Sand (parabola) soil profile with Fixed-SSI reference model.

| Ga | Dir. | J1 | J2 | J3 | J4 | J5 | J6 | J7 | J8 | J9 |
|---|---|---|---|---|---|---|---|---|---|---|
| 15 | X | 0.8526 | 0.7939 | 0.8423 | 0.0178 | 0.7122 | 0.6746 | 0.6185 | 0.4053 | 0.5478 |
| 15 | Y | 0.8683 | 0.8443 | 0.8203 | 0.0167 | 0.9153 | 0.6506 | 0.6436 | 0.8615 | 0.8012 |
| 25 | X | 0.8054 | 0.7523 | 0.9702 | 0.0178 | 0.7101 | 0.6413 | 0.5880 | 0.5382 | 0.5637 |
| 25 | Y | 0.7764 | 0.8152 | 0.6922 | 0.0175 | 0.8312 | 0.6058 | 0.6032 | 0.5618 | 0.7451 |
| 35 | X | 0.6780 | 0.6263 | 0.5710 | 0.0178 | 0.5934 | 0.6023 | 0.5000 | 0.3946 | 0.4390 |
| 35 | Y | 0.8193 | 0.8769 | 1.0382 | 0.0178 | 0.8263 | 0.5931 | 0.5953 | 0.7491 | 0.7201 |
| 50 | X | 0.6339 | 0.6112 | 0.7114 | 0.0178 | 0.4866 | 0.5596 | 0.4678 | 0.3964 | 0.4370 |
| 50 | Y | 0.6443 | 0.6754 | 0.8100 | 0.0174 | 1.0127 | 0.4375 | 0.4404 | 0.6441 | 0.5693 |
| 70 | X | 0.6767 | 0.6292 | 0.8719 | 0.0178 | 0.6375 | 0.4502 | 0.4134 | 0.4766 | 0.4297 |
| 70 | Y | 0.6915 | 0.7585 | 1.1723 | 0.0174 | 0.9124 | 0.5589 | 0.5821 | 0.9568 | 0.8895 |
| 100 | X | 0.7618 | 0.7175 | 0.6810 | 0.0178 | 0.7906 | 0.4069 | 0.3848 | 0.3452 | 0.4552 |
| 100 | Y | 0.7767 | 0.7616 | 0.9757 | 0.0175 | 0.8478 | 0.5916 | 0.5183 | 0.5731 | 0.6111 |
| Fixed | X | 0.8751 | 0.8961 | 0.7134 | 0.0178 | 0.9181 | 0.6154 | 0.5985 | 0.4850 | 0.6282 |
| | Y | 0.9320 | 0.9517 | 0.7451 | 0.0168 | 0.9752 | 0.4682 | 0.4743 | 0.5048 | 0.5730 |

Earthquake Corinth Greece, 2/24/1981, Corinth (RSN 313)

**Table D-29** Clay (linear) soil profile with SSI-SSI reference model.

| Ga | Dir. | J1 | J2 | J3 | J4 | J5 | J6 | J7 | J8 | J9 |
|---|---|---|---|---|---|---|---|---|---|---|
| 15 | X | 0.7727 | 0.7690 | 0.6505 | 0.0178 | 0.6498 | 0.5456 | 0.4254 | 0.2951 | 0.3796 |
| 15 | Y | 0.8650 | 0.8678 | 0.9359 | 0.0178 | 0.9894 | 0.8074 | 0.7952 | 0.8475 | 0.8855 |
| 25 | X | 0.8140 | 0.8378 | 0.8456 | 0.0178 | 0.8388 | 0.6678 | 0.6708 | 0.7637 | 0.6944 |
| 25 | Y | 0.8840 | 0.8728 | 0.7289 | 0.0178 | 0.9938 | 0.7927 | 0.7680 | 0.6577 | 0.8240 |
| 35 | X | 0.6199 | 0.5456 | 0.5688 | 0.0178 | 0.6670 | 0.5620 | 0.5115 | 0.3813 | 0.5263 |
| 35 | Y | 0.9374 | 0.9540 | 0.8101 | 0.0178 | 0.9436 | 0.8095 | 0.7432 | 0.5535 | 0.7289 |
| 50 | X | 0.8594 | 0.8035 | 0.9029 | 0.0178 | 1.0176 | 0.7864 | 0.7560 | 0.7119 | 0.7202 |
| 50 | Y | 0.9107 | 0.9017 | 0.7258 | 0.0178 | 0.8394 | 0.7721 | 0.7482 | 0.6183 | 0.7343 |
| 70 | X | 0.7758 | 0.8091 | 0.7846 | 0.0178 | 0.9170 | 0.7182 | 0.7132 | 0.6102 | 0.6871 |
| 70 | Y | 0.8685 | 0.8786 | 0.6283 | 0.0178 | 0.6764 | 0.7517 | 0.7510 | 0.5746 | 0.6035 |
| 100 | X | 0.6521 | 0.6059 | 0.5588 | 0.0178 | 0.9544 | 0.5801 | 0.5646 | 0.4348 | 0.5143 |
| 100 | Y | 0.8424 | 0.8214 | 0.9498 | 0.0178 | 0.9442 | 0.7011 | 0.7016 | 0.6531 | 0.5721 |
| Fixed | X | 0.9337 | 0.8849 | 0.8363 | 0.0178 | 0.9659 | 0.6182 | 0.6139 | 0.5678 | 0.6840 |
| | Y | 0.9383 | 0.9396 | 1.0992 | 0.0178 | 0.7980 | 0.7506 | 0.7394 | 0.6828 | 0.7742 |

**Table D-30** Clay (linear) soil profile with Fixed-SSI reference model.

| Ga | Dir. | J1 | J2 | J3 | J4 | J5 | J6 | J7 | J8 | J9 |
|---|---|---|---|---|---|---|---|---|---|---|
| 15 | X | 0.5992 | 0.5499 | 0.5745 | 0.0178 | 0.6485 | 0.5044 | 0.3505 | 0.2588 | 0.3715 |
| 15 | Y | 0.9018 | 0.9608 | 0.9794 | 0.0178 | 0.9868 | 0.8034 | 0.7927 | 0.8282 | 0.8799 |
| 25 | X | 0.7031 | 0.7140 | 0.8139 | 0.0178 | 0.7811 | 0.6189 | 0.6198 | 0.7084 | 0.6528 |
| 25 | Y | 0.8739 | 0.8736 | 0.6599 | 0.0178 | 1.0036 | 0.7333 | 0.7101 | 0.6443 | 0.8233 |
| 35 | X | 0.6108 | 0.5253 | 0.6343 | 0.0178 | 0.6717 | 0.5729 | 0.5205 | 0.3820 | 0.5099 |
| 35 | Y | 0.9037 | 0.9130 | 0.7809 | 0.0178 | 0.9304 | 0.7935 | 0.7178 | 0.5254 | 0.7140 |
| 50 | X | 0.7824 | 0.7410 | 0.9809 | 0.0178 | 1.0272 | 0.6842 | 0.6574 | 0.6956 | 0.6997 |
| 50 | Y | 0.8452 | 0.8305 | 0.7141 | 0.0178 | 0.8119 | 0.7541 | 0.7313 | 0.5939 | 0.7079 |
| 70 | X | 0.6578 | 0.6818 | 0.7749 | 0.0178 | 0.9147 | 0.5540 | 0.5493 | 0.5901 | 0.6633 |
| 70 | Y | 0.7988 | 0.8061 | 0.6007 | 0.0178 | 0.6480 | 0.5981 | 0.5986 | 0.5582 | 0.5577 |
| 100 | X | 0.5672 | 0.5556 | 0.5434 | 0.0178 | 0.9638 | 0.4047 | 0.3935 | 0.4117 | 0.5036 |
| 100 | Y | 0.7529 | 0.7609 | 0.9428 | 0.0178 | 0.9464 | 0.5658 | 0.5677 | 0.6397 | 0.5474 |
| Fixed | X | 0.9337 | 0.8849 | 0.8363 | 0.0178 | 0.9659 | 0.6182 | 0.6139 | 0.5678 | 0.6840 |
| | Y | 0.9383 | 0.9396 | 1.0992 | 0.0178 | 0.7980 | 0.7506 | 0.7394 | 0.6828 | 0.7742 |

Earthquake Corinth Greece, 2/24/1981, Corinth (RSN 313)

**Table D-31** Sand (parabola) soil profile with SSI-SSI reference model.

| Ga | Dir. | J1 | J2 | J3 | J4 | J5 | J6 | J7 | J8 | J9 |
|---|---|---|---|---|---|---|---|---|---|---|
| 15 | X | 0.8594 | 0.8270 | 0.6914 | 0.0178 | 0.8964 | 0.8203 | 0.8166 | 0.6605 | 0.9033 |
| 15 | Y | 0.8610 | 0.8716 | 0.9426 | 0.0178 | 0.9918 | 0.7823 | 0.7616 | 0.7806 | 0.8360 |
| 25 | X | 0.5981 | 0.5284 | 0.4477 | 0.0178 | 0.6007 | 0.5722 | 0.5258 | 0.3533 | 0.5021 |
| 25 | Y | 1.0069 | 1.0310 | 0.9000 | 0.0178 | 1.0174 | 0.7339 | 0.7552 | 0.9431 | 0.8712 |
| 35 | X | 0.8244 | 0.7678 | 0.8189 | 0.0178 | 1.0217 | 0.7763 | 0.7630 | 0.7613 | 0.7728 |
| 35 | Y | 0.9023 | 0.8783 | 0.6734 | 0.0178 | 0.7684 | 0.6268 | 0.6263 | 0.6117 | 0.6687 |
| 50 | X | 0.7763 | 0.7673 | 0.7879 | 0.0178 | 0.8880 | 0.6541 | 0.6518 | 0.7448 | 0.6909 |
| 50 | Y | 0.8745 | 0.8730 | 0.5841 | 0.0178 | 0.6174 | 0.7044 | 0.7009 | 0.5179 | 0.6116 |
| 70 | X | 0.7177 | 0.6564 | 0.6244 | 0.0178 | 0.8414 | 0.6216 | 0.6032 | 0.4534 | 0.5308 |
| 70 | Y | 0.8480 | 0.8700 | 0.8833 | 0.0178 | 0.8622 | 0.6700 | 0.6720 | 0.6968 | 0.5186 |
| 100 | X | 0.6655 | 0.6393 | 0.7524 | 0.0178 | 0.9525 | 0.5715 | 0.5641 | 0.4614 | 0.5104 |
| 100 | Y | 0.9118 | 0.9497 | 0.8668 | 0.0178 | 0.8948 | 0.7892 | 0.7833 | 0.7009 | 0.6962 |
| Fixed | X | 0.9337 | 0.8849 | 0.8363 | 0.0178 | 0.9659 | 0.6182 | 0.6139 | 0.5678 | 0.6840 |
| | Y | 0.9383 | 0.9396 | 1.0992 | 0.0178 | 0.7980 | 0.7506 | 0.7394 | 0.6828 | 0.7742 |

**Table D-32** Sand (parabola) soil profile with Fixed-SSI reference model.

| Ga | Dir. | J1 | J2 | J3 | J4 | J5 | J6 | J7 | J8 | J9 |
|---|---|---|---|---|---|---|---|---|---|---|
| 15 | X | 0.8049 | 0.8576 | 0.7419 | 0.0178 | 0.9208 | 0.7258 | 0.7265 | 0.7029 | 0.9114 |
| 15 | Y | 0.8820 | 0.9176 | 1.0147 | 0.0178 | 0.9913 | 0.7717 | 0.7569 | 0.8171 | 0.8248 |
| 25 | X | 0.5575 | 0.4662 | 0.5169 | 0.0178 | 0.6047 | 0.5502 | 0.5038 | 0.3504 | 0.4831 |
| 25 | Y | 0.9631 | 0.9898 | 0.8760 | 0.0178 | 1.0168 | 0.7048 | 0.7260 | 0.9076 | 0.8525 |
| 35 | X | 0.7824 | 0.7053 | 0.8368 | 0.0178 | 1.0319 | 0.6952 | 0.6844 | 0.7386 | 0.7513 |
| 35 | Y | 0.8056 | 0.8225 | 0.6435 | 0.0178 | 0.7660 | 0.6345 | 0.6292 | 0.5960 | 0.6599 |
| 50 | X | 0.6872 | 0.7259 | 0.8320 | 0.0178 | 0.8867 | 0.5491 | 0.5470 | 0.7583 | 0.6682 |
| 50 | Y | 0.7789 | 0.7360 | 0.5690 | 0.0178 | 0.5894 | 0.6245 | 0.6199 | 0.4919 | 0.5764 |
| 70 | X | 0.6109 | 0.5701 | 0.6185 | 0.0178 | 0.8483 | 0.4306 | 0.4172 | 0.4619 | 0.5169 |
| 70 | Y | 0.7630 | 0.7534 | 0.8963 | 0.0178 | 0.8754 | 0.5106 | 0.5130 | 0.6648 | 0.4799 |
| 100 | X | 0.5503 | 0.5279 | 0.7185 | 0.0178 | 0.9437 | 0.3516 | 0.3470 | 0.4561 | 0.4979 |
| 100 | Y | 0.7962 | 0.8077 | 0.8684 | 0.0178 | 0.8908 | 0.6572 | 0.6534 | 0.6467 | 0.6614 |
| Fixed | X | 0.9337 | 0.8849 | 0.8363 | 0.0178 | 0.9659 | 0.6182 | 0.6139 | 0.5678 | 0.6840 |
| | Y | 0.9383 | 0.9396 | 1.0992 | 0.0178 | 0.7980 | 0.7506 | 0.7394 | 0.6828 | 0.7742 |

# APPENDIX E

## NORMALIZATION OF SSI RESULTS WITH RESPECT TO FIXED SUPPORT RESULTS OF UNCONTROLLED SYSTEMS

Frame Building

Earthquake Managua Nicaragua-02, 12/23/1972, Managua (RSN 96)

**Table E-1** Clay (linear) soil profile.

| Ga | Direction | Max.Dis. Ratio | Max.Drift Ratio | Max. Acc. Ratio | Max. Base Shear Ratio |
|---|---|---|---|---|---|
| 15 | X | 0.7501 | 1.2803 | 2.2542 | 1.0700 |
| 15 | Y | 1.0459 | 1.1467 | 1.3741 | 1.0682 |
| 25 | X | 0.8592 | 1.1911 | 2.2525 | 1.0686 |
| 25 | Y | 1.1154 | 1.1691 | 1.3739 | 0.9405 |
| 35 | X | 0.9201 | 1.1274 | 2.2162 | 1.0527 |
| 35 | Y | 1.0929 | 1.1321 | 1.0764 | 0.9920 |
| 50 | X | 1.0038 | 1.1211 | 2.2930 | 1.0405 |
| 50 | Y | 1.0883 | 1.0804 | 1.1876 | 1.0056 |
| 70 | X | 1.0119 | 1.0908 | 2.3569 | 1.0163 |
| 70 | Y | 1.0743 | 1.0502 | 1.1415 | 1.0130 |
| 100 | X | 1.0068 | 1.0403 | 1.4468 | 1.0081 |
| 100 | Y | 1.0556 | 1.0386 | 1.1033 | 1.0071 |

**Table E-2** Medium top and soft bottom soil profile.

| Z/B | Direction | Max.Dis. Ratio | Max.Drift Ratio | Max. Acc. Ratio | Max. Base Shear Ratio |
|---|---|---|---|---|---|
| 0 | X | 0.8553 | 1.2141 | 2.8940 | 1.0656 |
| 0 | Y | 1.1137 | 1.1687 | 1.5937 | 0.9452 |
| 0.1 | X | 0.9655 | 1.1279 | 2.2178 | 1.0459 |
| 0.1 | Y | 1.1038 | 1.0862 | 1.3301 | 0.9898 |
| 0.25 | X | 0.9983 | 1.1418 | 2.2814 | 1.0341 |
| 0.25 | Y | 1.0846 | 1.0646 | 1.0460 | 0.9995 |
| 0.5 | X | 1.0143 | 1.0908 | 2.4307 | 1.0162 |
| 0.5 | Y | 1.0784 | 1.0463 | 1.1480 | 1.0088 |
| 1 | X | 1.0082 | 1.0622 | 1.7390 | 1.0072 |
| 1 | Y | 1.0626 | 1.0406 | 1.0258 | 1.0088 |
| 1.25 | X | 1.0057 | 1.0525 | 1.4858 | 1.0071 |
| 1.25 | Y | 1.0629 | 1.0394 | 1.1582 | 1.0068 |

Earthquake Managua Nicaragua-02, 12/23/1972, Managua (RSN 96)

**Table E-3** Sand (parabola) soil profile.

| Ga | Direction | Max.Dis. Ratio | Max.Drift Ratio | Max. Acc. Ratio | Max. Base Shear Ratio |
|---|---|---|---|---|---|
| 15 | X | 0.8566 | 1.3493 | 2.8372 | 1.0747 |
| 15 | Y | 1.0503 | 1.1286 | 1.1745 | 0.9984 |
| 25 | X | 0.9267 | 1.0978 | 2.6995 | 1.0565 |
| 25 | Y | 1.1043 | 1.1392 | 1.1713 | 0.9777 |
| 35 | X | 1.0031 | 1.0832 | 2.5392 | 1.0450 |
| 35 | Y | 1.0931 | 1.0873 | 1.3621 | 1.0027 |
| 50 | X | 1.0004 | 1.1138 | 2.3019 | 1.0232 |
| 50 | Y | 1.0789 | 1.0571 | 1.2411 | 1.0130 |
| 70 | X | 1.0073 | 1.0502 | 1.8609 | 1.0069 |
| 70 | Y | 1.0605 | 1.0395 | 1.0909 | 1.0094 |
| 100 | X | 1.0042 | 1.0350 | 1.3570 | 1.0119 |
| 100 | Y | 1.0457 | 1.0276 | 1.0819 | 1.0028 |

**Table E-4** Soft top and medium bottom soil profile.

| Z/B | Direction | Max.Dis. Ratio | Max.Drift Ratio | Max. Acc. Ratio | Max. Base Shear Ratio |
|---|---|---|---|---|---|
| 0 | X | 1.0022 | 1.0386 | 1.3071 | 1.0100 |
| 0 | Y | 1.0557 | 1.0370 | 1.1194 | 1.0025 |
| 0.1 | X | 1.0026 | 1.1177 | 2.3730 | 1.0247 |
| 0.1 | Y | 1.0783 | 1.0593 | 1.2494 | 1.0131 |
| 0.25 | X | 1.0061 | 1.0887 | 2.3727 | 1.0435 |
| 0.25 | Y | 1.0931 | 1.0847 | 1.3034 | 1.0039 |
| 0.5 | X | 0.9273 | 1.1281 | 2.1421 | 1.0503 |
| 0.5 | Y | 1.0907 | 1.1222 | 1.0973 | 0.9944 |
| 1 | X | 0.8802 | 1.0716 | 3.3678 | 1.0567 |
| 1 | Y | 1.1068 | 1.1215 | 1.2800 | 0.9655 |
| 1.25 | X | 0.8382 | 1.1002 | 3.2390 | 1.0590 |
| 1.25 | Y | 1.1072 | 1.1313 | 1.2943 | 0.9578 |

Earthquake Corinth Greece, 2/24/1981, Corinth (RSN 313)

**Table E-5** Clay (linear) soil profile.

| Ga | Direction | Max.Dis. Ratio | Max.Drift Ratio | Max. Acc. Ratio | Max. Base Shear Ratio |
|---|---|---|---|---|---|
| 15 | X | 1.5466 | 1.5673 | 2.2080 | 1.1149 |
| 15 | Y | 0.8595 | 0.9063 | 1.4285 | 1.5332 |
| 25 | X | 1.8659 | 1.8107 | 1.5801 | 1.0360 |
| 25 | Y | 1.0548 | 1.0744 | 1.2658 | 1.5256 |
| 35 | X | 1.5478 | 1.3404 | 2.0902 | 1.0842 |
| 35 | Y | 1.0512 | 1.0730 | 1.0772 | 1.2995 |
| 50 | X | 1.1238 | 1.1802 | 1.4663 | 1.0254 |
| 50 | Y | 0.9948 | 1.1066 | 1.1124 | 1.1491 |
| 70 | X | 1.0914 | 1.0885 | 1.1275 | 1.0091 |
| 70 | Y | 1.0073 | 1.0848 | 1.0393 | 1.0996 |
| 100 | X | 0.9875 | 0.9944 | 1.0492 | 0.9972 |
| 100 | Y | 1.0126 | 1.0571 | 1.0190 | 1.0371 |

**Table E-6** Medium top and soft bottom soil profile.

| Z/B | Direction | Max.Dis. Ratio | Max.Drift Ratio | Max. Acc. Ratio | Max. Base Shear Ratio |
|---|---|---|---|---|---|
| 0 | X | 1.8173 | 1.6475 | 1.8381 | 1.0317 |
| 0 | Y | 1.0449 | 1.0507 | 1.1832 | 1.5199 |
| 0.1 | X | 1.4282 | 1.3371 | 2.0510 | 1.0670 |
| 0.1 | Y | 1.0153 | 1.0634 | 1.0817 | 1.2455 |
| 0.25 | X | 1.1056 | 1.1735 | 1.3566 | 1.0161 |
| 0.25 | Y | 0.9517 | 1.0651 | 1.0322 | 1.1798 |
| 0.5 | X | 1.0774 | 1.0702 | 1.1511 | 1.0105 |
| 0.5 | Y | 0.9858 | 1.0605 | 1.1180 | 1.1218 |
| 1 | X | 0.9970 | 1.0071 | 1.0972 | 1.0057 |
| 1 | Y | 1.0051 | 1.0596 | 1.0983 | 1.0740 |
| 1.25 | X | 0.9904 | 1.0085 | 1.0131 | 1.0033 |
| 1.25 | Y | 1.0065 | 1.0578 | 1.0461 | 1.0619 |

Earthquake Corinth Greece, 2/24/1981, Corinth (RSN 313)

**Table E-7** Sand (parabola) soil profile.

| Ga | Direction | Max.Dis. Ratio | Max.Drift Ratio | Max. Acc. Ratio | Max. Base Shear Ratio |
|---|---|---|---|---|---|
| 15 | X | 1.8405 | 1.7243 | 2.1924 | 1.0693 |
| 15 | Y | 1.0408 | 0.9992 | 1.5164 | 1.6408 |
| 25 | X | 1.6045 | 1.4587 | 1.8997 | 1.0842 |
| 25 | Y | 1.0509 | 1.0554 | 1.1301 | 1.3961 |
| 35 | X | 1.2152 | 1.1971 | 1.5275 | 1.0367 |
| 35 | Y | 1.0030 | 1.1009 | 1.0272 | 1.1642 |
| 50 | X | 1.1061 | 1.0961 | 1.2878 | 1.0119 |
| 50 | Y | 1.0077 | 1.0872 | 1.1480 | 1.1056 |
| 70 | X | 1.0043 | 1.0034 | 1.1099 | 1.0036 |
| 70 | Y | 1.0106 | 1.0619 | 1.0497 | 1.0577 |
| 100 | X | 0.9823 | 0.9918 | 1.0386 | 0.9916 |
| 100 | Y | 1.0117 | 1.0456 | 1.0482 | 1.0074 |

**Table E-8** Soft top and medium bottom soil profile.

| Z/B | Direction | Max.Dis. Ratio | Max.Drift Ratio | Max. Acc. Ratio | Max. Base Shear Ratio |
|---|---|---|---|---|---|
| 0 | X | 0.9876 | 0.9976 | 1.0408 | 0.9957 |
| 0 | Y | 1.0095 | 1.0518 | 1.0708 | 1.0349 |
| 0.1 | X | 1.1056 | 1.0892 | 1.3004 | 1.0128 |
| 0.1 | Y | 1.0086 | 1.0918 | 1.1370 | 1.1060 |
| 0.25 | X | 1.1843 | 1.1857 | 1.5243 | 1.0404 |
| 0.25 | Y | 0.9950 | 1.1069 | 1.1379 | 1.1560 |
| 0.5 | X | 1.5170 | 1.3499 | 2.0867 | 1.0728 |
| 0.5 | Y | 1.0261 | 1.0806 | 1.0624 | 1.2724 |
| 1 | X | 1.7185 | 1.5343 | 1.9489 | 1.0909 |
| 1 | Y | 1.0481 | 1.0223 | 1.1202 | 1.4354 |
| 1.25 | X | 1.7565 | 1.6037 | 1.8134 | 1.0699 |
| 1.25 | Y | 1.0561 | 1.0615 | 1.3912 | 1.5011 |

Frame Shear Wall Building

Earthquake Managua Nicaragua-02, 12/23/1972, Managua (RSN 96)

**Table E-9** Clay (linear) soil profile.

| Ga | Direction | Max.Dis. Ratio | Max.Drift Ratio | Max. Acc. Ratio | Max. Base Shear Ratio |
|---|---|---|---|---|---|
| 15 | X | 1.4916 | 1.7877 | 2.0718 | 2.2960 |
| 15 | Y | 1.0610 | 1.1138 | 0.9711 | 1.5572 |
| 25 | X | 1.3081 | 1.5085 | 1.5994 | 1.6872 |
| 25 | Y | 1.3017 | 0.9942 | 0.8132 | 0.8926 |
| 35 | X | 1.5138 | 1.6988 | 1.8585 | 1.8196 |
| 35 | Y | 1.6142 | 1.2071 | 1.0703 | 1.1331 |
| 50 | X | 1.6140 | 1.8680 | 2.2068 | 1.8875 |
| 50 | Y | 2.2557 | 2.0127 | 1.9627 | 1.7280 |
| 70 | X | 1.4232 | 1.5219 | 1.4915 | 1.6898 |
| 70 | Y | 1.4256 | 1.1086 | 1.5124 | 1.2822 |
| 100 | X | 1.2044 | 1.2766 | 1.2028 | 1.4543 |
| 100 | Y | 1.2182 | 1.0835 | 1.5869 | 1.4302 |

**Table E-10** Medium top and soft bottom soil profile.

| Z/B | Direction | Max.Dis. Ratio | Max.Drift Ratio | Max. Acc. Ratio | Max. Base Shear Ratio |
|---|---|---|---|---|---|
| 0 | X | 1.2901 | 1.5017 | 1.6011 | 1.8148 |
| 0 | Y | 1.3764 | 1.1137 | 0.8425 | 0.9334 |
| 0.1 | X | 1.5964 | 1.9231 | 1.9454 | 1.9223 |
| 0.1 | Y | 1.8675 | 1.6187 | 1.9871 | 1.5108 |
| 0.25 | X | 1.5641 | 1.7440 | 2.2435 | 1.8125 |
| 0.25 | Y | 2.0292 | 1.7905 | 1.6490 | 1.4848 |
| 0.5 | X | 1.3891 | 1.4942 | 1.3779 | 1.6502 |
| 0.5 | Y | 1.6006 | 1.2139 | 1.3538 | 1.3123 |
| 1 | X | 1.2393 | 1.3668 | 1.2994 | 1.4455 |
| 1 | Y | 1.3111 | 1.0413 | 1.5625 | 1.3940 |
| 1.25 | X | 1.2141 | 1.3251 | 1.1345 | 1.4409 |
| 1.25 | Y | 1.2905 | 1.1014 | 1.5615 | 1.4343 |

Earthquake Managua Nicaragua-02, 12/23/1972, Managua (RSN 96)

**Table E-11** Sand (parabola) soil profile.

| Ga | Direction | Max.Dis. Ratio | Max.Drift Ratio | Max. Acc. Ratio | Max. Base Shear Ratio |
|---|---|---|---|---|---|
| 15 | X | 1.3927 | 1.6032 | 1.8994 | 1.6546 |
| 15 | Y | 0.9851 | 0.9606 | 0.7116 | 1.0090 |
| 25 | X | 1.4513 | 1.6041 | 1.5149 | 1.8109 |
| 25 | Y | 1.6902 | 1.3350 | 1.1237 | 1.2444 |
| 35 | X | 1.6348 | 1.9486 | 2.0095 | 1.9147 |
| 35 | Y | 1.9967 | 1.6855 | 1.3333 | 1.5750 |
| 50 | X | 1.4706 | 1.5859 | 1.6697 | 1.7425 |
| 50 | Y | 1.6074 | 1.2978 | 1.6273 | 1.2524 |
| 70 | X | 1.2369 | 1.3381 | 1.3656 | 1.4305 |
| 70 | Y | 1.3052 | 1.0528 | 1.4079 | 1.4239 |
| 100 | X | 1.0975 | 1.1509 | 1.0062 | 1.2469 |
| 100 | Y | 1.2047 | 1.2065 | 1.4850 | 1.5440 |

**Table E-12** Soft top and medium bottom soil profile.

| Z/B | Direction | Max.Dis. Ratio | Max.Drift Ratio | Max. Acc. Ratio | Max. Base Shear Ratio |
|---|---|---|---|---|---|
| 0 | X | 1.1665 | 1.2347 | 1.0212 | 1.4383 |
| 0 | Y | 1.2322 | 1.1366 | 1.5570 | 1.4008 |
| 0.1 | X | 1.4684 | 1.5878 | 1.6669 | 1.7317 |
| 0.1 | Y | 1.6588 | 1.3655 | 1.7280 | 1.2520 |
| 0.25 | X | 1.6370 | 1.9321 | 2.0407 | 1.9124 |
| 0.25 | Y | 2.1098 | 1.8462 | 1.5135 | 1.5787 |
| 0.5 | X | 1.5431 | 1.7857 | 2.1804 | 1.8418 |
| 0.5 | Y | 1.5437 | 1.1908 | 1.3418 | 1.1360 |
| 1 | X | 1.3662 | 1.5322 | 1.5697 | 1.7865 |
| 1 | Y | 1.6020 | 1.2276 | 1.0842 | 1.2194 |
| 1.25 | X | 1.3160 | 1.4522 | 1.6149 | 1.7693 |
| 1.25 | Y | 1.5508 | 1.2202 | 1.0653 | 1.1549 |

Earthquake Corinth Greece, 2/24/1981, Corinth (RSN 313)

**Table E-13** Clay (linear) soil profile.

| Ga | Direction | Max.Dis. Ratio | Max.Drift Ratio | Max. Acc. Ratio | Max. Base Shear Ratio |
|---|---|---|---|---|---|
| 15 | X | 1.0146 | 1.2980 | 2.6785 | 1.1735 |
| 15 | Y | 0.7520 | 0.6815 | 0.5488 | 0.9580 |
| 25 | X | 1.4379 | 1.4079 | 1.6149 | 0.9139 |
| 25 | Y | 0.9266 | 0.8784 | 0.9929 | 0.9729 |
| 35 | X | 1.4444 | 1.6318 | 2.1920 | 1.1601 |
| 35 | Y | 1.3034 | 1.3176 | 1.8055 | 1.5984 |
| 50 | X | 1.2096 | 1.2260 | 1.5791 | 0.8373 |
| 50 | Y | 1.8987 | 1.8919 | 2.2647 | 1.8595 |
| 70 | X | 1.2169 | 1.2804 | 1.9160 | 0.9739 |
| 70 | Y | 1.8716 | 1.7076 | 1.6993 | 1.5072 |
| 100 | X | 1.2653 | 1.3764 | 1.8736 | 0.9614 |
| 100 | Y | 1.6463 | 1.4732 | 1.2962 | 1.1525 |

**Table E-14** Medium top and soft bottom soil profile.

| Z/B | Direction | Max.Dis. Ratio | Max.Drift Ratio | Max. Acc. Ratio | Max. Base Shear Ratio |
|---|---|---|---|---|---|
| 0 | X | 1.5280 | 1.5612 | 1.6193 | 1.0177 |
| 0 | Y | 0.8741 | 0.8149 | 0.8403 | 1.0090 |
| 0.1 | X | 1.2119 | 1.2558 | 1.9042 | 0.8205 |
| 0.1 | Y | 1.3861 | 1.4649 | 2.2172 | 1.5346 |
| 0.25 | X | 1.1407 | 1.1329 | 1.8323 | 0.9556 |
| 0.25 | Y | 1.5266 | 1.6217 | 2.4511 | 1.8404 |
| 0.5 | X | 1.2216 | 1.2950 | 1.8101 | 0.9880 |
| 0.5 | Y | 1.7558 | 1.6515 | 1.7121 | 1.3195 |
| 1 | X | 1.2060 | 1.3760 | 1.7450 | 0.9989 |
| 1 | Y | 1.8073 | 1.6337 | 1.2677 | 1.3306 |
| 1.25 | X | 1.2371 | 1.3541 | 1.6409 | 0.9948 |
| 1.25 | Y | 1.7770 | 1.5870 | 1.2327 | 1.2673 |

Earthquake Corinth Greece, 2/24/1981, Corinth (RSN 313)

**Table E-15** Sand (parabola) soil profile.

| Ga | Direction | Max.Dis. Ratio | Max.Drift Ratio | Max. Acc. Ratio | Max. Base Shear Ratio |
|---|---|---|---|---|---|
| 15 | X | 1.0267 | 0.9989 | 1.8268 | 0.8096 |
| 15 | Y | 0.6877 | 0.6736 | 0.5872 | 0.9133 |
| 25 | X | 1.5296 | 1.7733 | 2.4263 | 1.2783 |
| 25 | Y | 1.0699 | 1.0710 | 1.5576 | 1.3628 |
| 35 | X | 1.2515 | 1.3111 | 1.6604 | 0.8119 |
| 35 | Y | 1.7166 | 1.7232 | 2.2552 | 1.7240 |
| 50 | X | 1.1918 | 1.2325 | 1.8586 | 1.0143 |
| 50 | Y | 1.9009 | 1.7876 | 2.0763 | 1.7713 |
| 70 | X | 1.2110 | 1.3737 | 1.7599 | 1.0321 |
| 70 | Y | 1.7849 | 1.6219 | 1.2751 | 1.1824 |
| 100 | X | 1.2461 | 1.2891 | 1.4949 | 0.9914 |
| 100 | Y | 1.3873 | 1.3033 | 1.2230 | 1.1646 |

**Table E-16** Soft top and medium bottom soil profile.

| Z/B | Direction | Max.Dis. Ratio | Max.Drift Ratio | Max. Acc. Ratio | Max. Base Shear Ratio |
|---|---|---|---|---|---|
| 0 | X | 1.2846 | 1.3696 | 1.5166 | 0.9573 |
| 0 | Y | 1.5805 | 1.3611 | 1.1700 | 1.2314 |
| 0.1 | X | 1.1942 | 1.2288 | 1.8463 | 1.0176 |
| 0.1 | Y | 1.9650 | 1.8910 | 2.2378 | 1.8855 |
| 0.25 | X | 1.2349 | 1.2745 | 1.6584 | 0.8189 |
| 0.25 | Y | 1.8444 | 1.8501 | 2.2582 | 1.6490 |
| 0.5 | X | 1.3380 | 1.4553 | 2.0408 | 0.9911 |
| 0.5 | Y | 1.3004 | 1.4090 | 2.0796 | 1.6596 |
| 1 | X | 1.5963 | 1.7404 | 2.3385 | 1.3403 |
| 1 | Y | 1.0455 | 1.0442 | 1.5390 | 1.3046 |
| 1.25 | X | 1.6161 | 1.7376 | 2.4056 | 1.3030 |
| 1.25 | Y | 0.9431 | 0.9028 | 1.2953 | 1.2051 |

APPENDIX F

NORMALIZED OF FOUNDATION RESULTS CHAPTER 7

Frame Building

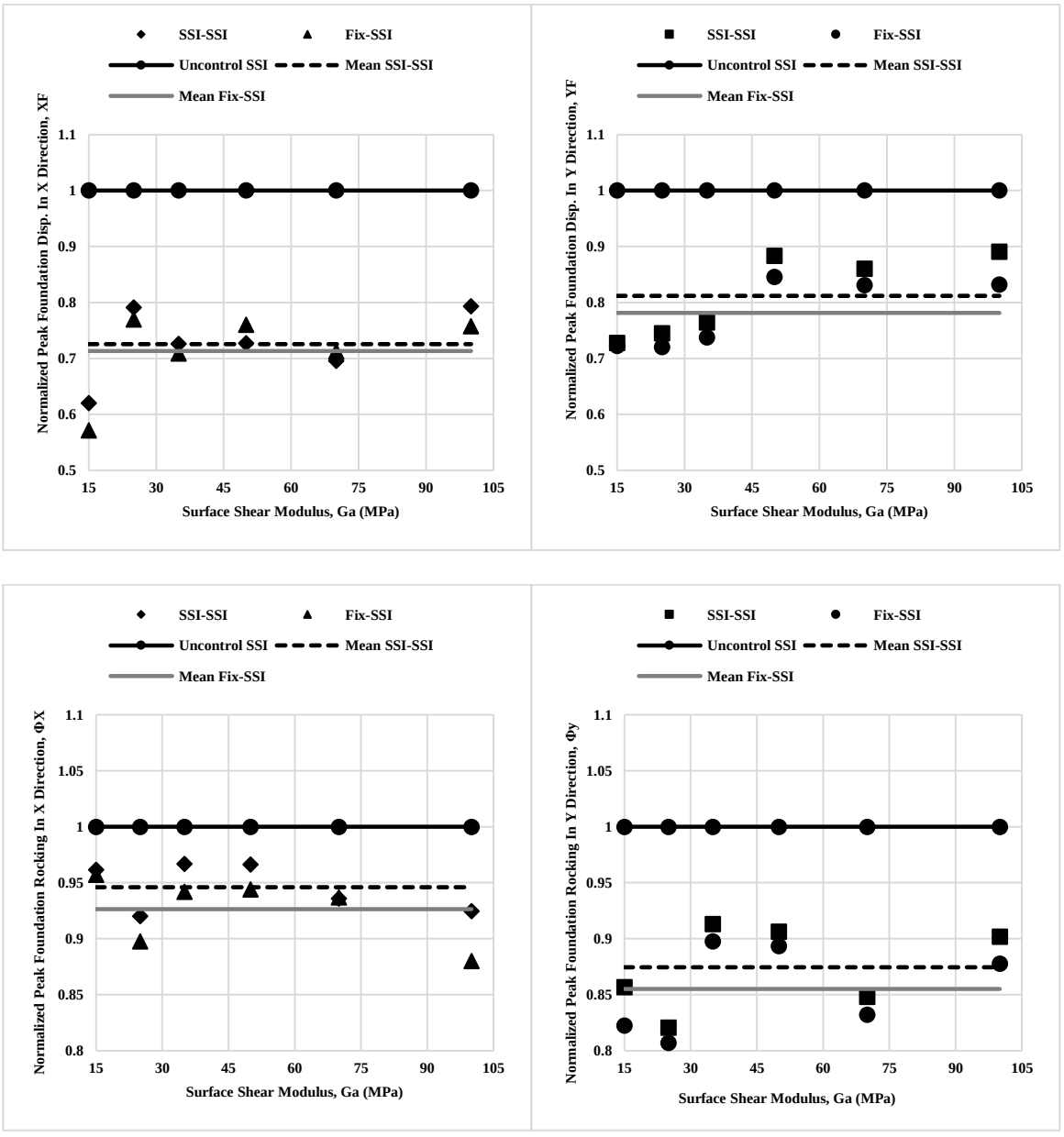


**Figure F-1** Clay (linear) soil profile under earthquake RSN96.

Frame Building

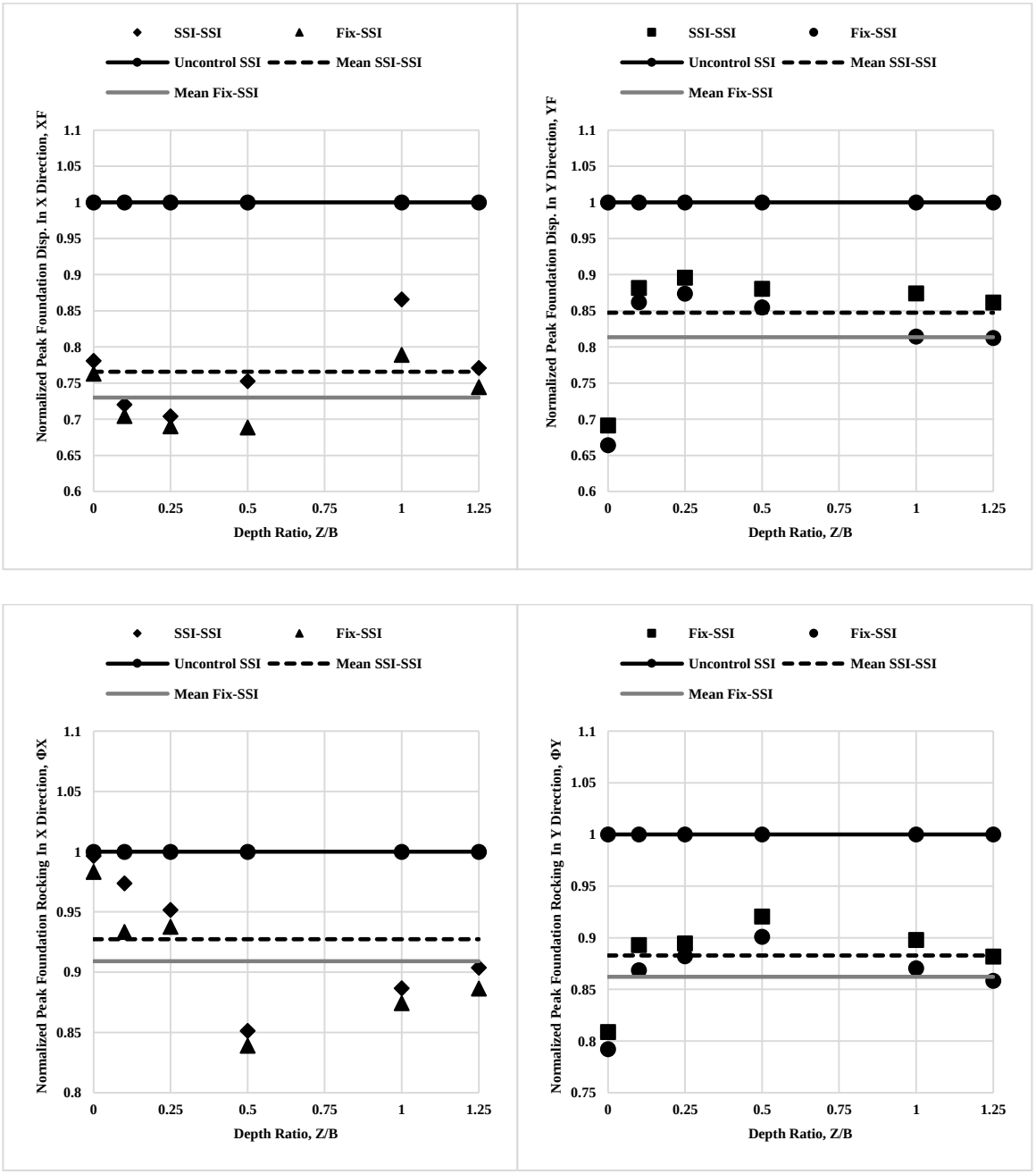


**Figure F-2** Medium soil top and soft soil bottom soil profile under earthquake RSN96.

Frame Building

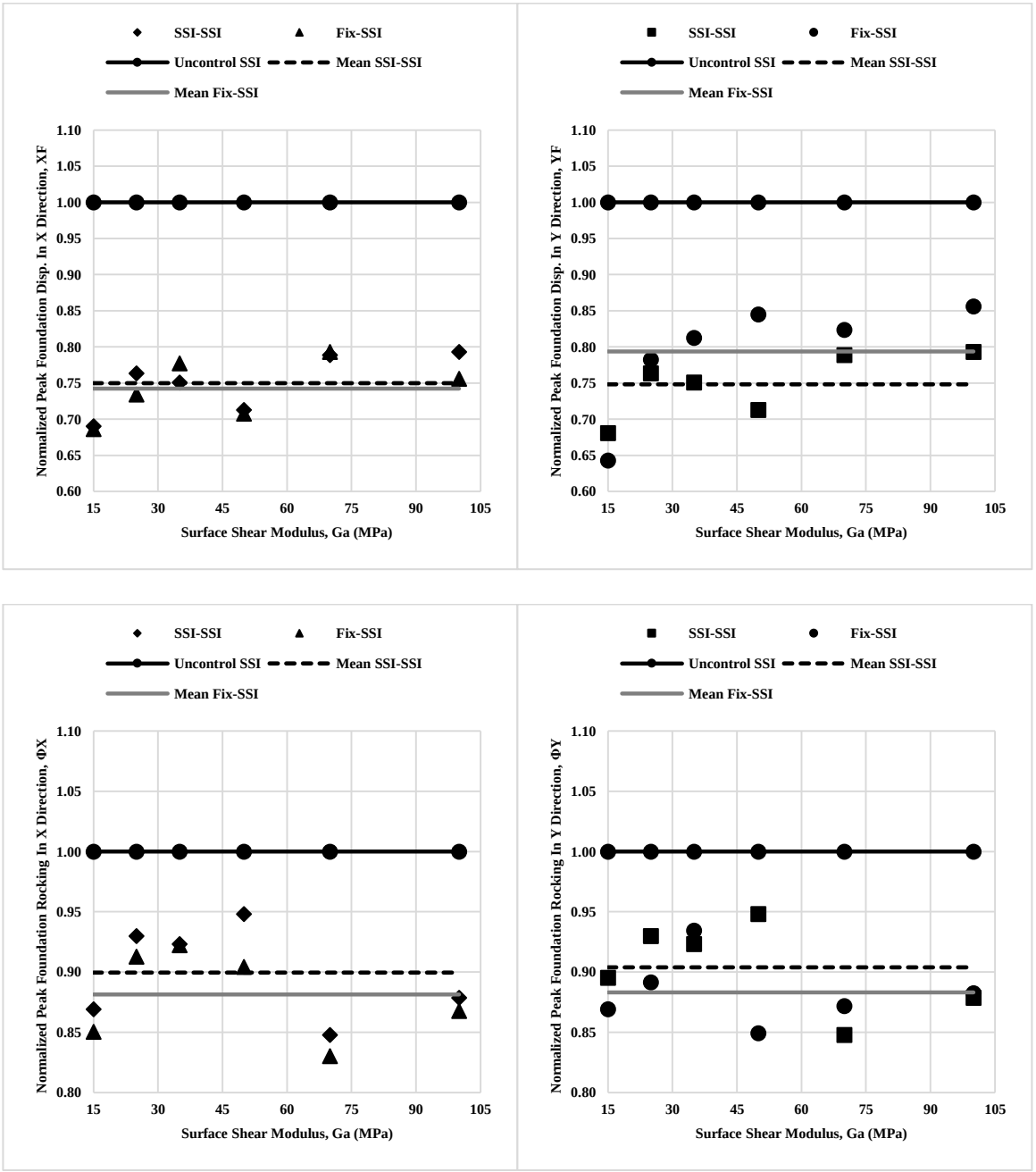


**Figure F-3** Sand (parabola) soil profile under earthquake RSN96.

Frame Building

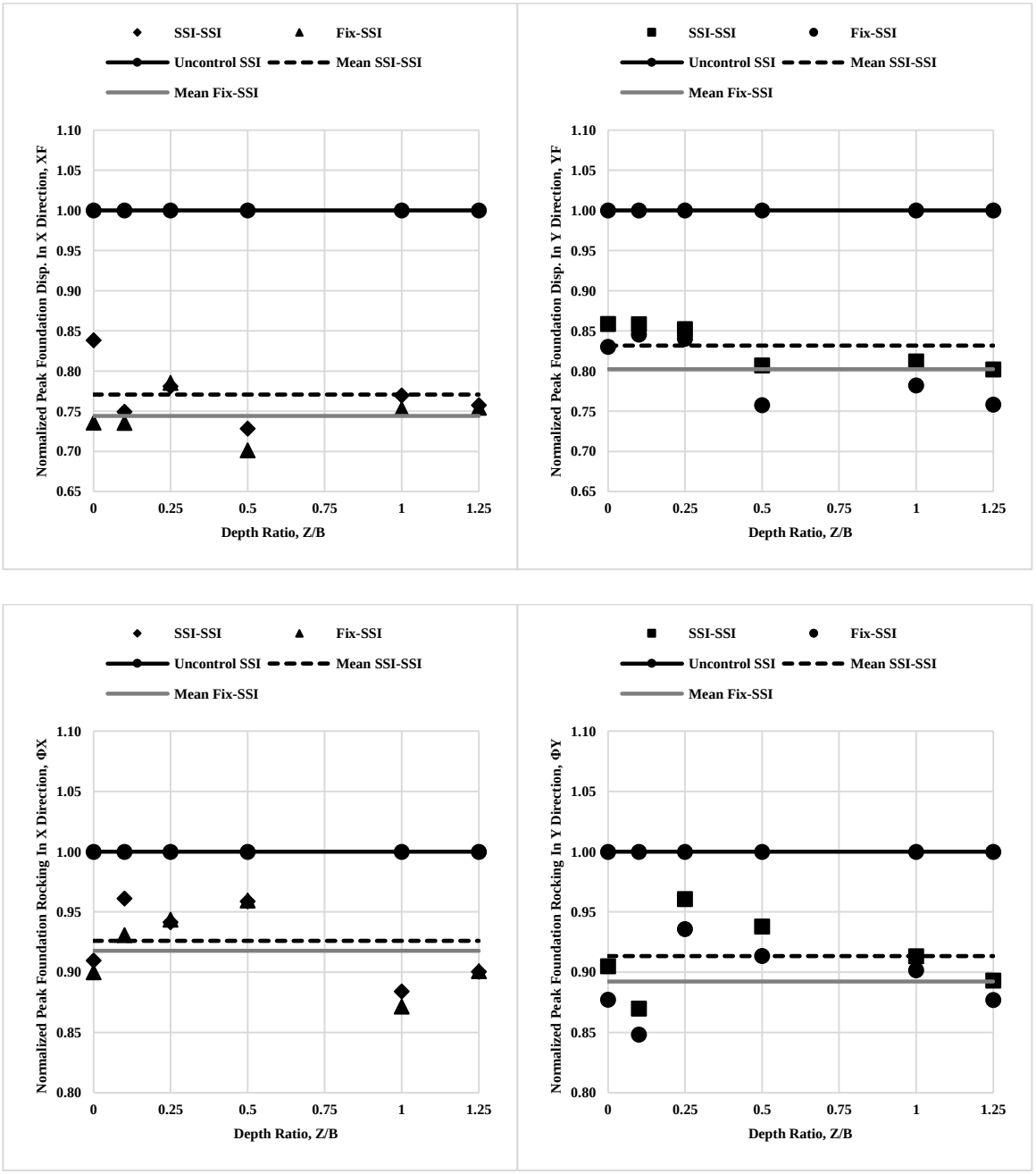


**Figure F-4** Soft soil top and medium soil bottom soil profile under earthquake RSN96.

Frame Building

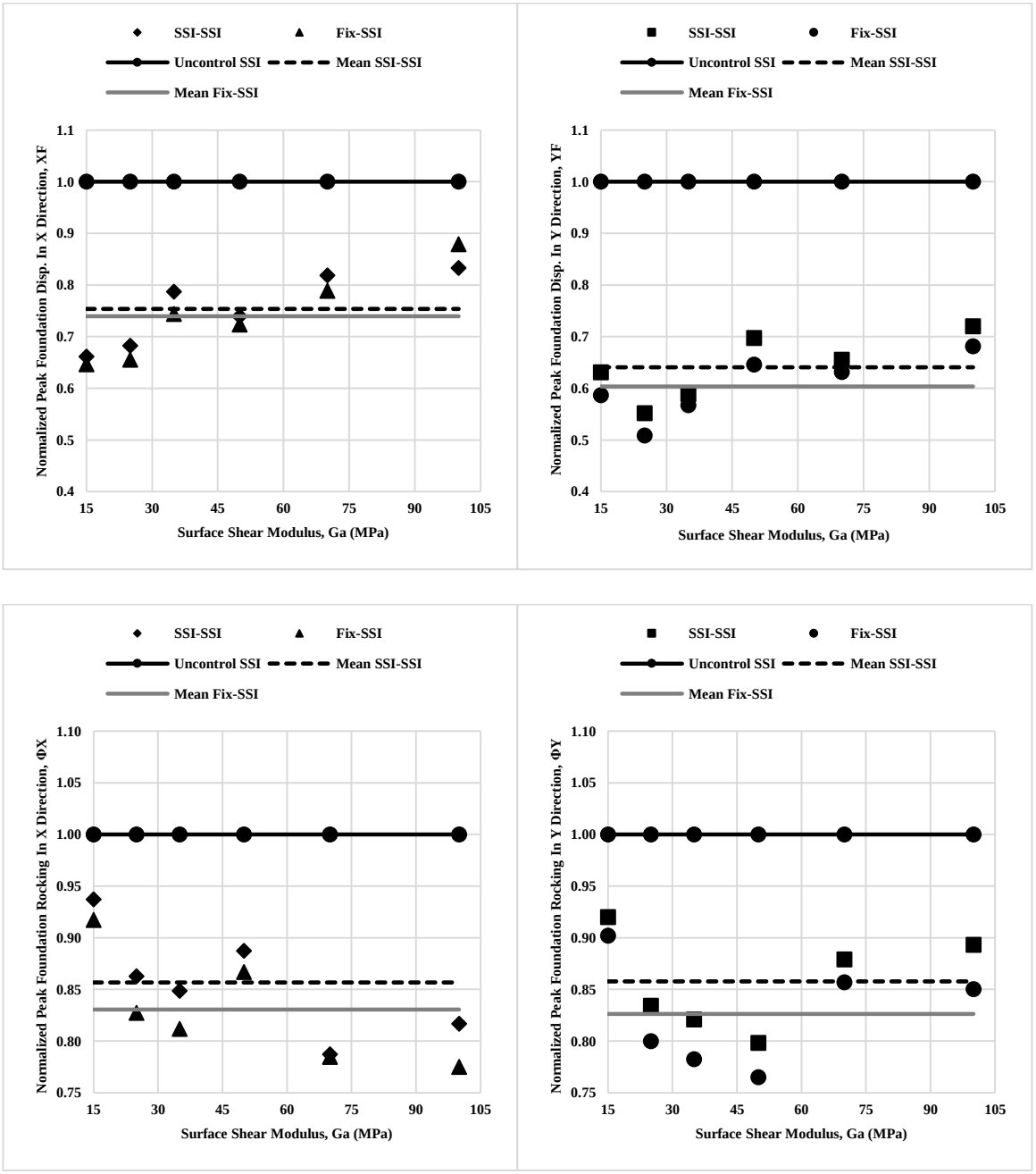


**Figure F-5** Clay (linear) soil profile under earthquake RSN313.

Frame Building

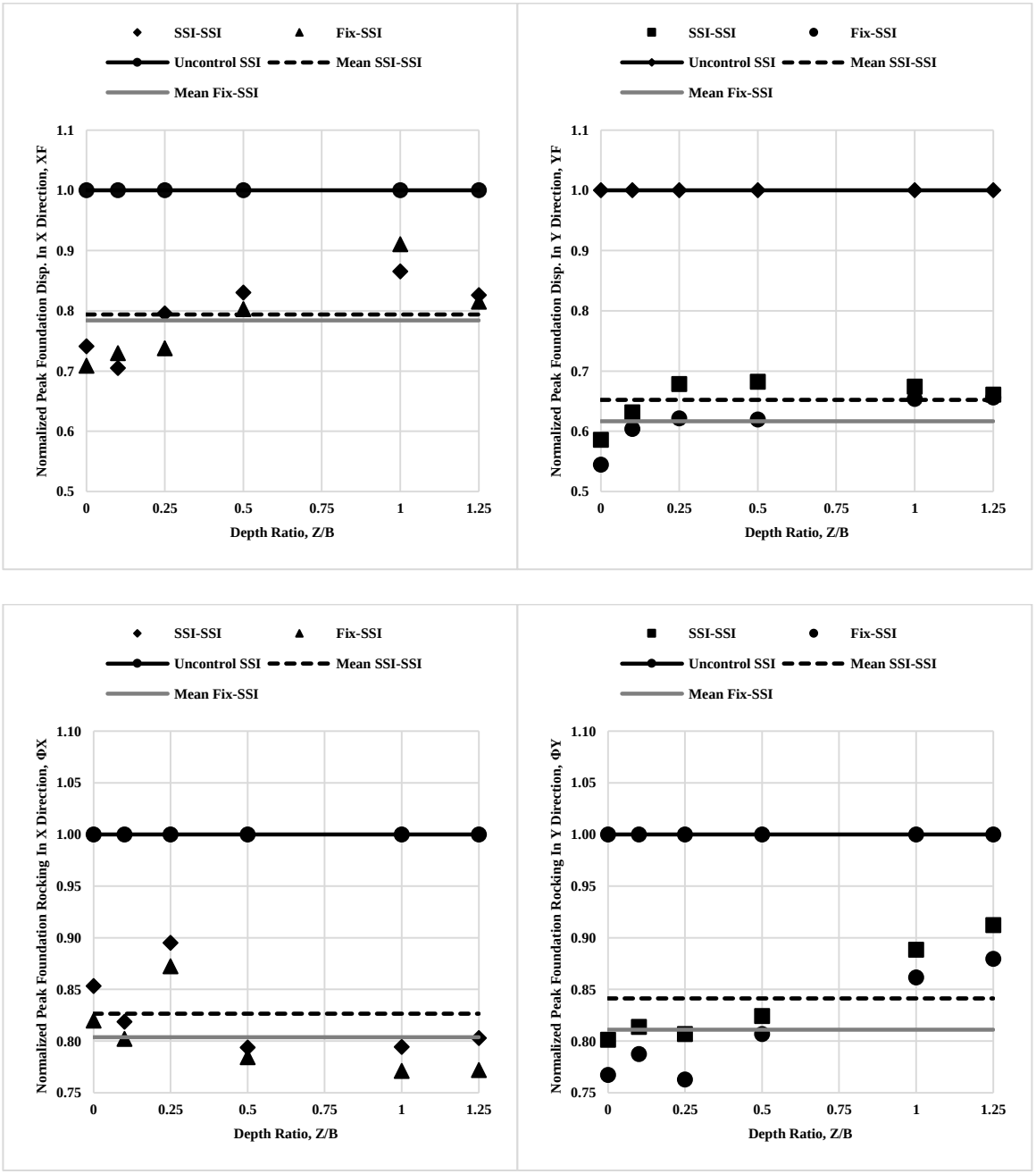


**Figure F-6** Medium soil top and soft soil bottom soil profile under earthquake RSN313.

Frame Building

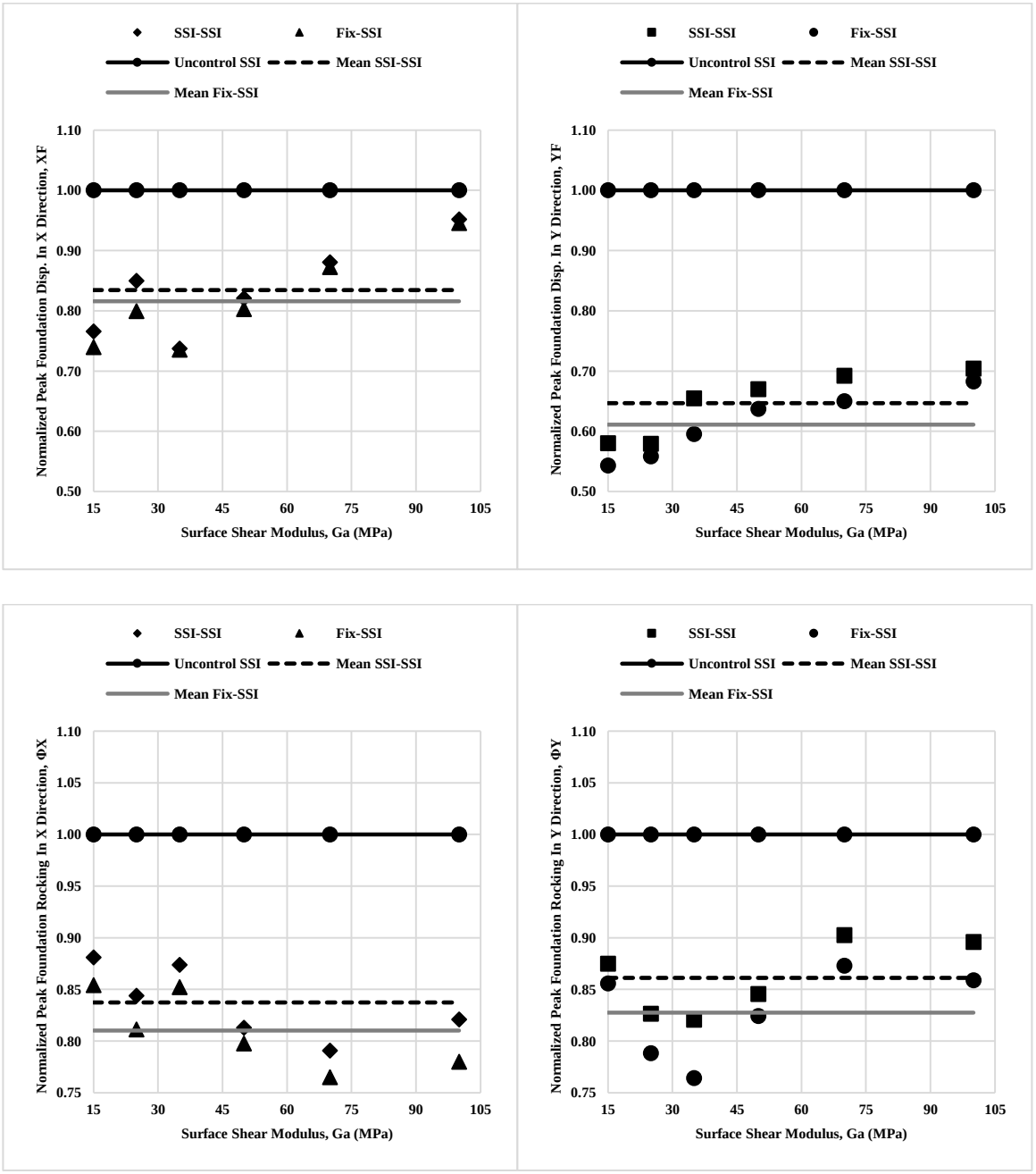


**Figure F-7** Sand (parabola) soil profile under earthquake RSN313.

Frame Building

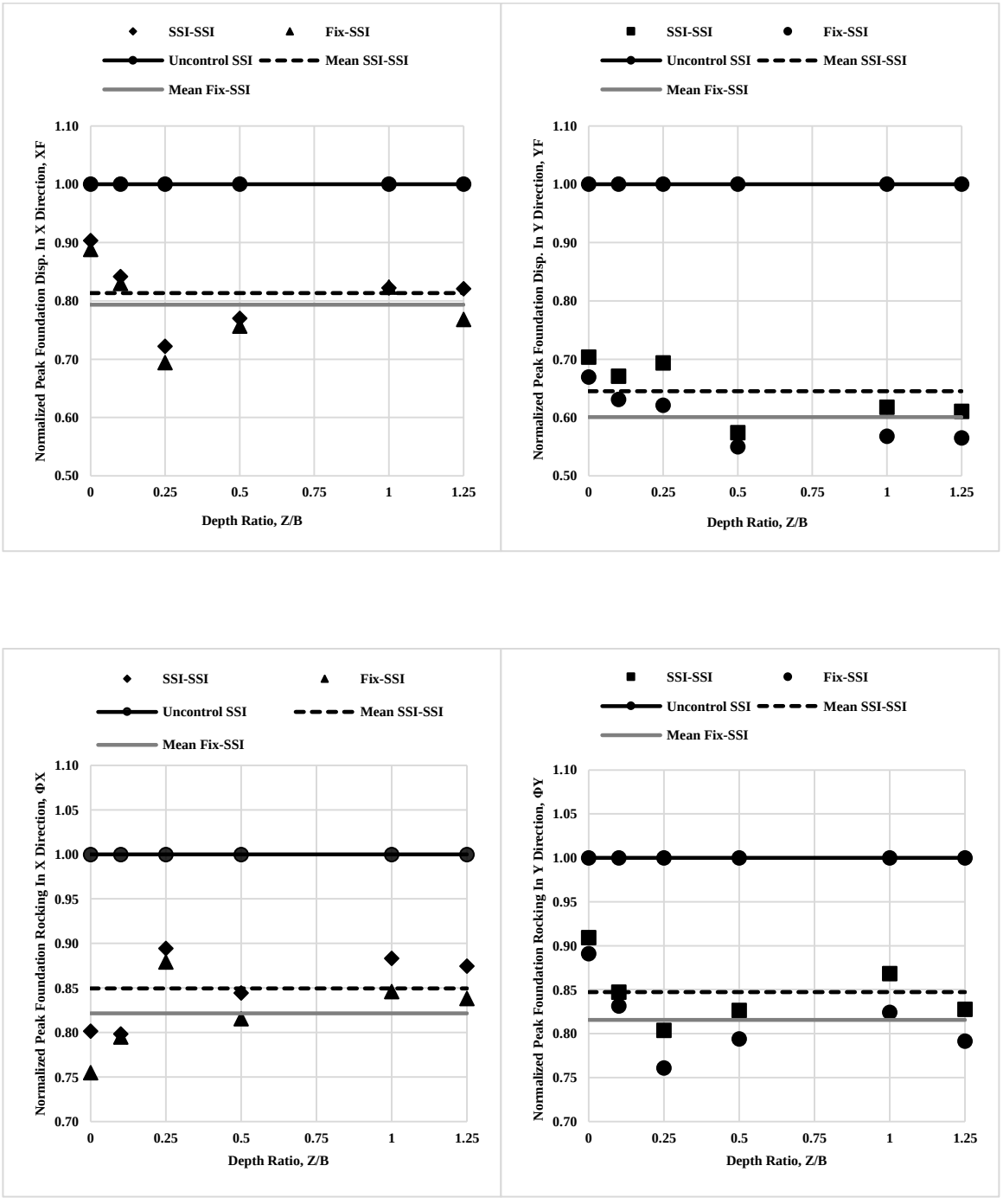


**Figure F-8** Soft soil top and medium soil bottom soil profile under earthquake RSN313.

Frame Shear Wall Building

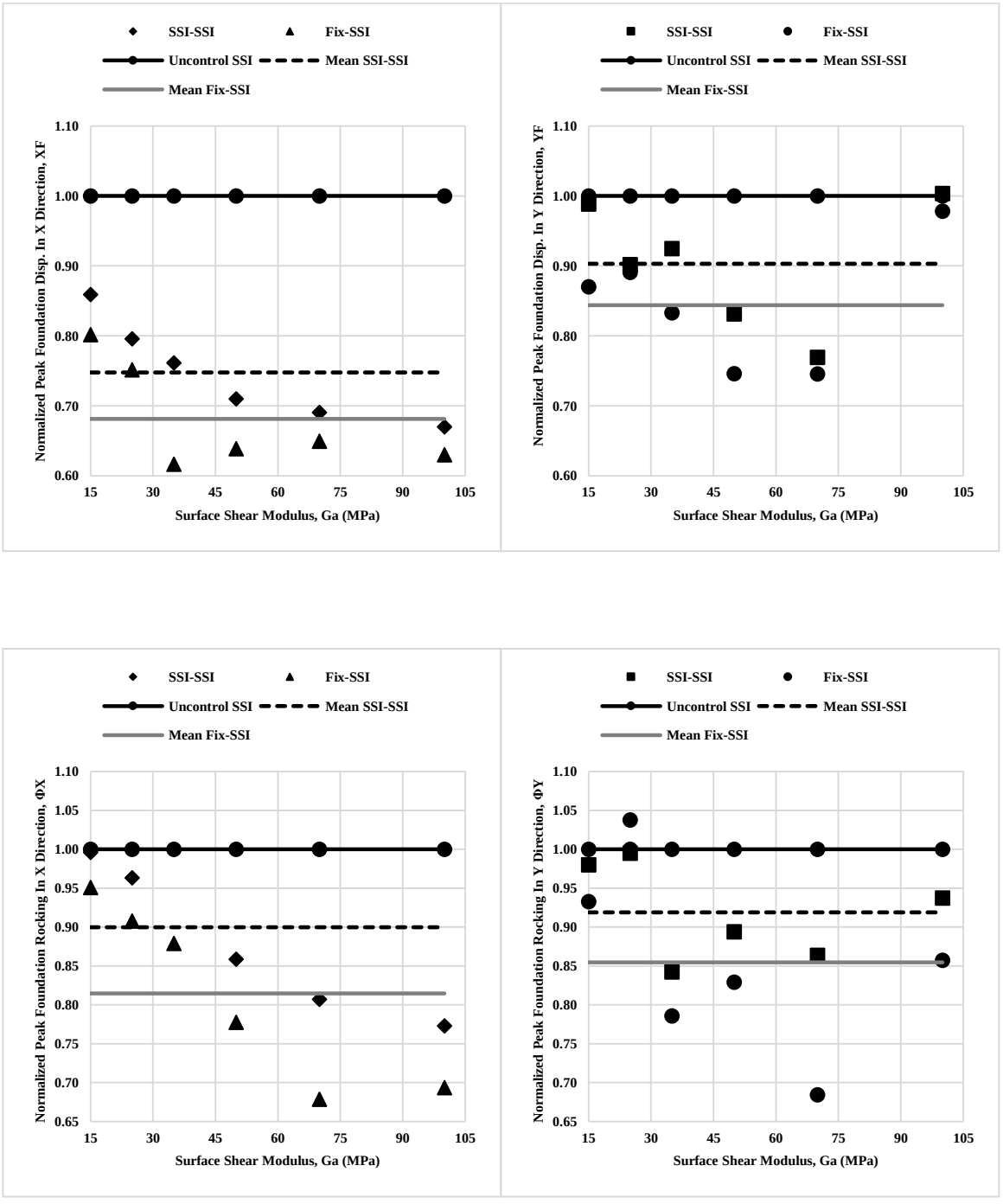


**Figure F-9** Clay (linear) soil profile under earthquake RSN96.

Frame Shear Wall Building

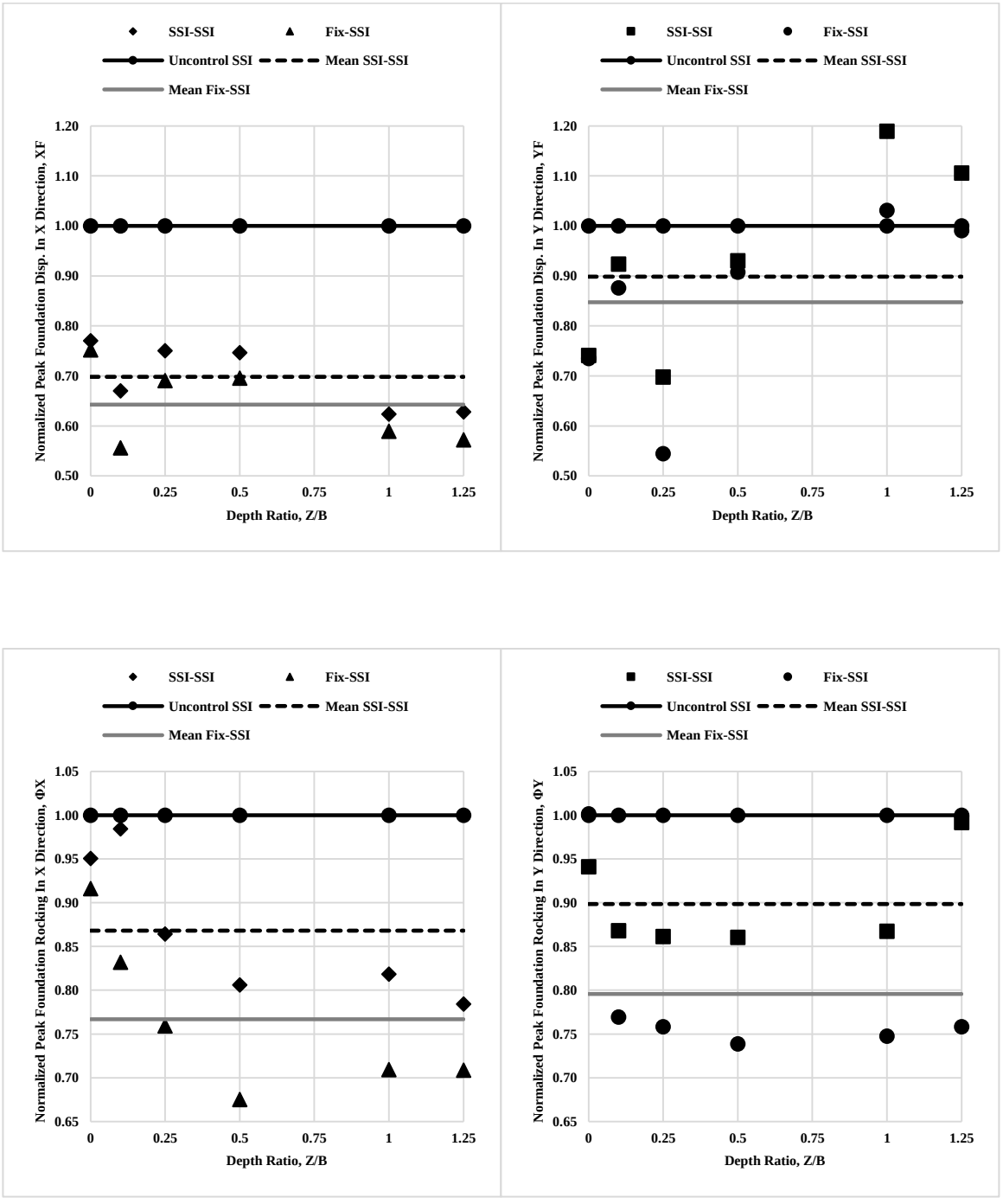


**Figure F-10** Medium soil top and soft soil bottom soil profile under earthquake RSN96.

Frame Shear Wall Building

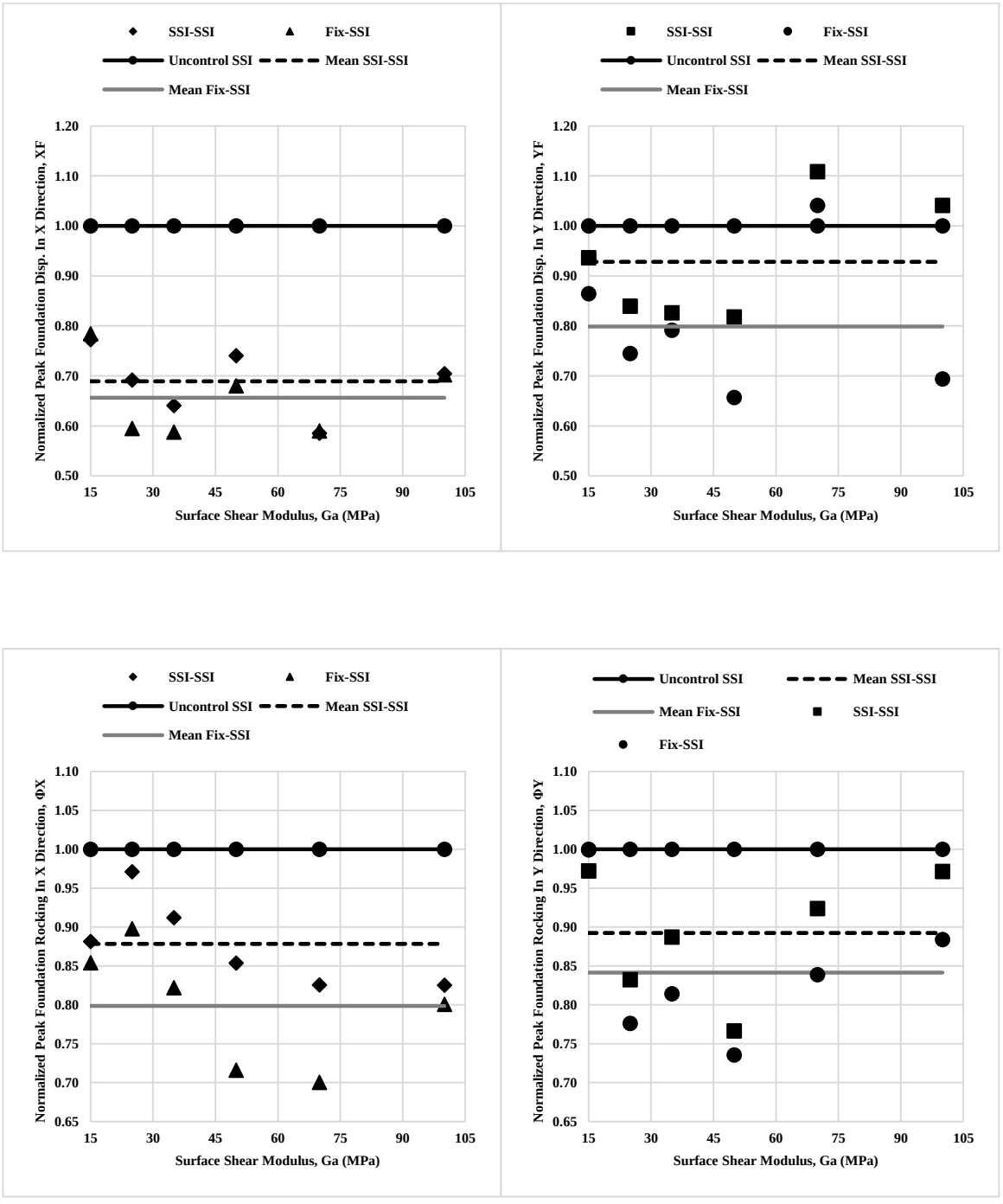


**Figure F-11** Sand (parabola) soil profile under earthquake RSN96.

Frame Shear Wall Building

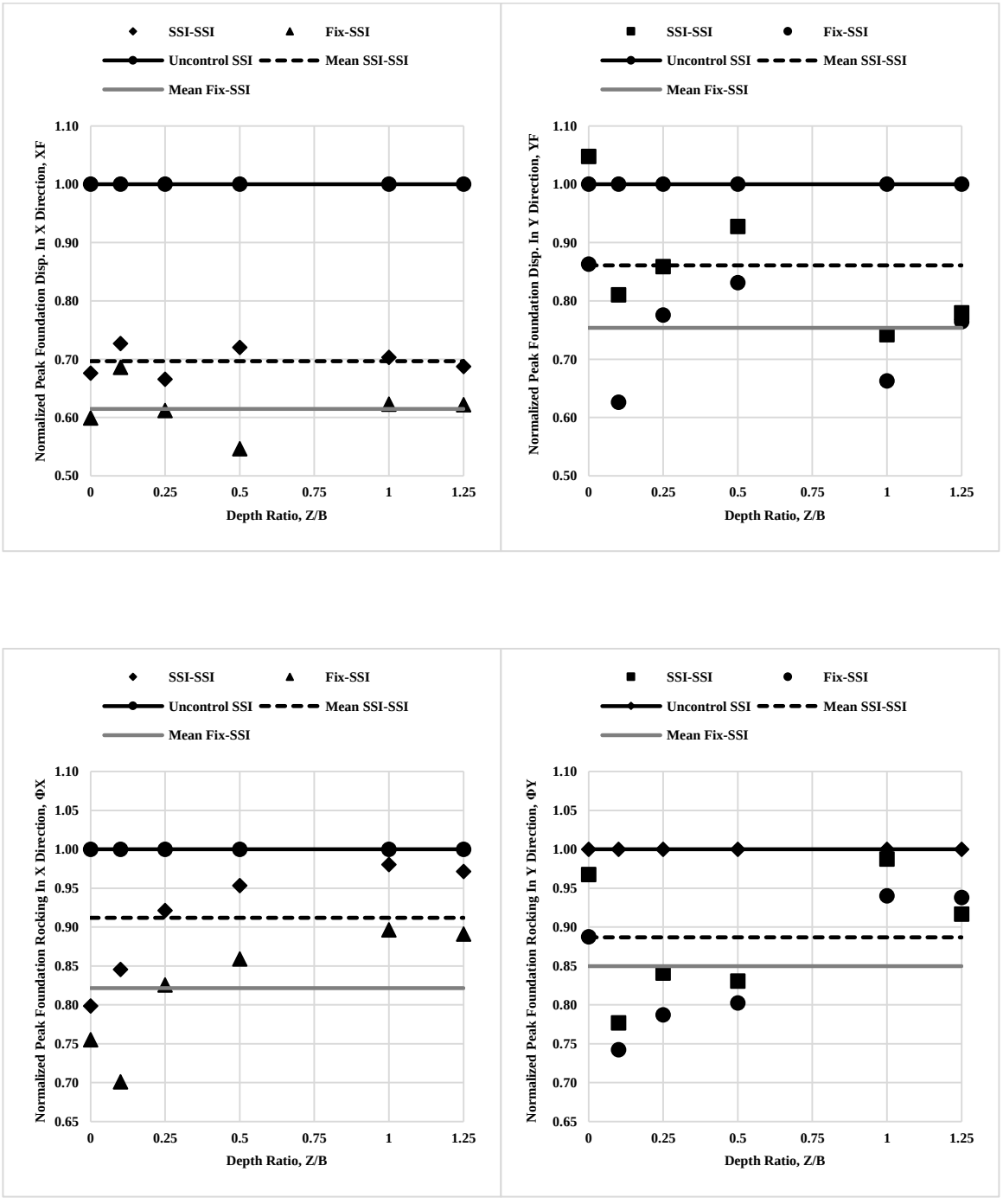


**Figure F-12** Soft soil top and medium soil bottom soil profile under earthquake RSN96.

Frame Shear Wall Building

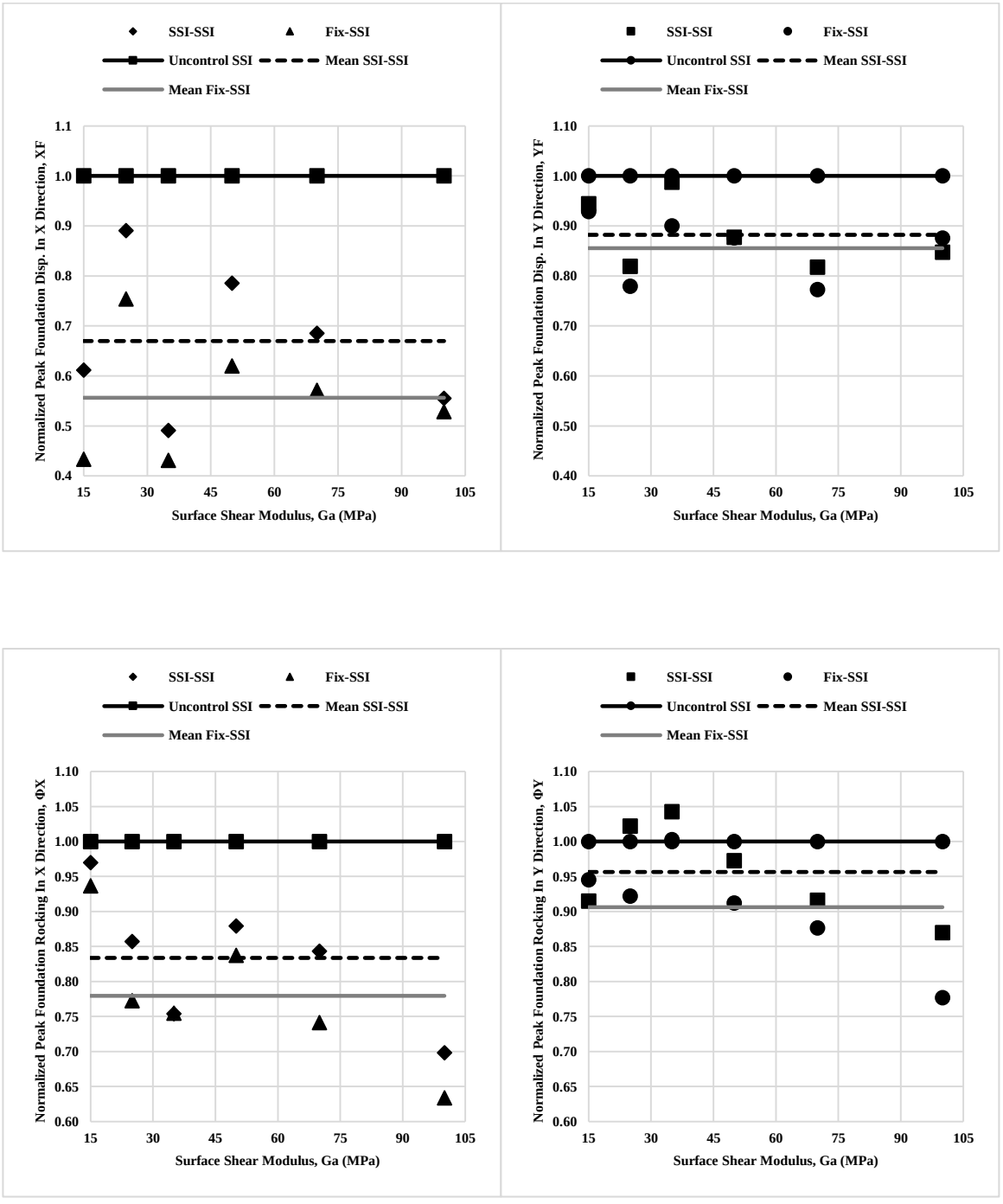


**Figure F-13** Clay (linear) soil profile under earthquake RSN313.

Frame Shear Wall Building

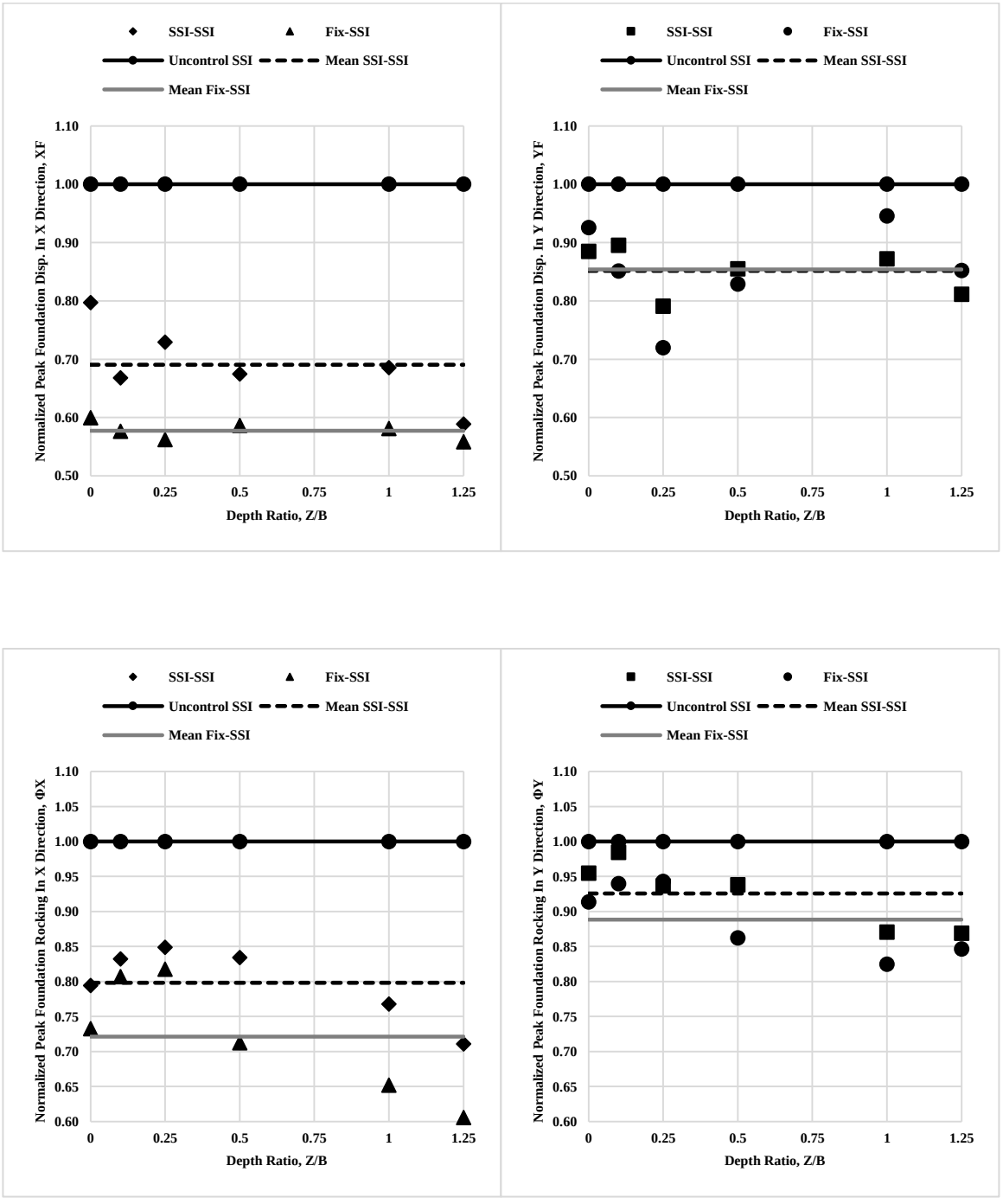


**Figure F-14** Medium soil top and soft soil bottom soil profile under earthquake RSN313.

Frame Shear Wall Building

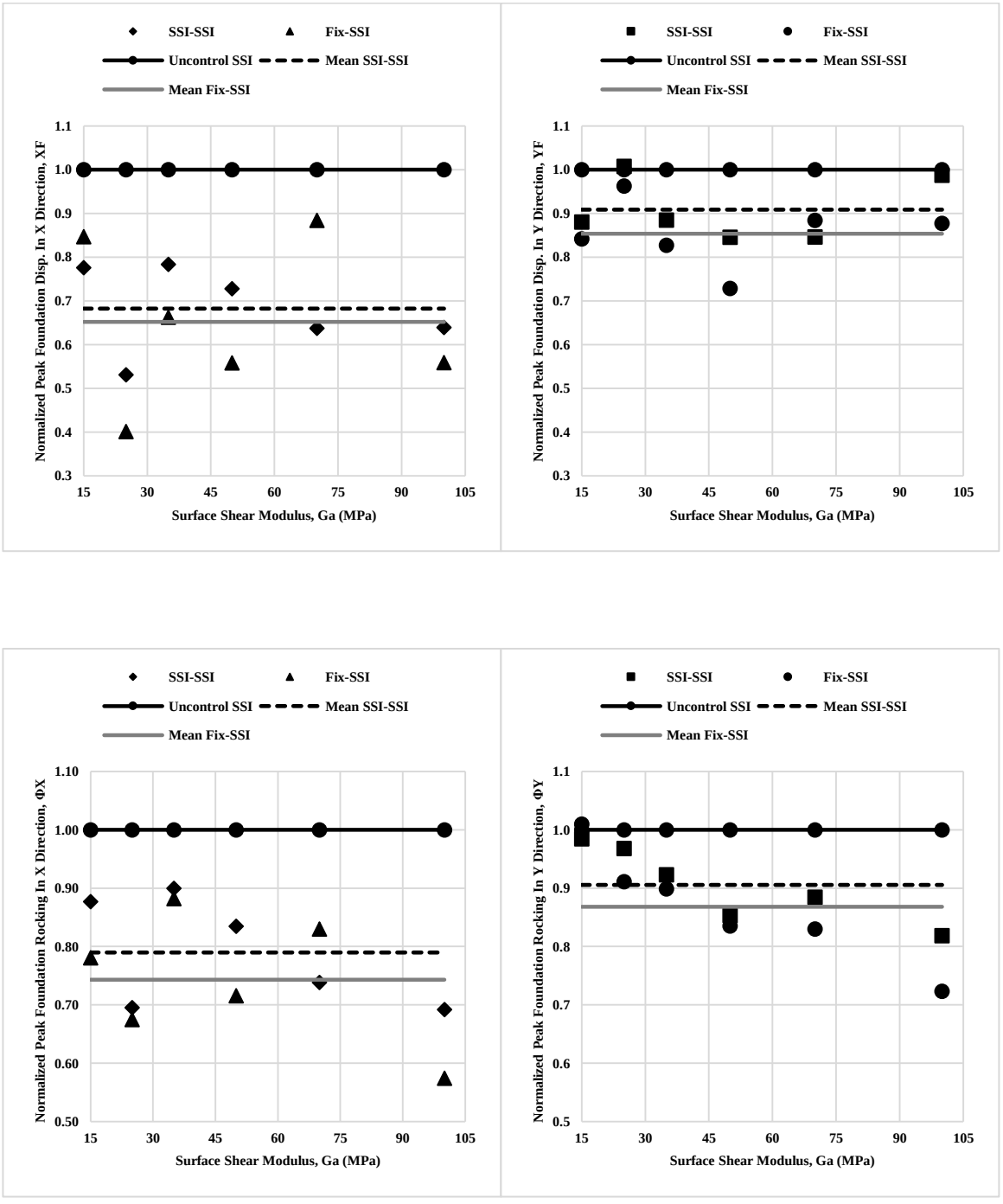


**Figure F-15** Sand (parabola) soil profile under earthquake RSN313.

Frame Shear Wall Building

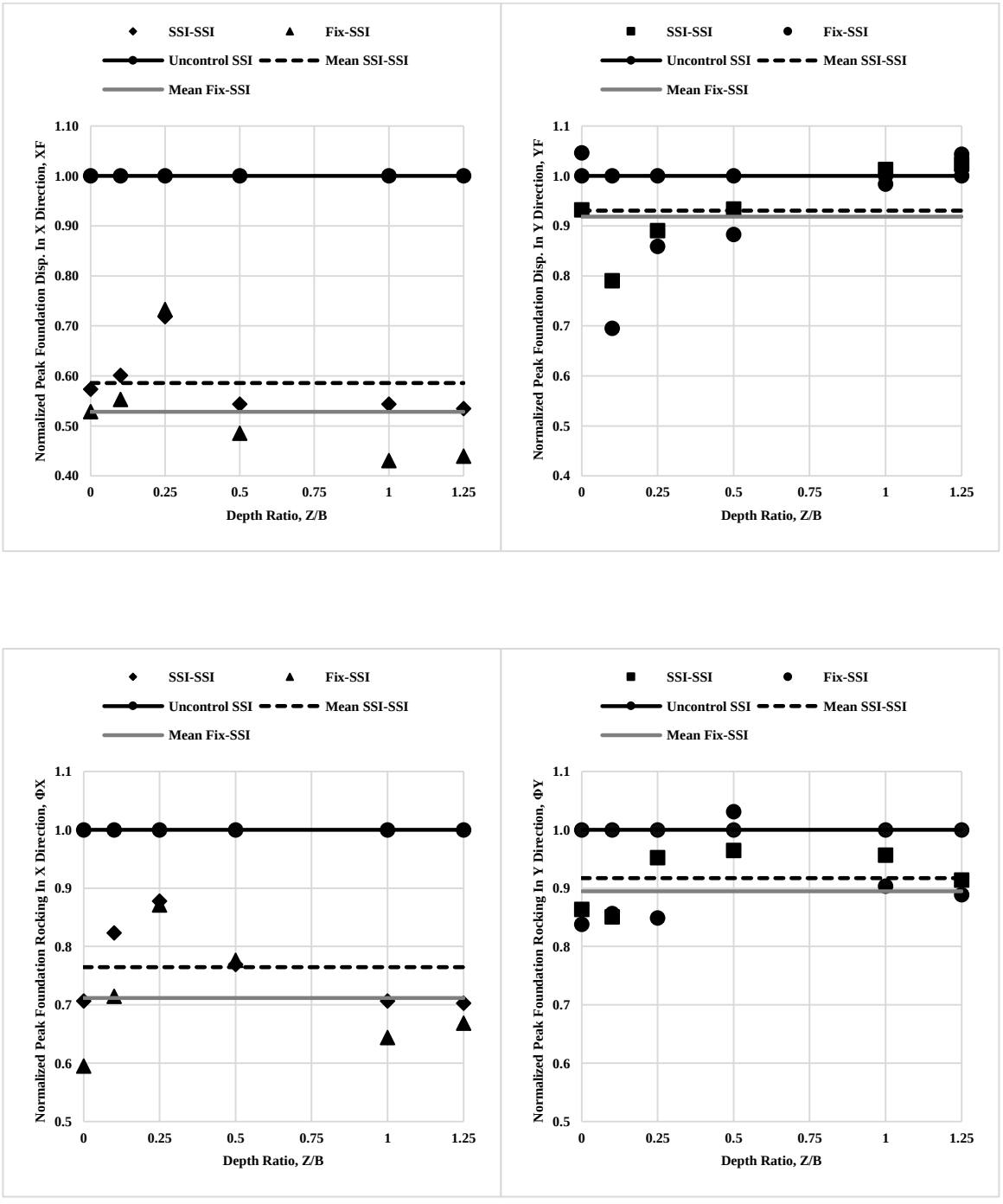


**Figure F-16** Soft soil top and medium soil bottom soil profile under earthquake RSN313.

APPENDIX G

RESULTS OF FLOORS

Frame Building

Soil profile medium top and soft bottom

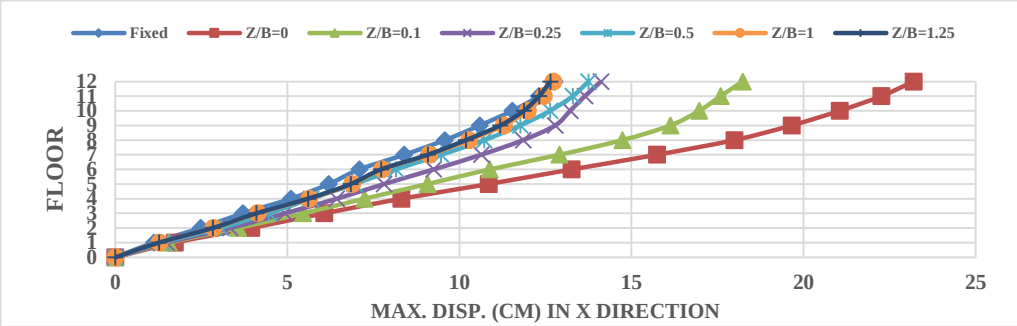


A) Uncontrolled Systems

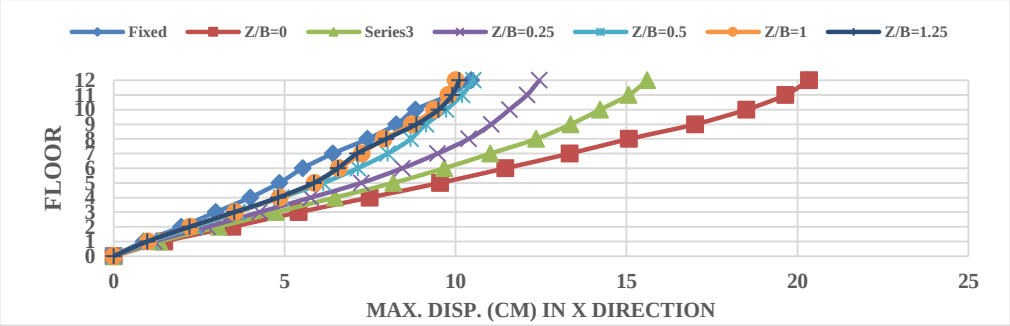


B) Controlled Systems SSI-SSI

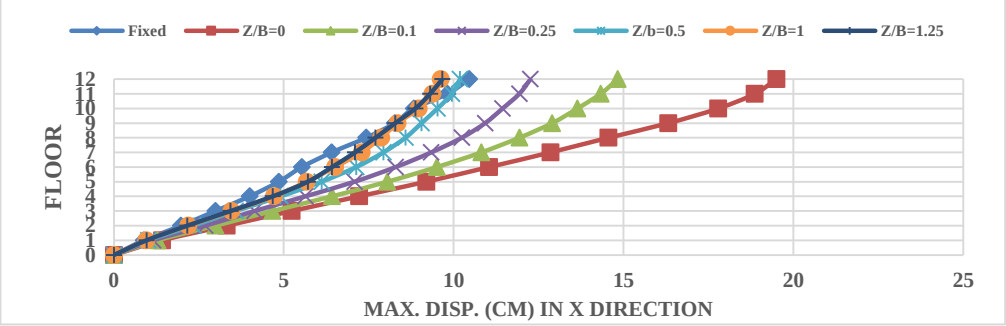


C) Controlled Systems Fixed-SSI

**Figure G-1** Max. displacements of the systems under earthquake Corinth Greece.

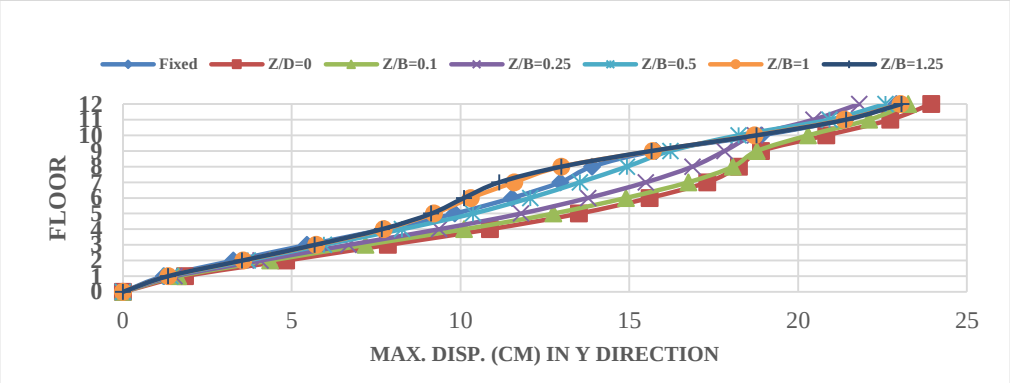


A) Uncontrolled Systems

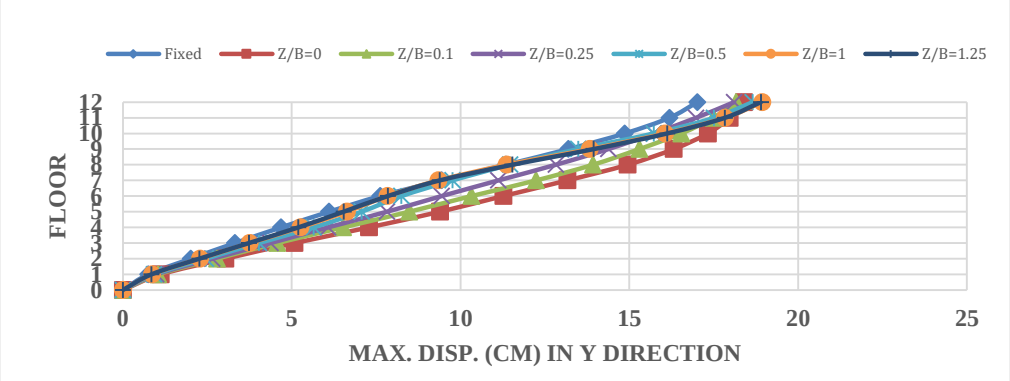


B) Controlled Systems SSI-SSI

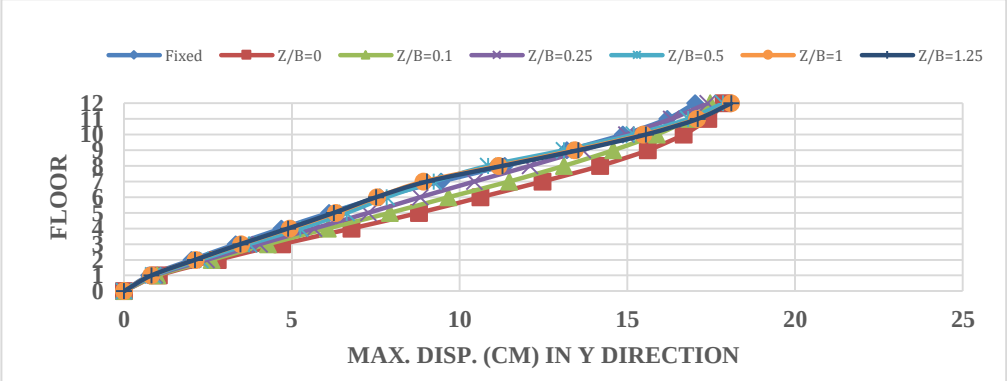


C) Controlled Systems Fixed-SSI

**Figure G-2** Max. displacements of the systems under earthquake Corinth Greece, 2/24/1981, Corinth (RSN 313)

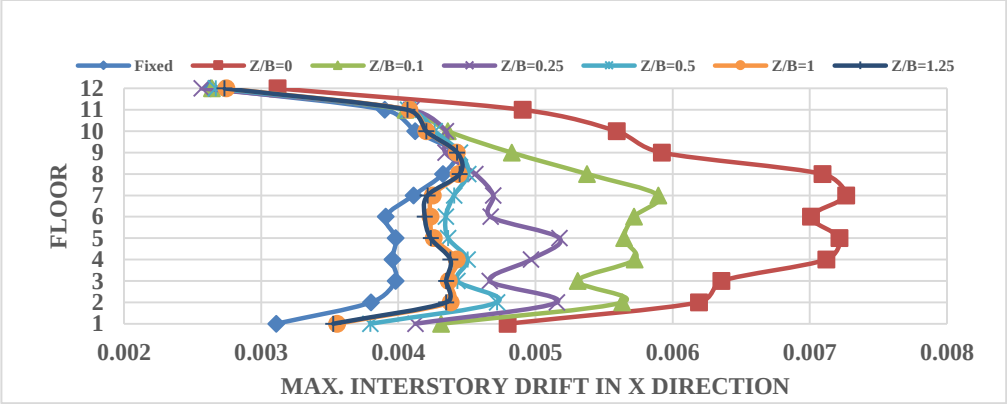


A) Uncontrolled Systems

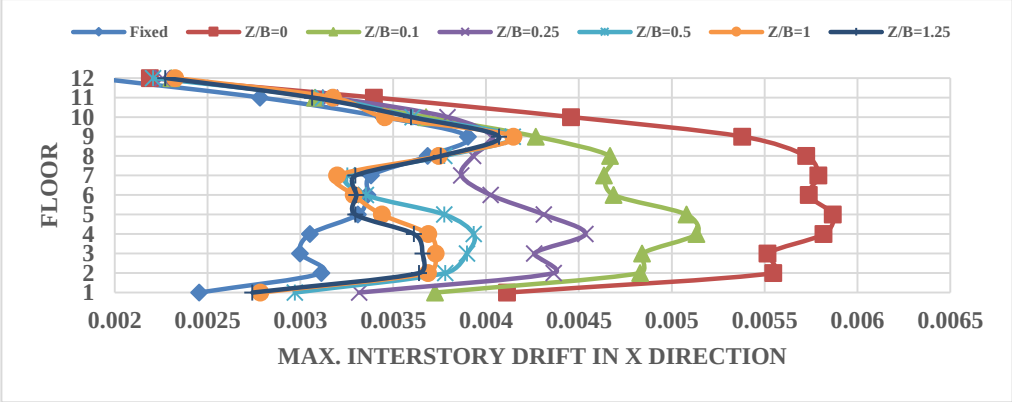


B) Controlled Systems SSI-SSI

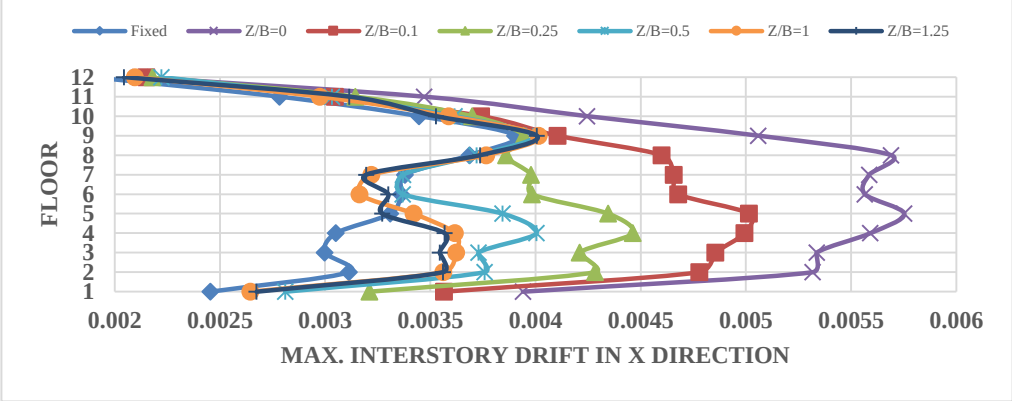


C) Controlled Systems Fixed-SSI

**Figure G-3** Max. interstory drift of the systems under earthquake Corinth Greece, 2/24/1981

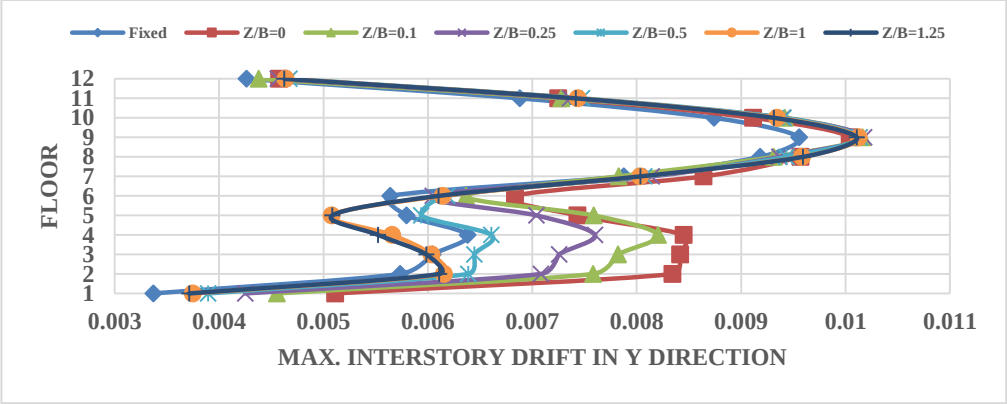


A) Uncontrolled Systems

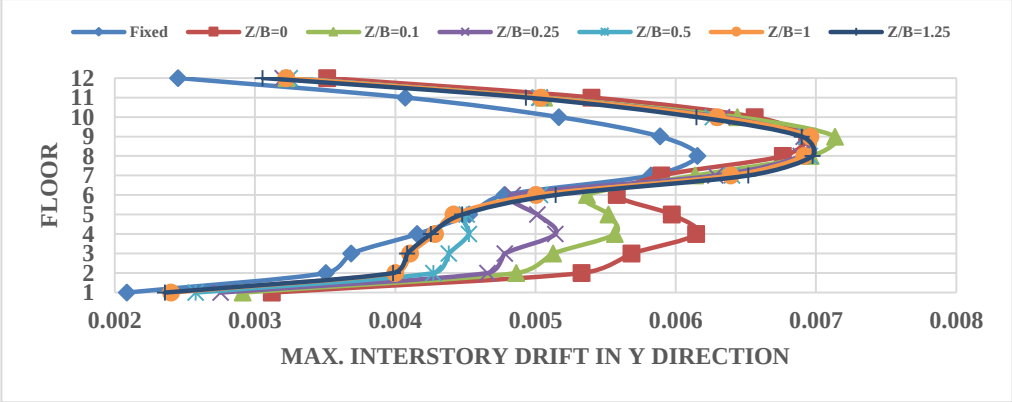


B) Controlled Systems SSI-SSI

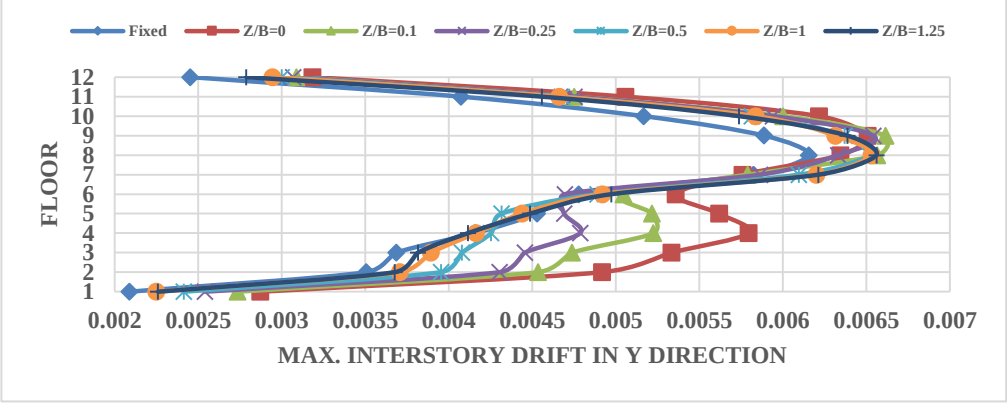


C) Controlled Systems Fixed-SSI

**Figure G-4** Max. interstory drift of the systems under earthquake Corinth Greece, 2/24/1981

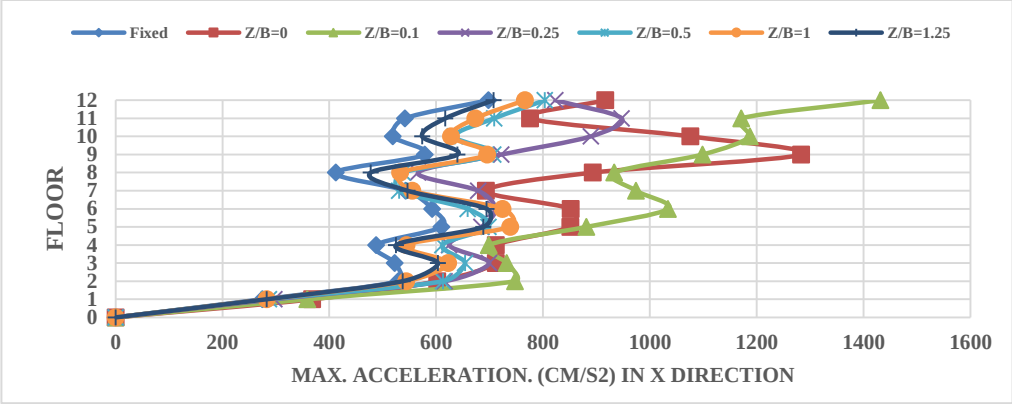


A) Uncontrolled Systems

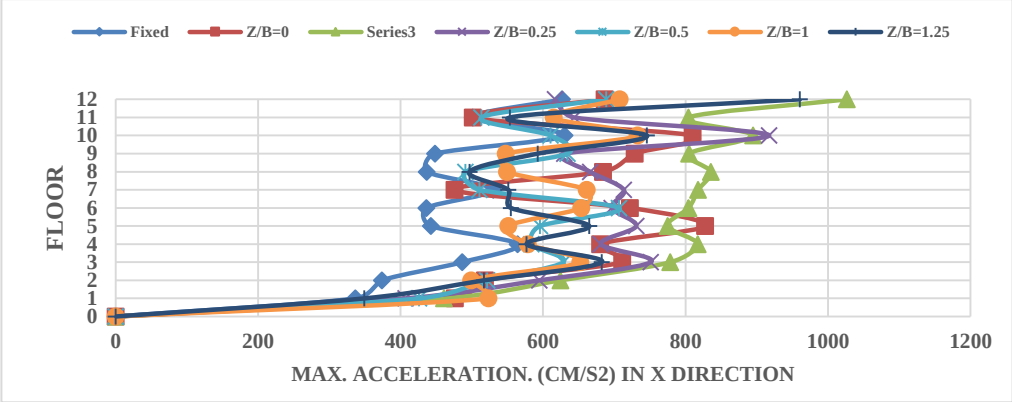


B) Controlled Systems SSI-SSI

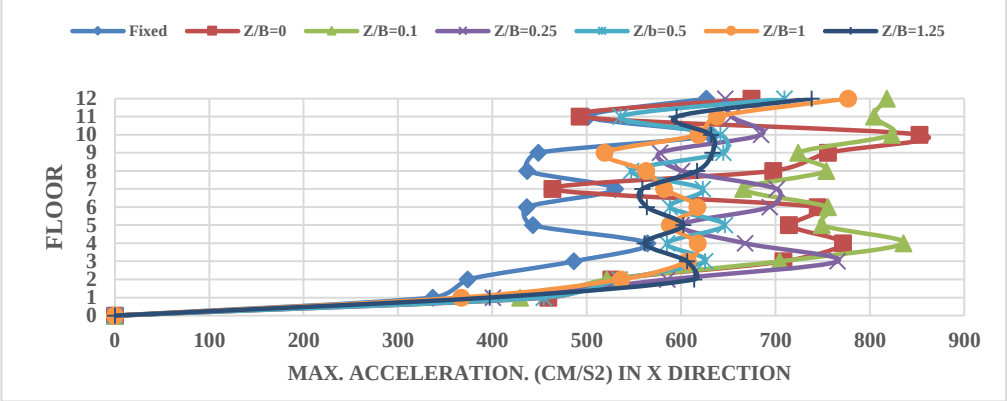


C) Controlled Systems Fixed-SSI

**Figure G-5** Max. acceleration of the systems under earthquake Corinth Greece, 2/24/1981

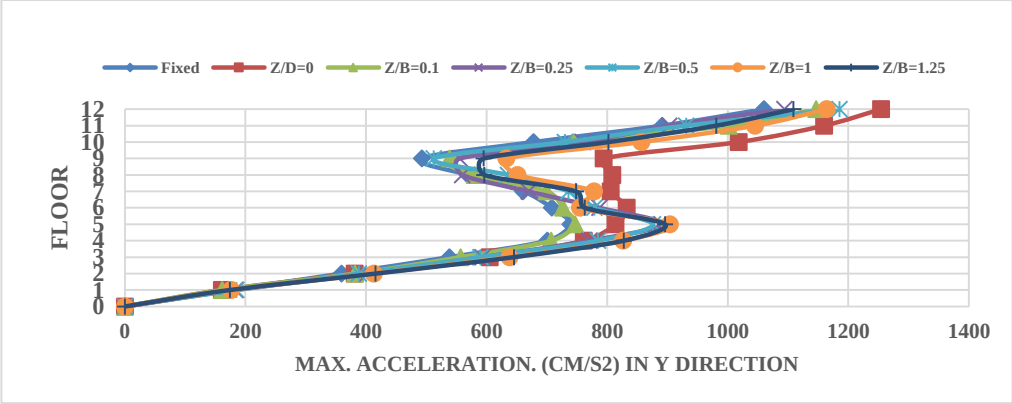


A) Uncontrolled Systems

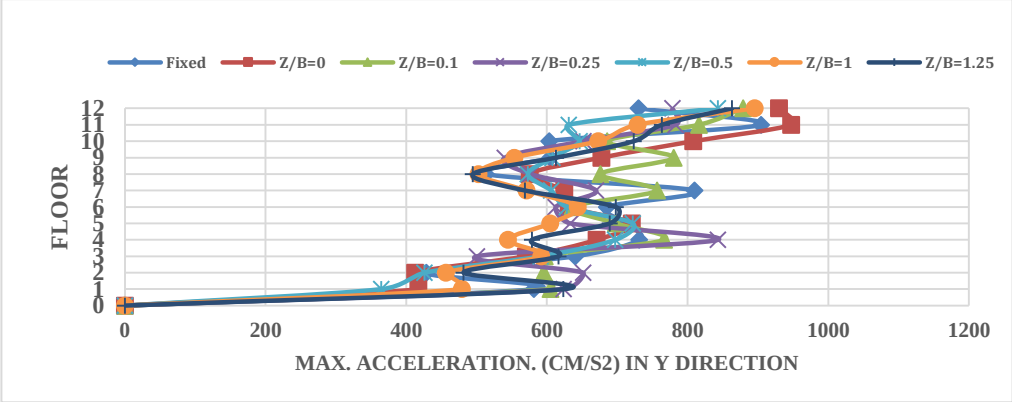


B) Controlled Systems SSI-SSI

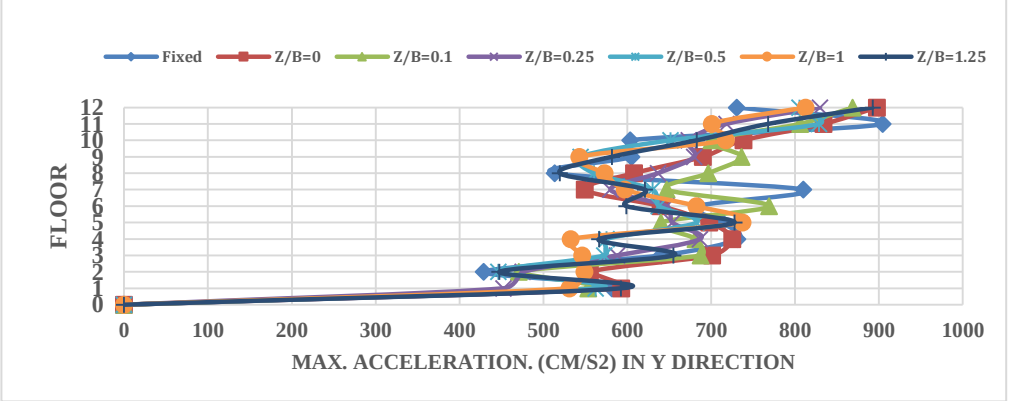


C) Controlled Systems Fixed-SSI

**Figure G-6** Max. acceleration of the systems under earthquake Corinth Greece, 2/24/1981

Soft top and medium bottom

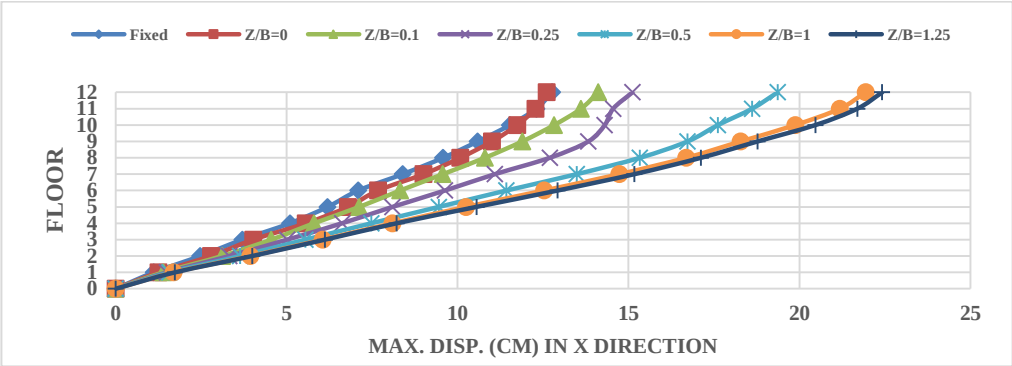


A) Uncontrolled Systems

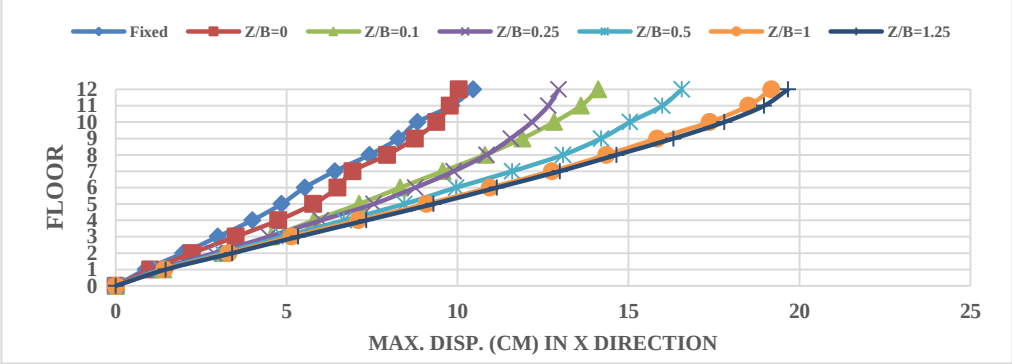


B) Controlled Systems SSI-SSI

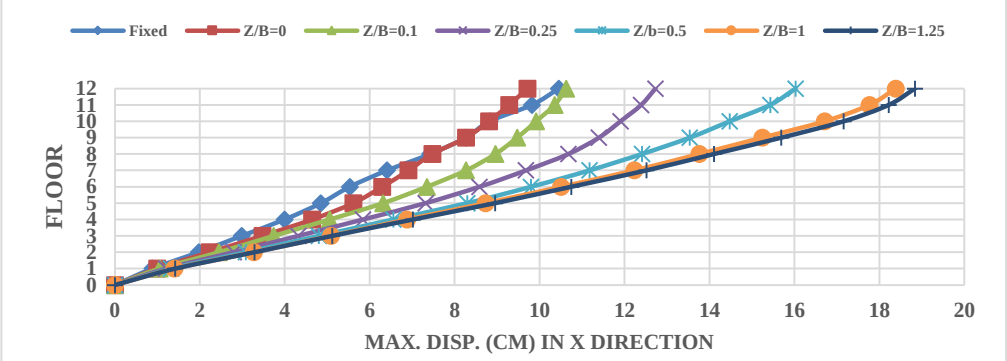


C) Controlled Systems Fixed-SSI

**Figure G-7** Max. displacements of the systems under earthquake Corinth Greece, 2/24/1981

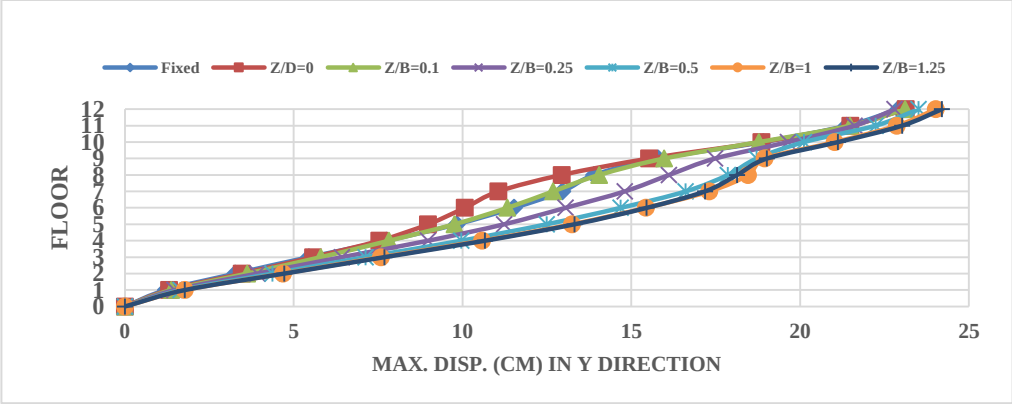


A) Uncontrolled Systems

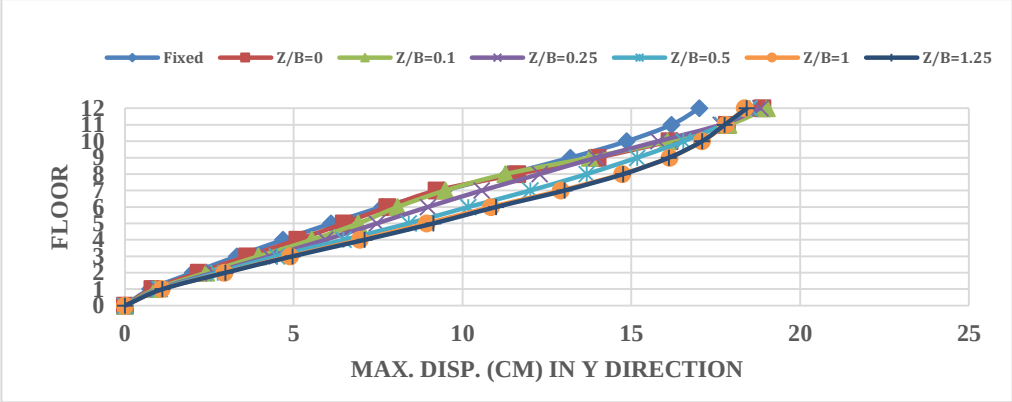


B) Controlled Systems SSI-SSI

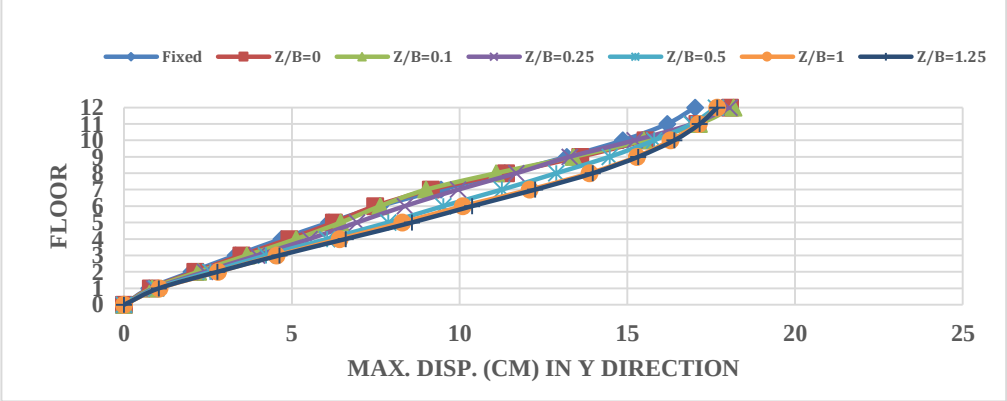


C) Controlled Systems Fixed-SSI

**Figure G-8** Max. displacements of the systems under earthquake Corinth Greece, 2/24/1981

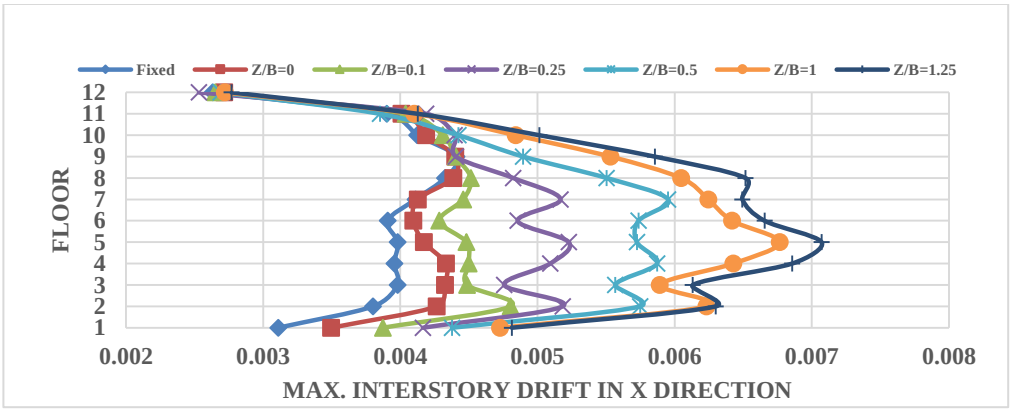


A) Uncontrolled Systems

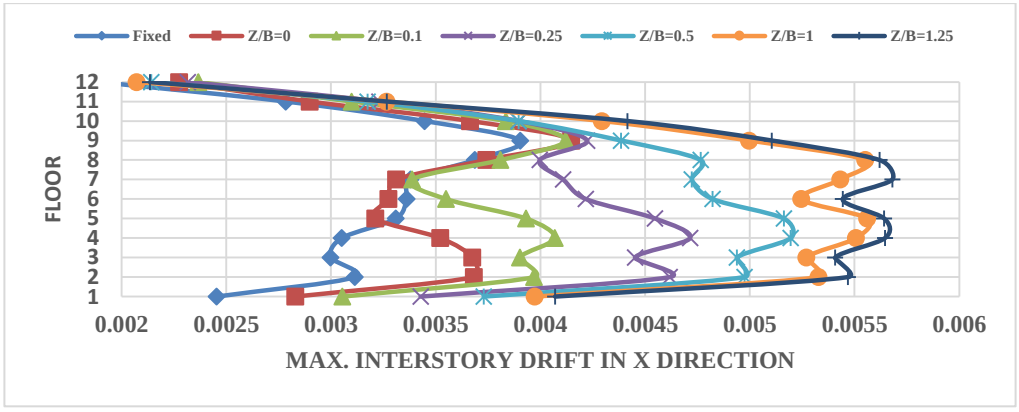


B) Controlled Systems SSI-SSI

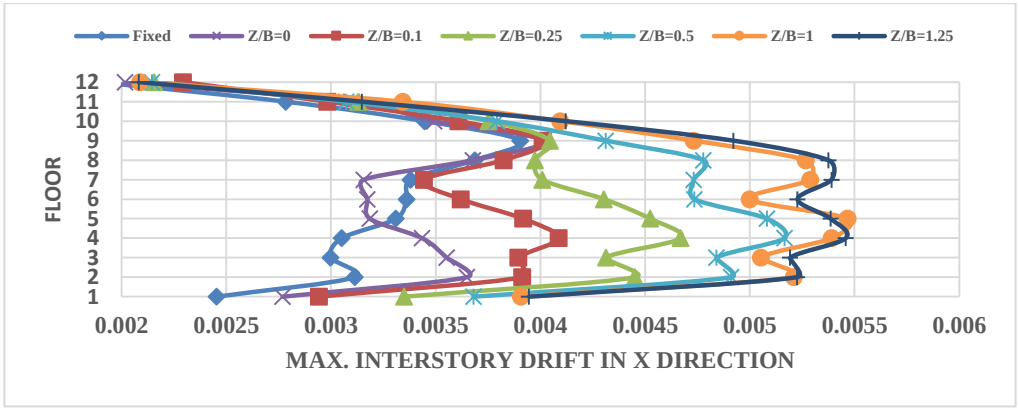


C) Controlled Systems Fixed-SSI

**Figure G-9** Max. interstory drift of the systems under earthquake Corinth Greece, 2/24/1981

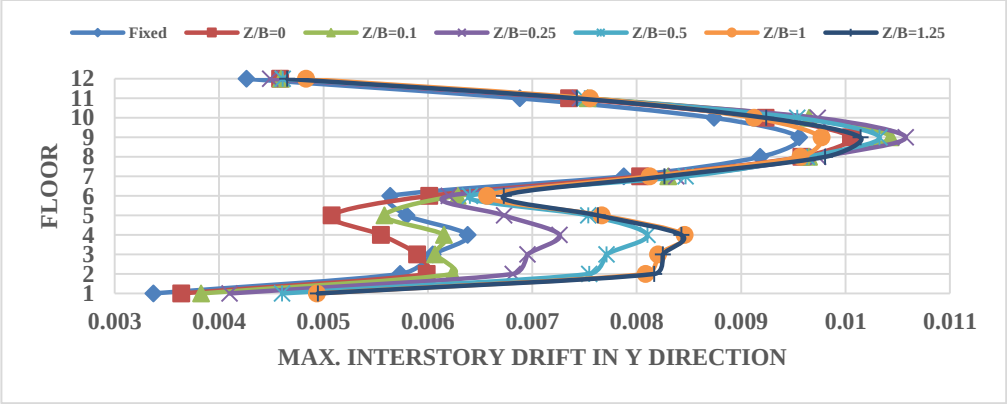


A) Uncontrolled Systems

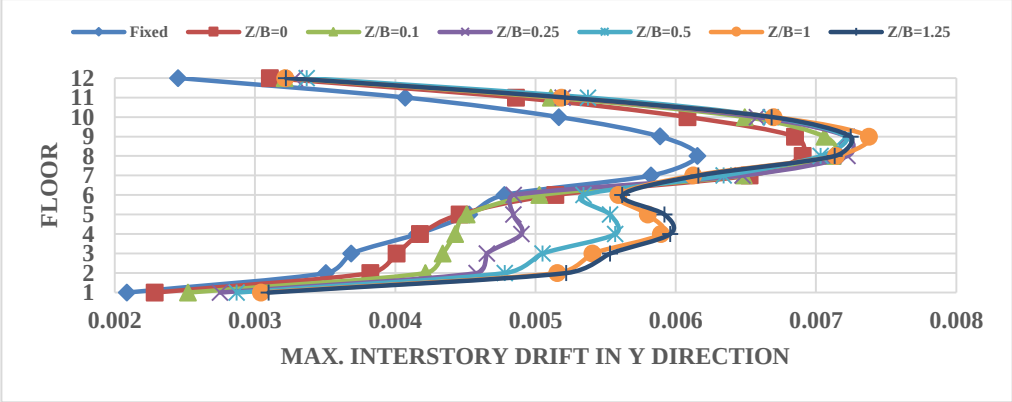


B) Controlled Systems SSI-SSI

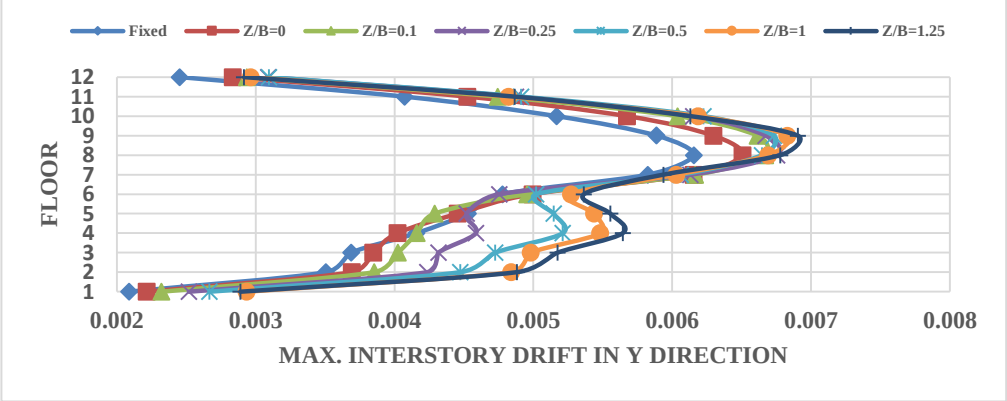


C) Controlled Systems Fixed-SSI

**Figure G-10** Max. interstory drift of the systems under earthquake Corinth Greece, 2/24/1981

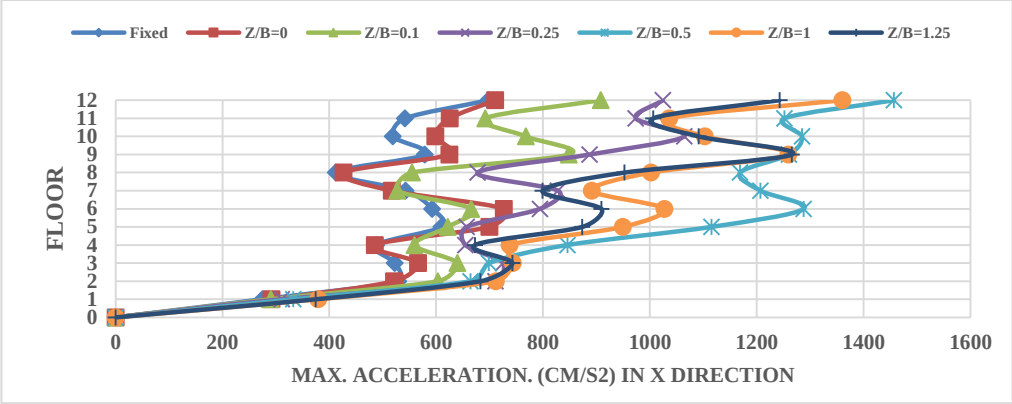


A) Uncontrolled Systems

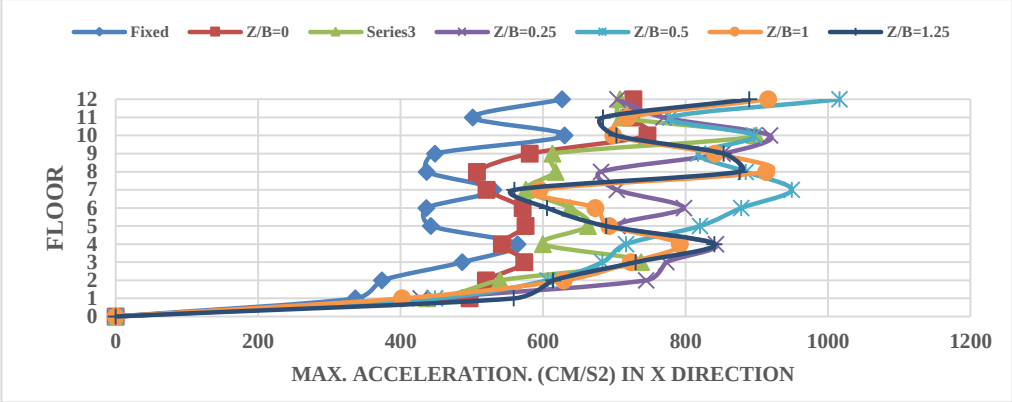


B) Controlled Systems SSI-SSI

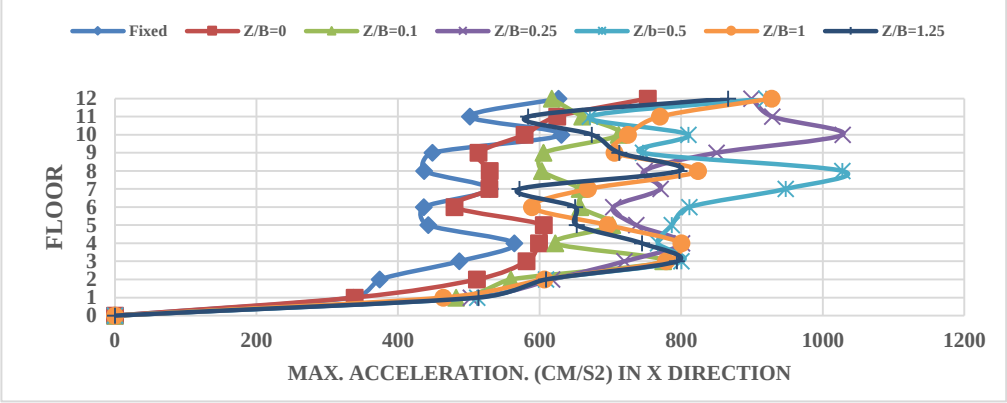


C) Controlled Systems Fixed-SSI

**Figure G-11** Max. acceleration of the systems under earthquake Corinth Greece,

2/24/1981

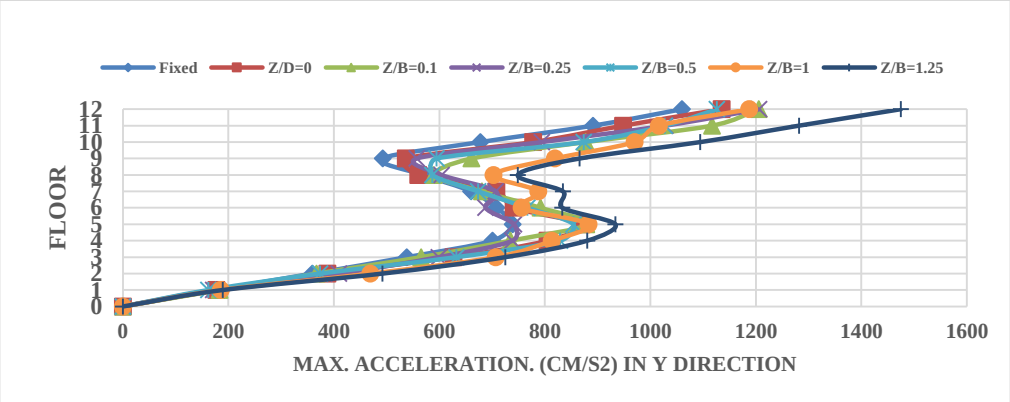


A) Uncontrolled Systems

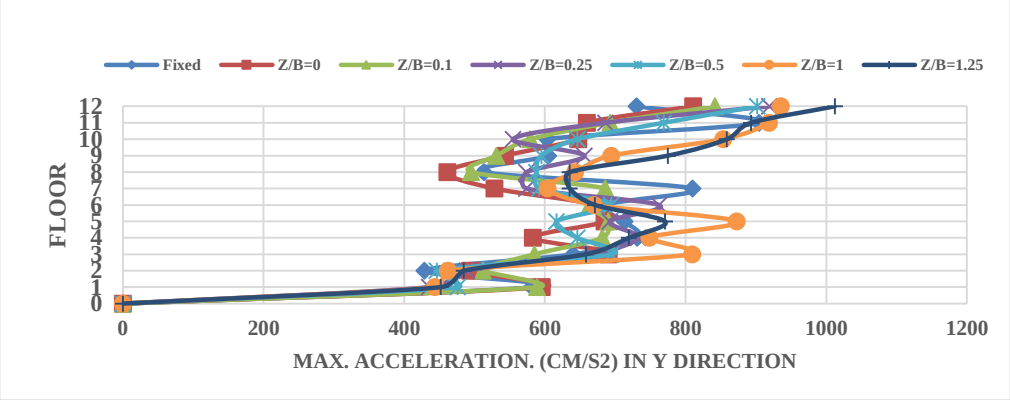


B) Controlled Systems SSI-SSI

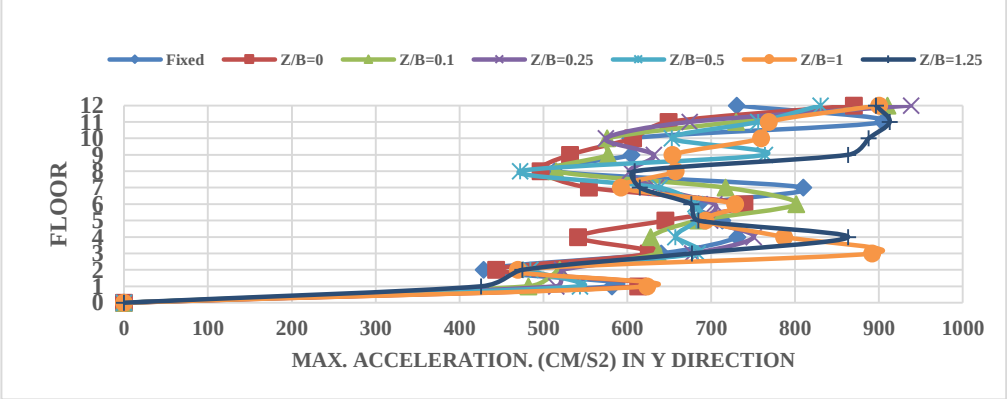


C) Controlled Systems Fixed-SSI

**Figure G-12** Max. acceleration of the systems under earthquake Corinth Greece, 2/24/1981

Medium top and soft bottom

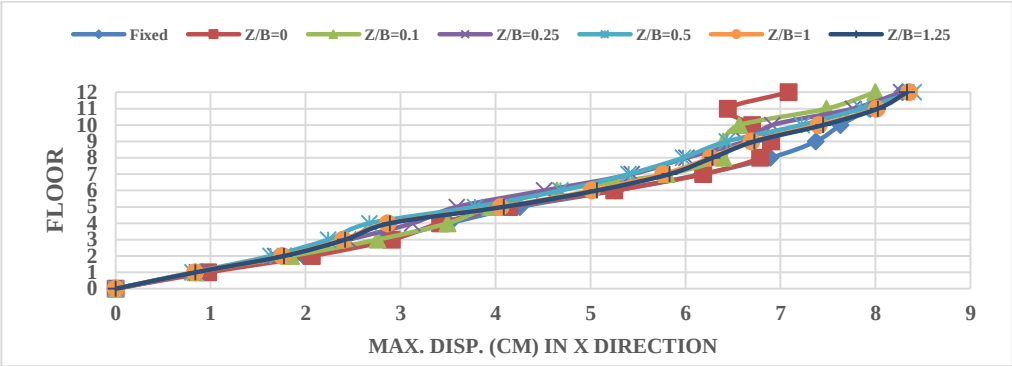


A) Uncontrolled Systems

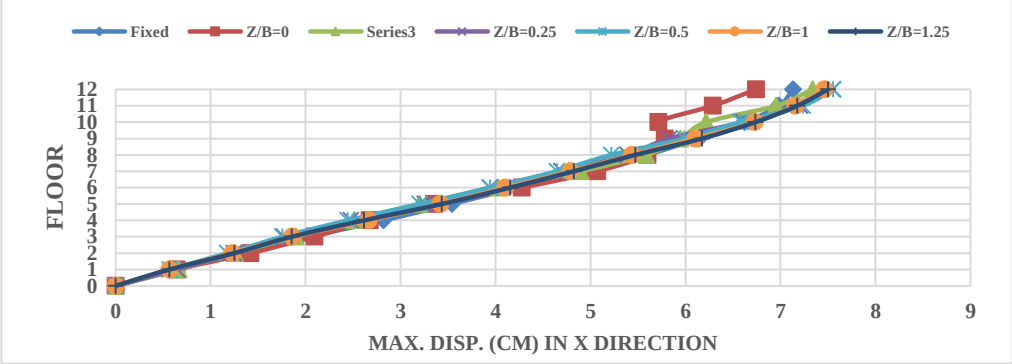


B) Controlled Systems SSI-SSI

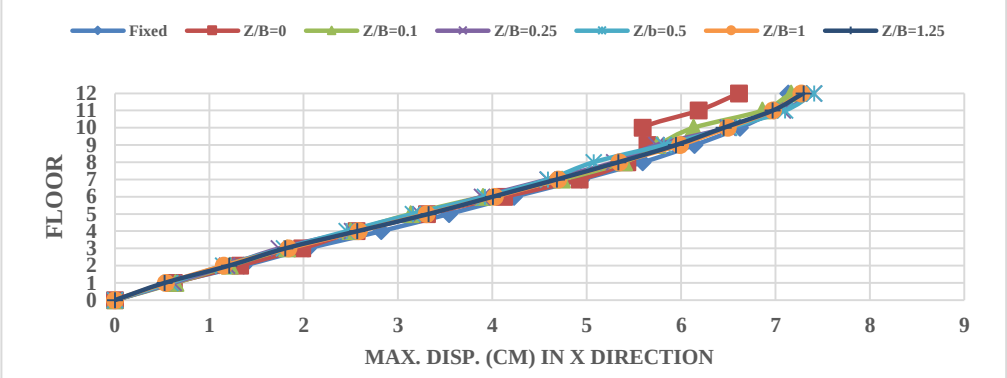


D) Controlled Systems Fixed-SSI

**Figure G-13** Max. displacements of the systems under earthquake Managua Nicaragua-02, 12/23/1972

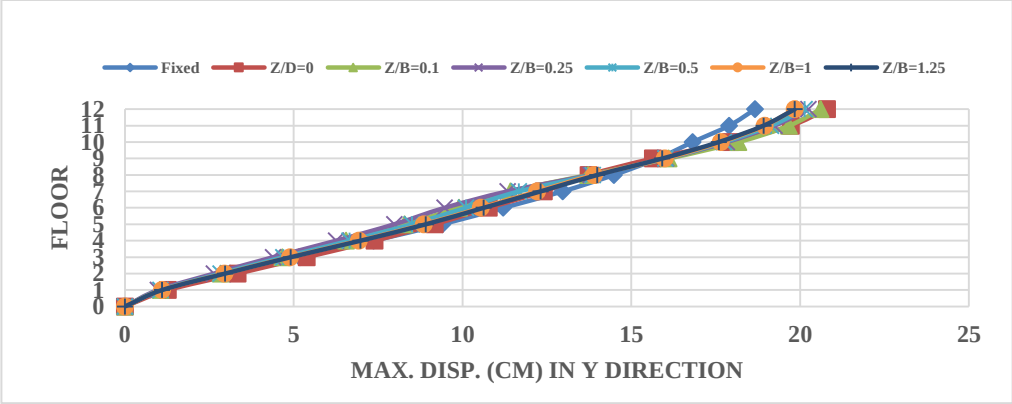


A) Uncontrolled Systems

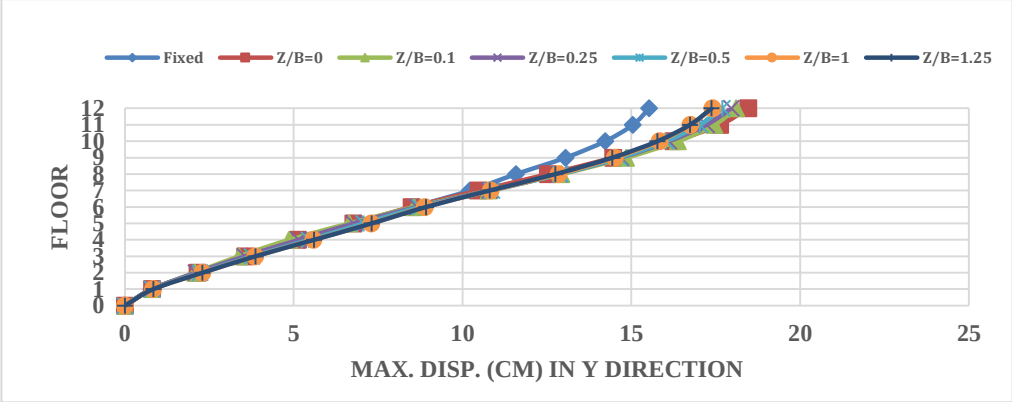


B) Controlled Systems SSI-SSI

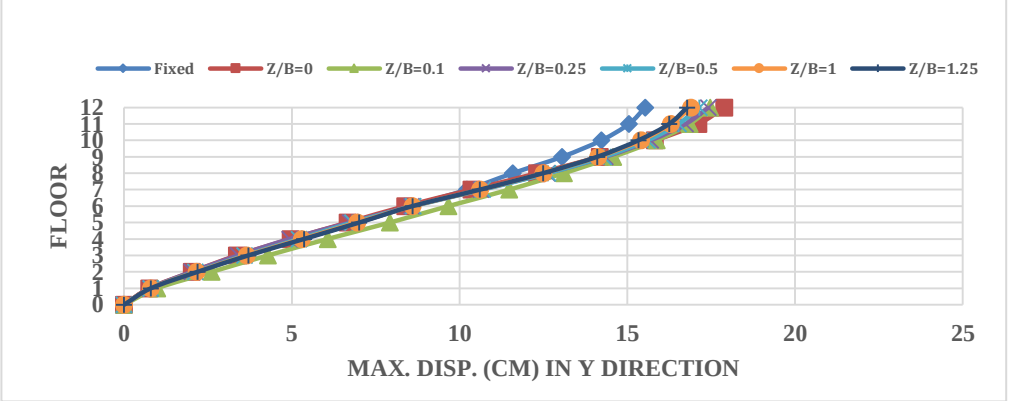


C) Controlled Systems Fixed-SSI

**Figure G-14** Max. displacements of the systems under earthquake Managua Nicaragua-02, 12/23/1972

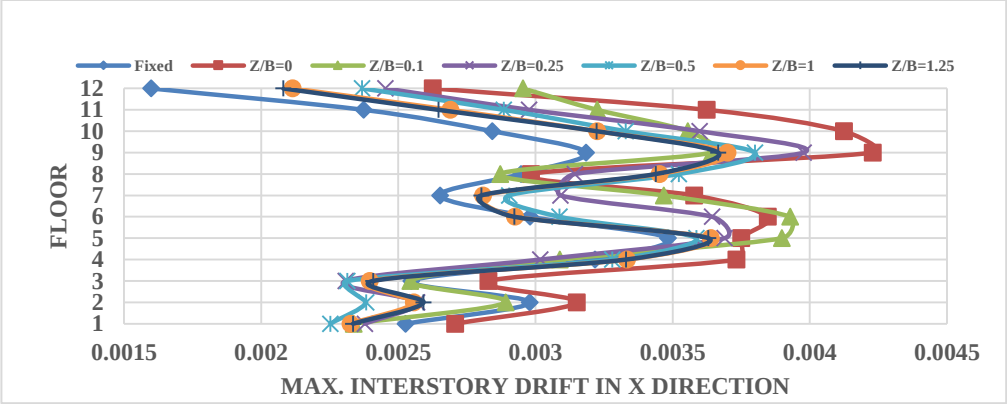


A) Uncontrolled Systems

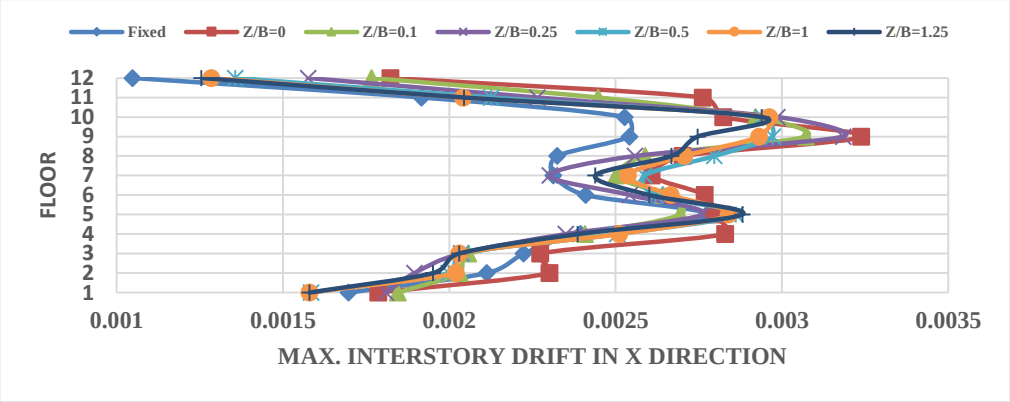


B) Controlled Systems SSI-SSI

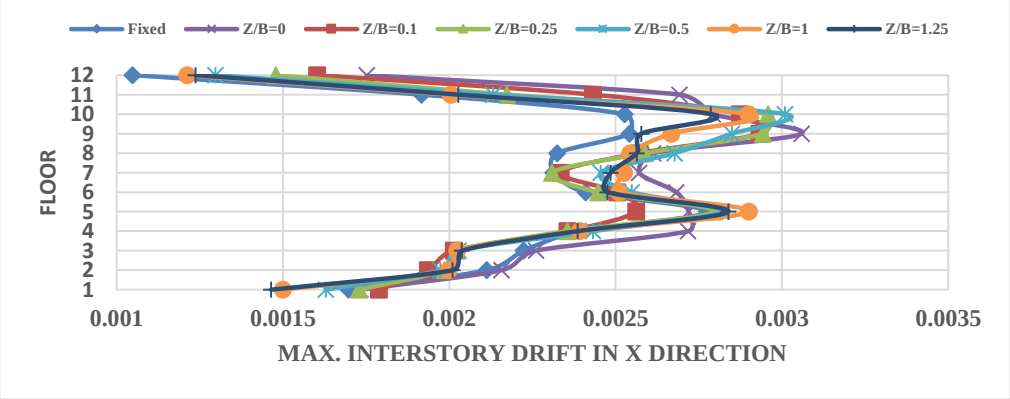


C) Controlled Systems Fixed-SSI

**Figure G-15** Max. interstory drift of the systems under earthquake Managua Nicaragua-02, 12/23/1972

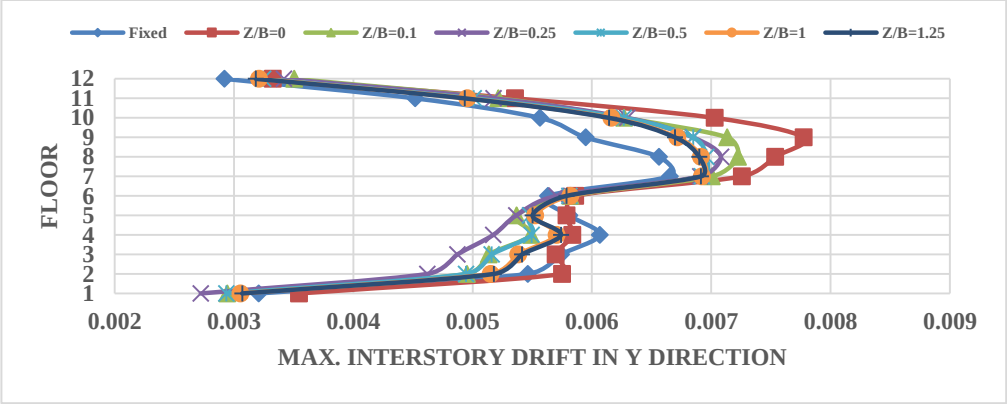


A) Uncontrolled Systems

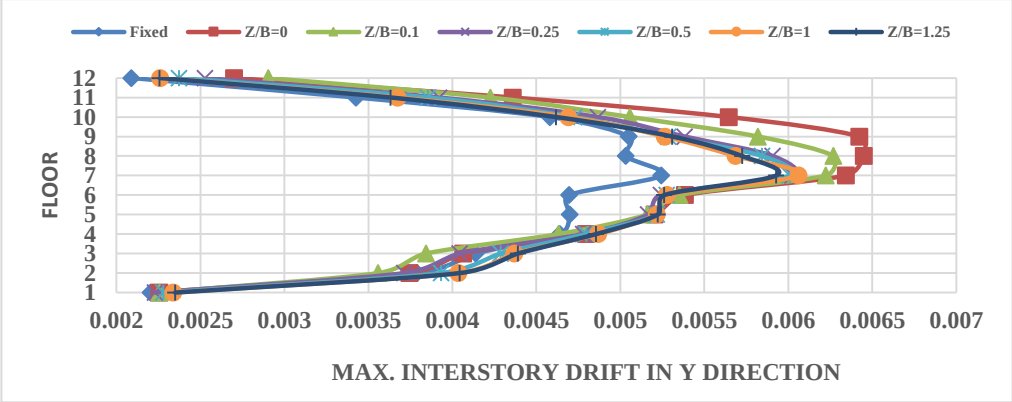


B) Controlled Systems SSI-SSI

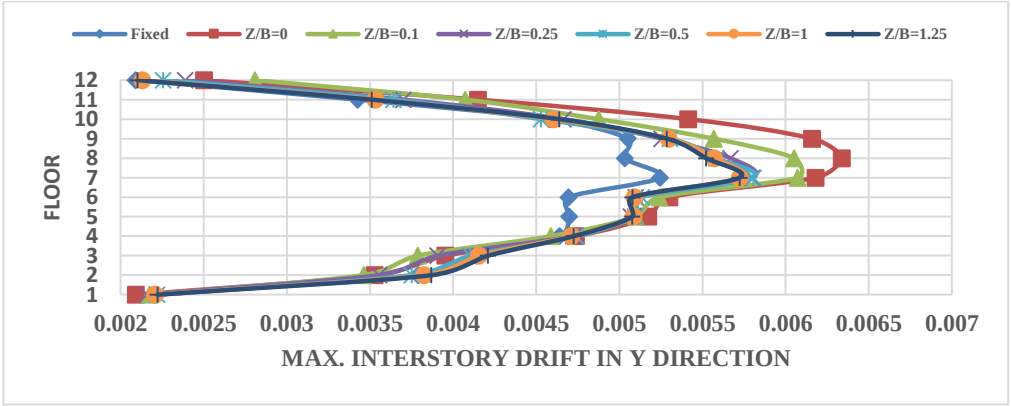


C) Controlled Systems Fixed-SSI

**Figure G-16** Max. interstory drift of the systems under earthquake Managua Nicaragua-02, 12/23/1972

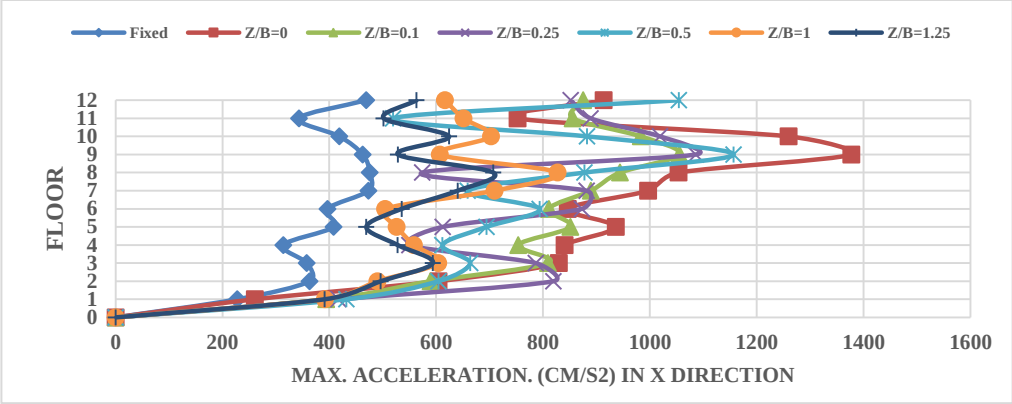


A) Uncontrolled Systems

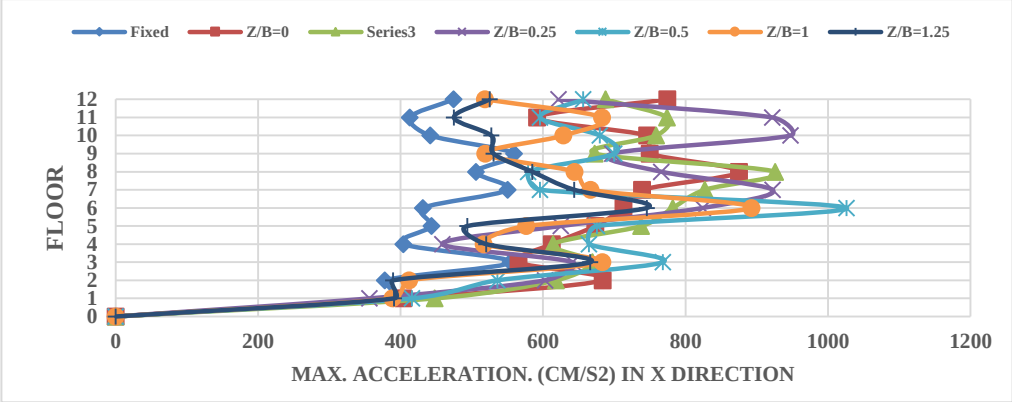


B) Controlled Systems SSI-SSI

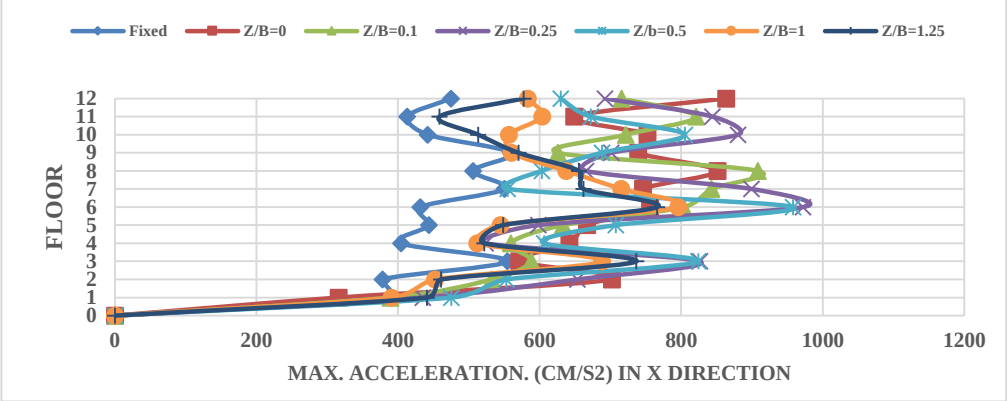


C) Controlled Systems Fixed-SSI

**Figure G-17** Max. acceleration of the systems under earthquake Managua Nicaragua-02, 12/23/1972

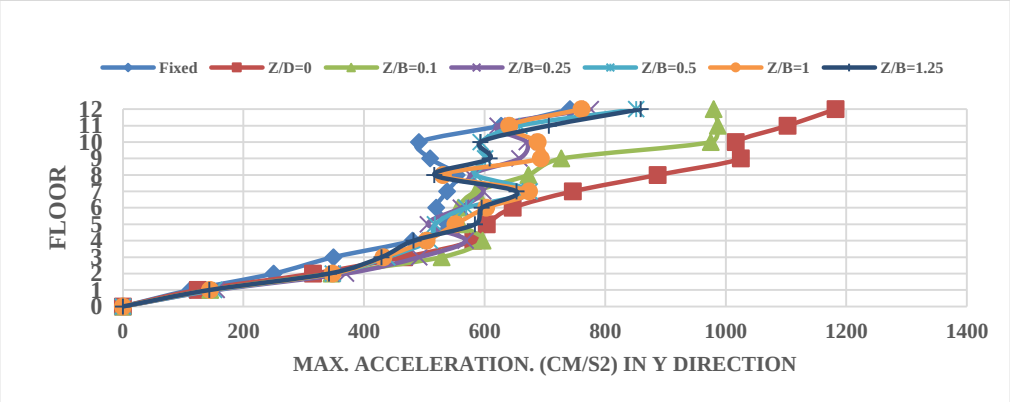


A) Uncontrolled Systems

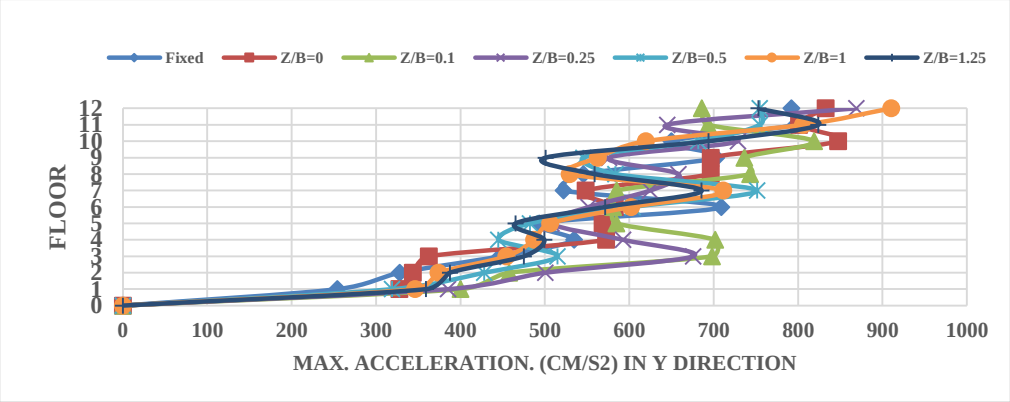


B) Controlled Systems SSI-SSI

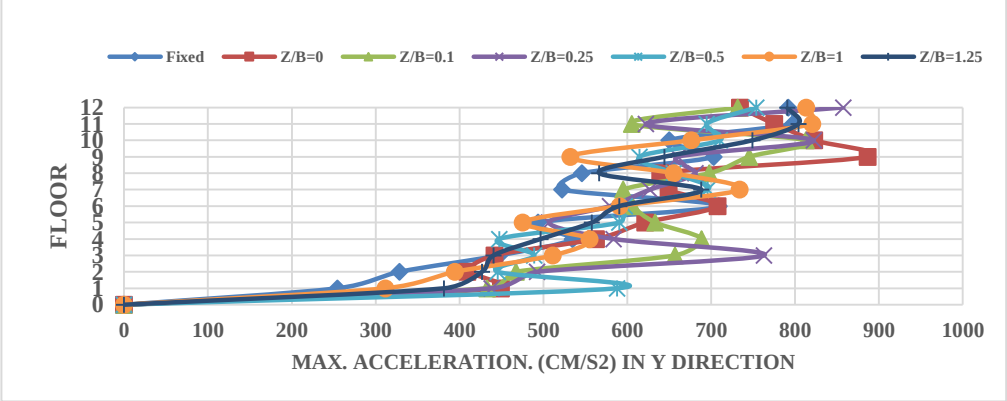


C) Controlled Systems Fixed-SSI

**Figure G-17** Max. acceleration of the systems under earthquake Managua Nicaragua-02, 12/23/1972

Soft top and medium bottom

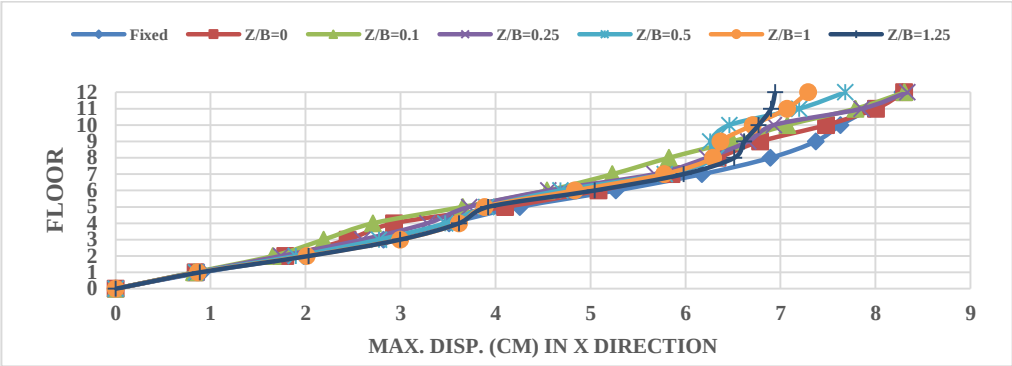


A) Uncontrolled Systems

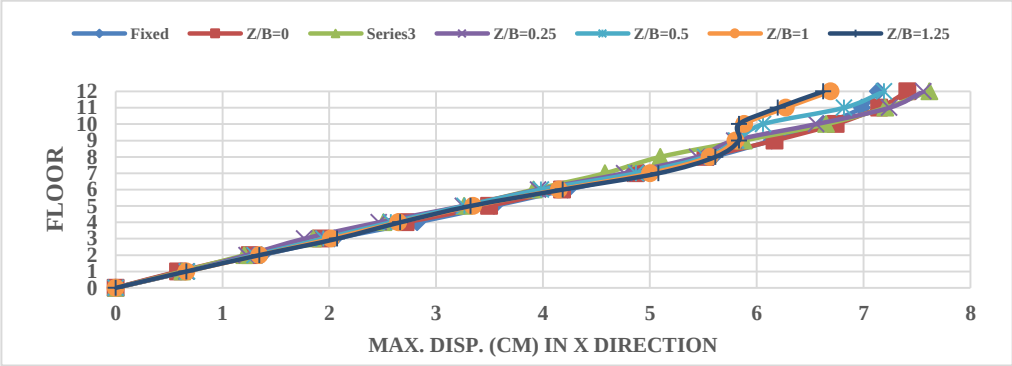


B) Controlled Systems SSI-SSI

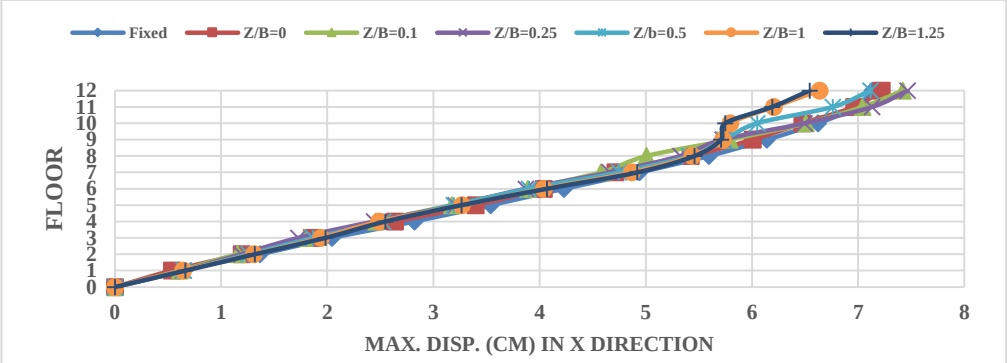


C) Controlled Systems Fixed-SSI

**Figure G-19** Max. displacements of the systems under earthquake Managua Nicaragua-02, 12/23/1972

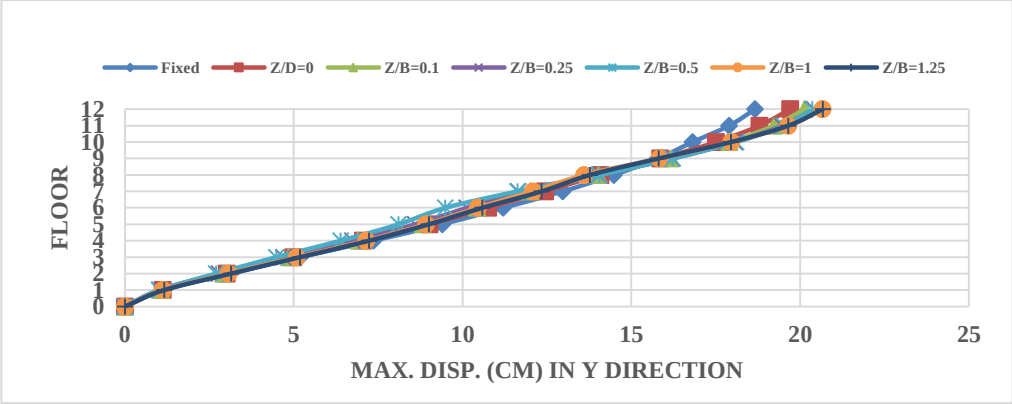


A) Uncontrolled Systems

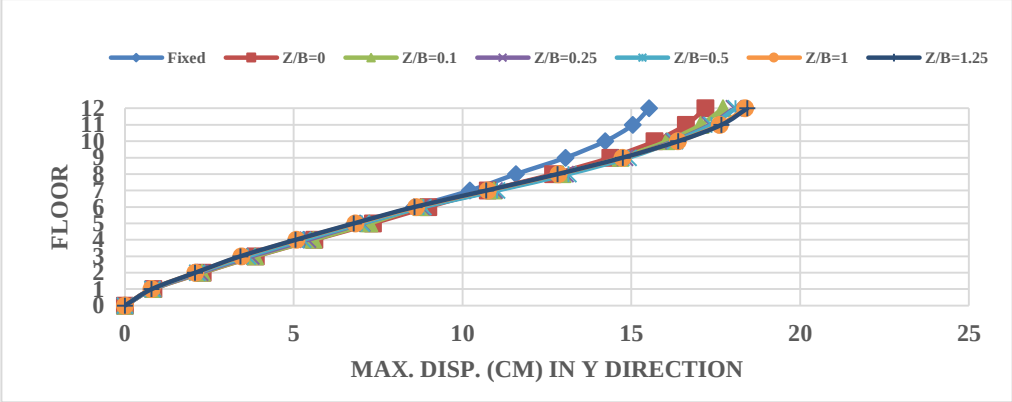


B) Controlled Systems SSI-SSI

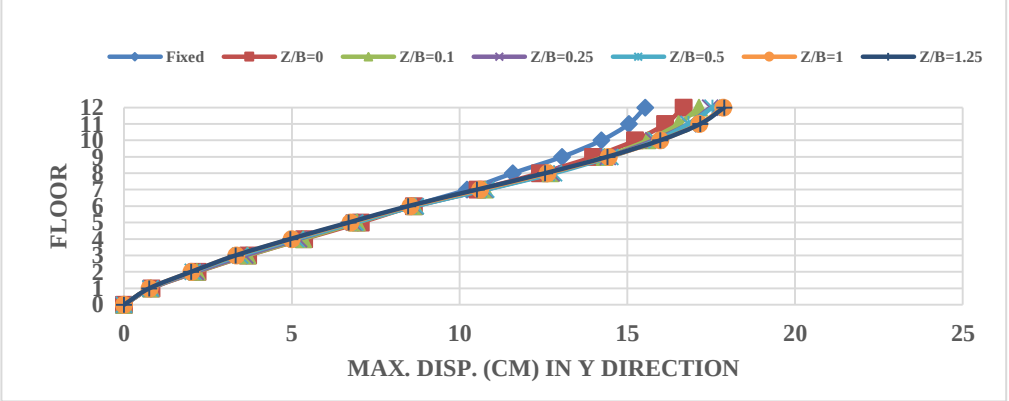


C) Controlled Systems Fixed-SSI

**Figure G-20** Max. displacements of the systems under earthquake Managua Nicaragua-02, 12/23/1972

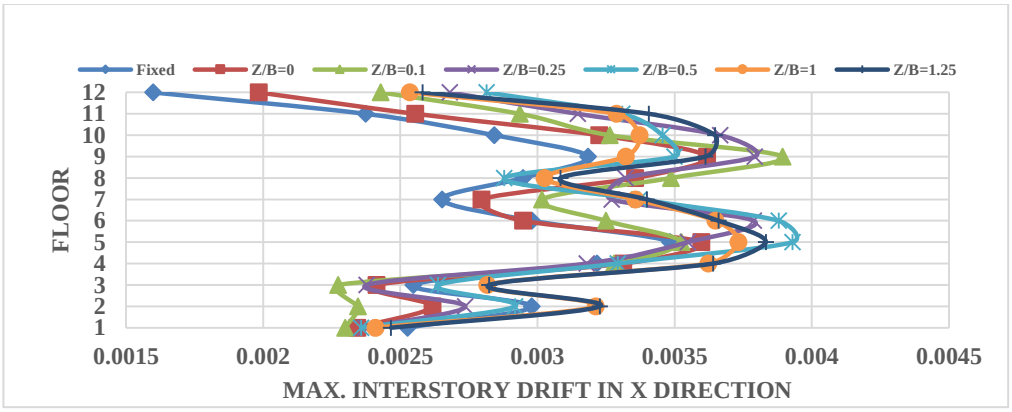


A) Uncontrolled Systems

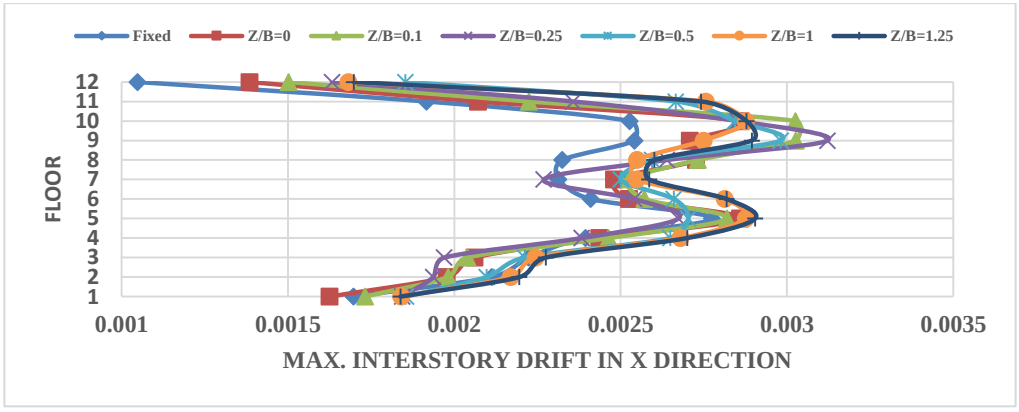


B) Controlled Systems SSI-SSI

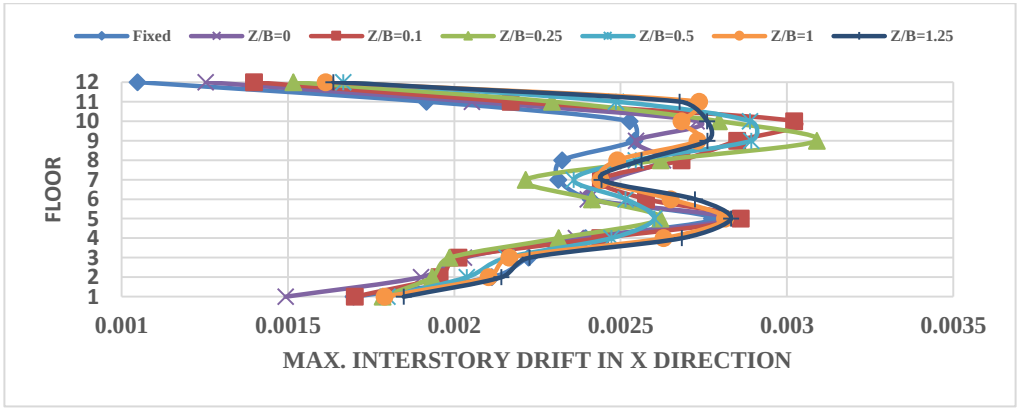


C) Controlled Systems Fixed-SSI

**Figure G-21** Max. interstory drift of the systems under earthquake Managua Nicaragua-02, 12/23/1972

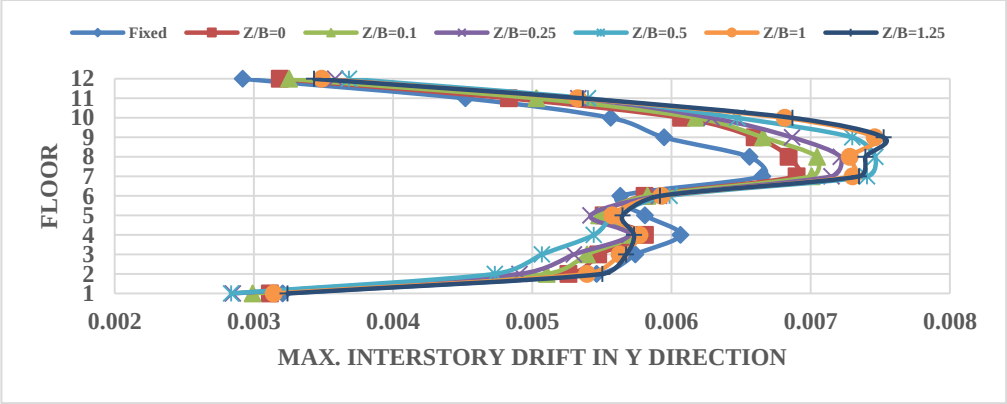


A) Uncontrolled Systems

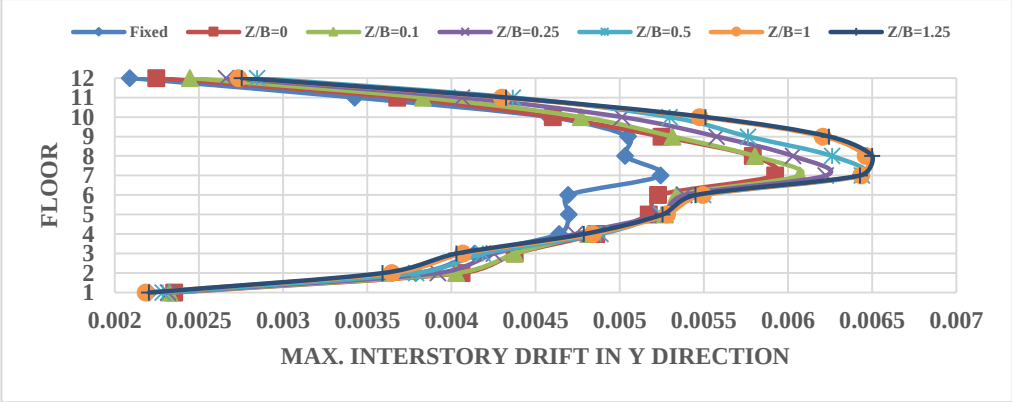


B) Controlled Systems SSI-SSI

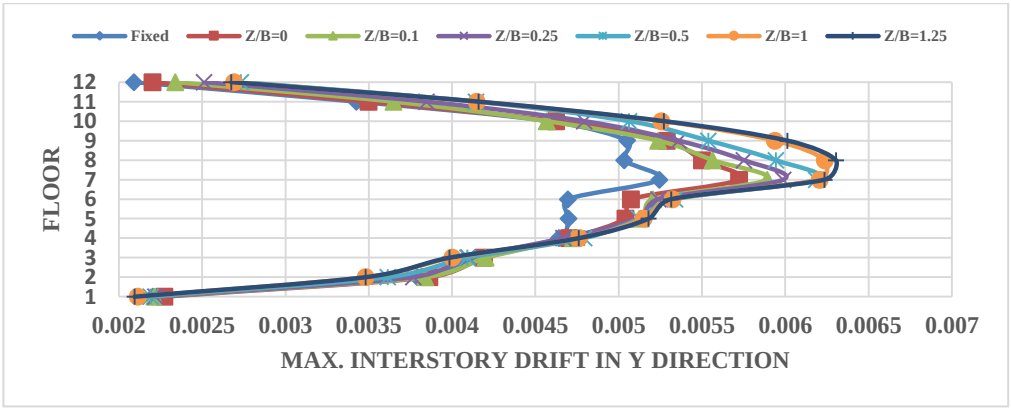


C) Controlled Systems Fixed-SSI

**Figure G-22** Max. interstory drift of the systems under earthquake Managua Nicaragua-02, 12/23/1972

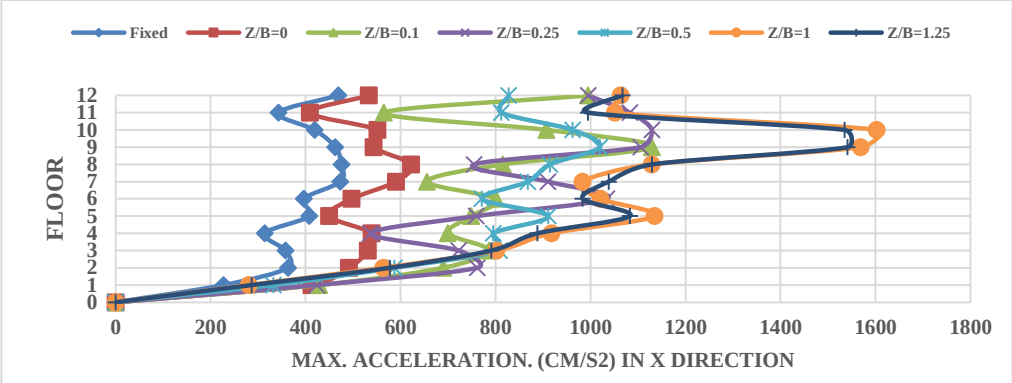


A) Uncontrolled Systems

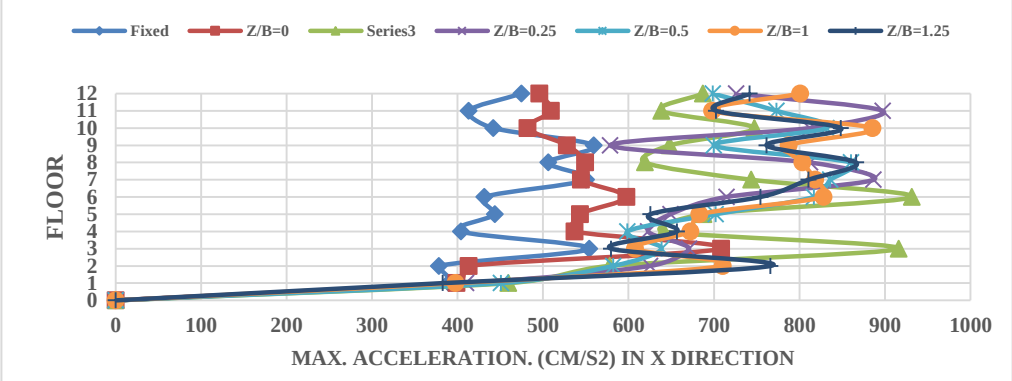


B) Controlled Systems SSI-SSI

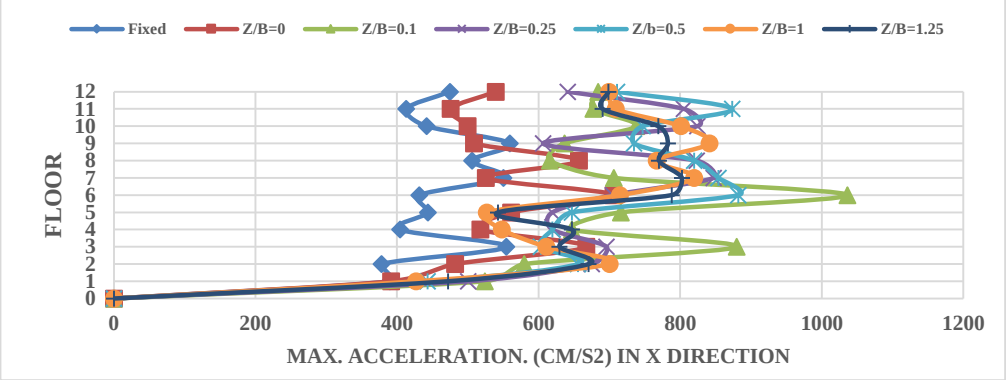


C) Controlled Systems Fixed-SSI

**Figure G-23** Max. acceleration of the systems under earthquake Managua Nicaragua-02, 12/23/1972

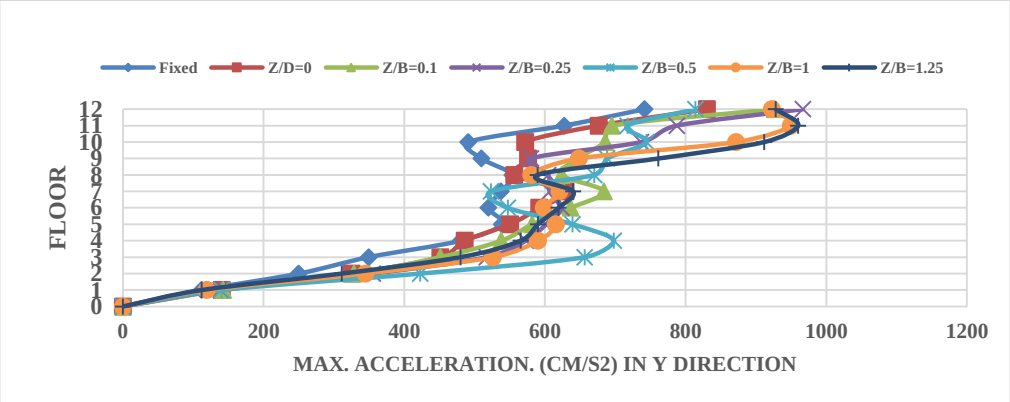


A) Uncontrolled Systems

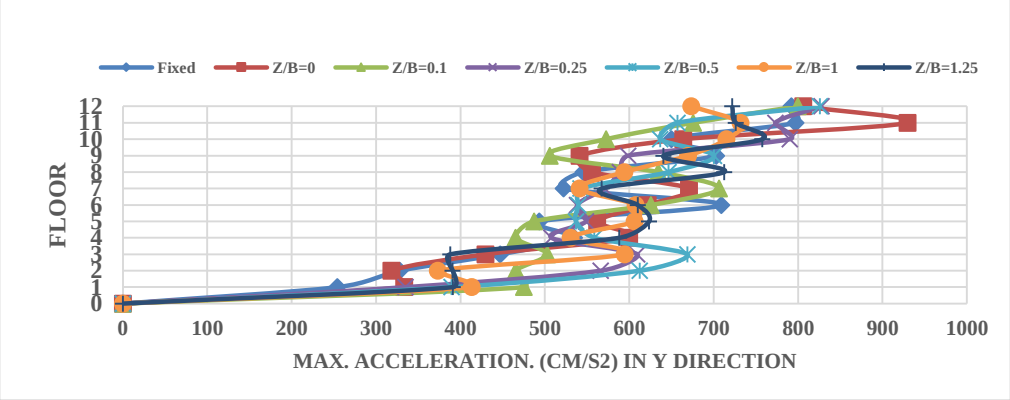


B) Controlled Systems SSI-SSI

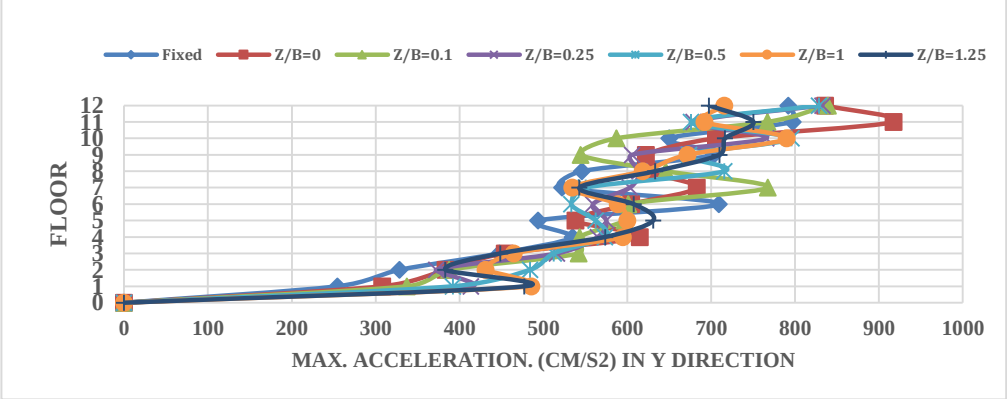


C) Controlled Systems Fixed-SSI

**Figure G-24** Max. acceleration of the systems under earthquake Managua Nicaragua-02, 12/23/1972

Soil profile clay (linear)

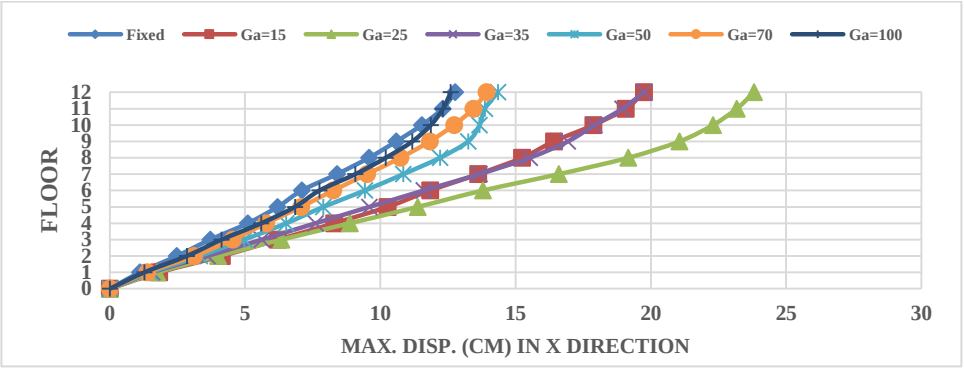


A) Uncontrolled Systems

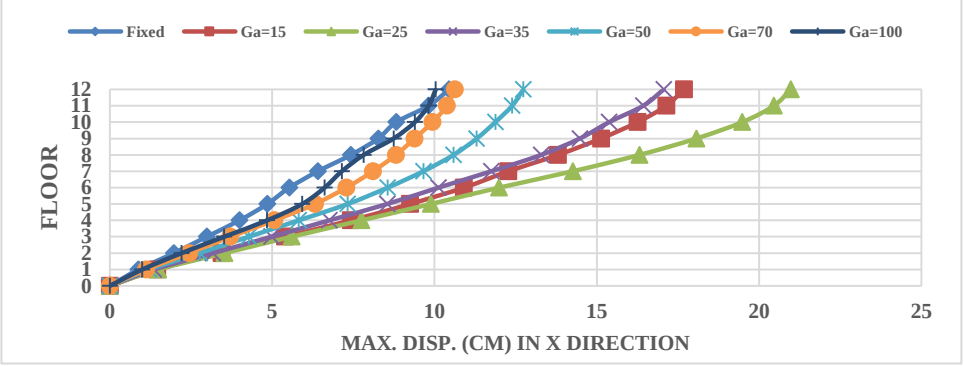


B) Controlled Systems SSI-SSI

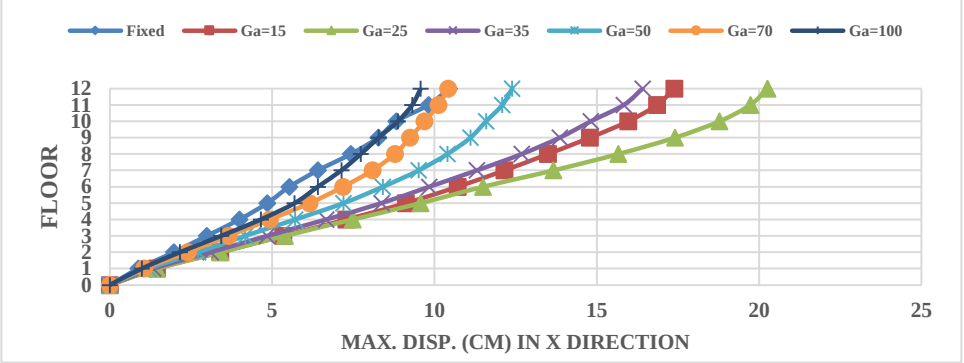


C) Controlled Systems Fixed-SSI

**Figure G-25** Max. displacements of the systems under earthquake Corinth Greece, 2/24/1981

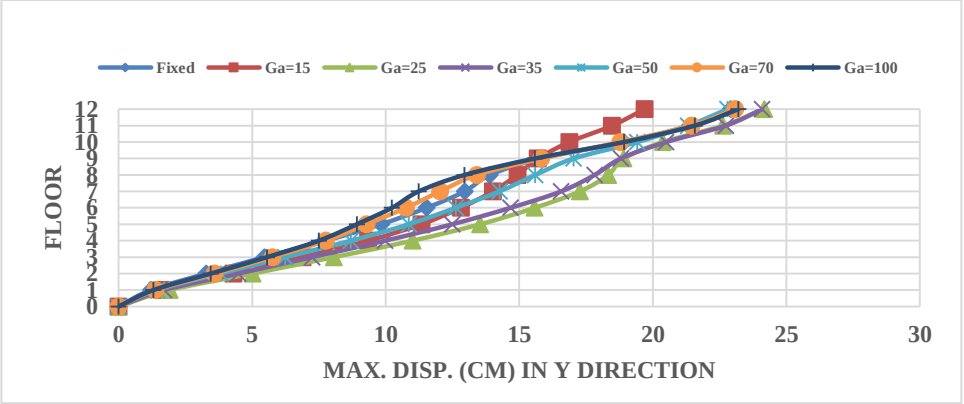


A) Uncontrolled Systems

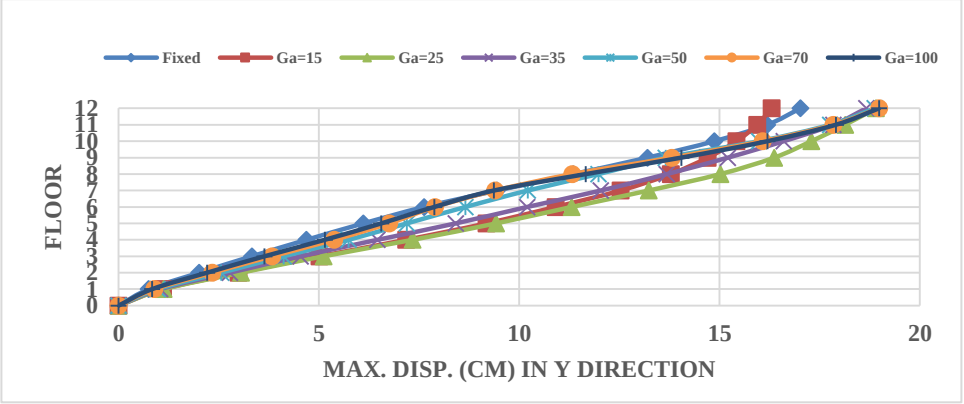


B) Controlled Systems SSI-SSI

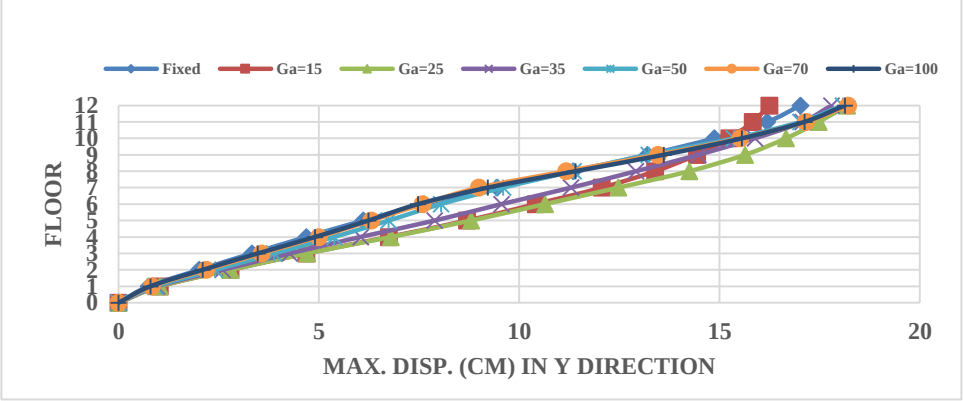


C) Controlled Systems Fixed-SSI

**Figure G-26** Max. displacements of the systems under earthquake Corinth Greece, 2/24/1981

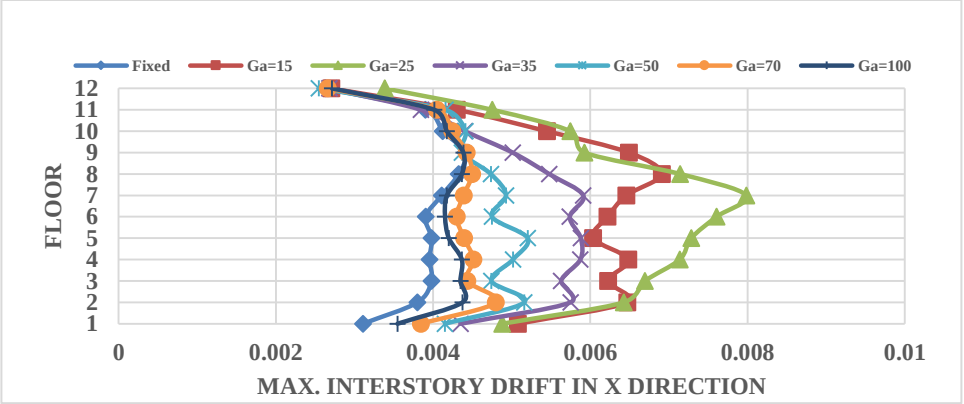


A) Uncontrolled Systems

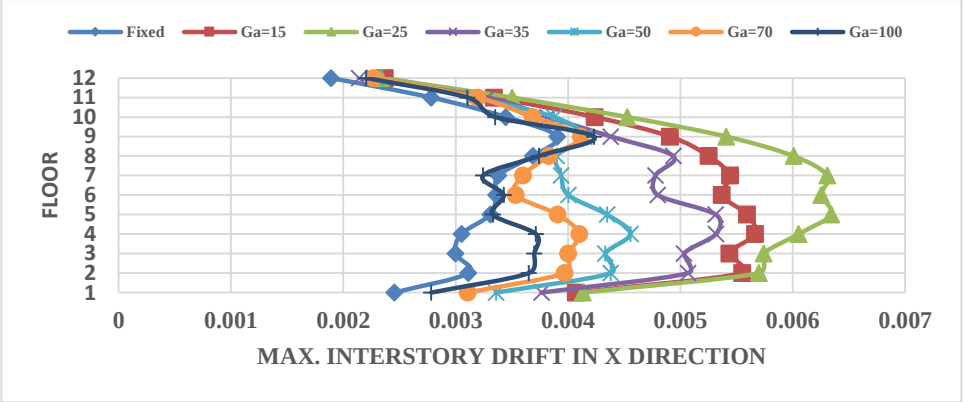


B) Controlled Systems SSI-SSI

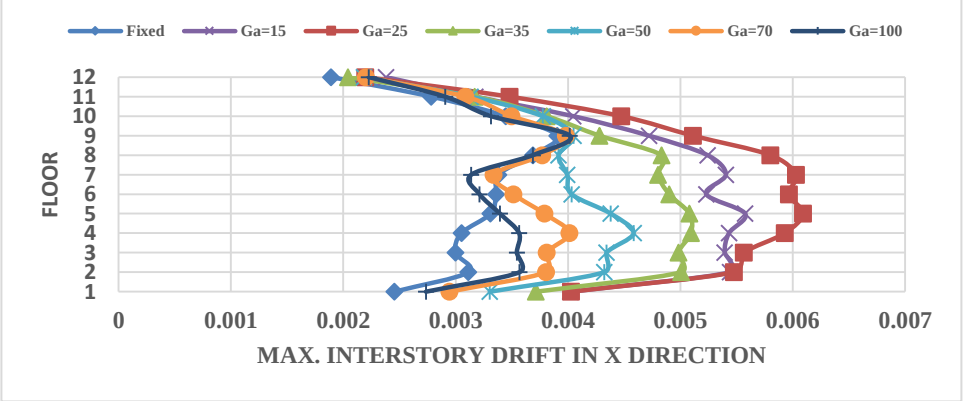


C) Controlled Systems Fixed-SSI

**Figure G-27** Max. interstory drift of the systems under earthquake Corinth Greece, 2/24/1981

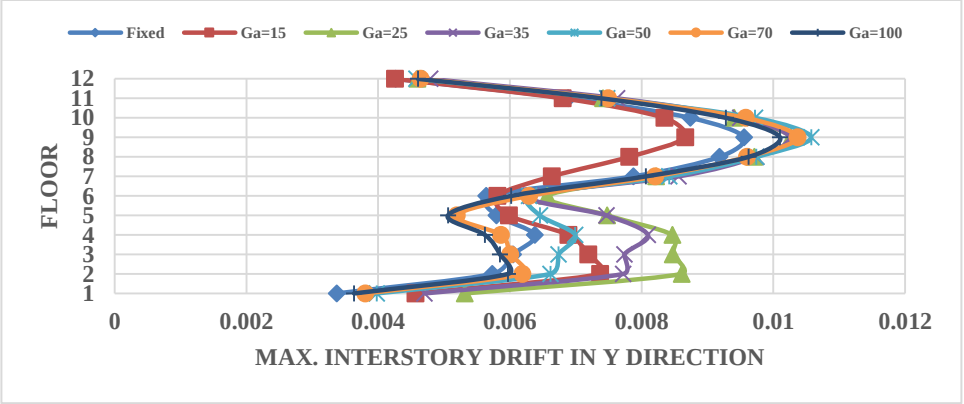


A) Uncontrolled Systems

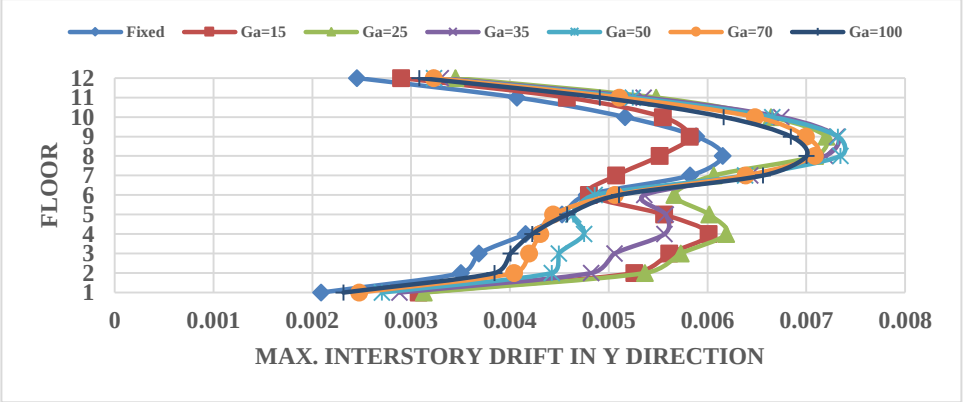


B) Controlled Systems SSI-SSI

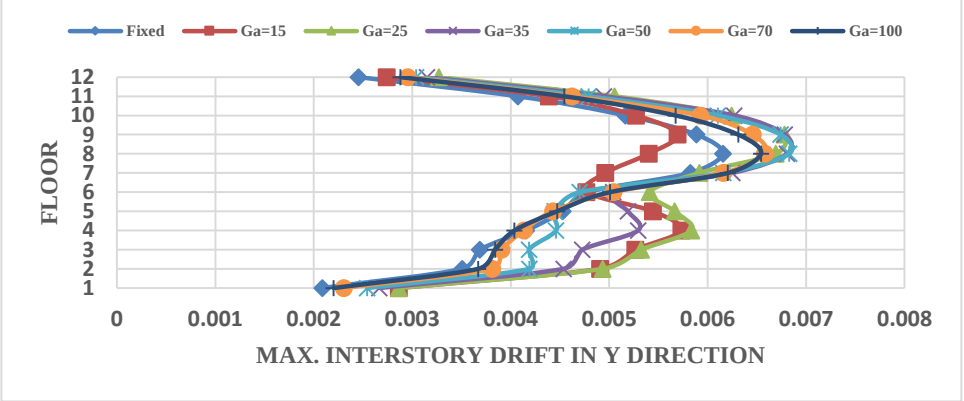


C) Controlled Systems Fixed-SSI

**Figure G-28** Max. interstory drift of the systems under earthquake Corinth Greece, 2/24/1981

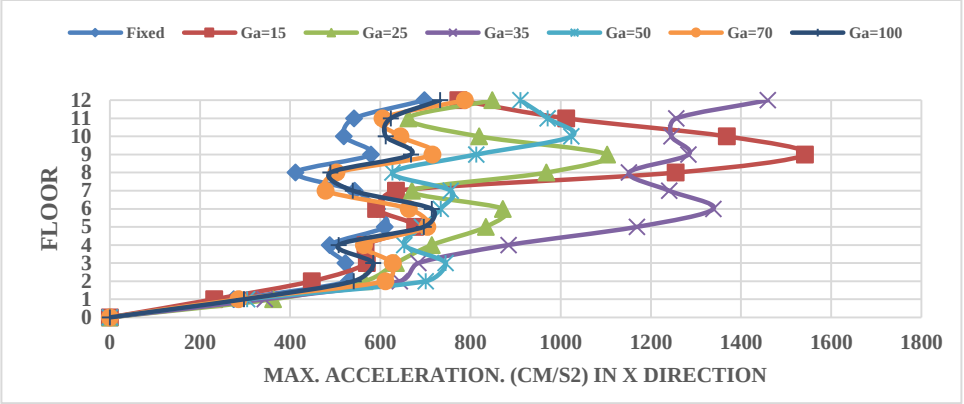


A) Uncontrolled Systems

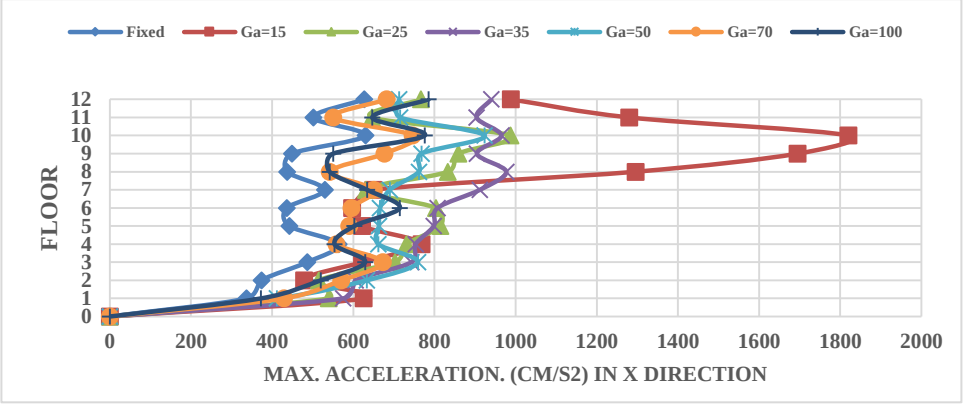


B) Controlled Systems SSI-SSI

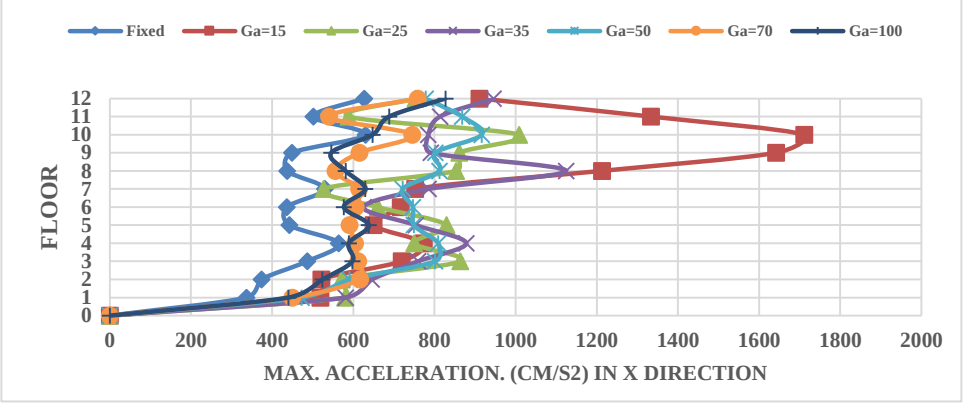


C) Controlled Systems Fixed-SSI

**Figure G-29** Max. acceleration of the systems under earthquake Corinth Greece, 2/24/1981

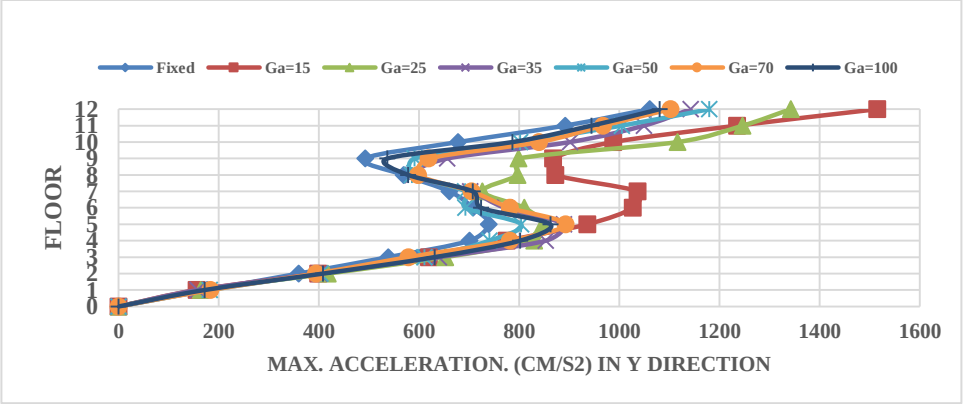


A) Uncontrolled Systems

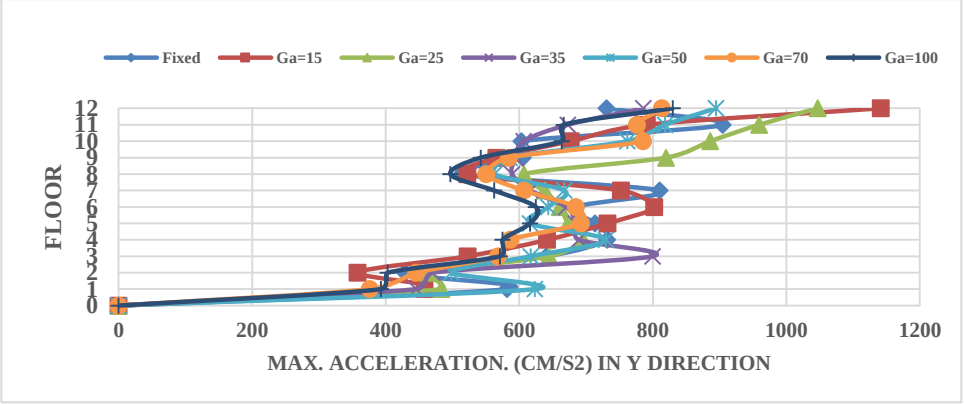


B) Controlled Systems SSI-SSI

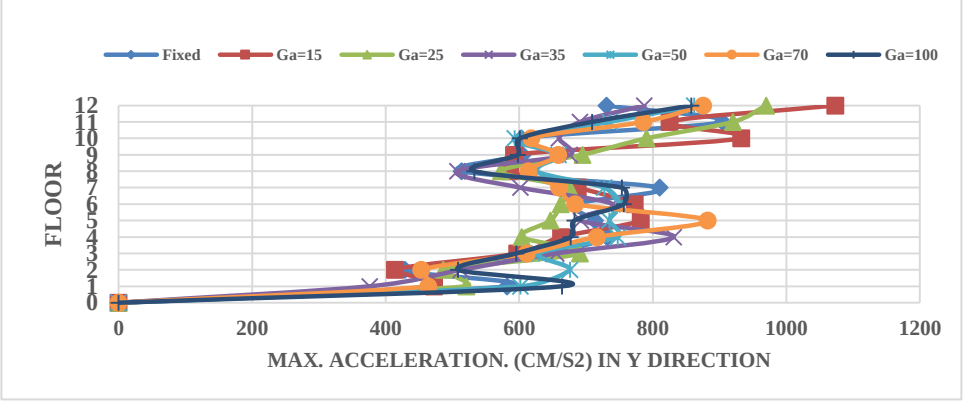


C) Controlled Systems Fixed-SSI

**Figure G-30** Max. acceleration of the systems under earthquake Corinth Greece, 2/24/1981

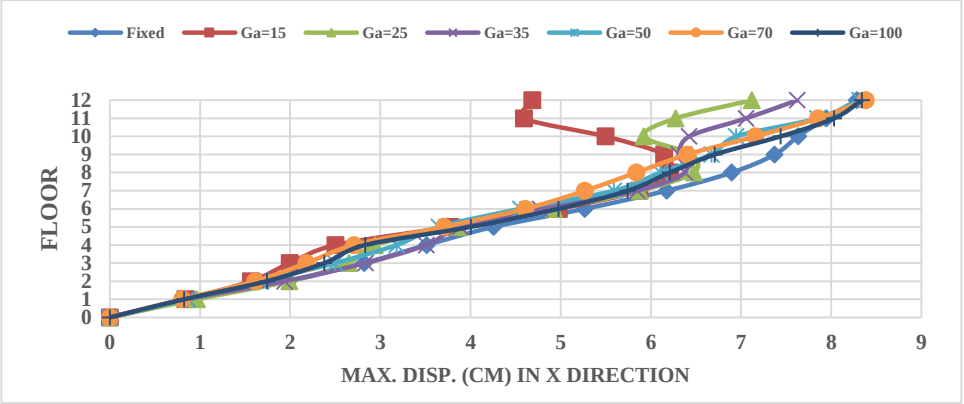


A) Uncontrolled Systems

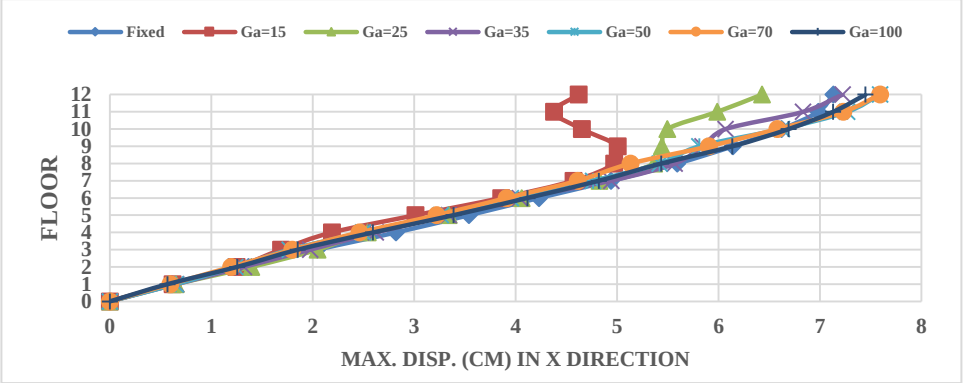


B) Controlled Systems SSI-SSI

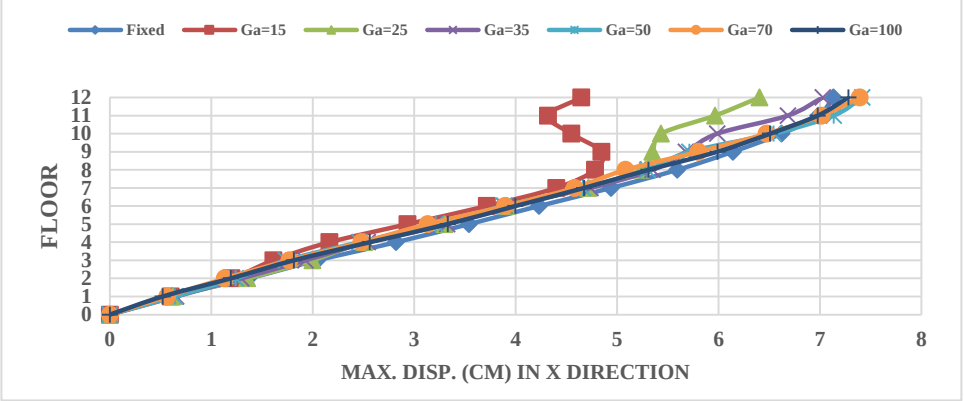


C) Controlled Systems Fixed-SSI

**Figure G-31** Max. displacements of the systems under earthquake Managua Nicaragua-02, 12/23/1972

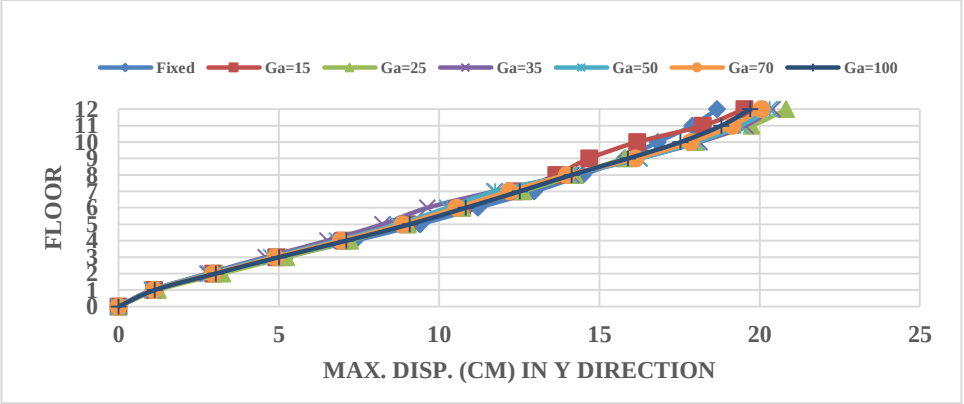


A) Uncontrolled Systems

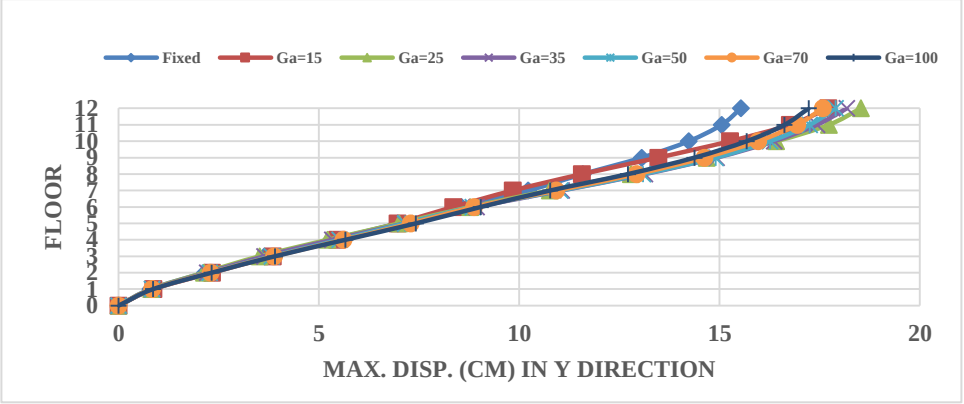


B) Controlled Systems SSI-SSI

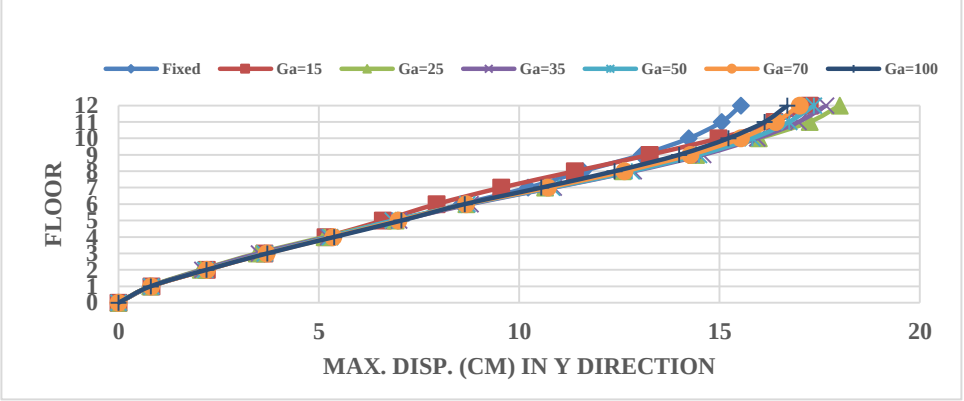


C) Controlled Systems Fixed-SSI

**Figure G-32** Max. displacements of the systems under earthquake Managua Nicaragua-02, 12/23/1972

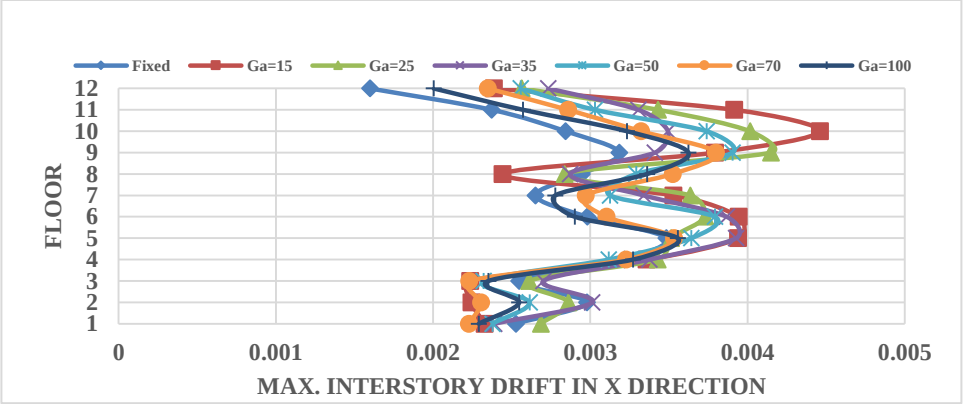


A) Uncontrolled Systems

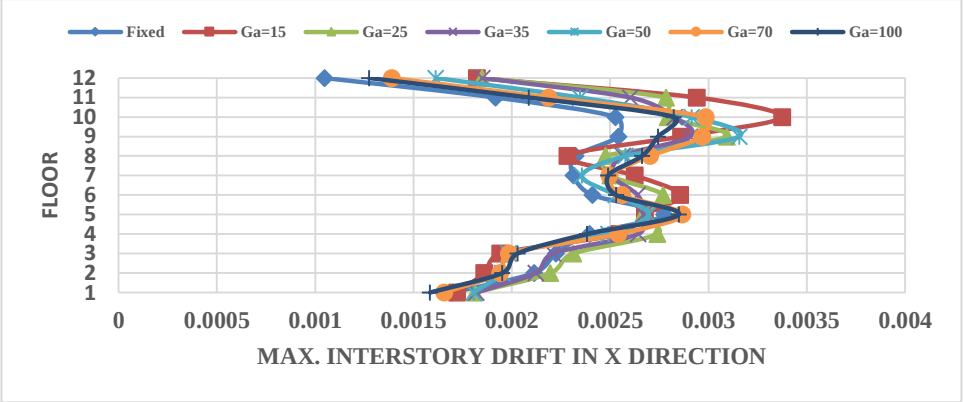


B) Controlled Systems SSI-SSI

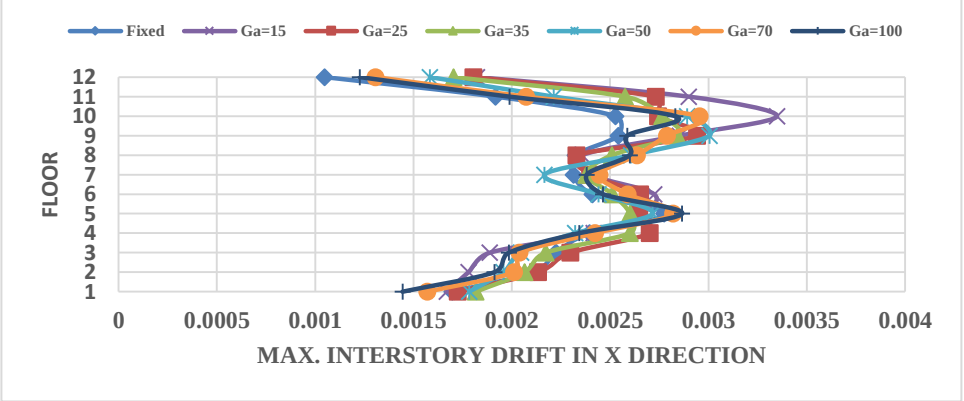


C) Controlled Systems Fixed-SSI

**Figure G-33** Max. interstory drift of the systems under earthquake Managua Nicaragua-02, 12/23/1972

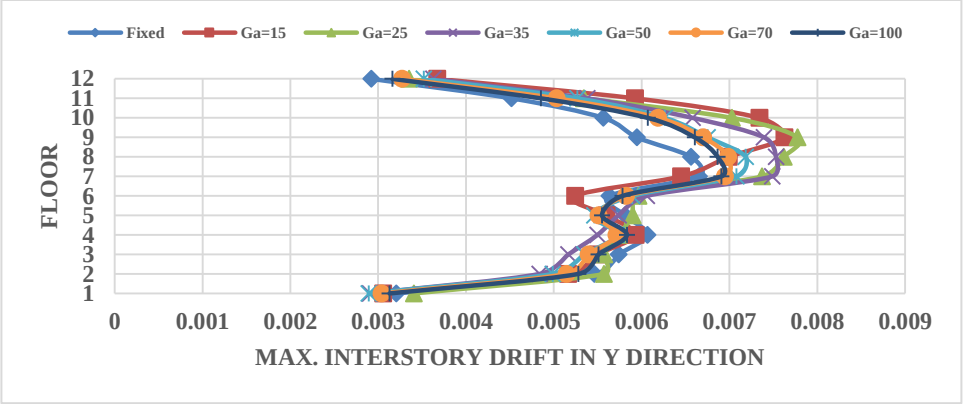


A) Uncontrolled Systems

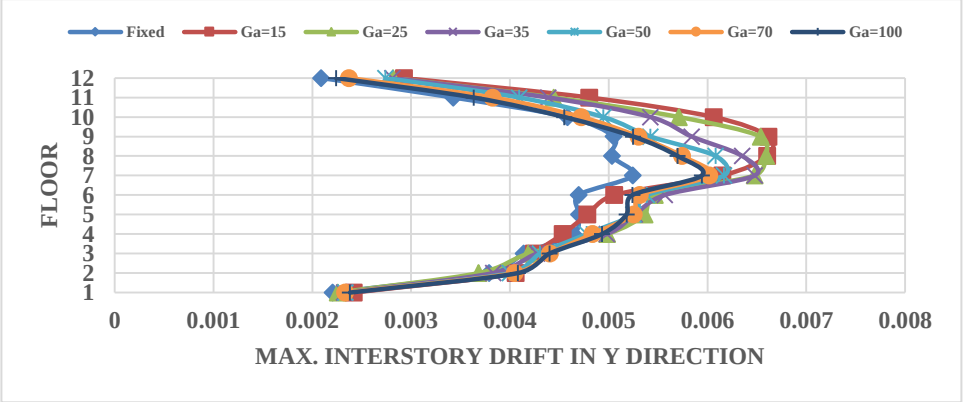


B) Controlled Systems SSI-SSI

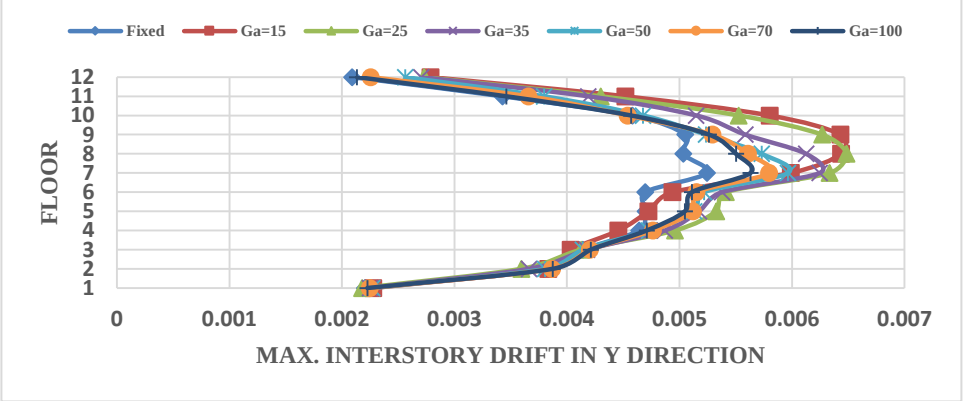


C) Controlled Systems Fixed-SSI

**Figure G-34** Max. interstory drift of the systems under earthquake Managua Nicaragua-02, 12/23/1972

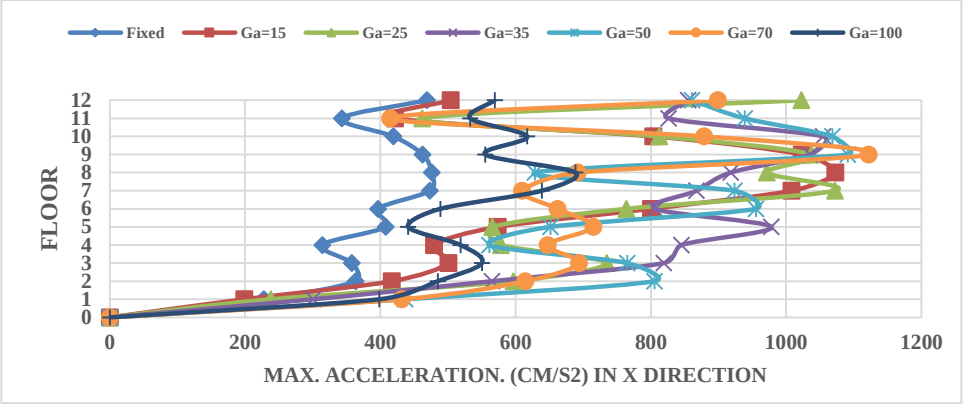


A) Uncontrolled Systems

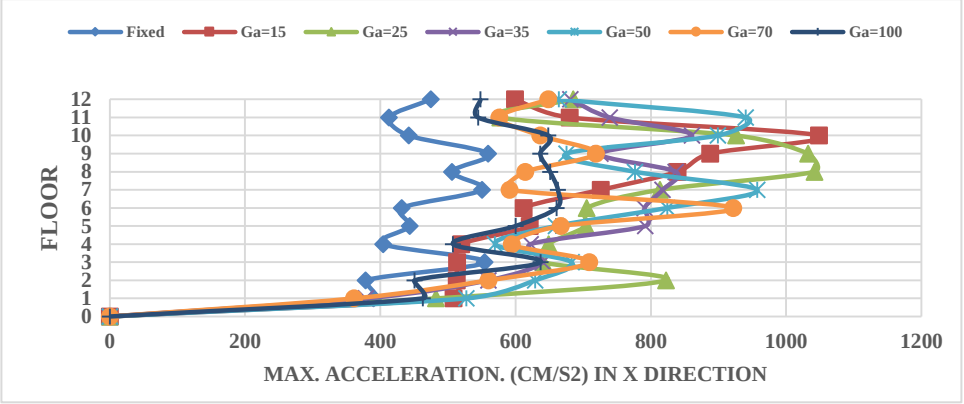


B) Controlled Systems SSI-SSI

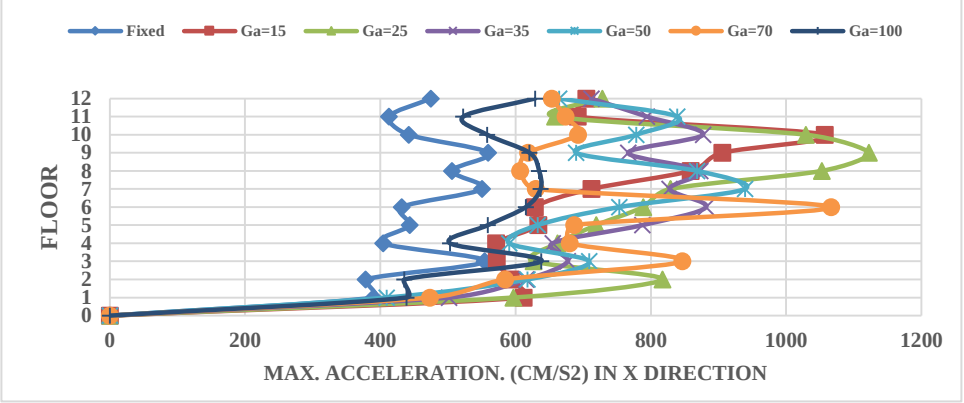


C) Controlled Systems Fixed-SSI

**Figure G-35** Max. acceleration of the systems under earthquake Managua Nicaragua-02,

12/23/1972

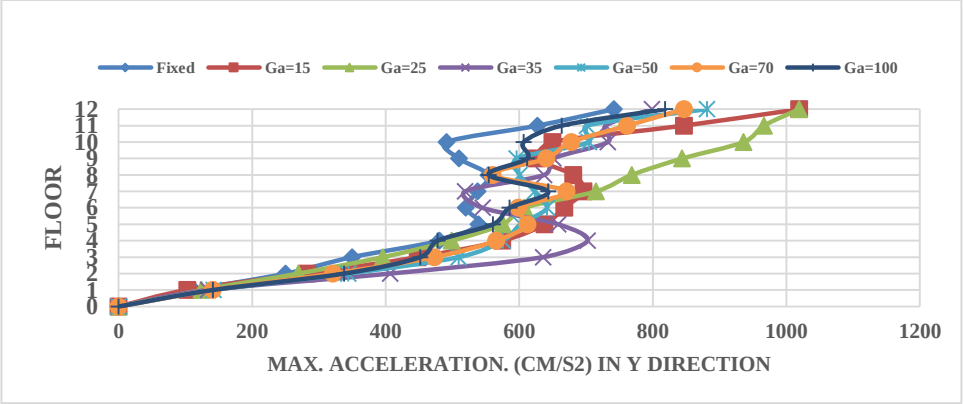


A) Uncontrolled Systems

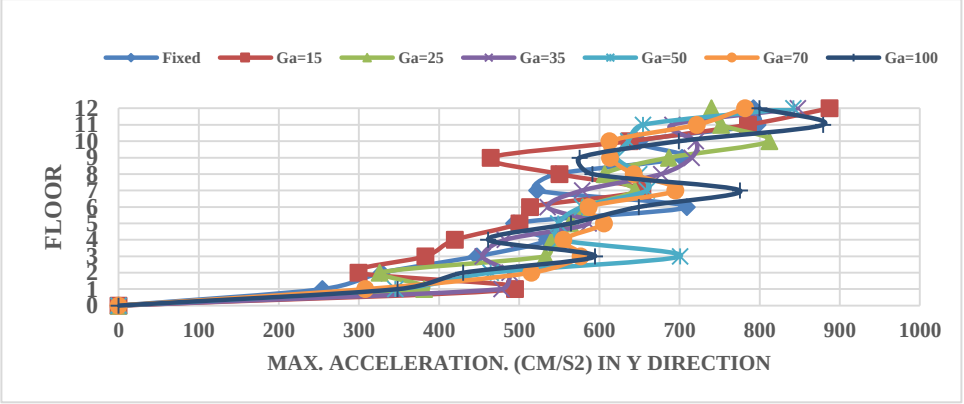


B) Controlled Systems SSI-SSI

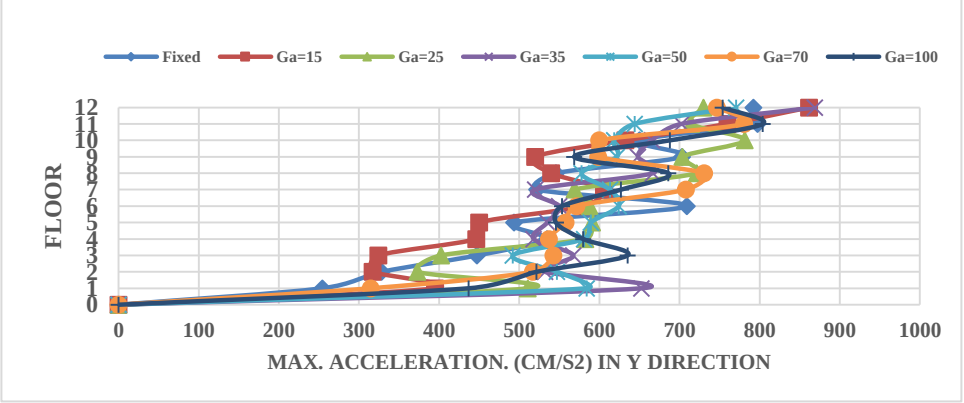


C) Controlled Systems Fixed-SSI

**Figure G-36** Max. acceleration of the systems under earthquake Managua Nicaragua-02, 12/23/1972

Soil profile sand (parabola)

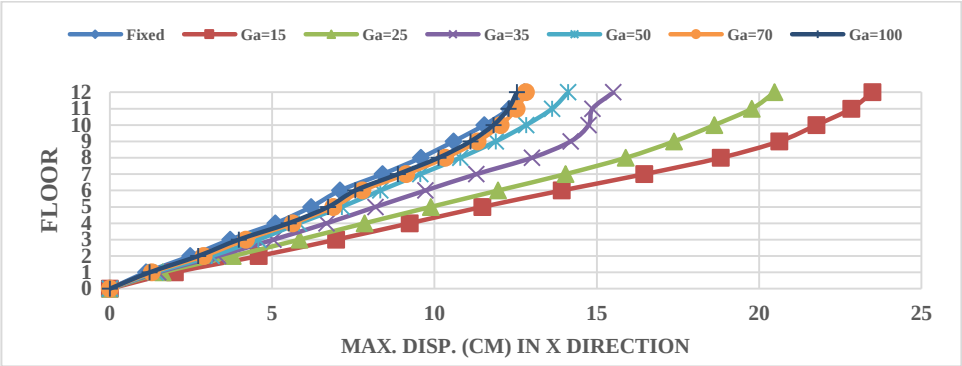


A) Uncontrolled Systems

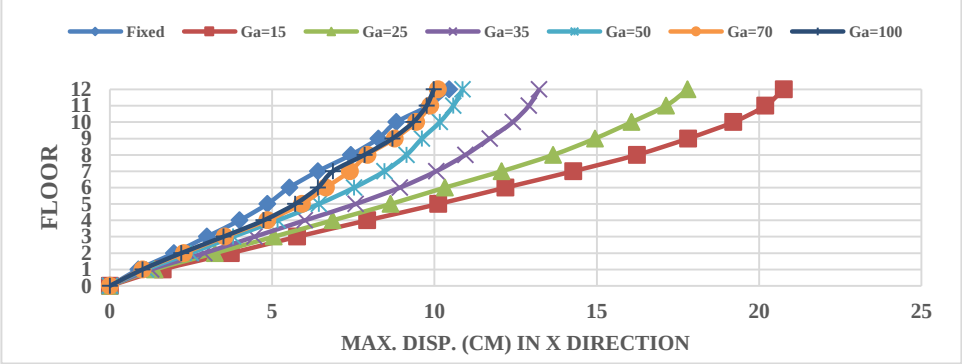


B) Controlled Systems SSI-SSI

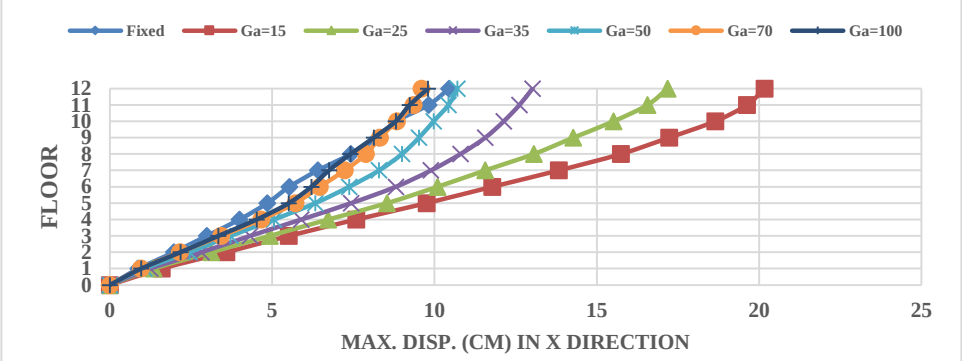


C) Controlled Systems Fixed-SSI

**Figure G-37** Max. displacements of the systems under earthquake Corinth Greece, 2/24/1981

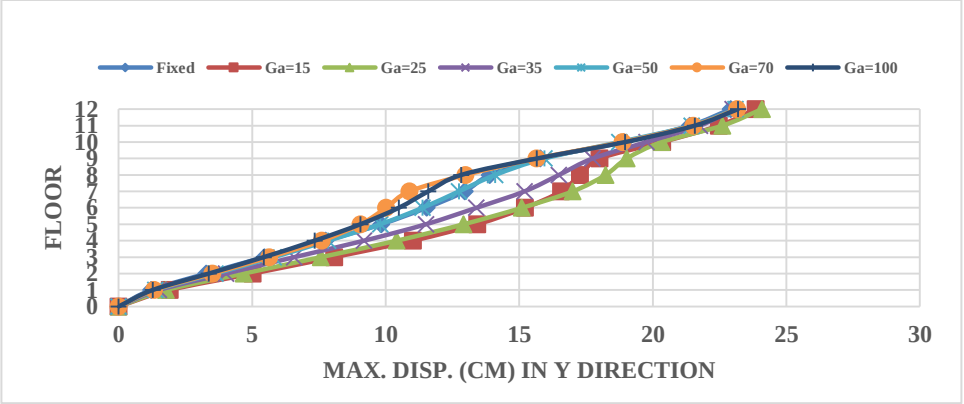


A) Uncontrolled Systems

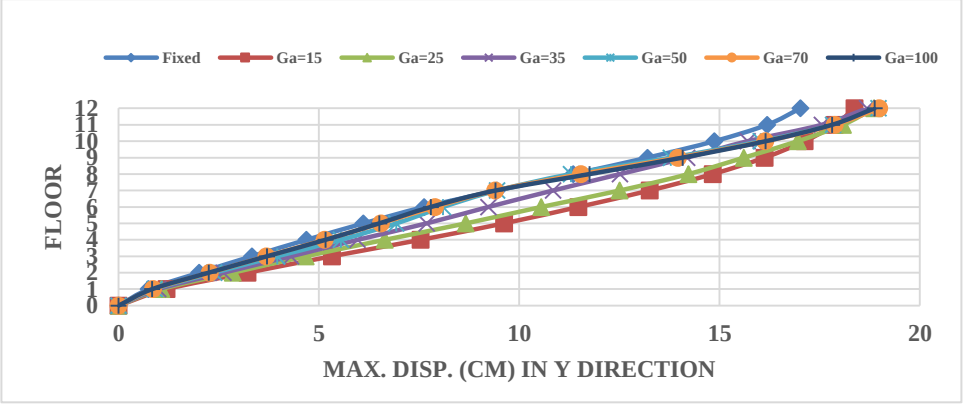


B) Controlled Systems SSI-SSI

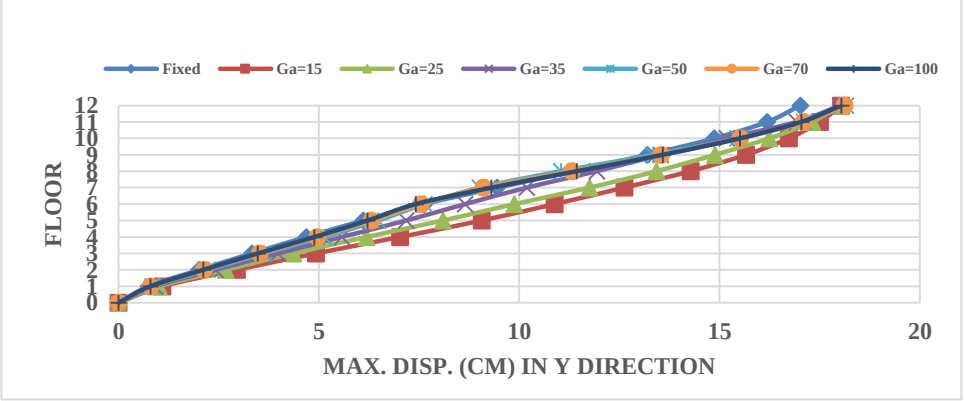


C) Controlled Systems Fixed-SSI

**Figure G-38** Max. displacements of the systems under earthquake Corinth Greece, 2/24/1981

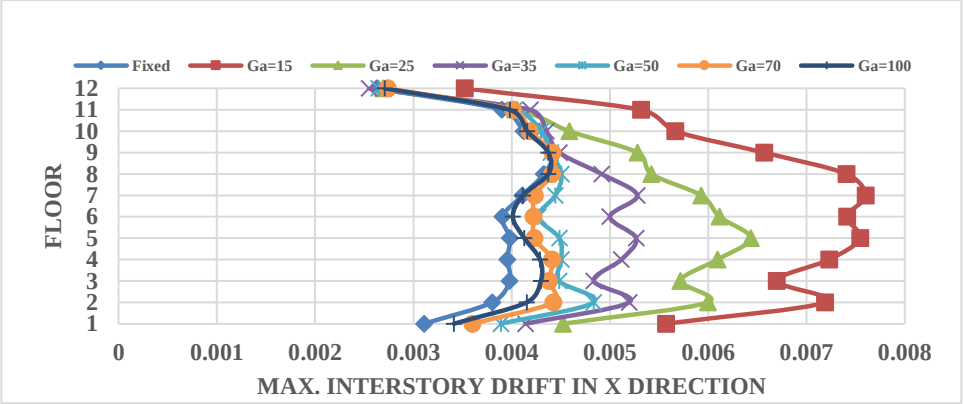


A) Uncontrolled Systems

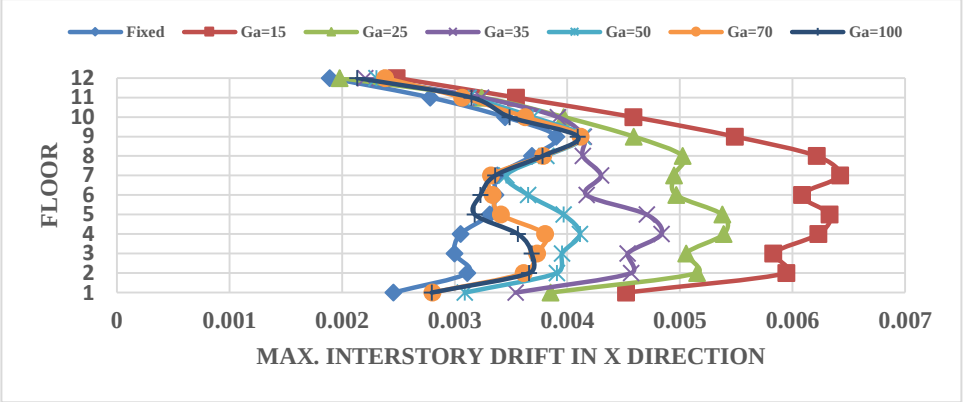


B) Controlled Systems SSI-SSI

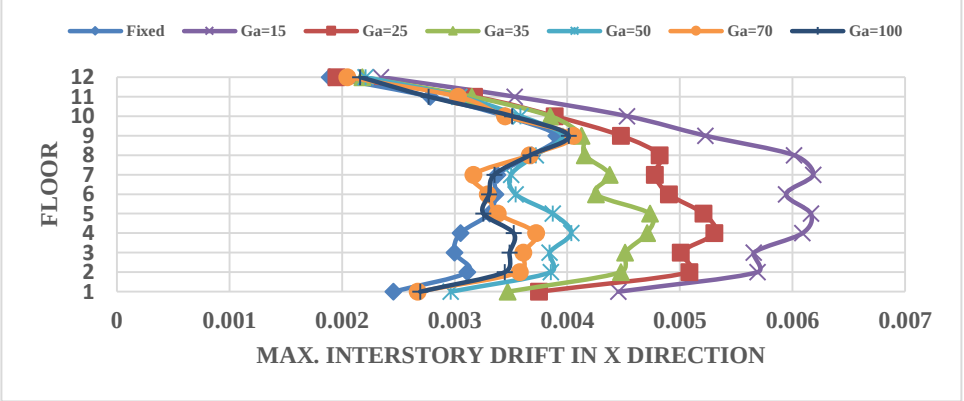


C) Controlled Systems Fixed-SSI

**Figure G-39** Max. interstory drift of the systems under earthquake Corinth Greece, 2/24/1981

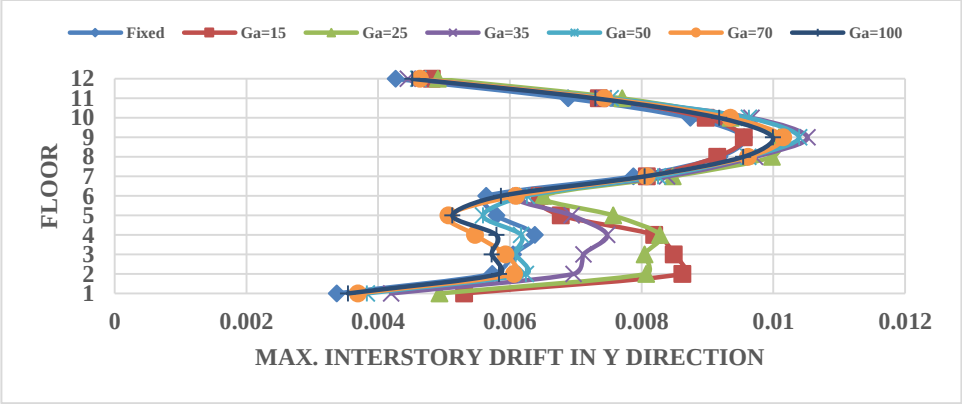


A) Uncontrolled Systems

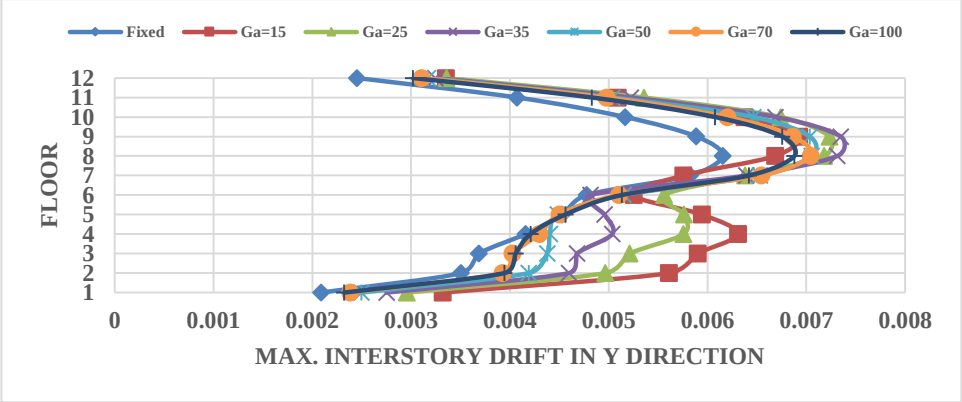


B) Controlled Systems SSI-SSI

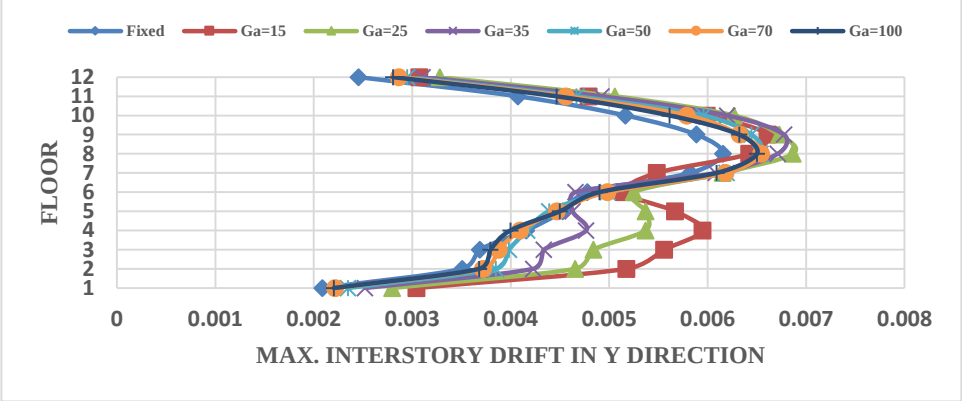


C) Controlled Systems Fixed-SSI

**Figure G-40** Max. interstory drift of the systems under earthquake Corinth Greece, 2/24/1981

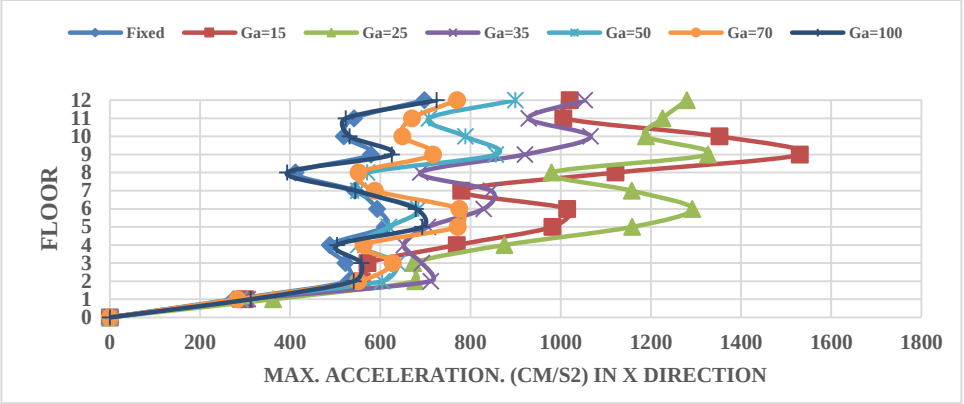


A) Uncontrolled Systems

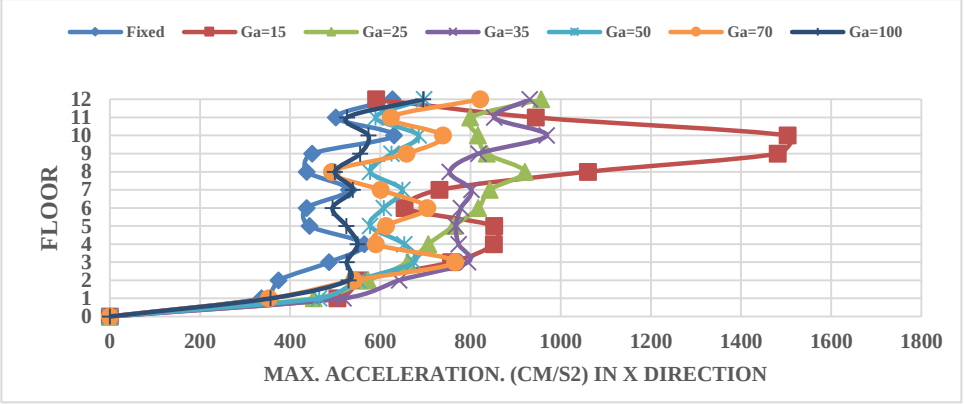


B) Controlled Systems SSI-SSI

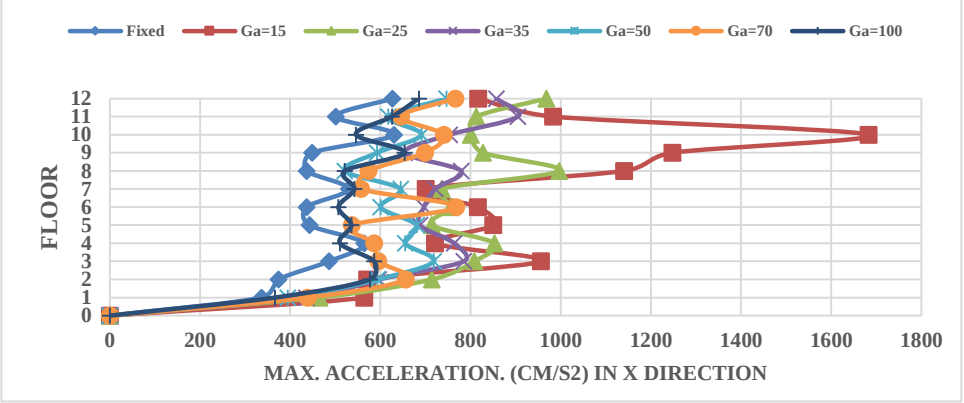


C) Controlled Systems Fixed-SSI

**Figure G-41** Max. acceleration of the systems under earthquake Corinth Greece, 2/24/1981

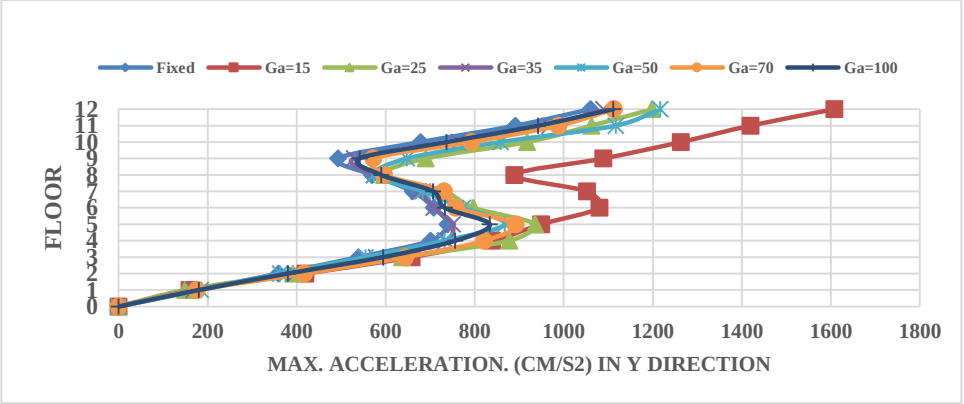


A) Uncontrolled Systems

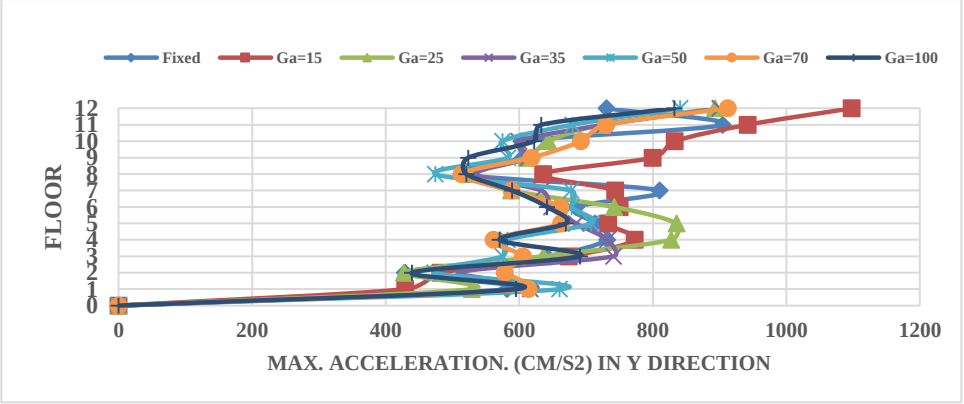


B) Controlled Systems SSI-SSI

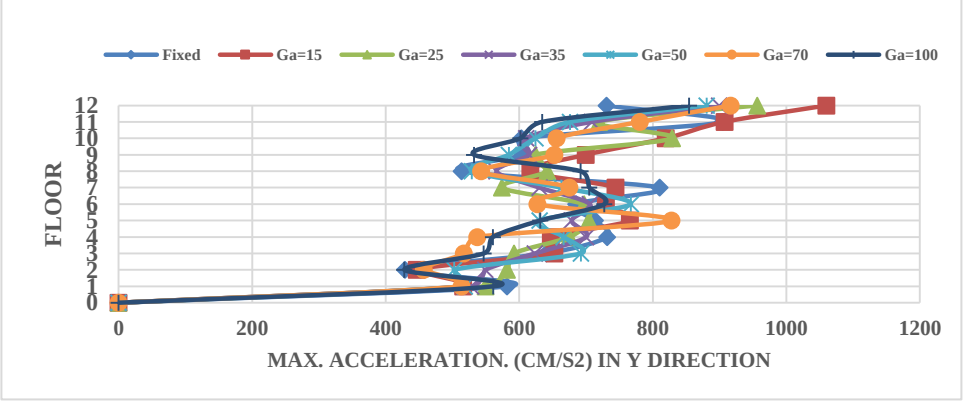


C) Controlled Systems Fixed-SSI

**Figure G-42** Max. acceleration of the systems under earthquake Corinth Greece, 2/24/1981

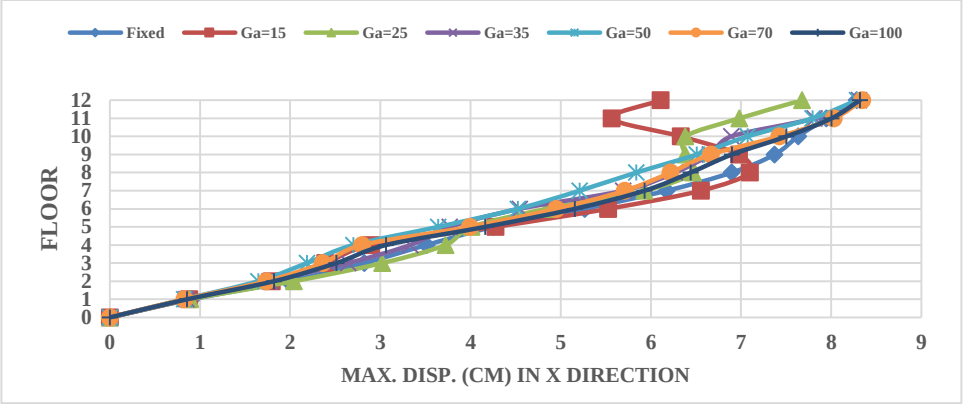


A) Uncontrolled Systems

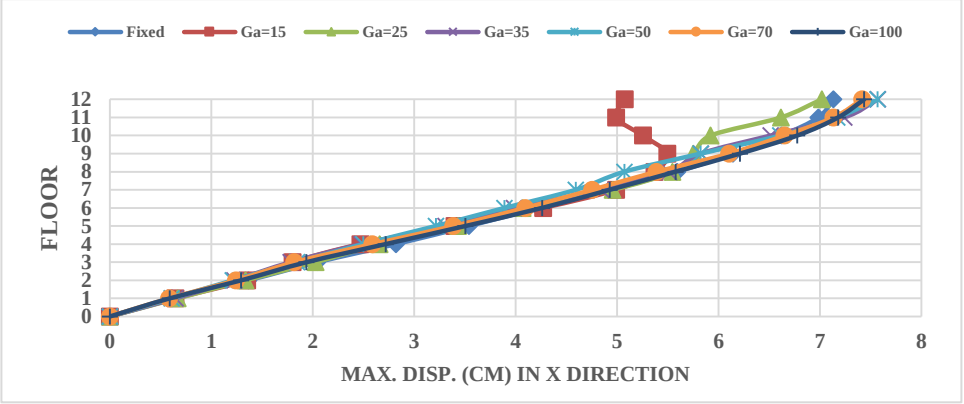


B) Controlled Systems SSI-SSI

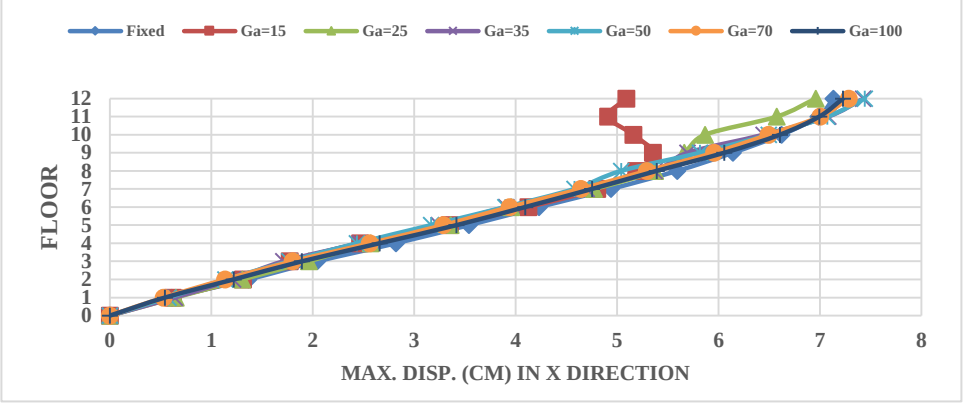


C) Controlled Systems Fixed-SSI

**Figure G-43** Max. displacements of the systems under earthquake Managua Nicaragua-02, 12/23/1972

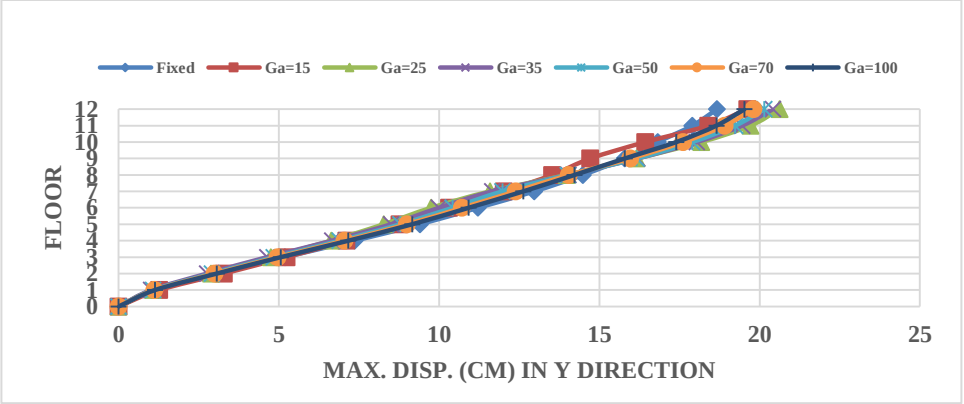


A) Uncontrolled Systems

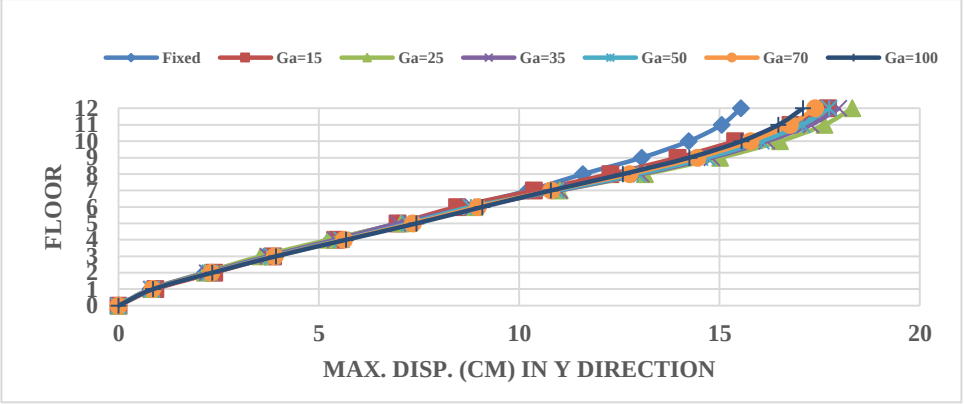


B) Controlled Systems SSI-SSI

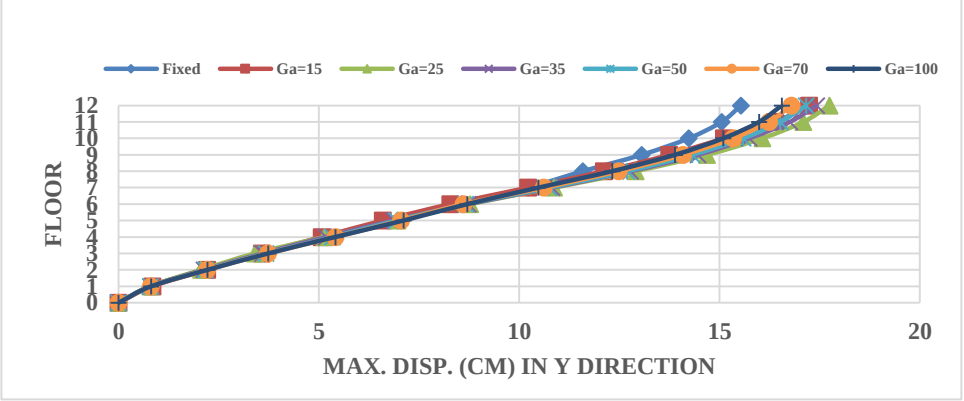


C) Controlled Systems Fixed-SSI

**Figure G-44** Max. displacements of the systems under earthquake Managua Nicaragua-02, 12/23/1972

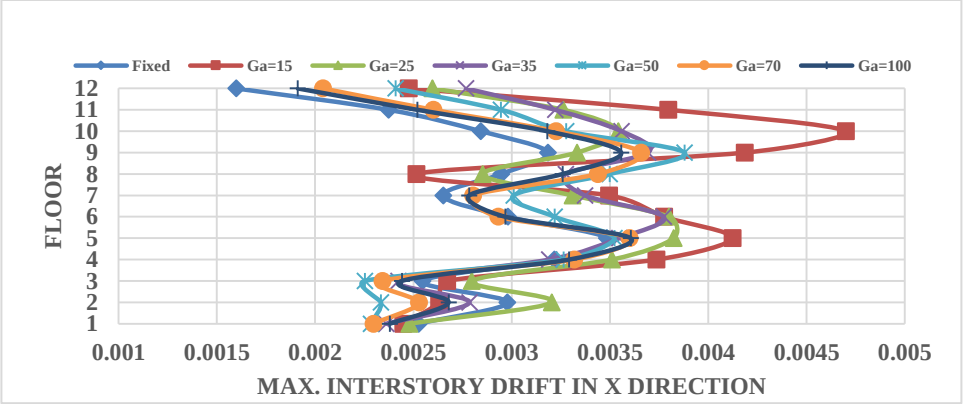


A) Uncontrolled Systems

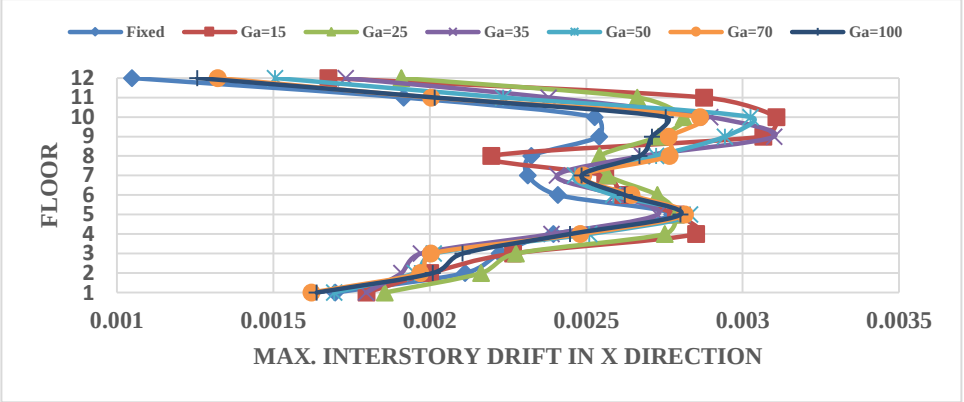


B) Controlled Systems SSI-SSI

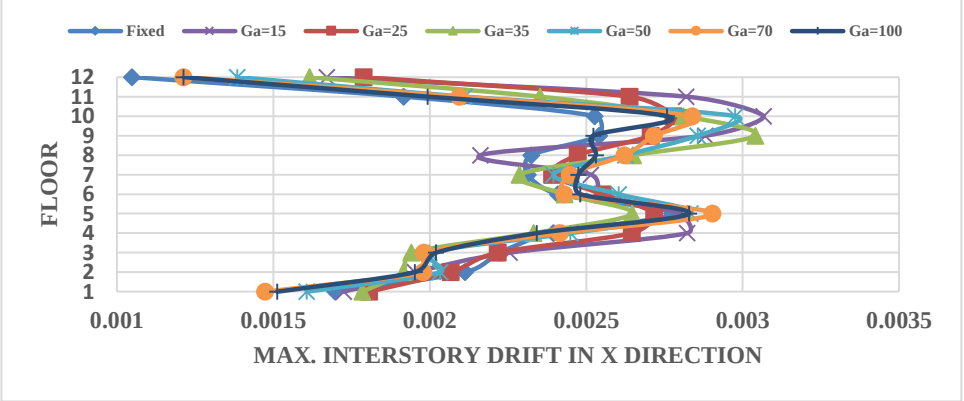


C) Controlled Systems Fixed-SSI

**Figure G-45** Max. interstory drift of the systems under earthquake Managua Nicaragua-02, 12/23/1972

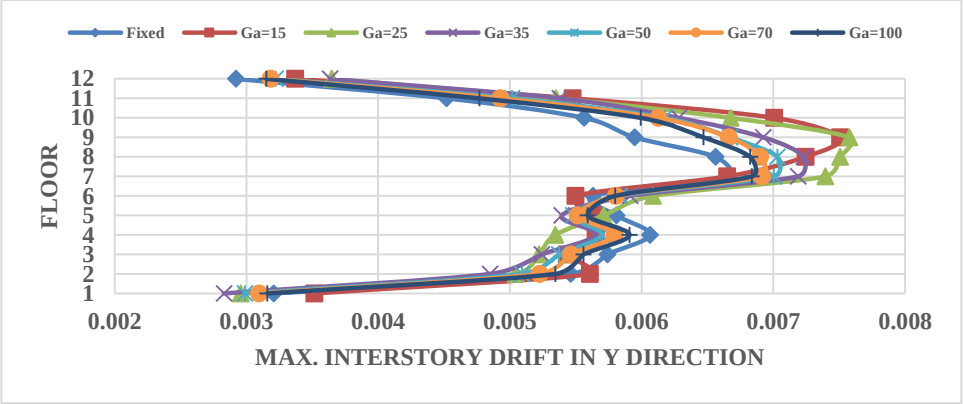


A) Uncontrolled Systems

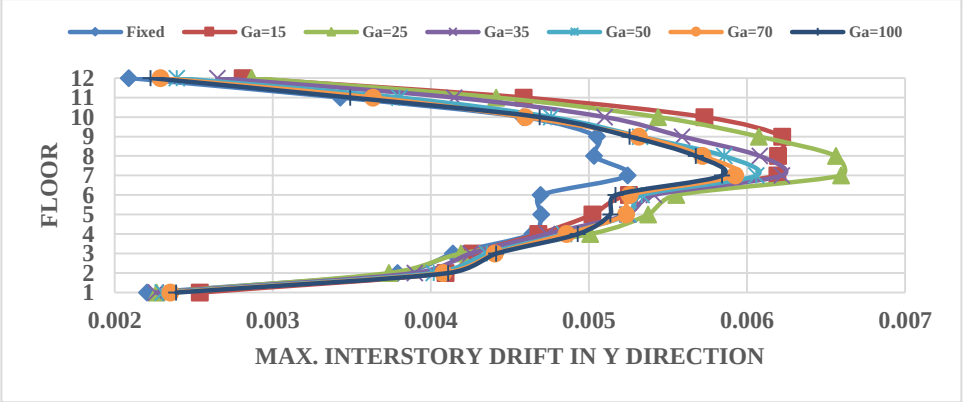


B) Controlled Systems SSI-SSI

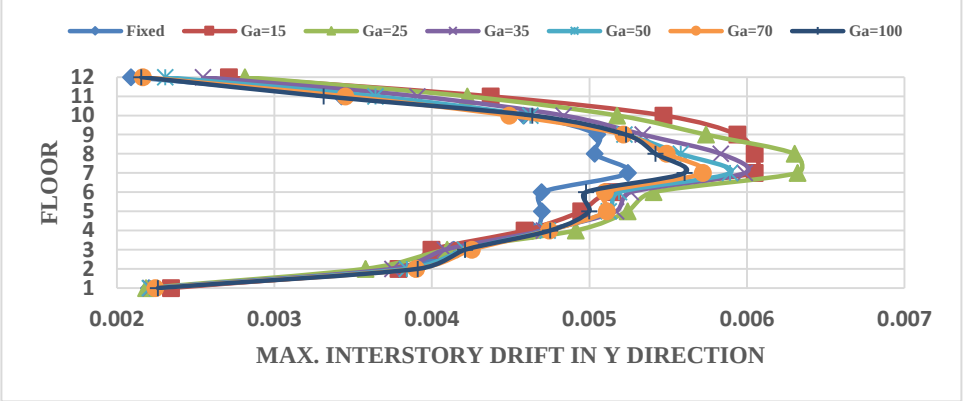


C) Controlled Systems Fixed-SSI

**Figure G-46** Max. interstory drift of the systems under earthquake Managua Nicaragua-02, 12/23/1972

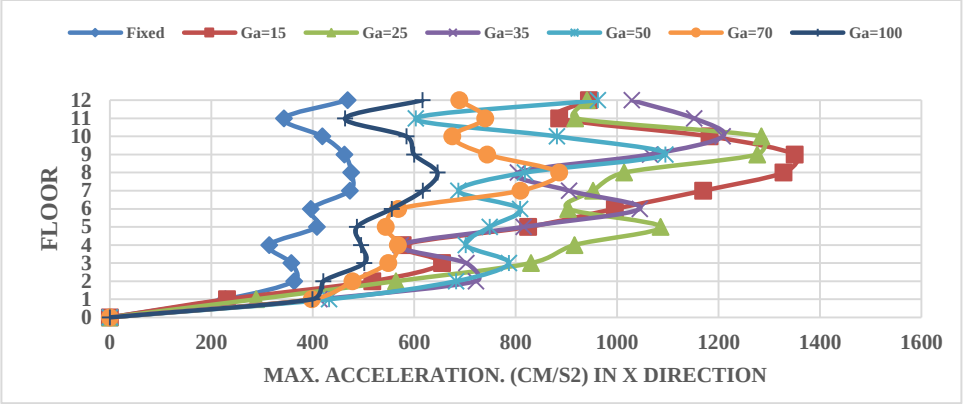


A) Uncontrolled Systems

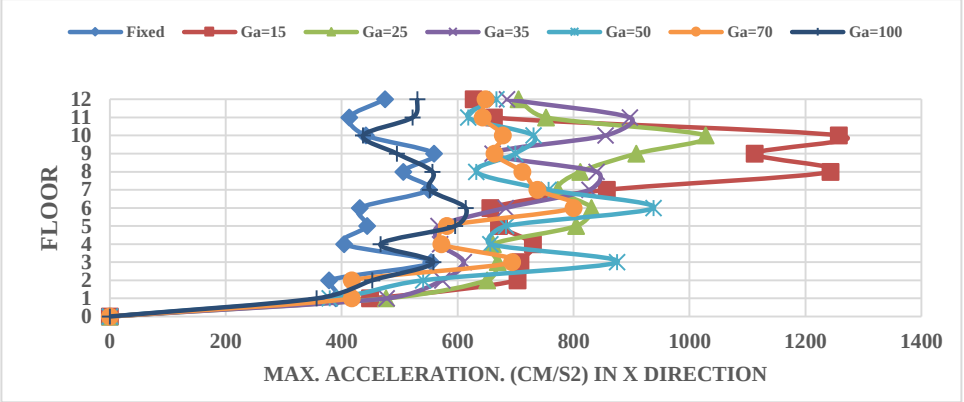


B) Controlled Systems SSI-SSI

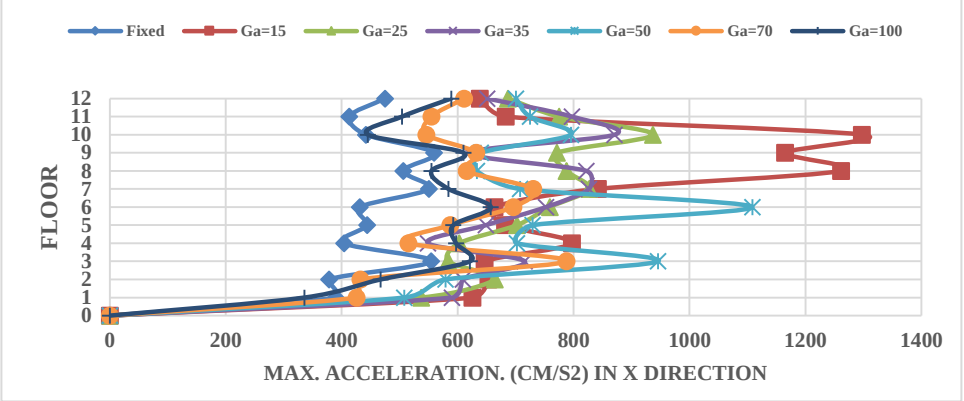


C) Controlled Systems Fixed-SSI

**Figure G-47** Max. acceleration of the systems under earthquake Managua Nicaragua-02, 12/23/1972

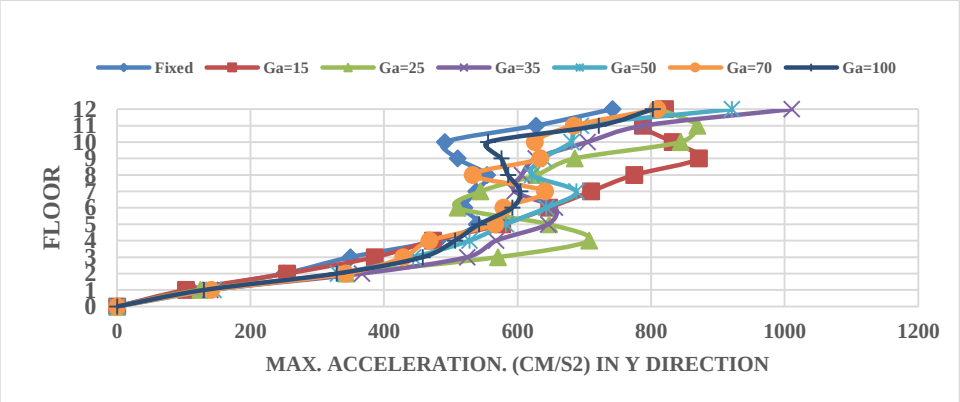


A) Uncontrolled Systems

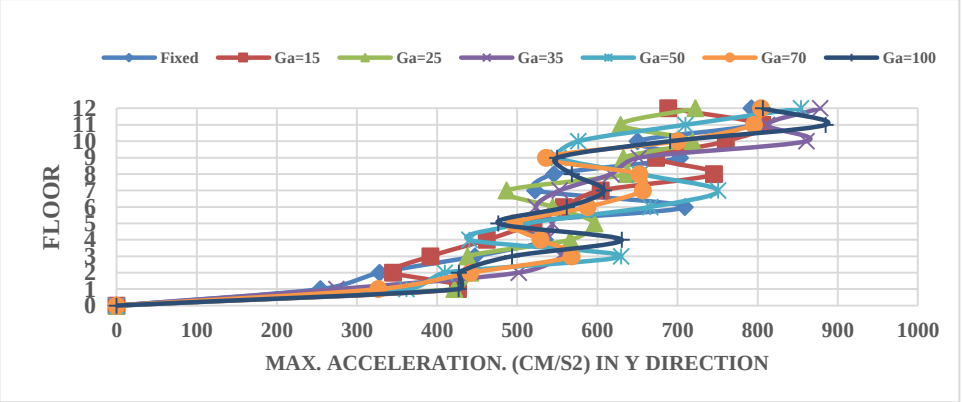


B) Controlled Systems SSI-SSI

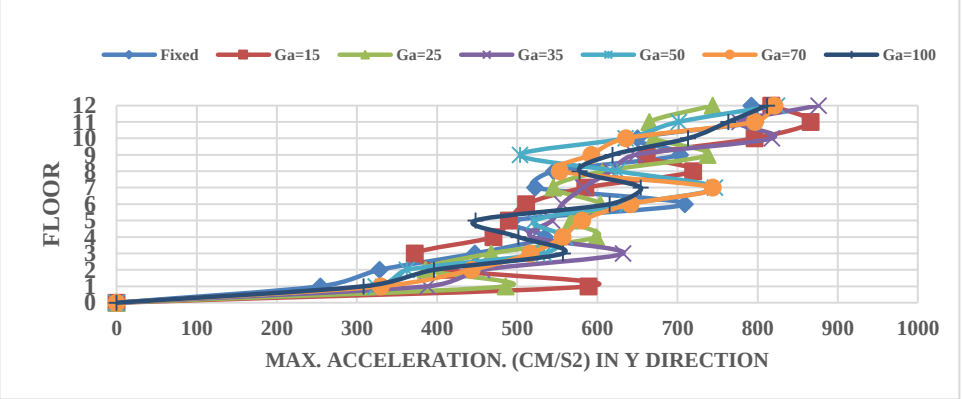


C) Controlled Systems Fixed-SSI

**Figure G-48** Max. acceleration of the systems under earthquake Managua Nicaragua-02, 12/23/1972

Frame Shear Wall Building

Medium top and soft bottom

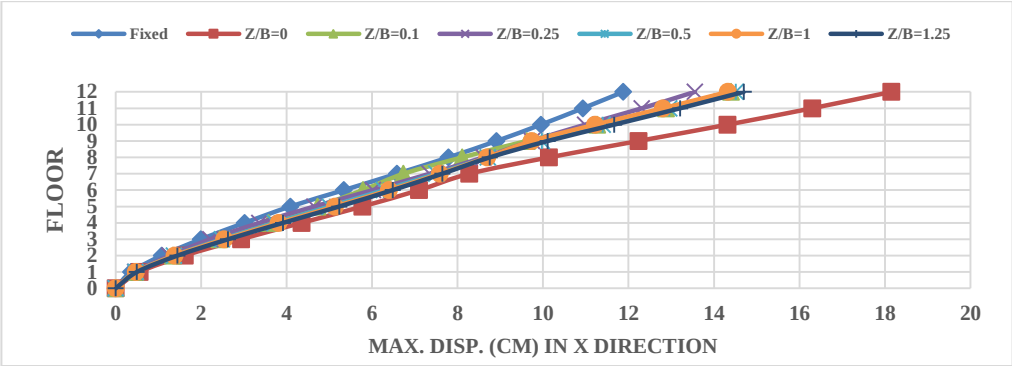


A) Uncontrolled Systems

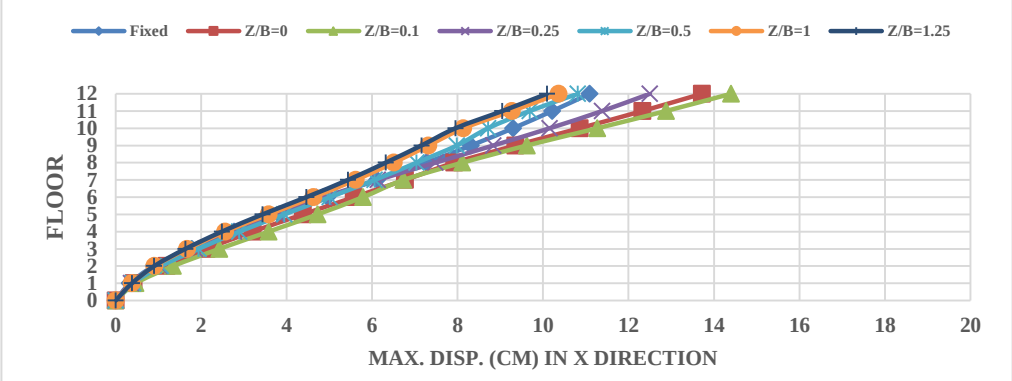


B) Controlled Systems SSI-SSI

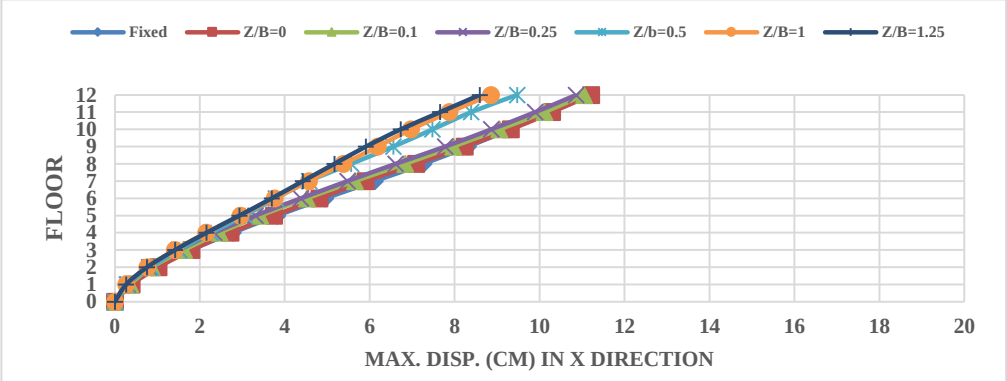


C) Controlled Systems Fixed-SSI

**Figure G-49** Max. displacements of the systems under earthquake Corinth Greece

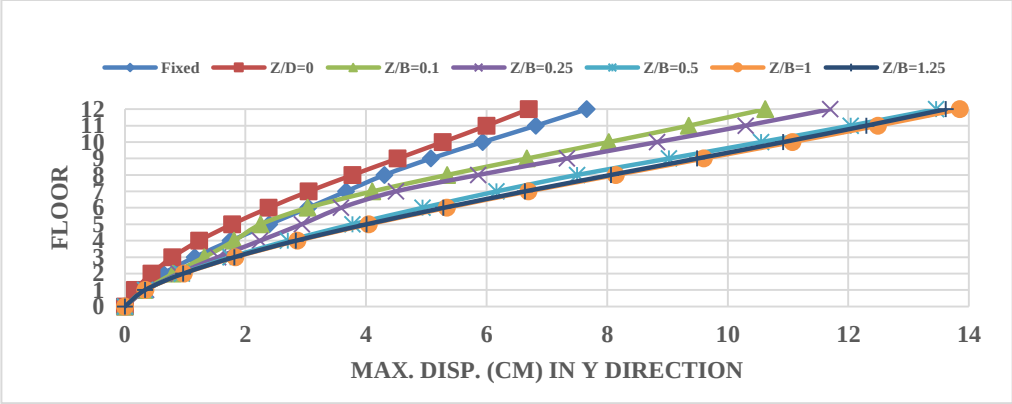


A) Uncontrolled Systems

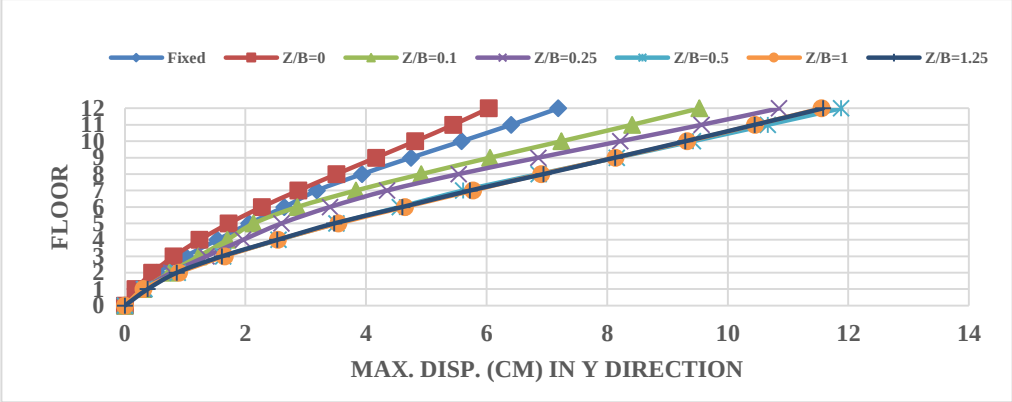


B) Controlled Systems SSI-SSI

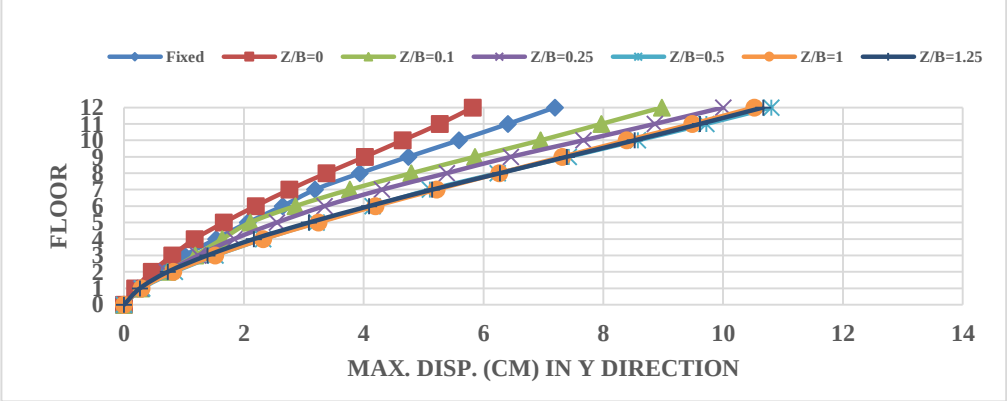


C) Controlled Systems Fixed-SSI

**Figure G-50** Max. displacements of the systems under earthquake Corinth Greece, 2/24/1981

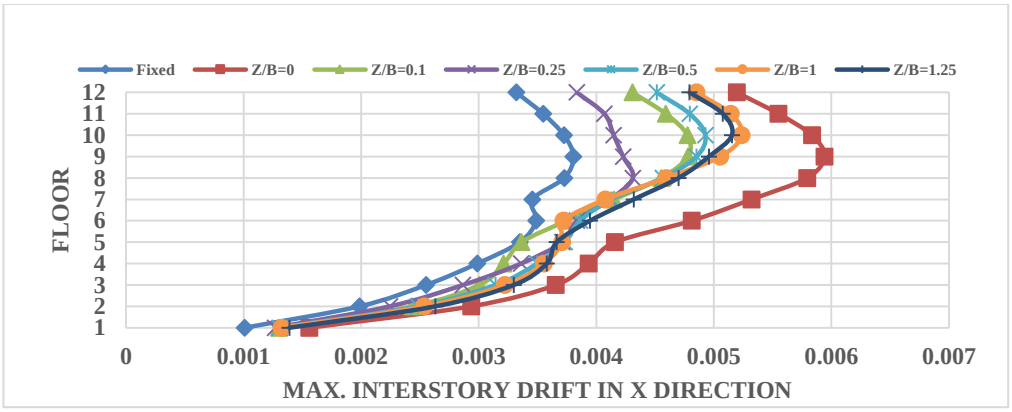


A) Uncontrolled Systems

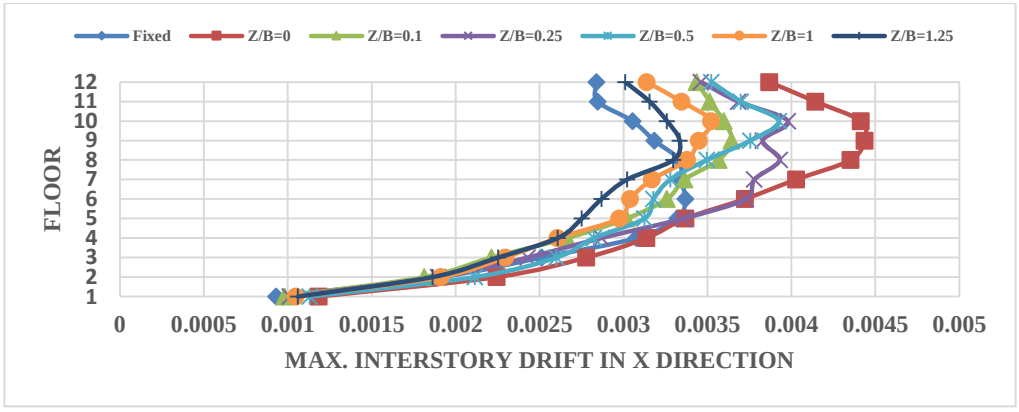


B) Controlled Systems SSI-SSI

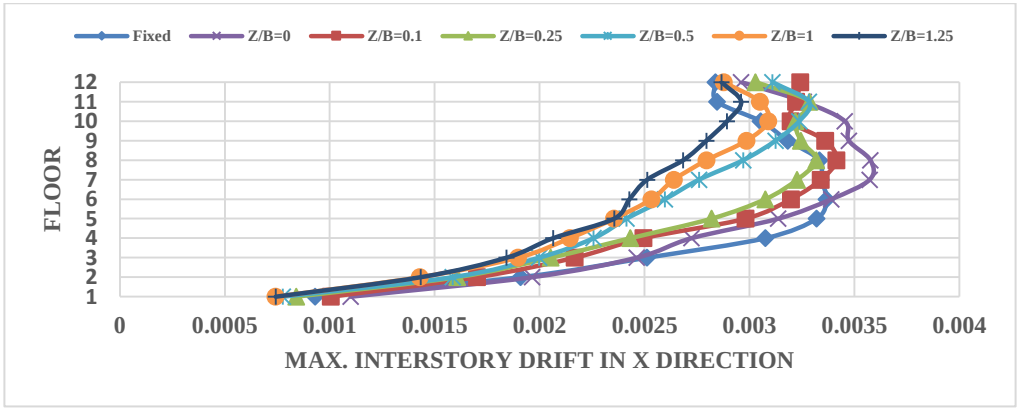


C) Controlled Systems Fixed-SSI

**Figure G-51** Max. interstory drift of the systems under earthquake Corinth Greece, 2/24/1981

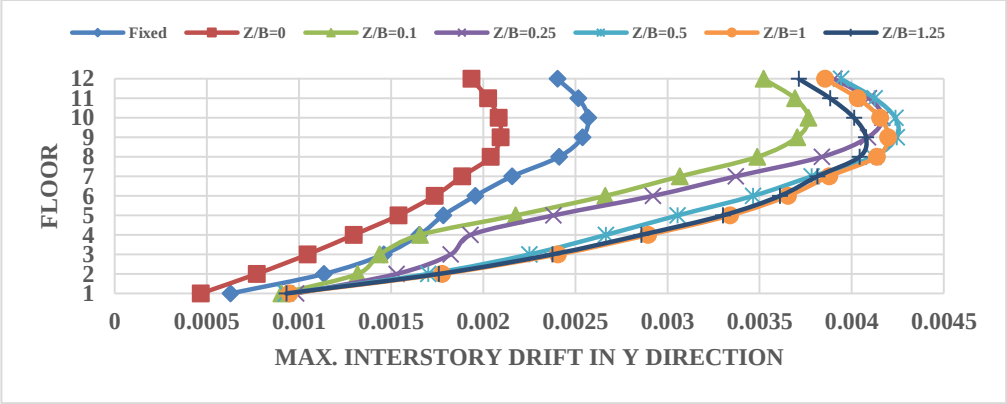


A) Uncontrolled Systems

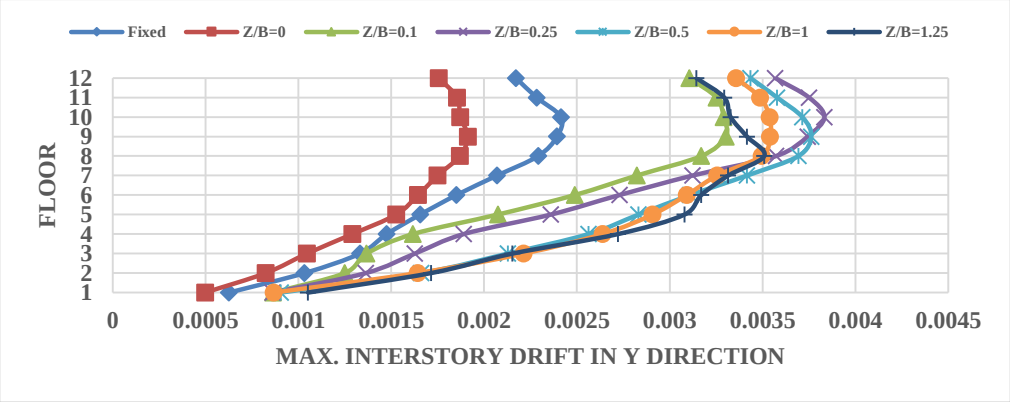


B) Controlled Systems SSI-SSI

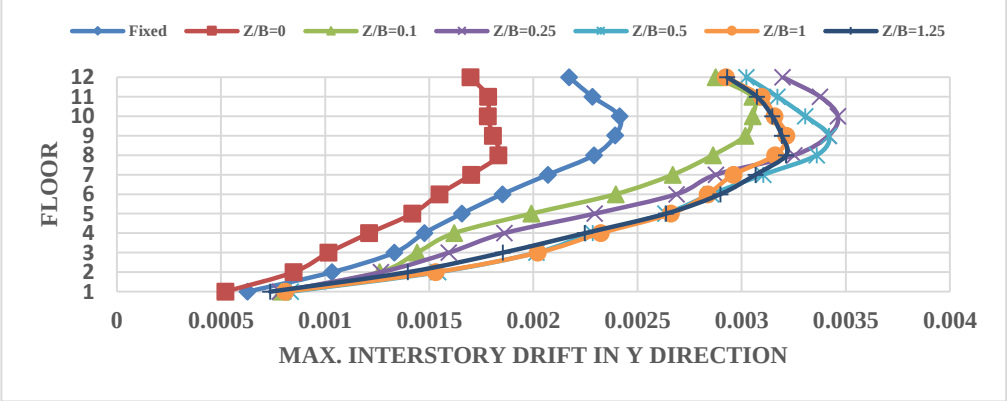


C) Controlled Systems Fixed-SSI

**Figure G-52** Max. interstory drift of the systems under earthquake Corinth Greece, 2/24/1981

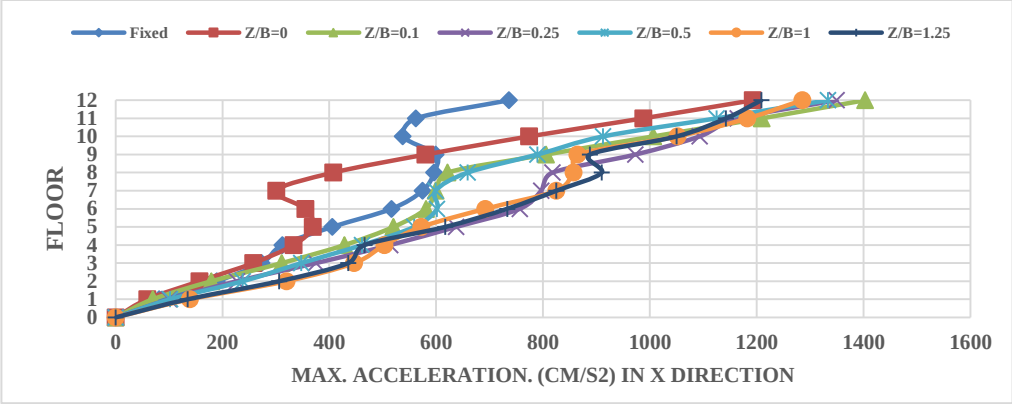


A) Uncontrolled Systems

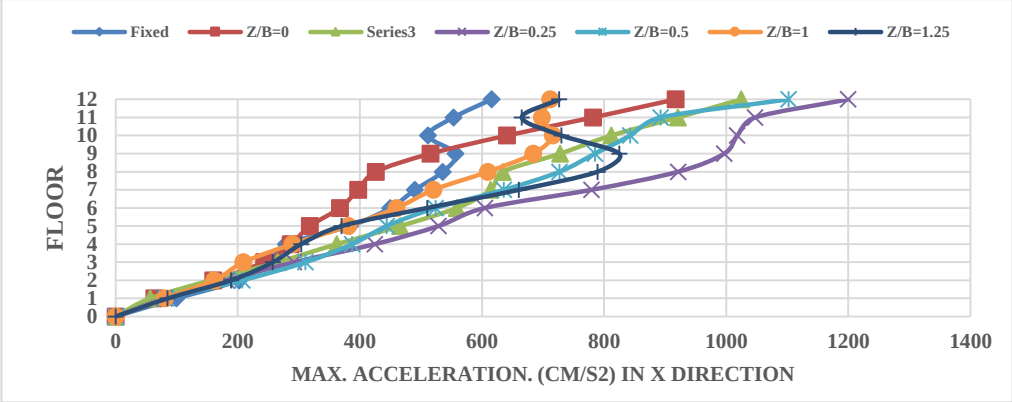


B) Controlled Systems SSI-SSI

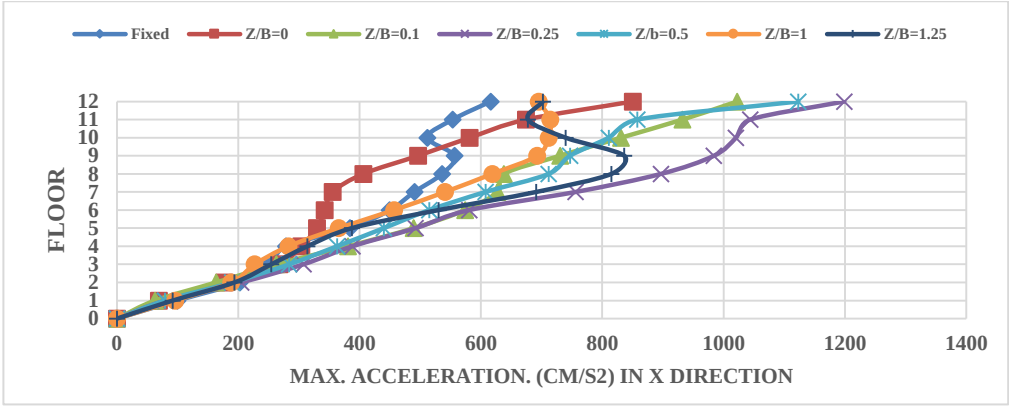


C) Controlled Systems Fixed-SSI

**Figure G-53** Max. acceleration of the systems under earthquake Corinth Greece,

2/24/1981

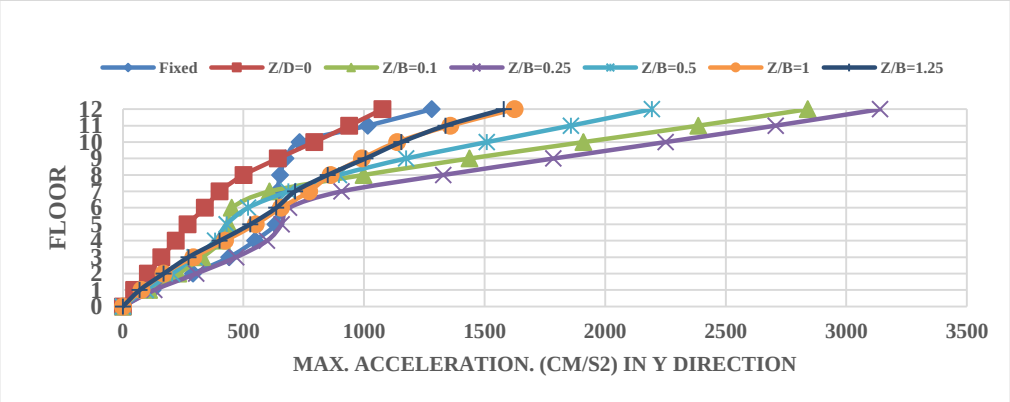


A) Uncontrolled Systems

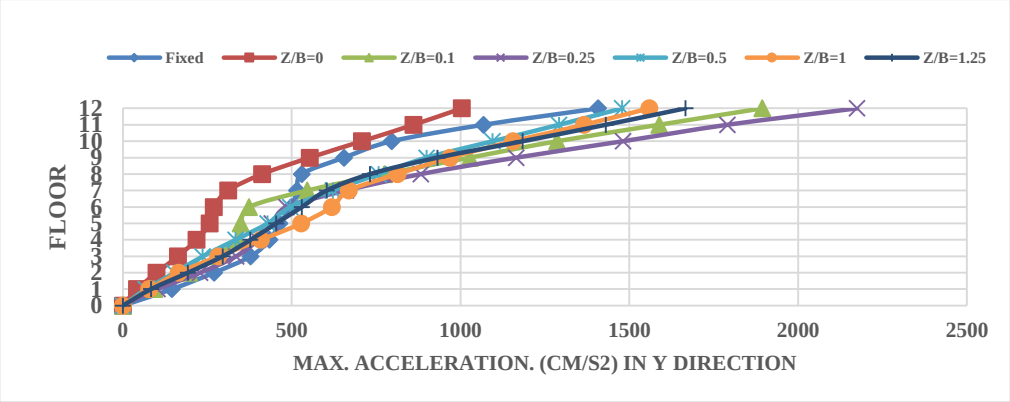


B) Controlled Systems SSI-SSI

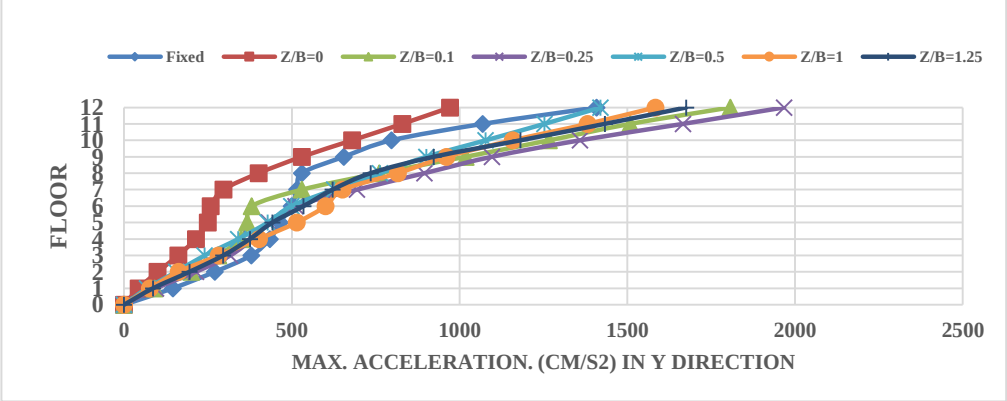


C) Controlled Systems Fixed-SSI

**Figure G-54** Max. acceleration of the systems under earthquake Corinth Greece, 2/24/1981

Soft top and medium bottom

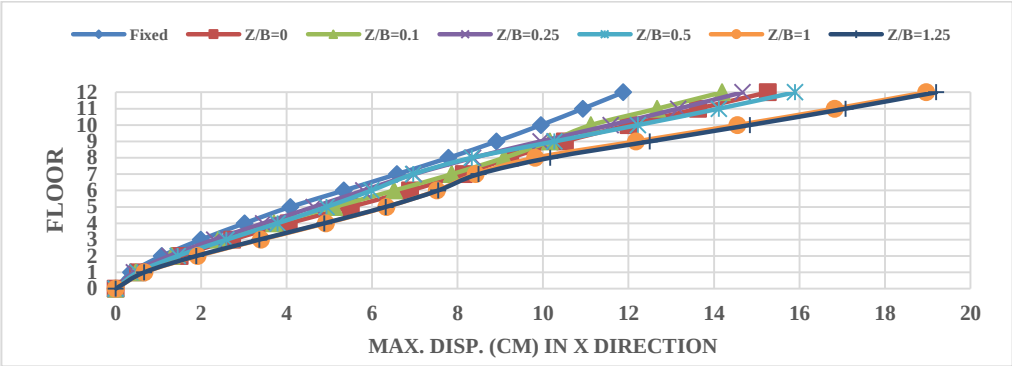


A) Uncontrolled Systems

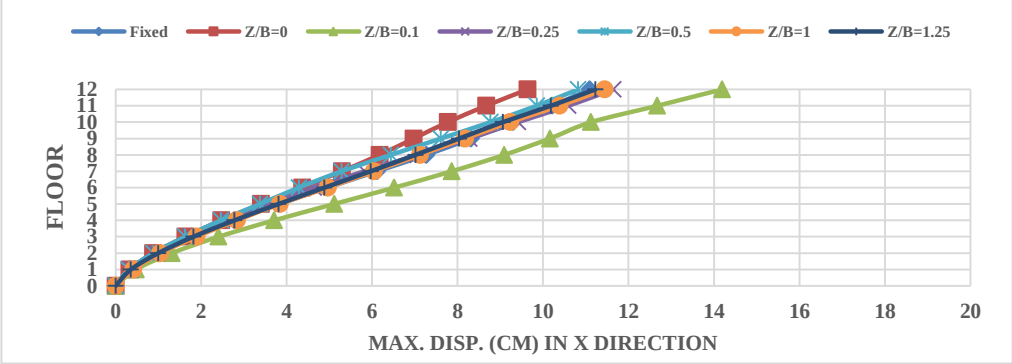


B) Controlled Systems SSI-SSI

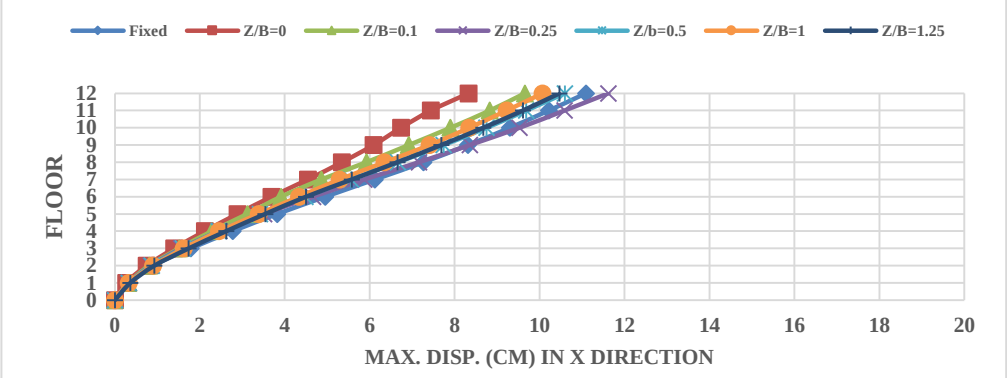


C) Controlled Systems Fixed-SSI

**Figure G-55** Max. displacements of the systems under earthquake Corinth Greece, 2/24/1981

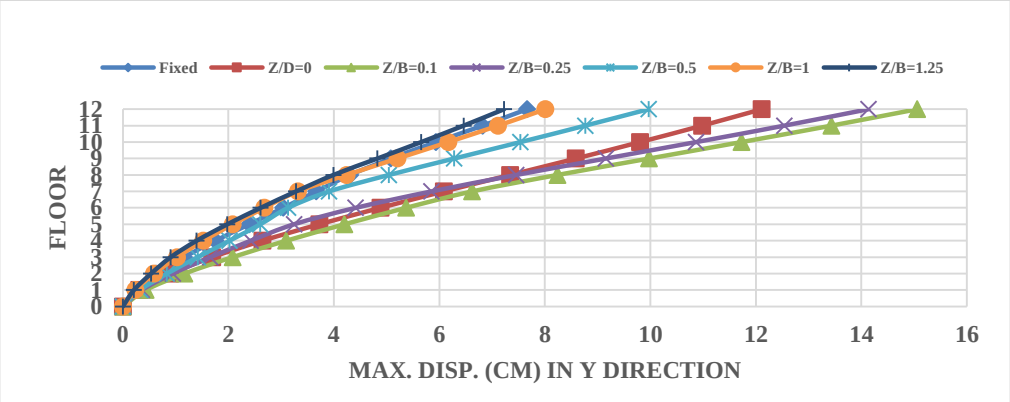


A) Uncontrolled Systems

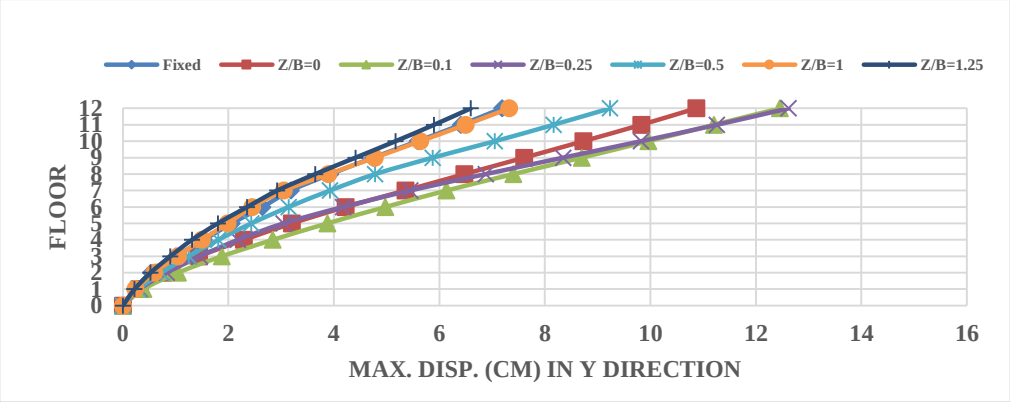


B) Controlled Systems SSI-SSI

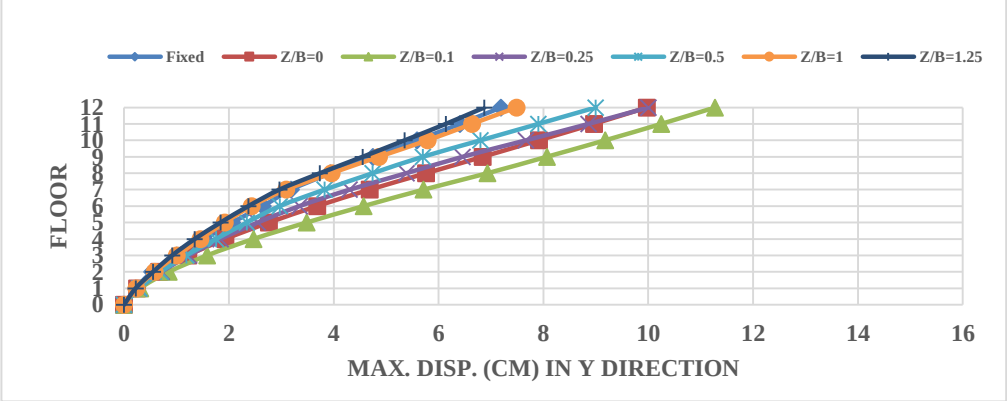


C) Controlled Systems Fixed-SSI

**Figure G-56** Max. displacements of the systems under earthquake Corinth Greece, 2/24/1981

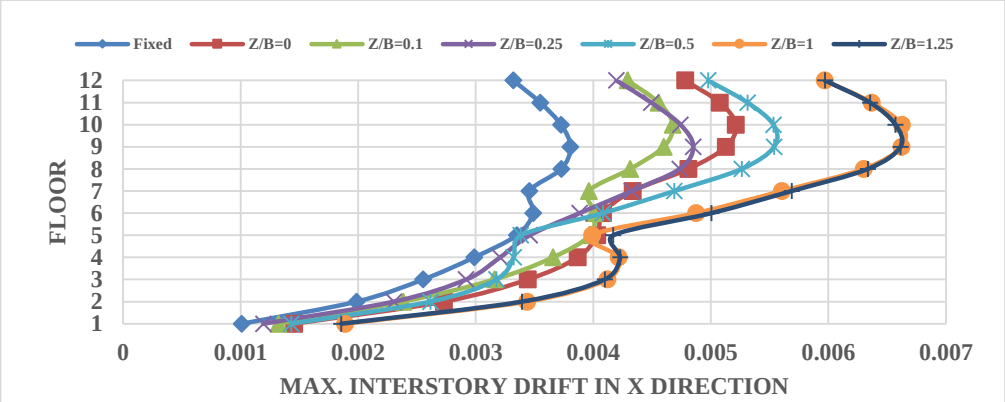


A) Uncontrolled Systems

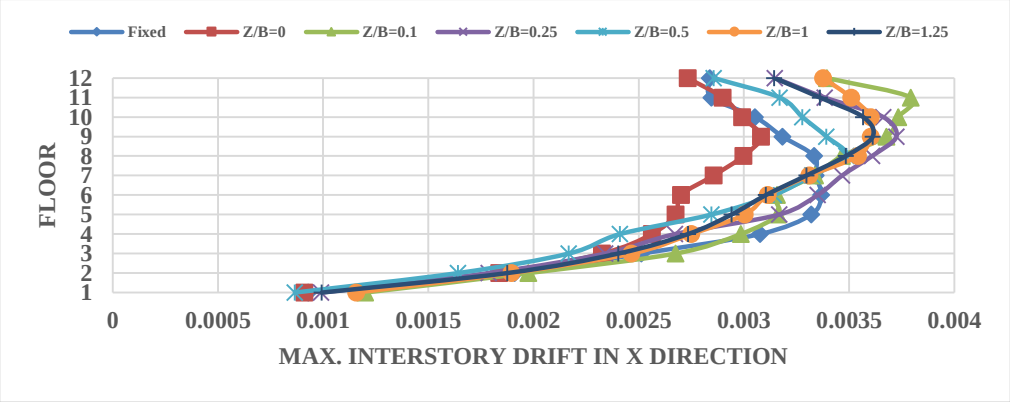


B) Controlled Systems SSI-SSI

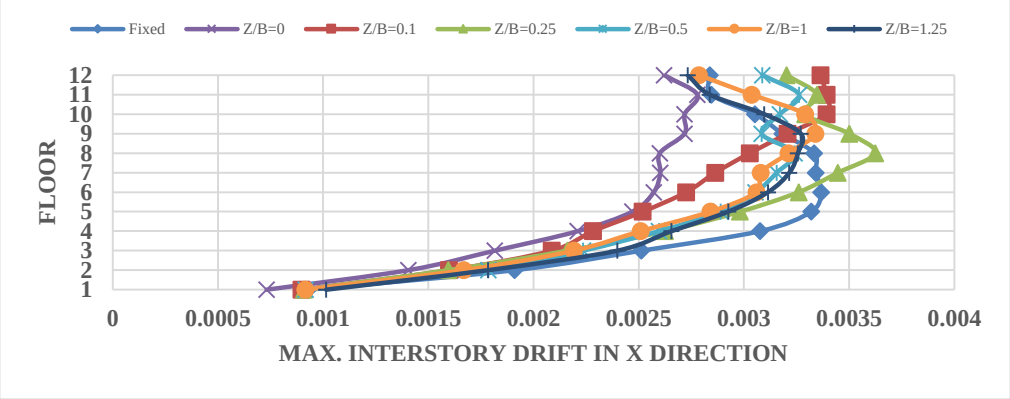


C) Controlled Systems Fixed-SSI

**Figure G-57** the max. interstory drift of the systems under earthquake Corinth Greece, 2/24/1981

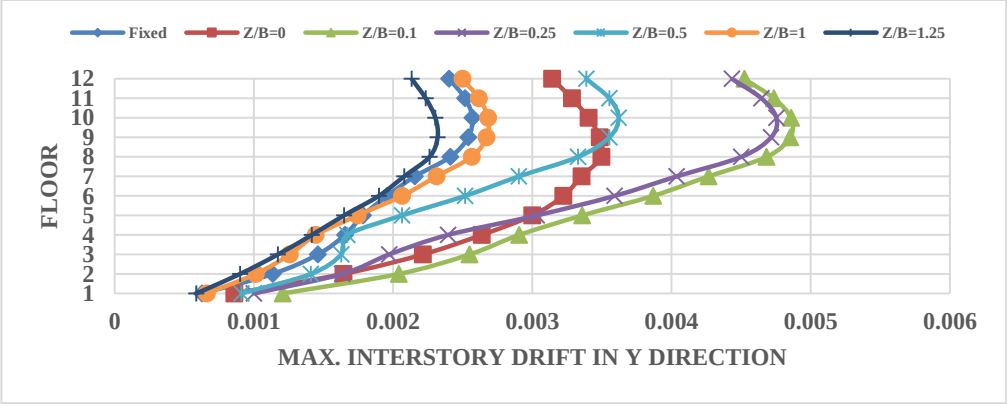


A) Uncontrolled Systems

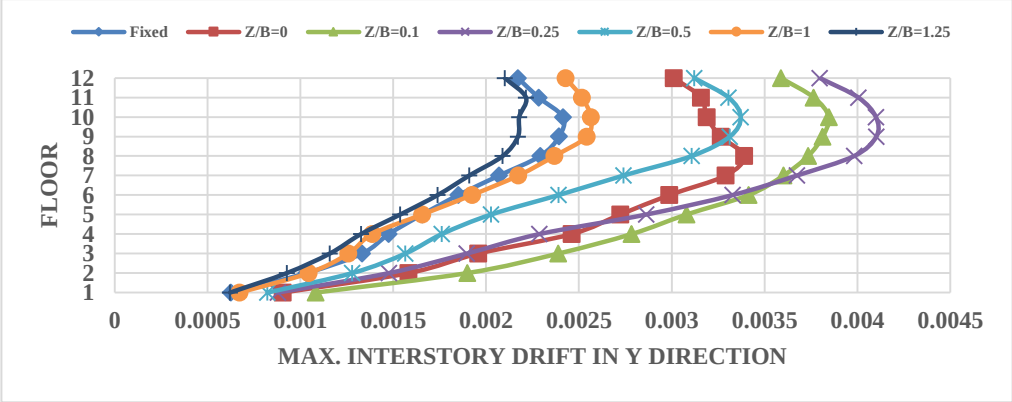


B) Controlled Systems SSI-SSI

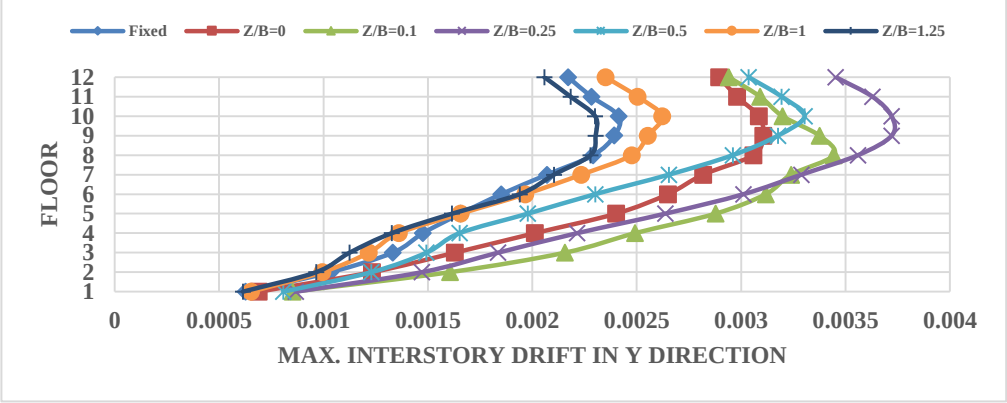


C) Controlled Systems Fixed-SSI

**Figure G-58** Max. interstory drift of the systems under earthquake Corinth Greece, 2/24/1981

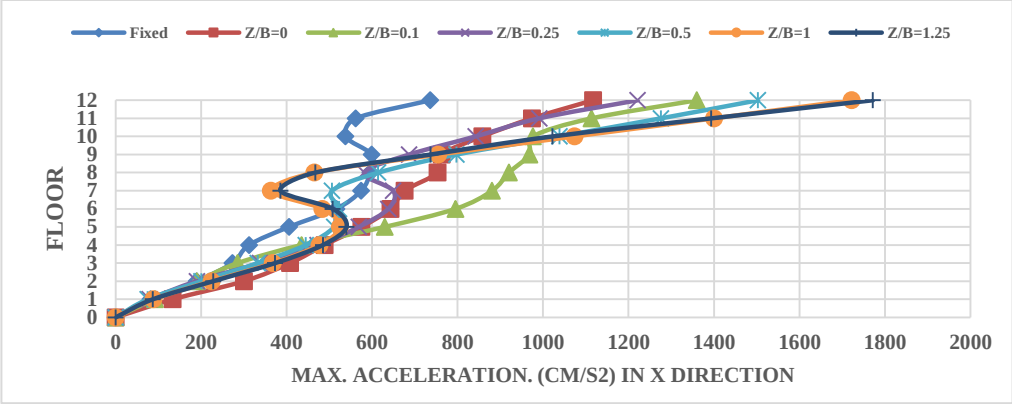


A) Uncontrolled Systems

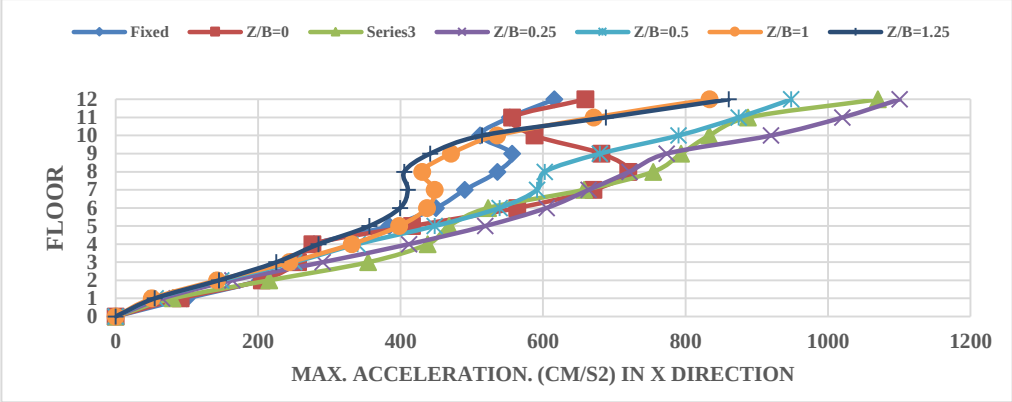


B) Controlled Systems SSI-SSI

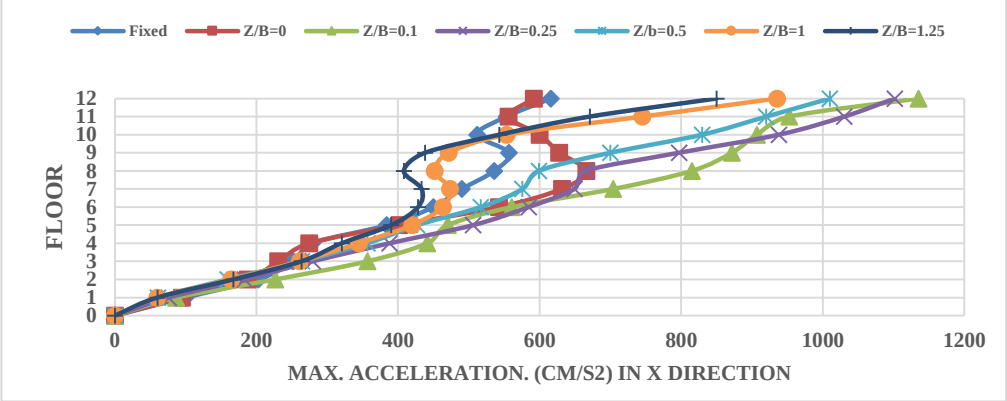


C) Controlled Systems Fixed-SSI

**Figure G-59** Max. acceleration of the systems under earthquake Corinth Greece,

2/24/1981

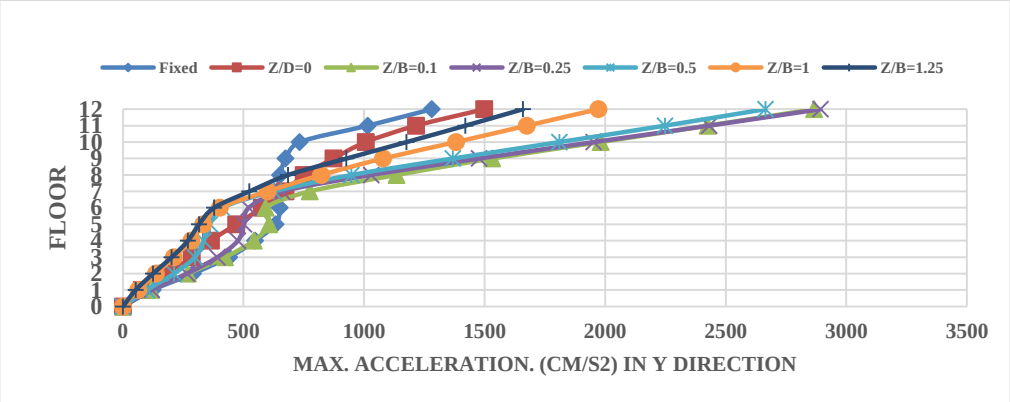


A) Uncontrolled Systems

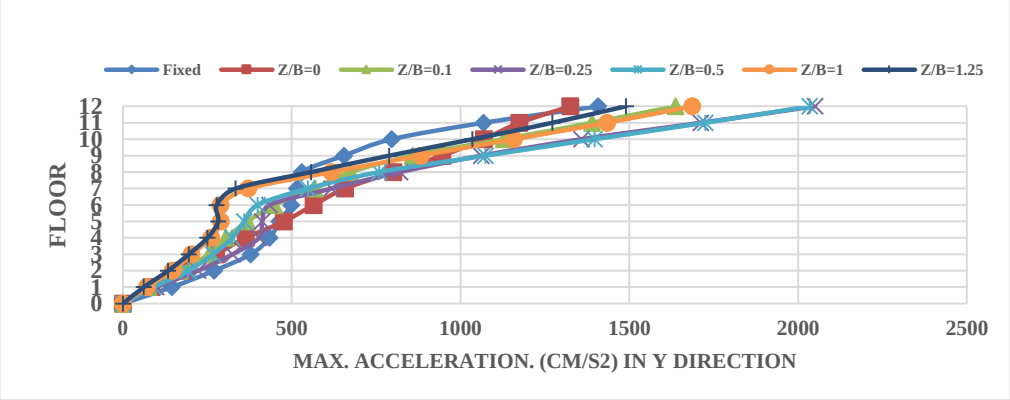


B) Controlled Systems SSI-SSI

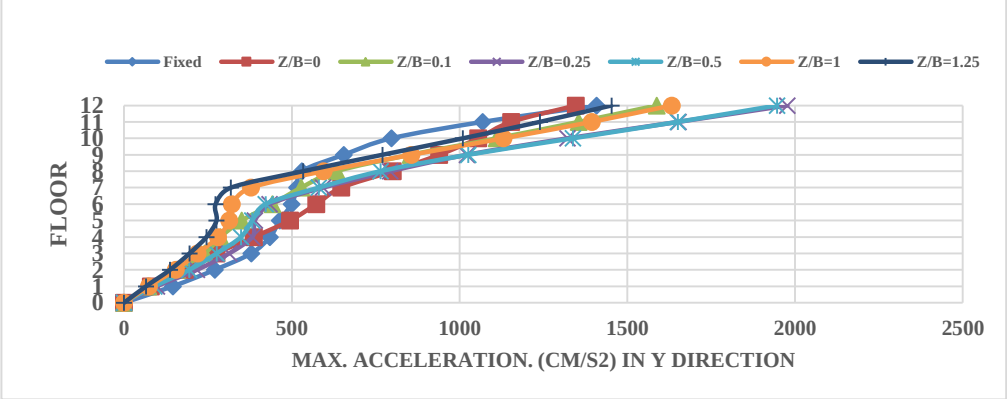


C) Controlled Systems Fixed-SSI

**Figure G-60** Max. acceleration of the systems under earthquake Corinth Greece, 2/24/1981

Medium top and soft bottom

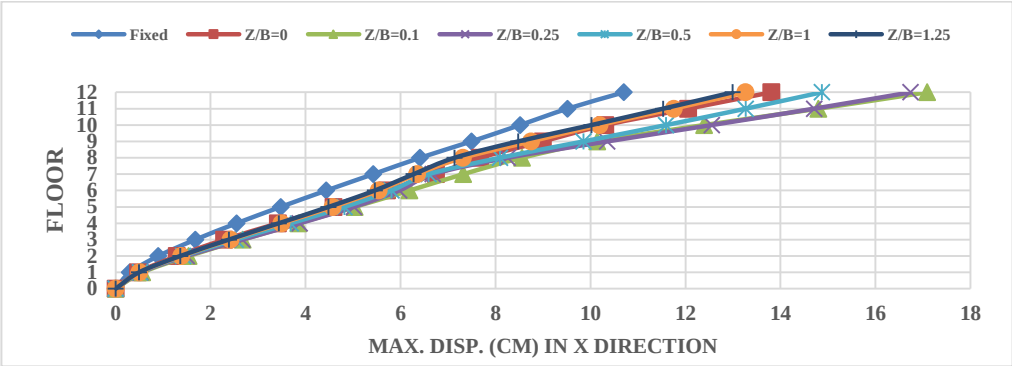


A) Uncontrolled Systems

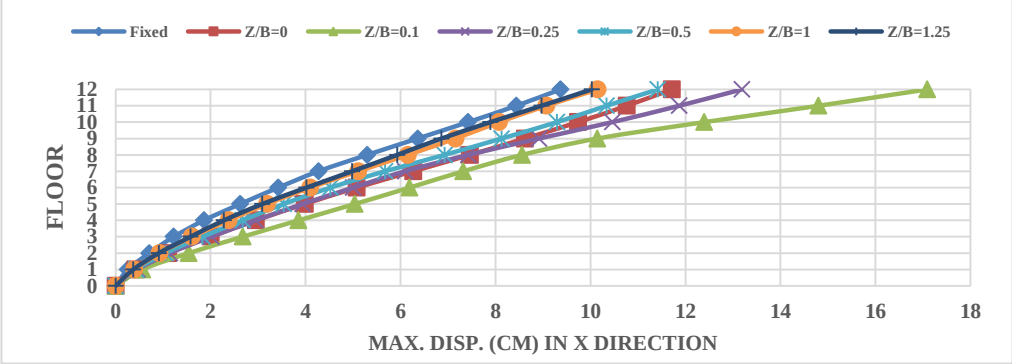


B) Controlled Systems SSI-SSI

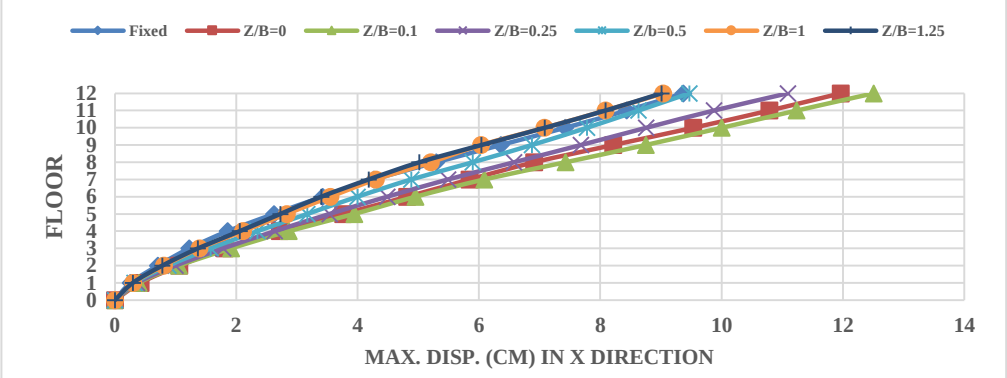


C) Controlled Systems Fixed-SSI

**Figure G-61** Max. displacements of the systems under earthquake Managua Nicaragua-02, 12/23/1972

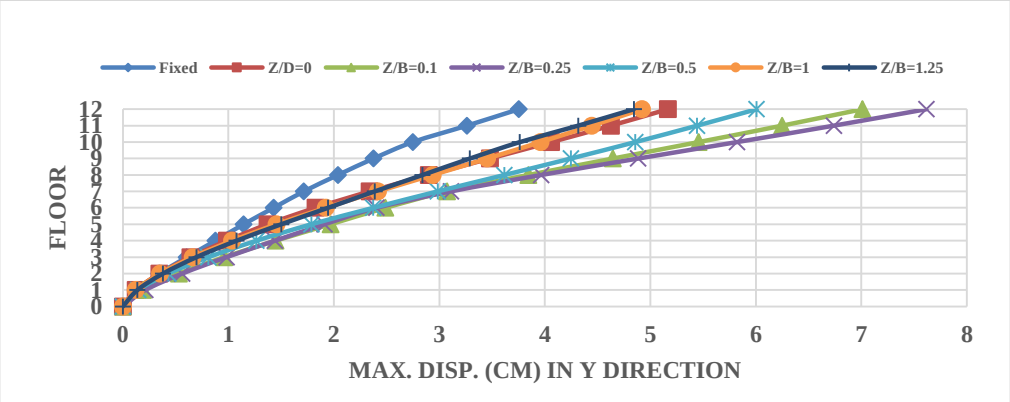


A) Uncontrolled Systems

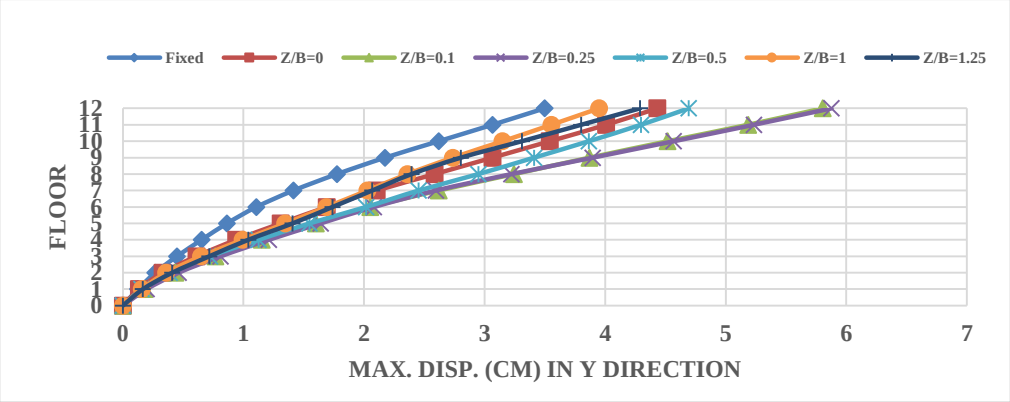


B) Controlled Systems SSI-SSI

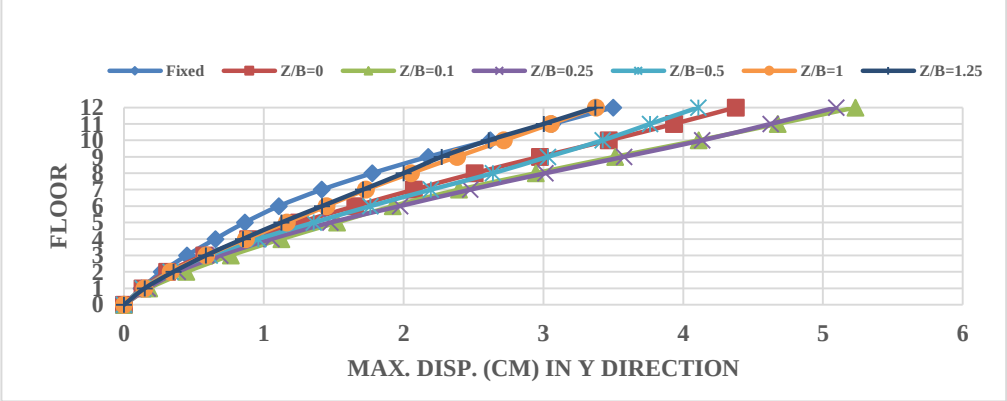


C) Controlled Systems Fixed-SSI

**Figure G-62** Max. displacements of the systems under earthquake Managua Nicaragua-02, 12/23/1972

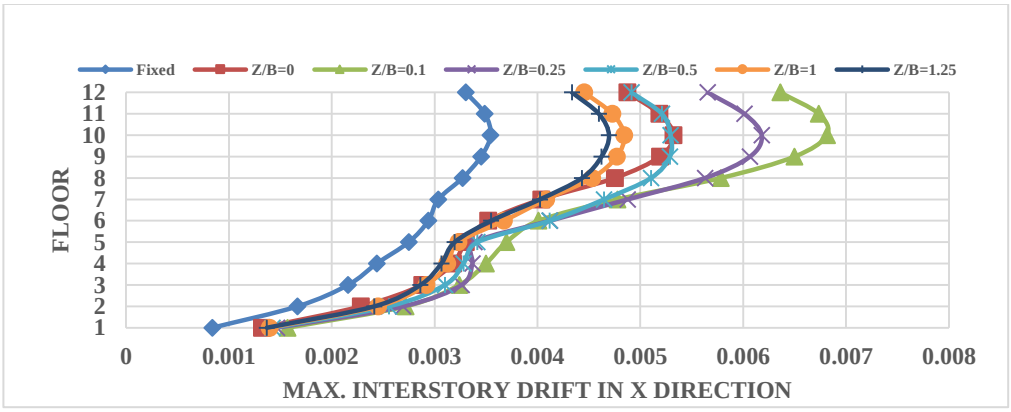


A) Uncontrolled Systems

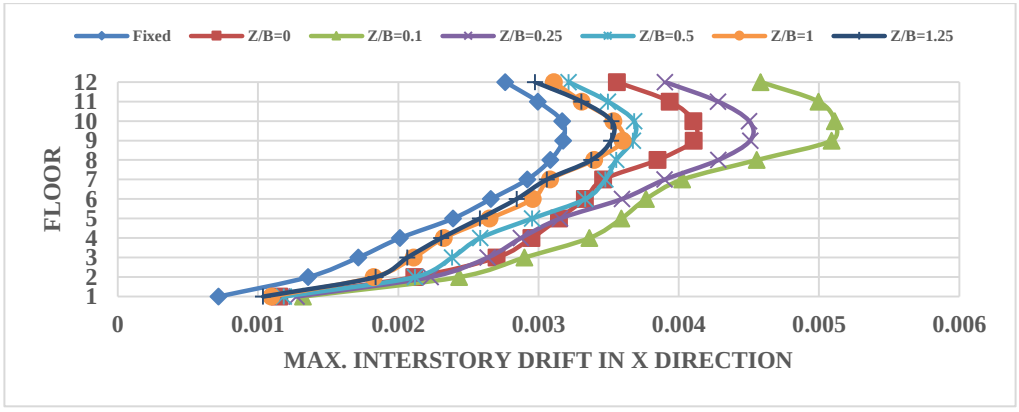


B) Controlled Systems SSI-SSI

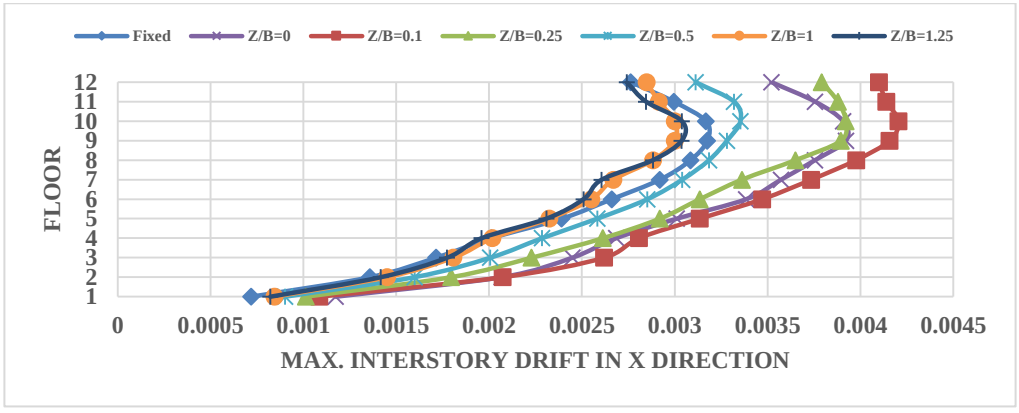


C) Controlled Systems Fixed-SSI

**Figure G-63** Max. interstory drift of the systems under earthquake Managua Nicaragua-02, 12/23/1972

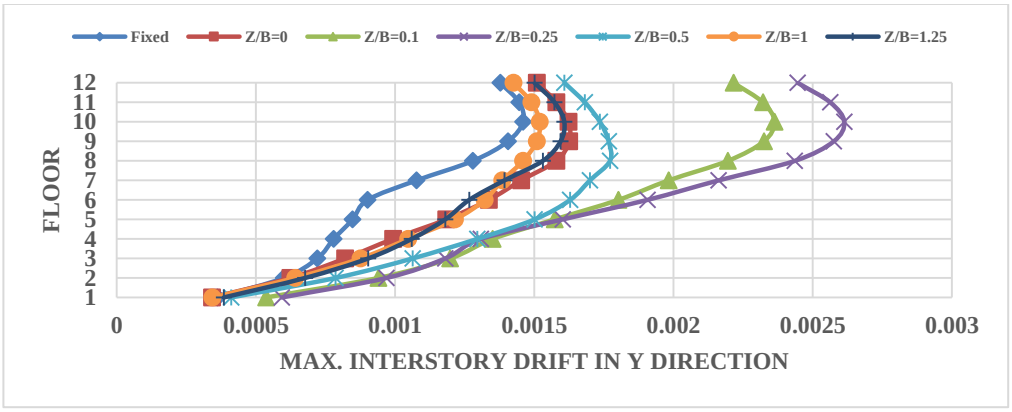


A) Uncontrolled Systems

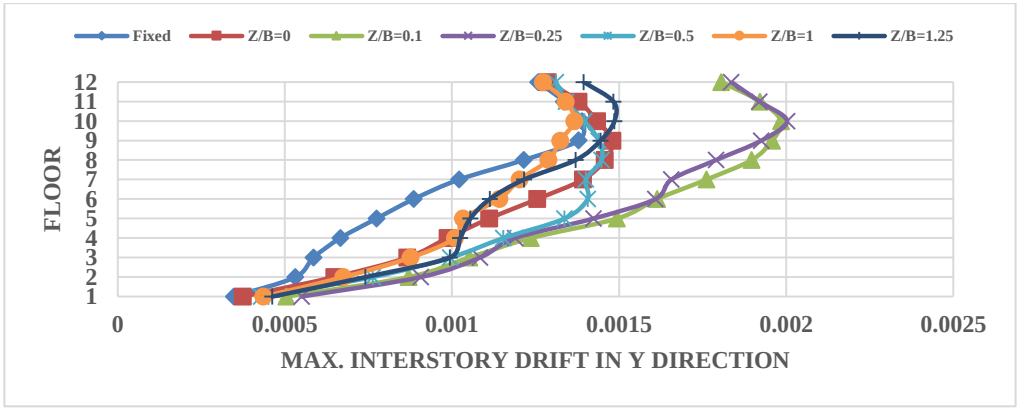


B) Controlled Systems SSI-SSI

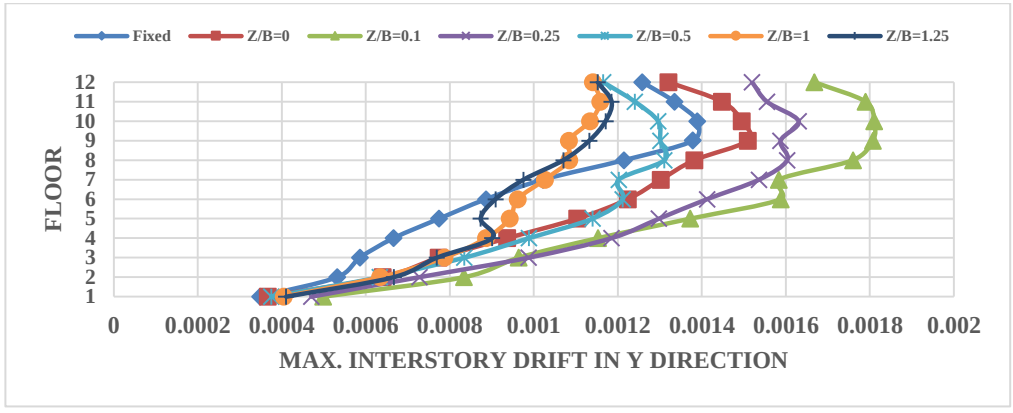


C) Controlled Systems Fixed-SSI

**Figure G-64** Max. interstory drift of the systems under earthquake Managua Nicaragua-02, 12/23/1972

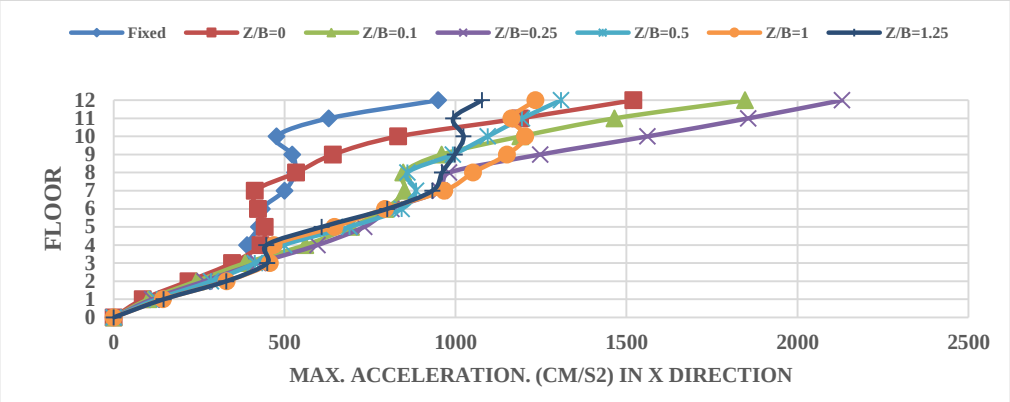


A) Uncontrolled Systems

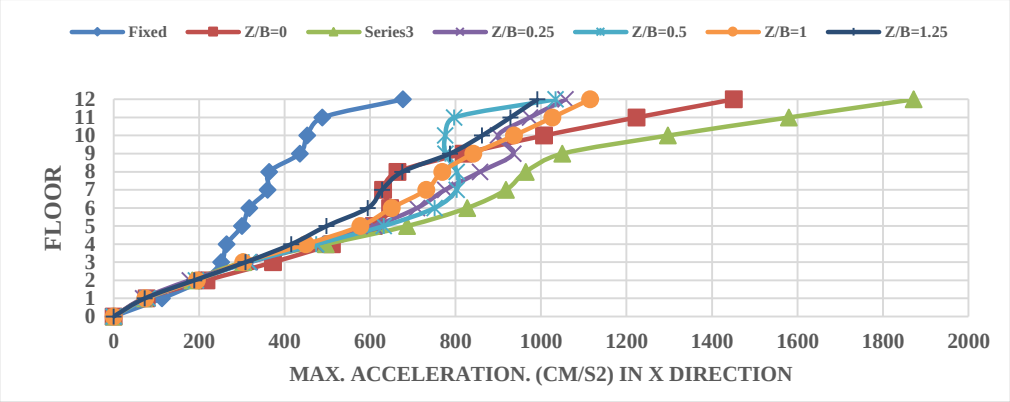


B) Controlled Systems SSI-SSI

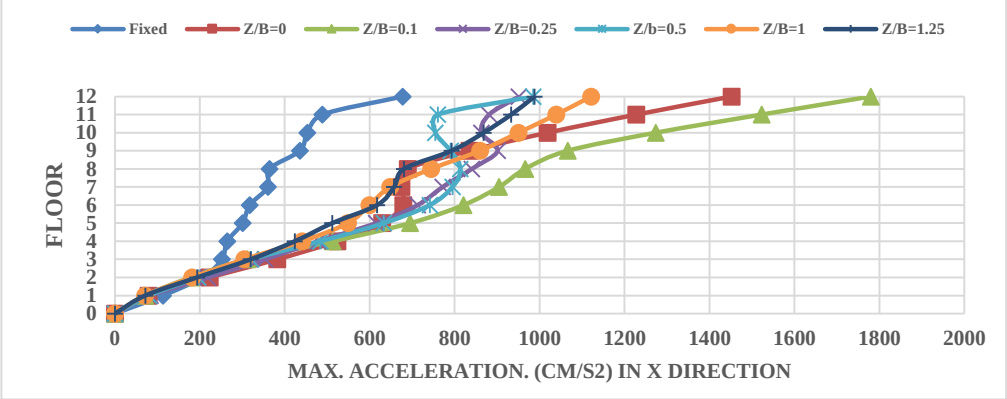


C) Controlled Systems Fixed-SSI

**Figure G-65** Max. acceleration of the systems under earthquake Managua Nicaragua-02, 12/23/1972

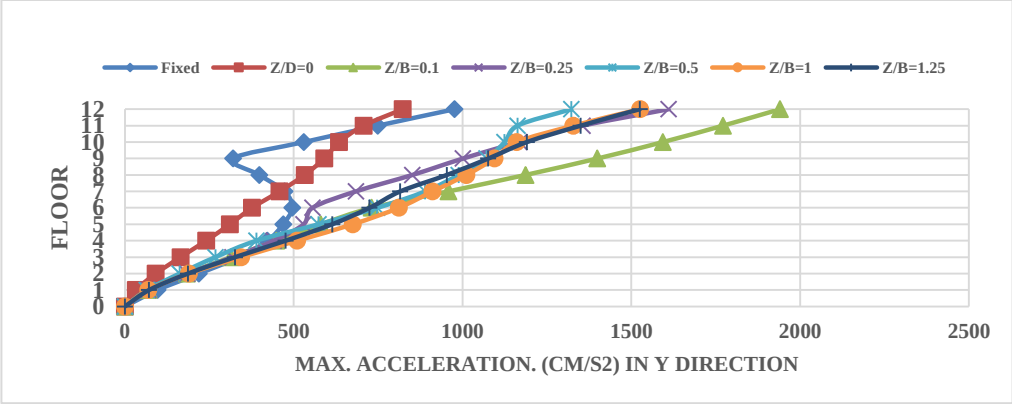


A) Uncontrolled Systems

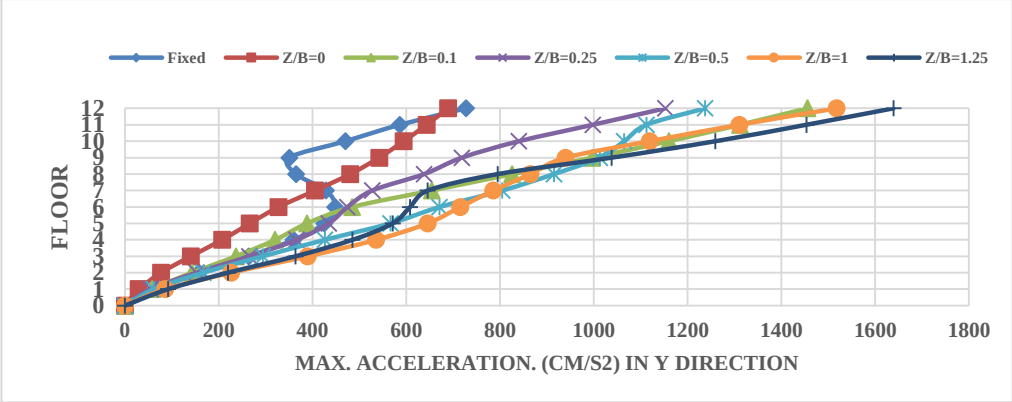


B) Controlled Systems SSI-SSI

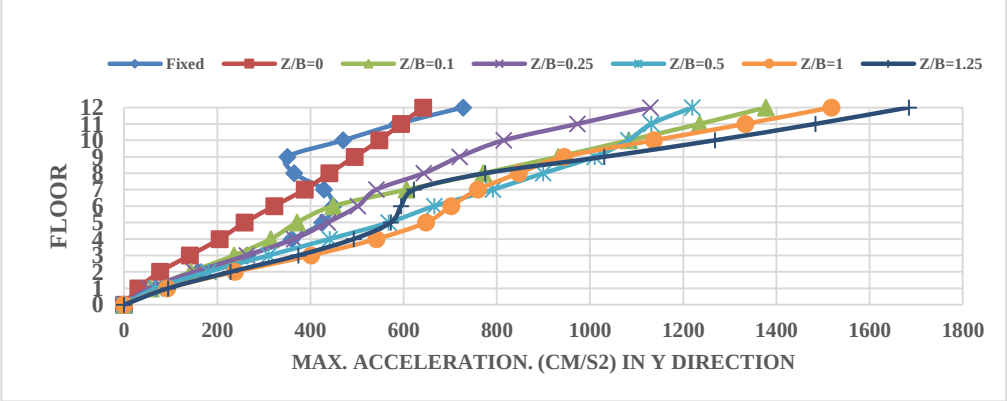


C) Controlled Systems Fixed-SSI

**Figure G-66** Max. acceleration of the systems under earthquake Managua Nicaragua-02, 12/23/1972

Soft top and medium bottom

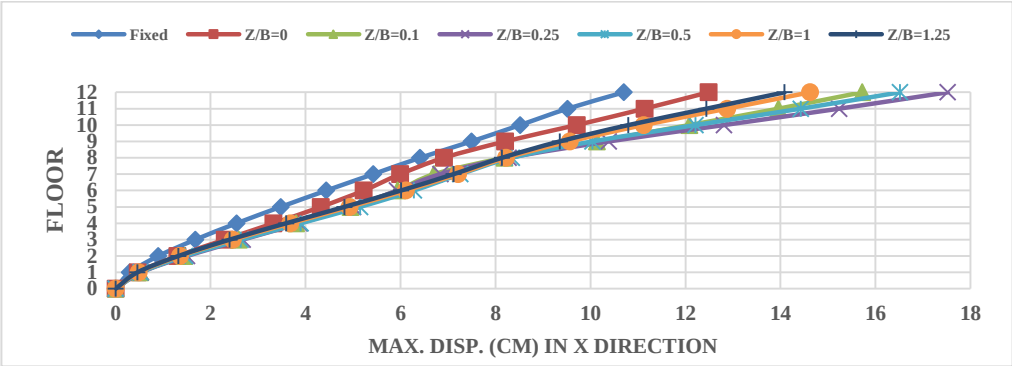


A) Uncontrolled Systems

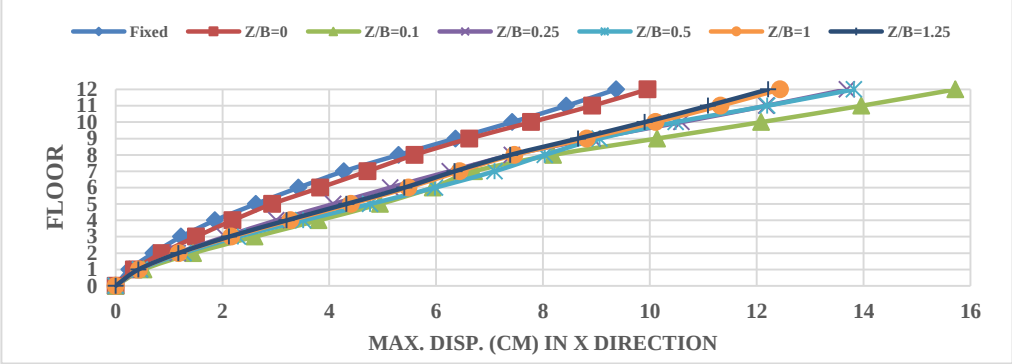


B) Controlled Systems SSI-SSI

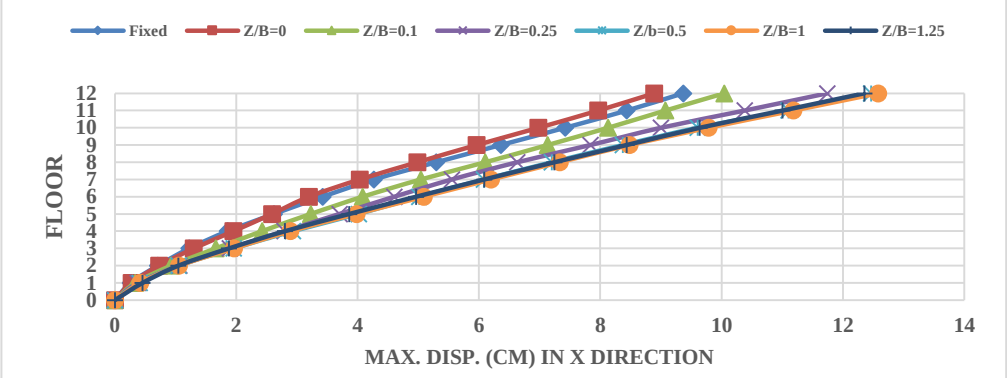


C) Controlled Systems Fixed-SSI

**Figure G-67** Max. displacements of the systems under earthquake Managua Nicaragua-02, 12/23/1972

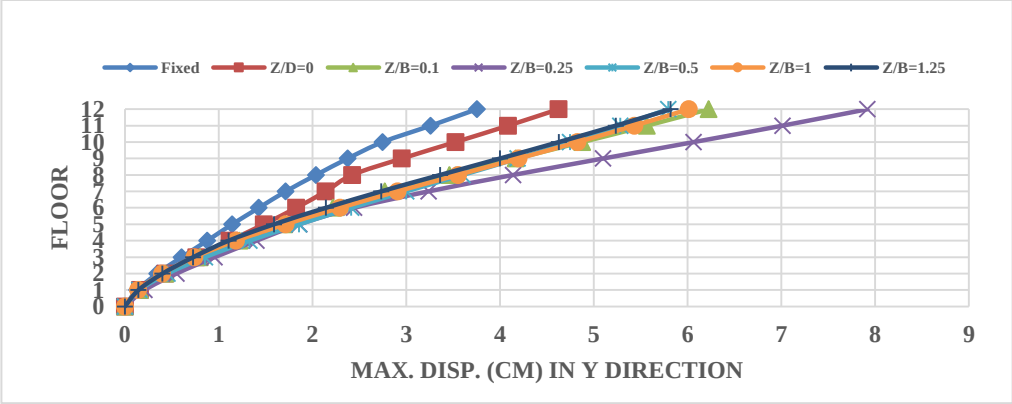


A) Uncontrolled Systems

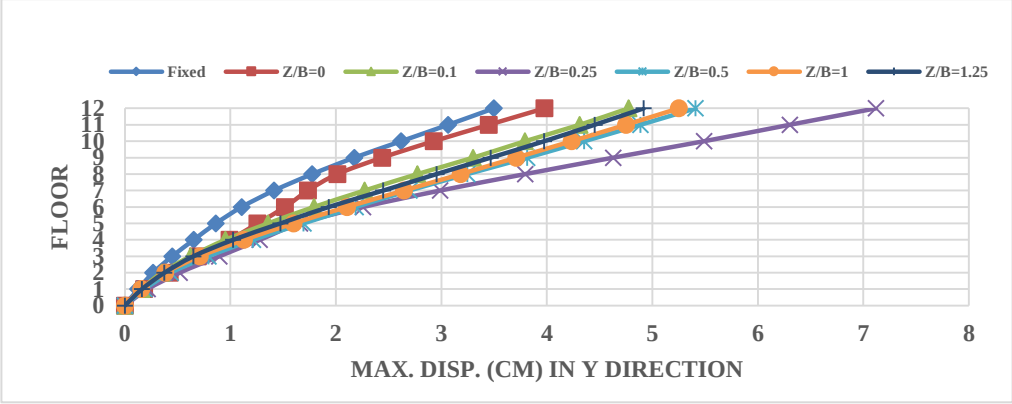


B) Controlled Systems SSI-SSI

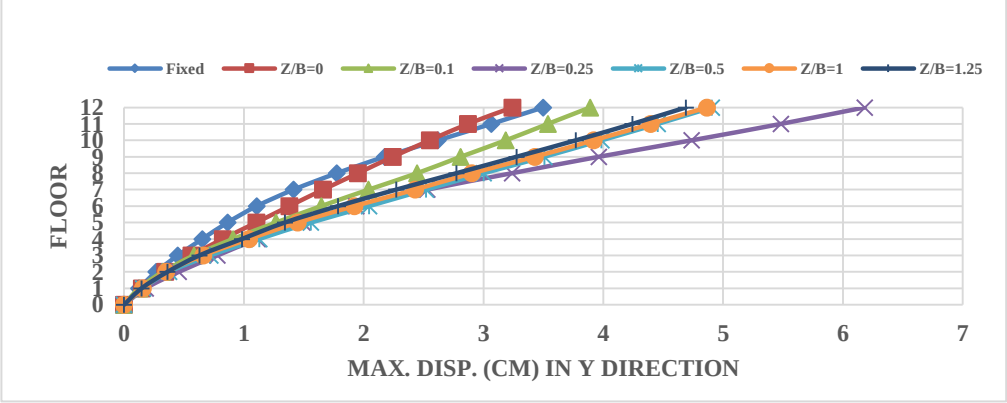


C) Controlled Systems Fixed-SSI

**Figure G-68** Max. displacements of the systems under earthquake Managua Nicaragua-02, 12/23/1972

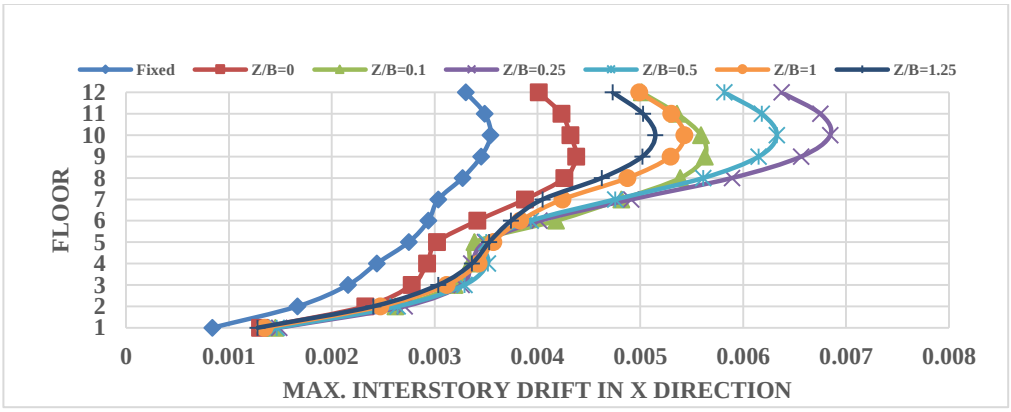


A) Uncontrolled Systems

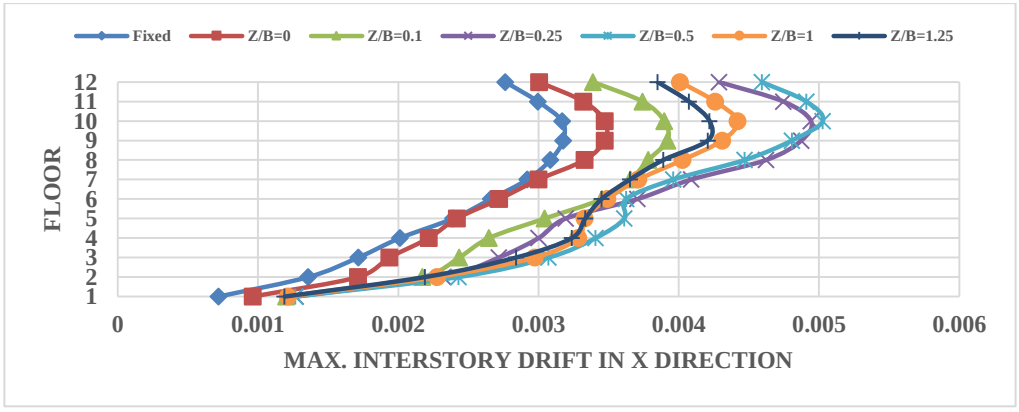


B) Controlled Systems SSI-SSI

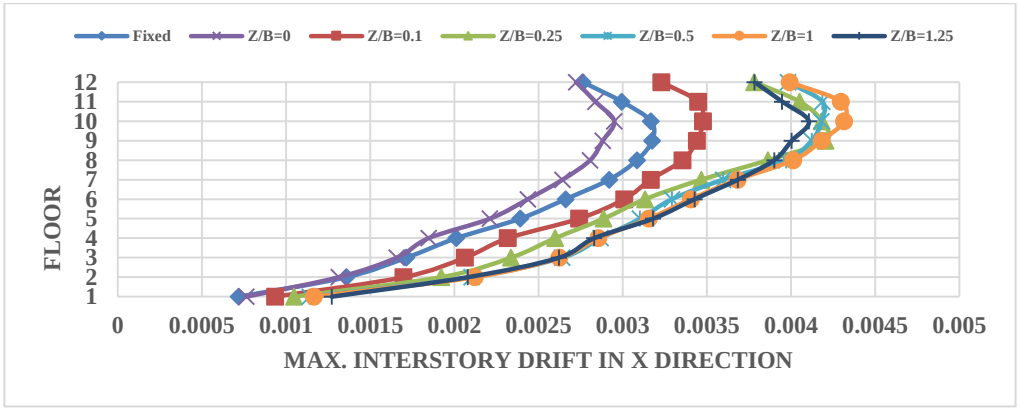


C) Controlled Systems Fixed-SSI

**Figure G-69** Max. interstory drift of the systems under earthquake Managua Nicaragua-02, 12/23/1972

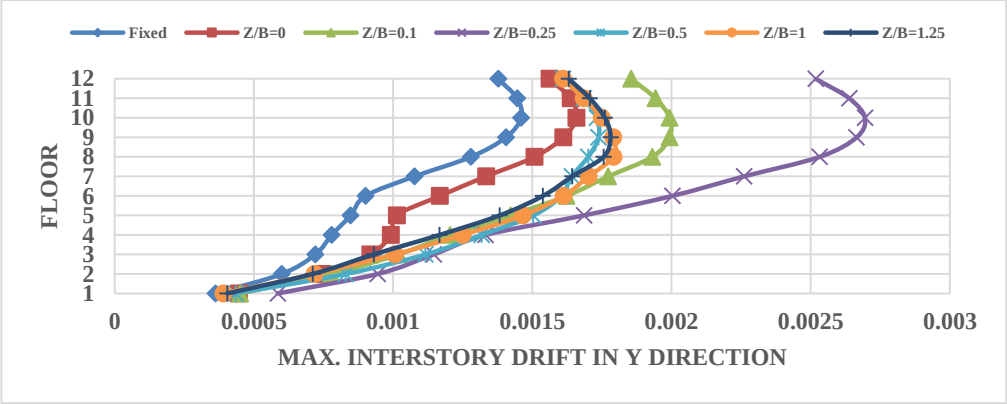


A) Uncontrolled Systems

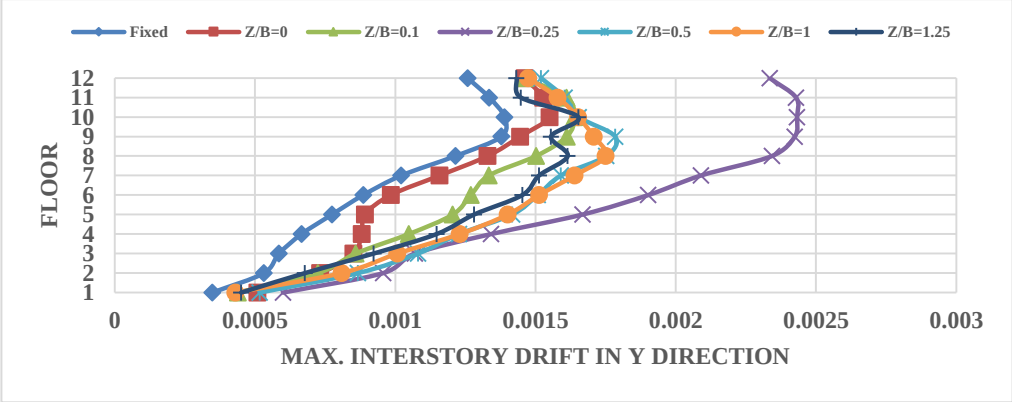


B) Controlled Systems SSI-SSI

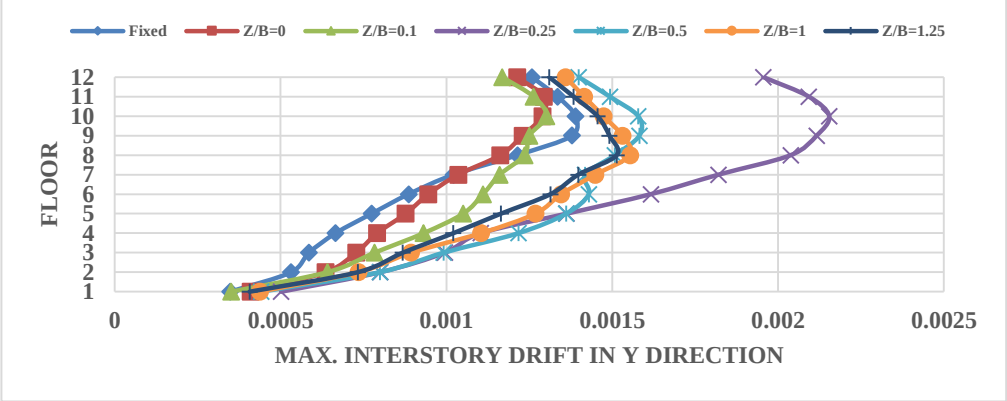


C) Controlled Systems Fixed-SSI

**Figure G-70** Max. interstory drift of the systems under earthquake Managua Nicaragua-02, 12/23/1972

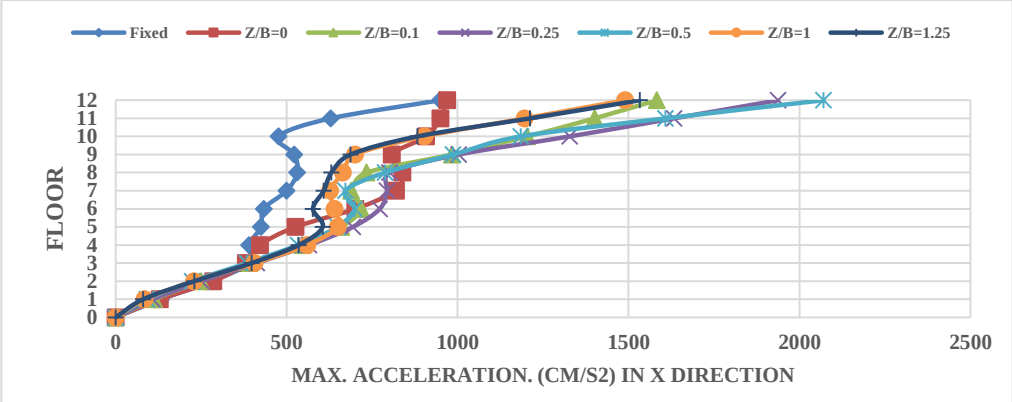


A) Uncontrolled Systems

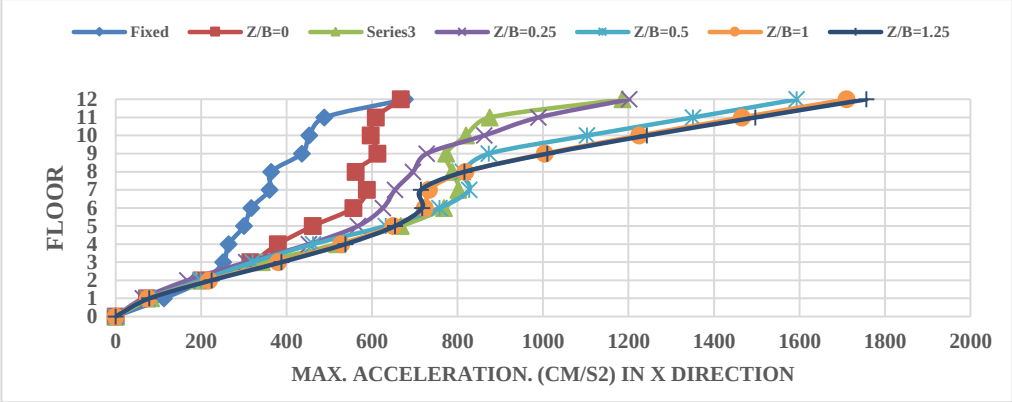


B) Controlled Systems SSI-SSI

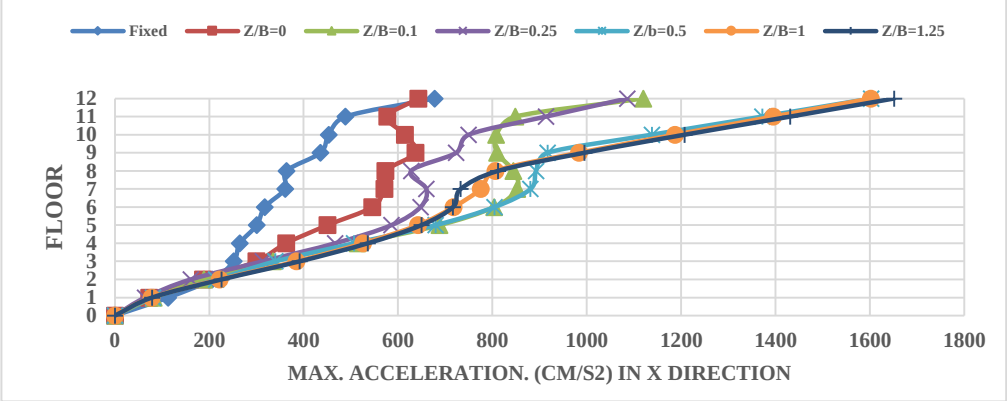


C) Controlled Systems Fixed-SSI

**Figure G-71** Max. acceleration of the systems under earthquake Managua Nicaragua-02, 12/23/1972

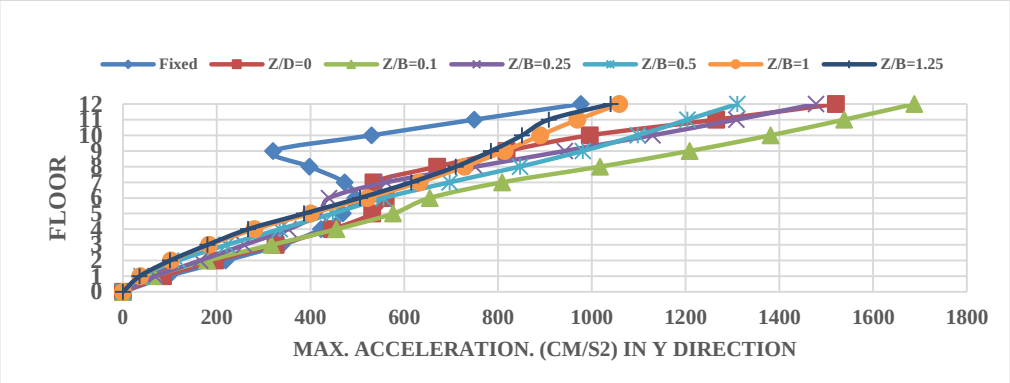


A) Uncontrolled Systems

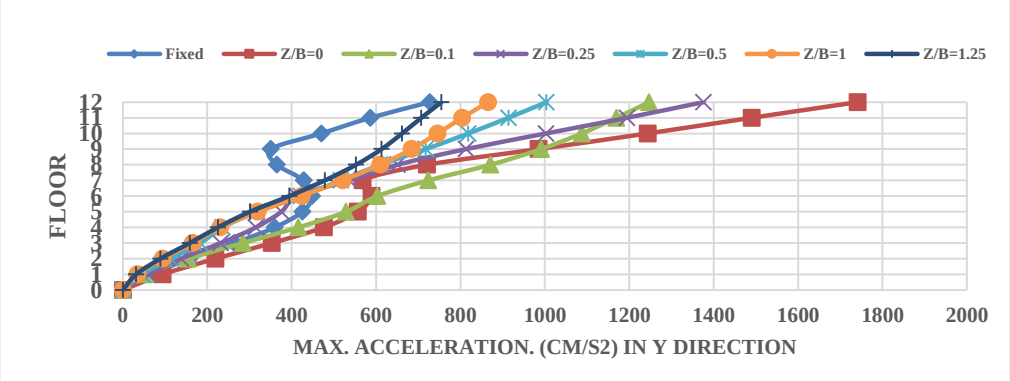


B) Controlled Systems SSI-SSI

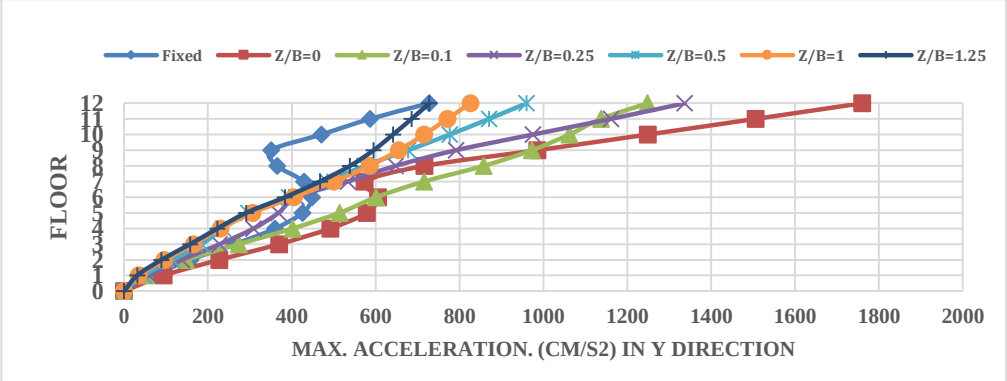


C) Controlled Systems Fixed-SSI

**Figure G-72** Max. acceleration of the systems under earthquake Managua Nicaragua-02, 12/23/1972

Soil profile clay (linear)

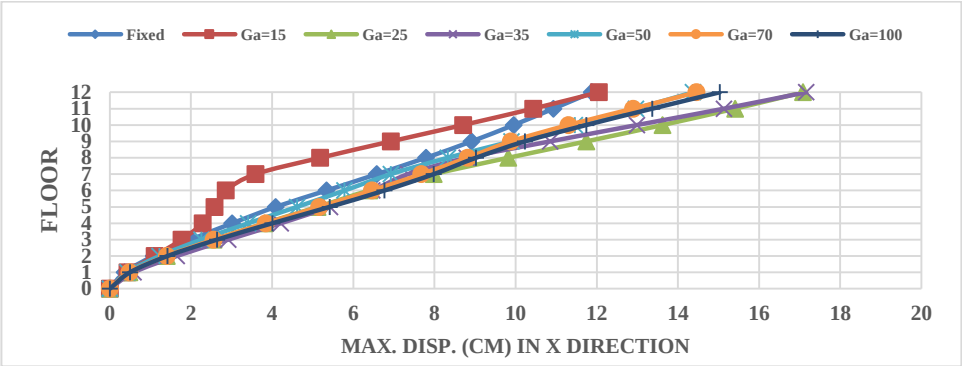


A) Uncontrolled Systems

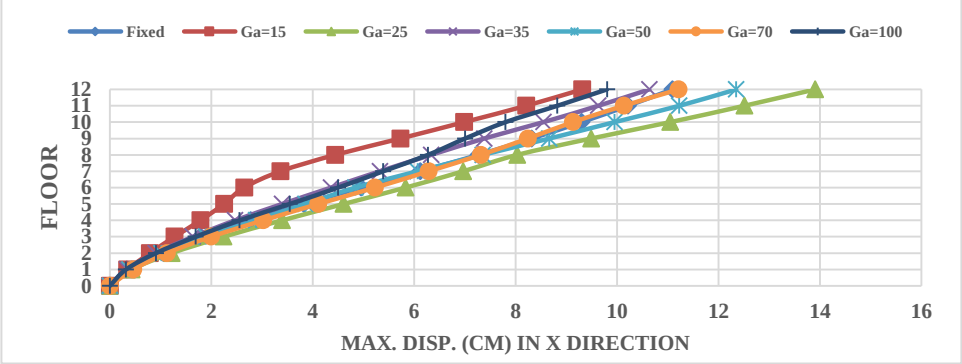


B) Controlled Systems SSI-SSI

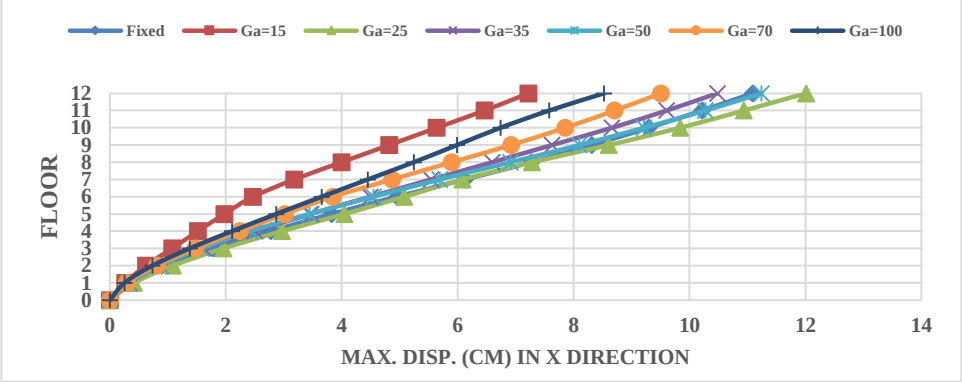


C) Controlled Systems Fixed-SSI

**Figure G-73** Max. displacements of the systems under earthquake Corinth Greece, 2/24/1981

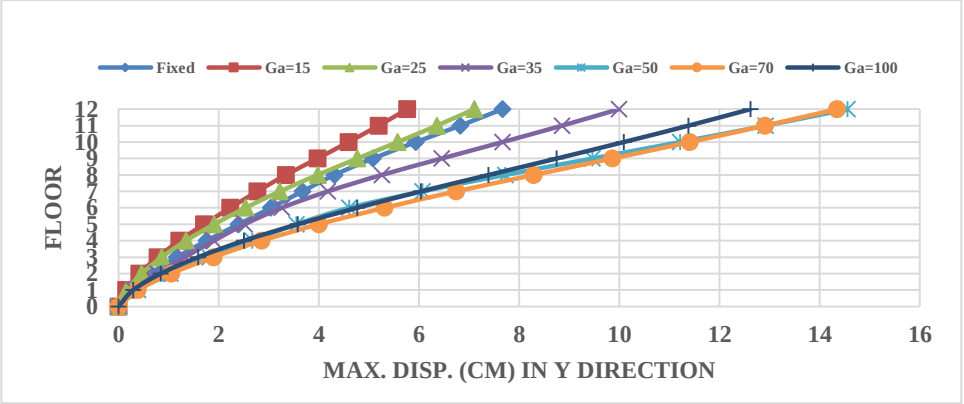


A) Uncontrolled Systems

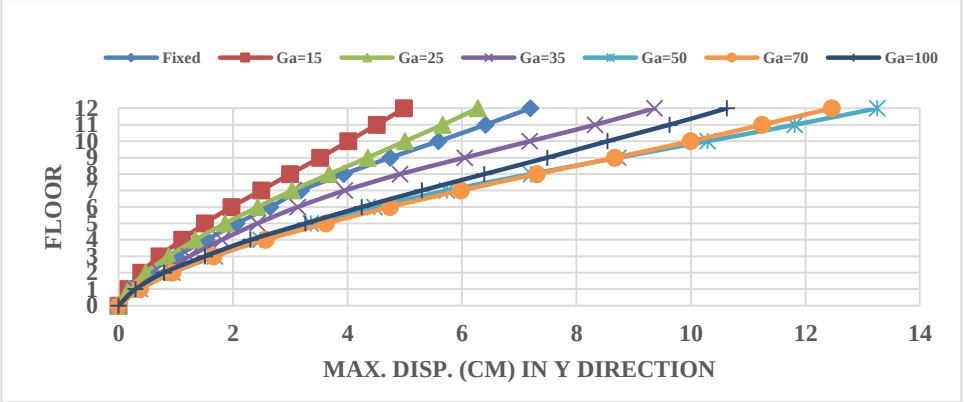


B) Controlled Systems SSI-SSI

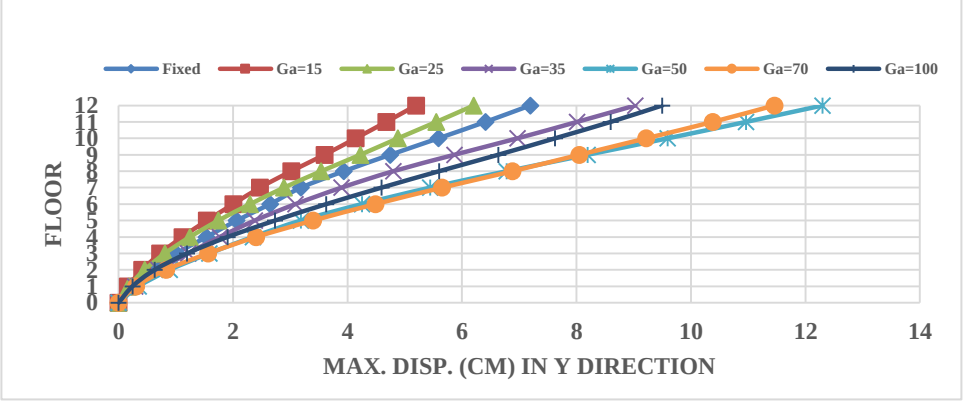


C) Controlled Systems Fixed-SSI

**Figure G-74** Max. displacements of the systems under earthquake Corinth Greece, 2/24/1981

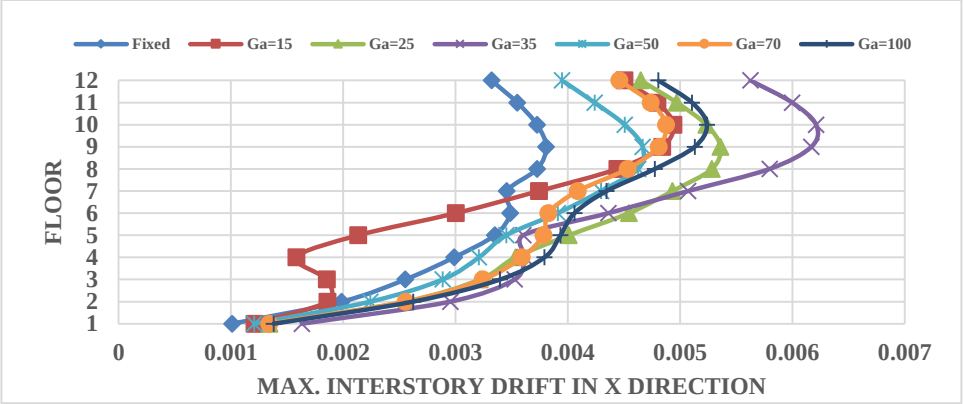


A) Uncontrolled Systems

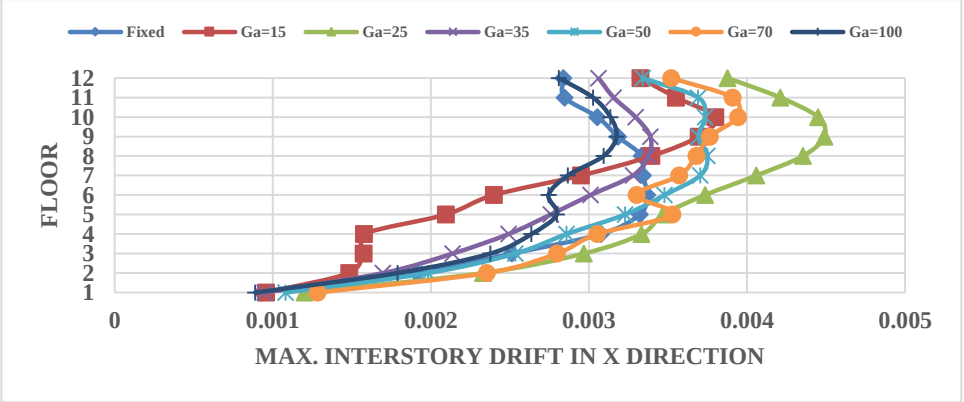


B) Controlled Systems SSI-SSI

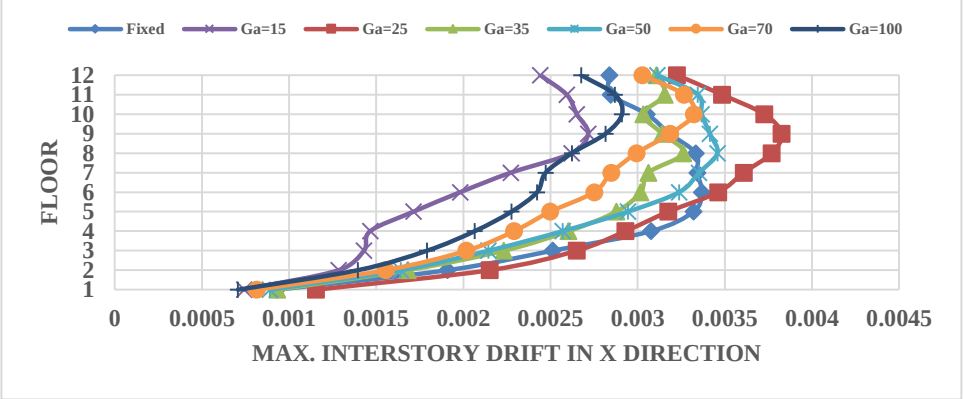


C) Controlled Systems Fixed-SSI

**Figure G-75** Max. interstory drift of the systems under earthquake Corinth Greece, 2/24/1981

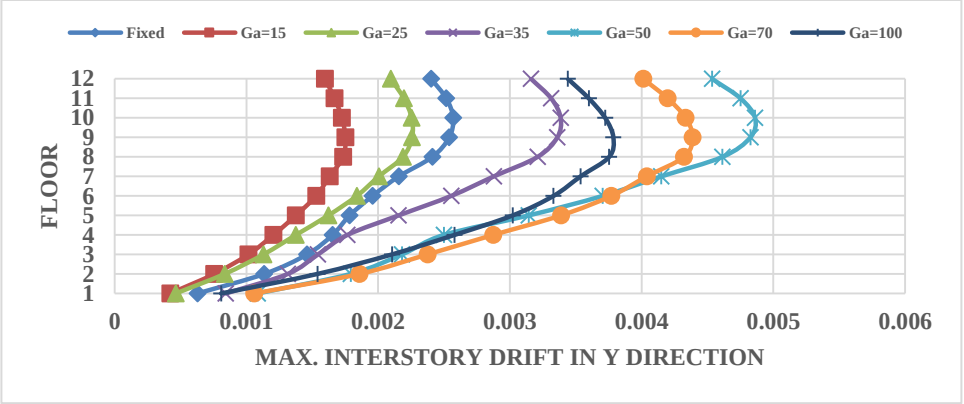


A) Uncontrolled Systems

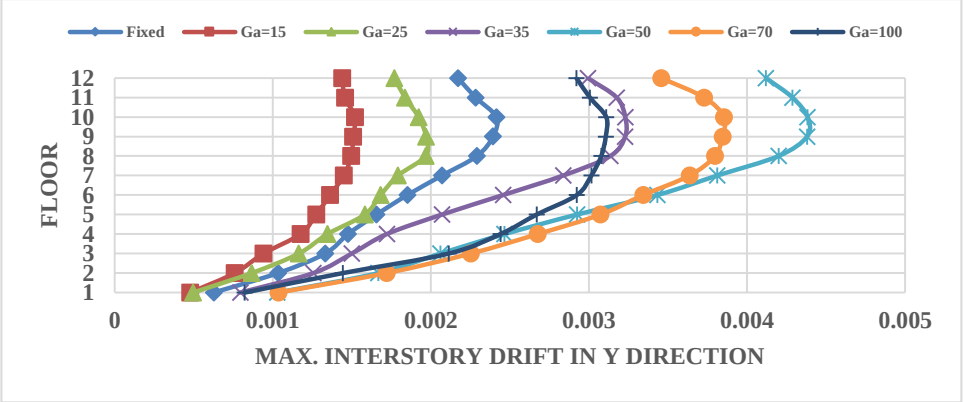


B) Controlled Systems SSI-SSI

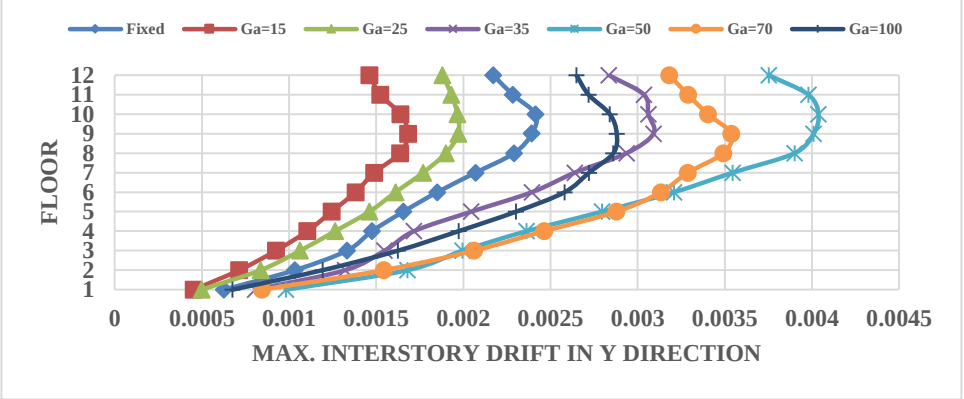


C) Controlled Systems Fixed-SSI

**Figure G-76** Max. interstory drift of the systems under earthquake Corinth Greece, 2/24/1981

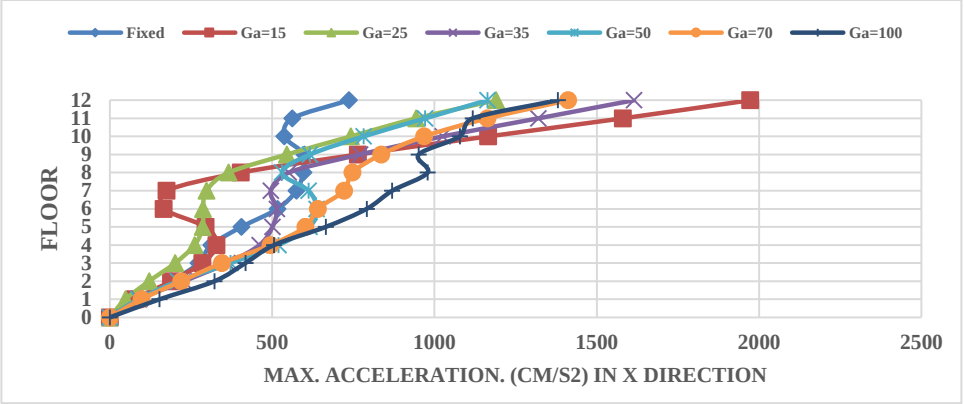


A) Uncontrolled Systems

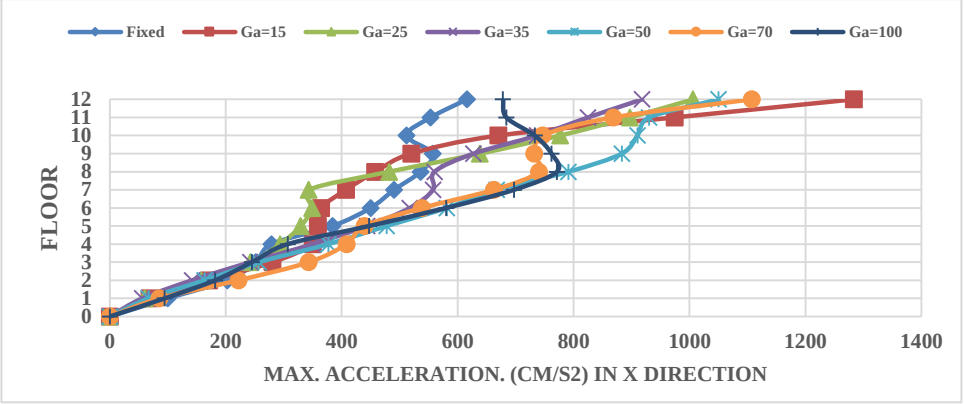


B) Controlled Systems SSI-SSI

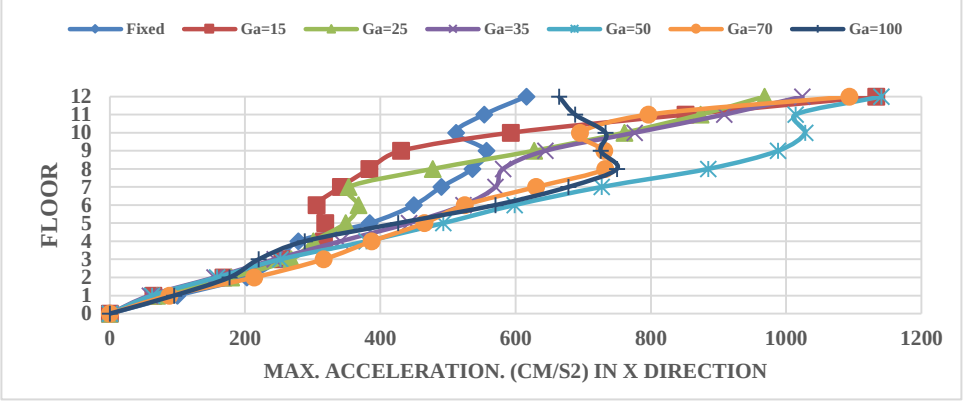


C) Controlled Systems Fixed-SSI

**Figure G-77** Max. acceleration of the systems under earthquake Corinth Greece, 2/24/1981

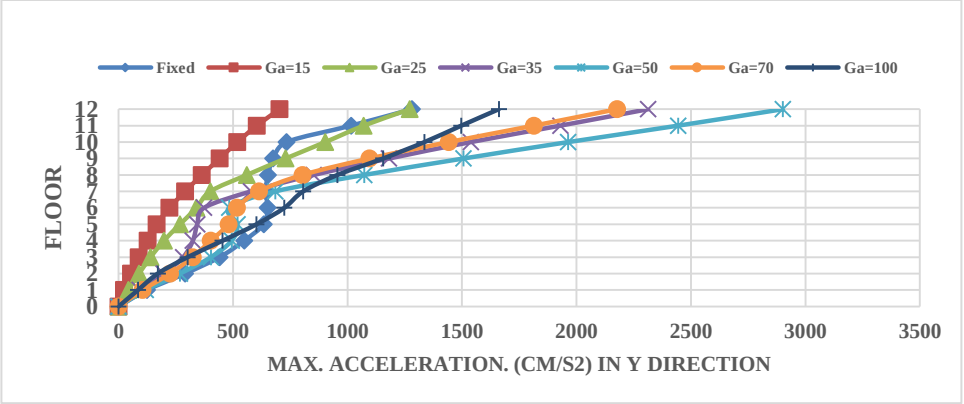


A) Uncontrolled Systems

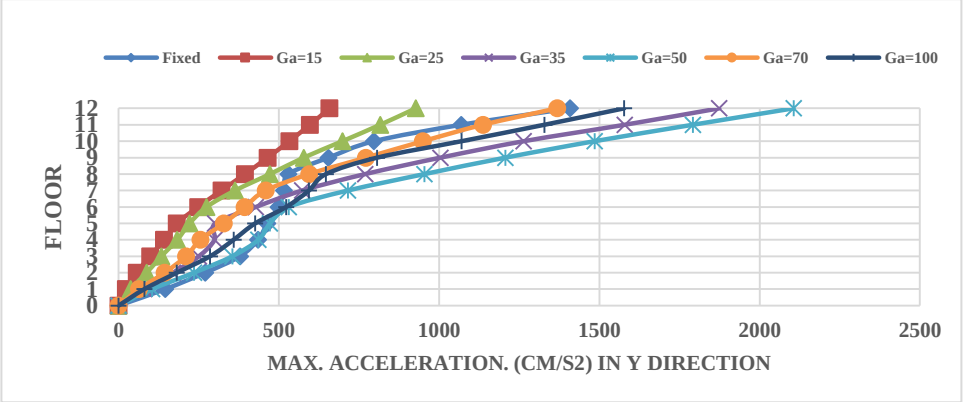


B) Controlled Systems SSI-SSI

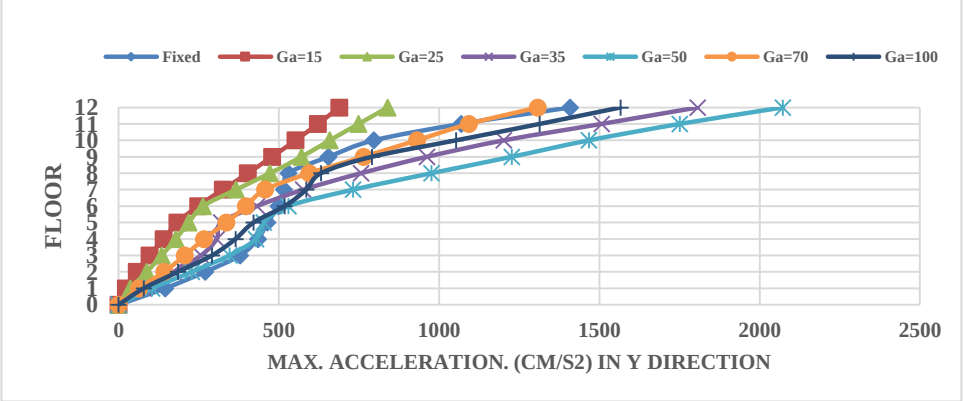


C) Controlled Systems Fixed-SSI

**Figure G-78** Max. acceleration of the systems under earthquake Corinth Greece, 2/24/1981

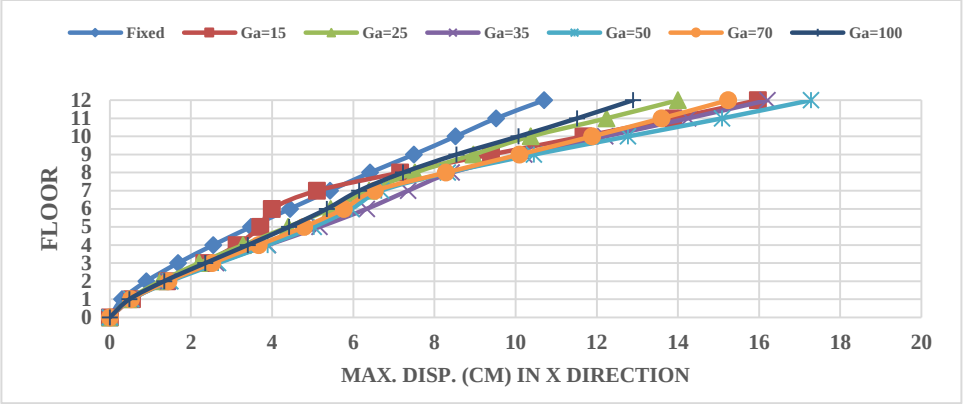


A) Uncontrolled Systems

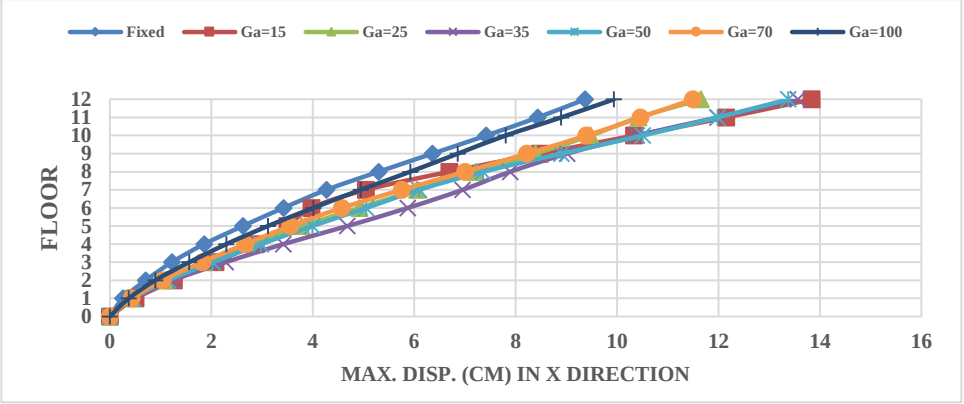


B) Controlled Systems SSI-SSI

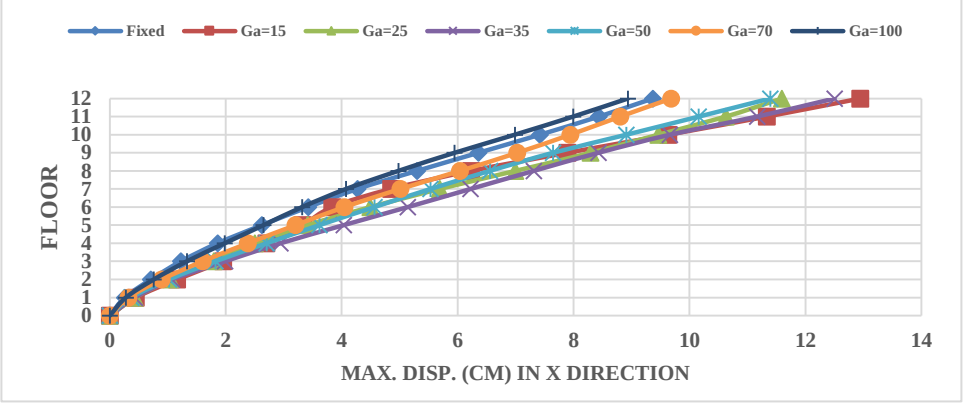


C) Controlled Systems Fixed-SSI

**Figure G-79** Max. displacements of the systems under earthquake Managua Nicaragua-02, 12/23/1972

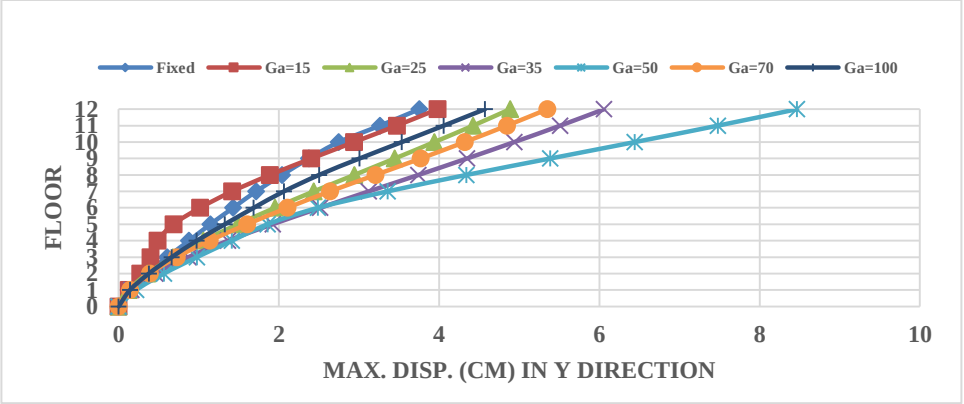


A) Uncontrolled Systems

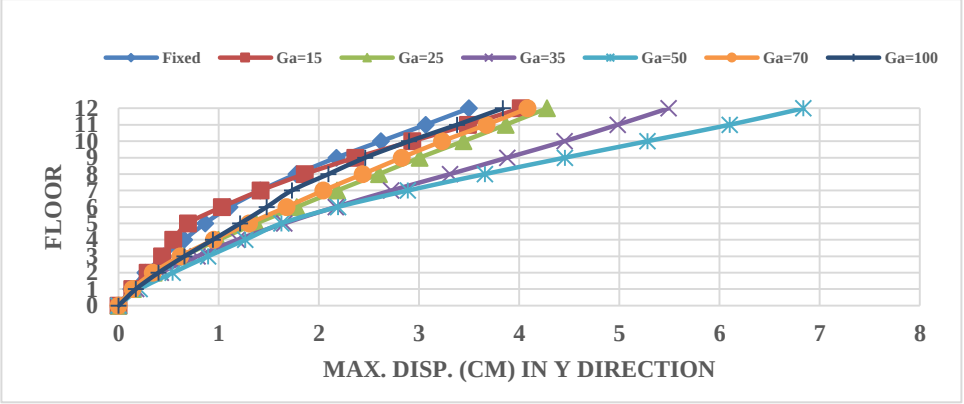


B) Controlled Systems SSI-SSI

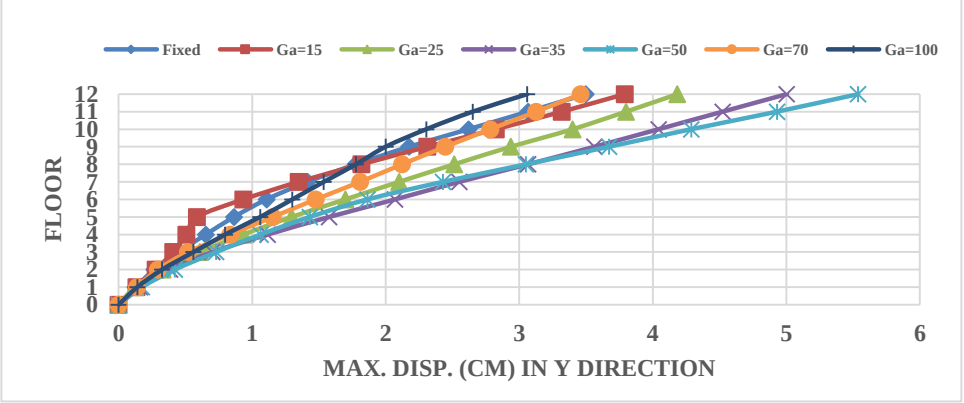


C) Controlled Systems Fixed-SSI

**Figure G-80** Max. displacements of the systems under earthquake Managua Nicaragua-02, 12/23/1972

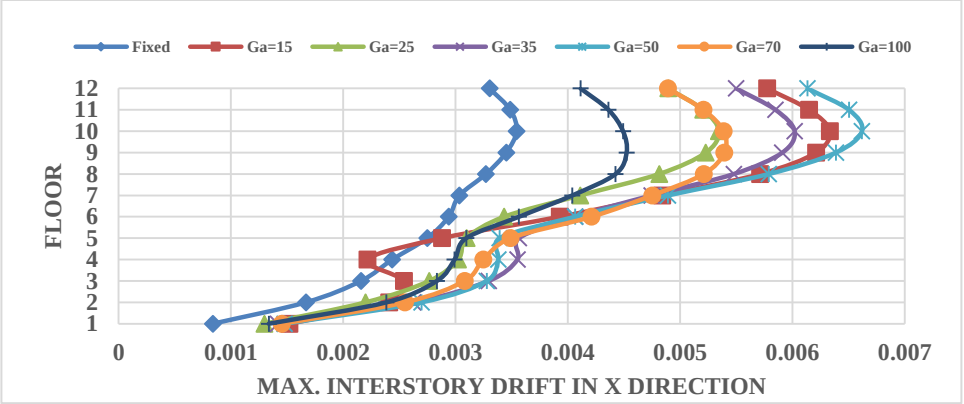


A) Uncontrolled Systems

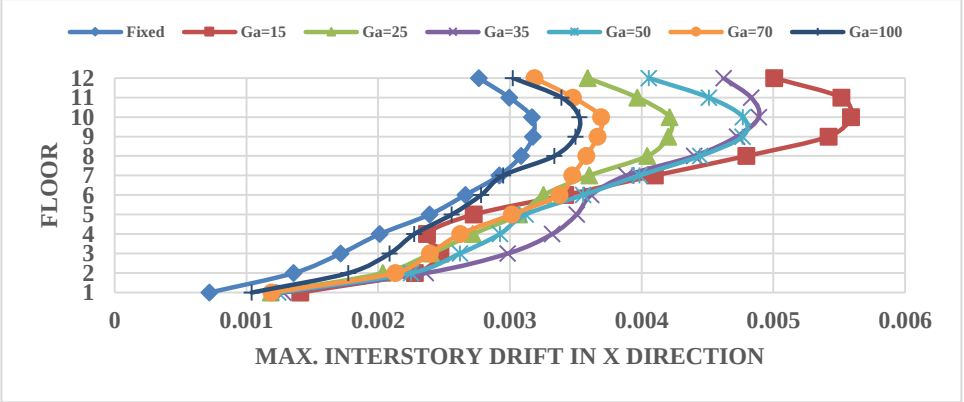


B) Controlled Systems SSI-SSI

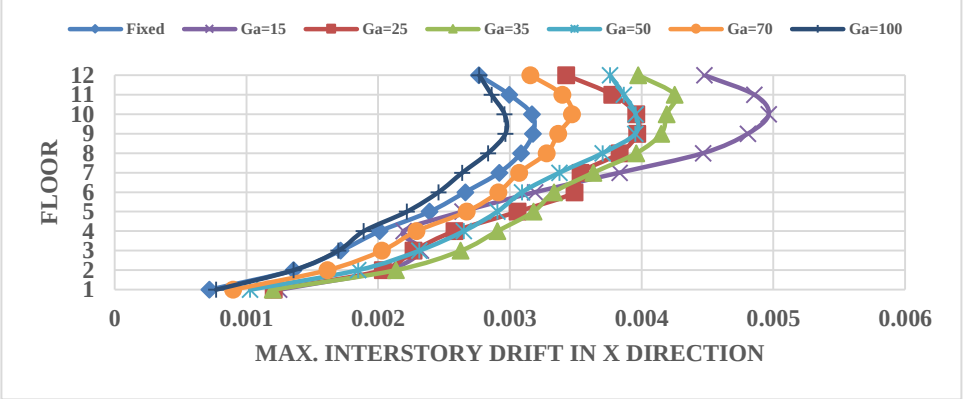


C) Controlled Systems Fixed-SSI

**Figure G-81** Max. interstory drift of the systems under earthquake Managua Nicaragua-02, 12/23/1972

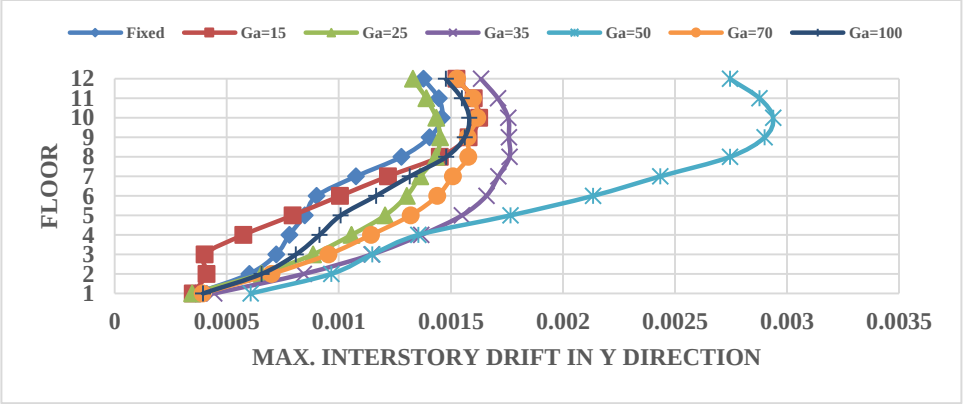


A) Uncontrolled Systems

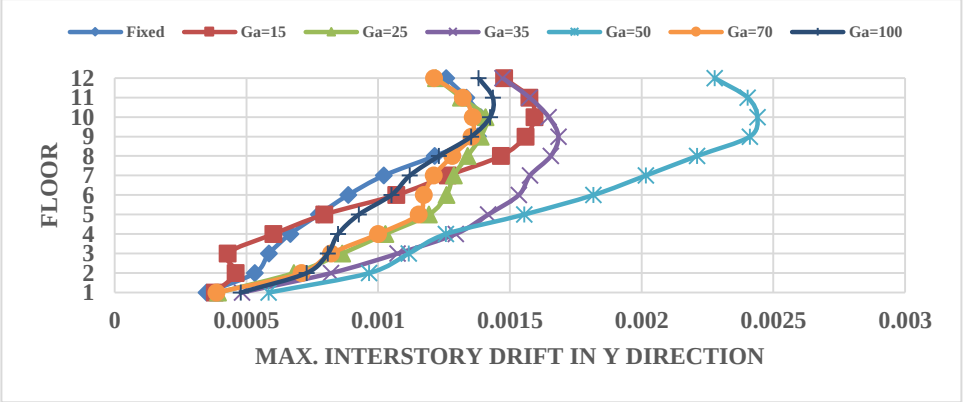


B) Controlled Systems SSI-SSI

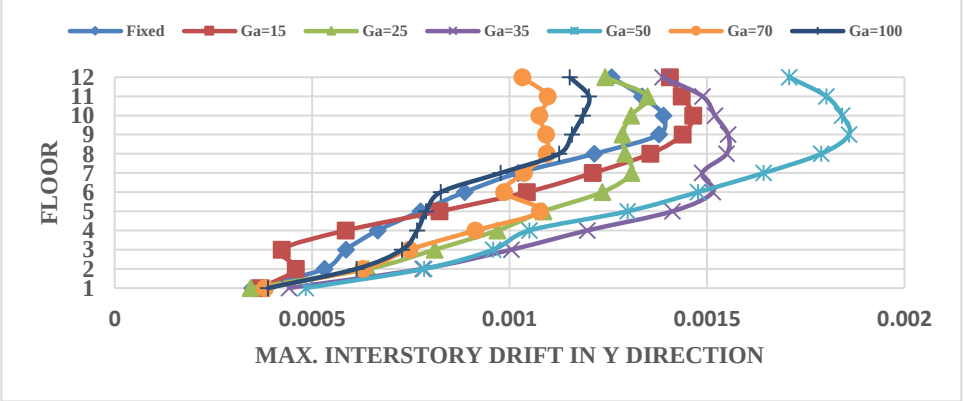


C) Controlled Systems Fixed-SSI

**Figure G-82** Max. interstory drift of the systems under earthquake Managua Nicaragua-02, 12/23/1972

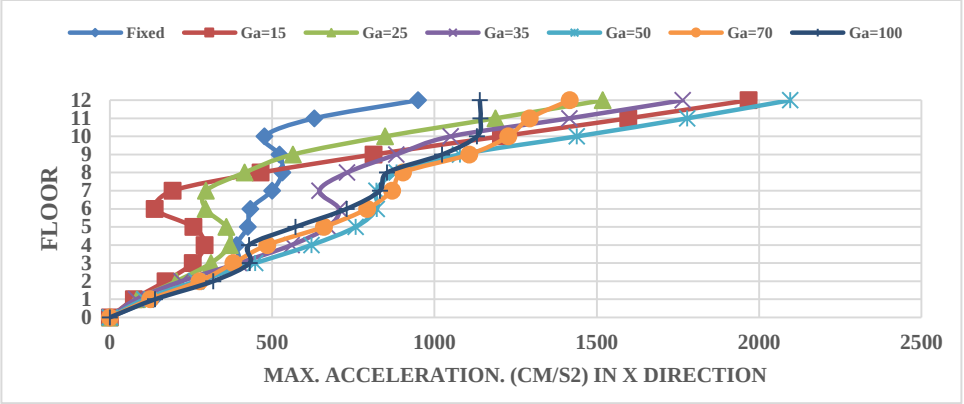


A) Uncontrolled Systems

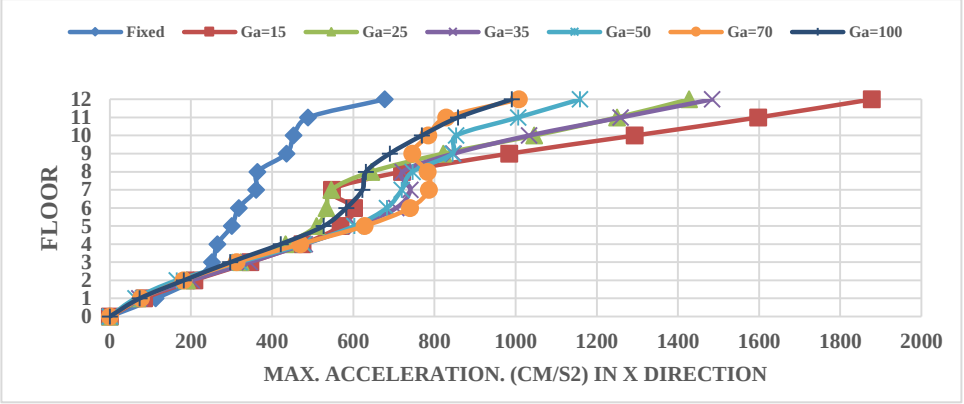


B) Controlled Systems SSI-SSI

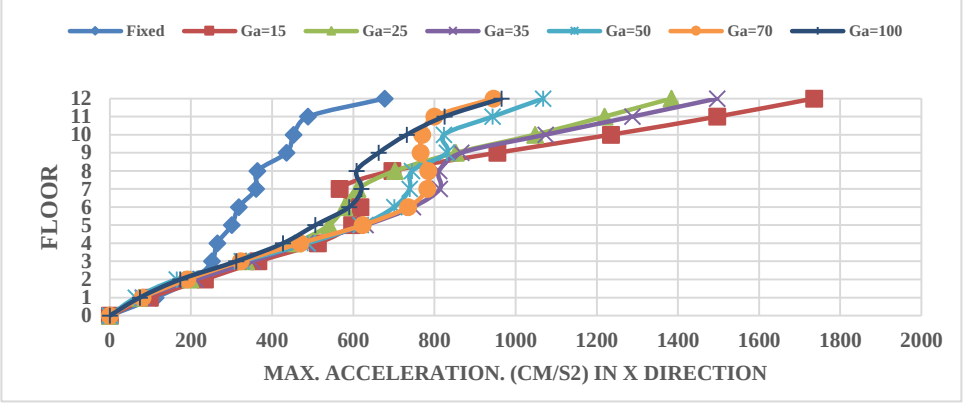


C) Controlled Systems Fixed-SSI

**Figure G-83** Max. acceleration of the systems under earthquake Managua Nicaragua-02, 12/23/1972

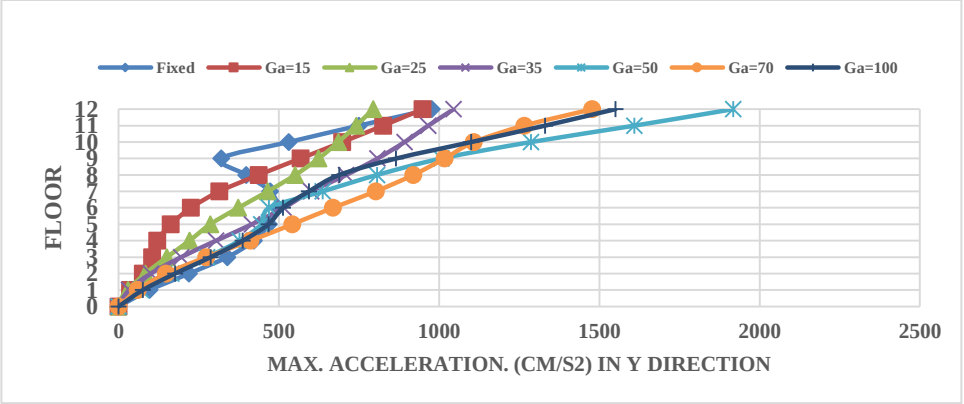


A) Uncontrolled Systems

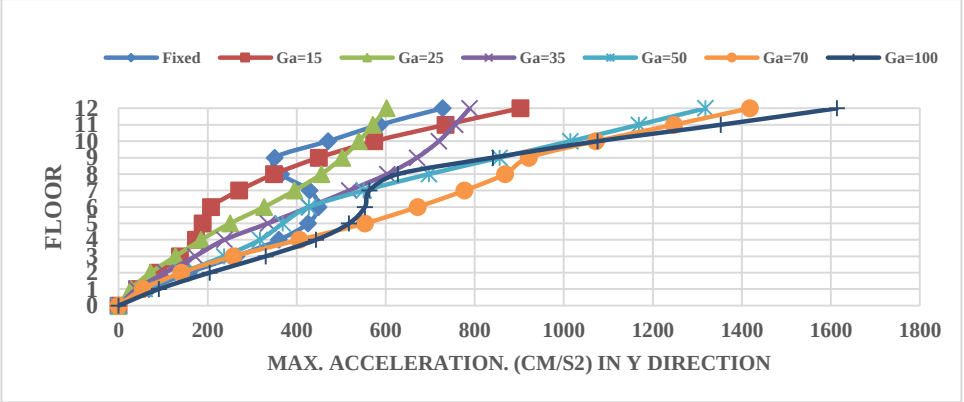


B) Controlled Systems SSI-SSI

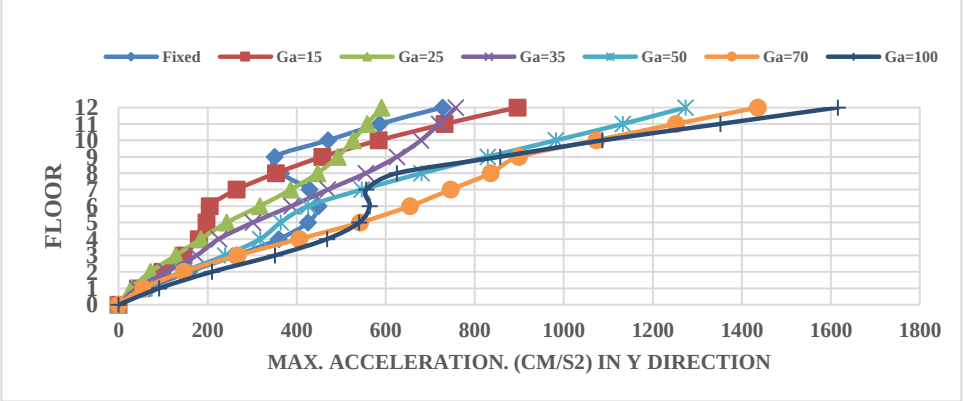


C) Controlled Systems Fixed-SSI

**Figure G-84** Max. acceleration of the systems under earthquake Managua Nicaragua-02, 12/23/1972

Soil profile sand (parabola)

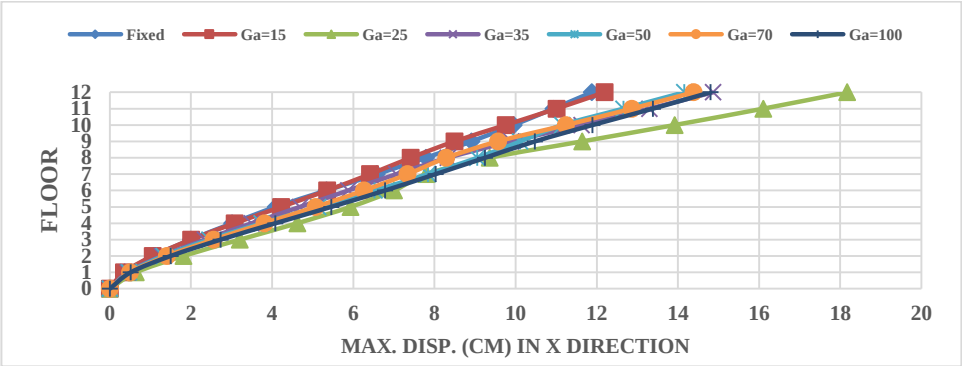


A) Uncontrolled Systems

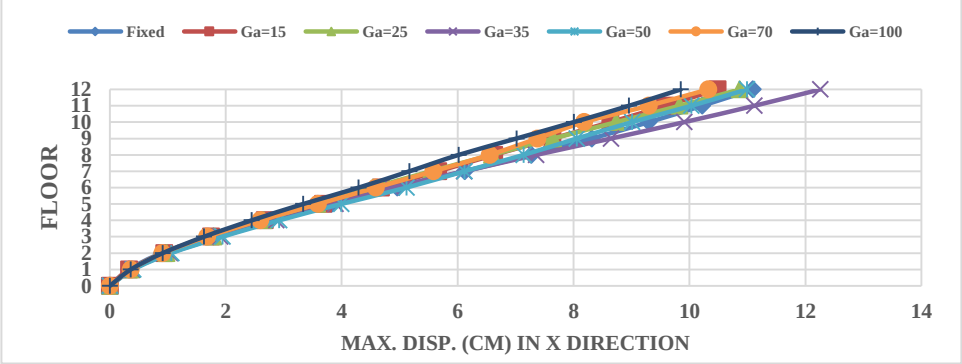


B) Controlled Systems SSI-SSI

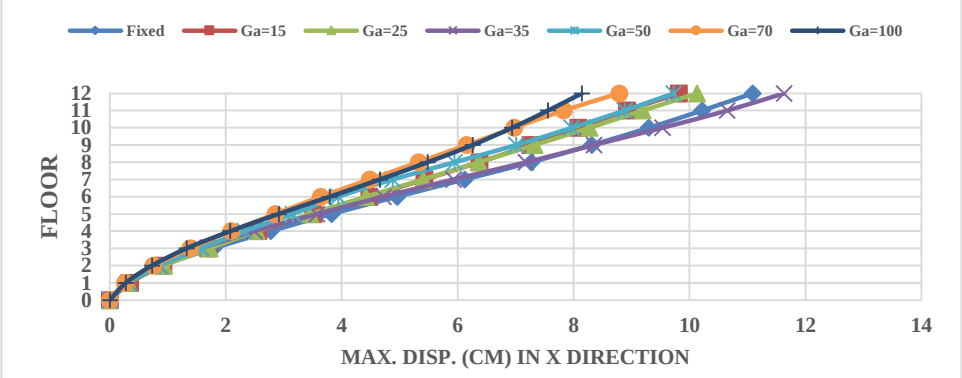


C) Controlled Systems Fixed-SSI

**Figure G-85** Max. displacements of the systems under earthquake Corinth Greece, 2/24/1981

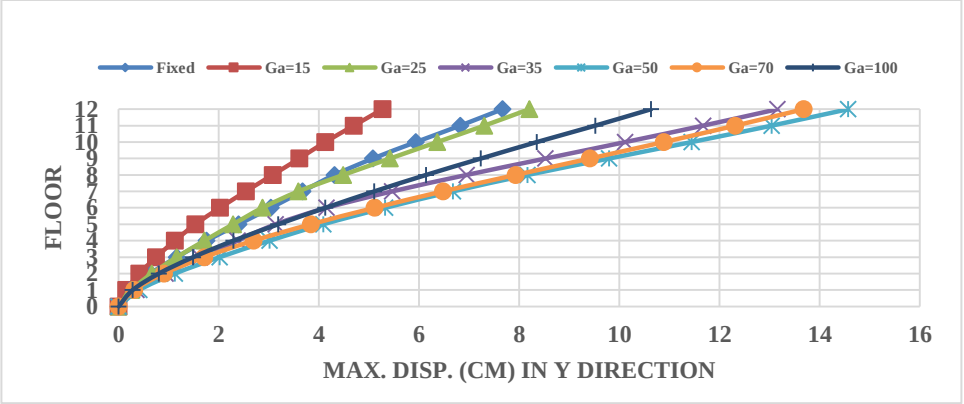


A) Uncontrolled Systems

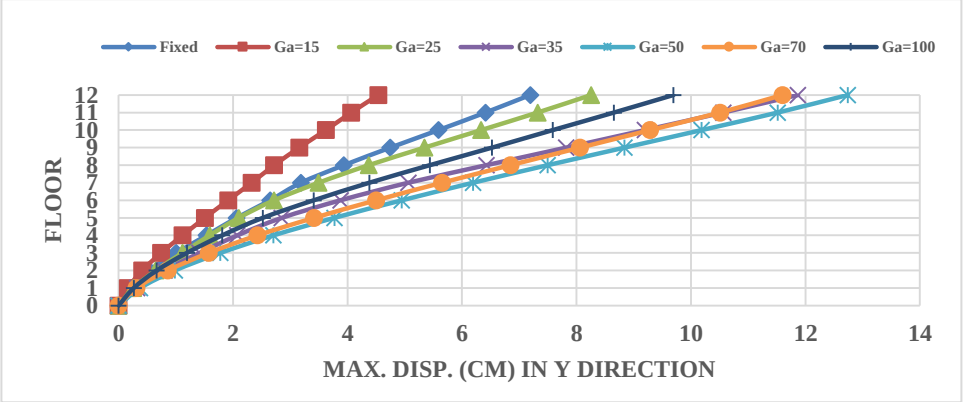


B) Controlled Systems SSI-SSI

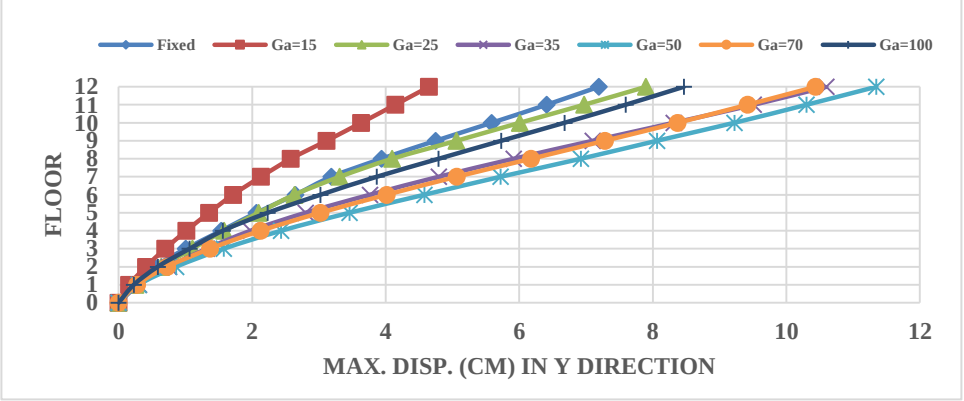


C) Controlled Systems Fixed-SSI

**Figure G-86** Max. displacements of the systems under earthquake Corinth Greece, 2/24/1981

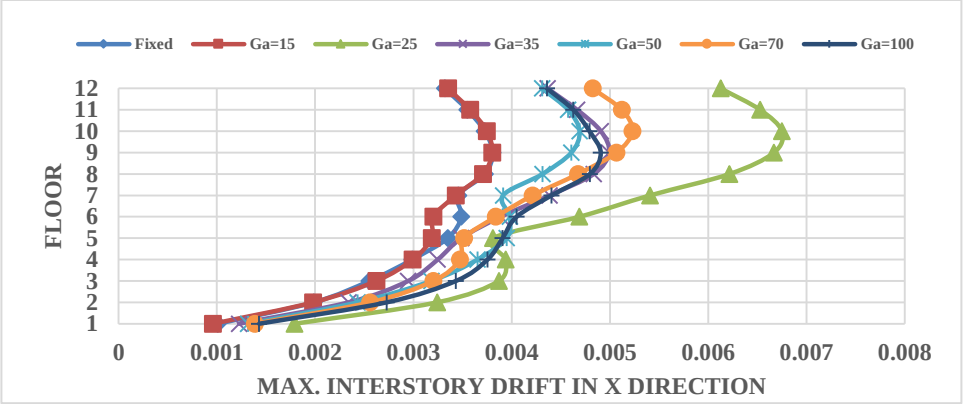


A) Uncontrolled Systems

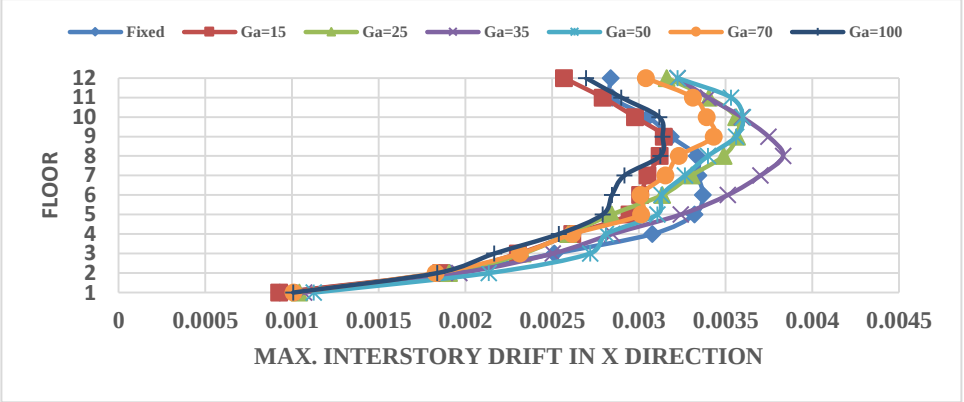


B) Controlled Systems SSI-SSI

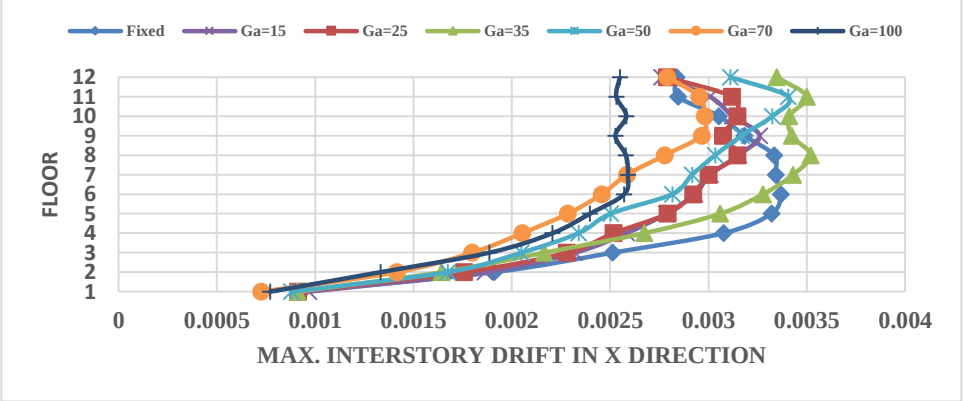


C) Controlled Systems Fixed-SSI

**Figure G-87** Max. interstory drift of the systems under earthquake Corinth Greece, 2/24/1981

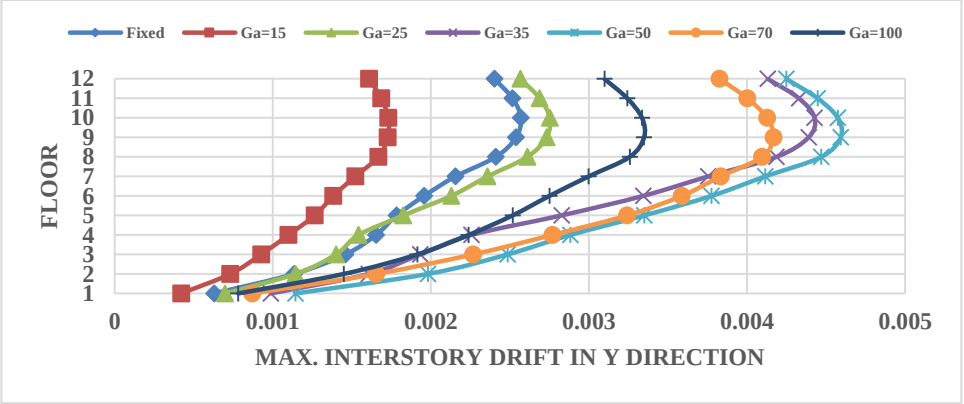


A) Uncontrolled Systems

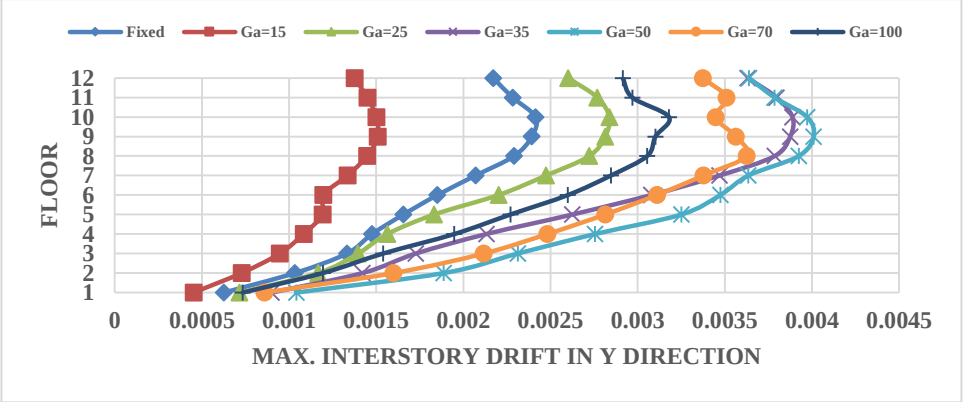


B) Controlled Systems SSI-SSI

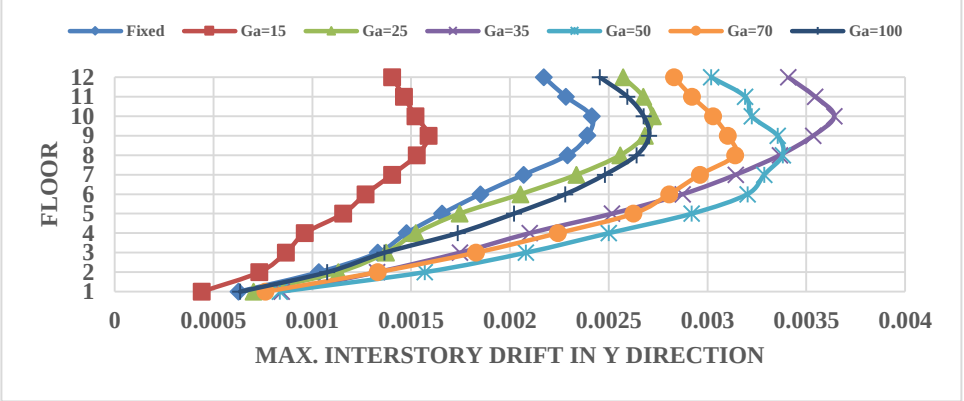


C) Controlled Systems Fixed-SSI

**Figure G-88** Max. interstory drift of the systems under earthquake Corinth Greece, 2/24/1981

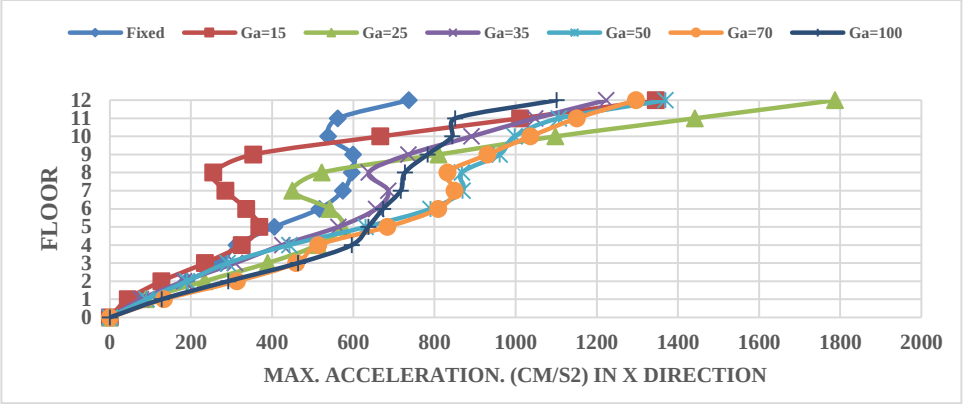


A) Uncontrolled Systems

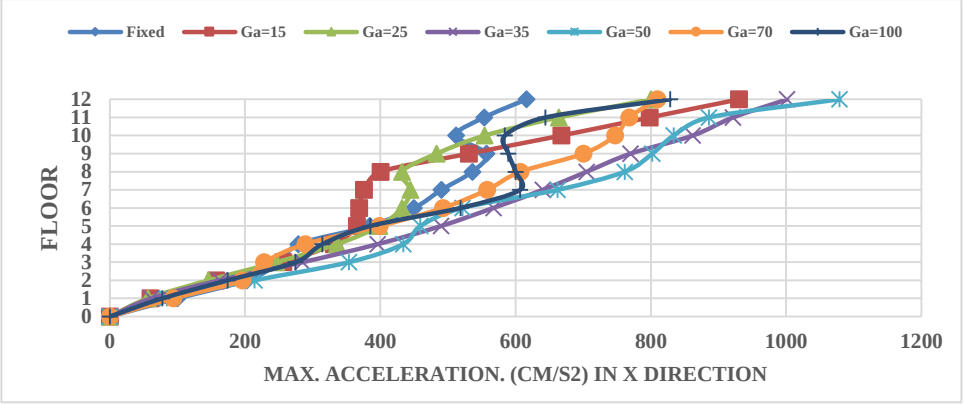


B) Controlled Systems SSI-SSI

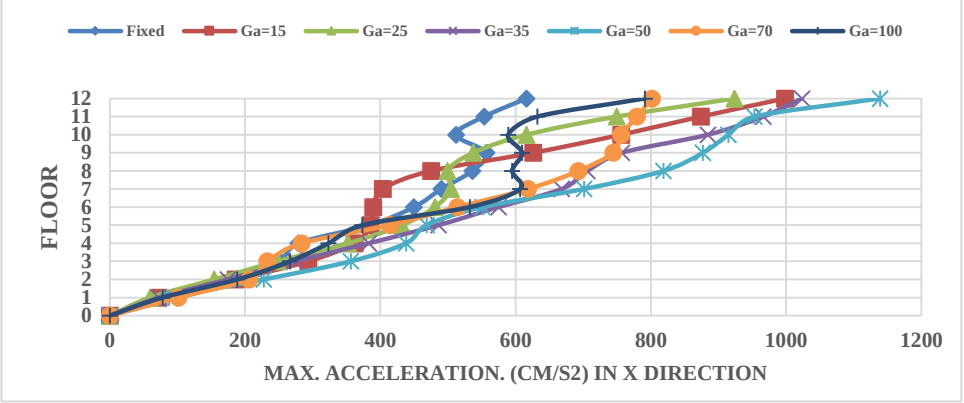


C) Controlled Systems Fixed-SSI

**Figure G-89** Max. acceleration of the systems under earthquake Corinth Greece, 2/24/1981

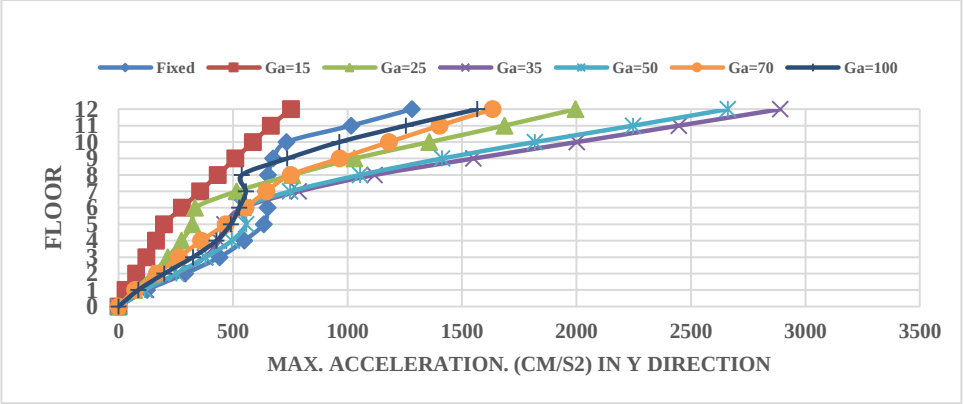


A) Uncontrolled Systems

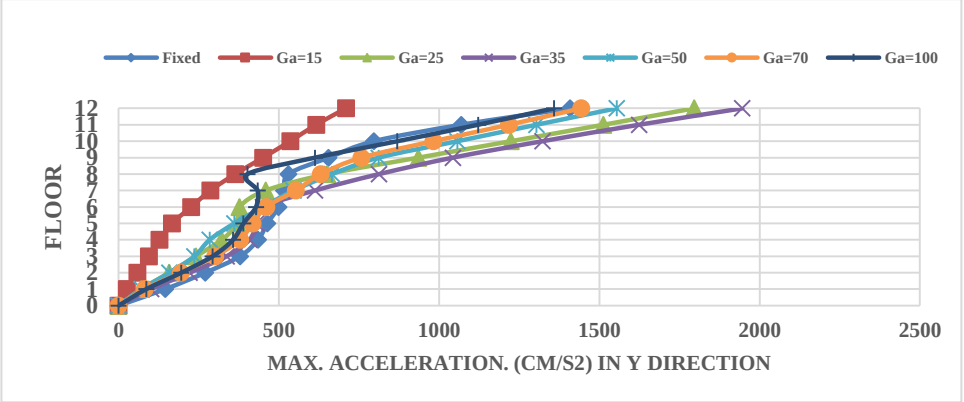


B) Controlled Systems SSI-SSI

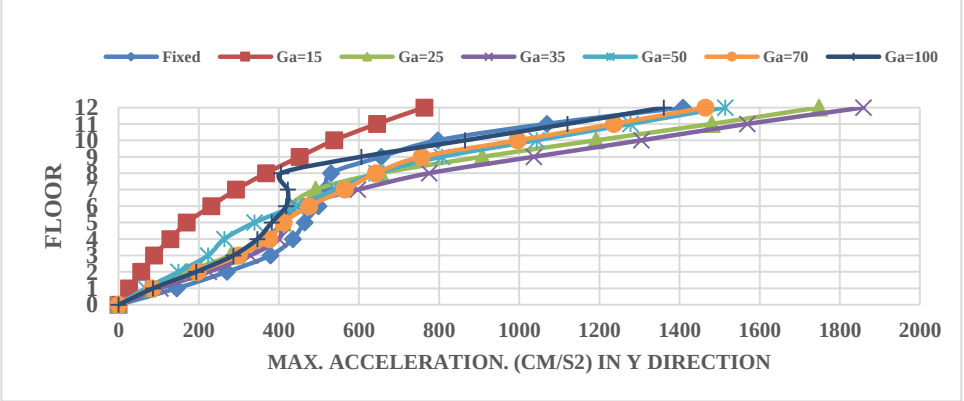


C) Controlled Systems Fixed-SSI

**Figure G-90** Max. acceleration of the systems under earthquake Corinth Greece, 2/24/1981

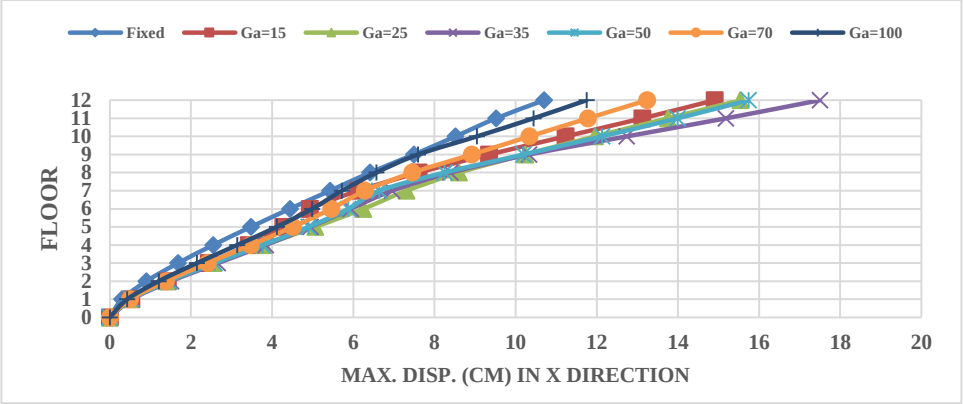


A) Uncontrolled Systems

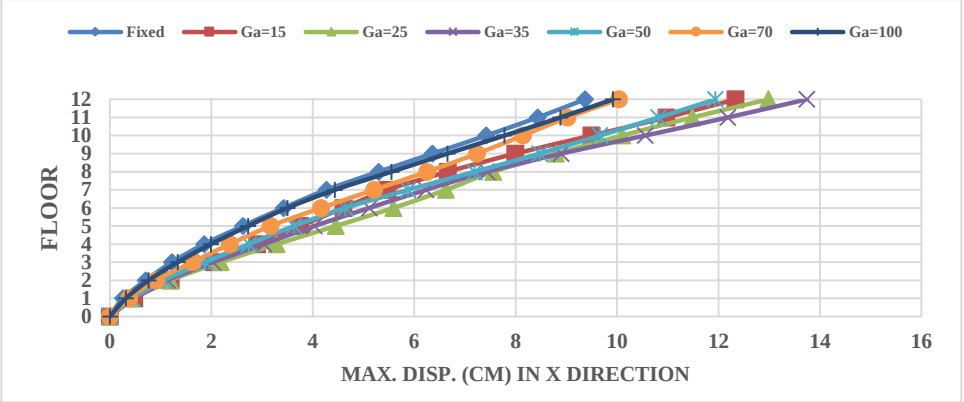


B) Controlled Systems SSI-SSI

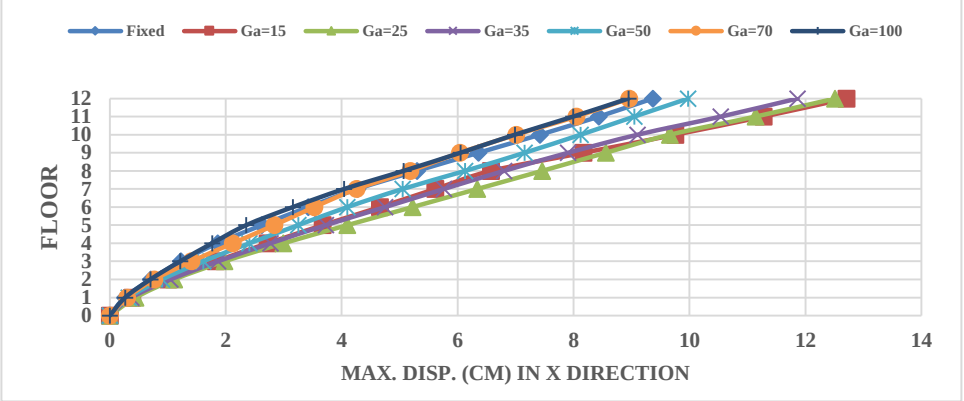


C) Controlled Systems Fixed-SSI

**Figure G-91** Max. displacements of the systems under earthquake Managua Nicaragua-02, 12/23/1972

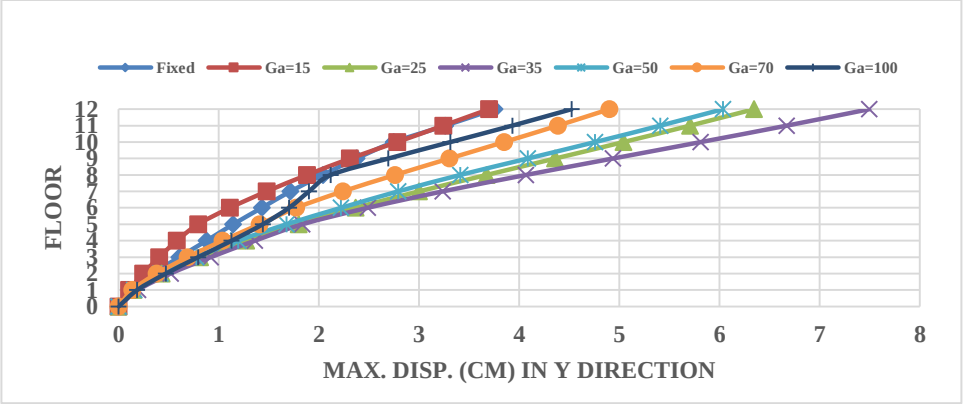


A) Uncontrolled Systems

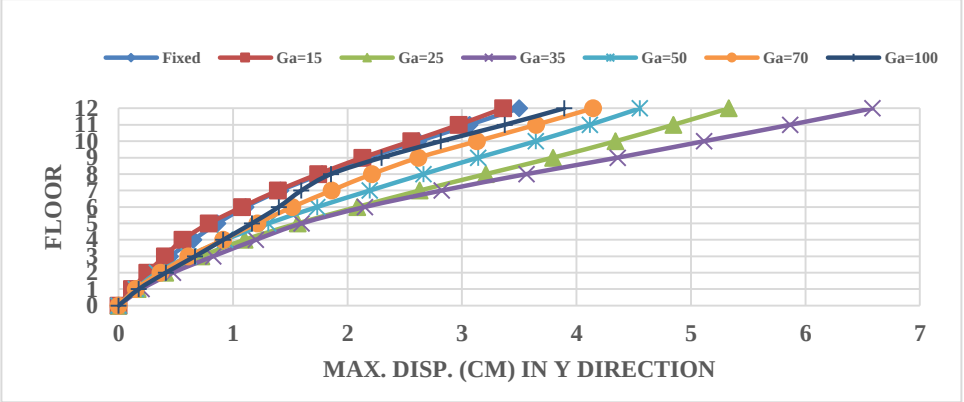


B) Controlled Systems SSI-SSI

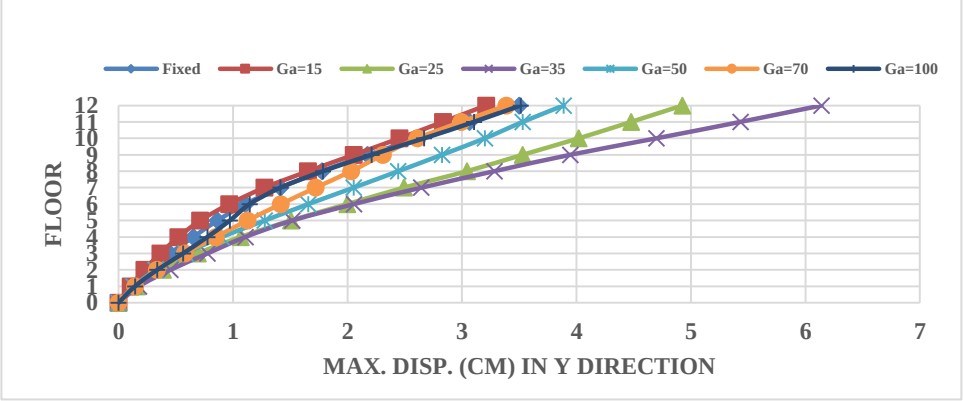


C) Controlled Systems Fixed-SSI

**Figure G-92** Max. displacements of the systems under earthquake Managua Nicaragua-02, 12/23/1972

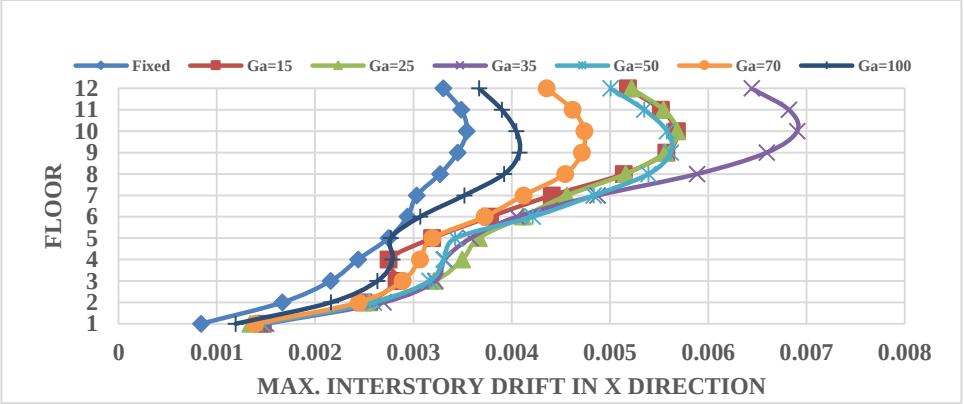


A) Uncontrolled Systems

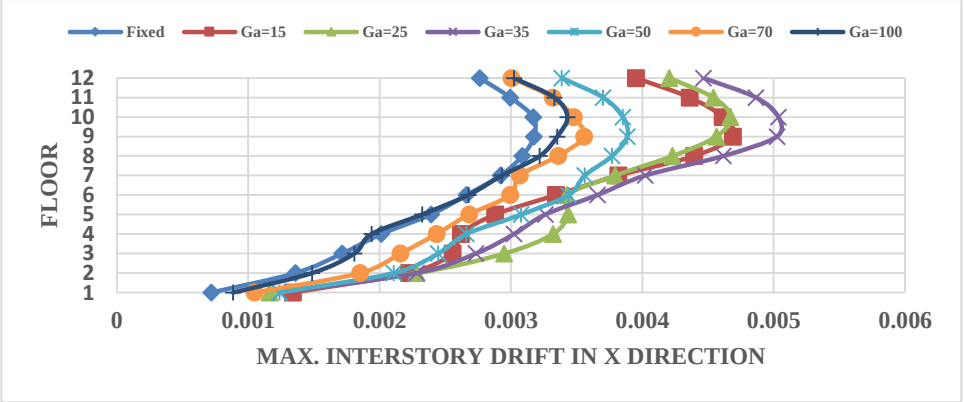


B) Controlled Systems SSI-SSI

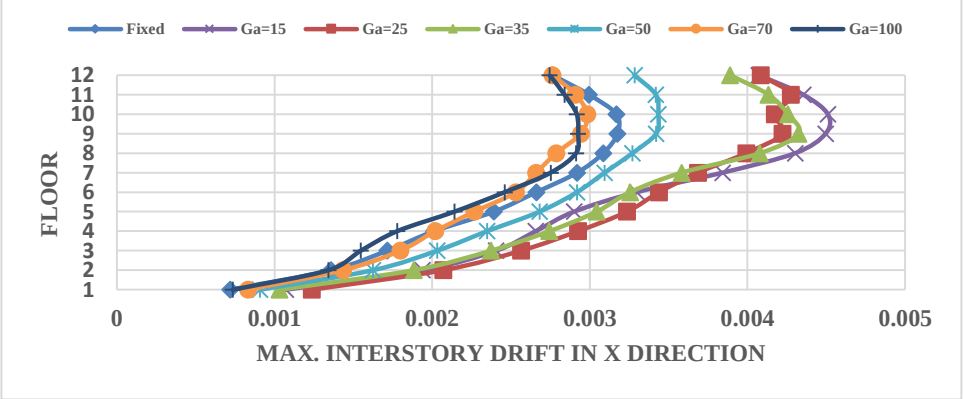


C) Controlled Systems Fixed-SSI

**Figure G-93** Max. interstory drift of the systems under earthquake Managua Nicaragua-02, 12/23/1972

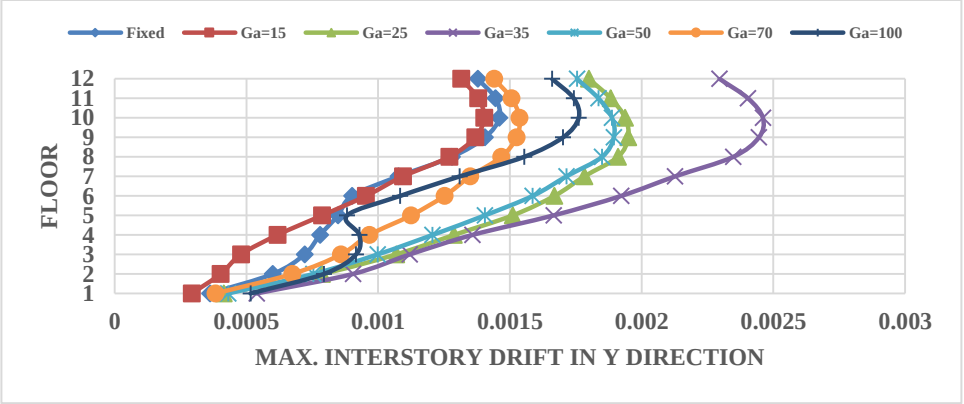


A) Uncontrolled Systems

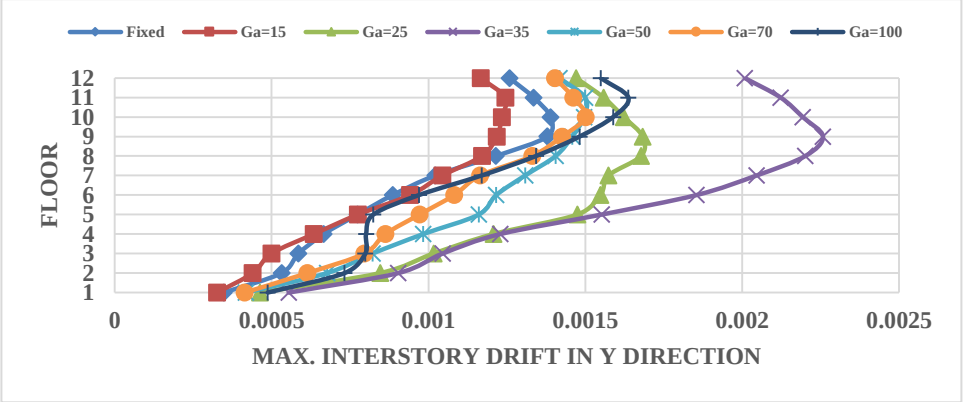


B) Controlled Systems SSI-SSI

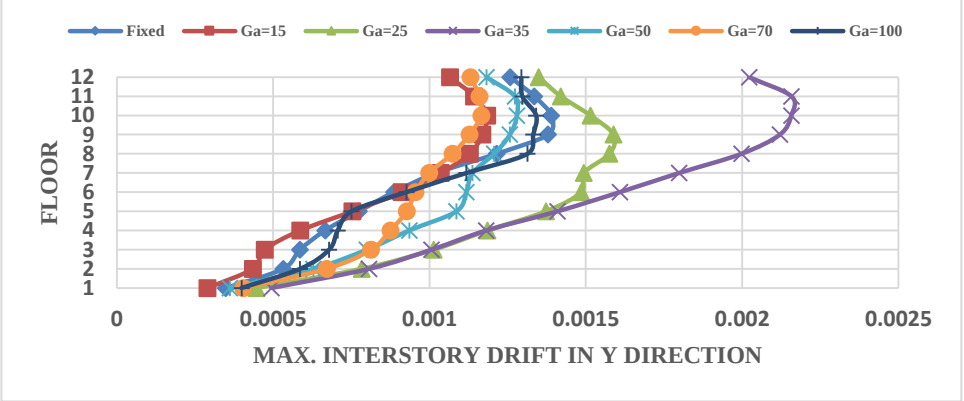


C) Controlled Systems Fixed-SSI

**Figure G-94** Max. interstory drift of the systems under earthquake Managua Nicaragua-02, 12/23/1972

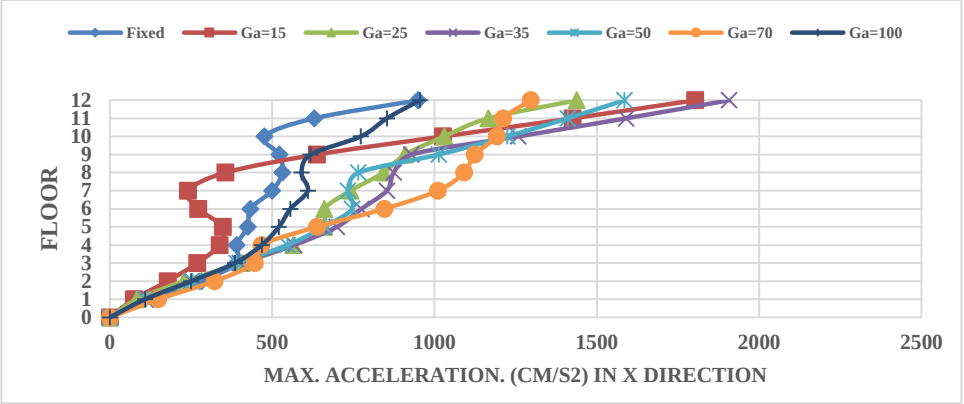


A) Uncontrolled Systems

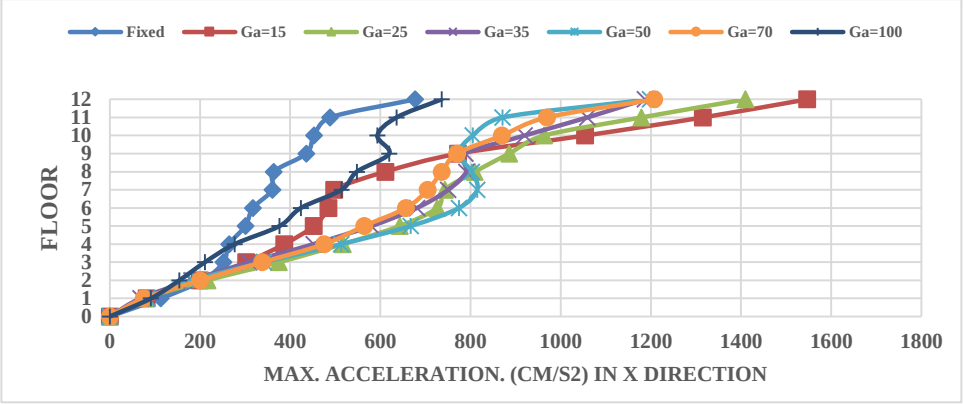


B) Controlled Systems SSI-SSI

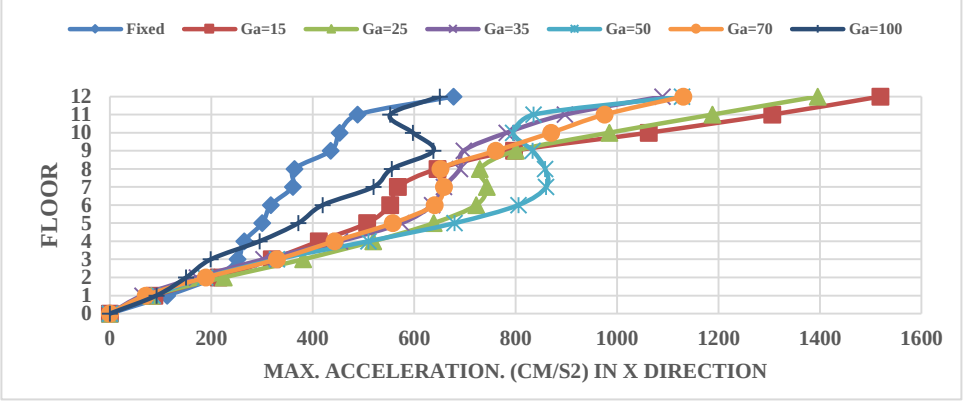


C) Controlled Systems Fixed-SSI

**Figure G-95** Max. acceleration of the systems under earthquake Managua Nicaragua-02, 12/23/1972

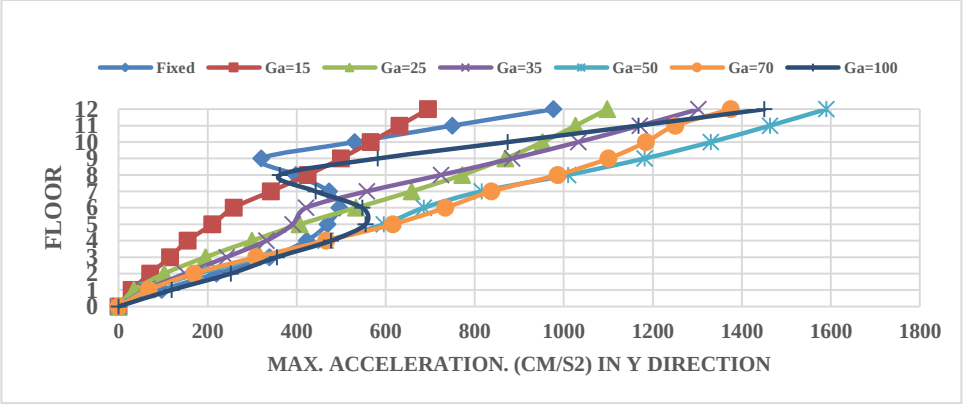


A) Uncontrolled Systems

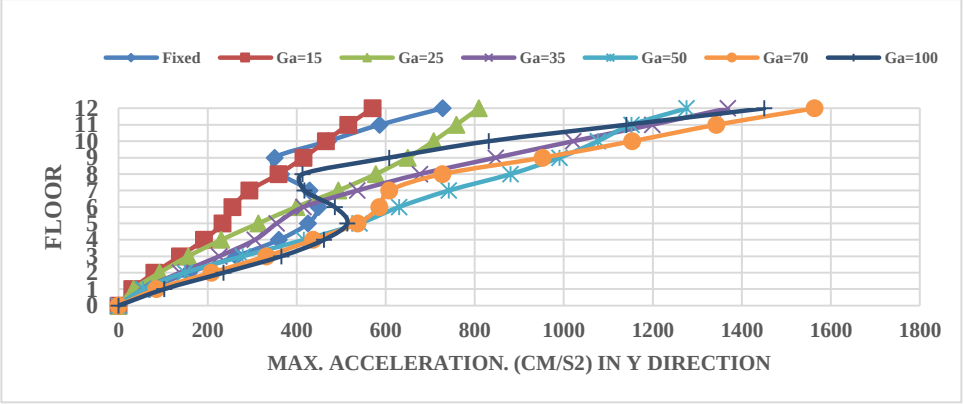


B) Controlled Systems SSI-SSI

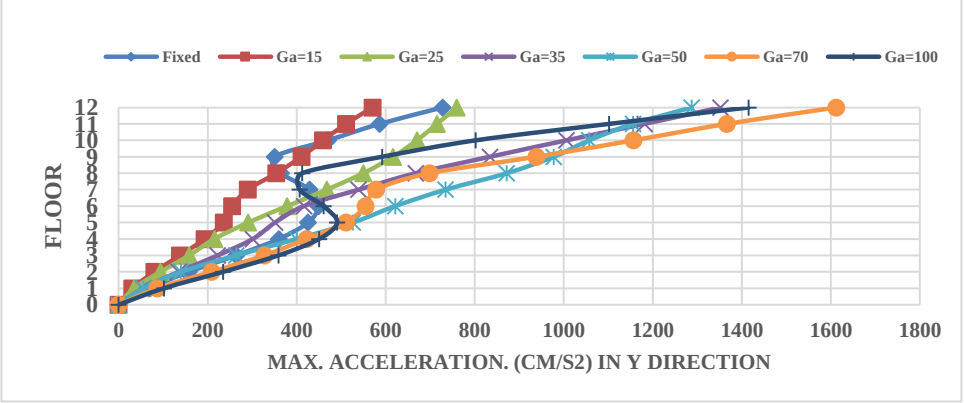


C) Controlled Systems Fixed-SSI

**Figure G-96** Max. acceleration of the systems under earthquake Managua Nicaragua-02, 12/23/1972

APPENDIX H

CONTROL SYSTEMS RESULTS IN RATIOS

Frame Building Control

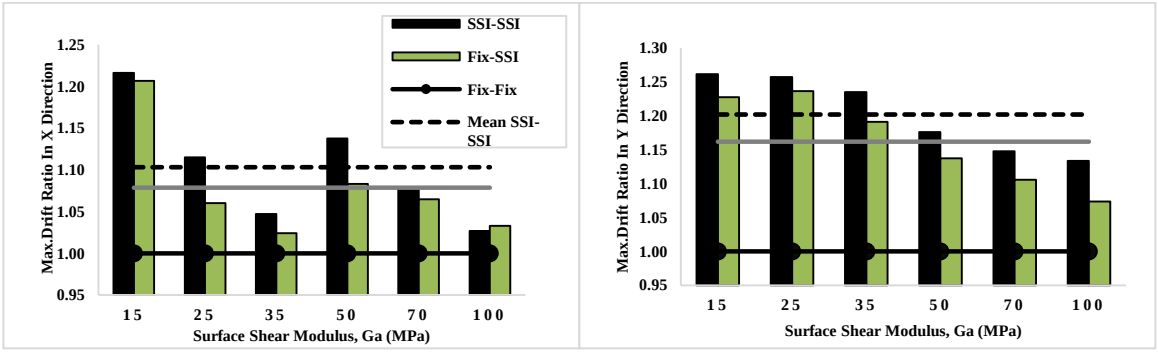


A) Max. Interstory Drift Ratio

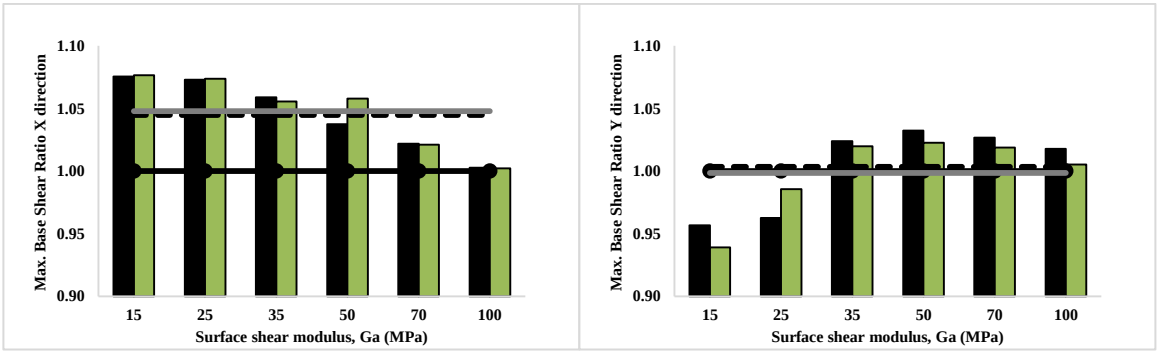


B) Max. Base Shear Ratio

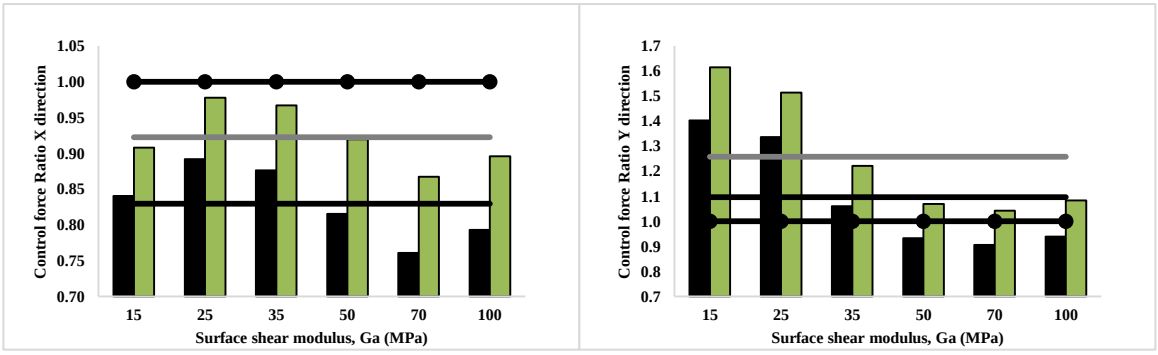


C) Max. Control force Ratio

**Figure H-1** The results of the clay (linear) soil profile under earthquake RSN96

Frame Building Control

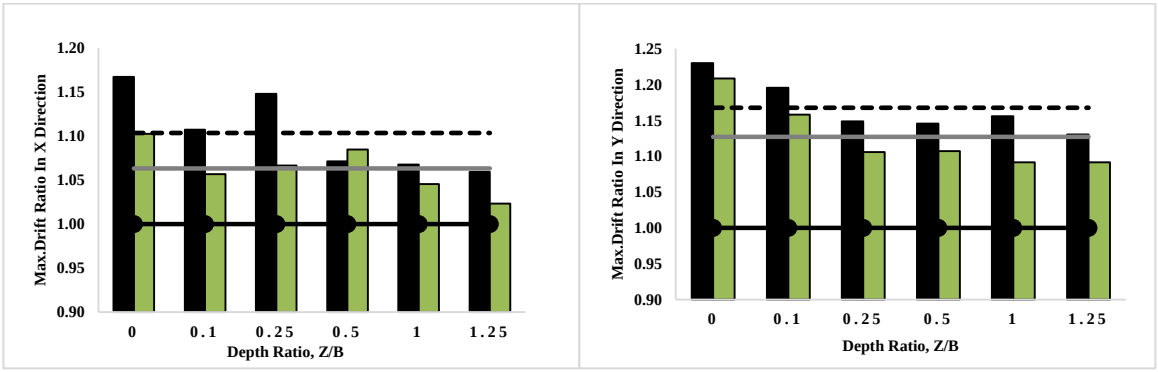


A) Max. Interstory Drift Ratio

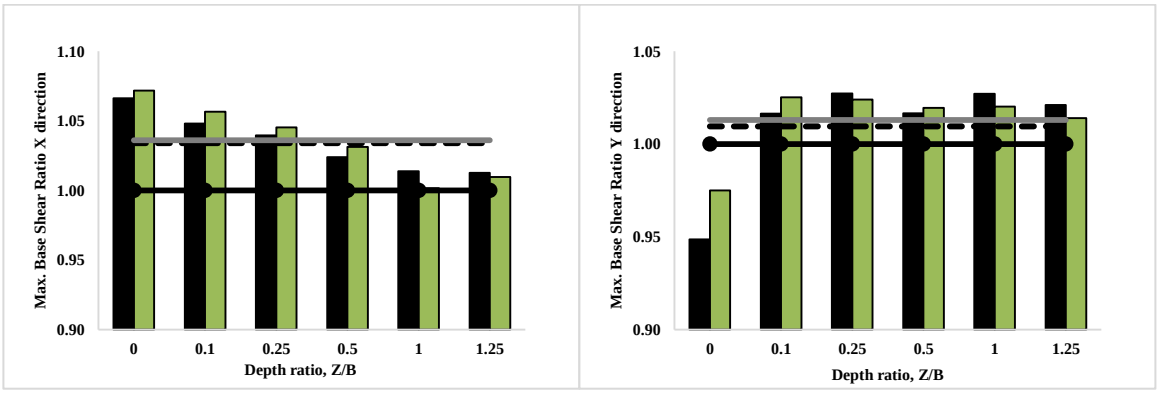


B) Max. Base Shear Ratio

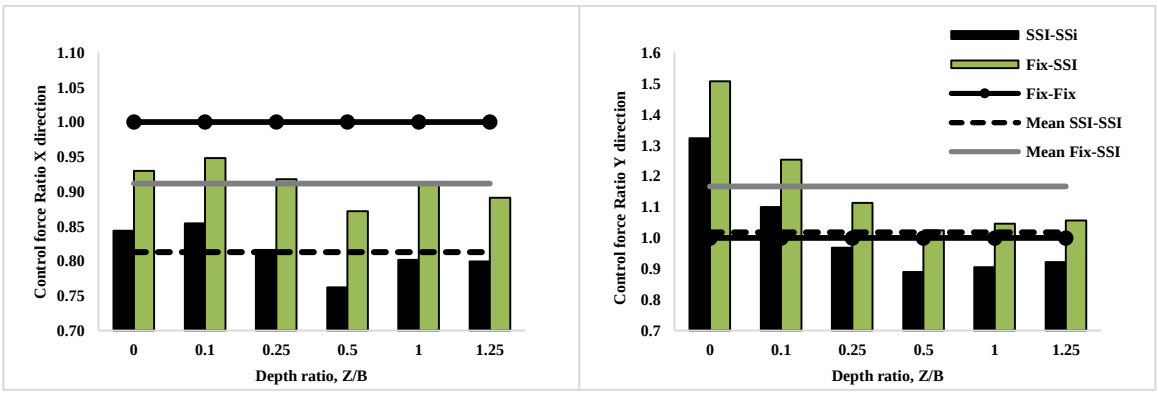


C) Max. Control force Ratio

**Figure H-2** The results of the medium soil top and soft soil bottom profile under earthquake RSN96.

Frame Building Control

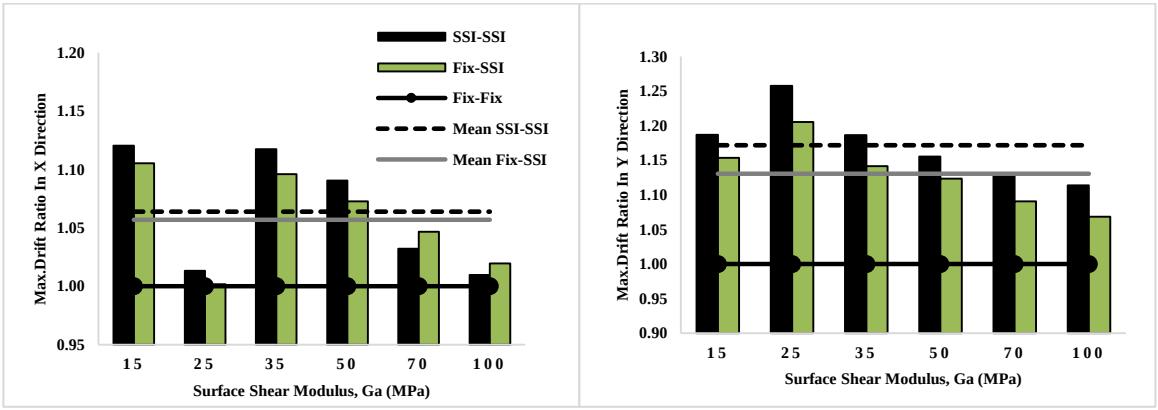


A) Max. Interstory Drift Ratio

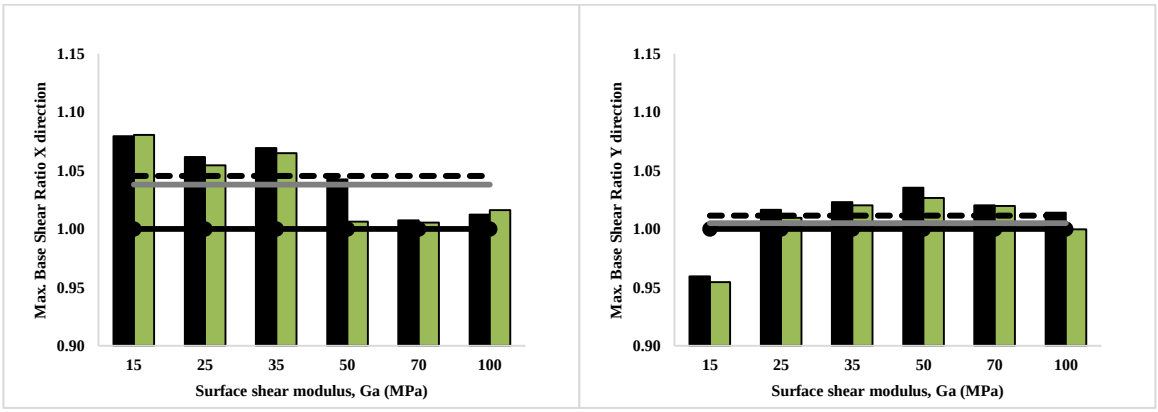


B) Max. Base Shear Ratio

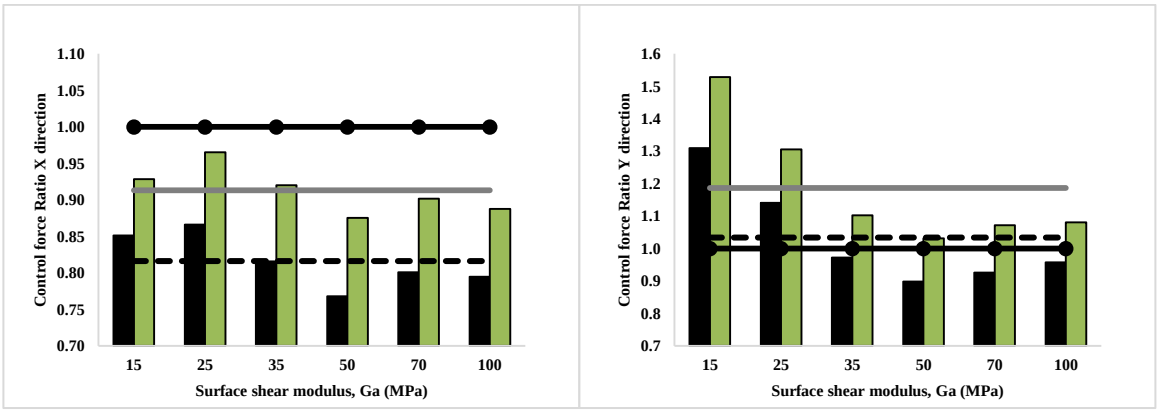


C) Max. Control force Ratio

**Figure H-3** The results of the sand (parabola) soil profile under earthquake RSN96.

Frame Building Control

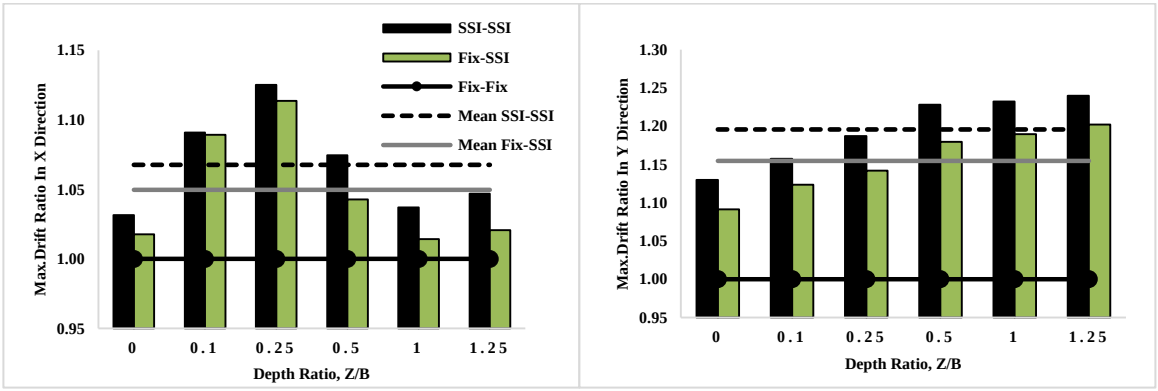


A) Max. Interstory Drift Ratio

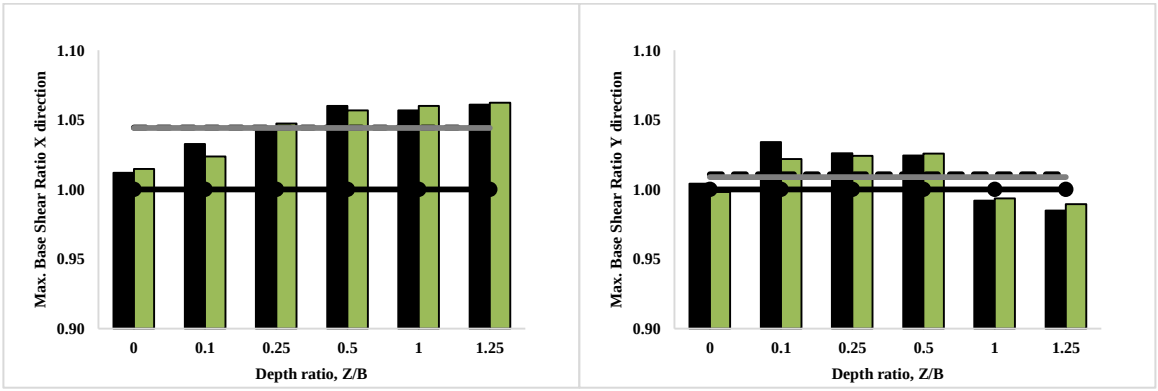


B) Max. Base Shear Ratio

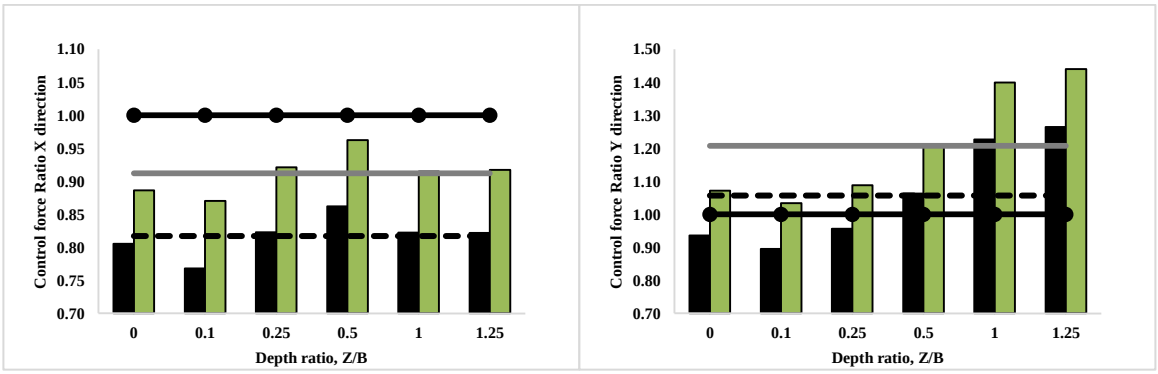


C) Max. Control force Ratio

**Figure H-4** The results soft soil top and medium soil bottom soil profile under earthquake RSN96.

Frame Building Control

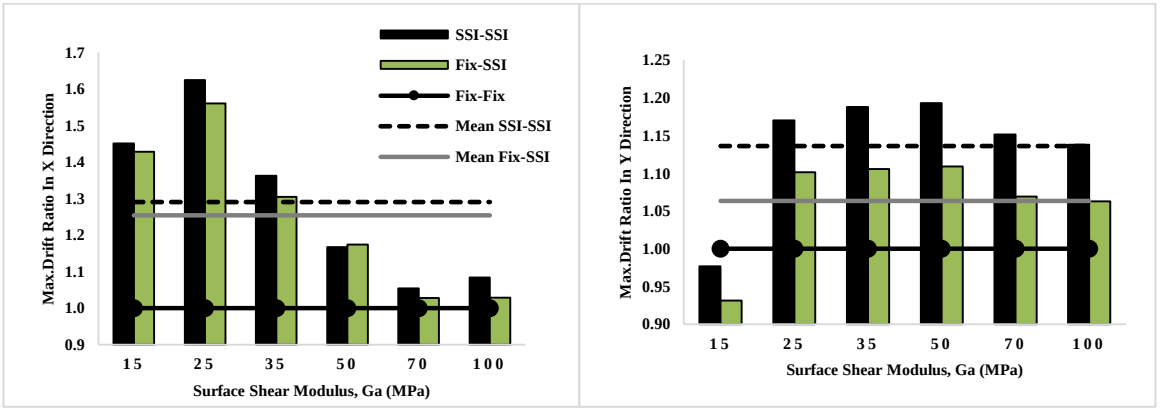


A) Max. Interstory Drift Ratio

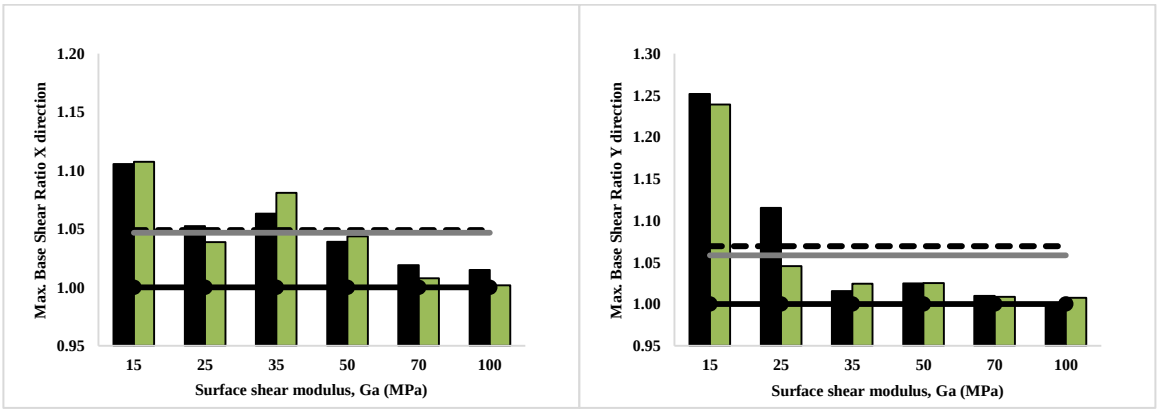


B) Max. Base Shear Ratio

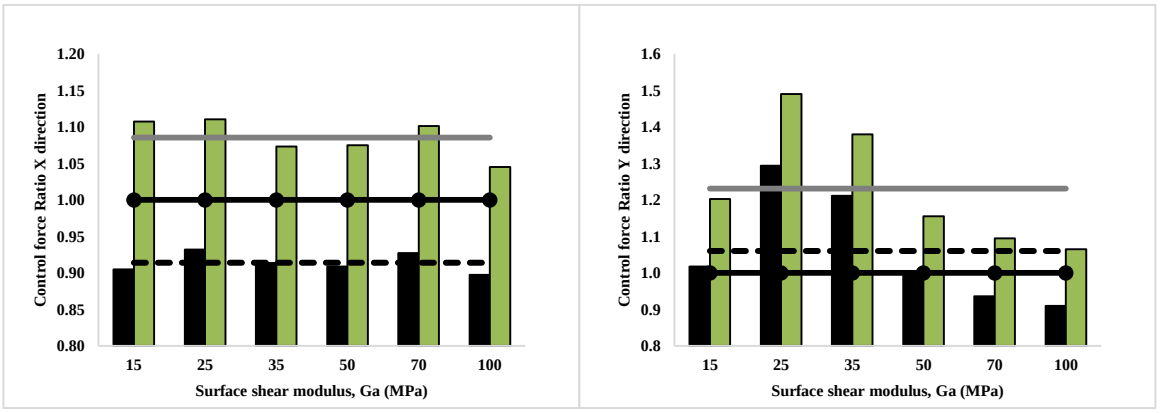


C) Max. Control force Ratio

**Figure H-5** The results clay (linear) soil profile under earthquake RSN313.

Frame Building Control

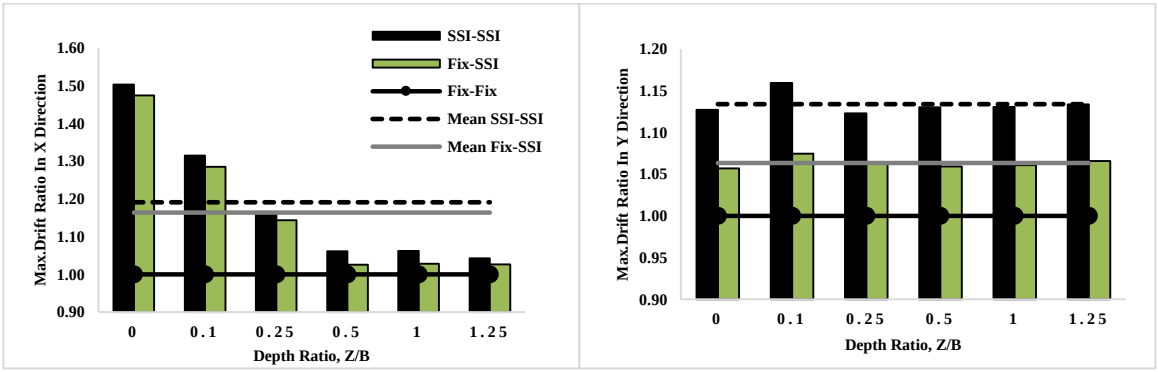


A) Max. Interstory Drift Ratio

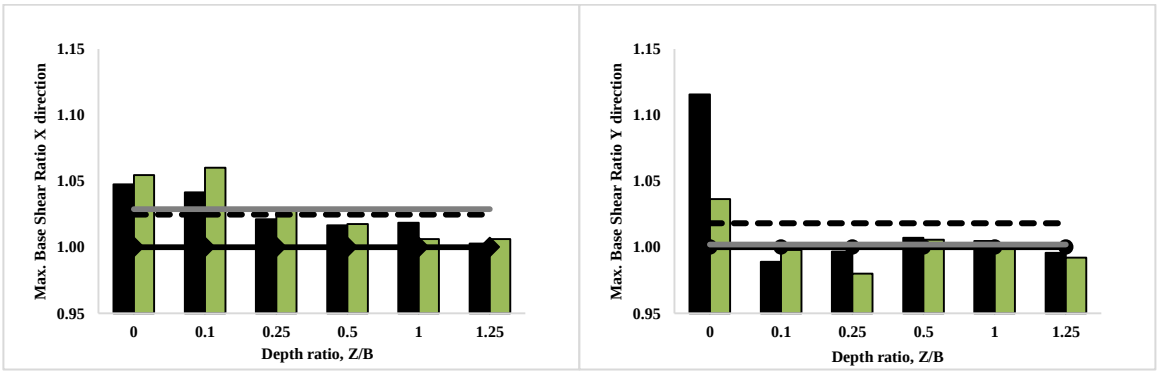


B) Max. Base Shear Ratio

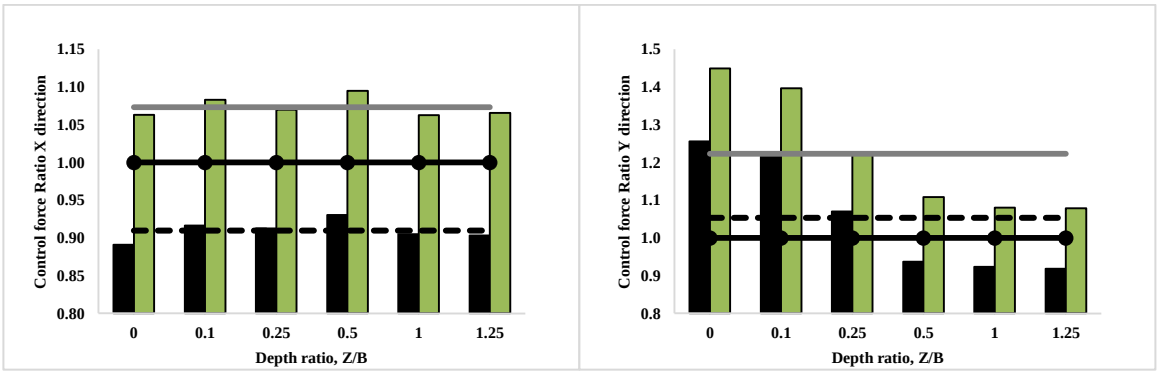


C) Max. Control force Ratio

**Figure H-6** The results of the medium soil top and soft soil bottom soil profile and earthquake RSN313.

Frame Building Control

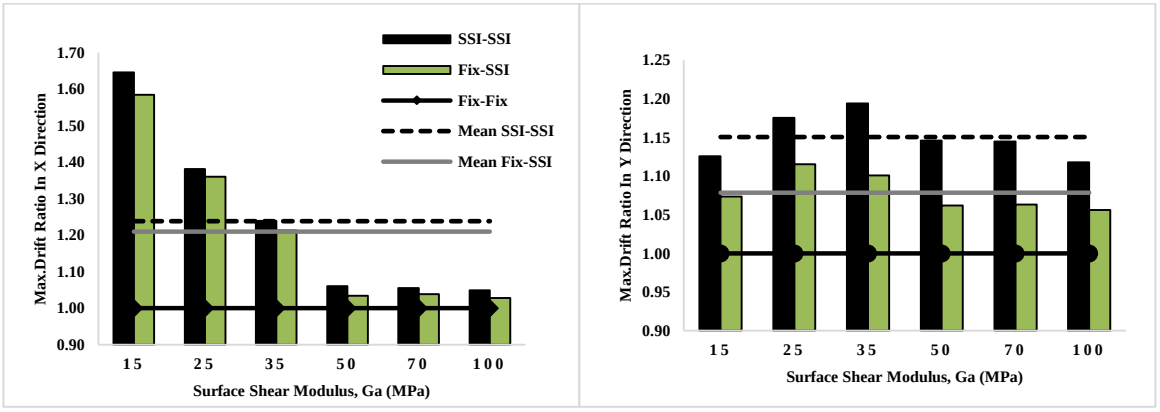


A) Max. Interstory Drift Ratio

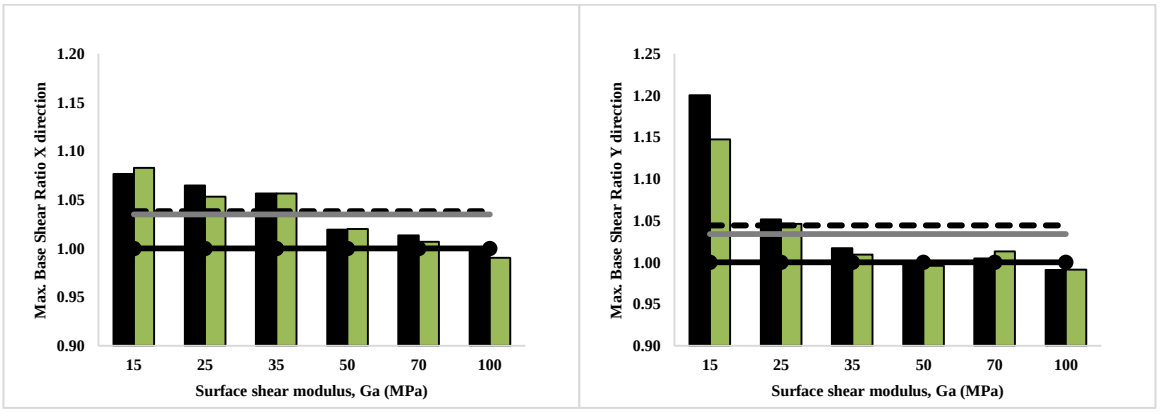


B) Max. Base Shear Ratio

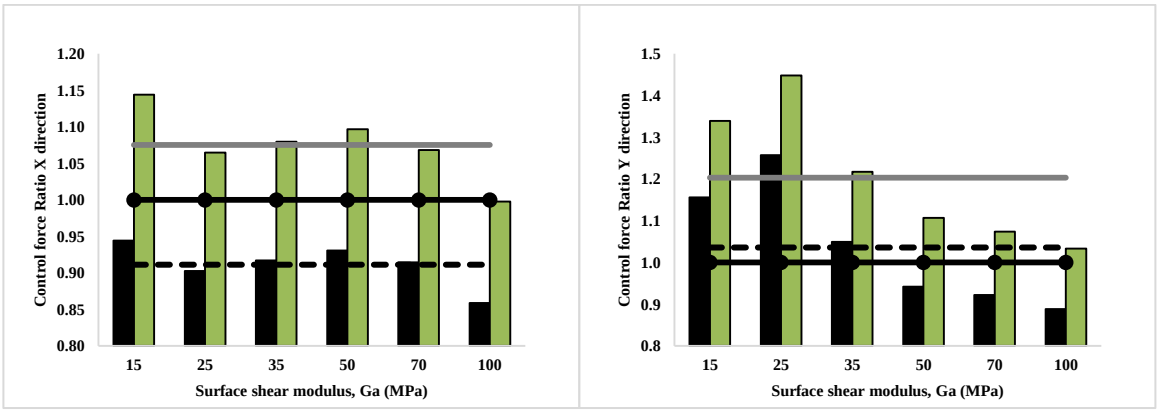


C) Max. Control force Ratio

**Figure H-7** The results of the sand (parabola) soil profile under earthquake RSN313.

Frame Building Control

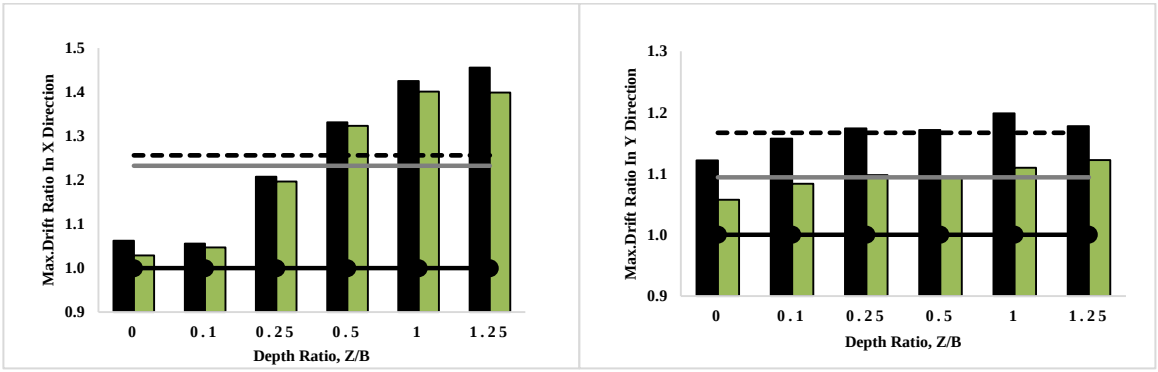


A) Max. Interstory Drift Ratio

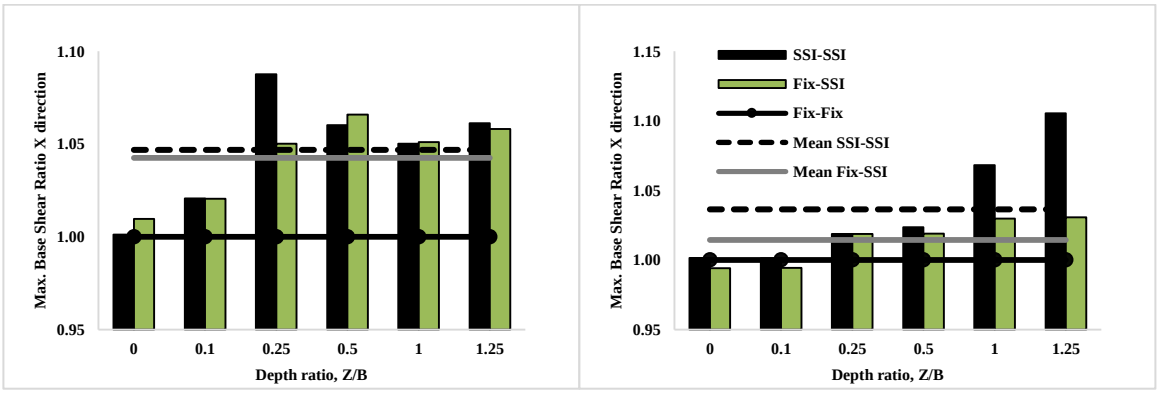


B) Max. Base Shear Ratio

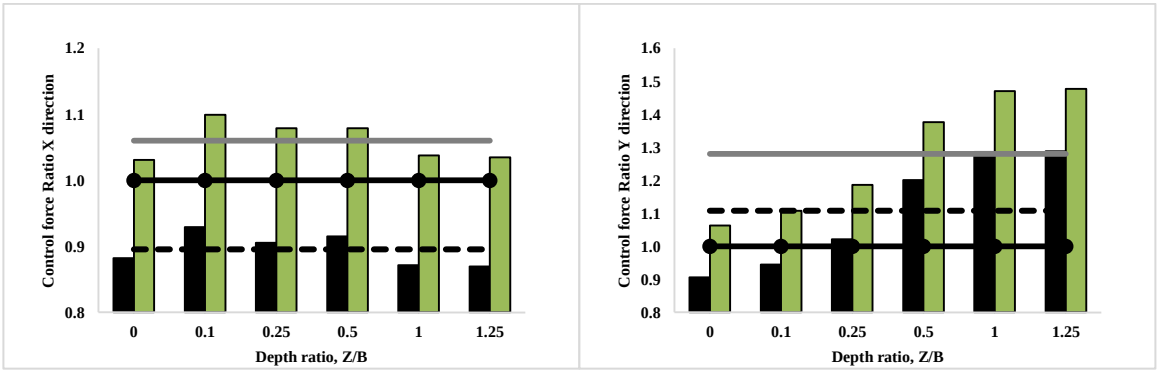


C) Max. Control force Ratio

**Figure H-8** The results of the soft soil top and medium soil bottom soil profile and earthquake RSN313.

Frame Shear Wall Building Control

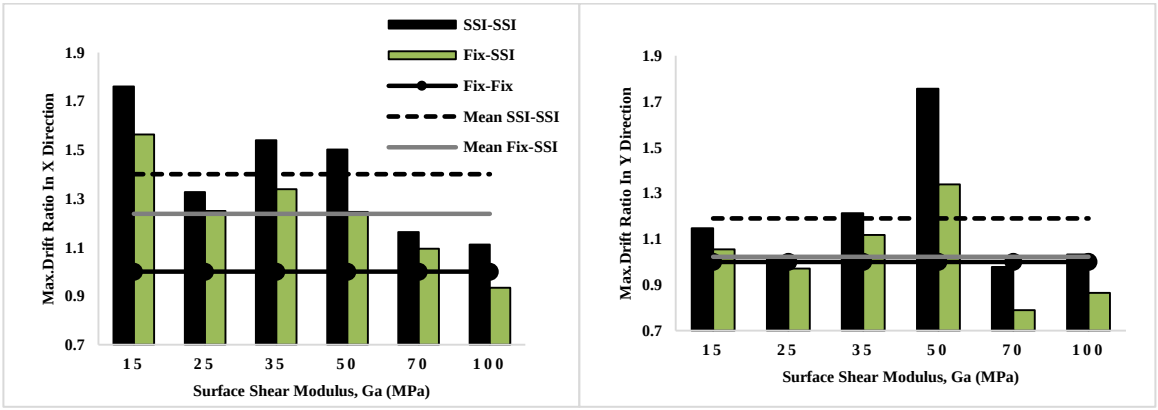


A) Max. Interstory Drift Ratio

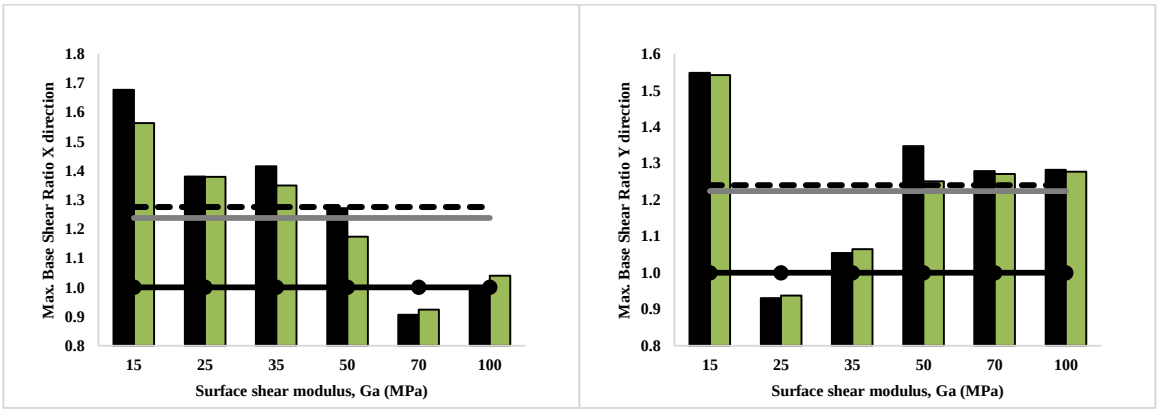


B) Max. Base Shear Ratio

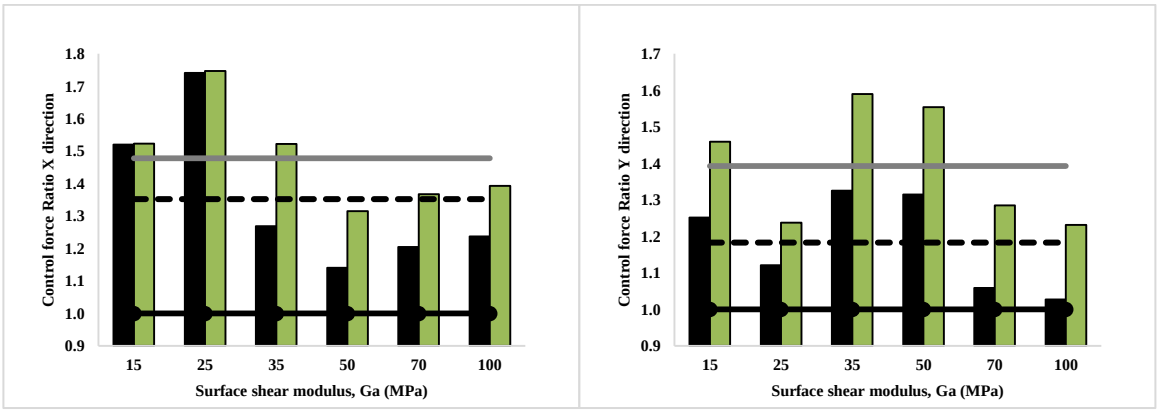


C) Max. Control force Ratio

**Figure H-9** The results of the clay (linear) soil profile under earthquake RSN96.

Frame Shear Wall Building Control

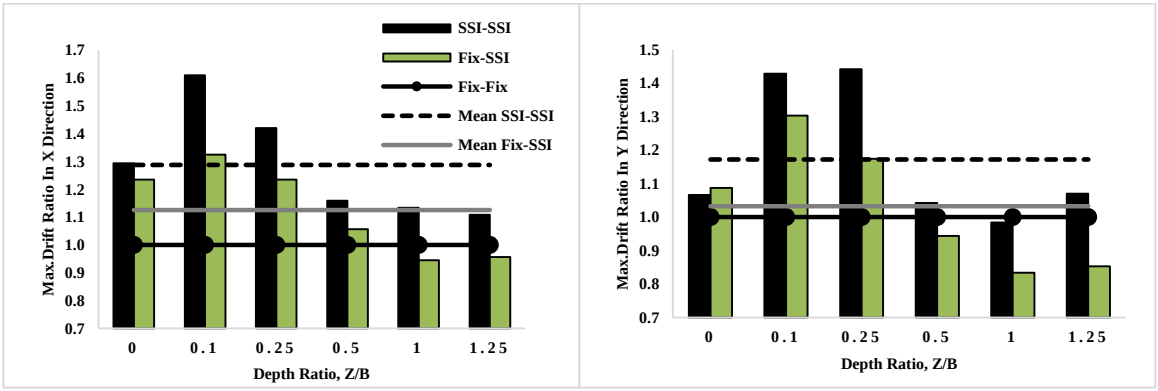


A) Max. Interstory Drift Ratio

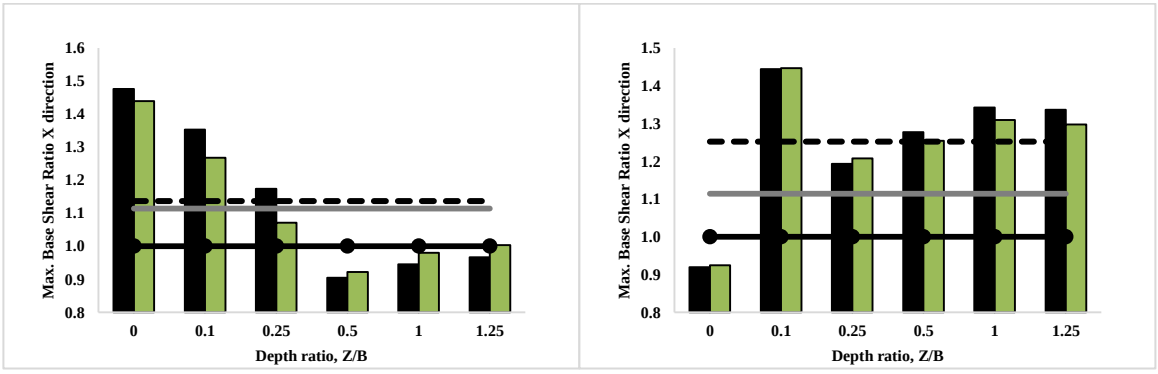


B) Max. Base Shear Ratio

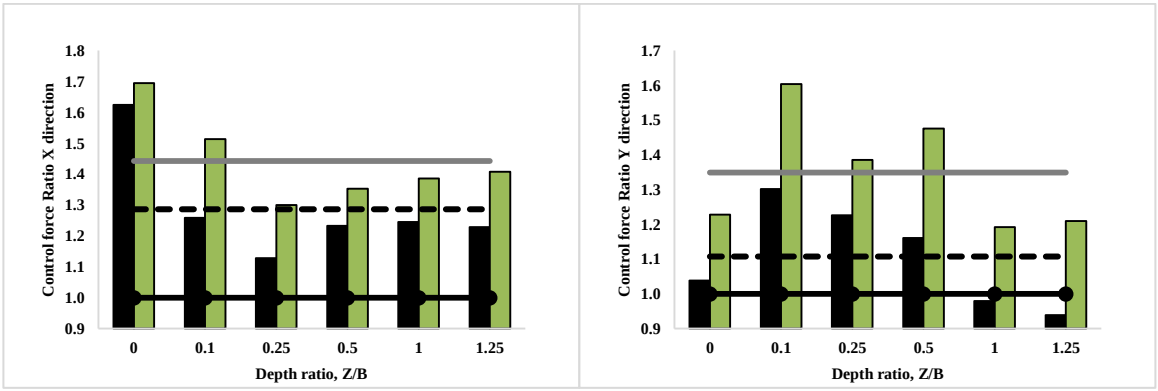


C) Max. Control force Ratio

**Figure H-10** The results of the medium soil top and soft soil bottom soil profile under earthquake RSN96.

Frame Shear Wall Building Control

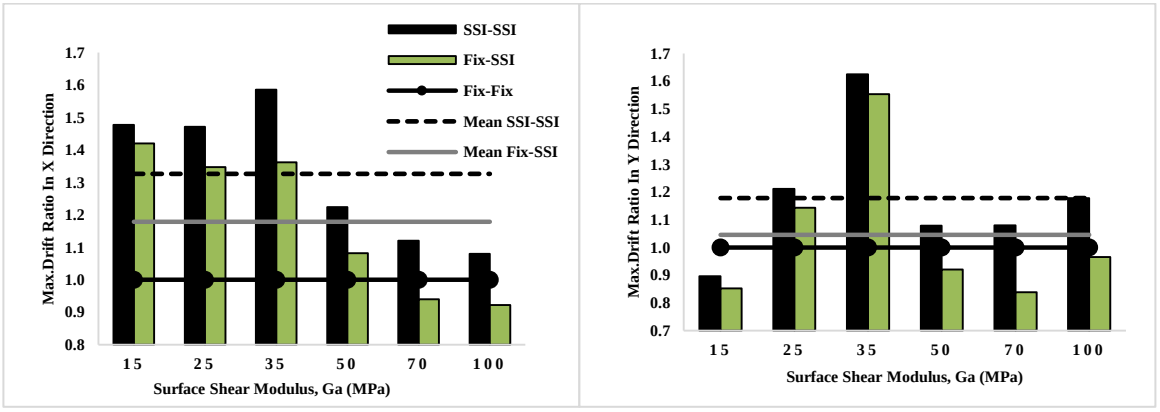


A) Max. Interstory Drift Ratio

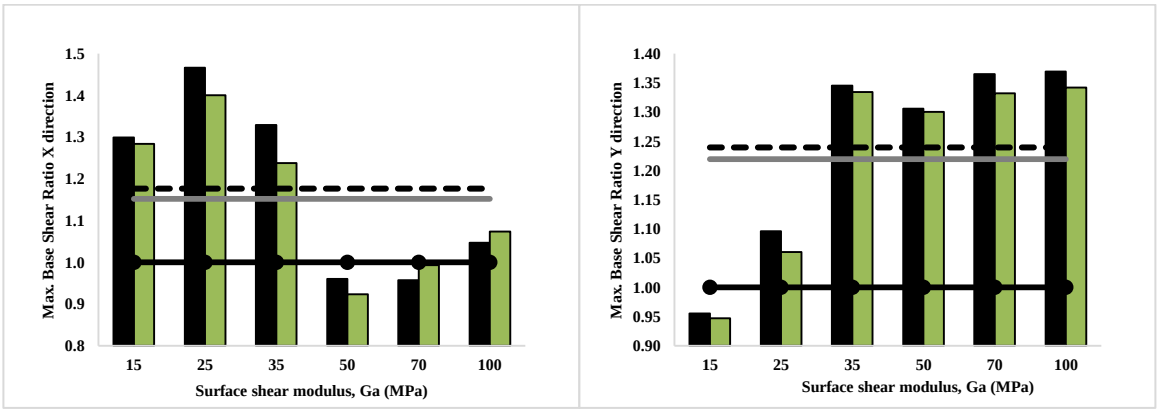


B) Max. Base Shear Ratio

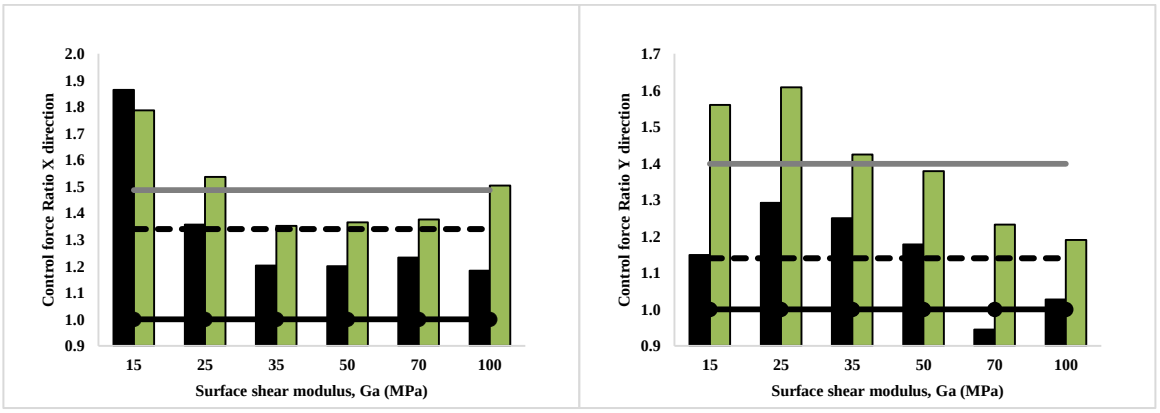


C) Max. Control force Ratio

**Figure H-11** The results of the sand (parabola) soil profile under earthquake RSN96.

Frame Shear Wall Building Control

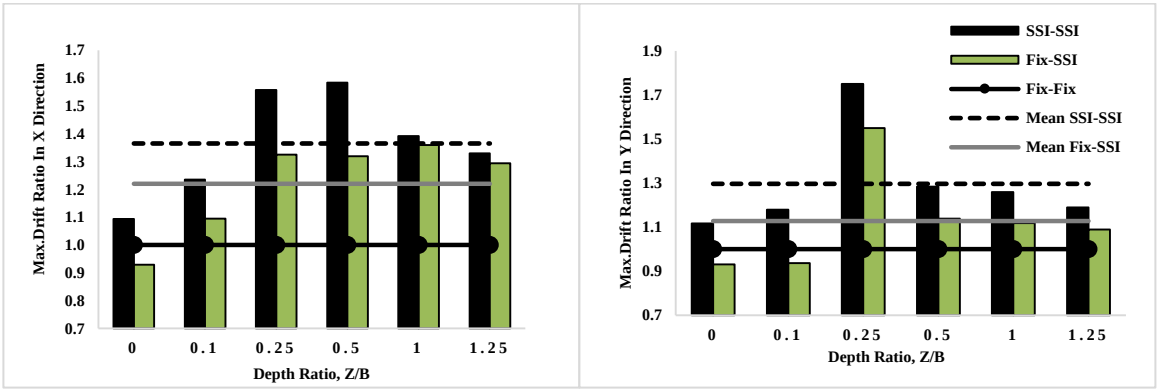


A) Max. Interstory Drift Ratio

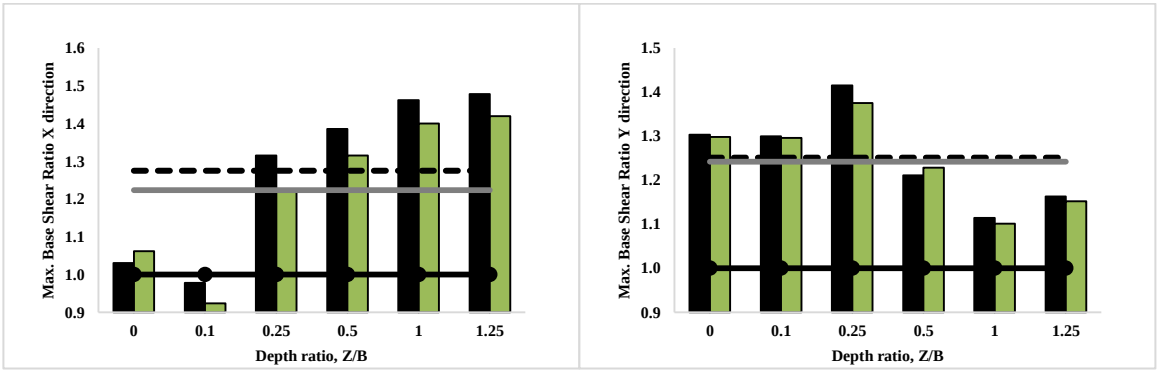


B) Max. Base Shear Ratio

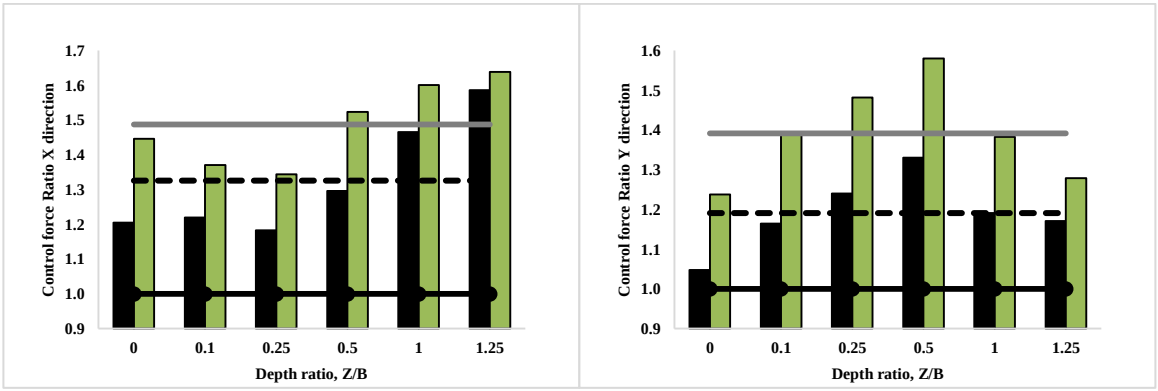


C) Max. Control force Ratio

**Figure H-12** The results of the soft soil top and medium soil bottom soil profile under earthquake RSN96.

Frame Shear Wall Building Control

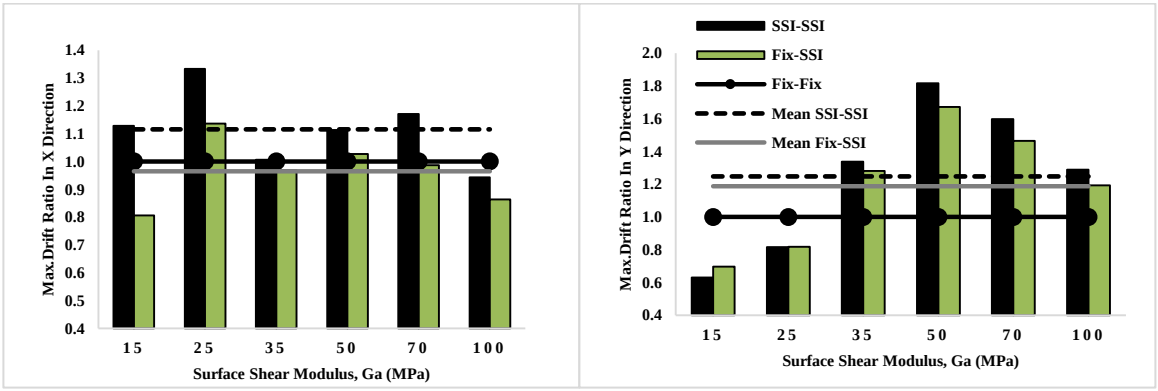


A) Max. Interstory Drift Ratio

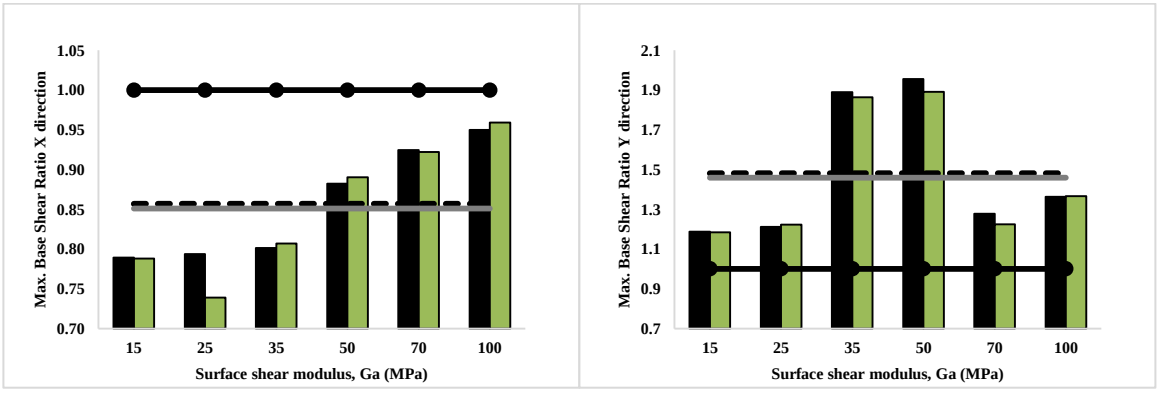


B) Max. Base Shear Ratio

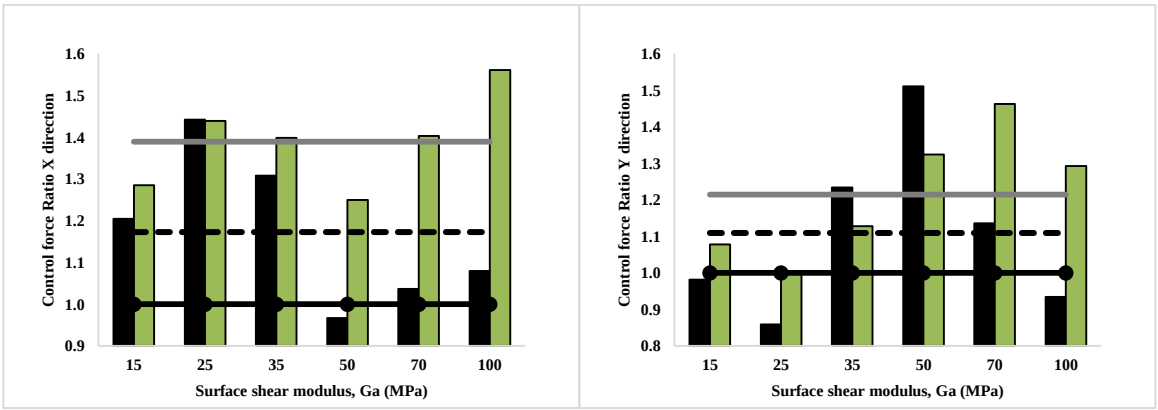


C) Max. Control force Ratio

**Figure H-13** The results of the clay (linear) soil profile under earthquake RSN313.

Frame Shear Wall Building Control

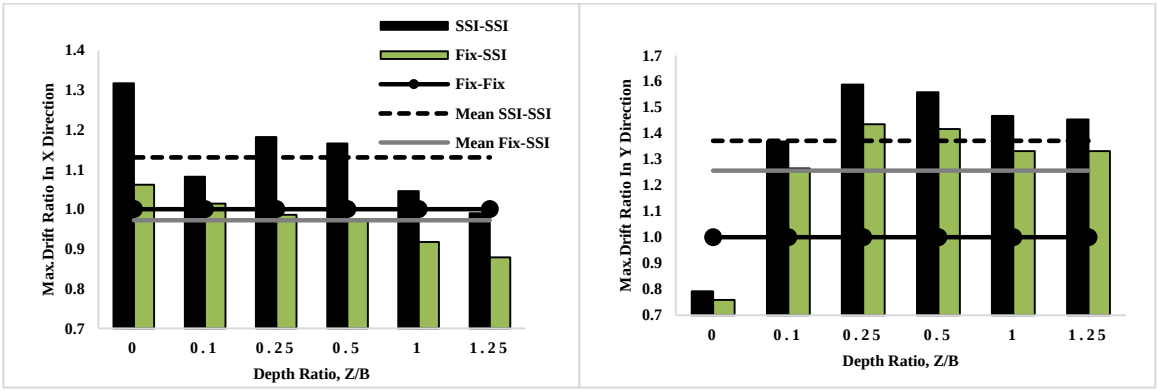


A) Max. Interstory Drift Ratio

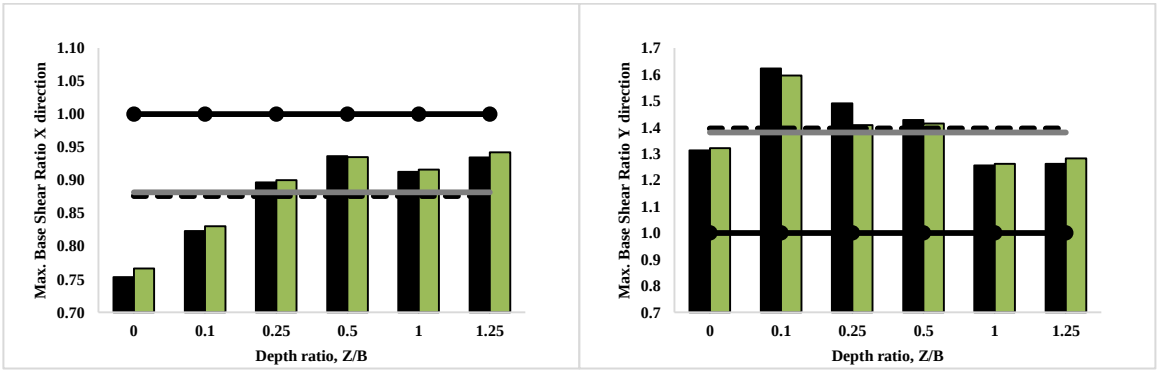


B) Max. Base Shear Ratio

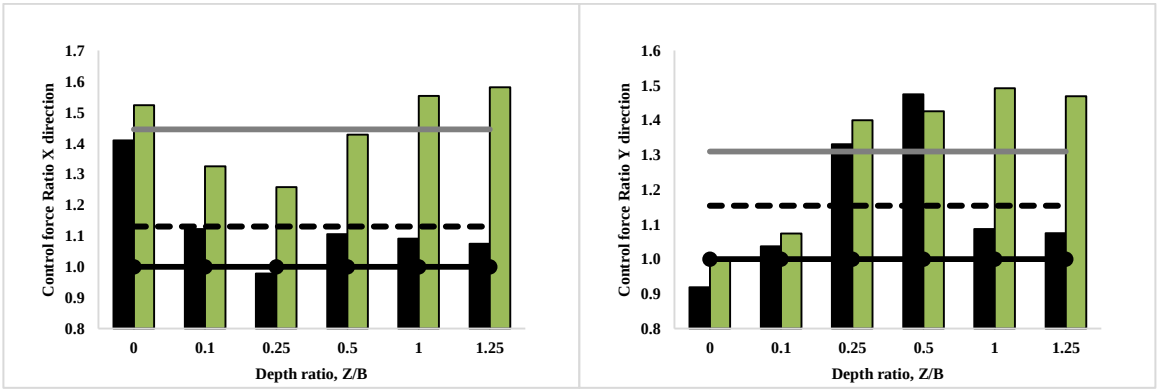


C) Max. Control force Ratio

**Figure H-14** The results of the medium soil top and soft soil bottom soil profile and earthquake RSN313.

Frame Shear Wall Building Control

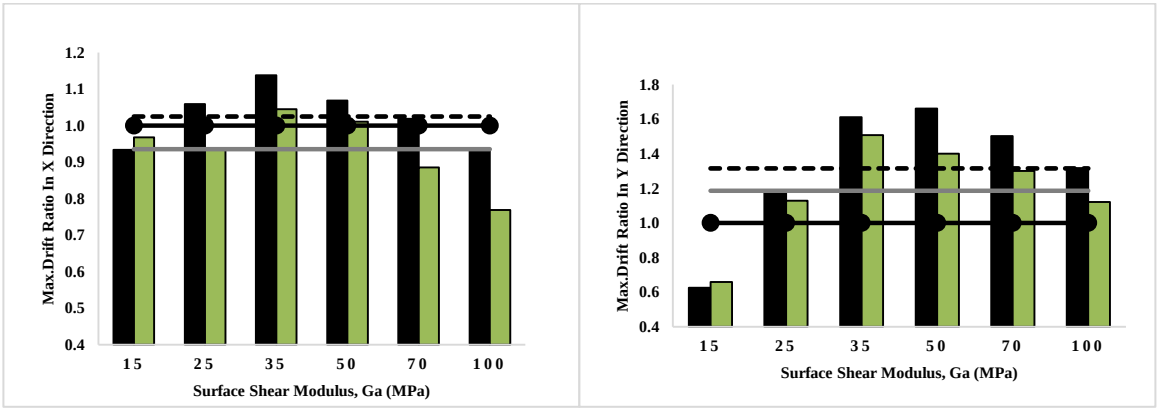


A) Max. Interstory Drift Ratio

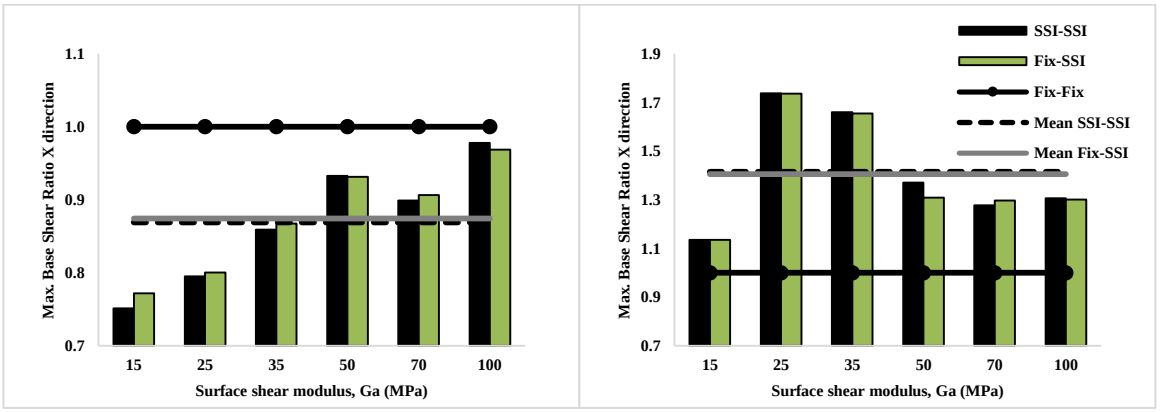


B) Max. Base Shear Ratio

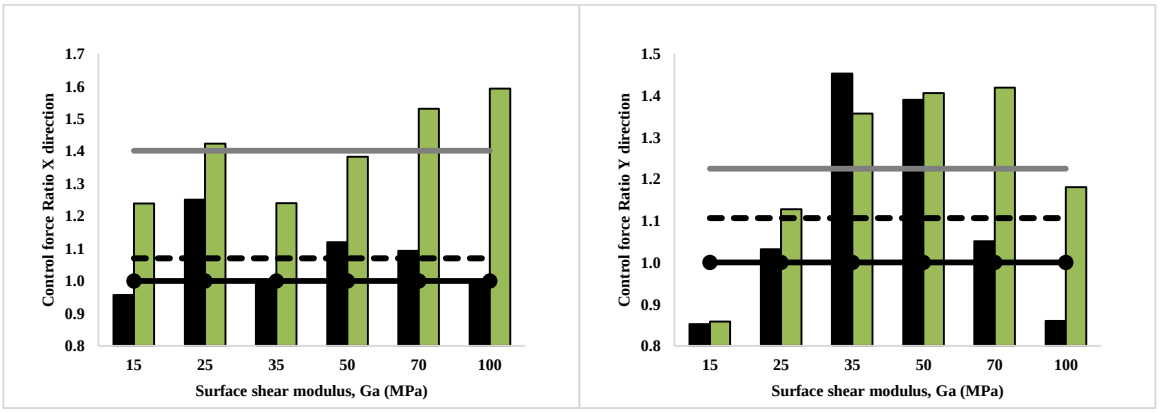


C) Max. Control force Ratio

**Figure H-15** The results of the sand (parabola) soil profile under earthquake RSN313.

Frame Shear Wall Building Control

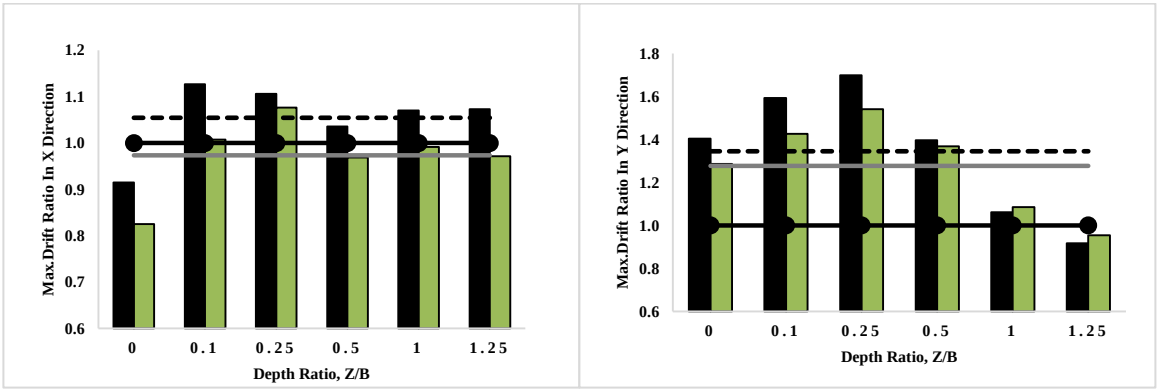


A) Max. Interstory Drift Ratio

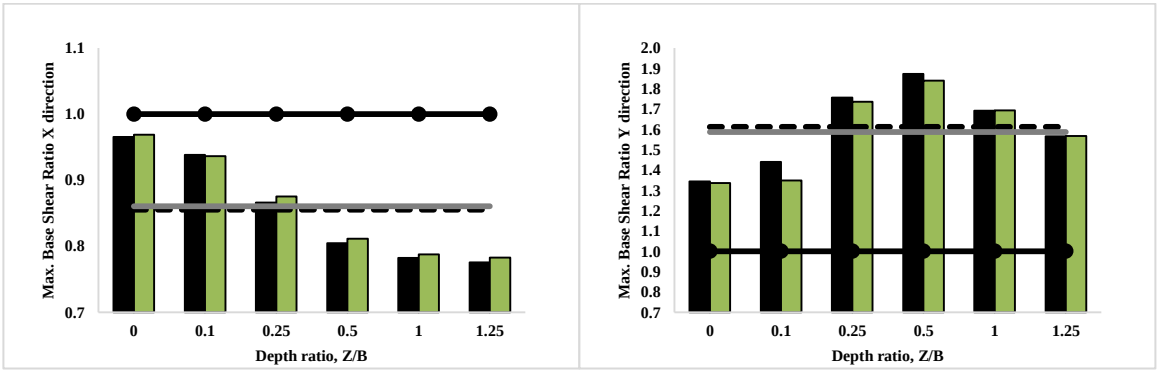


B) Max. Base Shear Ratio

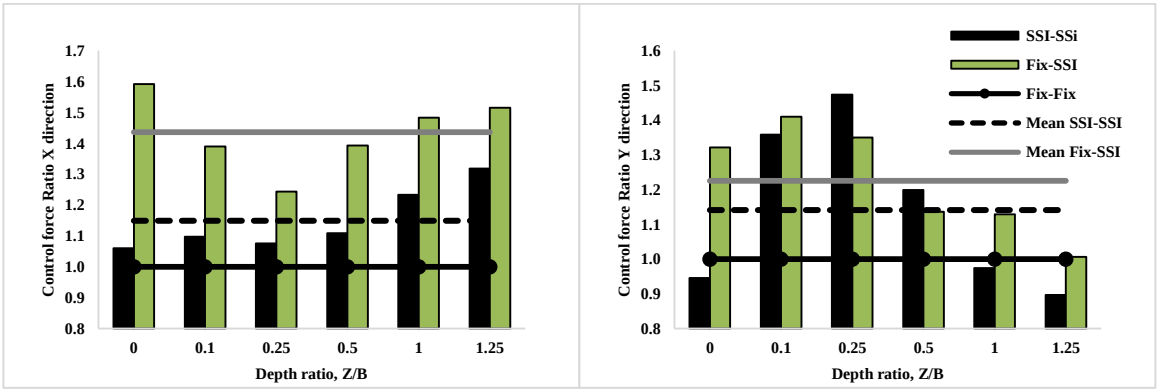


C) Max. Control force Ratio

**Figure H-16** The results of the soft soil top and medium soil bottom soil profile and earthquake RSN313.